Optimisation of a Novel Hydrogel for the Treatment of Cerebral Aneurysms

Sarah Brady, B.Eng. (Hons)

Dublin City University

School of Mechanical and Manufacturing Engineering

A dissertation submitted for the degree of Ph.D.

Under the supervision of

Dr. Owen Clarkin

Prof. Caitríona Lally

January 2018

Declaration

I hereby certify that this material, which I now submit for assessment on the programme of study leading to the award of PhD is entirely my own work, that I have exercised reasonable care to ensure that the work is original, and does not to the best of my knowledge breach any law of copyright, and has not been taken from the work of others save and to the extent that such work has been cited and acknowledged within the text of my work.

Signed: _____ (Candidate) ID No.: _____ Date: _____

Publications and Presentations

Papers

S.A. Brady, E.K. Fox, C. Lally, O.M. Clarkin, Optimisation of a Novel Glass-Alginate Composite for Treatment of Cerebral Aneurysms, *Carbohydr. Polym.*, vol. 176, pp. 227–35, 2017. Paper available in Appendix 9.1.1.1 (page 255)

S.A. Brady, E.K. Fox, F.R. Laffir, B. Phelan, C. Lally, O.M. Clarkin, Surface Modification of a Novel Glass for an Optimised Dispersion and Strength of an Injectable Alginate Composite*, J. Mater. Sci,.* Online 22nd August 2017. Paper available in Appendix 9.1.1.2 (page 270)

Conference Poster and Oral Presentations

Poster Presentation: S.A. Brady, E.K. Fox, C. Lally, O.M. Clarkin, Development of a Novel Hydrogel Filler to Treat Cerebral Aneurysms; Determination of the Influence of Molecular Weight and Alginate Concentration, Bioengineering in Ireland Conference, Carton House, Maynooth, 2015. Abstract available in Appendix 9.1.1.3 (page 283)

Poster Presentation: S.A. Brady, E.K. Fox, C. Lally, O.M. Clarkin, Determination of the Influence of Gamma Irradiation, Molecular Weight and Alginate Concentration of the Properties of a Novel Hydrogel for Vascular Applications, UK Society for Biomaterials Conference, The Merchant Hotel, Belfast, 2015. Abstract available in Appendix 9.1.1.4 (page 285)

Poster Presentation: S.A. Brady, E.K. Fox, F.R. Laffir, B. Phelan, C. Lally, O.M. Clarkin, Optimised Dispersion and Strength of an Injectable Alginate Composite, UK Society for Biomaterials Conference, University of Westminster, London, 2016. Abstract available in Appendix 9.1.1.5 (page 287)

Oral Presentation: S.A. Brady, C. Lally, O.M. Clarkin, Improved Adhesive Strength of a Novel Aneurysm Filler, RSC Biomaterials Special Interest Group Annual Meeting, Ulster University, Belfast, 2017. Abstract available in Appendix 9.1.1.6 (page 289)

Oral Presentation: S.A. Brady, C. Lally, O.M. Clarkin, Optimisation and In Vitro Analysis of a Novel Hydrogel for the Treatment of Cerebral Aneurysms, Faculty of Engineering and Computing Research Day, Dublin City University, Dublin, 2017. No abstract was required.

Acknowledgements

Firstly, I would like to thank my supervisors Dr. Owen Clarkin and Prof. Caitríona Lally for their support, guidance and patience. Their endless knowledge never ceased to amaze me and encourage me throughout this research. I sincerely appreciate the opportunities they have provided me by allowing me to work on this project.

Much of this research would not have been carried out without certain collaborations. In particular I would like to thank Prof. Paul Cahill for his advice and allowing me use his lab to carry out the *in vitro* analysis. Thank you to Dr. Alan O'Hare for his advice, constructive criticism and for testing the hydrogel throughout its development. I would also like to thank Fathima Laffir and Brendan Phelan, as much of the surface analysis of the glass would not be completed without their work.

I would like to thank all the PhD students and postdocs who have helped me, especially Eoin, Irina, Joe, Richard and Dr. Cahill's entire lab. I am grateful for their invaluable advice and willingness to help.

Many thanks to Michael, Chris, Liam and Alan in the School of Mechanical and Manufacturing Engineering for their technical support and training, and Jim, Cian and Dean for their support in the workshop.

Finally, I would like to thank my friends and family. My friends have always been there, especially on the days when I need them most. I am especially grateful to Michael for his support and for humouring me by listening. His encouragement particularly helped in the final stretch and I will always appreciate it. I am forever grateful to my parents and siblings, none of this would be possible without their belief, support and ability to put a smile on my face.

Contents

Chapter 1. Introduction 3

1.1. Aim 3

Chapter 2. Literature Review 7

2.1. Cerebral Vascular Structure and Cerebral Aneurysms 7

2.2. Cerebral Aneurysms 10

2.3. Cerebral Aneurysm Treatments 17

2.4. The Ideal Aneurysm Treatment Device 25

2.5. Novel Aneurysm Treatment 35

2.6. Novel Hydrogel 49

2.7. Rationale of work 50

Chapter 3. Background Theory 53

3.1. Alginate Classification 53

3.2. Glass Characterisation 54

3.3. Examination of the Hydrogel 60

3.4. Cell Culture 66

3.5. Platelet Activation 67

3.6. *In vivo* Analysis 69

Chapter 4. Materials and Methods 71

4.1. Alginate 71

4.2. Glucono Delta Lactone 73

4.3. Glass 73

4.4. Preparing Hydrogel 75

4.5. EDC and NHS 75

4.6. Examination of the Hydrogel 75

4.7. *In Vitro* Analysis 83

4.8. Ion dosing 86

4.9. Sterilisation 87

4.10. Direct Contact testing 87
4.11. Calcification 88
4.12. Platelet Adhesion 89
4.13. *In Vivo* Study 89
4.14. Statistical Analysis 92
Chapter 5. Results and Discussion 93
5.1. Effect of Molecular Weight and Chemical Composition 93
5.2. Effect of Gamma Irradiation of Alginate 109
5.3. Effect of Acid Washing Glass and Increasing Glass Content 117
5.4. Effect of the Addition of EDC and NHS 137
5.5. *In Vitro* Analysis 149
5.6. Optimising Sterilisation Techniques 167
5.7. Calcification Results 185
5.8. Direct Contact Analysis 193
5.9. Radiopacity 197
5.10. Platelet Adhesion 203
5.11. *In vivo* Analysis 209
5.12. Design of Injection Device 221
Chapter 6. Project Discussion 223
Chapter 7. Conclusion and Future Work 227
7.1. Conclusions 227
7.2. Future Work 229
Chapter 8. Bibliography 231
Chapter 9. Appendix 255
9.1. Appendix A 255
9.2. Appendix B 290
9.3. Appendix C 293
9.4. Appendix D 294
9.5. Appendix D 305

List of Figures

Figure 1.1.1 Schematic of a novel hydrogel being injected through a microcatheter into a cerebral aneurysm with a compliant balloon placed across the neck [15] 4
Figure 2.1.1 Comparison of the layers of intracranial and extracranial arteries [22] 8
Figure 2.2.1 Comparison of the cellular structure of cerebral arteries and an aneurysm wall [35] 10
Figure 2.2.2 Three aneurysm shapes; Saccular, fusiform and dissecting [60] 14
Figure 2.2.3 Circle of Willis with the common locations of cerebral aneurysms [62] 14
Figure 2.3.1 Clip Ligation of a Cerebral Aneurysm [1] 17
Figure 2.3.2 Coiling an aneurysm using a Guglielmi detachable coil [5] 19
Figure 2.3.3 Recurrent aneurysm formation [5] 20
Figure 2.3.4 Risks associated with aneurysm coiling [5] 21
Figure 2.3.5 a) Woven EndoBridge (WEB) dual layer device b) WEB single layer [104] 23
Figure 2.3.6. Balloon-assisted Onyx® embolization [70] 24
Figure 2.5.1 M-block (A), G-block (B) and alternating GM-blocks (C) of alginate [187] 38
Figure 2.5.2 Ionic gelation between the anionic alginate groups and Ca^{2+} to form the ”egg-box” structure [198] 40
Figure 2.5.3 Three steps involved in the binding of calcium to (a) short chain (low molecular weight) alginate and (b) long chain (higher molecular weight) alginate [207] 41
Figure 2.5.4 EDC and NHS coupling reaction [218] 44
Figure 2.5.5 Silica glass with bridging non-bridging oxygens as a result of the addition of a glass modifier (Ca^{2+}) [229] 46
Figure 2.6.1 Gelation of the alginate using multivalent ions released from the bioactive glass 49
Figure 3.1.1 Example of the 1H NMR Spectrum of Alginate Used for Quantitative Analysis [257] 54
Figure 3.2.1 Schematic of a DTA curve indicating glass transition (T_g), crystallisation onset (T_o), crystallisation peak (T_p) and liquidis (T_l) temperature [259] 55
Figure 3.2.2 XRD pattern of amorphous (SiO2 glass) and crystalline (Quartz and Cristobalite) material [261] 56
Figure 3.2.3 Scattering of light with large and small particles [264] 56
Figure 3.2.4 Formation of monolayer for determining a particle surface area and pore volume using the Brunauer-Emmett-Teller method and Barrett-Joyner-Halenda method [273] 60
Figure 3.3.1 Stress-Strain graph [286] 62
Figure 3.3.2 Example of gel point found using Winter-Chambon criterion [292] 64
Figure 3.3.3 Schematic of a T-peel test [298] 65

List of Figures

Figure 3.3.4 Schematic of the bond strength test using ASTM F2258-03[299] 66
Figure 3.5.1 Platelets in their (i) resting/non-activated state, (ii) spreading (dendritic, spread dendritic, spread and fully spread) state and (iii) attached state [310] 68
Figure 4.6.1 Hydrogel sample following compression testing 78
Figure 4.6.2 Setting Time testing jig 79
Figure 4.6.3 Bond strength test set-up 80
Figure 4.6.4 Testing the force required to inject the hydrogel through a microcatheter 81
Figure 4.6.5 Aneurysm flow model set-up 82
Figure 4.7.1 96 well plate dosed with varying concentrations of eluent 84
Figure 5.1.1 X-ray diffraction of the bioactive glass 93
Figure 5.1.2 GPC of alginates 94
Figure 5.1.3 Viscosity of 60kDa and 700kDa alginate at four increasing concentrations (n=5) 95
Figure 5.1.4 Compressive stress and strength up to 70% strain for the 60kDa (High-G) alginate following storage at 37^0C in DI (n=5) 96
Figure 5.1.5 Incremental modulus (30-50% strain) of the 60kDa (High-G) alginate following storage at 37^0C in DI (n=5) 96
Figure 5.1.6 Compressive stress and strength up to 70% strain of the 700kDa (High-M) alginate following storage at 37^0C in DI (n=5) 97
Figure 5.1.7 Incremental modulus (30-50% strain) of the 700kDa (High-M) alginate following storage at 37^0C in DI (n=5) 97
Figure 5.1.8 Compressive stress and strength up to 70% strain of the 60kDa and 700kDa following storage in DI at 37^0C for 7 days (n=5) 98
Figure 5.1.9 Incremental modulus (30-50% strain) of the 60kDa and 700kDa following storage in DI at 37^0C for 7 days (n=5) 99
Figure 5.1.10 Compressive strength of the 4.5% and 6.0% 700kDa alginate with an increased glass content following storage for 1 day in DI at 37^0C 100
Figure 5.1.11 Incremental modulus (30-50% strain) of the 4.5% and 6.0% 700kDa alginate with an increased glass content following storage for 1 day in DI at 37^0C 100
Figure 5.1.12 Size conservation after 7 days of 60kDa and 700kDa alginate at varying concentration with 4.6% glass and 4.15% (w/v) GDL (n=5) (n=5) 101
Figure 5.1.13 Working time of 60kDa and 700kDa alginate at varying concentration with 4.6% glass and 4.15% (w/v)GDL (n=5) 102
Figure 5.1.14 Hardening time of 60kDa and 700kDa alginate at varying concentration with 4.6% glass and 4.15% (w/v) GDL (n=5) 102
Figure 5.2.1 GPC of gamma irradiated and non-irradiated (700kDa - High-M) alginate 109

Figure 5.2.2 Viscosity of the gamma irradiated and non-irradiated alginate at four increasing concentrations (n=5) 110
Figure 5.2.3 Compressive stress up to 70% strain of the gamma irradiated and non-irradiated alginate following storage in DI at 37^0C for 7 days (n=5) 111
Figure 5.2.4 Incremental modulus (30-50% strain) of the gamma irradiated and non-irradiated alginate following storage in DI at 37^0C for 7 days (n=5) 112
Figure 5.2.5 Gamma irradiated and non-irradiated alginate size conservation after 7 days (n=5) 112
Figure 5.2.6 Gamma irradiated and non-irradiated alginate working time (n=5) 113
Figure 5.2.7 Gamma irradiated and non-irradiated alginate hardening time (n=5) 113
Figure 5.3.1 Particle size analysis of untreated and acid washed glass 117
Figure 5.3.2 High resolution O_{1s} spectra for untreated and acid washed glass. 119
Figure 5.3.3 High resolution $Ga_{2p3/2}$ spectra for untreated and acid washed glass. 120
Figure 5.3.4 Si_{2p} X-ray Photoelectron Spectroscopy trace for untreated and acid washed glass 120
Figure 5.3.5 Attenuated Total Reflectance Fourier Transform Infrared Spectroscopy of acid washed glass particles 121
Figure 5.3.6 Field Emission Scanning Electron Microscopy of a) untreated glass and b) acid washed glass at X100k. 122
Figure 5.3.7 Compressive stress up to 70% strain of the acid washed and untreated glass following storage at 37^0C in DI (n=5) 123
Figure 5.3.8 Incremental modulus (30-50% strain) of the acid washed and untreated glass following storage at 37^0C in DI (n=5) 123
Figure 5.3.9 Acid washed glass working time with varying glass and GDL content (n=5) 124
Figure 5.3.10 Acid washed glass hardening time with varying glass and GDL content (n=5) 125
Figure 5.3.11 Compressive stress up to 70% strain of the acid washed glass with varying glass and GDL content following storage at 37^0C in DI (n=5) 126
Figure 5.3.12 Incremental modulus (30-50% strain) of the acid washed glass with varying glass and GDL content following storage at 37^0C in DI (n=5) 126
Figure 5.3.13 Compressive stress up to 70% strain of 13.8% acid washed glass with 8.3% (w/v) GDL following storage at 37^0C in varying media (n=5) 127
Figure 5.3.14 Incremental modulus (30-50% strain) of 13.8% acid washed glass with 8.3% (w/v) GDL following storage at 37^0C in varying media (n=5) 127
Figure 5.3.15 Acid washed glass with varying glass and GDL content size conservation (n=5) 128
Figure 5.3.16 13.8% acid washed glass with 8.3% (w/v) GDL content size conservation after storage in varying media (n=5) 128

List of Figures

Figure 5.3.17 a) untreated glass compression testing sample and b) acid washed glass compression testing sample 129
Figure 5.3.18 Sample 3D XMT a) hydrogel with 4.6% untreated glass content and 4.15% (w/v) GDL b) hydrogel with 4.6% acid washed glass content and 4.15% (w/v) GDL c) hydrogel with 13.8% glass content and 8.3% (w/v) GDL 129
Figure 5.3.19 2D microtomography of a) a coil b) hydrogel with 4.6% glass content and 4.15% (w/v) GDL c) hydrogel with 13.8% glass content and 8.3% (w/v) GDL and a 99% aluminium step wedge 130
Figure 5.4.1 Bond strength of the hydrogel with varying EDC and NHS content with repeats after 1 hour (n=5) 137
Figure 5.4.2 Bond strength of the hydrogel with 0% and 0.83% (w/v) EDC and NHS following storage in SBF at 37^0C (n=5) 138
Figure 5.4.3 Working time of the hydrogel with 0% and 0.83% (w/v) EDC and NHS (n=5) . 138
Figure 5.4.4 Hardening time of the hydrogel with 0% and 0.83% (w/v) EDC and NHS (n=5) 139
Figure 5.4.5 Compressive stress up to 70% strain of the hydrogel with 0% and 0.83% (w/v) EDC and NHS after storage at 37^0C in DI (n=5) 139
Figure 5.4.6 Incremental modulus (30-50% strain) of the hydrogel with 0% and 0.83% (w/v) EDC and NHS after storage at 37^0C in DI (n=5) 140
Figure 5.4.7 Compressive stress up to 70% strain of hydrogel with 0.83% (w/v) EDC and NHS after storage at 37^0C in varying media (n=5) 141
Figure 5.4.8 Incremental modulus (30-50% strain) of the hydrogel with 0.83% (w/v) EDC and NHS after storage at 37^0C in varying media (n=5) 141
Figure 5.4.9 Compressive stress up to 70% strain of hydrogel with 0.83% (w/v) EDC and NHS after storage at 37^0C in varying media (n=5) 142
Figure 5.4.10 Volume conservation of the hydrogel with 0.83% (w/v) of EDC and NHS after storage in varying media 142
Figure 5.4.11 Volume conservation of the hydrogel with 0.83% (w/v) of EDC and NHS after storage in varying media 143
Figure 5.4.12 Hydrogel injected in to the aneurysm model with physiological flow applied 144
Figure 5.5.1 BAEC cell activity for cells dosed with eluent A at different eluent concentrations (n=3) 150
Figure 5.5.2 BAEC cell activity for cells dosed with eluent B at different eluent concentrations (n=3) 150
Figure 5.5.3 BAEC cell activity for cells dosed with eluent C at different eluent concentrations (n=3) 151

Figure 5.5.4 BAEC cell number change (%) of cells dosed with varying concentrations of eluent A (n=3) 152
Figure 5.5.5 BAEC cell number change (%) of cells dosed with varying concentrations of eluent B (n=3) 153
Figure 5.5.6 BAEC cell number change (%) of cells dosed with varying concentrations of eluent C (n=3) 153
Figure 5.5.7 ICP of eluent A (n=3) 154
Figure 5.5.8 ICP of eluent B (n=3) 154
Figure 5.5.9 ICP of eluent C (n=3) 155
Figure 5.5.10 BAEC cell activity for cells dosed with gallium chloride at different eluent concentrations (n=3) 156
Figure 5.5.11 BAEC cell number change (%) of cells dosed with varying concentrations of gallium chloride (n=3) 156
Figure 5.5.12 BAEC cell activity for cells dosed with gallium nitrate at different eluent concentrations (n=3) 157
Figure 5.5.13 BAEC cell number change (%) of cells dosed with varying concentrations of gallium nitrate (n=3) 158
Figure 5.5.14 BAEC cell activity for cells dosed with calcium chloride at different eluent concentrations (n=3) 158
Figure 5.5.15 BAEC cell number change (%) of cells dosed with varying concentrations of calcium chloride (n=3) 159
Figure 5.5.16 BAEC cell activity for cells dosed with silicic acid at different eluent concentrations (n=3) 159
Figure 5.5.17 BAEC cell number change (%) of cells dosed with varying concentrations of silicic acid (n=3) 160
Figure 5.5.18 BAEC cell activity for cells dosed with GDL at different eluent concentrations (n=3) 160
Figure 5.5.19 BAEC cell number change (%) of cells dosed with varying concentrations of GDL (n=3) 161
Figure 5.6.1 Compressive stress up to 70% strain of the 700kDa alginate and the ultrapure medium viscosity (MVM) alginate after storage at 37^0C in DI (n=5) 168
Figure 5.6.2 Incremental modulus (30-50% strain) of the 700kDa alginate and the ultrapure medium viscosity (MVM) alginate following storage at 37^0C in DI (n=5) 169
Figure 5.6.3 Compressive strength up to 70% strain of the alginate before and after autoclaving at varying concentrations following storage for 1 day in DI at 37^0C (n=5) 170
Figure 5.6.4 Incremental modulus (30-50% strain) of the alginate before and after autoclaving at varying concentrations following storage for 1 day in DI at 37^0C (n=5) 170

Figure 5.6.5 Alginate size conservation after 1 day following storage for 1 day in DI at 37^0C (n=5) 171
Figure 5.6.6 Force required to inject 6.75% autoclaved MVM hydrogel through a microcatheter 5 and 15 minutes after mixing 172
Figure 5.6.7 Force required to inject the hydrogel at various compositions through a microcatheter 5 and 15 minutes after mixing 172
Figure 5.6.8 Compressive strength up to 70% strain of the hydrogel with individual components sterilised using low temperature gamma irradiation following storage for 1 day in SBF at 37^0C (n=5) 173
Figure 5.6.9 Compressive strength up to 70% strain of the sterilised hydrogel with 4.5% alginate following storage in SBF at 37^0C (n=5) 174
Figure 5.6.10 Incremental modulus (30-50% strain) of the sterilised hydrogel with 4.5% alginate following storage in SBF at 37^0C (n=5) 174
Figure 5.6.11 Sterilised hydrogel with 4.5% alginate size conservation (n=5) 175
Figure 5.6.12 Ultimate tensile strength of the non-sterilised and sterilised hydrogel with 4.5% alginate following storage in SBF at 37^0C (n=5) 175
Figure 5.6.13 Bond strength of the hydrogel before and after sterilisation following storage for 1 day in SBF at 37^0C (n=5) 176
Figure 5.6.14 Working time of hydrogel with individual components sterilised using low temperature gamma irradiation (n=5) 177
Figure 5.6.15 Hardening time of hydrogel with individual components sterilised using low temperature gamma irradiation (n=5) 177
Figure 5.6.16 Hydrogels working time (n=5) 178
Figure 5.6.17 Hydrogels hardening time (n=5) 179
Figure 5.6.18 Glass transition temperature of glass 179
Figure 5.7.1 FTIR of glass after storage in DI (black line) and SBF (blue line) for 7 days 186
Figure 5.7.2 Raw alginate and alginate – bioactive glass hydrogel after storage in SBF FTIR 187
Figure 5.7.3 XRD of glass after storage in DI and SBF 188
Figure 5.7.4 XRD of hydrogels after storage in SBF for 7 days 188
Figure 5.7.5 Bioactive glass - Alginate hydrogel after Von Kossa staining 189
Figure 5.7.6 Hydroxyapatite - Alginate hydrogel before (a) and after (b) Von Kossa staining 189
Figure 5.8.1 Number of cells per cm^2 on the slide in contact with the hydrogel (n=3) 193
Figure 5.8.2 Cells on the slide in contact with the hydrogel 7 days after seeding 194
Figure 5.8.3 Cells on the hydrogel after a) 3 days and b) 7 days 194
Figure 5.8.4 Number of cells per cm^2 on the hydrogel (n=3) 195

Figure 5.9.1 Hydrogel radiopacity samples 197
Figure 5.9.2 Fluoroscopy images hydrogel samples of various tantalum content and thickness under a skull model from a) front view and b) side view 198
Figure 5.9.3 Fluoroscopy images of the hydrogel with 40% tantalum a) before, b) during and c) after injection into an aneurysm model. A balloon inflated with iodine contrast is placed at the neck of the aneurysm. 198
Figure 5.9.4 Compressive strength up to 70% strain of the hydrogel with 0% and 40% (w/v) tantalum following storage for 1, 3 and 7 days at 37^0C in SBF (n=5) 199
Figure 5.9.5 Incremental Modulus (30-40% strain) of the hydrogel with 0% and 40% (w/v) tantalum following storage for 1, 3 and 7 days at 37^0C in SBF (n=5) 199
Figure 5.9.6 Hydrogel with 0% and 40% tantalum size conservation after storage for 1, 3 and 7 days at 37^0C in SBF (n=5) 200
Figure 5.9.7 Working and hardening time with 0% and 40% (w/v) tantalum content (n=5) 200
Figure 5.10.1 Platelet attachment to the surface of the positive control (➞ indicates non-activated platelets, ⇨ indicates activated platelets) 204
Figure 5.10.2 Platelet attachment to the surface of the negative control (➞ indicates non-activated platelets, ⇨ indicates activated platelets) 205
Figure 5.10.3 Platelet attachment to the surface of the hydrogel (➞ indicates non-activated platelets, ⇨ indicates activated platelets, → indicates unfocused platelet) 206
Figure 5.11.1 A) Aneurysm B) Balloon inflated with Omnipaque™ occluding the aneurysm filled with Omnipaque™ 211
Figure 5.11.2 A) Balloon inflated with Omnipaque™ at the neck of the aneurysm B) Hydrogel being injected through the microcatheter into the aneurysm dome C) Balloon deformation D)No hydrogel observed post treatment 212
Figure 5.11.3 Hydrogel within the aneurysm dome 213
Figure 5.11.4 A) Balloon lumen trapped in aneurysm filled with hydrogel B) Hydrogel migrating downstream 214
Figure 5.11.5 Aneurysm fully occluded with hydrogel 214
Figure 5.11.6 Hydrogel being injected into the aneurysm 215
Figure 5.11.7 Histology of the aneurysm treated with the hydrogel 215
Figure 5.11.8 Kidney and renal artery embolized with hydrogel 216
Figure 5.11.9 Macroscopic image of the left kidney treated with the hydrogel 216
Figure 5.11.10 A) Hydrogel being injected into kidney B) Kidney embolized with hydrogel 217
Figure 5.11.11 Aneurysm A) during and B) after coiling 218
Figure 5.11.12 Histology of coiled aneurysm 218

Figure 5.11.13 Coil within renal artery 219
Figure 5.11.14 Macroscopic image of right kidney 219
Figure 5.12.1 Injecting 4.5% MVM alginate hydrogel through a 2.4F catheter 222
Figure 9.1.1 High resolution O 1s spectra for untreated and acid washed glass 277
Figure 9.3.1 Predicted mechanism of gallium ions cross-linking alginate [239] 293
Figure 9.4.1 Gel point of the 0.5% 700kDa alginate at a frequency of 40Hz 294
Figure 9.4.2 Gel point of the 0.5% 700kDa alginate at a frequency of 5Hz 295
Figure 9.4.3 Gel point of the 4.5% 700kDa alginate at a frequency of 40Hz 295
Figure 9.4.4 Gel point of the 4.5% 700kDa alginate at a frequency of 5Hz 296
Figure 9.4.5 Gel point of the 0.5% 700kDa using the Winter-Chambon Criterion 296
Figure 9.4.6 Gel point of the 4.5% 700kDa using the Winter-Chambon Criterion 297
Figure 9.4.7 Drawing of clamp used to keep the plate parallel 300
Figure 9.4.8 Drawing of the plate with template for placing hydrogel 301
Figure 9.4.9 Drawing of the plates used for bond strength testing 302
Figure 9.4.10 Assembly drawing of the bond strength testing clamp with plate 303
Figure 9.5.1 ^{1}H-NMR spectra of the 60kDa and 700kDa alginate 305
Figure 9.5.2 ^{1}H-NMR spectra of the non-irradiated (700kDa) and gamma irradiated (180kDa) alginate 305
Figure 9.5.3 Typical stress-strain graph of a 0.5% concentration of the 60kDa (High-G) alginate following storage for 1, 3 and 7 at 37^{0}C in DI 306
Figure 9.5.4 Typical stress-strain graph of a 2.5% concentration of the 60kDa (High-G) alginate following storage for 1, 3 and 7 at 37^{0}C in DI 306
Figure 9.5.5 Typical stress-strain graph of the 4.5% concentration of the 60kDa (High-G) alginate following storage for 1, 3 and 7 at 37^{0}C in DI 307
Figure 9.5.6 Typical stress-strain graph of the 6.0% concentration of the 60kDa (High-G) alginate following storage for 1, 3 and 7 at 37^{0}C in DI 307
Figure 9.5.7 Typical stress-strain graph of a 0.5% concentration of the 700kDa (High-M) alginate following storage for 1, 3 and 7 at 37^{0}C in DI 308
Figure 9.5.8 Typical stress-strain graph of the 700kDa (High-M) alginate following storage for 1, 3 and 7 at 37^{0}C in DI 308
Figure 9.5.9 Typical stress-strain graph of a 4.5% concentration of the 700kDa (High-M) alginate following storage for 1, 3 and 7 at 37^{0}C in DI 309
Figure 9.5.10 Typical stress-strain graph of a 6.0% concentration of the 700kDa (High-M) alginate following storage for 1, 3 and 7 at 37^{0}C in DI 309
Figure 9.5.11 Typical stress-strain graph of the 700kDa (High-M) alginate with varying glass content following storage for 1 at 37^{0}C in DI 310

Figure 9.5.12 Typical stress-strain graph of the acid washed glass (4.6% content) following storage for 1, 3 and 7 days at 37^{0}C in DI 311
Figure 9.5.13 Typical stress-strain graph of the acid washed glass (13.8% content) following storage for 1, 3 and 7 days at 37^{0}C in DI 311
Figure 9.5.14 Typical stress-strain graph of the acid washed glass (13.8% content) following storage for 1, 3 and 7 days at 37^{0}C in PBS 312
Figure 9.5.15 Typical stress-strain graph of the acid washed glass (13.8% content) following storage for 1, 3 and 7 days at 37^{0}C in SBF 312
Figure 9.5.16 Typical stress-strain graph of the hydrogel with 0.83% (w/v) of EDC and NHS following storage for 1, 3, 7 and 30 days at 37^{0}C in DI 313
Figure 9.5.17 Typical stress-strain graph of the hydrogel with 0.83% (w/v) of EDC and NHS following storage for 1, 3, 7 and 30 days at 37^{0}C in PBS 313
Figure 9.5.18 Typical stress-strain graph of the hydrogel with 0.83% (w/v) of EDC and NHS following storage for 1, 3, 7 and 30 days at 37^{0}C in SBF 314
Figure 9.5.19 Adhesive failure of hydrogel with 0.83% (w/v) of EDC and NHS 315
Figure 9.5.20 Cohesive failure of hydrogel with 0% (w/v) of EDC and NHS 315
Figure 9.5.21 BASMC cell activity for cells dosed with Eluent C at different eluent concentrations (n=3) 316
Figure 9.5.22 BASMC cell number change (%) of cells dosed with varying concentrations of Eluent C (n=3) 317
Figure 9.5.23 Typical stress-strain graph of the hydrogel with various components sterilised following storage for 1, 3 and 7 days at 37^{0}C in DI 318
Figure 9.5.24 BAEC cell activity for cells dosed with the hydrogel with MVM alginate at different eluent concentrations (n=3) 319
Figure 9.5.25 BAEC cell number change (%) of cells dosed with varying concentrations of the hydrogel with MVM alginate (n=3) 320
Figure 9.5.26 Typical stress-strain graph of the hydrogel with all components sterilised with 4.5% alginate following storage for 1, 3 and 7 days at 37^{0}C in SBF 321
Figure 9.5.27 Typical stress-strain graph of the hydrogel with all components sterilised with 6.75% alginate following storage for 1, 3 and 7 days at 37^{0}C in SBF 321
Figure 9.5.28 Compressive strength up to 70% strain of the sterilised hydrogel with 6.75% alginate following storage in SBF at 37^{0}C (n=5) 322
Figure 9.5.29 Incremental modulus (30-50% strain) of the sterilised hydrogel with 6.75% alginate following storage in SBF at 37^{0}C (n=5) 322
Figure 9.5.30 FTIR of hydroxyapatite powder [514] 323
Figure 9.5.31 Acellular DAPI stained hydrogel 324

List of Figures

Figure 9.5.32 Fluoroscopy images of an Iodine contrast agent and Onyx® under a skull model 325
Figure 9.5.33 X-ray diffraction of tantalum glass 326
Figure 9.5.34 Compressive strength of 700kDa alginate with varying glass content following storage in DI at 37^0C (n=5) 327
Figure 9.5.35 Compressive stress up to 70% strain of tantalum glass and original glass following storage in DI at 37^0C for 7 days (n=5) 327
Figure 9.5.36 Tantalum glass with 4.5% alginate size conservation following storage in DI at 37^0C for 7 days (n=5) 328
Figure 9.5.37 A) Structure of the kidney and B) the major blood vessels of the kidney [520] 329
Figure 9.5.38 Compressive stress up to 70% strain of the hydrogel mixed at a 1.2ml and 2.4ml volume following storage at 37^0C in DI (n=5) 334
Figure 9.5.39 Hydrogels working and hardening time mixed at a 1.2ml and 2.4ml volume (n=5) 335

List of Tables

Table 2.1.1 Normal diameters of cerebral arteries [17] 7
Table 2.1.2 Results obtained by Monson *et al.* (* standard deviation was not calculated when n<3) [32]. 9
Table 2.2.1 Classification of aneurysm by size [55] 13
Table 2.4.1 Design review table 33
Table 2.5.1 Varying chemical composition of alginate from various locations [194] 39
Table 3.3.1 Typical ion concentration of blood plasma and Simulated Body Fluid (c-SBF, r-SBF and n-SBF) 61
Table 3.3.2 Typical ion concentration of blood plasma and Phosphate Buffered Saline 61
Table 4.3.1 Novel bioactive glass constituents (grams) 73
Table 4.6.1 Pressure readings at increasing heights to calibrate physiologically correct flow model 83
Table 4.13.1 Embolization treatment and hydrogel delivery times for each rabbit 91
Table 5.1.1 Alginate chemical composition 94
Table 5.1.2 60kDa and 700kDa alginate design review table 107
Table 5.2.1 Alginate chemical composition 110
Table 5.2.2 Gamma irradiated and non-irradiated alginate design review 116
Table 5.3.1 Brunauer Emmett Teller (BET) adsorption and Barrett-Joyner-Halenda (BJH) desorption pore volume analysis 118
Table 5.3.2 Zeta potential measurements of untreated and acid washed glass. 118
Table 5.3.3 Composition (atomic %) from XPS of untreated and acid washed glass 118
Table 5.3.4 Sample 3D XMT analysis. 130
Table 5.3.5 Mean grey value 130
Table 5.3.6 Untreated and acid washed glass design review 135
Table 5.4.1 0% and 0.83% (w/v) EDC and NHS design review 147
Table 5.5.1 Hydrogel content for cell culture 149
Table 5.5.2 Design review table with in vitro analysis results 166
Table 5.6.1 Design review table with the hydrogel sterilised 183
Table 5.7.1 Design review table 191
Table 5.9.1 Design review table 202
Table 5.10.1 Design review table 208
Table 5.11.1 Embolization treatment tested for each rabbit 209
Table 9.2.1 Hydrogel formulae for corresponding sections 290

List of Equations

Equation 2.1.1 Hagen-Poiseuille equation [30] 8
Equation 2.5.1. Equation to determine the average G-block length [188] 38
Equation 3.1.1 Equation for calculating F_G [257] 54
Equation 3.1.2 Equation for calculating F_M [257] 54
Equation 3.2.1 Brunauer-Emmett-Teller method equation used to determine particle surface area[274] 58
Equation 3.2.2 Specific surface area of a solid using the Brunauer-Emmett-Teller method[272][275] 59
Equation 3.2.3 Barrett-Joyner-Halenda method equation to determine the pore volume and area in porous solids [276] 59
Equation 3.3.1 Normal stress equation 62
Equation 3.3.2 Normal strain equation 62
Equation 3.3.3 Young's modulus equation 63
Equation 3.3.4 Winter and Chambon loss tangent [296] 64
Equation 4.6.1 Equation to calculate pressure 82
Equation 4.7.1 Cell metabolic activity (% Growth) determined using resazurin blue 85
Equation 5.2.1 Chain Breaks per Molecule [357] 109
Equation 5.3.1 Estimation of the % of tetrahedrally coordinated ions 121
Equation 5.12.1 Hagen-Poiseuielle equation 221

Terms and Abbreviations

Al - Aluminium

ATR – FTIR – Attenuated Total Reflectance- Fourier Transform Infrared Spectroscopy

BAEC – Bovine Aortic Endothelial Cells

BASMC –Bovine Aortic Smooth Muscle Cells

BET – Brunauer-Emmett-Teller method

bFGF – Basic Fibroblast Growth Factor

BJH – Barrett-Joyner-Halenda method

BO – Bridging Oxygen

Ca^{2+} – Calcium

CA – Cerebral Aneurysm

$CaCl_2$ – Calcium Chloride

$CaCO_3$ – Calcium Carbonate

CFD - Computational Fluid Dynamic

CPP – Cerebral Perfusion Pressure

D_2O – Deuterium Oxide

DI – Deionised Water

DMSO – Dimethyl sulfoxide

DTA – Differential Thermal Analysis

ECM – Extracellular Matrix

EDC - (1-ethyl-3-(3-dimethylaminopropyl) carbodiimide hydrochloride)

EEL – External Elastic Lamina

EtO – Ethylene Oxide

EVAC – Ethylene Vinyl Alcohol Copolymer

EVOH – Ethylene Vinyl Alcohol

F_m – Mannuronic Fractions

F_g – Guluronic Fractions

FDA – Food and Drug Administration

FE – SEM – Field Emission Scanning Electron Spectroscopy

G - α-L-Guluronic Acid

G'- Elastic/Storage Modulus

G"- Viscous/Loss Modulus

Ga^{3+} – Gallium

$GaCl_3$ – Gallium Chloride

$Ga(NO_3)_3$ – Gallium Nitrate

GDL – D-(+)-Gluconic acid δ-lactone

GPC – Gel Permeation Chromatography

HCl – Hydrochloric Acid

^{1}H-NMR – Nuclear Magnetic Resonance Spectroscopy

IA – Intracranial aneurysm

ICP - Inductively Coupled Plasma – Atomic Emission Spectroscopy

IEL – Internal Elastic Lamina

ISO – International Standards Organization

K - Potassium

KOH – Potassium Hydroxide

M – β-D-mannuronic Acid

MCA – Middle Cerebral Artery

MMP - Matrix Metalloproteinases

MW – Molecular weight

MVM – Medium Viscosity High-M alginate

Na^{2+} - Sodium

NaCl – Sodium Chloride

$NaHCO_3$ - Sodium Bicarbonate

NC – Network Connectivity

NHS - N-Hydroxysuccinimide

NBO – Non-Bridging Oxygen

PBS – Phosphate Buffered Saline

PGA – Polyglycolic Acid

PLGA – Poly(lactic-co-glycolic) Acid

PSA – Particle Size Analysis

SAL – Sterility Assurance Level

SBF – Simulated Body Fluid

Si^{4+} – Silica

T_g – Glass Transition Temperature

WSS – Wall Shear Stress

VEGF – Vascular Endothelial Growth Factor

XMT – X-Ray Microtomography

XPS – X-Ray Photoelectron Spectroscopy

XRD – X-Ray Diffraction

Abstract

Optimisation of a Novel Hydrogel for the Treatment of Cerebral Aneurysms - Sarah Brady

Approximately 1-6% of adults have a cerebral aneurysm. Treatments include clipping and coiling; however, over 20% of coiled aneurysms recur. A novel bioactive glass-alginate hydrogel has been optimised to fill the aneurysm and prevent recurrence.

For successful aneurysm embolization, the hydrogel must be injectable and set *in situ*, as well as meeting other design requirements, including; injectability, strength, adhesiveness, radiopacity and cytocompatibility.

The hydrogel was optimised by examining the effect alginate concentration, chemical composition and molecular weight has on the hydrogel's properties. The glass was acid washed which improved homogeneity of the hydrogel and reduced glass agglomeration. The glass and GDL content were optimised and resulted in a hydrogel with a higher compressive strength compared to *in situ* gelling alginates reported in the literature. The addition of EDC and NHS improved the adhesive strength of the hydrogel without the need for cell attaching peptides. *In vitro* analysis showed cells can adhere and proliferate in direct contact with the hydrogel and its eluent. Proliferation was dose dependent and likely caused by silica ions and gluconic acid released. Although endothelial cells attached to the surface of the hydrogel, this was minimal. Platelet adhesion to the hydrogel was also marginal. The hydrogel was sterilised and radiopacity was improved, but with a loss in compressive strength. *In vivo* analysis indicated that issues occur in delivering this material into an aneurysm, though this hydrogel can be effectively used as an embolization treatment that supports the formation of a neointima layer.

This work highlights the influence each component has on the hydrogel's properties. Although this hydrogel was optimised for the treatment of cerebral aneurysms, the hydrogel is highly tuneable and would be suitable for a range of embolic applications. This bioactive *in situ* gelling hydrogel would also be suitable for tissue engineering and therapeutic drug delivery.

Chapter 1. Introduction

A cerebral aneurysm is an irregular out-pouching of a cerebral artery. It is estimated that 1% to 6% of the adult population has a cerebral aneurysm [1]. A ruptured aneurysm can lead to a stroke, resulting in disability or death. Treatments such as placing a clip at the neck of the aneurysm (clipping) or filling the aneurysm with wire coils (coiling) are currently used to prevent an aneurysm from rupturing. However, there are a number of problems associated with these procedures. Clipping the aneurysm involves a craniotomy and carries the risks of infection and scarring. In the United States, the most common treatment method for cerebral aneurysms is coiling. However, recurrence is common, happening in 20.8% of endovascular coiling cases, indicating that it is a suboptimal treatment method [2].

Liquid embolic materials have emerged as a promising option for the treatment of cerebral aneurysms. These materials are injected into the aneurysm, which allows the treatment to be minimally invasive. This has the advantage of reduced patient pain, recovery time and rate of infection. Liquid embolics also have the advantage of conforming to the irregular shape of the aneurysm and providing a complete embolization due to its ability to completely fill the aneurysm dome, reducing the risk of recurrence. However; many liquid embolic materials that have been tested have drawbacks such as rapid polymerisation, leaching of toxic organic solvents and complicated or prolonged delivery of the material [3]–[5].

Hydrogels are a possibility for the treatment of aneurysms as they have the ability to set *in situ* and are typically biocompatible. However, hydrogels typically have a low mechanical strength and degrade over time. Although mechanically stable hydrogels can be produced, they are usually covalently cross-linked which can affect the biocompatibility of the hydrogel [6]–[8].

To overcome the low inherent strength of hydrogels, inorganic materials such as bioactive glasses, salts and ceramics particles have been added to various compositions. To date, these composites have been extensively examined for the use in hard tissue applications due to their ability to calcify and promote bone cell growth. Yet, research to date on inorganic polymer composites has shown promising use in soft tissue applications. These composites are also designed to degrade overtime in order to permit new tissue growth [9]–[14].

1.1. Aim

The aim of this project is to optimise the composition of a hydrogel for the use as a cerebral aneurysm filler. The initial hydrogel will be composed of alginate, novel bioactive glass particles and glucono-delta lactone (GDL).

It is envisaged that the delivery procedure will involve inflating a balloon adjacent to the aneurysm neck, as is commonly carried out with endovascular coiling procedures (see Figure 1.1.1). This will ensure that the hydrogel does not leak into the surrounding vasculature during injection. The hydrogel will be injected into the aneurysm through a micro-catheter.

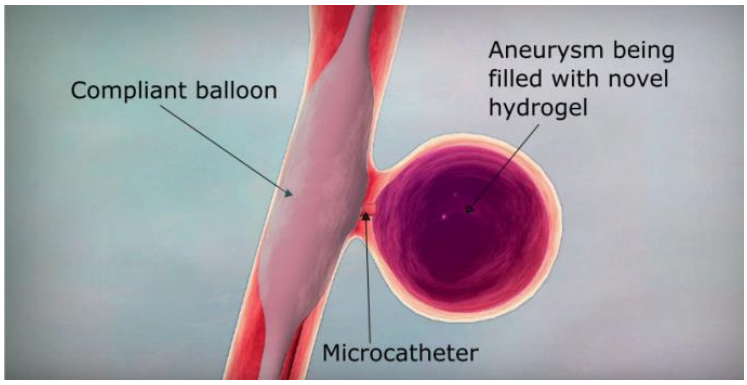

Figure 1.1.1 Schematic of a novel hydrogel being injected through a microcatheter into a cerebral aneurysm with a compliant balloon placed across the neck [15]

To optimise the compressive strength, sample volume conservation, working time and hardening time of the hydrogel, three alginates with varying concentration, molecular weight and chemical composition will be examined.

N-(3-Dimethylaminopropyl)-N′-ethylcarbodiimide hydrochloride (EDC) and N-Hydroxysuccinimide (NHS) will be examined in increasing increments, to increase the bond strength of the hydrogel. The bond strength, compressive strength, sample volume conservation, working time and hardening time of the hydrogel will be tested of the final composition.

In vitro analysis will be carried out by examining the cytotoxicity of the hydrogel eluent on bovine aortic endothelial cells and bovine aortic smooth muscle cells. Direct contact testing of the hydrogel with bovine aortic endothelial cells will also be carried out. To test for thrombotic potential, the hydrogel will be placed in contact with whole human blood to determine if platelets adhere to the surface. The hydrogel will also be injected into an aneurysm flow model to see how it performs when physiological blood flow and pressure is applied.

As bioactive glasses usually form an apatite layer *in vivo*, the hydrogel will be tested after storage in simulated body fluid to determine if the hydrogel calcifies. X-ray Diffraction, Fourier Transform Infrared spectroscopy and von Kossa staining will be carried out to examine if an apatite layer is present.

The optimum sterilisation technique for each component of the hydrogel will be determined, whilst the radiopacity of the hydrogel will be assessed and optimised to aid visualisation of the gel under fluoroscopic imaging.

Finally, *in vivo* testing of the optimum hydrogel will be carried out to assess the efficacy of the delivery mechanism and the effectiveness of this treatment modality for cerebral aneurysm treatment.

Chapter 2. Literature Review

2.1. Cerebral Vascular Structure and Cerebral Aneurysms

2.1.1. Cerebral Vascular Structure

The blood supply to the human brain comes from two pairs of arteries; the right and left internal carotid and the right and left vertebral arteries. The vertebral arteries join to form the basilar artery. The Circle of Willis is a ring of arteries which is formed when the basilar artery joins with the internal carotids. The Circle of Willis is found at the base of the brain and is composed of 3 pairs of arteries; the anterior, middle and posterior artery. These arteries divide into smaller arteries and arterioles [16]. The normal diameters of these cerebral arteries, when non-diseased are shown in Table 2.1.1.

Table 2.1.1 Normal diameters of cerebral arteries [17]

Artery	Normal diameters (mm)
Internal Carotid	3.7-4.5
Vertebral	0.9-4.1
Basilar	2.7-4.3
Anterior cerebral	1.2-2.4
Middle cerebral	1.8-3.1
Posterior cerebral	1.4-2.4

Arteries are composed of three layers, the intima, the media and the adventitia (Figure 2.1.1). The media and adventitia layers are thinner in cerebral arteries compared to those found elsewhere in the body. The innermost layer, the intima, is composed of endothelial cells attached to a basement membrane and an internal elastic lamina (IEL). Cerebral arteries have no external elastic lamina (EEL) which is compensated for by the thicker IEL. Endothelial cells do not provide much mechanical support to the cerebral artery but play a role protecting the vessel against haemodynamic forces and control exchanges between the blood and the brain. Platelets do not adhere to the surface of an intact endothelium, therefore inhibiting thrombus formation. The next layer is the muscular media. This is separated from the intima by the IEL [16] [18]–[20]. The media layer itself is composed of:

1. Elastin fibres
2. Vascular smooth muscle cells
3. Collagen fibres

The elastin fibres provide elasticity to cerebral arteries and vascular smooth muscle cells allow the vasoconstriction and vasodilation of the cerebral arteries. Cerebral arteries have a larger number of smooth muscle cells compared to that of extracranial arteries. The final

layer, the adventitia, is mainly made of collagen fibres. In healthy arteries, this layer ensures that there is no enlargement of the cerebral artery. Collagen fibres are constantly degrading and reforming. In healthy subjects collagen has a half-life of approximately two months and can withstand pressures up to 10 times that of blood pressure [16] [19] [21].

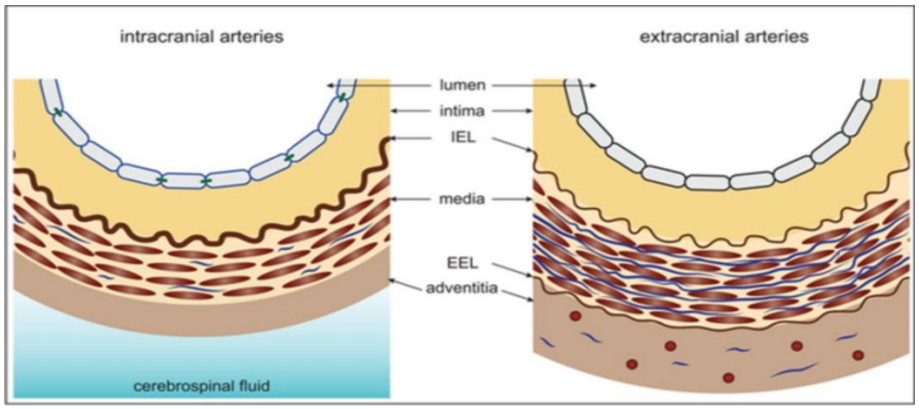

Figure 2.1.1 Comparison of the layers of intracranial and extracranial arteries [22]

2.1.2. Cerebral Haemodynamics

Cerebral perfusion pressure (CPP) is defined as the difference between the incoming mean arterial pressure and the intracranial pressure (pressure inside the skull due to cerebrospinal fluid) [23] [24]. CPP averages 70-85mmHg, with normal mean arterial pressure ranging 80-100mmHg and intracranial pressure ranging 5-10mmHg [25]. Between a CPP of 50mmHg and 160mmHg, blood flow is auto regulated and maintained at approximately 700ml/min, but can range from 550-930ml/min [16] [19] [24] [26]. Auto regulation is a myogenic response controlled by smooth muscle cells, which cause constriction and dilation of the vessels depending on the pressure. Therefore, CPP directly affects the cerebral blood flow when the perfusion pressure is outside the normal range. However, blood flow has been shown to vary throughout the brain [16] [26] [27]. CPP below 50mmHg may cause cerebral ischemia, with cell death occurring at 5mmHg [28].

Blood viscosity ranges from 3.28mPa.s to 4.33mPa.s [29]. Blood viscosity can also have an effect on blood flow as seen in the Hagen-Poiseuille equation (Equation 2.1.1), which can be used as an estimate for calculating cerebral blood flow [16] [26] [30].

Equation 2.1.1 Hagen-Poiseuille equation [30]

$$Cerebral\ blood\ flow\ (Q) = \frac{\Delta P \pi r^4}{8\mu L}$$

Where,
ΔP = the change in pressure (Pa)
r = the arteries internal radius (m)
μ = viscosity (Pa.s)
L = the length between the two pressures (m)

2.1.3. Mechanical Properties of Cerebral Arteries

Varying mechanical properties of cerebral arteries are reported in the literature. This is due to experimental variances such as testing *in vivo* and *ex vivo*, deformation mode (compressive, tensile, uniaxial, biaxial, *etc*.), experimental set-up, time since tissue excision, tissue hydration state, temperature and storage medium [31]. Another source of variance in results is the source of the cerebral tissue. A study by Monson *et al.* set out to determine the importance that source and size of cerebral blood vessels has on the mechanical properties. For this study, middle cerebral arteries (MCA) and small cortical cerebral vessels were obtained from autopsy and surgery. It should be noted that the average age of the autopsy subjects was twice that of surgical subjects. As uniaxial tension is the most common loading of arterial tissue, the cerebral vessels were extended longitudinally until failure. Table 2.1.2, shows mechanical properties that were obtained [32]. These results indicate that the time since tissue excision, patient age and source greatly affects the results and should be taken into consideration when examining data.

Table 2.1.2 Results obtained by Monson *et al.* (* standard deviation was not calculated when n<3) [32].

	Maximum Modulus (MPa)	**Yield Strain**	**Yield Stress (MPa)**	**Ultimate Strain**	**Ultimate Stress (MPa)**
Autopsy – Cortical	31.07 ±12.91	1.25 ±0.05	4.33 ±2.16	1.27 ±0.05	4.75 ±2.18
Surgical – Cortical	19.30 ±6.92	1.38 ±0.13	3.60 ±1.06	1.42 ±0.12	4.07 ±1.24
Autopsy – MCA	18.18 ±9.03	1.32*	2.52*	1.41*	3.23*

Analysis methods of the results obtained can also cause large variances in reported mechanical properties. The stress-strain response of a blood vessel is generally observed to be non-linear, but in fact it has two distinctly linear regions. This was highlighted by Dr. Ebrahimi, who showed that the tangent modulus of the lower region (up to 50% strain) of cerebral arteries is generally 0.2-0.6MPa. The upper, higher strain region is much stiffer with a tangent modulus of 2-6MPa [19]. These results show a significantly lower stiffness compared to the results of Monson *et al*., emphasising the large variances that can occur in reported results.

2.2. Cerebral Aneurysms

A cerebral aneurysm (CA) is an irregular out pouching of a cerebral artery [17].

2.2.1. Cerebral Aneurysm Structure

Many histological studies have shown either a lack of or a fragmented elastic layer throughout the aneurysm sac, with a broken media layer. In general, the aneurysm wall mainly consists of the adventitia layer and intima layer with collagen and fragmented internal elastic lamina remaining between these layers, as shown in Figure 2.2.1 [20] [33]. The endothelial layer of the aneurysm is often irregular with visible gaps between these cells [34].

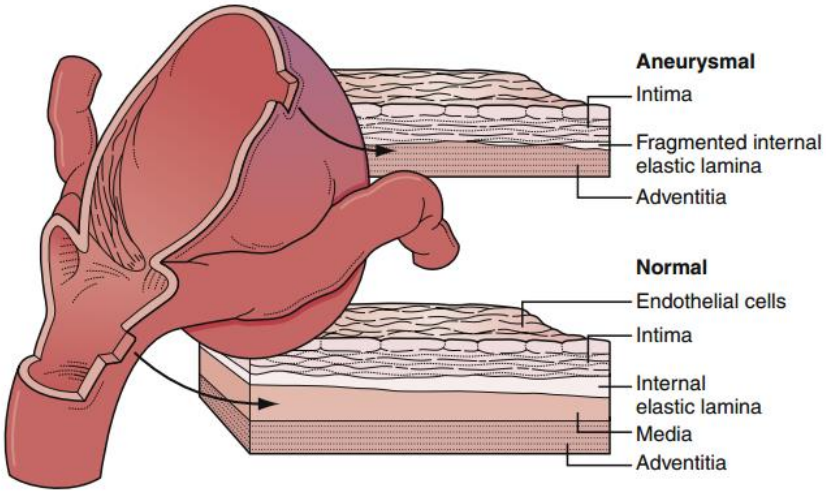

Figure 2.2.1 Comparison of the cellular structure of cerebral arteries and an aneurysm wall [35]

Aneurysm wall thickness has been reported as 16-400µm, with 78% of aneurysms having a varied thickness throughout the aneurysm [21] [36]. This is compared to the even wall thickness found in the basilar artery and middle cerebral artery which have a mean thickness of 600±120µm and 510±80µm, respectively [37].

2.2.2. Cause of Cerebral Aneurysm Formation and Rupture

It is generally thought that a combination of factors lead to a CA formation and eventually cause rupture, these factors include; hypertension, smoking-induced vascular changes, blood-flow dynamics, wall shear stresses (WSS), intrasaccular pressure, arterial wall composition, cell populations, and signalling pathways [1] [38].

CA formation is more common, compared to extracranial aneurysms, due to cerebral arteries thin walls and the absence of an external elastic lamina. Cerebral arteries also commonly have medial defects. An example of these medial defects is at bifurcations where the intima is thicker causing intimal pads. At these intimal pads there is a breakdown of the media. However, other medial defects are common throughout the cerebral vascular system [20].

Haemodynamic factors are also likely to cause aneurysms or be a factor in formation of a CA where medial defects are present and cause an aneurysm to rupture. Three haemodynamic factors are associated with blood flow through cerebral arteries; impact/dynamic, WSS and pressure [39]. Impacting/dynamic forces are caused by a perpendicular impact of blood. The dynamic pressure of the fluid is converted to static pressure where the flow impact occurs. WSS is caused by the friction of blood flow as it moves parallel to cerebral arteries. Wall shear stress in aneurysms range from 5-13Pa with the maximum stress occurring at the neck of the aneurysm [40]. Aneurysms usually occur in the Circle of Willis where arteries are tortuous and branching [41]. To be more precise, they generally occur at curved areas or bifurcations of the artery where high pressures and stresses occur [39]. Haemodynamic stresses are likely to be largest at bifurcations, due to the high impact force caused by central streams having a higher velocity, which may damage the internal elastic membrane. Once the membrane is damaged the arteries stretch in response to the pressure caused by blood flow [20] [35] [39]. CFD modelling has shown that the pressure within an aneurysm is higher compared to the parent artery caused by blood velocity being lower within the aneurysm. The pressure within the aneurysm is higher in aneurysms found at bifurcations compared to that of sidewall aneurysms [41].

Often cerebral arteries are required to undergo vascular remodelling due to injury caused by haemodynamic forces. Inflammation during vascular remodelling is also thought to be a contributing factor in cerebral aneurysm rupture. This is due to an increase in macrophages found in ruptured and un-ruptured aneurysms. Macrophages can produce the cytokine matrix metalloproteinases (MMP). MMP effects tissue development and remodelling, particularly MMP-9 which in excessive amounts can cause the degradation of elastin and collagen. The increase in the presence of macrophages will likely result is an abnormal remodelling of the artery and the progression of an aneurysm [42]–[44].

The development of an aneurysm can be broken up into four stages; commencement, growth, stabilisation and/or rupture [45]. A study by Selimovic *et al* used computational methods to recreate the four stages of an aneurysm life cycle [38]. To simulate the commencement stage, elastin was caused to degrade from a circular patch of the arterial wall. There is an increase in collagen fibres, following the loss of elastin, as the artery tries to regain homeostasis. The collagen fibre adapts and a CA evolves, this is due to the further degradation of elastin caused by the wall shear stresses [38].

A rupture occurs when there is a tear in the aneurysm. These tears can be large, causing an often fatal bleed or a small tear which causes a leak that can be repaired surgically. Rupture of a CA usually happens at the top (fundus) of the aneurysm with approximately 85% of ruptures reported here [46]. Either the larger aneurysm or the proximal aneurysm will

rupture first when more than one aneurysm exists, due to an increased intra-aneurysmal pressure. It is uncertain why aneurysms grow or the rate at which they grow but it has been shown that slower growing aneurysms have a lower risk of rupture [21] [47].

Computational fluid dynamic (CFD) models have shown aneurysms with complex flow patterns with a number of vortices are more likely to rupture compared to aneurysms with a single vortex. High intra-aneurysm pressure may cause rupture in low flow aneurysms [48] [49].

It has been shown that both high and low wall shear stresses can cause an aneurysm to form and rupture [31] [50]. Low WSS, caused by a reduced blood flow, can induce the formation of thrombi resulting in inflammation and endothelial apoptosis and wall remodelling. High WSS and a high WSS gradient can cause damaged to the elastic lamina, endothelium and a loss of smooth muscle cells [5] [39] [51].

CAs may also be associated with genetics, with approximately 10-12% of all aneurysms being associated with genetic factors. It is suggested that a genetic factor can result in weakened type III and V collagen in cerebral arteries. The symmetry of the Circle of Willis can also affect hemodynamic pressures and the symmetry may be a genetic factor. It is generally advised that people with 2 or more immediate relatives with a CA to undergo screening [1] [21] [35].

Certain conditions have been found to result in increased incidences of CA formation. These include; Fibro-muscular dysplasia, Marfan's syndrome, Elhers-Danlos syndrome type IV, arteriovenous malformations of the brain, and autosomal dominant polycystic kidney disease. Autosomal dominant polycystic kidney disease has a large association with CAs, with 5-40% of patients having a single CA, and 10-30% having multiple aneurysms [1] [35].

The risk of an aneurysm rupturing is generally based on haemodynamics and aneurysm location, grow rate, height, diameter and neck width [21] [35] [38] [45] [48] [49]. Other factors such as patient gender and age can influence rupture. Smoking has been shown to have the greatest influence on aneurysm rupture [52].

2.2.3. Mechanical Properties of Cerebral Aneurysms

Cerebral aneurysm walls are stiffer than healthy cerebral arteries. This is likely due to the structural differences; aneurysms consist of only collagen whereas cerebral arteries have both collagen and elastin [20]. When thin strips of 6 aneurysms were mechanically tested under uniaxial extension, the neck of aneurysms exhibited an average stress of 1.2MPa and are stiffer than the fundus, where tearing occurred at an average stress of 0.5MPa [53].

2.2.4. Cerebral Aneurysm Classification

CAs are usually classified by their size, shape and location. The size of an aneurysm is important as it is used to determine whether an aneurysm will likely rupture and the treatment that the patient will undergo. The various aneurysm sizes are usually described qualitatively; micro, small, medium, large, giant, supergiant [54]. However, these are usually grouped together under the titles small, large and giant aneurysms, the size ranges are shown in Table 2.2.1.

Table 2.2.1 Classification of aneurysm by size [55]

Classification	Diameter
Small aneurysm	Less than 11mm
Large aneurysm	11mm to 25mm
Giant aneurysm	Larger than 25mm

Giant aneurysms are rare, with approximately 5% of cerebral aneurysms being larger than 25mm in diameter [56].

Cerebral aneurysms are usually seen in three shapes; saccular, fusiform, and dissecting (Figure 2.2.2) [54]. Saccular aneurysms are also called berry aneurysms due to their shape. 59% of saccular aneurysms are round and 24% oval in shape. When a saccular aneurysm is fully developed it will tend to have a thin wall and a narrow neck connecting to the artery [57]. In women, the aneurysm neck is usually larger compared to aneurysms found in men. 43% of saccular aneurysms are thin at the neck, with thickness varying through the aneurysm body, 22% have a uniform thickness, 18% have a thick neck and 17% have a thick fundus [21].

Fusiform aneurysms are more commonly found in the abdominal aorta rather than in cerebral arteries, with approximately 0.1% of cerebral aneurysms having a fusiform shape [57] [58]. Fusiform aneurysms occur when an artery expands circumferentially, dilating the artery.

A dissecting aneurysm has a similar exterior shape to a fusiform aneurysm, however, it is formed when blood enters the media layer of the artery wall through a tear in the intima layer [59].

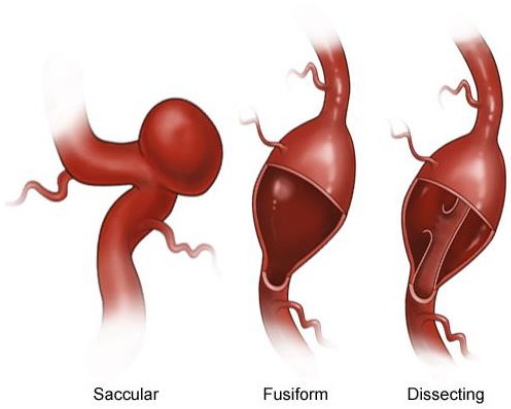

Figure 2.2.2 Three aneurysm shapes; Saccular, fusiform and dissecting [60]

The final aneurysm classification is the location of the CA. Location is another deciding factor for the type of treatment of the CA, as certain aneurysms may only be treated endovascularly due to location deep with the cerebral arteries. Location is usually described by its association with an intracranial branch vessel [54] [61]. Figure 2.2.3 shows the Circle of Willis with the most common locations of CAs and approximately how often they occur at each location. It can be seen that most aneurysms occur in the anterior, internal carotid and middle cerebral arteries.

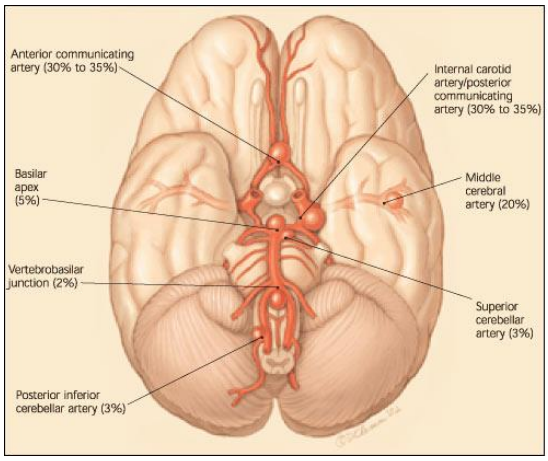

Figure 2.2.3 Circle of Willis with the common locations of cerebral aneurysms [62]

2.2.5. Diagnosis of Cerebral Aneurysms

Some CAs are not discovered until they rupture and lead to a subarachnoid haemorrhage. Subarachnoid haemorrhages have been described by patients as the “worst headache of my life”.

In some cases aneurysms can be diagnosed due to certain symptoms. As CAs grow they can exert a force on surrounding nerves, leading to cranial-nerve palsies, third nerve palsy or brain stem compression [55]. Hitting the nerve can cause:

- A sudden severe headache
- Nausea/vomiting
- Seizures
- Loss of consciousness
- Light sensitivity/ difficulty seeing
- Drooping eye lid

Patients with a suspected subarachnoid haemorrhage or unruptured aneurysm must undergo a computed tomography scan (CT) or magnetic resonance imaging (MRI) to confirm the diagnosis. There has been an increase in the number discovered before rupturing in recent years due to the improvement of non-invasive imaging [1] [55].

2.2.6. Prevalence of Cerebral Aneurysms and Rupture

It is unknown exactly how common CAs are, as they are not regularly checked for, but it is estimated that 1-6% of the entire population have a CA. This number is based on aneurysms found by accident, diagnosis, due to aneurysms rupturing and through autopsy [1] [35] [63]. CAs are more common in women (55-65%) and Asian and Finnish populations [35] [64]. Approximately 30% of people with one aneurysm have multiple aneurysms [35].

Up to 50% of aneurysms rupture during a person's lifetime [1]. However, it is generally noted that only between 0.1-1% of small aneurysms (<7mm) rupture [38].

2.2.7. Risks Associated with Aneurysm Rupture

An aneurysm ruptures when the tensile stress exerted on the aneurysm's walls exceeds the strength of the wall tissue. A ruptured aneurysm can cause many severe complications including;

- Subarachnoid haemorrhages (SAH)
- Disability
- Death

When a SAH stroke occurs, blood enters the subarachnoid space and requires immediate treatment. 1 in 10,000 people in the USA experience a SAH stroke caused by a ruptured aneurysm, with 35-50% of these resulting in death. SAHs are twice as likely to occur in women as in men and are most common in people aged between 55 and 60. 2-4% of CAs that rupture bleed again within the first 24 hours. There is a continued risk for the next 4 weeks, with approximately 15-30% re-rupturing. Patients who have had a bleed are 10 times more likely to suffer a subsequent haemorrhage [21] [35] [61] [65].

Hydrocephalus occurs in 15-20% of patients with a SAH stroke. Cerebral vasospasm is another complication of a SAH stroke, resulting in issues such as loss of speech, vision or

motor control, paralysis and death. Incidences of cerebral vasospasm result in a higher mortality rate within the 3 to 12 days following the haemorrhage [1] [63].

Up to 15% of SAH strokes are a result of an aneurysm. There is a 45% mortality rate for people who suffer a stroke from a ruptured aneurysm. Approximately 25-30% of the people who survive the stroke will have a disability [1] [38]. Around 10% of patients with a ruptured aneurysm die before reaching medical attention. Of those who do survive, many present in a coma or with neurological problems [63].

2.3. Cerebral Aneurysm Treatments

The aneurysm's size, shape and location and the patients' age and health are all taken into consideration when determining the best course of aneurysm treatment.

Aneurysm treatments can be broken into three categories; observation, surgical and endovascular treatments.

2.3.1. Observation

Active observation without any other treatment is used if the risk of aneurysm rupture is low or if the risk of treatment outweighs the benefits. The patient will be examined regularly to determine if there are any changes in the aneurysm. If changes in the aneurysm are present the course of treatment may change. In certain cases the patient will also be prescribed medication to reduce blood pressure [1] [66] [67].

2.3.2. Surgical Treatment

Surgical treatments are either clipping the aneurysm or parent vessel sacrifice.

2.3.2.1. Clipping

Clipping the aneurysm requires a neurosurgeon to perform a craniotomy. A craniotomy requires the patient to be under general anaesthesia and a lumbar drain to be placed to remove excess cerebrospinal fluid. A skin incision is performed to expose the skull and burr holes are drilled to allow the portion of skull to be removed. The dura mater, the brains protective layer, is then opened to gain access to the brain. The aneurysm must be freed if held by connective tissue. A clip is placed at the neck of the aneurysm to exclude the aneurysm from the blood flow, as shown in Figure 2.3.1. Following clipping, the aneurysm is punctured to insure total occlusion and the craniotomy is closed [68].

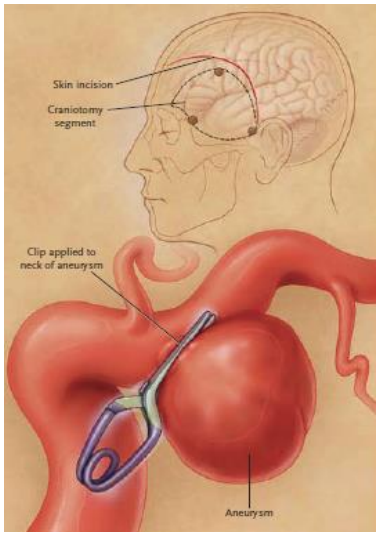

Figure 2.3.1 Clip Ligation of a Cerebral Aneurysm [1]

These clips are made from MRI compatible metal alloy, such as titanium [1] [68]. Clipping of an aneurysm can be performed on both ruptured and unruptured aneurysms [69].

Successful clipping of an aneurysm has a morbidity rate of 3-15.7% and a mortality rate of 1-3%. These percentages do not include the chances of technical failures which are incomplete occlusion (5.2%) and SAH (0.26%) [1]. However, the chances of recurrence after aneurysm clipping is low with reports showing rates up to 2.9% [69].

There are many risks associated with such an invasive surgery such as infection, allergy to anaesthesia, swelling of the brain, vasospasm and stroke [68].

2.3.2.2. Parent Vessel Sacrifice

Parent vessel sacrifice is only used as a last resort for giant aneurysms when clipping and endovascular treatment is considered too risky. Coil occlusion, clip occlusion and detachable balloon embolization are used [56] [70].

To gain a better understanding of the aneurysm neck and direction of blood flow, a three-dimensional reconstruction of the aneurysm is found using a catheter-based angiography. It is important that after giant aneurysms are treated, the aneurysm is excluded from blood flow but the neural tissues preserve their function. Depending on the patient's age and the location of the aneurysm, morbidity and mortality rates of unruptured giant aneurysms are between 20 and 45%. Risks with parent vessel sacrifice is delayed ischemia and the formation of new aneurysms due to induced stress on the artery [56] [71] [72].

2.3.3. Endovascular Embolization Treatment

Endovascular embolization of the aneurysm dome is a minimally invasive treatment to block the flow of blood into the aneurysm. Endovascular treatments of aneurysms can be carried out with coils, hybrid coils, flow diverters, intrasaccular devices and polymers [5] [61].

2.3.3.1. Coiling

In 1995 the Food and Drug Administration (FDA) approved the Guglielmi Detachable Coil (GDC), designed by Boston Scientific. Since then endovascular treatment of aneurysms, such as coiling, has become the primary method of treating an unruptured aneurysm, with approximately 42,500 aneurysms being coiled in the USA in 2013 [1] [73].

Coiling an aneurysm can be completed by a neuroradiologist or a neurologist with the patient under general anaesthesia. Coiling an aneurysm involves inserting a guiding catheter followed by micro-catheter from the femoral artery, at the patients' groin, to the site of the aneurysm. The coil is then pushed through the micro-catheter into the aneurysm. This coil then fills the aneurysm, blocking of blood flow, as shown in Figure 2.3.2 [1].

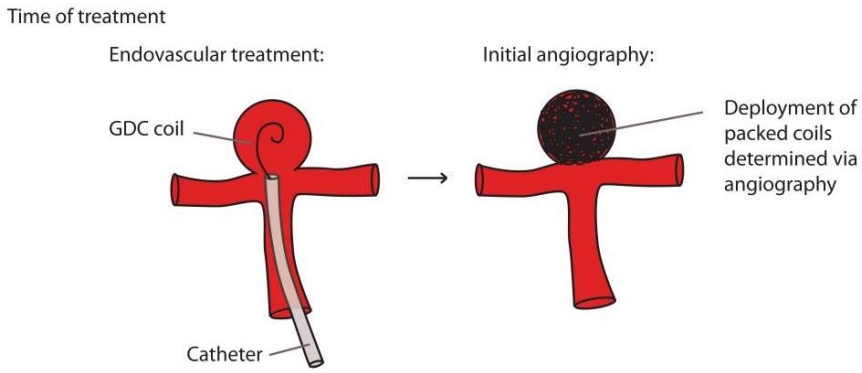

Figure 2.3.2 Coiling an aneurysm using a Guglielmi detachable coil [5]

The ideal healing of aneurysms treated with coils has been observed through histopathological studies. In the first week a thrombus forms within the aneurysm dome. This is caused by stasis due to the presence of the coils. This is followed by macrophages, fibroblasts, foreign body giant cells and inflammatory cells attaching to the clot and proliferating. Fibroblasts begin to differentiate into myofibroblasts. By week 2, fibrin usually begins to cover the coils and a thin fibrin membrane forms across the neck of the aneurysm. 2 to 4 weeks following treatment the coils are covered in fibrin. Fibroblasts, myofibroblasts, inflammatory cells and macrophages continue to invade the clot within the aneurysm. The fibrin layer at the neck of the aneurysm usually thickens. After 3 months, no inflammatory cells or myofibroblasts should be present in the aneurysm dome. Fibroblasts and endothelial cells have migrated and proliferated across the neck of the aneurysm. Endothelialisation of the aneurysm neck can occur by the movement of endothelial cells and the circulation of endothelial progenitor cells (EPCs). These cells can adhere, differentiate and proliferate across the treated aneurysm neck. EPCs, formed from bone marrow, are found in low numbers in the bloodstream [74] [75]. After one year the dome is filled with connective tissue and is completely occluded from the parent artery by a layer of fibrous tissue and endothelial cells [75].

The strength and compliance of the coil is important as recurrence can be observed due to the compaction of the coil with arterial blood flow [76]. This compaction leaves the neck of the aneurysm susceptible to growth, as shown schematically in Figure 2.3.3. This compaction is due to the low coil packing density, poor thrombus formation and incomplete neointimal formation. It is assumed that these coils will cause a thrombus to form in the aneurysm dome and undergo the ideal healing discussed previously. This will improve the mechanical strength of the coils and will continue to improve with the granulation of tissue present between the coils. However, this rarely occurs in bare metal coils [5] [75] [77]–[79]. One study has shown a compaction of 28% of coiled aneurysms within 6 months of coiling [80]. Recurrence rate have been reported to be 20.8% - 33.6% depending on aneurysm size and packing density [1] [2] [75].

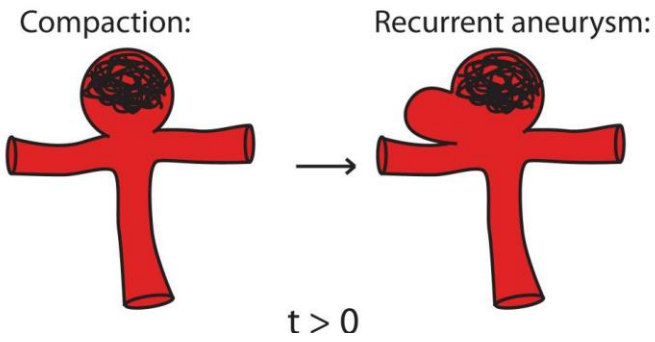

Figure 2.3.3 Recurrent aneurysm formation [5]

Coils are made from biocompatible soft materials such as platinum, tungsten and nitinol, in the form of a fine wire. This wire can be of varying diameter, which determines the coils primary structure. The fine wire, of the selected metal, is wound around a mandrel to form a spring like structure. This is the coils secondary structure and can vary by the number of times the coil is wound and the diameter. This spring is then shaped into its final form (tertiary structure), such as helical or spherical. Depending on the type of coil used and the skill of the clinician, coiling of the aneurysm fills between 20% and 73% of the aneurysm [81].

The number of coils varies depending on aneurysm size with an average of 4.6 coils used to treat small aneurysms and an average of 8.2 coils for medium aneurysms [82]. Compliant balloons and various stents can be placed across the neck of the aneurysm during coiling in an attempt to achieve an increased coil packing density [73]. Balloon assisted coiling is especially used in the case of wide neck aneurysms to stop coil migration through distal arteries during aneurysm embolization. For this, the micro-catheter is placed at the aneurysm fundus and the balloon catheter is placed across the aneurysm neck. The balloon is inflated while the coils are being placed and can be deflated and reflated as needed between coil placements to reduce the chance of cerebral ischemia and allow angiography to be carried out. Once the aneurysm is coiled the balloon is deflated and removed [70].

The Raymond-Roy Occlusion Classification (RROC) can be used to describe how successful the occlusion of the aneurysm is. The RROC is broken into Class I, Class II and Class III. Class I indicates a complete occlusion of the aneurysm dome and neck, Class II is used to describe an aneurysm with a residual neck and Class III is used when the aneurysm dome is not occluded successful. Typically, aneurysm occlusion rates are discussing number or percentage of aneurysm that are completely occluded (Class I) [83]. Coils have a lower occlusion rate of 77.6% compared to the clipping which can achieve a 92.5% occlusion rate. As a result, the risk of a SAH in coiled aneurysms is higher than those of clipped aneurysms [1] [2]. Despite

this, endovascular coiling has become the gold standard due to reduced risk associated with the procedure and reduced operating and recovery times [61].

The minor risks associated with endovascular treatment are reactions to the material, groin hematomas, infections and pseudo-aneurysms. Major risks are arterial dissection (0.7%) parent-artery occlusion (2%) and thromboembolic phenomena (2.4%). There is also a risk of aneurysm rupture caused by advancing the catheter too far, which happens in 1-2.7% of patients, of which, 30-40% die. Loose coils migrating into the surrounding vasculature can also occur (see Figure 2.3.4) and result in parent artery occlusion resulting in ischemic stroke [84]. Overall, for endovascular aneurysm coiling, there is a mortality rate of between 1.1 and 1.5% and a morbidity rate of 3.7-5.3% [1].

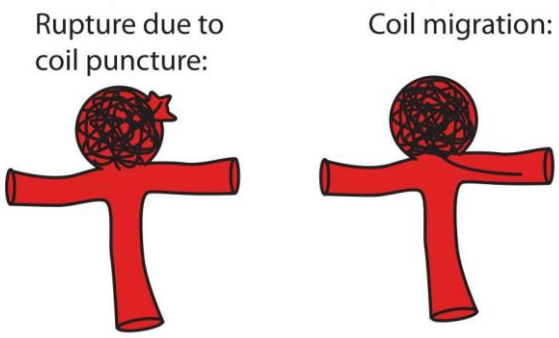

Figure 2.3.4 Risks associated with aneurysm coiling [5]

Generally, aneurysms are treated by endovascular coiling but up to 15% of aneurysms are unable to be treated by endovascular coiling as their location makes it too difficult to access *via* catheter [1] [85]. Aneurysms are also typically not coiled if the patient has intracerebral or subdural hematomas, a large neck-to-dome ratio, an artery incorporated into the aneurysm dome, a fusiform aneurysm, an aneurysm that is filled with a clot, if the aneurysm is a giant aneurysm or if the aneurysm is in an unfavourable location, such as the middle cerebral artery. If one or more of these instances occurs an alternative course of treatment, such as clipping, is chosen [85] [86].

2.3.3.2. Hydrogel Coated Coils

Coils used for the treatment of CAs can be coated with a hydrogel to reduce the chances of recurrence. The hydrogel coating on the coils can expand up to 900% which improves the packaging density of the aneurysm. Typically, the hydrogel coating is made with polyglycolic acid (PGA) or poly(lactic-co-glycolic) acid (PLGA). Surgery time is increased when using coils coated with a hydrogel as they are stiffer than bare coils. Hydrogel coated coils are inserted in the same manner as uncoated coils [5] [87].

Coating coils with a bioactive hydrogel encourages an inflammatory response which encourages clot organisation and maturation. It is also thought to induce neointimal formation [78].

A study by Fareed *et al* found that recurrence rates with coils without hydrogel coatings were 13 to 33% [87]. To attempt to overcome this they coated a platinum coil with a hydrogel that expands to its maximum capacity in 20 minutes, after coming in contact with blood. They inserted these coils into 3 patient's aneurysms and found they had reduced recurrence and packing rates between 35% and 72%. This was higher than the 30 – 32% seen in bare coils.

Reinges *et al* induced aneurysms in rabbits and inserted hydrogel coated coils into these aneurysms. After 12 months they found that the loops of the coils were adhering to themselves and created a smooth surface at the neck of the aneurysm. In this study they found that the aneurysm was completely occluded and leading to full wall healing [78].

One disadvantage associated with the use of hydrogel coated coils is that the coil may become stuck in the micro-catheter as its coating expands [88]. Recurrence rates remain high due to the degradation rate of the polymer coating being faster than that of thrombus formation [5]. To overcome this non-resorbable coils coated with a poly(ethylene glycol) hydrogel have been designed to provide a permanent occlusion [89].

2.3.3.3. Flow Diverters

Flow diverters are a newer treatment designed to cause a blood flow redirection which should cause aneurysm thrombosis without the need for coiling. Flow diverters are flexible devices similar in structure to stents that conform to the shape of the parent vessel [5] [70].

A flow diverter is placed across the neck of the aneurysm, causing blood stagnation within the aneurysm and promoting thrombus formation [5]. Complete closure of the aneurysms with flow diverters is unpredictable, generally occurring between 6 weeks and 6 months following the placement of the flow diverter [90] [91].

Flow diverters most commonly are used for the treatment of fusiform and side wall wide neck aneurysms. These flow diverting stents are made of a self-expanding, cylindrical high-coverage mesh. Metal coverage varies depending on the flow diverter design but can range from 20-35% [92]. Flow diverters have been made of braided nitinol strands of woven platinum tungsten and cobalt chromium strands [93] [94].

A study of 26 patients showed a mortality rate of 4% and a morbidity rate of 15% [93]. Concerns of the flow diverter covering unobserved artery side branches during stent placement remain [95]. An increase in intra-aneurysm pressure has also been observed with flow diverters, which causes a delayed aneurysm rupture. This increase has been postulated

to be caused by a decrease resistance in blood inflow than outflow when the diverters are not placed correctly and resistance in the parent artery [96]–[98].

2.3.3.4. Intrasaccular Flow Disrupter

Intrasaccular flow disrupter, such as the Woven EndoBridge (WEB), is a flow diverter that is placed in the sac of the aneurysm. The device is made of nitinol wire that is braided into a 'globular shell shape'. A concave shape at the base of the device is intended to avoid thrombosis on the device. Platinum markers are used to hold the shape and for visualisation purposes. The device is placed into the aneurysm through a micro-catheter and is detached distally using an electro-thermal system (Figure 2.3.5). The WEB device is designed to attach to the aneurysm wall like a stent. The device has high-attenuation mesh that reduces blood flow in the aneurysm, which allows the device to be used in both ruptured and unruptured aneurysms [99] [100]. However, this device may cause issues as the device should be of similar size and shape as the aneurysm to ensure the aneurysm does not recur [101]. Studies involving this device have resulted in the dual layer version of the WEB device being removed from the market and replaced by a single layer device. The evidence suggests the WEB device has not reduced aneurysm recurrence compared to aneurysm coiling [73] [102]–[104].

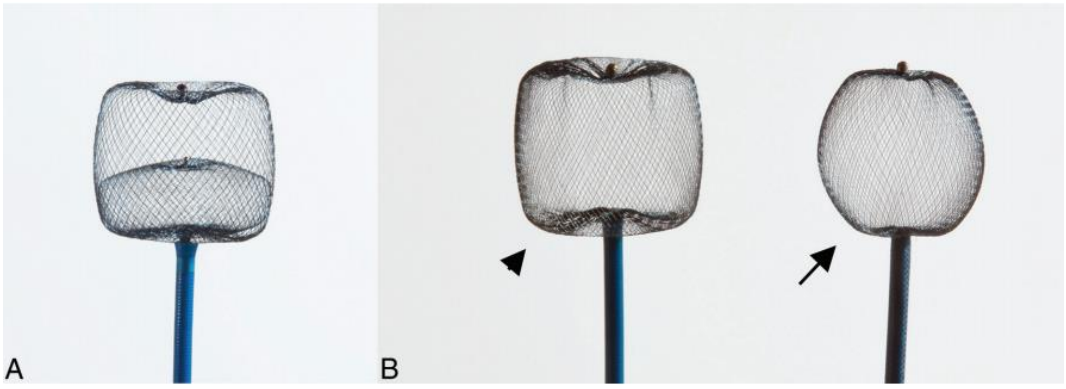

Figure 2.3.5 a) Woven EndoBridge (WEB) dual layer device b) WEB single layer [104]

2.3.3.5. Balloon-Assisted liquid Embolization

Liquid embolization can be carried out with Onyx® 500, a non-adhesive material that was developed for the treatment of CAs, shown in Figure 2.3.6. Onyx® is made of 20% ethylene vinyl alcohol (EVAC) which is dissolved in dimethyl sulfoxide (DMSO). Onyx® also contains 30% (w/v) tantalum to improve radiopacity. This is a micronized tantalum powder with a maximum particle size of 22µm but with 68% of the powder having a particle size <5.5µm [105]. This composition must be mixed for 20 minutes prior to injection. This treatment involves inserting a balloon-assisted micro-catheter adjacent to the patient's aneurysm. This micro-catheter and balloon must be DMSO compatible, which limits the surgeons catheter and balloon choice. The balloon is then inflated and tested to ensure it is in the correct position. A syringe is filled with Onyx® and injected through the micro-catheter. A rate of

0.1mL/minute is used to inject the Onyx®. An injection rate quicker than 0.5ml/min has been shown to have angiotoxic effects caused by the presence of DMSO in the Onyx® solution. The EVAC component of the material polymerizes in contact with blood due to the diffusion of the DMSO. To allow the material to precipitate the injection should be stopped and the balloon deflated every 0.2 to 0.3mL. Failure to inject the material correctly can cause arterial necrosis and induce vasospasms. Vessel damage can also be caused by the numerous cycles of inflating and deflating the balloon. Once the aneurysm is filled, the balloon is then deflated and removed. The micro-catheter is left in place for 10 minutes to ensure the material sets within the aneurysm. In total, it takes approximately 90 minutes to complete an aneurysm treatment with Onyx® [3] [5] [70] [88] [106] [107].

Figure 2.3.6. Balloon-assisted Onyx® embolization [70]

One study carried out on 97 patients found a morbidity rate of 8.3% and a mortality rate of 2.1% associated with this procedure. 11% of patients who have undergone this treatment have needed retreatment [70].

The FDA has issued a safety communication with the use of Onyx® for cerebral AVMs as the catheter commonly became trapped in the Onyx® gel as it set [108].

2.3.3.6. N-butyl cyanoacrylate

N-butyl cyanoacrylate is usually used for the treatment of cerebral arteriovenous malformations (AVM), though it has been examined for embolization of cerebral aneurysms. N-butyl cyanoacrylate becomes a solid adhesive material when in contact with blood. This polymer induces thrombosis which helps with occlusion of aneurysms and AVMs [109] [110]. However, N-butyl cyanoacrylate is thought to be too adhesive as it can block the tip of the catheter during injection and cause the catheter to adhere to the embolized aneurysm [91] [107] [111].

2.4. The Ideal Aneurysm Treatment Device

A number of studies discuss various aspects of an ideal aneurysm treatment but none provide a complete picture [3] [5] [112]–[114]. Combining these studies, the design requirements for the ideal aneurysm treatment device/therapy can be determined. Ideally the device is initially a liquid material that sets within the aneurysm dome and should be:

- Mechanically stable over time and have adequate mechanical properties
- Injectable
- Adhesive
- Biocompatible
- Sterilisable
- Radiopaque

2.4.1. Optimum Mechanical Properties for an Embolic Agent

A CFD model by Wang *et al*. was used to show that a liquid embolic agent reduced the risk of aneurysm rupture as it eliminates jet flows and causes a uniform distribution of pressure and WSS, whereas coils only reduced these factors [115]. FEA has shown that increasing the Young's modulus of an aneurysm thrombus, up to 1MPa, decreases the wall shear stresses in the aneurysm as it can "absorb" the stress caused by blood flow. A Young's modulus of 1.0MPa decreased the wall shear stresses by up to 100% compared to a thrombus with a lower Young's modulus of 0.05MPa [116] [117]. Although these studies made assumptions such as a homogenous artery wall that undergoes linear elastic deformation and that the thrombus was homogenous, these results indicate that a full occlusion with a material that can reduce hemodynamic forces within the aneurysm are advantageous and will reduce the risk of rupture. Although wall shear stresses play a role in aneurysm rupture, intrasaccular pressure is thought to be the leading factor in aneurysm rupture. A material that completely occludes the aneurysm would reduce these pressures, provided the material does not induce stresses due to excessive expansion [5].

The material should be mechanically stable over time as this both maintains support and allows endothelialisation of the aneurysm neck. It has been suggested that the mechanical stability of the material may be more important to aneurysm closure than the bioactivity of the material, as a stable surface is required for endothelialisation [5]. Onyx® has shown improved endothelialisation of the aneurysm neck compared to coiled aneurysms. This is likely due to the material completely filling the aneurysm and providing a stable surface for the cells to migrate across [118] [119]. Stiffness can also affect cell attachment; fibroblasts, endothelial cells and smooth muscle cells proliferate on and move towards areas of stiffer materials [120] [121]. Cell migration is important for wound healing and relies on adhesion and traction [122]. Cell attachment is caused by focal adhesion points that anchor the cell to the material. It has been shown that cells form more stable focal adhesions and a more

organised F-actin when seeded onto stiffer gels. Cells also show an increase in spreading on stiff materials [120] [123] [124]. Therefore, the mechanical properties of a biomaterial can be as influential in determining cell proliferation and differentiation as the chemical properties [123]–[126]. Depending on their composition, hydrogels can provide both chemical and mechanical stimulus for cell growth [127].

Ideally, the mechanical properties of the device should also be similar to the native tissue, as a mismatch in mechanical properties can result in inflammation, fibrosis or necrosis [5] [128]. Without the formation of a thrombus, coiled aneurysms typically become compressed over time. Coils with clots have a compressive strength of approximately 4.24±1.26kPa [129]. Although no maximum strength or stiffness of a material for embolization has been discussed in the literature two materials for aneurysm embolization with high strengths are Onyx®, which has compressive strength of approximately 3MPa [130] and a poly(propylene glycol) diacrylate and pentaerythritol tetrakis (3-mercaptopropionate) (PPODA–QT) material, which was examined for the treatment of cerebral aneurysm and has a Young's modulus of approximately 2MPa [3]. Although these materials do not have the same material properties as the cerebral artery, these results indicate that high strength and stiffness materials can be tolerated and used for the treatment of cerebral aneurysms. Overall, the materials compressive strength and strain should not be excessively high as this may lead to the transfer of stress to the aneurysm wall. At a minimum, the strength of the hydrogel should be able to withstand hypertensive blood pressure which is 160mmHg (22kPa) and should not fracture and a low strain.

Neither swelling nor shrinking of the hydrogel after injection is ideal. Shrinkage will cause a gap between the material and the aneurysm wall which may cause the material to migrate or the aneurysm to grow. Excessive swelling may exert pressurisation on the aneurysm wall, resulting in rupture. Small amounts of swelling may be tolerable and may reduce the chance of recanalization [131].

The structure of the device should not affect the blood flow patterns in the parent artery. Sharp edges may cause turbulent flow in the parent artery, which should be avoided [5]. A smooth and complete closure of the aneurysm neck is preferred.

2.4.2. Injectability of an Embolic Agent

The embolization of an aneurysm using a device that can be placed into the aneurysm dome endovascularly has the advantage of reducing patient pain and surgery time [5] [6]. Injectable biomaterials that form *in situ* will likely conform to the shape of the dome and completely fill and occlude the aneurysm. This has the advantage of not relying on unpredictable blood clotting mechanisms to stabilise the aneurysm [112].

Due to the narrow and treacherous nature of the cerebral vascular system, only micro-catheters can be used to endovascular treatment of cerebral aneurysms. Typically 0.021" (1.6F) to 0.027" (2.1F) distal inner diameter micro-catheters are used for aneurysm coiling. Larger, 0.033" (2.5F) distal inner diameter micro-catheters, are used with the WEB device [73]. These microcatheters are supplied in several lengths typically ranging from 90cm to 150cm [132].

The materials viscosity and the micro-catheters inner diameter and length can affect the force required to inject a material. If the material is to be injected easily into the aneurysm, the restrictions of current market micro-catheters inner diameter and length need to be taken into consideration.

The material must have an injection time that is sufficiently long to fill the aneurysm without blocking the microcatheter. Then, the material must harden after injection to ensure it does not migrate into the parent artery. Typically, embolic materials are injected into the aneurysm with a balloon across the neck of the aneurysm in order to ensure no material migration occurs. For this reason, the material should harden within 5 minutes of injection, as a balloon inflated in the cerebral vasculature for longer periods will likely result in irreversible cerebral ischemia [3] [133].

2.4.3. Adhesive Properties of the Embolic Agent

Materials that adhere to the aneurysm wall would be an advantage as it would reduce the risk of the material migrating due blood flow or high pressures [112]. They also may improve the distribution of the stress, caused by blood flow, across the aneurysm wall. Yet, the material should not adhere to the microcatheter or the balloon. This is a common problem in embolization with the adhesive material cyanoacrylate [91] [107] [111]. As a result, the material ideally should be selectively adhesive, adhering only to selective functional groups on the natural artery and not to the synthetic surfaces of the microcatheter and balloon. Catheters are typically made of silicone, polyvinyl chloride, polytetrafluoroethylene (PTFE) or latex rubber [134]. Balloons are made of a variety of materials including latex, polyethylene terapthelate and polyolefin copolymer [135] [136].

2.4.4. Biocompatibility

Biological evaluation must be carried out to ensure there is no toxic effect, either locally or systemically, when the device is in contact with the body. The intended use of the product dictates which testing is required to ensure a device is biocompatible. Biocompatibility is "the ability of a material to perform with an appropriate host response in a specific application" [137]–[139]. The appropriate host response depends on the materials application, but generally it should not induce cytotoxicity or carcinogenesis [139].

The International Standard Organization (ISO) has written the standard for the evaluation of the biocompatibility of medical devices (ISO 10993). This standard is used to select testing to be carried out to determine the biocompatibility for each device. In some cases, literature may already exist showing the biocompatibility of some, or the entire device, and in this case a reduced amount of testing is required. The type of test selected for each medical device depends on factors such as the location of the device, if it is surface contact or implanted and the duration the device is in contact with the body. Examples of these tests include [137] [138]:

- Haemocompatibility
- Cytotoxicity
- Immunotoxicity

Haemocompatibility testing examines how the material interacts with the components of blood. Typically, this involves examining whether platelets adhere to the surface of the material and if there is formation of a thrombus. Platelet adhesion to certain embolization treatments, such as coils, is an advantage as it improves the strength and reduces blood flow within the aneurysm [88] [140]. For the majority of vascular devices, however, platelet adhesion is seen as a disadvantage as it can cause thrombus formation and result in irreversible ischemia [141]. Haemolysis is the damaging of erythrocytes (red blood cells) and must also be examined for biomaterials [142].

Cytotoxicity testing examines if the material or its eluent is toxic to surrounding cells and tissues. For an item to be considered non-cytotoxic the percentage of cells remaining after testing must be above 70% compared to that of the control cells [143] [144].

Immunotoxicity examines whether the material will cause tissue damage, typically by an inflammatory response [145]. An inflammatory response usually occurs following the implantation of a device. Initially there is an acute inflammatory response which typically lasts a maximum of a week. An acute inflammatory response involves the movement of neutrophils, monocytes and macrophages to the site of injury. Phagocytosis by neutrophils and macrophages may occur, but this is not always the case with biomaterials due to the size difference. This may be followed by a chronic inflammatory response. In some cases, the chronic inflammatory stage can last several months. This is typically necessary for wound healing but may result in a negative effect on tissue remodelling and should be avoided where possible for vascular devices. In the case of aneurysm treatments, inflammation cause can a further remodelling of the aneurysm wall and results in a weakened aneurysm. Chronic inflammation is when lymphocytes, macrophages and plasma cells are found at the site of injury. Macrophages often coalesce to form foreign body giant cells. As 5μm is the largest particle size that can be engulfed during phagocytosis, a material with a larger surface area

will often stimulate frustrated phagocytosis. This involves the release of leukocyte products, in an attempt to degrade the material. The final stage of the immune response is the formation of a fibrous capsule which occludes the material from the surrounding tissue. The immunotoxic response of the material is usually determined by the intensity and duration of the inflammatory response. Tissue necrosis occurs when an implant causes a toxic reaction, resulting in cell death. This response indicates the material is not biocompatible [139] [145]–[151].

2.4.5. Sterilisation of Medical Devices

Devices intended for implantation must be able to withstand sterilisation. Before sterilisation the manufacturing of the device must be carried out in a clean room, which is a controlled environment with a low number of potential contaminants, according to the FDA Good Manufacturing Practices guidelines [152].

Not every sterilisation type is suitable for each device and testing must be carried out to determine a suitable type of sterilisation for each component of a device [153] [154]. The sterilisation type selected must not damage the product, as it may chemically and physically alter the material. The type of sterilisation selected must also insure an acceptable sterility level called the Sterility Assurance Level (SAL) of a minimum 10^{-6} (a maximum of one device per million is non-sterile) [155] [156].

There are many types of sterilisation used to remove microorganisms, pyrogens, spores and bacteria from a medical device. These sterilisation types can be either physical or chemical and some examples are:

- Wet/Steam sterilisation
- Dry heat sterilisation
- Gas sterilisation – Ethylene oxide, formaldehyde and hydrogen peroxide
- Irradiation – gamma and e-beam
- Sterile filtration

Wet/Steam sterilisation requires using a pressurised autoclave to expose the product to temperatures between 121^0C to 134^0C. Steam sterilisation is a quick process; only requiring 3 to 15 minutes depending on the product and temperature. However, a quarantine time post-sterilisation is required as the product has to dry and allow to return to ambient temperatures. Wet/steam sterilisation should not be used on certain materials, such as hydrophobic materials, powders and corrosive materials [157] [158]. Typically, materials are packaged in a material which allows appropriate steam penetration while acting as microbial barrier, such as Tyvek® [159].

Ethylene oxide (EtO) sterilisation is one of the most commonly used methods of sterilisation. EtO sterilisation has advantages such as not discolouring packaging or products, can be used on products that degrade at high temperatures and does not damage electrical components [160]. EtO can be used to sterilise both the surface of products and products sealed in gas penetrable packaging. Other gases such as steam formaldehyde and hydrogen peroxide can be used for sterilisation. EtO has many advantages over these other gases. It can be used at elevated temperatures to reduce sterilisation time, is permeable and is relatively molecularly stable [154]. There are disadvantages associated with the use of EtO sterilisation such as residues being left in some materials. This is caused by the material absorbing EtO and releasing it slowly over time. Usually, sterilised materials have a quarantine period following sterilisation as EtO is neurotoxic. Depending on the polymer type, EtO residues can be high, as EtO reacts with the polymers functional groups. These polymers need extended quarantine periods and the residual EtO level needs to be examined [155] [161]–[164].

Both gamma ray and electron beam (e-beam) radiation can be used to sterilise medical devices. Gamma and e-beam irradiation has the advantage of not requiring a quarantine time after sterilisation; it can be used to sterilise dense materials and can be used on closed products without a need for increased temperature. E-beam is a quicker sterilisation method compared to gamma rays; however, it is less effective for dense materials. Gamma and e-beam irradiation carries disadvantages such as discolouration of some products and it can degrade polymers [155] [165]. The amount of degradation can be reduced by lowering the irradiation dose, placing the samples in a vacuum during irradiation or irradiating at low temperatures [166]. Most countries accept an exposure of 25kGy of gamma rays for a product to be considered sterile but lower doses can be used on degradable material once sterility assurance level is confirmed [155] [167].

Sterile filtration is an aseptic technique that can be used on liquid materials which are unsuitable for other forms of sterilisation. This involves passing the liquid through a filter, or a number of filters, to remove all microorganisms from the solution [168] [169]. Sterile filtering through a 0.2μm filter is ideal for polymers as it has no apparent effect on their structure. However, this is not often feasible as it is time consuming, difficult to achieve for high viscosity materials and needs to be completed in a sterile environment [156].

2.4.6. Radiopacity of Embolic Agents

Typically, fluoroscopy is used during the treatment of aneurysms. Fluoroscopy uses low intensity X-rays to identify radiopaque material. Therefore, aneurysm treatment devices must also be radiopaque to allow the material to be placed with minimal invasiveness [170]. CT is also a commonly used tissue imaging technique that allows a non-invasive three dimensional visual reconstruction and segmentation of soft tissues [7].

Contrast agents are low viscosity dyes that have been developed to be injected into blood vessels to allow the vasculature to be visualised. These contrast agents can be both ionic and non-ionic. A number of these contrast agents have been approved for medical use in cerebral vasculature. These include; Ultravist (Bayer Healthcare), Isovue (Bracco Imaging) and Hexabrix (Mallinckrodt Imaging) [171]. Contrast agents have been mixed with embolization materials to improve their radiopacity [110] [172] [173]. Though, they can affect the usability of the embolization material depending on their ionic nature, additives and viscosity [171].

Other additives such as tantalum powder have been added to embolization materials such as Onyx® to improve radiopacity [110]. However, tantalum can increase the viscosity of the material and cause permanent skin discolouration [174].

Although the ideal radiopacity of a material is not discussed in the literature, a material must have a sufficient radiopacity to be easily observed during placement. The radiopacity of a material can be too high and make it difficult to determine if the aneurysm is fully occluded.

2.4.7. Summary

Summarising the above criteria, for the hydrogel to be injected safely into the aneurysm and perform as a suitable embolization material, the hydrogel should;

- Have sufficient mechanical strength to withstand 22kPa (160mmHg) of compression, which relates to hypertensive blood pressure, while distributing stress across the wall of the aneurysm [16].
- Not shrink or excessively expand, to ensure the material does not migrate or cause aneurysm rupture. Small amounts of expansion (<10%) of the material will likely be tolerated by the aneurysm wall, without protruding and blocking the parent artery
- Be injectable through a microcatheter (ideally 2.1F distal inner diameter and a length of 1.5m) into the aneurysm to allow for a minimally invasive procedure.
- Have a working time between 10 and 30 minutes.
- Have maximum hardening time of 5 minutes, as this is the maximum time a balloon can be inflated in the cerebral vasculature without causing irreversible cerebral ischemia [133].
- Ideally adhere to the aneurysm wall to reduce the chance of migration of the hydrogel and aneurysm recurrence.
- Not result in any cytotoxic effect to the surrounding vasculature.
- Be sufficiently radiopaque to be observed by fluoroscopy, in order for the hydrogel to be injected in a minimally invasive manner.
- Platelets should not adhere to the material and result in thrombus formation.

A design review table can be formed from this discussion, as shown in Table 2.4.1.

Table 2.4.1 Design review table

Compressive Strength >22kPa?	**Is the material size conserved? (<10% expansion with no shrinkage)**	**Is the hydrogel injectable?**	**Working time between 10 and 30 mins?**	**Hardening time <5 mins?**	**Is the material adhesive?**	**Is the material cytocompatible? (>70% cell viability)**	**Is the material sterilisable?**	**Is the material suitably radiopaque?**	**Is the material haemocompatible?**
Yes/No	Yes/No	Yes/No	Yes/No	Yes/No	Yes/No	Yes/No	Yes/No	Yes/No	Yes/No

2.5. Novel Aneurysm Treatment

The aim of this work is to design a material that will fulfil the criteria of Table 2.4.1 From Section 2.4, it can be deduced that an injectable material, such as a hydrogel, may be applicable.

2.5.1. Hydrogels

A hydrogel is described as being a three-dimensional water-swollen, cross-linked polymeric structure. Hydrogels are generally biocompatibility materials that can be tailored to have various mechanical properties and degradation rates. The varying mechanical properties allow hydrogels to be biomimetic and can induce cell proliferation as a result of physical cues [7] [175] [176].

Hydrogels were the first materials specifically designed for human use. Although the term hydrogel was first reported around 1900, the first hydrogel for medical use (the contact lens), was not created until 1960. Since then, hydrogels have been produced in various forms, such as scaffolds, adhesives, carriers for cells and delivering drugs [6] [177].

Hydrogels are hydrophilic which is shown by their ability to hold a large amount of water [175] [176]. Swelling occurs as the material absorbs water as a result of osmotic forces. A swelling equilibrium is reached when the cross-links cause a retraction force [176]. The high permeability allows the transfer of necessary nutrients and oxygen through the hydrogel structure [5] [178].

Hydrogels can be classified by their type of cross-linking or by the type of polymer chain used [175] [176]. Cross-linking of polymers can occur by either physical or chemical linking of macromolecular chains. Physical cross-linking of polymer chains causes the connections to be strong or weak and can be reversed if needed. Reversible cross-links are utilized when a biodegradable material is required, such as in tissue engineering and drug delivery. Chemical cross-linking of polymer chains is strong and permanent. Chemical cross-linking is typically achieved by addition of covalent cross-linking agents, which are generally cytotoxic [7] [175] [176] [179].

Types of physical cross-links are chain entanglement and secondary interactions such as electrostatic forces, hydrogen bonds, hydrophobic interactions and ionic bonds. Ionic gelation occurs when cross-linking divalent and trivalent cations come into contact with anionic polymers [176] [179].

Types of chemical cross-links are polymerization, radiation, small-molecule cross-linking and polymer-polymer cross-linking [179].

Hydrogels can also gel due to combined chemical and physical stimuli. pH, ions and chemical compositions are examples of such chemical stimuli. Physical stimuli include temperature, pH, light and ion content [180].

Both natural and synthetic polymers can be used to form a hydrogel. Natural polymers tend to be biocompatible, however, they tend to have a low and variable mechanical strength and have a high batch inconsistency which limits their use [175] [176] [181]. Despite this, natural polymers have been extensively used in hydrogels, such as gelatin, collagen, fibrin, hyaluronate, alginate, agarose and chitosan [7]. Examples of synthetic polymers are polycaprolactone (PCL), polyethylene glycol (PEG), poly(acrylic) acid (PAA), poly(lactic) acid (PLA), poly(glycolic) acid and their copolymer PLGA. Synthetic polymers tend to have a higher strength than natural polymers, however, they tend not to be as biocompatible [7] [175] [176] [181].

It is important that both the hydrogel and its degradation products do not cause an adverse chronic immune response. Hydrogels are generally considered to be biocompatible. Cells do not adhere to hydrogels due to their hydrophilic surfaces and surrounding tissues are not irritated by them, as the hydrogel can mimic the tissue flexibility, which limits the foreign body response [176]. When designing a hydrogel it is important to take 5 factors into consideration for biocompatibility [7] [182]:

1. Degradation rates
2. Bioadhesion
3. Bioactivity
4. Transport/release of bioactive molecules
5. Mechanical properties

Hydrogels can undergo controlled degradation due to hydrolysis, proteolysis, disentanglements and environmental triggers. Controlled degradation rates are an ideal characteristic for cell transporting biomaterials. Due to these characteristics, hydrogels are used in various medical devices such as drug delivery, wound dressings, contact lenses and tissue engineering scaffolds [7] [175] [176].

Bioadhesion and bioactivity are important factors for tissue engineering scaffolds in that they control how the cells will attach, differentiate and proliferate on the biomaterial [7].

Ideally, hydrogel's should have similar mechanical properties to the surrounding native tissue. The mechanical properties of hydrogels are controlled by the type of polymer used, as different polymers have varying chain rigidity. The type of cross-linking and cross-linking density will also greatly affect the strength and biocompatibility of the hydrogel [7] [182].

To increase deliverability and minimise trauma, the hydrogel should gel under physiological conditions. Ideally, the hydrogel will be injectable, lending itself to minimally invasive delivery techniques, which can reduce the pain and recovery time for the patient. Injectability and gelation under physiological conditions can usually be achieved by *in situ* forming hydrogels. Current *in situ* forming hydrogels are either cross-linked by physical reactions such as a change in pH or temperature and introduction of ions, but these usually have poor mechanical properties. Chemical reactions, such as Michael-type addition, can be used to improve the mechanical properties but such hydrogels usually have a reduced biocompatibility [6] [180] [183] [184]. *In situ* forming hydrogels have been of considerable interest as they allow currently invasive techniques to be accomplished in a non-invasive manner. *In situ* forming hydrogels allow for delivery of acellular and cellular scaffolds directly into defects. These hydrogels can provide a complete filling of the defect, which can improve tissue repair. These hydrogels are also more efficient, with higher cell and growth factor survival rates compared to materials processed prior to implantation. *In situ* forming hydrogels are also used in drug delivery as they allow the drugs to be delivered directly to the site, where required. The rate of gelation is important as fast gelation is optimal for delivering cells and drugs but a slower gelation may be needed to fill irregularly shaped defects [6] [180] [183] [184].

Alginate hydrogels that are cross-linked with multivalent ions are *in situ* gelling hydrogels that are typically biocompatible, as they are natural polymers. Alginates and their ability to form hydrogels are discussed in more detail below.

2.5.2. Alginate

2.5.2.1. Alginate Structure

Alginate, also called alginic acid, is polysaccharide found in the cell walls of brown seaweeds [109]. Alginate is a linear polymer, containing blocks of β-D-mannuronic acid (M-block), α-L-guluronic acid (G-block) and regions of alternating structure (GM-blocks). Alginates M-block units are in a $^4C_1$ chair conformation and the G-blocks are in a $^1C_4$ chair confirmation. Alginate polymers are formed when the monomers join at the $^4C_1$ and $^1C_4$ position, which gives the M-block its flat polymer shape and the G-block a buckled shape, as shown in Figure 2.5.1 [185] [186].

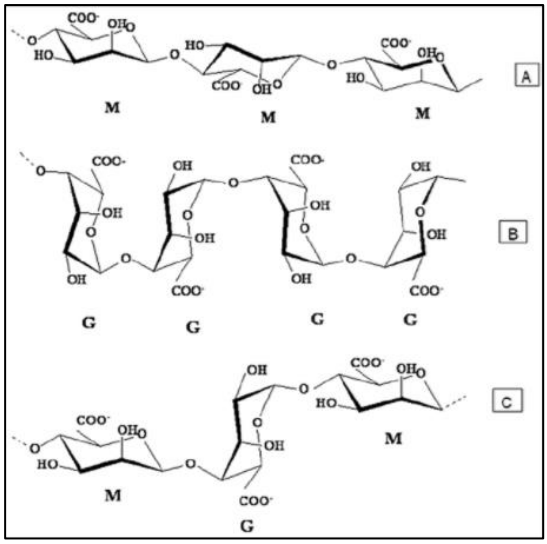

Figure 2.5.1 M-block (A), G-block (B) and alternating GM-blocks (C) of alginate [187]

Alginate is usually described by its chemical composition (M/G ratio or monad, diad and triad sequences) and molecular weight. There are four diad sequences (MM, GM, MG, and GG) and eight triad sequences (MMM, MMG, MGM, MGG, GMM, GMG, GGM and GGG) [188] [189]. If the alginate has a higher G-block content the hydrogel will be strong and brittle. If the M-block content is larger than the G-block content the hydrogel will be weak but flexible. Increasing the G-block length generally increases mechanical properties, due to an increased rigidity of the chains [190]–[192]. The average length of the G is found using Equation 2.5.1.

Equation 2.5.1. Equation to determine the average G-block length [188]

$$\overline{N}_{G>1} = \frac{F_G - F_{MGM}}{F_{GGM}}$$

Where,
$N_{G>1}$ = Average G-block length
F_G = Frequency of the G-block
F_{MGM} = Frequency of the triad MGM
F_{GGM} = Frequency of the triad GGM

Alginate's chemical composition (M/G ratio) and its molecular weight can vary greatly depending on the location the alginate was collected and the extraction and purification process. Table 2.5.1 shows the effect location has on the chemical composition of some alginates. Average alginate molecular weights range from 20kDa to 500kDa [193] [194]. The molecular weight and M/G ratio greatly affects the compressive strength, viscosity, gel uniformity and gelation rate of the hydrogel [195] [196].

Table 2.5.1 Varying chemical composition of alginate from various locations [194]

Species	Origin	F_G	F_M	M/G	F_{MM}	F_{GG}	F_{GM}	F_{MG}
Laminaria digitata	Norway	0.41	0.59	1.44	0.43	0.25	0.16	0.16
Laminaria japonica	China	0.35	0.65	1.86	0.48	0.18	0.17	0.17
Macrocystis pyrifera	Argentina	–	–	1.17	–	–	–	–
Laminaria hyperborea (stipe)	Norway	0.71	0.29	0.41	0.17	0.59	0.12	0.12
Laminaria hyperborea (leaf)	Norway	0.51	0.49	0.96	0.34	0.36	0.15	0.15
Laminaria digitata	France	0.40	0.60	1.5	–	–	–	–
Laminaria digitata	Morocco	0.47	0.53	1.12	0.47	0.41	0.06	0.06

Alginate generally has a high viscosity at low concentrations due to intramolecular electrostatic repulsion [181]. Despite alginate's high viscosity, it has the ability to be injected through micro catheters as it is a shear thinning material [197].

Alginate is removed from algae by using hydrochloric acid, followed by washing, filtering and neutralizing the solution with an alkaline buffer. This process can be repeated to further purify the alginate by removing phenols and endotoxins. Sodium alginate is precipitated by adding the alginate solution to alcohol, such as ethanol or methanol [109] [198].

2.5.2.2. Alginate Hydrogels

Alginate is commonly used in hydrogels as it is cheap, biocompatible, easily purified, and can form a gel under physiological conditions. Alginate has the ability to form a gel by ionic cross-linking when introduced to multivalent ions, covalently cross-linked or by acidification below its pK_a value of 3.38 for mannuronic acid and 3.65 for guluronic acid. Alginate can be processed in soft and elastic materials of different forms, such as gels, fibres, foams and nanoparticles [188] [190] [193] [199].

Cells and platelets do not adhere to alginate due to its high hydrophilicity and negative charge [188]. The molecular weight, M-block and G-block content also affects the biocompatibility of the alginate. Alginates with a high G-content or with a high molecular weight do not usually cause a chronic immune response. High M-content alginates have been seen to causes

cytokine production by monocytes. An increased cytokine production can cause the inflammatory stage to be prolonged. Alginate with a molecular weight below 20kDa can cause lower molecular weight M-block material to leak, causing cytokine production and therefore should be avoid for use as a biomaterial [151] [188].

Alginate binds preferentially with divalent ions in the following order $Pb^{2+} > Cu^{2+} > Cd^{2+} > Ba^{2+} > Sr^{2+} > Ca^{2+} > Co^{2+}$, Ni^{2+}, $Zn^{2+} > Mn^{2+}$ [200]. These cations generally bind preferentially to the G-block forming a three-dimensional "egg-box" structure when cross-linked, see Figure 2.5.2 [190]. The "egg-box" structure is caused by the cations coordinating with monomer moieties which cause inter-chain complexes between alginate strands. Ca^{2+} will only cross-link with the G-block of alginate, and therefore will not gel 100% M-block alginates. While Ba^{2+} and Sr^{2+} bind both with the M-block and the G-block of alginate, which produces stronger gels [188] [201]. Despite forming a weaker hydrogel, Ca^{2+} is preferred to Ba^{2+} and Sr^{2+} as it has a reduced cellular toxicity [188] [195].

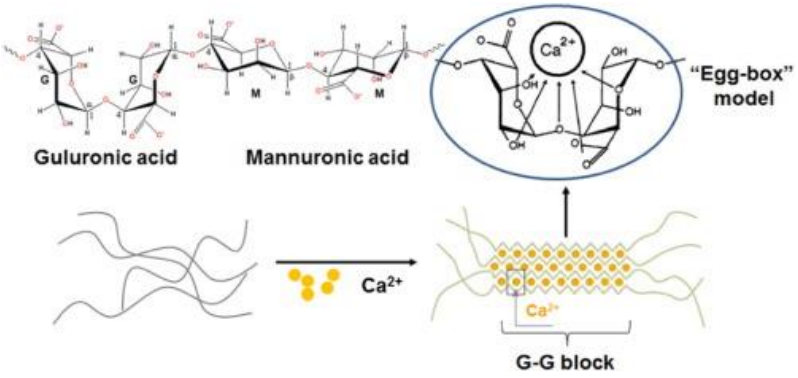

Figure 2.5.2 Ionic gelation between the anionic alginate groups and Ca^{2+} to form the "egg-box" structure [198]

Ionic alginate cross-linking can occur by diffusion or *in situ* gelation. Gelation by diffusion involves the alginate solution being placed in a reservoir of the multivalent ions. A typical source of cations for forming alginate hydrogels is the highly soluble calcium chloride salt ($CaCl_2$). This method produces an inhomogeneous gel caused by rapid gelation, with the cross-linking density being highest on the surface of the hydrogel. This method is generally only used in the formation of gel beads. *In situ* gelation involves mixing an alginate solution and GDL with a non-soluble (at neutral pH) cation source, such as calcium carbonate ($CaCO_3$). GDL, as it hydrolyses, will lower the pH of the solution and cause Ca^{2+} to dissociate from the alkaline $CaCO_3$, resulting in a slow, controlled gelation of the alginate. A slow gelation causes a strong and homogenous gel to form. *In situ* gelling alginates are ideal for tissue engineering as they allow the hydrogel to be implanted by a minimally invasive surgery, they have improved mechanical properties and can be moulded *in situ* to the required shape [188] [191] [193] [195] [201] [202].

The crosslinking density can be controlled by varying the ion content and alginate concentration. An increase in crosslinking density can greatly increase the gelation and strength of alginate and stability of the hydrogel. Alginate concentration can also greatly affect the viscosity of the hydrogel due to an increase in chain entanglements [191] [203] [204].

Studies have also shown that the M-blocks and G-blocks do not alone play a role in alginate gelation, as pure MGM sequence alginate was shown to gel with the addition of calcium ions. However, this did not produce as strong a gel as G-block only calcium alginates [205] [206].

It is generally considered that the gelation of alginate with Ca^{2+} ions is a 3 step process and varies depending on molecular weight see Figure 2.5.3. Step 1 involves individual alginate chains shrinking/collapsing, which causes an initially decrease in viscosity. As there is more flexibility in alginate chains with a high molecular weight, they can shrink further causing a greater decrease in viscosity than low molecular weight chains. A monocomplex between Ca^{2+} ions and the G-block of the alginate is formed causing an alginate intramolecular attraction. Step 2 involves the formation of egg-box dimers. Step 3 sees a decrease in molecular size for high molecular weight alginates, whereas the short molecular weight chains continue to grow in molecular size. It is suggested that due to low molecular weight alginate's short chains there is an inter-cluster association. High-molecular weight alginates form individual clusters. It is also suggested that calcium binds more easily in Step 3 compared to Step 1 and 2, as the egg-box structure has been formed [207].

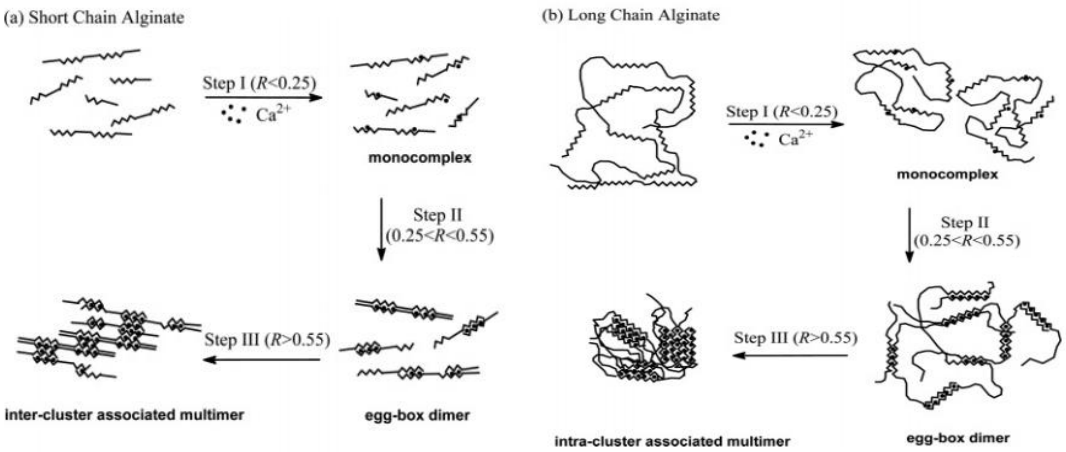

Figure 2.5.3 Three steps involved in the binding of calcium to (a) short chain (low molecular weight) alginate and (b) long chain (higher molecular weight) alginate [207]

In vivo, ionically cross-linked alginate hydrogels decrease in strength and swell due to a loss of crosslinks as the Ca^{2+} ions in the hydrogel exchange with sodium ions in blood but alginate is otherwise stable at physiological pH and temperature [188] [198] [203]. Alginates can degrade in a solvent with a pH below 5 or greater than 10. If the pH is below 5, degradation

occurs by proton-catalysed hydrolysis. ß-alkoxy-elimination occurs at a pH above 10. Enzymes such as alginate lyase or depolymerases can also degrade alginate, but they are not found in humans. Alginate lyase causes scissions in the polymer chains by ß-elimination [208]. Alginate hydrogels formed with ions like barium are more stable long term under physiological conditions [209].

Alginate can also be covalently cross-linked, to produce a more stable hydrogel. Methacrylated alginates can be produced using carbodiimide chemistry. These alginates can then cross-link in the presence of UV light or a photo initiator [188] [191]. Thermally setting alginates have also been used by polymerising N-isopropylacrylamide (NIPAAm) with sodium alginate which has the ability to gel at approximately 32^0C [191].

Alginates are hydrophilic and have a negative charge, which makes cell attachment difficult. Although alginate alone cannot adhere to cells, covalent bonding and carbodiimide chemistry can be used to increase the alginates adhesive properties. One example is covalently attaching RGD (Arginine-Glycine-Aspartic acid), a peptide found in the extracellular matrix (ECM) proteins, to the alginate by the addition of (1-ethyl-3-(3-dimethylaminopropyl) carbodiimide hydrochloride) (EDC) and N-Hydroxysuccinimide (NHS), discussed in more detail in section 2.5.3 [188].

Alginate beads have been used for drug delivery and to encapsulate cells. The basic method is achieved by producing a cell/alginate mixture by dripping the alginate cell solution from a needle into a $CaCl_2$ solution. Other methods such as using an electrostatic potential, vibrating capillary jets and rotating capillary jets have been developed to produce smaller beads and control bead size. The cells remain viable due to the alginates limited cell adhesion properties and gelation under mild conditions [181] [188] [202].

Alginate foams have been used in tissue engineering and wound healing due to their macroporous scaffolds allowing an increase in cell invasion and the transfer of nutrients through the hydrogel. Foam alginates are typically formed by freeze drying the cross-linked alginate or by the passage of gases through the hydrogel. Alginate foams loaded with cells have been used in repairing soft tissue, the regeneration of bone and to encourage angiogenesis. Acellular alginate foams can be used for sustained local delivery of drugs and growth factors [181] [188].

Alginate fibres have been used in wound healing and tissue engineering. Macrofibres can be produced by extruding an alginate solution into a solution of multivalent ions. Microfibers can be produced by electrospinning [188] [191].

In situ gelling alginates allow for alginate to be minimally invasively implanted into the body. Alginate/cell mixtures have been injected with a calcium sulphate or a calcium carbonate with GDL for the repair of bone defects [181]. As mentioned, a significant disadvantage of these hydrogels is their poor mechanical properties and stability *in vivo* due to calcium exchange with sodium in blood [191] [197] [202]. These gels can often require a prolonged gelation time to produce a homogenous material [202].

2.5.3. EDC and NHS

N-(3-Dimethylaminopropyl)-N′-ethylcarbodiimide hydrochloride (EDC) is a water soluble carbodiimide. This is a zero length cross-linker that has the ability to form amide bonds between carboxylic and amine groups without becoming part of the amide bond [193] [210] [211]. As EDC is water soluble and no other (potentially toxic) solvents are required in the reaction [212].

EDC, in the presence of carboxylic acid, forms an o-acylisourea intermediate. EDC reacts with the carboxyl group of mannuronic acid in alginate. This intermediate undergoes a nucleophilic attack and forms a stable amide bond when in contact with primary amines. However, if there is an excess of EDC or a lack of primary amines, the unstable o-acylisourea hydrolyses to form a stable N-acylurea, which can't form an amide bond. Therefore, an increased amount of EDC will be required to increase the bond strength. However, EDC has been found to have cytotoxic effects in mice in high concentrations (>12.9mg/ml) [213]. N-Hydroxysuccinimide (NHS) is typically added to a hydrogel with EDC as it reduces the rate of hydrolysis, therefore reducing the production of N-acylurea, while allowing amide bond formation [212] [214]–[216]. This allows for a reduced EDC content without compromising the bond strength and, in turn, a reduction in any possible cytotoxic effects [214] [217]. The EDC and NHS reaction can be seen in Figure 2.5.4.

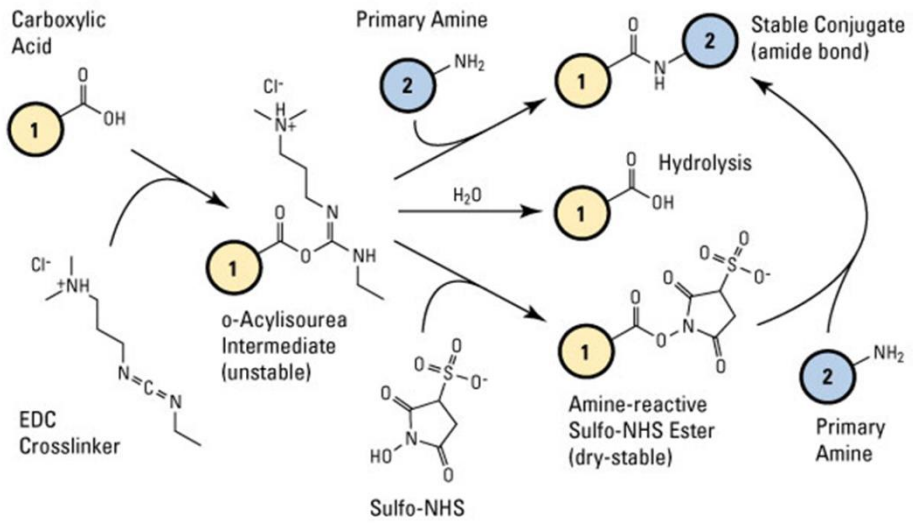

Figure 2.5.4 EDC and NHS coupling reaction [218]

The water content and pH can vary the time required for the adhesion to occur. The activation of the EDC/NHS reaction is most effective in a pH of 4.5-7.2 [219].

2.5.4. Glass

Glass is a hard, amorphous, brittle material made by fusing one or more oxides [138]. The glass transition temperature (T_g) is the temperature at which the glass melt moves from a liquid state to a solid state [220]. Below the T_g the material is considered a glass. The glass transition temperature is associated with the passage of glass through a temperature range where the thermal coefficient of expansion exhibits a large change in slope [221]. Glass can be produced by either a melt-quench frit or by a sol-gel process [222].

A melt-quench glass is formed by weighing out the correct mole/weight fraction of the glass ingredients. The ingredients are then added to a platinum or ceramic crucible and placed in a high temperature furnace at a specified temperature for a specified amount of time. Typically, the mixture is heated to between 1200 and 1500^0C. Platinum crucibles are more commonly used to insure there is no oxide contamination from the ceramic crucible. After this specified amount of time, the melted glass is quickly quenched by pouring into water. The produced glass frit has granules of different sizes that can be ground into a powder [223] [224]. Crystallisation can occur if the glass is not cooled rapidly enough. However, potassium oxide, magnesia and boron oxide can be added to the glass formulation to reduce the crystallisation [220].

A sol-gel technique can be used to produce a bioactive glass without requiring the high temperatures needed for a melt quench. Sol-gel materials can be achieved by gelling colloidal powders by varying the pH or by the hydrolysis and condensation of the metal alkoxide

followed by drying. Sol-gel produces a more bioactive material as the surface area, particle size and particle morphology can be controlled [225] [226].

The materials used to produce a glass can be divided into different roles; the glass former, modifier and intermediate [221]. Formers are oxides that may be used alone to form glass. For example; silica oxide is used as the glass former in silicate glass. More than one material can be used as a glass former in one glass [221]. Typically, glasses are formed in either an octahedral, tetrahedral or triangle structure. Silica oxide glasses are formed when the SiO_4 tetrahedron is connected to the neighbouring SiO_4 tetrahedron by Si-O-Si bonds, giving it a high network connectivity (NC) [221] [224].

The NC is described by the number and arrangement of the bridging oxygens (BO) and non-bridging oxygen (NBO) bonds. The Q_n notation is used to describe the number of BO per tetrahedron in the glass, where n is the number of bridging ions. As discussed, silica glass is typically formed in a silicon-oxygen tetrahedron structure, of one cation surrounded by four oxygen ions. This gives silica glass a coordination of 4 (Q_4). Each of these oxygen atoms is connected to two silicon atoms. In this respect, silica glass has a high degree of order with all four corners of the tetrahedron structure being linked but this is a disordered network with broad ring distribution. The Si-O-Si structure can be varied to introduce further disorder to the structure. This can affect the properties of the glass, such as chemical resistance and strength. NBO's are formed by the addition of glass modifiers to the glass and this decreases the connectivity of the glass network. A fully linked tetrahedron glass theoretically has a structure of Q_4 and a glass with no bridging oxygens is described as Q_0 [221] [224] [227].

Alkali oxides, such as calcium and sodium can act as glass modifiers and break the Si-O-Si bridge to form non-bridging oxygens. This break occurs in the glass structure as the bridging oxygen anion attempts to charge to balance the positive charge introduced by modifying cation (*e.g.* Ca^{2+}, Na^{+}). The addition of calcium oxide (CaO) to a glass composition increases the number of NBOs and, therefore, decreases the NC, see Figure 2.5.5. This addition allows the glass the undergo acid dissolution, as NBOs are hydrophilic [221] [224] [228].

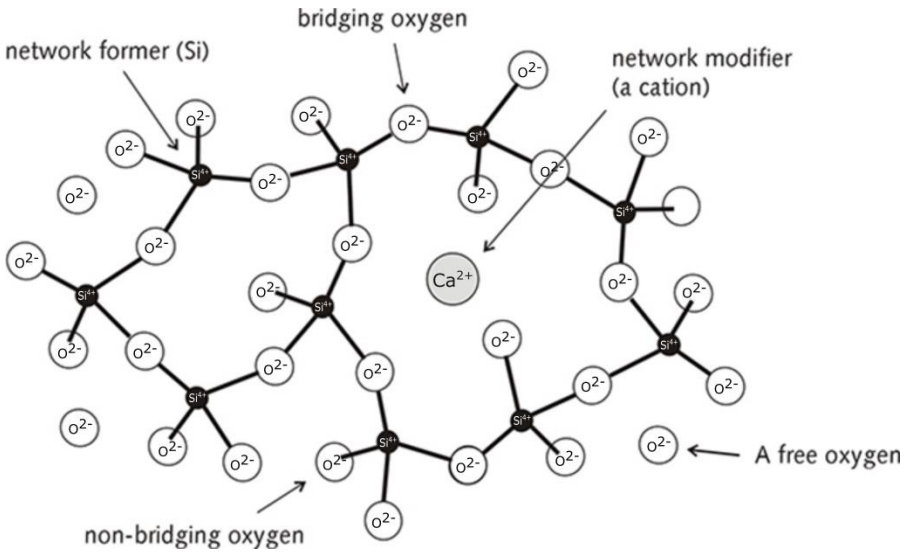

Figure 2.5.5 Silica glass with bridging non-bridging oxygens as a result of the addition of a glass modifier (Ca^{2+}) [229]

Non-silica glasses can dissolve in high or low pH solutions and, in certain cases, may even dissolve in water. Aluminium-silica glasses undergo dissolution in acidic solutions as the acid attacks the Al-O bonds. The Si/Al ratio must be high in order for the glass to be degradable by acid. A Si/Al mole ratio between 3:1 and 2:1 has been shown in glass with cement-forming ability to produce a cement that has a reasonable setting time. A mole ratio above 3:1 does not set and below a mole ratio of 2:1 will give a setting time below 10 minutes. As gallium and aluminium glasses are often structurally similar, it can be assumed that gallium-silica glasses will undergo the same dissolution [221] [228]. Calcium or sodium ions not only play an important role in charge balancing NBOs but are important in increasing the network connectivity in glass with trivalent ions, such as aluminium-silica glasses. A silica glass network with aluminium ions requires calcium or sodium to charge balance the network and results in a tetrahedral coordination. Excess calcium or sodium will interrupt the network, causing NBOs to occur [228] [230]. This indicates the importance not only in the Si/Al ratio but the Al/Ca ratio of the glass composition.

Some oxides such as aluminium oxide (Al_2O_3) and gallium oxide (Ga_2O_3) cannot form a glass unless mixed with another glass former. This occurs due to the gallium or alumina substituting for part of the silica (former) in the glass network. These oxides also can act as modifiers in the network and, therefore, is called an intermediate [221] [224] [231].

The random network model of Zachariasen suggests that glass is a random assembly of oxygen polyhedral. A central glass cation is surrounded by oxygen atoms to form this polyhedral. The random network theory is three-dimensional and composed of Q_3 and Q_4 units only. However, it is also possible to produce glasses with a predominantly Q_1 and Q_2 structure [221] [228].

2.5.4.1. Bioactive Glass

A bioactive material is described as a material that is designed to elicit, modulate or induce a specific biological activity. A bioactive glass is an amorphous inorganic solid that displays bioactive characteristics. The glass is not adhesive but can form a chemical bond with hard and soft tissues in appropriate *in vivo* and *in vitro* conditions [138].

Bioactive glasses, such as Bioglass™ (45S5), are designed to cause biological activity. However, the level of the bioactive response depends on the quantity of ions released from the glass and the types of ions being released [232] [233].

Bioactive glasses, like all glasses, have an amorphous structure but typical network connectivity of 2 or 3 to allow ions to be released from the glass [224] [234]. Silicon dioxide (SiO_2) and phosphorous pentoxide (P_2O_5) are generally used as the network formers in bioactive glasses. Examples of commonly used network modifiers are Na^+, K^+, Ca^{2+} and Mg^{2+} [77] [224]. Due to the reduced network connectivity the glass can be dissolved in water or acid, which allows ions to be continuously released over time. The ions released from the glass can affect cell proliferation and mineralisation [224] [235]. Ions typically released from bioactive glasses, such as calcium and strontium have been shown to stimulate osteoblast differentiation and proliferation. Silver and gallium are used for their antibacterial properties [224] [236]. Bioactive glasses have been shown to improve vascularization, by upregulating growth factors such as vascular endothelial growth factor (VEGF) and basic fibroblast growth factor (bFGF) and causing endothelial cells and fibroblasts to proliferate. It is thought that the silica ions released from the glass are the main contributing factor to this [10] [11] [224] [237]–[243].

Research into bioactive glass was started in 1969 by Larry Hench. This research found that a silicate-based material that had an amorphous structure could form a strong bond with bone. This was due to the formation of an apatite layer, a component in hard tissues, caused by the release of calcium and phosphate ions. This glass can then be resorbed during bone formation. Due to the calcium and phosphate of the glass being similar to those found in hydroxyapatite of bone, the glass does not disturb the surrounding tissue [220] [224] [244]. Larry Hench's bioactive glass composition, Bioglass® 45S5, is still used in the commercially available products PerioGlas® and NovaBone® [222]. Bioglass® 45S5 has a network connectivity of 2.11, which allows it to be dissolved in body fluids [224]. Extensive research has been carried out examining the use of bioactive glass for hard tissue applications such as bone repair and dentistry [244].

It has been shown that soft tissues can bind to the surface of bioactive glasses [12] [243] [245]. The binding mechanics of soft tissue to glass are currently unknown [244]. Though

binding of hard tissue to bioactive glass is encouraged by the formation of a hydroxyapatite layer on the surface of the glass, the binding of soft tissue to bioactive glass is thought to be encouraged by the ions released from the bioactive glass influencing the cellular process [238].

Bioactive glasses can be sintered into porous scaffolds, processed into glass fibres and used as a bioactive coating on implants [224] [228] [232]. Bioactive glasses have been used to strengthen and improve the bioactivity of hydrogels and scaffolds. Such hydrogels include, PEG hydrogels fillers for bone tissue repair and alginate hydrogels scaffolds for bone tissue and periodontium regeneration [239] [246]–[249]. Varying the glass content can be used to vary the strength and gelation rate in acid based cements [228].

2.5.5. Glucono Delta-Lactone

Glucono Delta-Lactone (GDL) is a water soluble crystalline powder that acts as an acidifier. GDL is formed by removing water from gluconic acid and when hydrolysed, GDL forms gluconic acid. Hydrolysis of GDL is a slow reaction that continues until there is a balance between gluconic acid and its delta-lactone ester [250].

GDL has been used to form acid gels and ionically cross-linked alginate hydrogels. For ionically cross-linked alginates, smaller amounts of GDL can be used to cause the slow and homogenous gelation of alginate hydrogels, as the slow decrease in pH causes a slow release of multivalent ions such as calcium from calcium ceramic sources, such as hydroxyapatite, calcium carbonate and calcium sulphate [199] [251] [252]. GDL can also be used to control the rate of gelation, as an increased GDL content causes a faster decrease in pH and greater release rate of multivalent ions [252].

2.6. Novel Hydrogel

The novel hydrogel optimised in this thesis is composed of alginate, a novel bioactive glass and glucono delta-lactone.

As discussed, alginate has the ability to form a gel when in contact with multivalent ions. The novel glass used in this hydrogel is a gallium-calcium-silicate glass [253]. The role of the glass in this hydrogel is to deliver a steady release of these multivalent ions, controlling the rate of gelation and the strength of the hydrogel, see Figure 2.6.1. The bioactive glass contains calcium and gallium which can both cross-link alginate. Calcium's cross-link mechanisms are discussed in 2.5.2 and gallium is shown in Figure 9.3.1. The more stable the glass the slower the rate of gelation. A glass that contains more ions will form a more highly crosslinked hydrogel.

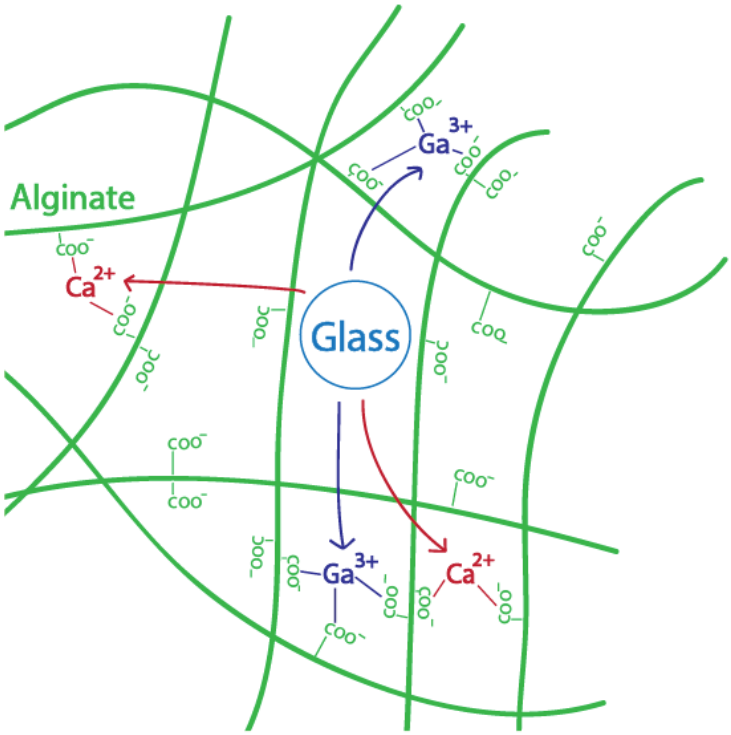

Figure 2.6.1 Gelation of the alginate using multivalent ions released from the bioactive glass

The role of GDL in the novel hydrogel is to acidify the solution. This in turn releases multivalent ions, contained in the glass, allowing them to cross-link with the alginate. The gelation rate of the hydrogel can be tightly controlled by both the composition of the glass phase and the ratio of constituent components of the gel. An increased amount of GDL results in increased acidity, causing a more rapid glass ion release and a more rapid gelation.

2.7. Rationale of work

The aim of this work is to design a hydrogel that fits the criteria of Table 2.4.1. In order to fit these criteria, the hydrogel's composition must be fully analysed and optimised. This analysis and optimisation will be carried out in the following manner:

1. Ideally, this hydrogel will have a strength similar to the surrounding vasculature but at a minimum its compressive strength must exceed hypertensive blood pressure of 22kPa. The hydrogel should not shrink or degrade over time to ensure that the aneurysm does not recur and to provide a stable structure to allow cells to migrate across. The hydrogel will be injectable through a microcatheter (2.1F distal inner diameter and a length of 1.5m) to ensure the aneurysm treatment can remain minimally invasive. As discussed, an alginate hydrogel's strength, size conservation and viscosity/injectability can be affected by its chemical composition and molecular weight. The concentration of the alginate used in a hydrogel will also greatly affect these properties. To examine the effect of these factors on the hydrogel, two alginates of different molecular weights and chemical composition will be examined at four concentrations. In order to determine the optimum alginate type and concentration; the hydrogels compressive strength, sample size conservation, working time, hardening time and injectability will be assessed. GPC and NMR will be used to determine each alginate's molecular weight and chemical composition. The viscosity of each alginate will also be examined at the four concentrations.

2. One of the alginates will be gamma irradiated, to examine the effect that this change in the molecular weight from radiation has on the hydrogel properties.

3. When the optimum alginate is determined, the glass and GDL content can be modified to further optimise the material. Changes to the content of these elements will likely affect the strength, sample size conservation, injectability and working and hardening time of the hydrogel due to changes in the hydrogel's cross-linking density. Each of these characteristics will be fully assessed. Increasing the glass content may also improve the radiopacity of the hydrogel and this will also be examined.

4. Current aneurysm treatments do not adhere to the aneurysm wall without adhering to the micro-catheter or balloon. This can cause many issues and restraints on the treatment procedure. However, a treatment that adheres to the aneurysm will likely reduce the chance of aneurysm recurrence and revascularisation caused by blood ingress between the aneurysm wall and the hydrogel. The addition of EDC and NHS has been used to improve the adhesive strength of alginate hydrogels. However, it is

uncertain how it will affect the overall properties of the hydrogel. To examine this, EDC and NHS will be added at increasing concentrations to the hydrogel composition and the effect it has on the hydrogel's bond strength will be examined. Subsequently, the effects of EDC and NHS on the hydrogel's strength, sample size conservation, working and hardening time and injectability will be examined.

5. The hydrogel and its eluent should not have a cytotoxic effect on the surrounding vasculature. Components from the hydrogel, such as ions released from bioactive glass, can have both positive and negative influences on the surrounding tissue. To examine this, bovine aortic endothelial cells will be dosed with the hydrogel's eluent at increasing concentrations and its effect evaluated by examining metabolic activity and cell number.

6. As this is an implanted device, each component of the hydrogel must be sterile. The optimum sterilisation technique for each component of the hydrogel will need to be determined. The effect that sterilisation has on each individual component of the hydrogel and the hydrogel as a whole will be determined by examining the strength, sample size conservation, bond strength, working and hardening time and injectability of the hydrogel. GPC and DTA will be used to evaluate the effects of sterilisation on the components structure. Sterilisation typically has negative effects on alginate and bioactive glass. If necessary, the hydrogels composition will be modified to accommodate for the effects of sterilisation.

7. Bioactive glass and calcium alginate hydrogels are typically used to promote formation of bone. In cerebral vasculature, a material that causes calcification of tissue will have a negative effect, including a prolonged immune response or stroke. Testing will be carried out to determine if the material calcifies under *in vivo* conditions. This will be determined using von Kossa staining, XRD and FTIR.

8. Once sterilised, direct contact testing can be carried out without the problems of contamination. Bovine aortic endothelial cells will be placed in direct contact with the hydrogel. This will be done to assess cell attachment and spreading which will give an indication of whether endothelialisation of the hydrogel will occur *in vivo.*

9. The radiopacity of the hydrogel will need to be evaluated and, if required, improved for endovascular treatment. Tantalum can be added to the hydrogel to increase its radiopacity in two ways; the addition of tantalum powder to the hydrogel

composition or the addition of tantalum oxide to the bioactive glass. Both of these methods will be examined and the effect they have on the radiopacity, mechanical properties and setting times of the hydrogel will be determined.

10. Platelet adhesion will be examined to determine if the material is thrombogenic. This will be carried out by placing whole human blood in contact with the hydrogel for 1 hour. The samples will be stained to determine if platelets adhere and become activated in the presence of the material.

11. *In vivo* testing will be conducted to evaluate the injectability and the effectiveness of this material for treating cerebral aneurysms. This will be carried out by embolizing 8 rabbit's vessels using the hydrogel or a control (coils). The general health of the rabbits will be examined by monitoring their blood and weight. After 30 days, the rabbits will be euthanized and histopathology will be used to examine the surround tissue.

12. Alginate hydrogels typically have a high viscosity. To reduce the force required to inject the material; a deliver device will be designed. Ideally, this will allow the material to be injected easily and at a controlled rate.

Chapter 3. Background Theory

3.1. Alginate Classification

3.1.1. Gel Permeation Chromatography

Gel permeation chromatography (GPC) is a form of size exclusion chromatography that is commonly used to determine the molecular weight of alginate. A GPC consists of a pump which pushes the solvent through the instrument, an injection port for adding the polymer samples to the columns, columns to hold the stationary phase and detectors for monitoring the polymer chains as they move through the columns. These columns are composed of porous particles to separate the molecules. First the polymer is dispersed in a mobile phase to cause the molecular chains to coil up on themselves to form sphere-like structures. The molecules are added to a mobile phase and pumped through the columns. The small molecular weight chains form small spheres, while the largest molecular weight chains form the largest spheres. The molecules are separated as the pores in the columns are of varying sizes. The largest molecules cannot pass through the pores and exit the column, while the small molecules move through the pores into the next column and the process is repeated. This means that the large molecular weight chains are eluted from the column first and plotted followed by the next molecular weight chains [254].

3.1.2. Nuclear Magnetic Resonance Spectroscopy

Nuclear magnetic resonance (NMR) spectroscopy is an analytical technique that can be used to determine the molecular structure of a sample. NMR involves applying an external magnetic field to a nuclei. As nuclei are electrically charged, there can be a transfer of energy. The transfer of energy takes place at a wavelength, which is related to a frequency. The frequency that this energy transfer takes place at can be effected by electron shielding (chemical shift) and the orientation of the neighbouring nuclei (spin-spin coupling). There are several types of NMR analysis, but the two most common are proton NMR (^{1}H-NMR) and carbon NMR (^{13}C-NMR). A NMR spectrum is produced, which can be used to determine a sample's molecular structure [255] [256].

^{1}H-NMR spectra can be used to determine the chemical composition of alginate.

Equations, stated in ASTM standard F2259-10 are used to integrate the intensities of the signals produced by alginate; A, B1, B2, B3, B4 and C, shown in Figure 3.1.1 [257]. These equations are used to find the diad and triad sequences discussed in 2.5.2.

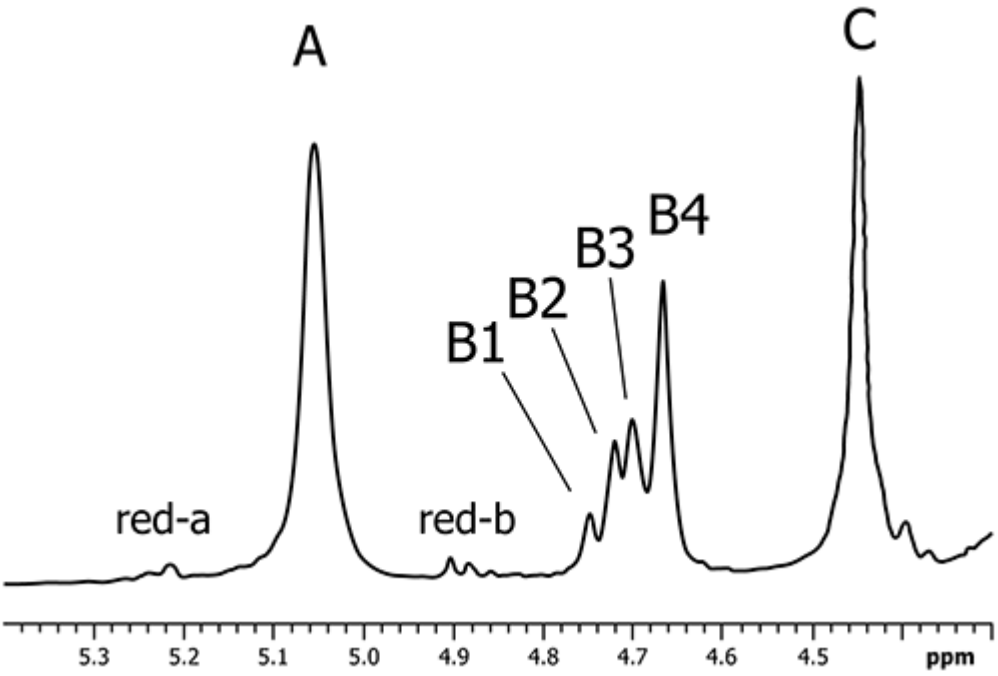

Figure 3.1.1 Example of the 1H NMR Spectrum of Alginate Used for Quantitative Analysis [257]

Examples of these equations are Equation 3.1.1 and Equation 3.1.2 which are used to calculate F_G and F_M respectively.

Equation 3.1.1 Equation for calculating F_G [257]

$$F_G = \frac{G}{M+G}$$

Equation 3.1.2 Equation for calculating F_M [257]

$$F_M = \frac{M}{M+G}$$

Where
G = 0.5(A+C+0.5(B1+B2+B3))
M = B4+0.5(B1+B2+B3)

3.2. Glass Characterisation

3.2.1. Differential Thermal Analysis

Differential thermal analysis (DTA) can be used for determining the glass transition temperature (T_g), crystallisation onset temperature (T_o), crystallisation peak temperature (T_p) and liquidis temperature (T_l), as shown in Figure 3.2.1. T_g is the temperature the glass melt transforms into a non-crystalline structure upon rapid cooling. T_o and T_p are the temperature associated with crystallisation of the glass upon heating. These temperatures are important if the glass is going to be processed at high temperatures following formation. The T_l is the melting point of the glass. A DTA measures the temperature difference (ΔT)

between the sample of glass (T_s) and a thermally inert reference sample (T_r). A DTA curve is produced where the temperature difference is plotted against voltage [238] [258] [259].

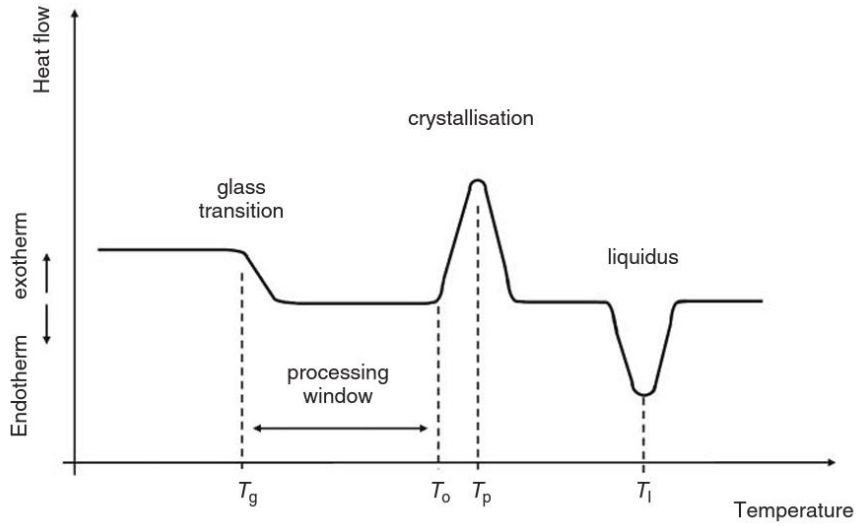

Figure 3.2.1 Schematic of a DTA curve indicating glass transition (T_g), crystallisation onset (T_o), crystallisation peak (T_p) and liquidis (T_l) temperature [259]

3.2.2. X-ray Diffraction

X-ray Diffraction (XRD) of glass powder can be used to determine whether a glass is crystalline or amorphous. X-ray beams are known to diffract when they pass through a crystal and this knowledge is used in XRD to compare crystalline and amorphous materials. An XRD typically consist of an X-ray source, a sample stage, an X-ray detector and slits to focus the X-ray beam. During XRD, X-rays are produced in a cathode ray tube and directed towards the sample which is on a sample stage. A diffraction pattern is produced when the conditions of Bragg's Law is satisfied ($n\lambda = 2d\sin\theta$). The XRD scans the samples through a range of 2θ angles to ensure all possible diffraction directions are accounted for. This diffraction pattern is then detected, counted and plotted in terms of intensity versus degrees-2θ [260].

Amorphous materials such as glass, will show a broad amorphous hump/peak but no sharp peaks such as those observed in crystalline structures, as shown in Figure 3.2.2 [261]. However, XRD can produce inaccurate results due to limitations on detectable crystalline structure size [262].

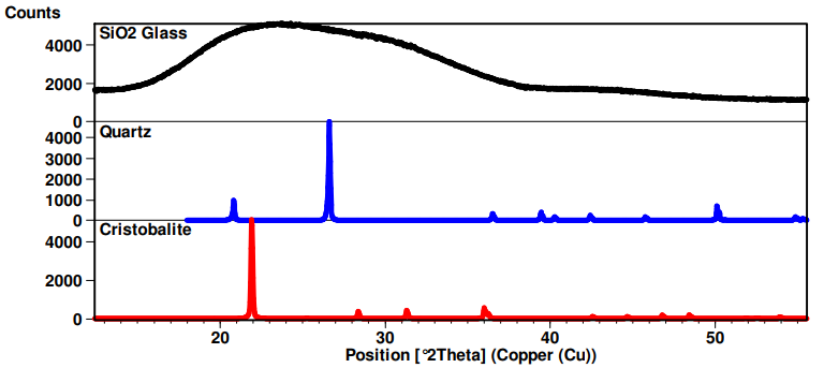

Figure 3.2.2 XRD pattern of amorphous (SiO2 glass) and crystalline (Quartz and Cristobalite) material [261]

3.2.3. Particle Size Analysis

Particle size analysers use laser diffraction to measure the size of the particles. A laser passes through a fluid containing the particles and the particles cause the laser to diffract. Large particles passing the laser cause the light to diffract at small angles relative to the beam and small particles cause the light to scatter at large angles, see Figure 3.2.3. Mie theory of light scattering is used to calculate the size of the particles. The particle size is calculated assuming the particle is a sphere, with the particle size being reported at a volume equivalent sphere diameter. Therefore, errors in measurements can occur when examining non-spherical particles [263].

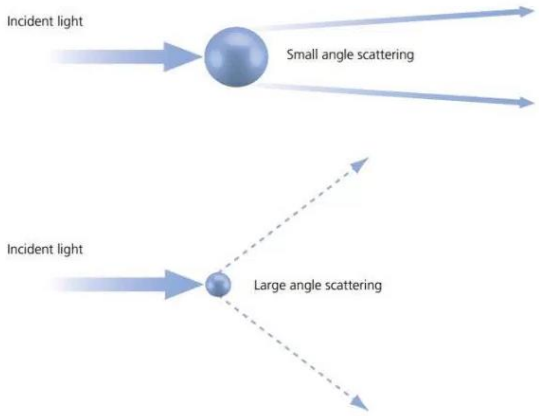

Figure 3.2.3 Scattering of light with large and small particles [264]

3.2.4. X-ray Photoelectron Spectroscopy

X-ray photons colliding with a sample cause photoelectrons to be released. This displaced photoelectron is filled by an electron from a higher level which causes either X-ray fluorescence or the de-excitation processes. X-ray photoelectron spectroscopy (XPS) is used to determine the electron binding energy using the kinetic energy of the displaced photoelectron. The electron binding energy can be found using information about the element and atomic level that the photoelectron was emitted from [265]. The electron binding energy relates to the oxidation state or charge of the atom. The binding energies are

shown as chemical shifts when graphed. The surface network connectivity of glass can be determined using XPS [266].

3.2.5. Scanning Electron Microscopy

Scanning Electron Microscopy (SEM) can be used to examine the physical shape and surface texture of fine particles, such as glass. A fine probe is used to focus electrons at the surface of the sample. These electron energies can reach tens of thousands of eV. The electron interaction between the beam and the sample can cause two types of interactions; elastic interactions and inelastic interactions. Elastic interactions are a result of the deflection of the incident electron by electrons from the outer shell of similar energy of the sample. Elastic scattered electrons are backscattered through an angle of $\geq 90^0$. The interactions have a negligible energy loss and are useful for imaging and compositional information. Inelastic interactions are caused by significant energy lost. The amount of energy lost varies with the binding energy of the sample and the whether the electrons are excited. Inelastic interactions are used to see surface texture and roughness. The probe scans across the sample in a raster or a pattern of parallel lines to produce a signal from the electrons. The signal from each position of the electron probe is amplified. The ratio between the dimensions of the image and the area scanned on the sample is used to determine the magnification [267] [268].

3.2.6. Fourier-Transform Infrared Spectroscopy

The molecular structure of a sample can be found using Fourier-Transform Infrared spectroscopy (FTIR). When infrared radiation is passed through a sample some is absorbed while the rest is transmitted. The absorption levels relate to the frequency of vibrations between atomic bonds. The absorption and transmittance levels can be used to produce a spectrum that determines the molecular structure, as no two molecules have the same spectrum. An Attenuated Total Reflection (ATR) accessory allows the surface of the sample to be examined [269].

3.2.7. Zeta Potential

The zeta potential of a glass is the difference in electrical potential between the dispersion medium and the stationary layer of fluid attached to the glass particle. Zeta potential relates to the repulsion between adjacent particles where a glass with a higher zeta potential (positive or negative) will have a reduced amount of agglomerations [225]. The zeta potential of molecules is measured by applying an electrical field to a solution containing molecules. This electric field causes the molecules to move and the velocity of this is measured using light scattering measurements. The zeta potential of these molecules can be determined from their velocity [270].

3.2.8. Nitrogen Adsorption/Desorption

Nitrogen adsorption/desorption is used to characterise particle surface area and the pore volume of porous materials such as glass. The two most commonly used methods using nitrogen absorption are the Brunauer-Emmett-Teller (BET) method and the Barrett-Joyner-Halenda (BJH) method [271].

The BET method is the standard method used to determine particle surface area [271]. BET can only be used to determine the surface area of disperse, nonporous, macroporous or mesoporous solids. Solids which may absorb the gas cannot be examined reliably. The BET equation calculates the amount of adsorptive gas required to complete a monolayer on the external and internal pore surface of a solid. The gas used must be able to be physically absorbed by weak bonds at the solid's surface and can be desorbed with an increase in pressure [272]. Multilayer nitrogen adsorption can occur at liquid nitrogen temperature [271]. The sample is cooled under a vacuum to cryogenic temperature and dosed with an adsorptive gas. After dosing, the pressure is brought to equilibrium and the quantity of gas adsorbed is calculated. This is repeated and the sample is dosed in increments, see Figure 3.2.4. The quantity of gas absorbed at each pressure gives an adsorption isotherm that can be used to find the quantity of gas required to form a monolayer [273]. The amount of gas absorbed (v) is plotted against the relative pressure (p/p_0) to give the adsorption isotherm. The BET equation (Equation 3.2.1) is used to determine the volume absorbed in a monolayer (v_m) [272].

Equation 3.2.1 Brunauer-Emmett-Teller method equation used to determine particle surface area[274]

$$\frac{p}{v(p_0 - p)} = \frac{1}{v_m c} + \frac{c - 1}{v_m c}\frac{p}{p_0}$$

Where,
p = equilibrium pressure of the gas
p_0 = saturation pressure of the gas
p/p_0 = relative pressure
v = volume of gas absorbed at standard pressure
v_m = volume of gas absorbed in one unimolecular layer
c = BET parameter

When the results of the BET equation are plotted against the relative pressure, a straight line should be given between a relative pressure of 0.05 and 0.3. Using the slope of the line and the intercept, both the monolayer amount (v_m) and BET parameter (c) can be calculated. The specific surface area (a_s) is the calculated using Equation 3.2.2 [272].

Equation 3.2.2 Specific surface area of a solid using the Brunauer-Emmett-Teller method[272][275]

$$a_s = v_m a_m N_a$$

Where,
v_m = volume of gas absorbed in one unimolecular layer
a_m = molecular cross-sectional area
N_a = Avogadro's number

BET method is generally recognised as being over-simplified. BET assumes that the adsorption of one site is independent of neighbouring sites and that lateral interactions between absorbed molecules do not exist. Therefore, they first acts as a site for the molecules of the second layer and so on. All layers above the first layer are assumed to behave like liquids. The absorption system and operational temperature affects the location and extent of the linear region [271]

The Barrett-Joyner-Halenda method (BJH) is used to determine the pore volume and area in porous solids, this is done by examining the desorption of gases from porous samples. By extending the BET process, the gas can be allowed to condense in the pores of the sample (see Figure 3.2.4). An increase in pressure can cause gas to condense, causing the pores to fill with liquid. The pressure is then reduced in increments which cause the condensed gas to evaporate. The pore volume, size and area can be calculated using by observing the adsorption and desorption of the gas [273]. Equation 3.2.3 is used to calculate the pore volume [276].

Equation 3.2.3 Barrett-Joyner-Halenda method equation to determine the pore volume and area in porous solids [276]

$$V_{p_n} = R_n \Delta V_n - R_n c \Delta t \sum_{j=1}^{n-1} A_{pj}$$

Where,
V_{pn} = Pore volume
$R_n = r^2_{pn}/(r_{kn} + \Delta t_n)^2$
ΔV_n = observed volume of gas desorbed
c = constant
Δt = change in thickness of the physically adsorbed layer
A_{pj} = pore area from where the adsorbed gas is desorbed

The BJH method assumes that all pores are cylindrical [276].

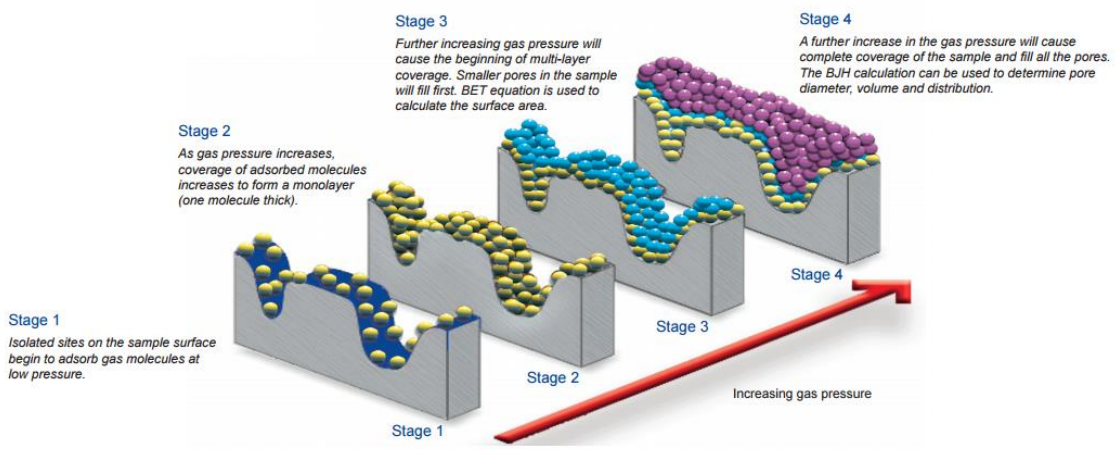

Figure 3.2.4 Formation of monolayer for determining a particle surface area and pore volume using the Brunauer-Emmett-Teller method and Barrett-Joyner-Halenda method [273]

3.3. Examination of the Hydrogel

3.3.1. Storage Media

3.3.1.1. Deionised Water

Water contains impurities in the form of negatively and positively charged ions. Ions with a positive charge are called cations and with a negative charger are called anions. Water can be deionised using ion exchange resins [277].

3.3.1.2. Simulated Body Fluid

Simulated body fluid (SBF) is an acellular liquid with a similar pH and ion concentration of those found in human blood plasma. SBF is commonly used to examine the effects that ions in blood have on biomaterials *in vitro*, such as surface apatite formation [278].

Kokubo's c-SBF is commonly used in the examination of ion exchange and apatite formation on alginate hydrogels [279] [280]. Table 3.3.1 shows the ion concentration of human blood plasma and SBF described by Kokubo et al. There are difference in the ion concentration of chloride (Cl^-) and bicarbonate (HCO^{3-}) of c-SBF compared to blood plasma. Two SBFs (r-SBF and n-SBF) have been prepared with improved ion concentrations; however, r-SBF has been shown to easily precipitate and n-SBF has shown to produce the same results in apatite formation as c-SBF. Both c-SBF and n-SBF are stable for up to 4 weeks when refrigerated [281] [282].

Table 3.3.1 Typical ion concentration of blood plasma and Simulated Body Fluid (c-SBF, r-SBF and n-SBF)

	Ion Concentration (mM)			
	Blood plasma	**c-SBF**	**r-SBF**	**n-SBF**
Sodium (Na^+)	142.0	142.0	142.0	142.0
Potassium (K^+)	5.0	5.0	5.0	5.0
Magnesium (Mg^{2+})	1.5	1.5	1.5	1.5
Calcium (Ca^{2+})	2.5	2.5	2.5	2.5
Chloride (Cl^-)	103.0	147.8	103.0	103.0
Bicarbonate (HCO^{3-})	27.0	4.2	27.0	4.2
Hydrogen phosphate (HPO^-)	1.0	1.0	1.0	1.0
Sulphate (SO^-)	0.5	0.5	0.5	0.5
pH	7.2-7.4	7.4	7.4	7.4

3.3.1.3. Phosphate Buffered Saline

Phosphate buffered saline (PBS) is a water-based buffer salt solution. The ion concentrations of potassium and sodium are similar to that of human blood plasma, see Table 3.3.2 [283].

Table 3.3.2 Typical ion concentration of blood plasma and Phosphate Buffered Saline

	Ion Concentration (mM)	
	Blood plasma	**PBS**
Phosphate (PO^-)	1	10
Sodium (Na^{2+})	142.0	137.0
Potassium (K^+)	5.0	2.7
pH	7.2-7.4	7.4

3.3.2. Homogeneity and Radiopacity

X-ray Microtomography (XMT) is a non-destructive method of visualising the internal structure of X-ray opaque materials. An XMT passes X-rays through the material being examined and these X-rays are attenuated according to the density and atomic number of the material. The XMT produces cross-sectional images from varying angles that are used to reconstruct a 3D image of the sample. XMT can also be used in 2D for determining the radiopacity of materials when compared to standard materials [284].

3.3.3. Compression and Tensile Testing

The mechanical properties of a hydrogel can be determined, among other techniques, by compression and tensile testing the hydrogel.

The stress-strain graph produced when a sample is compressed or tensile tested can be used to find the ultimate strength of the material, which is the maximum stress reached followed by failure. The yield strength and modulus of elasticity can also be found. The yield strength shows the maximum stress that can be applied to the hydrogel without permanent deformation of the hydrogel. Modulus of elasticity, also called Young's modulus is the ratio of stress to strain for the linear range, see Figure 3.3.1 [285].

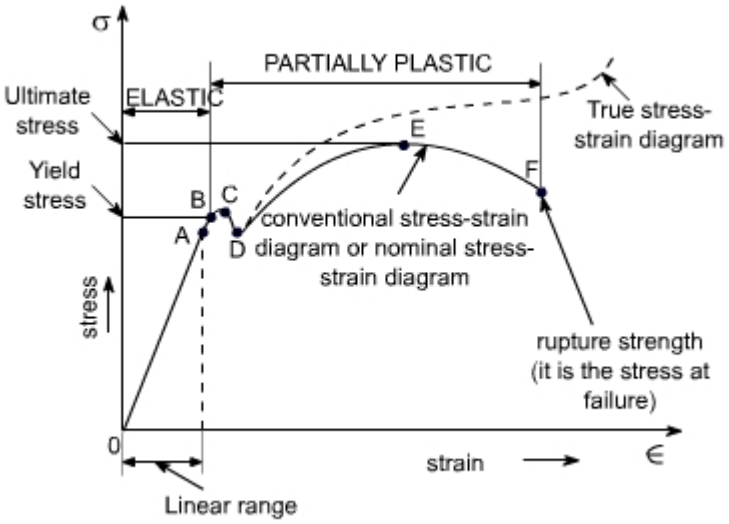

Figure 3.3.1 Stress-Strain graph [286]

Mathematically, normal stress can be found using Equation 3.3.1, normal strain can be found using Equation 3.3.2 and Young's modulus can be found using Equation 3.3.3 for a linear elastic material.

Equation 3.3.1 Normal stress equation

$$\sigma = \frac{F}{A_O}$$

Where,
σ = Normal stress
F = Applied load
A_0 = Original cross-sectional area

Equation 3.3.2 Normal strain equation

$$\varepsilon = \frac{\Delta L}{L_O}$$

Where,
ε = Normal strain
ΔL = Change in length
L_0 = Original length

Equation 3.3.3 Young's modulus equation

$$E = \frac{\sigma}{\varepsilon}$$

Where,
E = Young's modulus
σ = Normal stress
ε = Normal strain

Normal stress and strain does not take into account the changes of materials length or cross sectional area during testing. This can result in errors when there are large changes to the length and cross sectional area during testing. These errors can be reduced by calculating the materials true stress ($\bar{\sigma}$) and strain ($\bar{\varepsilon}$), where the instantaneous length and cross sectional area are determined throughout testing, rather than the original used for normal stress and strain [287]. Determining the true stress and strain of a material can be difficult as the length and cross sectional area needs to be continuously monitored throughout testing [288].

As discussed previously, biological tissue does not produce a typically linear stress-strain response. To overcome this, a secant modulus of elasticity or an incremental modulus of elasticity can be determined. The secant modulus of elasticity considers the stress at a certain strain to be proportional to the strain at that level. An incremental modulus of elasticity considers increments of stress are proportional to increments of strain [289].

Other aspects of experimental set up, such as strain rate and sample hydration and temperature can affect the results obtained when examining the compressive and tensile strength of a material, particularly viscoelastic materials such as polymers [287].

3.3.4. Rheology/Working and Hardening Time

Determining the working time of a material is important as the polymer must be shaped or injected before this time. The working time is defined here as the time measured from the start of mixing, during which it is possible to manipulate the hydrogel without causing damage. The setting time is defined here as the time it takes the hydrogel to set, such that it can hold a 17kPa load [290] [291]. The hardening time is defined as the time difference between the working and setting time.

Rheology is often used to determine the gel point of a cross-linked polymer such as alginate. The gel point is when the alginate is cross-linked and moves from a liquid to a solid. There are two different methods used to determine the gel point; the storage and loss modulus cross method and the Winter-Chambon criterion [290] [292].

The storage and loss modulus cross method considers the gel point as being the time, when graphed, that the complex storage/elastic (G') and loss/viscous (G") modulus cross. However, there is an issue with determining the gel point from this method as it is frequency dependent. Weak gels are highly frequency dependent and the G' increases with an increase in frequency. Strong, highly cross-linked gels show little frequency dependency [292] [293].

The Winter-Chambon criterion is frequency independent. The loss tangent of the hydrogel is found at varying frequencies using Equation 3.3.4 [292] [294] [295].

Equation 3.3.4 Winter and Chambon loss tangent [296]

$$tan\delta = \frac{G"}{G'} = \tan(\frac{n\pi}{2})$$

Where
n = the relaxation exponent.

The relaxation exponent (n) must be a value between 0 and 1 as a completely viscous liquid would have a value of 1 and a completely elastic solid would have an n value of 0. A decrease in n value indicates an increase in the viscoelastic behaviour of the material [296].

The varying loss tangents, as a function of frequency, are graphed against time and the gel point is considered the time when there is a single intercept, see Figure 3.3.2 for graphed example [292] [294] [295].

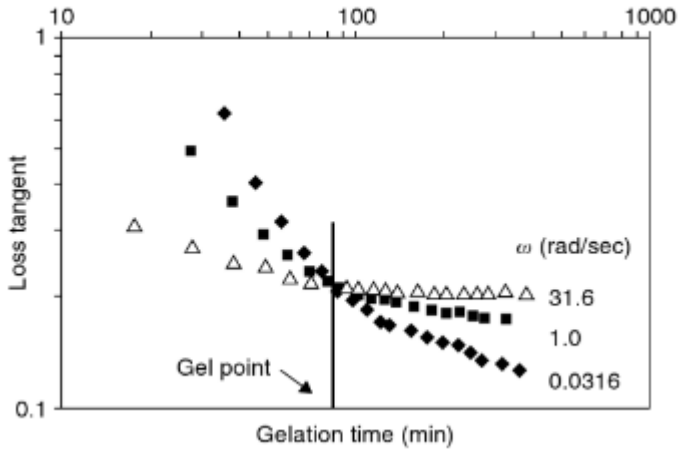

Figure 3.3.2 Example of gel point found using Winter-Chambon criterion [292]

3.3.5. Bond Strength

Three ASTM standards are in place for determining the bonding or adhesive strength of a tissue adhesive. These standards are

- ASTM F2255 – 03 Standard Test Method for Strength Properties of Tissue Adhesives in Lap-Shear by Tension Loading.

This method involves a porcine skin graft being glued to two test fixtures. The tissue adhesive is then placed uniformly between the two test fixtures and allowed set for 1 hour at 37^0C in PBS. A load of 1-2N is placed on the bond area for this hour. The test fixtures are then placed into the testing machines grips and a load is applied with the long axis at a cross-head speed of 5mm/min [297].

- ASTM F2256 – 03 Standard Test Method for Strength Properties of Tissue Adhesives in T-Peel by Tension Loading.

  This method involves two sections of porcine skin graft to be cut to an equal size, 25mm x 150mm. The adhesive is placed uniformly on the pig skin to cover an area of 25mm x 125mm. The adhesive is allowed set with a weight of 5-10N applied to the bond area. After the required amount of time, the porcine skin graft is clamped to the testing machine using the 25mm of unbonded area (Figure 3.3.3). The specimen is tested at a cross-head speed of 250mm/min [298].

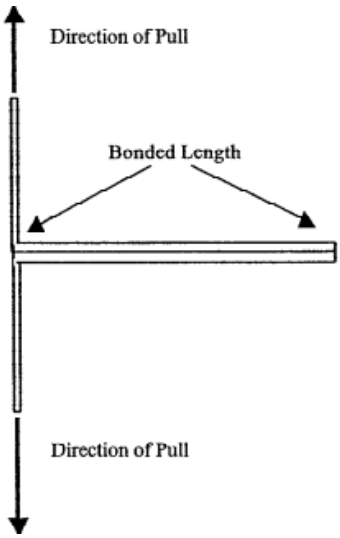

Figure 3.3.3 Schematic of a T-peel test [298]

- ASTM F2258 – 03 Standard Test Method for Strength Properties of Tissue Adhesives in Tension.

  For the method two square pieces of porcine skin graft (25mm x 25mm) at glued to the surface of two specimen holders. The adhesive is the placed between the specimen holders and allowed set for 1 hour. The specimen holder is then attached to the testing machine (Figure 3.3.4) and is tested at a cross-head speed of 2mm/min.

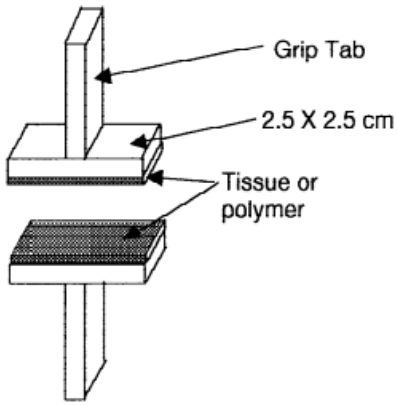

Figure 3.3.4 Schematic of the bond strength test using ASTM F2258-03[299]

3.4. Cell Culture

According to ISO 10993, the examination of cytotoxicity of the medical device can be carried out by conducting an elution test, direct contact testing or by an agar diffusion test. The elution test involves taking the eluent of the material and adding it at different concentrations to cell cultures. Direct contact testing involves placing the cells in direct contact with the test material. Agar diffusion testing involves placing agar between the cells and the test material, as agar will allow eluent to diffuse through to the cells. Cell death or growth is then examined. Generally, there is a correlation between these cell culture assays and what happens to the device *in vivo* [98]. For an item to be considered non-cytotoxic the percentage of cells remaining after testing must be above 70% compared to that of the control cells [99].

Two common methods of quantifying cell proliferation is using metabolic assays such as resazurin blue or by counting cells stained with a nucleic acid binding dye such as DAPI [300].

3.4.1. Staining cells

3.4.1.1. Resazurin Blue

Resazurin blue, also known as alamarBlue® is used to evaluate the metabolic function of cells to assess cellular health. Resazurin blue is non-toxic, water-soluble and permeates through cell membranes. Resazurin blue is a non-fluorescent dye that is reduced to a pink highly fluorescent resazurin with a transfer of electrons. Mitochondrial and cytoplasm enzymes such as reductases and dehydrogenanase are thought to be responsible for this exchange of electrons [301]. There are limitations to using this type of assay as metabolic activity of cells naturally varies greatly throughout its lifecycle [300]. However, quiescing the cells prior to examining the metabolic activity can reduce this variance.

3.4.1.2. DAPI

4′,6-diamidino-2-phenylindole (DAPI) is a fluorescent stain used to label DNA to allow the nucleus of cells to visualized using a fluorescent microscope [302]. This can be used to image cells and complete a cell count.

3.4.1.3. Phalloidin

Phalloidin is used to label the F-actin of the cytoskeleton to examine cell attachment and level of spreading (an indicator of cellular health) [303].

3.5. Platelet Activation

According to ISO 10993-4, all materials that will be in contact with blood must be haemocompatibility tested [304]. For an implant to be considered completely biocompatible, platelets would not adhere to the surface of the material, as platelet adhesion is the first step of the coagulation cascade [18]. Materials that cause platelet adhesion and result in thrombus formation are a major complication concerning vascular implants [141]. Although in some, cases such as coiled aneurysms and certain embolization materials, the formation of a clot is advantageous and it further supports the material and provides a more complete occlusion [88] [140]. Proteins are typically adsorbed on to the surface of a device after implantation, followed by the adhesion of platelets. A device's chemical composition, topography, surface charge and tension can affect the adsorption of proteins and platelet adhesion [18] [305]. Proteins such a fibrinogen and albumin are adsorbed within minutes from blood onto the surface of a material. Ideally, a material will adsorb more albumin as the protein is more haemocompatible and reduces platelet adhesion and activation [305]–[308].

Platelets are anucleated fragments of blood cells found in blood and are in a discoid shape in their resting non-activated state [309] [310]. The typical diameter of a platelet in its discoid shape is 2-3 μm [311]. Platelets do not adhere to the surface of an intact endothelium but adhere to the surface of injured endothelial cells, exposed ECM or when a foreign material is introduced and become activated [312]. Cells in their activated state are seen in 4 states; dendritic, spread dendritic, spread and fully spread, as shown in Figure 3.5.1 [310].

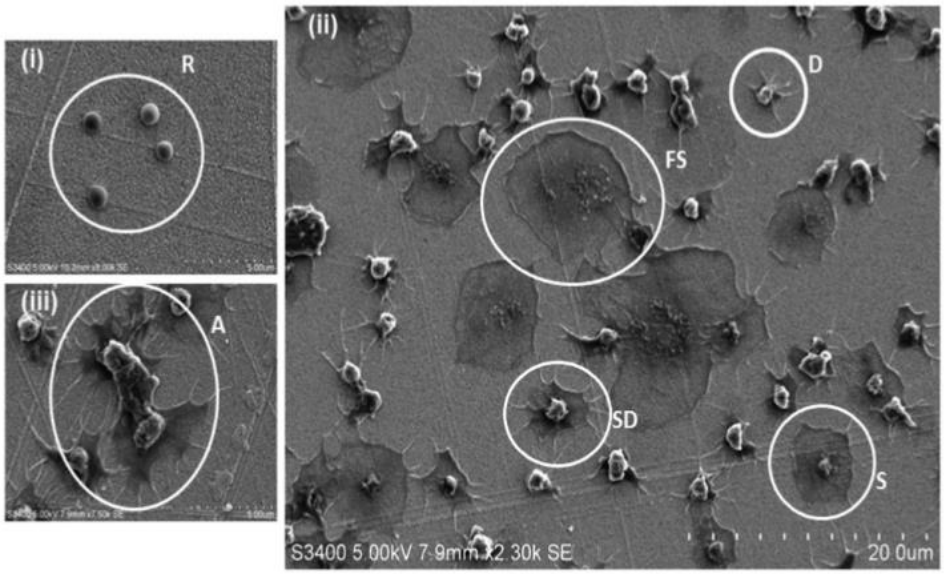

Figure 3.5.1 Platelets in their (i) resting/non-activated state, (ii) spreading (dendritic, spread dendritic, spread and fully spread) state and (iii) attached state [310]

3.5.1. Platelet Adhesion

In accordance with ISO 10093-4, a positive and negative control is required to examine platelet adherence [304]. This is due to blood being delicate and experimental set-up may cause activation prior to and during the experiment. Blood is typically collected in tubes that contain sodium citrate, as sodium citrate chelates the extracellular calcium and reduces the chances of the blood coagulating [313] [314]. Although this chelater still allows for the platelets to activate it typically is a at a reduced amount [141] [313]–[316]. A positive control will also be necessary for assuring the sodium citrate has not affected the results.

Although ISO 10993-4 indicates that both human and animal blood is acceptable for examination, blood composition is species specific and may result in an under or over estimation of platelet attachment [317].

3.5.2. Staining Cells

3.5.2.1. CD62P

P-selectin (CD62p) is a glycoprotein that is found in the α-granules of platelets. Once the platelet is activated, α-granules move to the periphery of the cells. PE-CD62P can stain the α-granules and therefore can be used to examine if the platelet is activated [318] [319].

3.5.2.2. Phalloidin

As platelets have no nucleus, DAPI cannot be used to count the number of cells adhered to the surface of the material. Phalloidin is typically used to stain the F-actin of the platelets to allow the number of adhered cells to be counted and the shape to be assessed [310] [319].

3.6. *In vivo* Analysis

3.6.1. Aneurysm formation

Animal selection for an *in vivo* study is important. There is a large variance across each species such as blood pressure, blood flow rate, metabolic rate and vessel size. Cost is commonly taken into consideration, with small animals such as mice, rats, rabbits and guinea pigs typically having reduced maintenance costs compared to dogs or pigs. Dogs, rats, pigs, rabbits and monkeys have all been used for examining the treatment of cerebral aneurysm with various devices. Larger animals such as pigs and dogs have vasculature dimensions similar to that of humans but results from these models show increased thrombus formation compared to humans. Rabbits have a similar coagulation system to humans and have been used in increasing amounts for the study of aneurysm treatments [320] [321].

Natural aneurysm formation in animals is extremely rare. For *in vivo* testing, the aneurysm will have to be induced. This can be done surgically or by an enzymatic method of inducing the aneurysm. Surgical models involve grafting a venous pouch using the external jugular vein. This is typically grafted at the common carotid artery at a lateral wall or a bifurcation. Enzymatic models involve placing enzymes in contact with the common carotid artery. Typically, elastase or papain is used. Elastase induced aneurysm occur due to the elastase causing injury to the artery and triggering an inflammatory response. This induced inflammation is thought to cause degradation of the elastin and collagen of the artery which results in the formation of an aneurysm. Papain is able to degrade elastic fibers and collagen without relying on an inflammatory response [320].

3.6.2. Histopathology

Histopathology is carried out to examine sections of tissue, such as those of animals involved in an *in vivo* study. These sections can be used to test for presence of changes or abnormalities such as inflammation, endothelial cell proliferation, and necrosis. For a histopathology study, a biopsy or section of tissue is fixed onto a glass slide. The samples are stained and examined under a microscope. Haematoxylin and Eosin (H&E) and the Verhoeff/van Geison stain are two commonly used stains to examine details of the tissue [322].

H&E stain is used to stain tissue structures. Haematoxylin contains aluminium salts and is a basic dye (positively charged) that reacts with basophilic (negatively charged) cells, such as nucleic acid. Eosin on the other hand is an acidic dye that stains acidophilic tissue components. Haematoxylin is a blue stain and Eosin stains pink [323].

Elastic fibres of histology samples are stained using the Verhoeff/van Geison stain. Samples are initially stained with a hematoxylin-ferric chloride-iodine solution which overstains the

sections. The samples are the differentiated and counterstained with a Van Gieson solution. The stain colour varies for the tissue being stained. Elastic fibers are a blue-black, collagen is red and muscle is orange. Van Geison stains the cytoplasm yellow [324].

Chapter 4. Materials and Methods

4.1. Alginate

The hydrogel was tested at four varying alginate concentrations; 0.5%, 2.5%, 4.5% and 6.0% (w/v). The alginate concentrations were determined using design of experiments. Two alginate purification techniques were used to produce two varying alginates. A sample of alginate produced by Technique 2 was sent for gamma irradiation.

4.1.1. Alginate Purification

All reagents used were purchased from Sigma-Aldrich (Wicklow, Ireland), unless stated otherwise. Two different alginate purification techniques were used to produce two different molecular weight hydrogel compositions.

Technique 1: 8g of alginic acid was dissolved in 400ml of deionised water (DI). The alginate pH was raised to 7.0 by adding the required amount of a 0.5M potassium hydroxide (KOH), 20mmol/l sodium chloride (NaCl) solution. The alginate was then precipitated by adding 200ml of methanol per 100ml of alginate. The alginate was filtered through a 500µm sieve after 10 minutes. The alginate was then freeze-dried.

Technique 2: 9g of alginic acid sodium salt from brown algae was dissolved in 900ml of 1mmol/l sodium Egtazic acid (EGTA). The solution was then filtered through 11µm and 2.5µm filter paper, respectively. The alginate was then precipitated on ice by reducing the pH to 1.5 by adding the required quantity of a 2M hydrochloric acid (HCl), 20mmol/l NaCl solution. The alginate was decanted through a 500µm stainless sieve and stirred 30 minutes in 200ml of a 0.01M HCl, 20mmol/l NaCl solution and decanted again. This stirring and decanting was repeated three times. To remove proteins the alginate was stirred for 30 minutes in 100ml of a 0.01M HCl, 20mmol/l NaCl solution with 20ml of chloroform and 5ml of buthanol, and collected in a 500µm stainless sieve. This washing and collecting was repeated three times. 350ml of DI was added and the pH was raised to 7.0 by adding the required quantity of a 0.5M KOH, 20mmol NaCl solution. The alginate was stirred in a solution of 20ml chloroform and 5ml of buthanol per 100ml of alginate and centrifuged at a rate of 5000rpm for 5 minutes. The alginate was then separated using a pipette from the chloroform/buthanol solution. This washing and centrifuging was repeated once. Finally, the alginate was precipitated by adding 200ml of ethanol per 100ml of alginate and filtered after 10 minutes. The alginate was then washed twice with 50ml of diethyl ether and freeze-dried [325].

After freeze drying the required amount of alginate was added to 12ml of DI to produce the required alginate concentration, for example a 4.5% alginate concentration was prepared by adding 540mg of freeze-dried alginate to 12ml of DI.

4.1.1.1. Gamma Irradiation

A sample of the freeze dried alginate from Technique 2 (see Section 4.1.1) was gamma irradiated by Synergy Healthcare (Westport, Ireland) at 25kGy over 114 minutes, to sterilise the alginate and to achieve a third molecular weight.

4.1.2. Design of Experiments

Design of experiments was carried out using Design Expert 9 (Stat-Ease, Minneapolis, USA).

4.1.3. Alginate Classification

4.1.3.1. Gel Permeation Chromatography

GPC was carried out using a liquid chromatography system (Agilent 1200, USA) equipped with a Suprema Linear GPC column (PSS, Germany). The mobile phase used consisted of 0.1M disodium hydrogen phosphate containing 0.5g/L of sodium nitrate buffered to pH 9.0. All samples were injected at a concentration of 1mg/mL and at a flow rate of 0.5mL/min. Pullulan polysaccharide standards were injected to construct a calibration curve.

Pullulan is a straight chain polysaccharide of maltotriose units. This is not an ideal standard as it can overestimate the molecular weight but this standard is typically used as a standard for alginate when using a refractive index detector. Other standards are stated in the literature; however, these use a UV detector. No alginate standards provide 100% accurate values of molecular weight but do provide a comparative standard to which other researchers can compare samples [326]–[329].

4.1.3.2. Nuclear Magnetic Resonance Spectroscopy

^{1}H-NMR of the alginate was tested using a modified version of the standard ASTM F2259–10. The alginate solution was prepared by mixing the alginate to 0.1% (w/v) in DI. 1M HCI was used to bring the alginate pH to 5.6 and the alginate solution was stored in a water bath at 100°C for 1 hour. 1M HCl was used to further adjust the pH of the alginate to 3.8. The solution was stored again in a water bath at 100°C for 30 minutes. The pH was then raised to 7.0 using 1M NaOH and the alginate was freeze dried. The alginate was then re-dissolved in 5ml of 99% D_2O and freeze dried overnight. 12mg of alginate was dissolved in 1 ml of D_2O and placed in a NMR tube. The NMR of the alginate was carried out using a Bruker Advance 400 (Massachusetts, USA) at 80°C. 64 scans were carried out using a 2s relaxation delay. The produced graph is then used to calculate the alginates diad and triad sequences as per ASTM F2259-10.

4.1.4. Viscosity

The viscosity of each alginate at varying concentrations was determined at 24^{0}C using a SV-10 tuning forks Vibro Viscometer (A&D Company, Japan) running a sine wave formation at a constant frequency of 30Hz and amplitude of less than 1mm. This viscometer measures up to 10,000mPa.s.

4.2. Glucono Delta Lactone

D-(+)-Gluconic δ-lactone (GDL) was purchased from Sigma-Aldrich (Wicklow, Ireland). The GDL particle size was reduced by grinding 30g at 500rpm for 5 minutes using 5mm zirconia balls in a planetary ball mill (Pulverisette 6 classic Mono planetary ball mill, Fritsch GmbH, Germany).

4.3. Glass

4.3.1. Glass Production

The gallium-silicate glass had a composition of $0.33SiO_2 \bullet 0.18Ga_2O_3 \bullet 0.23CaO \bullet 0.11P_2O_5 \bullet 0.15CaCl_2$ [253]. The glass frit was produced by melting the raw materials (see Table 4.3.1) in a platinum 10% rhodium crucible at 1480°C for 1 hour. The molten mixture was then shock quenched into water. A glass powder was then produced by grinding 30g of glass frit using 15mm diameter zirconia balls in a planetary ball mill (Pulverisette 6 classic Mono planetary ball mill, Fritsch GmbH, Germany) at 500rpm for 10 minutes. Particles over 500µm were removed by sieving the glass powder through a 500µm sieve. 7.5g of the <500µm particles were mixed with 22.5ml of DI and milled using 5mm zirconia balls in a planetary ball mill at 500rpm for 10 minutes. The glass mixture was dried in the oven at 130^{0}C

Table 4.3.1 Novel bioactive glass constituents (grams)

Raw Materials:	**SiO_2**	**Ga_2O_3**	**$CaCO_3$**	**$Ca(H_2PO_4)_2.H_2O$**	**$CaCl_2$**
Mass (g):	19.8	33.76	12.00	27.72	16.64

4.3.2. Glass with Tantalum Production

The gallium-silicate glass with added tantalum for radiopacity, had a composition of $0.33SiO_2 \bullet 0.18Ga_2O_3 \bullet 0.19CaO \bullet 0.11P_2O_5 \bullet 0.15CaCl_2 \bullet 0.04TaO$. The glass frit was produced in the same way as discussed in Section 4.3.1.

4.3.2.1. Acid Washing Treatment of Glass

To acid wash the glass, 7g of ground glass was stirred in 280ml of 2 vol.% acetic acid for 1 hour. The glass was then centrifuged at 5,000rpm for 5 minutes and the supernatant was removed. The glass was then stirred in 560ml of DI for 1 hour and then centrifuged at

5,000rpm for 5 minutes. The glass was then separated by centrifugation and dried in a convection oven at 160^0C for 1.5 hours.

4.3.3. Glass Analysis

4.3.3.1. Differential Thermal Analysis

DTA was carried out using a Stanton Redcroft STA 1640 (Rheometric Scientific, England). A minimum of 30mg of the glass sample was placed in a platinum crucible. A matched blank platinum crucible was used as the inert reference sample. The sample was heated to 900^0C at a rate of 10^0C/min. RSI Orchestrator software was used to monitor the ΔT and to calculate the T_g of the glass.

4.3.3.2. X-ray Diffraction

XRD of the powdered glass sample was carried out using a Brucker D8 Advance XRD (Bruker, Billerica, USA). The sample was examined at a range of $10^0<2\theta<80^0$ at a step size of 0.05^0 and a step time of 10 seconds.

4.3.3.3. Particle Size Analysis

Particle size analysis was carried out using a 632.8 nm He-Ne laser Malvern Mastersizer S (Malvern, UK). Particles were pre-sonicated for 15 seconds and analysed in DI. Laser obscuration was in the range 10-15% and particles were analysed in the range 0.05μm to 900μm.

4.3.3.4. X-Ray Photoelectron Spectroscopy

X-Ray Photoelectron Spectroscopy (XPS) was completed in the Materials and Surface Science Institute, University of Limerick, Limerick, Ireland by Fathima Laffir. XPS was carried out on glass powders in a Kratos Axis 165 Spectrometer (Kratos Analytical, Manchester, UK) using monochromatic Al Kα radiation of energy 1486.6eV. Surface charge was efficiently neutralised by flooding the sample surface with low energy electrons. C_{1s} peak at 284.8eV was used as the charge reference in determining the binding energies. Elemental analyses were obtained from a survey spectrum scanning the entire binding energy and then high resolution spectra were taken at a number photoelectron transitions, including O_{1s}, Ga_{2p} and Si_{2p}, with a 20eV pass energy. The Ga_{2p} region was chosen instead of the more commonly used Ga_{3d} region to avoid interference of the Ga_{3d} peaks with the O_{2s} peak. Photoelectrons were collected at a normal take off angle relative to the sample surface. Construction and peak fitting in the narrow range spectra used a Shirley type background and the synthetic peaks were of a mixed Gaussian-Lorenzian type.

4.3.3.5. Field emission scanning electron Microscope

Glass samples were embedded in graphene resin, attached to sample stubs and analysed using a Hitachi S5500 (Hitachi, Tokyo). Images were captured at 100,000X magnification. An accelerating voltage of 25kV and a current of 4300nA were applied. FE-SEM analysis was carried out by Dr. Eoin Fox in Dublin City University.

4.3.3.6. Attenuated Total Reflectance-Fourier Transform Infrared Spectroscopy

Glass samples were analysed using a Spectrum 100 ATR-FTIR (Perkin Elmer, Waltham, USA) equipped with Grams Analyst data analyser. All spectra were obtained between 600 and 4000cm^{-1} at 4cm^{-1} resolution after averaging four scans.

4.3.3.7. Zeta Potential Measurements

Zeta potential measurements were performed at 25°C in DI using a Zetasizer NanoZS (Malvern Instruments, Malvern, UK). The values reported are averages of three measurements, each measurement consisting of an average of > 30, 10 second runs.

4.3.3.8. Nitrogen Adsorption/Desorption Measurements

Nitrogen Adsorption/Desorption Measurements was completed by Serguei Belochapkine at the Materials and Surface Science Institute, University of Limerick, Limerick, Ireland. The Brunauer, Emmett and Teller (BET) surface area and porosimetry analysis was measured by nitrogen gas adsorption in a Micrometrics Gemini V gas adsorption analyser. The pore size distribution and pore volume were estimated using the Barrett-Joyner-Halenda (BJH) scheme [276].

4.4. Preparing Hydrogel

1.2ml of the required alginate was mixed with the required glass and GDL content. The initial glass and GDL content were determined during previous testing [330][331]. 9.2 Appendix B (page290) details the hydrogel formulas examined.

4.5. EDC and NHS

N-(3-Dimethylaminopropyl)-N′-ethylcarbodiimide hydrochloride (EDC) and N-Hydroxysuccinimide (NHS) were purchased from Sigma-Aldrich (Wicklow, Ireland). The EDC and NHS were used as received.

A 1:1 EDC:NHS ratio (w/w) was used as this has been shown previously to cause alginate bonding [332] [333].

4.6. Examination of the Hydrogel

4.6.1. Storage Medium

For the results to be comparable the samples were stored in DI; however, this is not comparable to the effects of the sample *in vivo,* as calcium ions typically exchange with the

sodium ions of blood. To overcome this some samples were tested after storage in simulated body fluid. Although not exactly the same as blood, SBF is a better storage medium for estimation of *in vivo* strengths. As SBF is only stable for a maximum of 4 weeks at 4^0C, samples will also be tested after storage in phosphate buffered saline (PBS) as it allows the samples to be stored for an extended amount of time at 37^0C.

5 samples (10mm diameter and 14mm height) were stored together in 16.5ml of the varying storage mediums.

4.6.1.1. Simulated Body Fluid

All reagents used were purchased from Sigma-Aldrich (Wicklow, Ireland). To ensure the temperature was kept at 36.5^0C throughout producing the SBF a temperature controller (IC 901, Eliwell, Italy) was used to set the temperature of the liquid using a thermistor (NTC, Eliwell, Italy) and a silicon heating mat (100 x 150mm, Radionics, Ireland). The temperature must be as exact as possible throughout the preparation, as temperature affects pH.

cSBF was produced by following the method specified by Kokubo *et al*. [281]. 700ml of DI was placed in a plastic beaker with a stirring bar and placed on top of a magnetic stirrer and heating mat. The DI was heated to 36.5^0C. The thermistor and a thermometer were placed in the DI to monitor and control the temperature and the beaker was covered with Parafilm. The following agents were added slowly allowing each to fully dissolve before adding the next; 8.035g sodium chloride (NaCl), 355mg sodium hydrogen carbonate ($NaHCO_3$), 225mg potassium chloride (KCl), 231mg di-potassium hydrogen phosphate trihydrate ($K_2HPO_4.3H_2O$), 311mg magnesium chloride hexahydrate ($MgCl_2.6H_2O$), 39ml 1M-HCl, 292mg calcium chloride ($CaCl_2$), 72mg sodium sulphate (Na_2SO_4). 200ml of DI was added and the temperature was allowed to adjust to 36.5^0C. Approximately 6.7g of Tris-hydroxymethyl aminomethane ($(HOCH_2)_3CNH_2$) was added slowly until the solution had a pH of 7.40 at a temperature of 36.5^0C. The solution was added to a volumetric flask. The beaker used, stirring bar, thermometer and thermistor was washed with DI and the washings were also added to the volumetric flask. The solution was allowed cool to 20^0C and DI was added until the solution had a final volume of 1000ml.

4.6.1.2. Phosphate Buffered Saline

PBS tablets were purchased from Sigma-Aldrich (Wicklow, Ireland). PBS was produced by dissolving one tablet in 200ml of DI, as per user's instructions.

4.6.2. X-ray Microtomography

XMT was carried out using a Phoenix Nanotom S (GE Measurement & Control Solutions, Billerica, USA). A voltage of 80kV and a current of 220µA were maintained to achieve a voxel size of 4.30µm. 3D-XMT was used to examine the agglomeration size and distribution

throughout the hydrogel by taking a 3D image, isolating a 4.725mm^3 of the image of the hydrogel and reconstructing it using VGStudio Max (Volume Graphics, Heidelberg, Germany). 2D-XMT images were used to determine the radiopacity of the hydrogel and ImageJ was used for comparing the radiopacity of the hydrogel to a 99% aluminium step wedge. This work was carried out in Waterford Institute of Technology by Brendan Phelan.

4.6.2.1. ImageJ

The mean greyscale value was measured using ImageJ software (National Institute of Health, MD). Note: 255=White and 0=Black.

4.6.3. Volume Conservation

To examine whether the hydrogel's volume was conserved over time, the hydrogel sample volume was measured after 1, 3 and 7 days. The novel hydrogel was mixed and poured into a cylindrical mould (10mm diameter and 14mm height). The hydrogel was left to set for 1 hour and incubated in the required medium (DI, PBS or SBF) at 37°C for the required amount of time. After the required time the hydrogel dimensions were measured using callipers. 'Volume conservation' was calculated by calculating the change in volume compared to the original (pre-incubated) volume.

4.6.4. Compression Testing

To examine the mechanical properties of the novel hydrogel, unconfined compression testing was carried out. The compression test samples were made as described in Section 4.6.3. After storage at 37^{0}C for the required amount of time, the hydrogel sample was compressed using a mechanical testing machine (Zwick Roell, Z005, Germany) equipped with a 5kN load cell. A 0.005N pre-load was applied. The samples were compressed up to 70% strain at a crosshead speed of 2mm/min.

Figure 4.6.1 Hydrogel sample following compression testing

4.6.5. Tensile Testing

Tensile testing samples were prepared by preparing rectangular shaped hydrogel samples in a mould (40 mm x 15m x 2mm). Once set the samples were cut into a dogbone shape (width 4mm, length 20mm) and stored in SBF. After storage at 37^0C for the required amount of time the hydrogel sample was tensile tested using a mechanical testing machine (Zwick Roell, Z005, Germany) equipped with a 5kN load cell. The samples were tensile tested until failure at a crosshead speed of 2mm/min, which is specified in ASTM D3039 – 14 Standard Test Method for Tensile Properties of Polymer Matrix Composite Materials.

4.6.6. Rheological Gelation Time

Rheology is typically used to determine the gelation point of the hydrogel. However, due to the nature of the hydrogel, the gelation point could not be determined using rheology and it was decided to examine these using an alternative method. The results from rheology testing can be seen in Appendix 9.4.1.

4.6.7. Working and Hardening Time

The working and setting time of each alginate was determined using a modified version of ISO 9917.

To find the working time, the timer was started at the start of mixing the hydrogel sample. Once mixed, the hydrogel was placed in a cylindrical holder and every minute was stirred with a spatula. The end of the hydrogel's working time was considered as the time when the hydrogel was no longer fluid enough to return to the shape of the cylindrical holder (diameter 10mm, height 5mm) after stirring.

The setting time was found by starting the timer at the point of mixing the hydrogel and placing a circular indenter (diameter: 6mm, weight: 20g) on the sample every 60 seconds. The hydrogel was considered set when it held the indenter without causing an indentation in the hydrogel, see Figure 4.6.2.

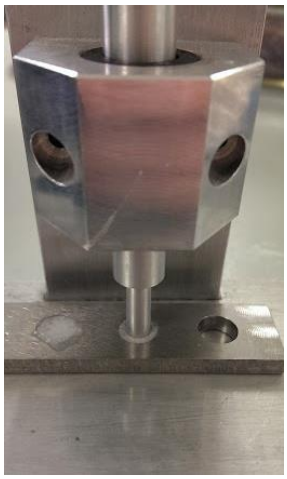

Figure 4.6.2 Setting Time testing jig

The hardening time is defined as the difference between the working time and setting time of the hydrogel.

4.6.8. Bond Strength

4.6.8.1. Bond Strength Testing Clamp Design

As stated in the ASTM standard F2255-03, when examining the bond strength of the material, a tissue and adhesive material sample should have a width of 25mm [297]. The length of the of the sample is not specified, however, ATSM standard F2258-03 "Strength Properties of Tissue Adhesives in Tension" states that the sample specimen must be square with dimensions of 25mm X 25mm [299]. It was decided to use the square sample to correlate with the two standards.

To insure that each sample of the hydrogel was 25mm x 25mm, a plate with a square hole of this size was designed to act as a template. The plate could be placed on the porcine skin graft, the hydrogel could then be added evenly and the template was removed.

Two plates with a width of 30mm and a length of 60mm were designed to glue the porcine skin graft to. This was a brushed stainless steel to ensure that porcine skin graft would adhere to the surface.

Two clamps were also designed, these would attach to the mechanical testing machine while keeping the plates parallel to one another.

Drawings for each component can be seen in Appendix 9.4.3.

4.6.8.2. Bond Strength Testing

The bond strength was tested in accordance to ATSM standard F2255-03, which is used to examine the strength properties of adhesives in Lap-Shear. It was decided to carry out bond strength testing according to ASTM F2255-03 as the adhesive will be experiencing shear stress in vivo.

To prepare the samples, 25mmx25mm sections of porcine xenograft (131703-01 Ez-Derm 9x10 cm Patches non-perforated, Fannin Limited) were glued, using cyanoacrylate to stainless steel, plates and allowed set for 20 minutes. 25mmx25mm of the hydrogel was then placed between the porcine graft sections and a weight was placed on the plates. A weight of between 1–2 Newton is described in ATSM F2255-03. However, this strength was too large and caused the hydrogel to move from between the plates before setting. It was therefore decided to use a smaller weight of 0.5N which has been used in previous bond strength testing studies [332] [334]. The hydrogel was tested following storage at 37^0C for 1 hour. The optimum concentration was subject to further testing by examining the bond strength of storage in SBF at 37^0C for 1 hour and 24 hours. The bond strength of the hydrogel to tissue was determined using a mechanical testing machine (Zwick/Roell, Z005, Germany) equipped with a 5kN load cell. The samples were tested to failure at a cross-head speed of 5mm/min, Figure 4.6.3. The bond strength was the peak force exhibited.

Figure 4.6.3 Bond strength test set-up

4.6.9. Deliverability

To examine the deliverability of the hydrogel through a micro-catheter, the force required to inject the hydrogel through a 2.1F micro-catheter (Headway® microcatheter, MicroVention Terumo, USA) was measuring using a mechanical testing machine (Zwick/Roell, Z005, Germany), see Figure 4.6.4. The effects of the syringe size and flow rate were examined. The crosshead speed varied depending on the syringe size and required flow rate.

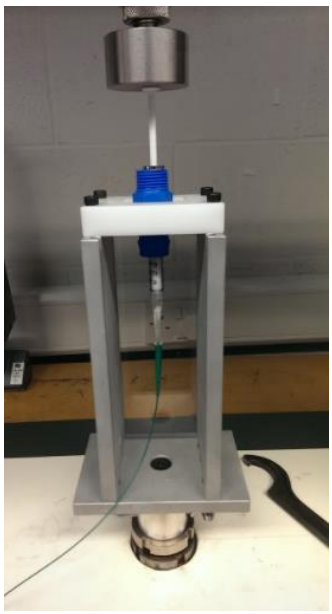

Figure 4.6.4 Testing the force required to inject the hydrogel through a microcatheter

The hydrogels that could be delivered through a micro-catheter were injected into an aneurysm model with physiological blood pressure and flow, discussed in detail in Section 4.6.9.1. A 5mm diameter compliant balloon (Scepter C compliant occlusion balloon catheter, MicroVention Terumo, USA) was inflated adjacent to the aneurysm neck, to facilitate placement.

4.6.9.1. Flow Model

An aneurysm model was purchased from Elastrat (Genève, Switzerland). This model (H+N-S-A-005) has two sized aneurysms; aneurysm 1 is spherical and has a diameter of 10-11mm and a neck of 2.5x2.5mm and aneurysm 2 has a diameter of 10mm, a height of 16.5mm and a neck of 2.5x2.5mm.

A pulsatile flow pump for large animals (Harvard Apparatus, Massachusetts, USA) was used to pump the liquid through the aneurysm model. This pump is used to control the pressure and the flow rate of the system. The flow rate and pressure can be modified by a combination of the pump rate (rpm) and the stroke volume. A water reservoir was placed above the pump to provide a base pressure,

A pressure transducer (DTX-plus, BD Medical systems, Utah, USA) was placed at the inlet and the outlets of the aneurysm model in order to monitor the pressure in the system and to calculate the flow rate. The pressure transducer was wired to a bridge (NI 9949 RJ-50, National Instruments, USA). This bridge was then connected to a bridge analog input (NI 9237, National Instrument, USA) in order to graph the signal. The flow model set-up is shown in Figure 4.6.5.

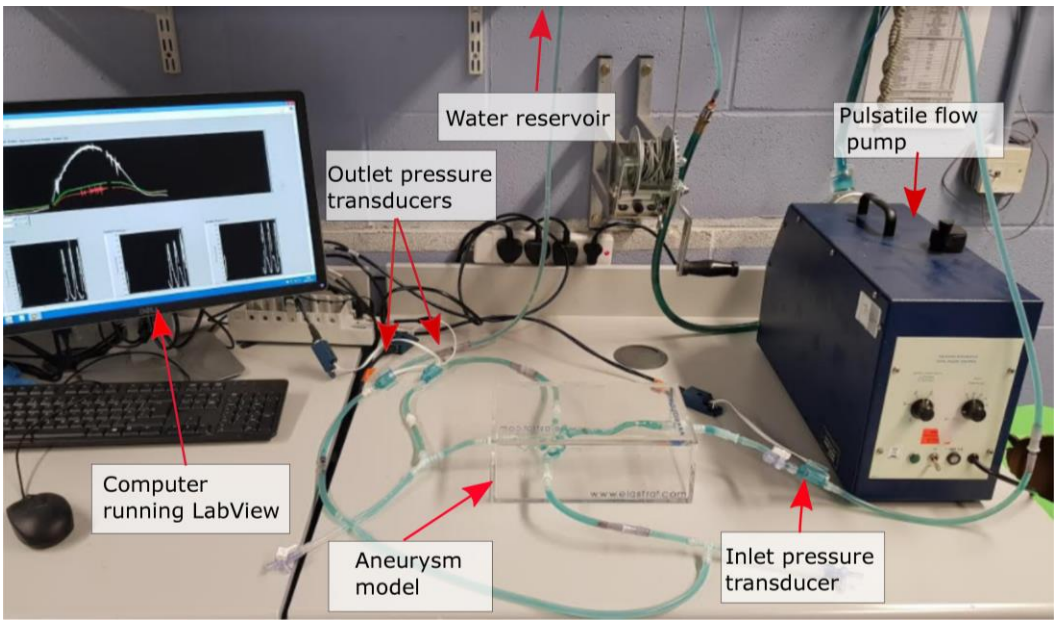

Figure 4.6.5 Aneurysm flow model set-up

The flow rate was calculated using the Hagen-Poiseuille equation (Equation 2.1.1). There are some limitations involved with this equation as it requires the inner diameter of the artery in order to calculate flow. However the inner diameter changes throughout the aneurysm model. In order to minimise this error, the same diameter tubing was used at the aneurysm model inlet and the outlet. Larger tubing had to be used at the inlet and the outlet of the pump due to the pumps design but this did not affect the flow rate as the pressure was calculated before and after this tubing change.

A custom LabVIEW program was used to produce a graph of the pressure in the aneurysm model and to calculate the flow. The LabVIEW program can be seen in Appendix 9.4. The program had to be calibrated to convert the voltage signal, read by the bridge, to blood pressure (mmHg). To calibrate this, the pressure transducer was connected to a container of water and the pressure was found at increasing height increments using Equation 4.6.1.

Equation 4.6.1 Equation to calculate pressure

$$Pressure\ (\frac{N}{m^2}) = \rho g h$$

Where,
ρ = density of the fluid. Water has a density of 1000kg/m^3
g = gravity (9.8066m/s^2)
h = height of the bucket (m)

Table 4.6.1 shows the voltage readings of the NI 9237 compared to the calculated pressure (R^2=0.9979). The calculated pressure was an average of 4.25 times larger than that of the of

the voltage found using the NI 9237 and therefore the signal was multiplied by this in order to calculate the pressure in the aneurysm model.

Table 4.6.1 Pressure readings at increasing heights to calibrate physiologically correct flow model

Height (m)	Calculated pressure (N/mm²)	Calculated pressure (mmHg)	Bridge reading (v)	Calibration factor
0.5	4905	36.79	8.23	4.47
0.75	7357.5	55.18	12.74	4.33
1	9810	73.58	17.47	4.21
1.25	12262.5	91.97	22.23	4.14
1.5	14715	110.36	25.74	4.29
1.75	17167.5	128.76	30.85	4.17
2	19620	147.15	34.78	4.23
2.25	22072.5	165.54	37.95	4.36
2.5	24525	183.94	44.24	4.16

The literature presents three solutions that have a similar viscosity of blood [335]–[337]. The viscosity of the solutions was tested at 37^{0}C in order to find a solution with a similar viscosity to that of blood. A 36:64 water glycerol solution had a viscosity of 4.15mPa.s, which was the most similar to that of blood (3.28mPa.s to 4.33mPa.s [29]). The solution was heated to 37^{0}C, placed in the water reservoir and pumped throughout the system.

4.7. *In Vitro* Analysis

Initially, a resazurin blue assay was carried out to assess the metabolic activity of the bovine aortic endothelial cells (details in 4.7.3). As this only indicates cellular metabolic activity, rather than exact cell numbers, cells were dosed 20% and 100% eluent and were stained with DAPI and Phalloidin in order to determine the specific cell numbers (discussed further in 4.7.4).

The cell culture medium, DMEM, is free of lipids, proteins and growth factors. As a result of this, DMEM was supplemented with 10% foetal bovine serum (FBS) and 1% Penicillin-Streptomycin (PS) for high serum DMEM and 0.5% FBS and 1% PS for low serum DMEM. The same batch of FBS and PS were used. All reagents for cell culture were purchased from Sigma-Aldrich (Wicklow, Ireland).

4.7.1. Preparation of Eluent

Hydrogel samples were prepared in cylindrical silicone moulds (Ø15 mm, height: 1 mm) and allowed to set for one hour before being placed in 2.75 ml of DMEM cell culture media (as per ISO10993-5) with 1 vol.% penicillin-streptomycin (Sigma Aldrich, Wicklow, Ireland). Samples

were stored in 24 well plates for both 24 hours and 48 hours before being filter through a 0.22µm sterile filter. The eluent was supplemented to 10 vol.% FBS for high serum eluent and 0.5 vol.% FBS for low serum eluent.

4.7.2. Eluent Dosing

To examine the effects of the eluent on the BAEC cells, the elution media was added to the cells at varying concentrations of eluent (0, 20, 40, 60, 80, 100 vol.%) mixed with corresponding non-eluent media and incubated for 24 and 48 hours. Each concentration was analysed using both high serum and low serum media.

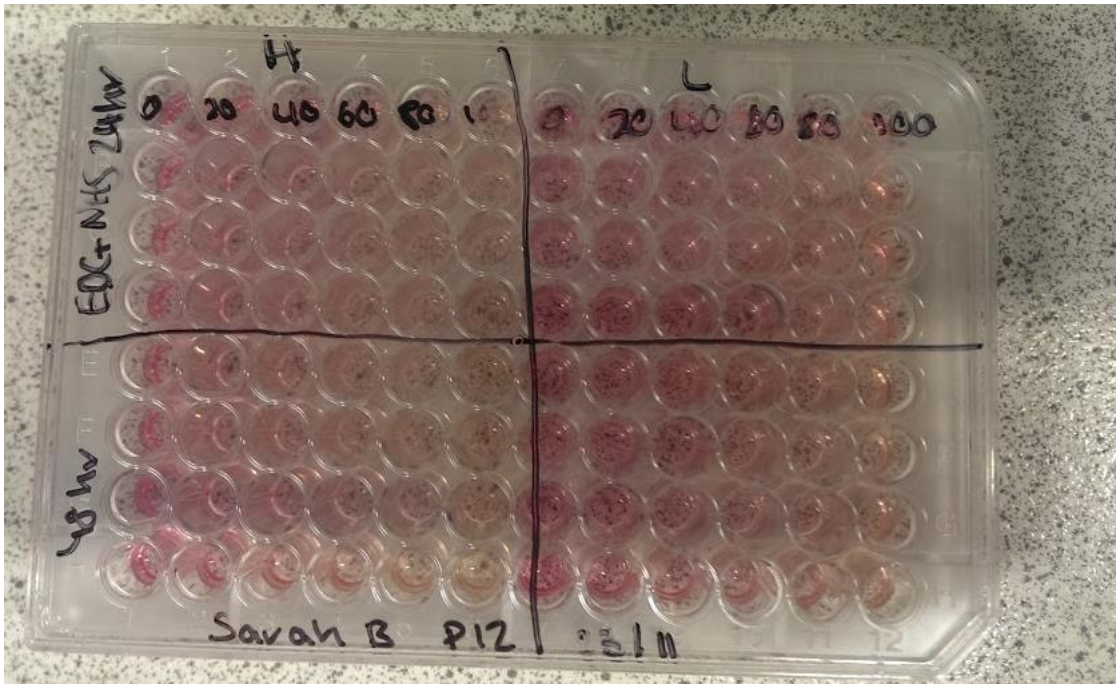

Figure 4.7.1 96 well plate dosed with varying concentrations of eluent

4.7.3. Metabolic Activity

Bovine aortic endothelial cells (BAECs) were cultured in high serum DMEM until they formed a sub-confluent monolayer (37°C, 5% CO_2). The cells were then seeded at 1,800 cells per 100µl of high serum media in a 96 well plate and incubated for 24 hours. The high serum media was then aspirated off and 100µl of low serum media was added to each well and incubated for a further 24 hours, in order to quiesce the cells. Following this, the cells were stained with resazurin blue. Resazurin sodium salt was purchased from Sigma-Aldrich (Wicklow, Ireland). 100 µL of resazurin blue solution (0.01 mg/mL media) was placed per well. This was removed at 4.5 hours and analysed in order to provide an initial cellular activity profile. The cells were then dosed with the eluent as described in Section 4.7.2. After 24 hours the metabolic activity of the cells was again examined using resazurin blue. Cell growth was calculated as a percentage of untreated control cells using Equation 4.7.1. Cell growth was normalised for starting cell number and untreated cell growth. Resazurin blue

was measured using a fluorescent plate reader with an excitation 560nm, emission of 590nm and a bandwidth of 10nm.

Equation 4.7.1 Cell metabolic activity (% Growth) determined using resazurin blue

$$\%\ Growth = \frac{Absorbance_{540nm} of\ treated\ cells}{Absorbance_{540nm} of\ untreated\ cells}$$

4.7.4. Cell Counting

Glass coverslips were sterilised and placed in each well of a 6 well plate. The cells were then seeded at 50,000 cells per 2.5ml and incubated for 24 hours in high serum DMEM until they formed a sub-confluent monolayer (37˚C, 5% CO_2). The high serum media was then aspirated off and the cells were quiesced by adding 2.5ml of low serum media to each well and incubated for a further 24 hours. Following this, the cells were dosed with 2.5ml of the eluent as described in 4.7.2. The cells were then stained using Phalloidin and DAPI for imaging and counting.

4.7.4.1. Phalloidin

The cells were fixed by placing 400µl of 3.7% formaldehyde in PBS solution to each well. The formaldehyde solution was removed after 5 minutes and washed three times with 300µl of PBS. The cells were permeabilized by placing 300µl of a 0.1% Triton X-100 in PBS solution to each well and left for 3 minutes. The Triton X-100 solution was removed and the cells were washed 3 times with PBS. 200µl of 1% Phalloidin in DMSO was then added to each well and left for 40 minutes. The Phalloidin was removed and the cells were washed, again, with PBS three times.

4.7.4.2. DAPI

Following Phalloidin stain, the cells were stained with DAPI. 5mg/ml of DAPI was diluted in DI. 300µl of the diluted DAPI was added to each well and left for 5 minutes. The DAPI was removed and each well was washed 3 times with PBS.

4.7.4.3. Microscopy

Images of the cells were taken using a fluorescence microscope (BX51, Olympus, MA, USA) using Cell^F software.

4.7.4.4. Image J

ImageJ software (National Institutes of Health, MD) was used for counting DAPI stained cells using the “Analyze Particles” feature. The Watershed feature was also used prior to counting to ensure each cell was counted individually.

4.7.5. Inductively Coupled Plasma – Atomic Emission Spectroscopy

Inductively Coupled Plasma – Atomic Emission Spectroscopy (ICP) was carried out to determine the gallium, calcium and silica ions released from the hydrogel into the eluent. 100µl of eluent was removed from each eluent and diluted to 50ml in 1M HNO_3. Each sample was run with a minimum of three calibration concentrations for each elemental standard. ICP-AES was carried out on a Liberty 220 Emission Spectrometer (Agilent, Santa Clara, USA) at a coil power of 1.1kW using argon gas as a carrier

4.8. Ion dosing

Cells were dosed with each of the individual ions for 24 hours. Cell metabolic activity was examined and cell counts were carried out as described previously (Section 4.7.3 and Section 4.7.4).

Due to the acidic nature of the ion solutions, the sodium bicarbonate ($NaHCO_3$) levels of the DMEM was increased by adding to 370mg/100mL. This content was selected to effectively buffer the pH when the ions and GDL were added, unless otherwise stated. The ion solutions were prepared in the following methods. Calculations are shown in Appendix 9.4.4.

4.8.1. GDL

83mg/mL of GDL was added to the high $NaHCO_3$ DMEM. This was allowed to dissolve and added to the cells at the required concentration.

4.8.2. Calcium

Calcium chloride ($CaCl_2$) was added at a concentration of 1.9mg/mL in the high $NaHCO_3$ DMEM. This was allowed to dissolve and added to the cells at the required concentration.

4.8.3. Gallium

Gallium is a hard acid that can drop the pH of a solution to 2 when the gallium content is above 100mM. Gallium is insoluble at a neutral pH and neutralising a solution will cause the gallium to precipitate forming amorphous gallium hydroxide. Certain forms of gallium are insoluble in a aqueous solution [338]. These restrictions make ion dosing with gallium difficult.

Gallium chloride and gallium nitrate are two forms of gallium that are soluble in aqueous solution but cause a large decrease in pH. As DMEM contains chloride, gallium chloride was used in order to provide more accurate results. However, it should be noted that gallium chloride is more acidic than gallium nitrate. Cells were dosed with solutions of gallium nitrate and gallium chloride solutions at the required concentrations.

Gallium nitrate ($Ga(NO_3)_3$) solution was prepared by adding 4.3mg/ml of $Ga(NO_3)_3$ to the high $NaHCO_3$ DMEM. This solution had a pH of 6.8.

Gallium chloride ($GaCl_3$) solution was prepared by adding 0.7ml/ml of a 0.703M $GaCl_3$ solution to the high $NaHCO_3$ DMEM. This solution had a pH of 6.0.

4.8.4. Silica

Most forms of silica ions are also insoluble in aqueous solutions. To examine the effects of silica ions on the cells, silicic acid was added at a concentration of 0.5mg/mL in the high $NaHCO_3$ DMEM. This was allowed to dissolve and added to the cells at the required concentration.

4.9. Sterilisation

4.9.1. Autoclaving

Alginate was weighed in an amber vial and sealed in an autoclave bag. The vial was not sealed with a cap, to allow for adequate steam penetration. The samples were autoclaved at 121^0C for 15 minutes using a SX-700E autoclave (Tomy, California, USA).

4.9.2. Gamma Irradiation

As discussed previously, the damage caused by gamma irradiation can be reduced by storing the samples under cold conditions during irradiation. Glass, GDL, EDC and NHS were sealed separately in screw cap vials. The vials were added to a dry ice box, along with 20kg of dry ice pellets. The samples were then gamma irradiated by Synergy Healthcare (Westport, Ireland) at a minimum dose of 15.7kGy and a maximum dose of 20.2kGy (for approximately 7minutes/kGy), to effectively sterilise the powder samples.

4.10. Direct Contact testing

4.10.1. Cells on Slide

Coverslips were sterilised by placing them under a UV lamp for 1 hour. The coverslips were then placed at the bottom of each well of a 6 well plate. BAECs were then seeded at 90,000 cells per 2.5ml in each well and incubated for 24 hours. A higher density of cells was used compared to previous analysis in order to achieve a confluent layer and encourage cell movement. The high serum media was then aspirated off and the cells were quiesced by adding 2.5ml of low serum media to each well and incubated for a further 24 hours. Cell seeded coverslips were then removed from 6 well plates.

The hydrogel was sterilised, mixed and poured into a well of a fresh 6-well plate. Cell seeded coverslips were then placed on top of each hydrogel prior to the end of working time. When being placed on the hydrogel, the coverslips were inverted to ensure the cells were directly in contact with the hydrogel. 2.5ml of DMEM was placed on the hydrogel and the samples were incubated for 1, 3 and 7 days. The media was initially changed after 24 hours and every 48 hours thereafter.

After the required amount of time, the cells were stained using DAPI and Phalloidin and counted, as described previously.

4.10.2. Cells Seeded on the Hydrogel

The hydrogel was sterilised, mixed and set in a 6 well plate. Once the hydrogel was set, 90,000 cells per 2.5ml was added to each well and incubated for 1, 3 and 7 days. The media was initially changed after 24 hours and every 48 hours thereafter.

After the required amount of time, the cells were stained and counted, as described previously.

4.11. Calcification

4.11.1. Sample Preparation

Bioactive glass samples (without any alginate) were stored in both DI and SBF separately for 7 days. The samples were then dried at 170^0C for 1.5 hours.

Alginate and bioactive glass hydrogel samples were prepared by mixing 1.2ml of 4.5% alginate with 13.8% (w/v) of glass, 8.3% (w/v) of GDL and 0.83% (w/v) of EDC and NHS. The mixed samples were placed in moulds (⌀ = 15mm, height = 1mm) and allowed set for one hour. The samples were stored in SBF for 7 days and then lyophilized.

As a control, hydroxyapatite and alginate samples were prepared. The samples were prepared in the same manner but 13.8% hydroxyapatite (Sigma-Aldrich, Wicklow, Ireland) was used as a replacement for bioactive glass with 8.3% (w/v) of GDL.

4.11.2. X-ray Diffraction

XRD was carried out as described in 4.3.3.2.

4.11.3. Attenuated Total Reflectance-Fourier Transform Infrared Spectroscopy

Samples were analysed using a Perkin Elmer Spectrum Two with a diamond universal ATR accessory (Perkin Elmer, Waltham, USA) equipped with Grams Analyst data analyser. All spectra were obtained between 450 and 4000cm^{-1} at 4cm^{-1} resolution after averaging four scans. A force of 85N was applied to each sample.

4.11.4. Von Kossa Staining

Samples were Von Kossa stained by placing samples in a 1% silver nitrate solution (Sigma-Aldrich, Wicklow, Ireland) in DI for 20 minutes under Blak-Ray B-100 UV light (UVP, Upland, CA). The silver nitrate was removed and the samples were washed several times with DI. Any unreacted silver nitrate was removed by soaking the samples in 5% sodium thiosulfate (Sigma-Aldrich, Wicklow, Ireland) in DI for 5 minutes. The samples were then washed again using DI.

4.12. Platelet Adhesion

4.12.1. Positive Control

For a positive control, a Thermo Scientific Nunclon Delta plate (Thermo Fisher, USA) is used. The Nunclon Delta plate is a hydrophilic polystyrene that promotes platelet adhesion.

4.12.2. Negative Control

For a negative control, clean coverslips are placed at the bottom of a 6 well plate. 1ml of Sigmacote® (Sigma Aldrich, Ireland) was added to each well and left for 30 minutes. After 30 minutes the Sigmacote® was removed and the coverslips/wells were left to dry overnight. The coverslips/well were then washed with DI and left to dry overnight. Sigmacote® is a siliconizing reagent that will cause glass to become hydrophobic. This hydrophobicity will limit platelet adhesion.

4.12.3. Hydrogel Sample

The hydrogel was sterilised, mixed and poured into a well of a fresh 6 well plate.

4.12.4. Platelet Adhesion

40ml of whole blood was collected into a blood collection tube with sodium citrate. 1.5ml of citrated whole human blood was placed into each well and stored at 37^0C for 1 hour. After 1 hour the blood was removed and 1.5ml of a 3% bovine serum albumin/PBS solution was added to each well. The bovine serum albumin/PBS solution was used as a blocking agent to reduce background noise caused by the fluorescent stain. The samples were left for 1 hour at room temperature. After an hour the media was aspirated off and the samples were gently washed with PBS.

4.12.5. Platelet staining

4.12.5.1. CD62P

A PE-CD62P solution is prepared by dilution 1/100 in PBS. 300µl of PE-CD62P was added to each well and incubated at 37^0C for 15 minutes. The stain was removed and the samples were washed 3 times using PBS.

4.12.5.2. Phalloidin

Cell fixing, permeabilising and Phalloidin staining was carried out as per Section 4.7.4.1.

4.12.5.3. Platelet imaging

Platelets were imaged and analysed as per Section 4.7.4.3 and 4.7.4.4.

4.13. *In Vivo* Study

4.13.1. Hydrogel packaging and sterilisation

Each component of the hydrogel was weighed out and packaged into glass vials in a Class 100 cleanroom. The uncapped vials of alginate were packaged into an autoclave pouch and

autoclaved. The bioactive glass, GDL, EDC and NHS were packaged into a foil pouches and gamma irradiated at 15.7 – 20.2kGy on dry ice.

4.13.2. *In vivo* Study

The *in vivo* study was carried out by an interventionalist in CBSET, Inc., Lexington, Massachusetts, USA. This study involved creating aneurysms in 8 female New Zealand White (NZW) rabbits. The following information details the method of creating the aneurysms and treating the rabbits. Fluoroscopy was used for visualisation purposes throughout the aneurysm creation and treatment. Unless otherwise stated, the rabbits were euthanized 30 days following treatment and histology was carried out to examine the success of the treatment.

4.13.3. Aneurysm Creation

Each rabbit received antiplatelet therapy (40mg of aspirin) for 3 days prior to and up to 14 days post aneurysm creation. The antiplatelet therapy was required to reduce the chance of thrombotic events. The rabbits were anesthetised using a combined injection of 35mg/kg ketamine and 5mg/kg xylazine, which was administered subcutaneously. Throughout the procedure, the rabbits had Isoflurane as an inhalant anaesthesia and IV fluids. Aneurysms were created at either 66 or 90 days prior to treatment. Variance was caused by treatment time.

The right common carotid artery (RCCA) was exposed by an incision in the rabbit's neck and an introducer sheath was placed into the artery. A balloon was placed and inflated to isolate the proximal carotid artery. Porcine elastase (8 units/mg, 25mg/ml) was mixed with a contrast agent, for visualisation purposes and injected through the introducer sheath. This was left in place for 10-20 minutes and aspirated off with a syringe. The balloon was deflated and removed with the introducer sheath. The RCCA was ligated and the incision at the neck was closed with sutures. The procedure used here to create the aneurysm is similar to those of other studies examining aneurysm embolization [321][339][340].

4.13.4. Embolization Treatment

The rabbits were approximately 7 months old when the embolization device was delivered and weighed between 3.68kg and 4.80kg. The rabbits did not receive antiplatelet therapy prior to treatment. The rabbits were anesthetised as discussed in 4.13.3 Aneurysm Creation. Incisions were cut in the left and right hind leg of the animals to place the microcatheter and balloon in the femoral artery. If only a microcatheter was used, the incision was cut in the left hind leg.

The hydrogel was used as the test material and platinum coils were used as a comparative control device. Due to limited success in occluding the rabbit's aneurysm, the hydrogel was

examined for the use of renal artery embolization. The treatment each rabbit received is shown in Table 4.13.1. The difficulties of treating cerebral aneurysm with the hydrogel will be discussed in more detail in results. Although not ideal, results from renal artery embolization will provide an indication on the safety of the hydrogel *in vivo* and if neointima formation is likely to occur. The structure of the kidneys can be found in Appendix 9.5.9.

Rabbit 1 and Rabbit 2 were treated with the hydrogel formula used in Section 9.5.4.4. Rabbit 3 – Rabbit 7 were treated with the hydrogel in Section 5.6. For treatment with the hydrogel; the timer was started and the hydrogel was mixed. To deliver the hydrogel, a microcatheter (0.027" Renegade HI-FLO microcatheter, Boston Scientific) was placed over a guidewire into the aneurysm or renal artery. A balloon (Over-the-Wire Fogarty Thru-Lumen Embolectomy Catheter, Edwards) was placed at the neck of the aneurysm. A balloon was used for embolization of one renal artery; another animal was embolized with no balloon. The guidewire was removed and the microcatheter was filled with the hydrogel. The balloon was inflated and the hydrogel was injected into the aneurysm see Table 4.13.1. The balloon inflation/injection time relates to the end of the hydrogel's working time. After the relevant time, the balloon was deflated (Table 4.13.1). Variance in times was due to issues with injectability that will be discussed in more detail in the results. The balloon and microcatheter were removed and a post-treatment angiogram was carried out.

For treatment with the coils; a microcatheter was placed over a guidewire into the aneurysm or renal artery. The guidewire was removed and the coils were placed through the microcatheter into the aneurysm. The microcatheter was removed and contrast agent was injected to examine if occlusion was achieved.

After treatment, the femoral artery was ligated and the hind legs were closed with sutures.

Table 4.13.1 Embolization treatment and hydrogel delivery times for each rabbit

Rabbit	Treatment	Area treated	Balloon inflation/Injection time (since start of mixing) (MM:SS)	Total time balloon was inflated (MM:SS)
1	Hydrogel	Aneurysm	17:00	02:37
2	Hydrogel	Aneurysm	14:26	04:55
3	Hydrogel	Aneurysm	20:30	08:00
4	Hydrogel	Aneurysm	23:00	08:00
5	Hydrogel	Aneurysm	23:00	02:00
6	Hydrogel	Renal Artery	23:55	06:40
7	Hydrogel	Renal Artery	23:00	N/A
8	Coil	Aneurysm and Renal Artery	N/A	N/A

4.13.5. Observation

Blood samples were taken and the rabbits' weights were monitored post treatment to ensure the rabbits were healthy.

4.13.6. Euthanasia

The rabbits were anesthetised using a combined injection of 30mg/kg ketamine and 3mg/kg xylazine, which was administered subcutaneously. Throughout the euthanasia procedure, the rabbits had Isoflurane as an inhalant anaesthesia and an IV of Heparin and Nitroglycerin which was administered as needed. An overdose of euthanasia solution or a potassium chloride solution by IV was administered to euthanize the rabbits.

4.13.7. Tissue Collection and Histology

Histology samples were taken, stained and examined by a pathologist at CBSET Inc. The areas to be examined were dissected from the surrounding tissue and stored in 10% neutral buffered formalin until histology could be carried out.

The treated sites of 4 rabbits were examined. The treated sites were resin-processed. Longitudinal sections of the aneurysms and cross-sections of the renal arteries and kidneys were examined. To examine the treated sites, each sample stained with Haemotoxylin and Eosin (H&E) and Verhoff/van Gieson elastin stain and examined using light microscopy.

4.14. Statistical Analysis

Student T-test and ANOVA with Bonferroni's post hoc test was carried out using IBM SPSS (IBM, Armonk, NY). Asterisks will be used to indicate the p-value, where * indicates a value of $P \leq 0.10$, ** indicates a value of $P \leq 0.05$, *** indicates a value of $P \leq 0.01$ and **** indicates a value of $P \leq 0.001$.

Chapter 5. Results and Discussion

5.1. Effect of Molecular Weight and Chemical Composition

In this section, the alginate concentration, molecular weight and chemical composition (M/G ratio) were varied and the effect that this variation had on the hydrogel's mechanical properties, sample volume conservation and deliverability were determined. The alginates produced by the two techniques were characterised and examined at 4 concentrations. The four alginate concentrations used in this study were determined using Design Expert 9. The two methods of producing these alginates are discussed in Section 4.1.1.

Following characterisation of the two alginates; the hydrogel's viscosity, compressive strength, sample volume conservation, working time, hardening time and deliverability were determined at the 4 varying alginate concentrations; 0.5%, 2.5%, 4.5% and 6.0%. The glass and GDL content of the hydrogel were kept constant at 4.6% (w/v) and 4.15% (w/v), respectively, unless otherwise stated. This glass and GDL content were determined from testing conducted previously [330] [331].

5.1.1. X-ray diffraction

Figure 5.1.1 shows XRD spectra of the bioactive glass. From the spectra it is clear that the bioactive glass used in the hydrogel is fully amorphous, with no evidence of crystallisation.

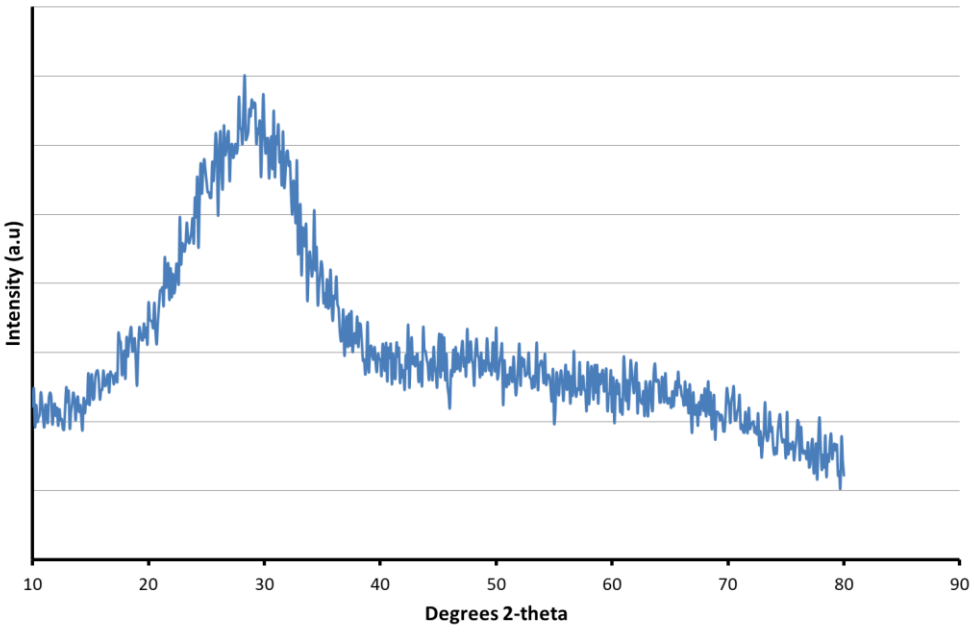

Figure 5.1.1 X-ray diffraction of the bioactive glass

5.1.2. Gel Permeation Chromatography

GPC was carried out to examine the molecular weight of the two alginates. Figure 5.1.2 shows the GPC results of the two alginates produced. Technique 1 produces an alginate with a low

molecular weight of 60kDa, while Technique 2 produced an alginate with a greater molecular weight of 700kDa.

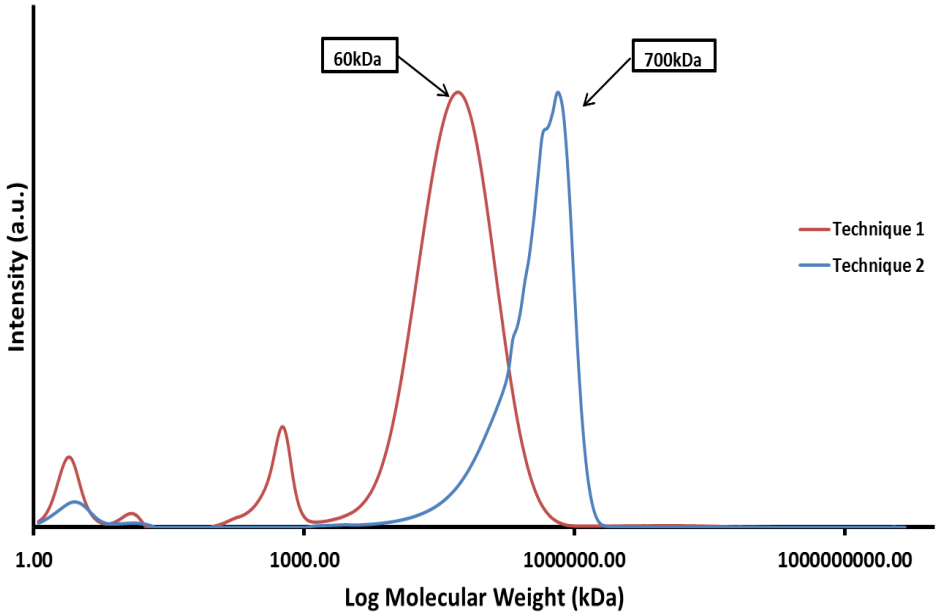

Figure 5.1.2 GPC of alginates

5.1.3. Nuclear Magnetic Resonance Spectroscopy

The ^{1}H-NMR spectrum (Figure 9.5.1) was used to determine the guluronic acid (F_G) and mannuronic acid (F_M) fractions of the alginate. Table 5.1.1 shows the ^{1}H-NMR results, calculated using the equations discussed in Section 3.1.1. The 60kDa alginate is a High-G alginate with an average G-block length of 7.08. The 700kDa is a High-M alginate with a much shorter average G-block length of 3.59.

Table 5.1.1 Alginate chemical composition

Molecular weight	F_G	F_M	M/G	F_{GG}	F_{MM}	F_{MG}	$\bar{N}_{G>1}$
60kDa	0.52	0.48	0.92	0.38	0.33	0.14	7.08
700kDa	0.37	0.63	1.7	0.18	0.45	0.18	3.59

5.1.4. Viscosity

The viscosity of the ungelled alginate, without the addition of glass or GDL, can be seen in Figure 5.1.3. The viscosities of both the 60kDa and 700kDa alginate are similar at each alginate concentration tested and the viscosity increases with increasing alginate concentration. The 6.0% alginate concentration of both alginates has a viscosity greater than 10,000mPa.s, which is the upper limit of the viscometer used. Alginate's viscosity typically increases greatly with small increases of alginate concentration [341] [342].

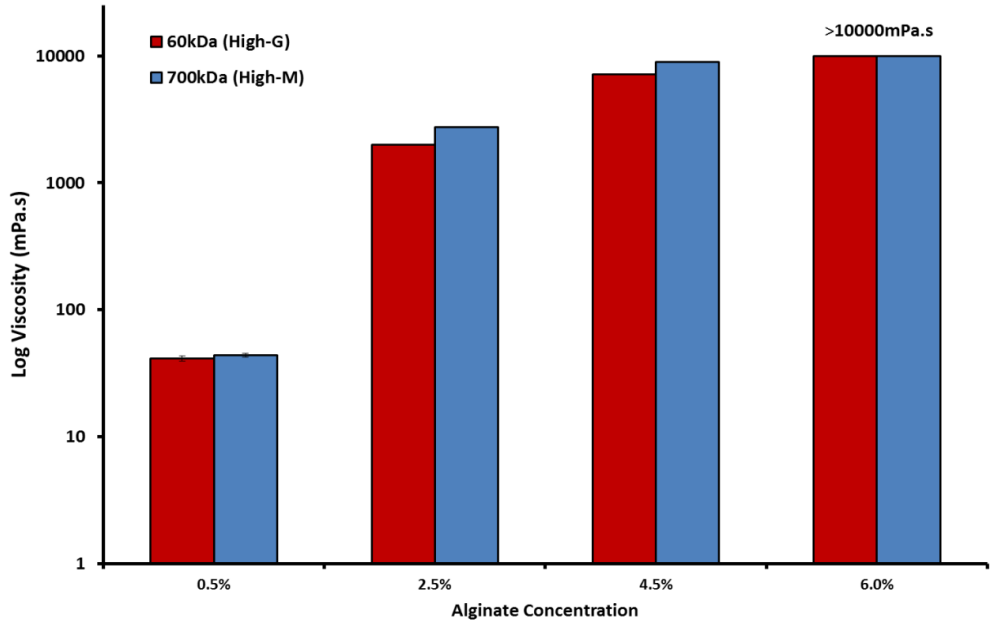

Figure 5.1.3 Viscosity of 60kDa and 700kDa alginate at four increasing concentrations (n=5)

5.1.5. Compressive Strength

Figure 5.1.4 and Figure 5.1.5 examines the effect of alginate concentration and incubation time has on the compressive strength and incremental modulus of the resultant hydrogels. In this case, compressive strength and incremental modulus, between 30-50% strain, is examined for the 60kDa alginate at 4 varying alginate concentrations; 0.5%, 2.5%, 4.5% and 6.0%. The samples were tested following storage in DI at 37^0C for 1, 3 and 7 days. Typical stress strain graphs for each sample are shown in the appendix (Figure 9.5.3-Figure 9.5.6).

There is no significant increase in the strength or incremental modulus of the hydrogel over time for the 0.5% and 2.5% alginate, as shown in Figure 5.1.4 and Figure 5.1.5. There is a significant increase over time for the 4.5% and 6.0% alginate concentrations. This suggests that the hydrogel is highly cross-linked for the lower alginate concentrations, however, cross-linking continues for a minimum of 7 days for the higher alginate concentrations, presumably as a result of a continued release of cross-linking ions from the glass phase.

Only the 4.5% and 6.0% alginate concentration samples fractured when compressed after storage for 1, 3 and 7 days, which likely accounts for the large standard deviation. No other samples tested fractured up to 70% strain. This fracturing may be caused by the gel initially having an inhomogeneous structure due to a lack of crosslinking ions to accommodate the higher alginate concentration.

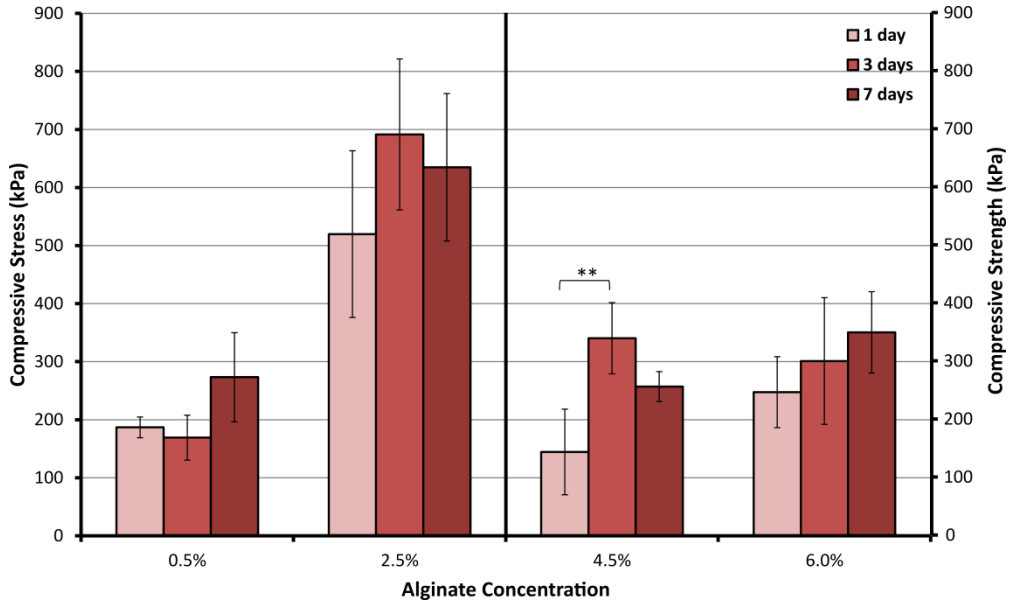

Figure 5.1.4 Compressive stress and strength up to 70% strain for the 60kDa (High-G) alginate following storage at 37^{0}C in DI (n=5)

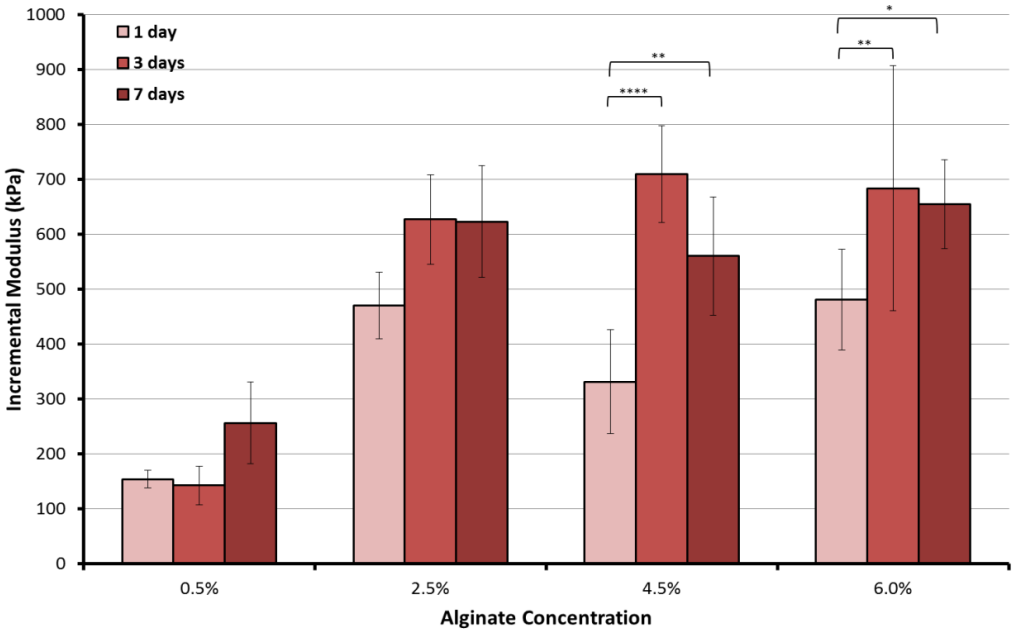

Figure 5.1.5 Incremental modulus (30-50% strain) of the 60kDa (High-G) alginate following storage at 37^{0}C in DI (n=5)

As with the 60kDa alginate, the 700kDa alginate samples fracture after 1, 3 and 7 days storage at an alginate concentration of 4.5% and 6.0%. However, it can be seen in Figure 5.1.6 and Figure 5.1.7 that there is a significant increase in both compressive strength and incremental modulus over the 7 days of storage for each concentration examined when compared to day 1. This may suggest gelation of the M-block occurs later then the gelation of the G-block. This may suggest that G-block cross-linking ions such as calcium are released from the glass before M-block cross-linking ions such gallium.

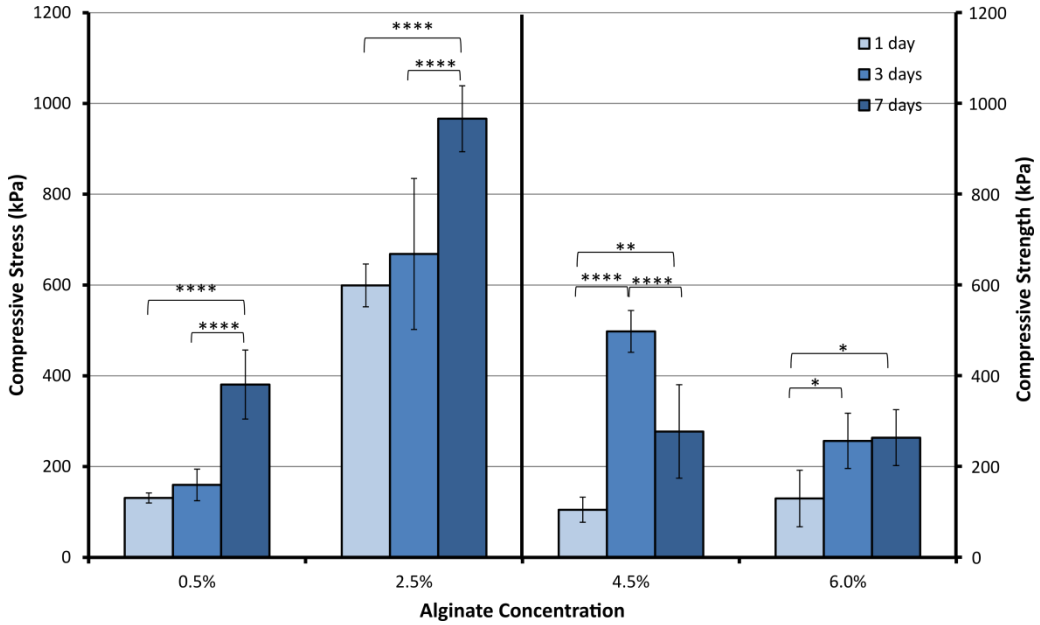

Figure 5.1.6 Compressive stress and strength up to 70% strain of the 700kDa (High-M) alginate following storage at 37^{0}C in DI (n=5)

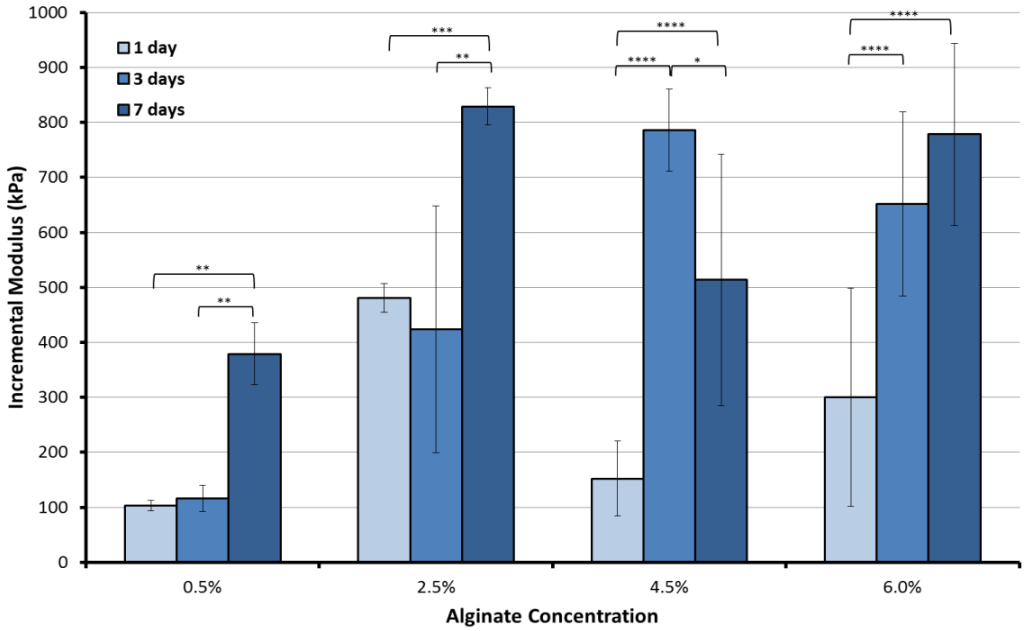

Figure 5.1.7 Incremental modulus (30-50% strain) of the 700kDa (High-M) alginate following storage at 37^{0}C in DI (n=5)

Figure 5.1.8 and Figure 5.1.9 examine the effect of alginate molecular weight and concentration on the compressive strength and incremental modulus of the resultant hydrogels after 7 days of incubation. It can be seen that both hydrogels exhibited strengths greater than 22kPa, which is important if the material is to withstand the compressive forces of blood flow. A significant difference in the strength and incremental modulus is seen between the two different molecular weight alginates at a 2.5% alginate concentration, with the 700kDa alginate generally having an increased strength at each concentration. Typically, the High-G alginate has the highest strength and stiffness at low alginate concentrations

[343]; however, this is not observed here and this variation is likely caused by the increased molecular weight of the High-M alginate, providing strength through increased chain entanglement.

The hydrogel's strength increases for alginate concentrations 0.5% to 2.5% and, overall, is at its highest when the alginate concentration is 2.5%. It has been observed elsewhere that the strength increases with a continued increase in alginate concentration [109] [202], however, this is not seen here. In contrast, here the strength is seen to reduce at alginate concentrations greater than 2.5%. It is hypothesised that this may be due to a shortage of ions available for crosslinking. This shortage may be caused by a lack of relative increase in the glass or GDL content of the hydrogel with the increase in available chains. This shortage of ions will likely result in a hydrogel with a low strength caused by a reduced cross-linking density or an inhomogeneous hydrogel with areas of varying cross-linking density.

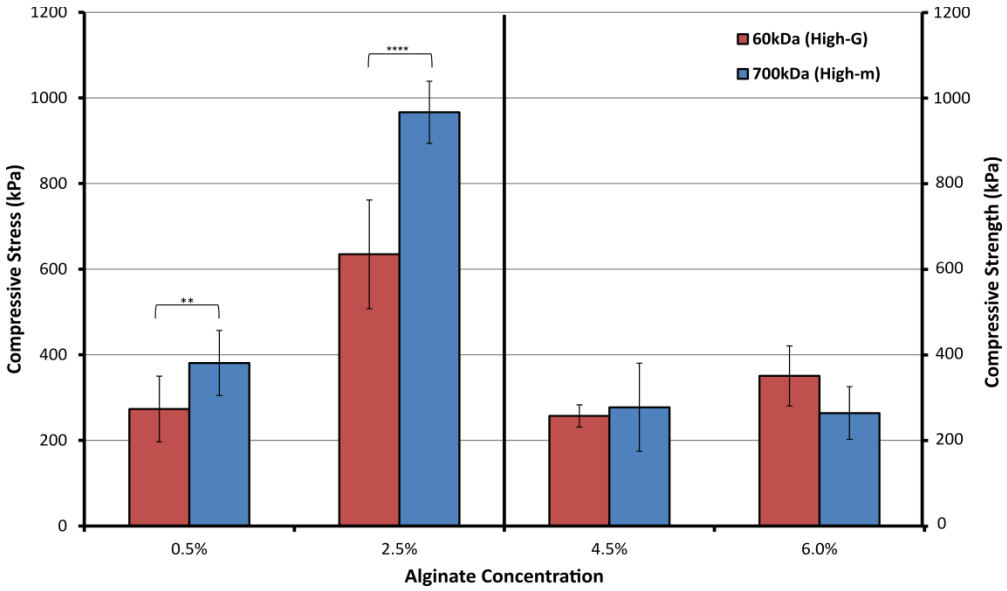

Figure 5.1.8 Compressive stress and strength up to 70% strain of the 60kDa and 700kDa following storage in DI at 37^{0}C for 7 days (n=5)

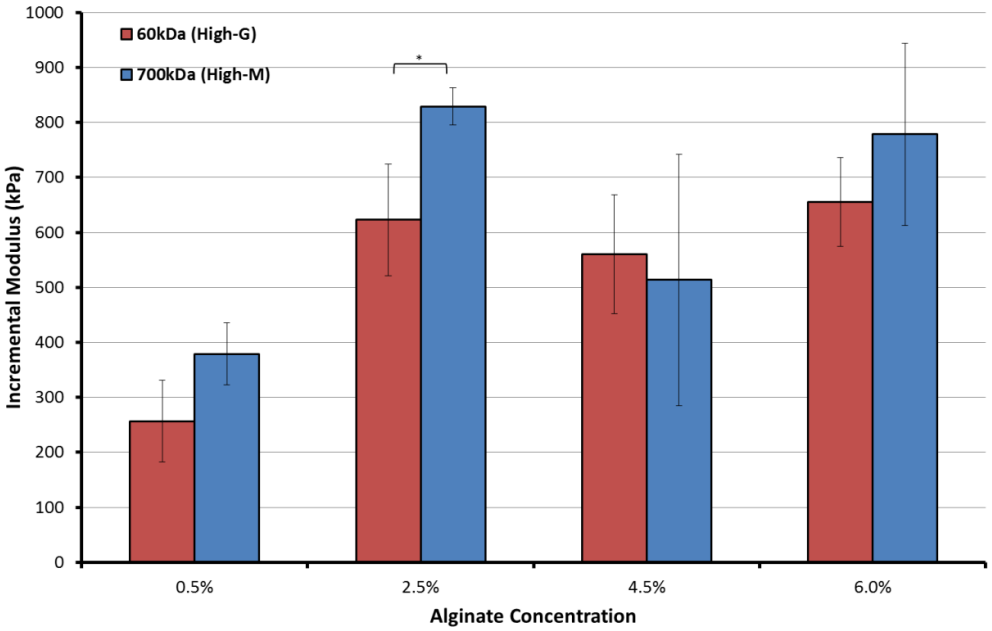

Figure 5.1.9 Incremental modulus (30-50% strain) of the 60kDa and 700kDa following storage in DI at 37^0C for 7 days (n=5)

To test this hypothesis and to examine the effects of increasing the crosslinking density, by increasing the availability of crosslinking ions, the 4.5% and 6.0% alginate concentration of the 700kDa alginate were tested with increasing glass contents (9.2% and 13.8%), shown in Figure 5.1.10 and Figure 5.1.11. The 700kDa alginate was examined here as it provided the highest compressive stress with the 4.6% glass content. Typical stress-strain graphs can be seen in Figure 9.5.11.

Increasing the glass content provided a significant increase in the strength and incremental modulus of the hydrogel at both a 4.5% and 6.0% alginate concentration. There is no significant difference in the strength when the glass content is increased from a 9.2% glass content to the 13.8% glass content. This is likely due to the GDL content of the alginate not being increased. This may cause the solution to not acidify sufficiently to cause a sufficient release of multivalent ions from the glass.

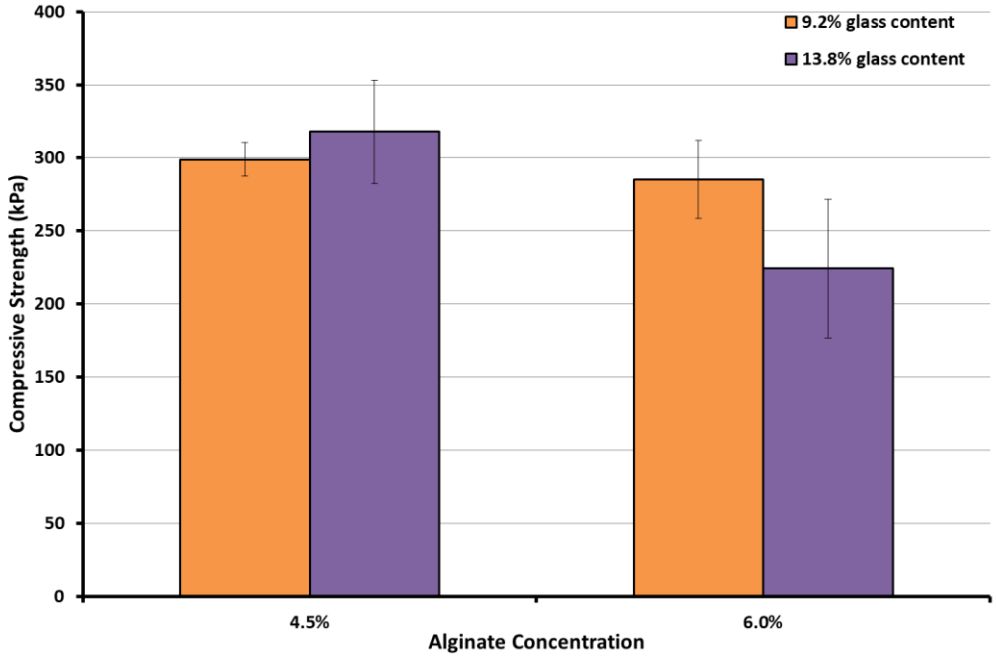

Figure 5.1.10 Compressive strength of the 4.5% and 6.0% 700kDa alginate with an increased glass content following storage for 1 day in DI at 37^0C

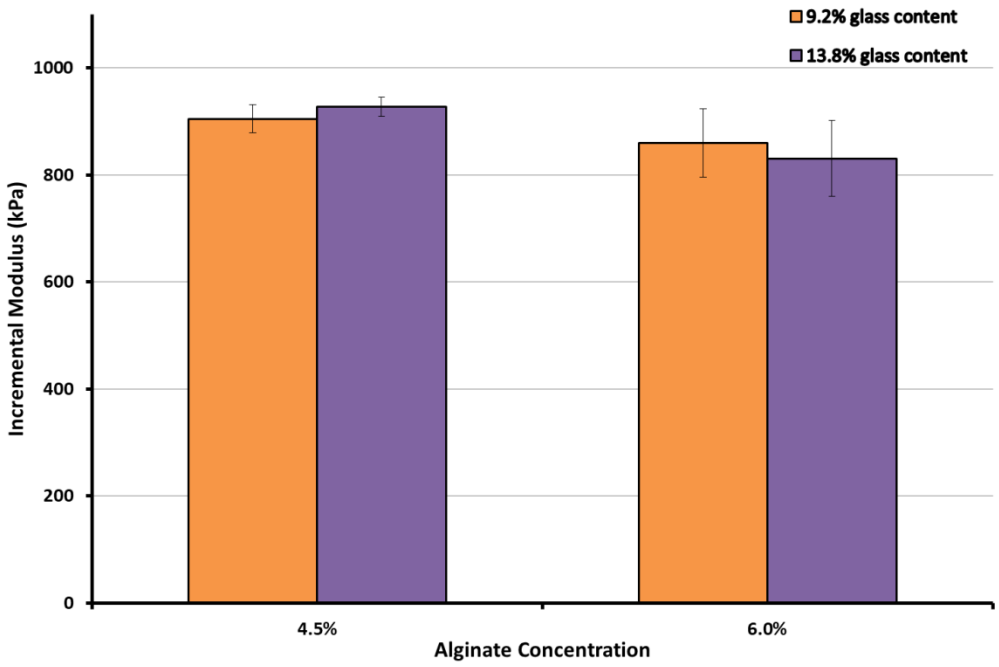

Figure 5.1.11 Incremental modulus (30-50% strain) of the 4.5% and 6.0% 700kDa alginate with an increased glass content following storage for 1 day in DI at 37^0C

5.1.6. Volume Conservation

In Figure 5.1.12 a considerable shrinkage of the samples at a 0.5% and 2.5% alginate concentration is observed when stored in DI for 7 days. The 4.5% alginate maintains the samples volume (<5% expansion), while the 6.0% expands considerably (~60%). There is a significant difference between the alginates' volumes at the 2.5% alginate concentration,

where the 700kDa shrinks 23% more compared to the 60kDa alginate. This is likely caused by the increased physical cross-linking density provided by an increased chain entanglement.

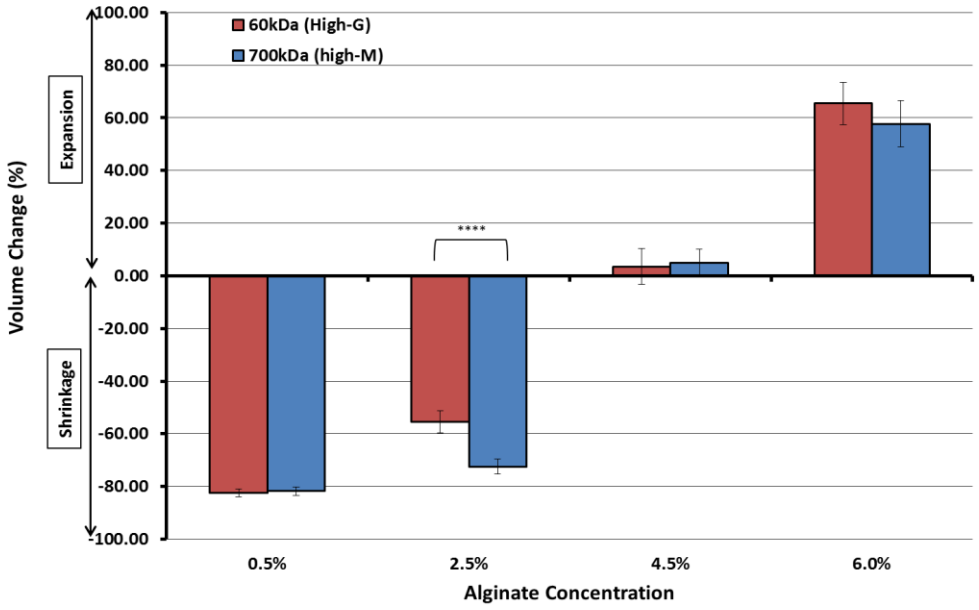

Figure 5.1.12 Size conservation after 7 days of 60kDa and 700kDa alginate at varying concentration with 4.6% glass and 4.15% (w/v) GDL (n=5) (n=5)

5.1.7. Working and Hardening Time

Figure 5.1.13 compares the working time of the 60kDa and the 700kDa alginate at 4 concentrations. As discussed previously, there is an optimum working time limit of between 10 and 30 minutes. The 60kDa is within this working time limit at each concentration, with working time decreasing linearly with increasing alginate concentration (R^2= 0.91). The 700kDa also decreases linearly with increasing alginate concentration (R^2= 0.94), however, only the 4.5% and 6.0% alginate concentrations are within the working time limits for this alginate. The hydrogel's working time decreases at a rate of 1 minute per 1% increase in alginate concentration for the 60kDa alginate and a 4 minutes decrease per 1% increase in alginate concentration for the 700kDa alginate.

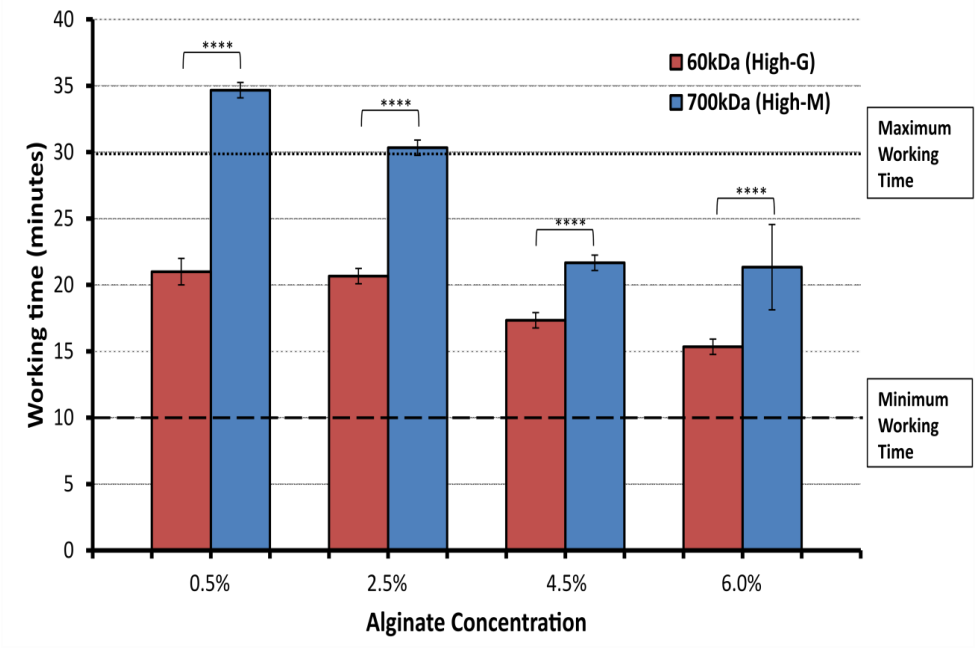

Figure 5.1.13 Working time of 60kDa and 700kDa alginate at varying concentration with 4.6% glass and 4.15% (w/v)GDL (n=5)

The hardening time, shown in Figure 5.1.14, shows a linear decrease with increasing alginate concentration for the 700kDa alginate (R^2= 0.93). Both the 60kDa and 700kDa alginate are only within the required hardening time requirements at the 4.5% and 6.0% alginate concentrations.

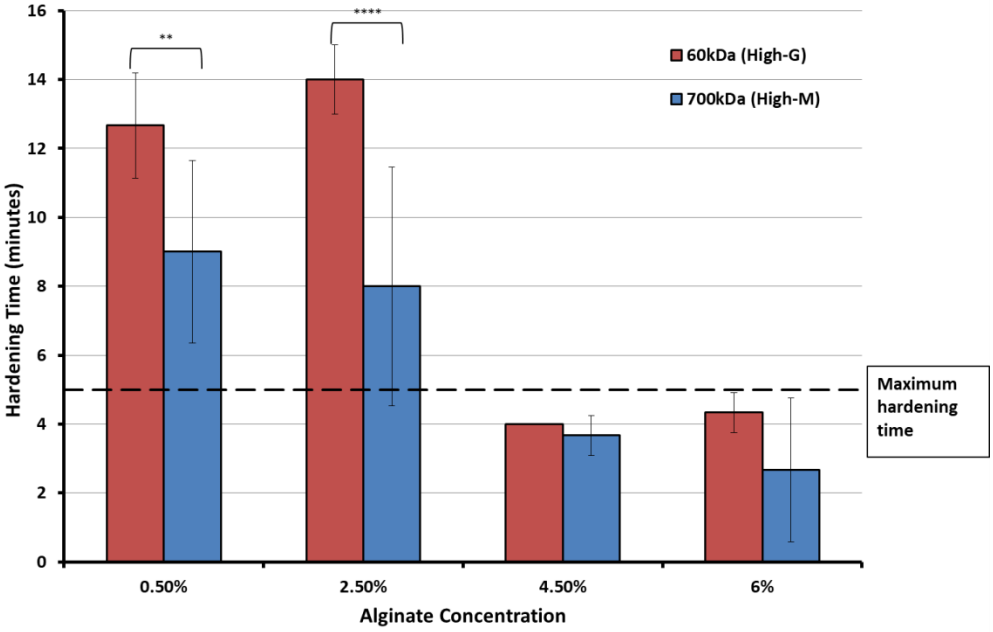

Figure 5.1.14 Hardening time of 60kDa and 700kDa alginate at varying concentration with 4.6% glass and 4.15% (w/v) GDL (n=5)

5.1.8. Deliverability

The deliverability of the hydrogel was examined by injecting the hydrogel through a 3F micro-catheter. The 0.5% alginate concentration of both the 60kDa and 700kDa was not sufficiently viscous (41-44mPa.s) to stay in the aneurysm when blood flow was applied. Both the 2.5% and 4.5% of the 60kDa and 700kDa could be injected through the micro-catheter up to 20 minutes following mixing. However, the 6.0% alginate concentration of the 60kDa and 700kDa alginate was too viscous (>10,000mPa.s) and could not inject through the 3F micro-catheter 2 minutes following mixing the hydrogel.

5.1.9. Discussion

From the GPC (Figure 5.1.2) and ^{1}H-NMR (Table 5.1.1) results it is clear that the two alginate manufacturing techniques produce two alginates with vastly different molecular weight and chemical composition. The alginate produced by Technique 1 is a low molecular weight (~60kDa), High-G alginate (F_g = 0.52) and the alginate produced using Technique 2 is a high molecular weight (~700kDa), High-M alginate (F_m = 0.63). 60kDa is an extremely low molecular weight compared to alginates discussed in the literature, while the 700kDa is extremely high [194] [202] [344] [345].

Small molecular weight chains (600Da) are visible in the 60kDa GPC results (Figure 5.1.2) which are absent from the 700kDa alginate. This may be caused by small polyphenol chains remaining in the 60kDa alginate that may have been removed from the 700kDa during the chloroform wash of the alginate during purification [346]. Failure to remove these small chains may cause an immune response as they are not involved in the gelling of the alginate and can leak from the hydrogel [347].

Viscosity typically relates to the molecular weight of the alginate [348]. However, it can be seen in Figure 5.1.3 that although the 700kDa alginates molecular weight is significantly greater than the 60kDa alginate, the viscosities are similar at each concentration. This may be caused by the different M/G ratio of the two alginates as the 60kDa alginate has a High-G content, with higher G content alginates typically being stiffer and more viscous [189] [349] [350]. It has been shown that varying the alginate purification method results in alginates with significantly different viscosities, when the alginates starting molecular and chemical composition was constant. The varying alginates and purification methods used here may have an additional effect on the viscosity of the alginate due to variances in residual salts and impurities and the resulting pH of the alginate solution [191] [346] [351].

As discussed previously, the strength of the hydrogel increased when the alginate content was increased from a 0.5% alginate concentration to a 2.5% alginate concentration and decreases with a further increase in alginate concentration. This is likely caused by a shortage

of cross-linking ions, reducing the cross-linking density. Figure 5.1.10 shows that increasing the glass content resulted in an increase in strength for the 4.5% and 6.0% alginate concentration suggesting that increasing the cross-linking density will provide the expected increase in strength.

Typically, the alginate with a high G-block content would provide the highest hydrogel strength due to increased chain stiffness and ions preferentially binding with G-blocks [349]. However, this is not observed to be the case here (Figure 5.1.8). As discussed previously, this may be caused by the significant increase in molecular weight of the 700kDa alginate providing an increase in chain entanglements, as both the M/G ratio and molecular weight can affect the strength of the hydrogel [186]. The effect of this variation on the incremental modulus (Figure 5.1.9) is reduced compared to that of the strength. This may be associated with alginates of a High-G content being stiffer [352]. It has also been suggested that the MG-blocks of alginate can also bind with Ca^{2+} ions [353] [354]. From Table 5.1.1 it can be seen that the 700kDa alginate has an increased MG-block compared to the 60kDa alginate which may contribute to the strength increase observed.

The results of the 700kDa alginate show a significant increase in strength of the hydrogel from 1 to 7 days of storage. Typically, ionically cross-linked hydrogels degrade over time, unless stored in solutions containing cross-linking ions [209]. This observed increase is likely due to the continued release of ions from the glass phase, which has previously been observed to occur in Glass Polyalkonate Cements (GPCs) [228].

The sample volume reduces (shrinks), following storage for 7 days in DI, at an alginate concentrations of 0.5% and 2.5% and expands at higher alginate concentrations of 4.5% and 6.0%. It is suggested that at the lower alginate concentration (<2.5%) there is an increased cross-linking density. An increased cross-linking density causes an increase in the elastic forces that can resist the swelling caused by water molecules diffusing into the hydrogel. As the alginate concentration increases, without an increase in available cross-linking cations, the cross-linking density decreases which allows water to diffuse into the hydrogel, increasing the samples size. These results are similar to results observed by Kuo *et al* [209], where increasing the cross-linking density caused shrinkage of the sample. This theory is supported by evidence presented in Figure 5.1.10, which shows that increasing the glass content causes an increase in strength, indicating that lack of availability of cross-link ions in the lower glass content results in a lower cross-link density. In the application, significant shrinking of the sample, as observed at a 0.5% and 2.5% alginate concentration, may cause blood ingress and recurrence when used as an aneurysm filler and significant expansion of the hydrogel may cause the aneurysm to rupture or blockage of the parent artery. Of the alginates tested, an alginate concentration of 4.5% causes the least change in sample volume

and suggests this alginate concentration with the glass and GDL content provided is the optimum cross-linking density to conserve the hydrogel volume.

Figure 5.1.13 shows that the 60kDa alginate has the shorter working time; while Figure 5.1.14 shows that the 700kDa alginate has the faster hardening time. This may be caused by the 60kDa alginate's increased G-block content, as multivalent ions preferentially bind with the G-block of alginate to form an egg-box dimer. As the hydrogels reach the end of the working time it is likely that the formation of egg-boxer dimers is reduced and the molecular weight of the alginate has a more dominant effect on the hydrogel. This suggests that the chemical composition of the alginate predominantly affects the working time of the hydrogel and the molecular weight of the alginate predominantly affects the hardening time [207]. Increasing the alginate concentration increases the chain entanglements and available locations for cross-linking, causing a reduction in working time and hardening time.

In situ forming alginate hydrogels have a wide range of gelation times, varying from 2 – 200 minutes, varying with alginate type, alginate concentration, cross-linker type and concentration. The hydrogel produced is within the wide gelation rate range but has a higher strength than hydrogels with similar gelation rates [195] [202] [344] [355] [356].

The viscosity of the ungelled alginate affects the deliverability of the hydrogel. The injected hydrogel's viscosity must be sufficient to stay within the aneurysm with applied blood flow while not being too viscous that it requires excessive force to inject through a micro-catheter. The hydrogels with an initial alginate viscosity of 2000-9000mPa.s (2.5% and 4.5% alginate concentrations) are injectable through a 3F micro-catheter. Hydrogels with an alginate of an initial viscosity >10,000mPa.s could not inject through a micro-catheter.

It can be seen from the results that the alginate molecular weight, chemical composition and concentration affects compressive strength, viscosity, working time, hardening time and deliverability of the hydrogel. The cross-linking density of the hydrogel is also important to control the strength and volume conservation. At a 0.5% alginate concentration there is likely a shortage of alginate chains and an excess of cations. At 4.5% and 6.0% alginate concentrations there is a shortage of cross-linking ions and, as a results, there are alginate chains that are not completely cross-linked. The gelation rate of the hydrogel can be easily controlled by the alginate concentration, with is indicated by the linear decrease in working and hardening times. This may be an advantage if the gelation rate needs to be altered; however the effects alginate concentration has on strength, size conservation and injectability need to be taken into consideration. The hydrogels tested can be used for a wide range of applications; however, only the 4.5% alginate concentration of the 60kDa and 700kDa alginate met the requirements discussed for the use of the hydrogel as a cerebral

aneurysm filler. These requirements are shown in Table 5.1.2. It was decided to only continue testing with 700kDa due to this alginate producing a higher strength hydrogel compared to the 60kDa.

Table 5.1.2 60kDa and 700kDa alginate design review table

Sample	Alginate Concentration	Compressive Strength >22kPa?	Is the material size conserved? (<10% expansion with no shrinkage)	Is the hydrogel injectable?	Working Time between 10 and 30 mins?	Hardening Time <5 mins?	Is the material adhesive?	Is the material cytocompatible? (>70% cell viability)	Is the material sterilisable?	Is the material suitably radiopaque?	Is the material haemocompatible?
60kDa	0.5%	Yes	No	No	No	No	TBD	TBD	TBD	TBD	TBD
	2.5%	Yes	No	Yes	No	No	TBD	TBD	TBD	TBD	TBD
	4.5%*	Yes	Yes	Yes	Yes	Yes	TBD	TBD	TBD	TBD	TBD
	6%	Yes	No	No	Yes	Yes	TBD	TBD	TBD	TBD	TBD
700kDa	0.5%	Yes	No	No	No	No	TBD	TBD	TBD	TBD	TBD
	2.5%	Yes	No	Yes	No	No	TBD	TBD	TBD	TBD	TBD
	4.5%**	Yes	Yes	Yes	Yes	Yes	TBD	TBD	TBD	TBD	TBD
	6%	Yes	No	No	Yes	Yes	TBD	TBD	TBD	TBD	TBD

** Provided improved compressive strength (277 kPa) compared to * (257 kPa) after 7 days.

5.2. Effect of Gamma Irradiation of Alginate

In order to examine a third molecular weight with no change to chemical composition, a sample of the 700kDa alginate was gamma irradiated at 25kGy. Gamma irradiation was selected as it has been shown to cause chain scissions while sterilising the alginate [357]. The samples were gamma irradiated at 25kGy as it is the accepted dose for complete sterilisation. The molecular weight, chemical composition, viscosity, compressive strength, volume conservation, working time, hardening time and deliverability were examined to determine the effects that gamma irradiation has on the alginate and hydrogel produced.

The results of the non-irradiated 700kDa (High-M) alginate were discussed previously in Section 5.1. The gamma irradiated alginate was tested under the same conditions and alginate concentrations as the 60kDa (High-G) and 700kDa (High-M) alginate.

5.2.1. Gel Permeation Chromatography

Figure 5.2.1 shows that gamma irradiation of the alginate causes a large decrease in the alginate molecular weight. This decrease is likely due to scissions in the glycosidic bonds, as observed elsewhere [217] [357]–[359].

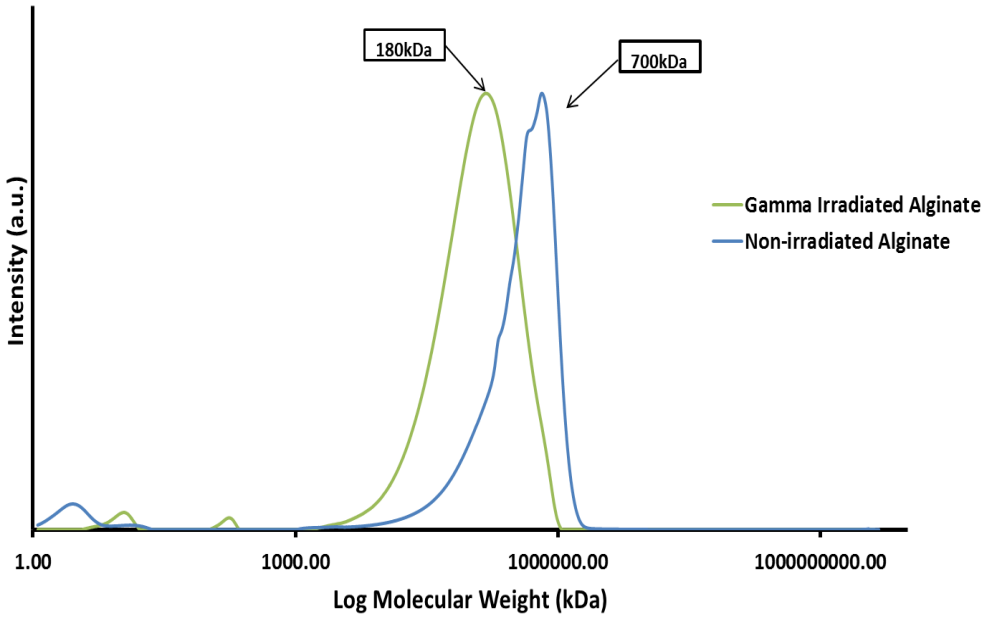

Figure 5.2.1 GPC of gamma irradiated and non-irradiated (700kDa - High-M) alginate

Using Equation 5.2.1 it was calculated that gamma irradiation causes approximately 2.88 chain breaks per molecule.

Equation 5.2.1 Chain Breaks per Molecule [357]

$$N = \frac{M_o}{M} - 1$$

Where;

M_o = original molecular weight
M = molecular weight of the alginate following irradiation

5.2.2. Nuclear Magnetic Resonance Spectroscopy

It has been observed elsewhere that gamma irradiation can cause a change in the M/G ratio of alginate at a lower rate of irradiation [357]. In this case, Table 5.2.1 shows that gamma irradiation has no significant effect on the chemical composition of the alginate tested here. However, there is a shortening in the average G-block length due to a reduction in the MGM-block.

Table 5.2.1 Alginate chemical composition

	Molecular weight	F_G	F_M	M/G	F_{GG}	F_{MM}	F_{MG}	$\bar{N}_{G>1}$
Gamma irradiated alginate	**180kDa**	0.37	0.63	1.7	0.18	0.45	0.18	3.59
Non-irradiated alginate	**700kDa**	0.37	0.63	1.7	0.18	0.45	0.18	2.68

5.2.3. Viscosity

Gamma irradiation of the alginate has a large effect on the alginate viscosity, shown in Figure 5.2.2. Although the alginate viscosity increases with increasing alginate concentration, there is a significant difference in viscosity at each concentration when compared to the non-irradiated alginate.

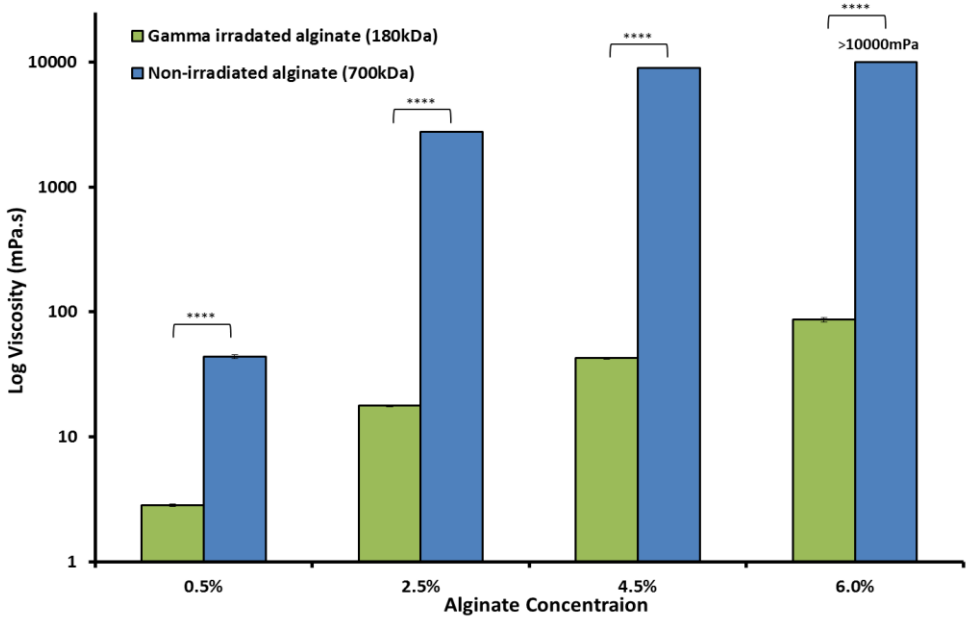

Figure 5.2.2 Viscosity of the gamma irradiated and non-irradiated alginate at four increasing concentrations (n=5)

5.2.4. Compressive Strength

Figure 5.2.3 and Figure 5.2.4 shows that the reduced molecular weight causes a significant decrease in compressive strength and incremental modulus after storage for 7 days. There is a linear reduction in hydrogel strength with increased alginate concentration for the 180kDa (R^2 = 0.90). As with the 60kDa and 700kDa, this strength decreases with increasing alginate concentration was not expected and may be caused by a number of reasons such as reduction in chain entanglements, cross-linking density, swelling of the hydrogel or an increase in chain ends. The gamma irradiated alginate is still providing the required strength (22kPa) at 6.0% alginate concentration despite a significant decrease in strength.

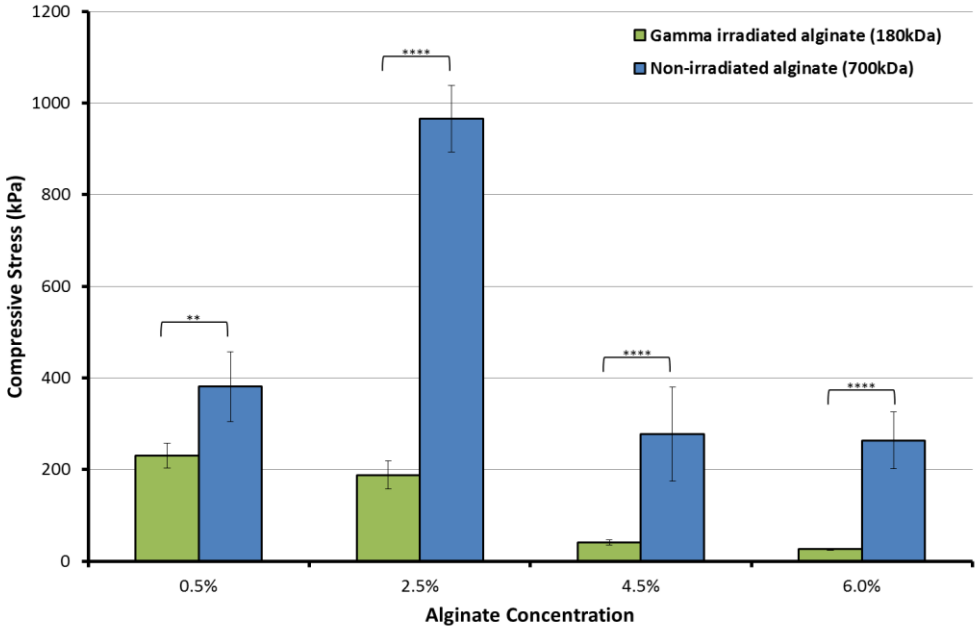

Figure 5.2.3 Compressive stress up to 70% strain of the gamma irradiated and non-irradiated alginate following storage in DI at 37^0C for 7 days (n=5)

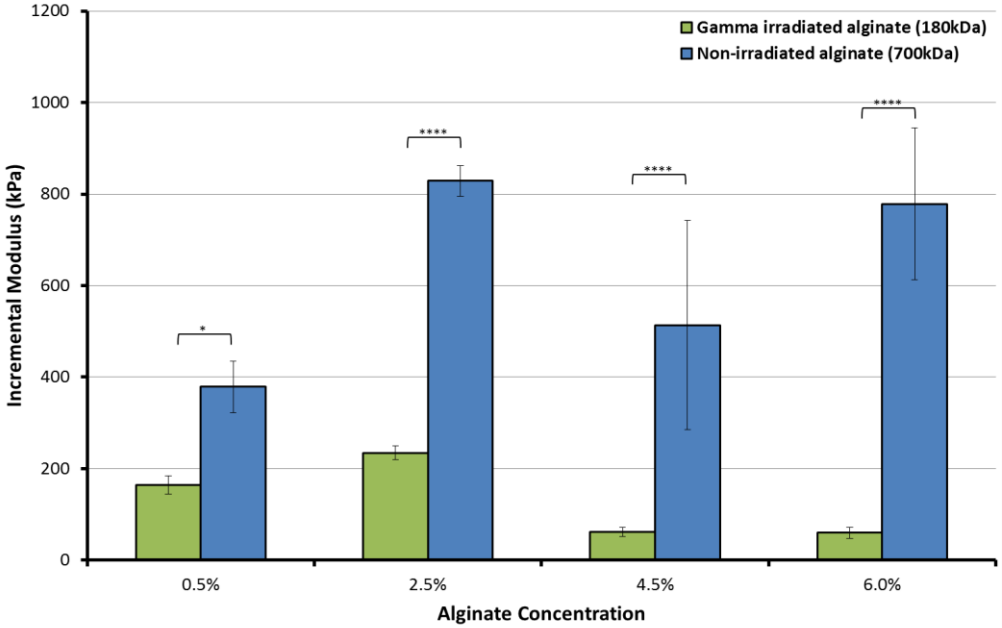

Figure 5.2.4 Incremental modulus (30-50% strain) of the gamma irradiated and non-irradiated alginate following storage in DI at 37^0C for 7 days (n=5)

5.2.5. Volume Conservation

Figure 5.2.5 shows a shrinking of the alginate at 0.5% and 2.5% for both alginates. There is also an expansion of both the alginate at 4.5% and 6.0% alginate concentration. Although there is a significant difference the irradiated and non-irradiated sample at the 2.5% and 6.0% alginate concentration, the change in volume remains significant when compared to the original sample size. The alginate concentration of 4.5% provides the minimum change in volume after 7 days.

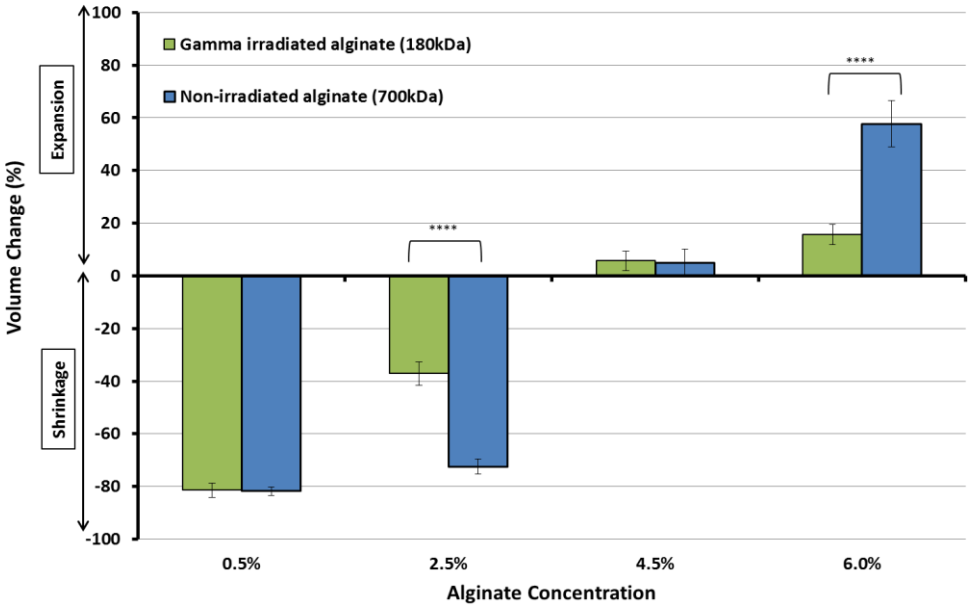

Figure 5.2.5 Gamma irradiated and non-irradiated alginate size conservation after 7 days (n=5)

5.2.6. Working and Hardening Time

Gamma irradiation causes a significant increase in the working time of the hydrogel, see Figure 5.2.6. The gamma irradiated alginate working time decreases linearly with increased alginate concentration (R^2 = 0.91) but remains outside the working time requirements at each alginate concentration tested.

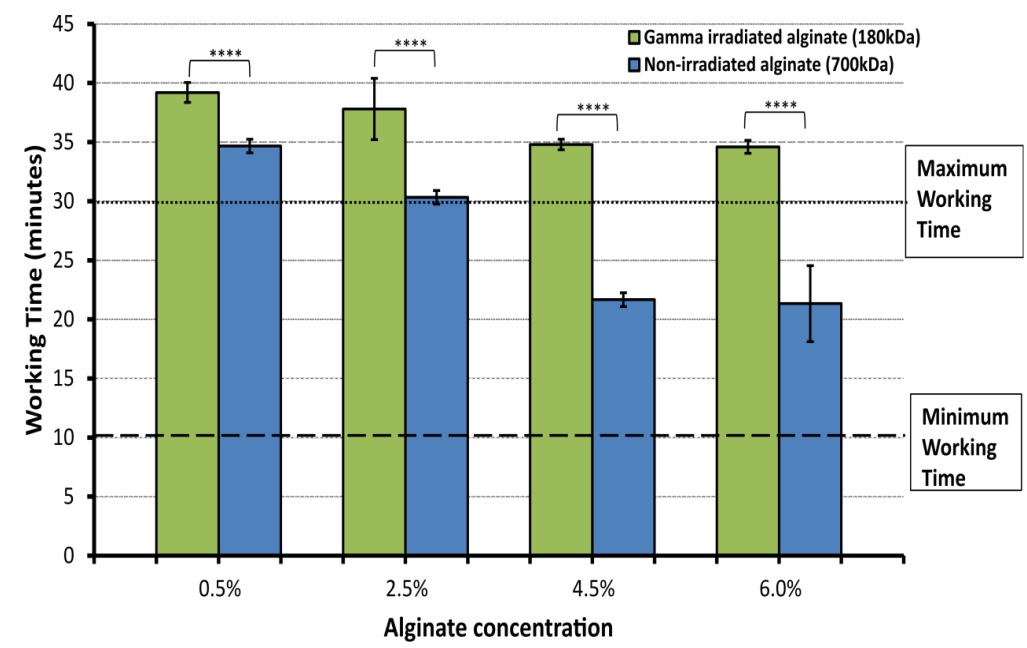

Figure 5.2.6 Gamma irradiated and non-irradiated alginate working time (n=5)

It can be seen in Figure 5.2.7 that the gamma irradiated alginate hardening time also decreases linearly (R^2 = 0.91) but remains outside the hardening time requirements.

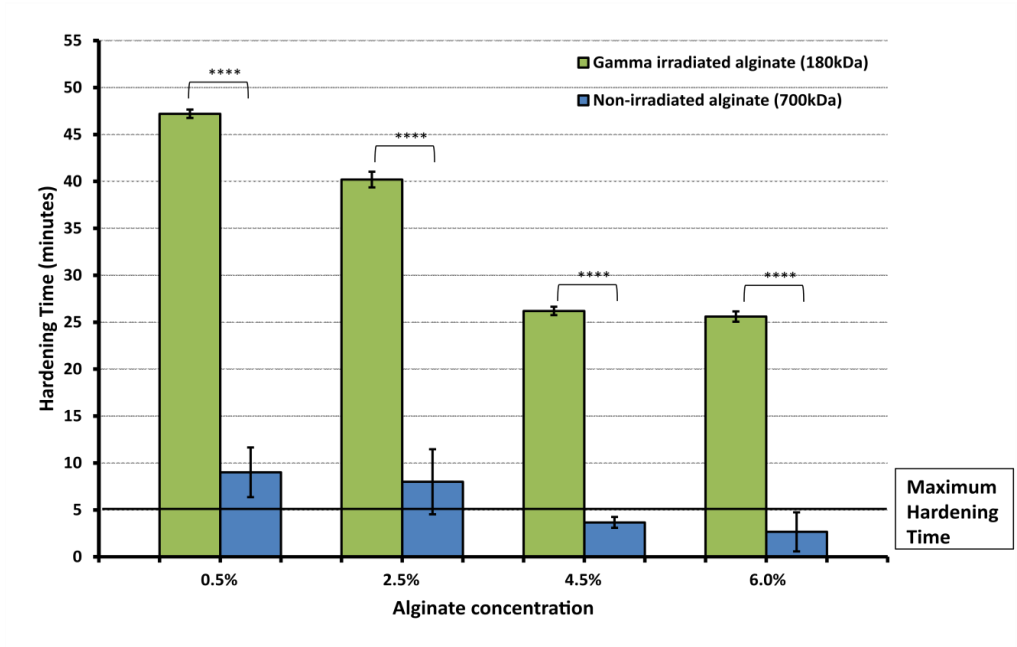

Figure 5.2.7 Gamma irradiated and non-irradiated alginate hardening time (n=5)

5.2.7. Deliverability

The hydrogels produced with the gamma irradiated alginate at each concentration tested could inject through a micro-catheter but did not exhibit the required viscosity to remain in the aneurysm when blood flow was applied.

5.2.8. Discussion

Gamma irradiation has no significant effect on the alginate chemical composition but greatly affects the molecular weight. This decrease in alginate molecular weight is likely caused by a scission of glycosidic bonds occurring during gamma irradiation [357]. There was approximately 2.88 chain breaks per molecule, which has been closely observed elsewhere for a 25kGy dose [357].

The decrease in alginate molecular weight shows a significant decrease in the ungelled alginates viscosity (Figure 5.2.2). This has been previously observed and is caused by a decrease in chain entanglements [195] [202] [346] [360].

Along with a significant decrease in alginate viscosity, gamma irradiated alginate exhibits strengths significantly decreased when compared to the non-irradiated alginate. As with the 60kDa and 700kDa, the hydrogels strength was expected to increase with increasing alginate concentration. This was not seen here, with the hydrogel's strength linearly decreasing with increasing alginate concentration. This may be caused by a combination of factors with the reduced molecular weight. The results indicate that the cross-linking density is reduced with increasing alginate concentration, as the hydrogel swells. The reduction in molecular weight will likely reduce steric hindrance, providing an increased number of available carboxylic bonds, resulting in a lack of sufficient cross-linking cations at a lower alginate concentration than its high molecular weight counterpart. A further increase in the alginate concentration reduces the hydrogel's cross-linking density further. This lower cross-linking and hydrogel swelling will reduce physical cross-links caused by chain entanglements. Another possible explanation is the reduced molecular weight of the alginate may have an increased number of "weak spots" caused by an increase in chain ends. [175] [361] [362] [359].

The volume change of the hydrogel is likely related to the hydrogel's cross-linking density. It can be seen in Figure 5.2.5 that the gamma-irradiated alginate hydrogel has no significant difference in volume change at 0.5% and 4.5% compared to the non-irradiated alginate hydrogel. However, the shrinkage at a 2.5% alginate concentration and the expansion at a 6.0% alginate concentration are significantly reduced in the gamma irradiated alginate. The similar shrinkage of approximately 80% in both the gamma irradiated and non-irradiated samples at a 0.5% alginate concentration suggests that both hydrogels have a high cross-linking density and have reduced in size the maximum amount permitted by the hydrogel. At

a 2.5% concentration, the gamma irradiated alginate has a reduced volume change compared to the non-irradiated samples. This is likely caused by a decrease in cross-linking density. This increased expansion of the hydrogel would be expected to continue, though this does not occur. This may be caused by the ion release from the gamma irradiated hydrogel being increased compared to the non-irradiated sample. This may cause the cross-linking ion content of the storage medium to increase, which would reduce sample volume change [363].

Figure 5.2.6 and Figure 5.2.7 shows a significant increase in the working time and hardening time of the gamma irradiated alginate hydrogel compared to the non-irradiated alginate hydrogel at each concentration tested. There is a greater difference in the hardening time between the gamma irradiated alginate hydrogel and non-irradiated alginate hydrogel compared to the working time. This correlates with the previous hypothesis that the alginates molecular weight has a predominate effect on the hardening time of the hydrogel. The gelation of the alginate is likely caused by the ionic cross-linking of the alginate chains and the physical chain entanglements. As 180kDa has a reduced number of chain entanglements, steric hindrance is reduced which allows ionic gelation to occur at a quicker rate compared to a high molecular weight alginate. However, high molecular weight alginates have increased chain entanglements to increase their viscosity, without the requirement of ionic cross-linking [195]. The reduced steric hindrance is likely improving the working time of the gamma irradiated hydrogel. However, the hardening time of the alginate relies on the hydrogel to have a sufficient strength to hold 17kPa. The gamma irradiated alginate will likely require an increase in ionic cross-linking density compared to that of the 700kDa alginate due to reduced chain entanglements. This is achieved by the release of ions from the bioactive glass over time.

The decrease in strength, increase in working time and hardening time and poor injectability of the resulting hydrogel at each concentration does not fulfil the requirements of the hydrogel for the use as a cerebral aneurysm treatment. The strength, working time, hardening time, viscosity and deliverability of the hydrogel with the gamma irradiated alginate may be improved by increasing the alginate concentration, glass and GDL content. However, other methods of sterilisation such as filtration or autoclaving, discussed in Section 2.4.5, may be a more cost effective solution for sterilising the alginate. The gamma irradiated alginate may have other uses in applications which allow a greater working and hardening time and where strength is not required to be as high, such as cell and growth factor delivery, nerve regeneration and wound healing [61] [191]. Due to the results shown in Table 5.2.2, for this particular application, it was decided to continue testing with the non-irradiated 700kDa High-M alginate at an alginate concentration of 4.5%.

Table 5.2.2 Gamma irradiated and non-irradiated alginate design review

Sample	Alginate Concentration	Compressive Strength >22kPa?	Is the material size conserved? (<10% expansion with no shrinkage)	Is the hydrogel injectable?	Working Time between 10 and 30 mins?	Hardening Time <5 mins?	Is the material adhesive?	Is the material cytocompatible? (>70% cell viability)	Is the material sterilisable?	Is the material suitably radiopaque?	Is the material haemocompatible?
Gamma irradiated alginate	**0.5%**	Yes	No	No	No	No	TBD	TBD	TBD	TBD	TBD
	2.5%	Yes	No	No	No	No	TBD	TBD	TBD	TBD	TBD
	4.5%	Yes	Yes	No	No	No	TBD	TBD	TBD	TBD	TBD
	6%	Yes	No	No	No	No	TBD	TBD	TBD	TBD	TBD
Non-irradiated alginate	**0.5%**	Yes	No	No	No	No	TBD	TBD	TBD	TBD	TBD
	2.5%	Yes	No	Yes	No	No	TBD	TBD	TBD	TBD	TBD
	4.5%	Yes	Yes	Yes	Yes	Yes	TBD	TBD	TBD	TBD	TBD
	6%	Yes	No	No	Yes	Yes	TBD	TBD	TBD	TBD	TBD

5.3. Effect of Acid Washing Glass and Increasing Glass Content

The hydrogel tested to date had visible agglomerations/clumps of glass; producing an inhomogeneous hydrogel, which is commonly observed [239] [364]. In an attempt to increase the homogeneity of the hydrogel it was decided to examine the effects of acid washing the glass, as this has been shown to reduce agglomerations in other glass containing composites [228][365]. From the results discussed in Section 5.1 and 5.2, it was decided to use the 700kDa alginate at a 4.5% alginate concentration and the effects of varying the glass and GDL content were examined. The results of the untreated glass have been examined in Section 5.1 and will be compared here to the acid washed glass.

5.3.1. Particle size analysis

Figure 5.3.1 shows the particle size analysis of the acid washed glass and untreated glass. Acid washing the glass reduced the relative quantity of the fine particles.

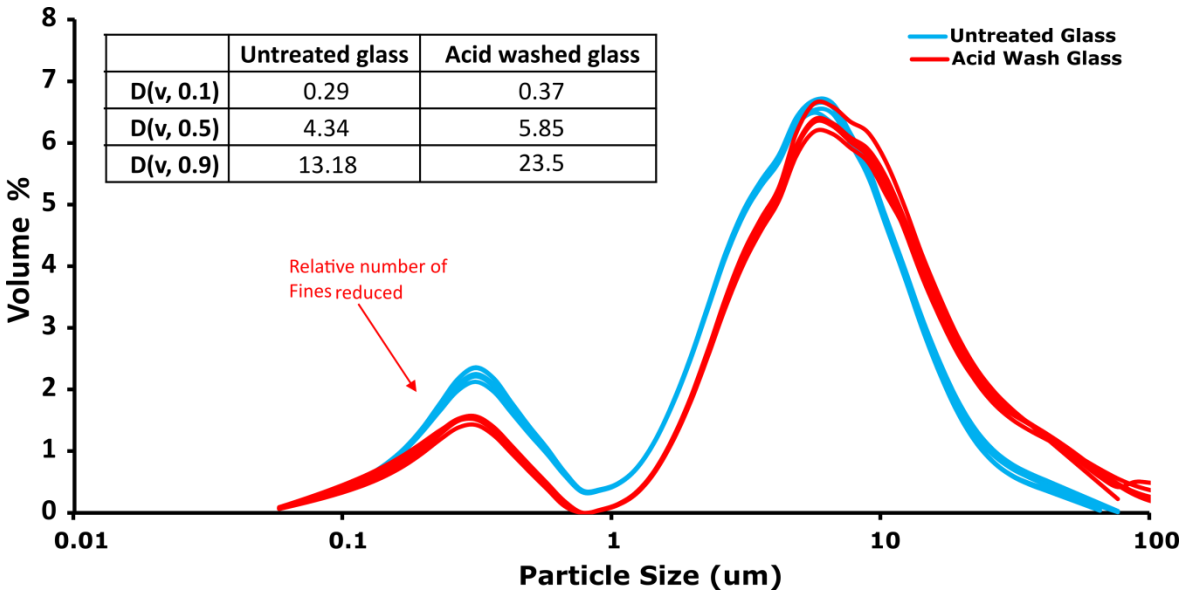

Figure 5.3.1 Particle size analysis of untreated and acid washed glass

5.3.2. Nitrogen Adsorption/Desorption Measurements

The nitrogen adsorption results (Table 5.3.1) indicates an increased BET calculated surface area of the acid washed glass particles compared to that of the untreated glass. Nitrogen adsorption results, calculated by BJH, indicate an increased pore diameter and decreased pore volume, which would indicate a widening and decrease in depth of the pores, most likely indicating some surface erosion.

Table 5.3.1 Brunauer Emmett Teller (BET) adsorption and Barrett-Joyner-Halenda (BJH) desorption pore volume analysis.

	BET Surface Area (m^2/g):	BJH Pore Volume (cc/g):	BJH Pore Radius (nm):
Untreated Glass	2.375	0.009	1.5466
Acid washed Glass	2.552	0.007	1.9399

5.3.3. Zeta Potential Measurements

Acid washing was shown to decrease the negative zeta potential on the glass surface (Table 5.3.2) which in the case of glasses is indicative of increased hydrophilicity.

Table 5.3.2 Zeta potential measurements of untreated and acid washed glass.

	Zeta (mV):	Zeta Stdev:
Untreated Glass	-18.8	0.603
Acid Washed Glass	-9.31	0.276

5.3.4. X-Ray Photoelectron Spectroscopy

Quantitative XPS was carried out on untreated and acid washed glass to characterise the surface properties. It can be seen in Figure 5.3.3 that the surface Ca/Ga ratio decreases from 1.5 in the untreated glass to 0.3 in the acid washed glass, indicating that calcium is being preferentially leached from the surface of the glass particles, which is a noted result of acid washing glass [228]. This may also indicate migration of the Ga^{3+} from the internal structure to the surface of the glass, as the Ga/Si ratio increases from 0.94 to 1.5 with acid washing. A significant decrease in the surface Ca/P ratio is observed after acid washing the glass. This reduction from 2.2 to 0.49 will likely have a significant effect on the potential formation of a hydroxyapatite layer on the surface of the glass [366].

Table 5.3.3 Composition (atomic %) from XPS of untreated and acid washed glass

Sample:	O	Ga	Ca	Si	P	C
Untreated Glass	55.4	5.7	8.7	6.0	3.9	20.4
Acid Washed Glass	58.6	9.0	2.9	5.8	5.9	17.7

Figure 5.3.2 shows the high resolution O_{1s} XPS spectra for the untreated and acid washed glasses, indicating a peak at 531.4eV for the untreated sample and 532.0eV for the acid washed sample. This shift in O_{1S} to a higher binding energy with acid washing indicates a higher glass network connectivity (NC) of the acid washed glass surface. Deconvolution of these peaks into their bridging oxygen (BO, 532.0 eV) and non-bridging oxygen (NBO, 531.0 eV) components indicates a considerably lower non-bridging oxygen content on the surface of the acid washed sample. The ratio of non-bridging oxygens to bridging oxygens on the surface of the untreated glass are calculated as 1.1, indicating a Q_2 type surface structure, however, after acid treatment this decreases to 0.1, indicating a shift to a higher NC type

surface structure (Q_3/Q_4). This higher network connectivity may be the result of silica condensation or repolymerisation in the surface layer following removal of the divalent calcium ions, which usually acts as a network modifier. Similar results were observed by Tsomaia et al. in aluminosilicate glasses [367].

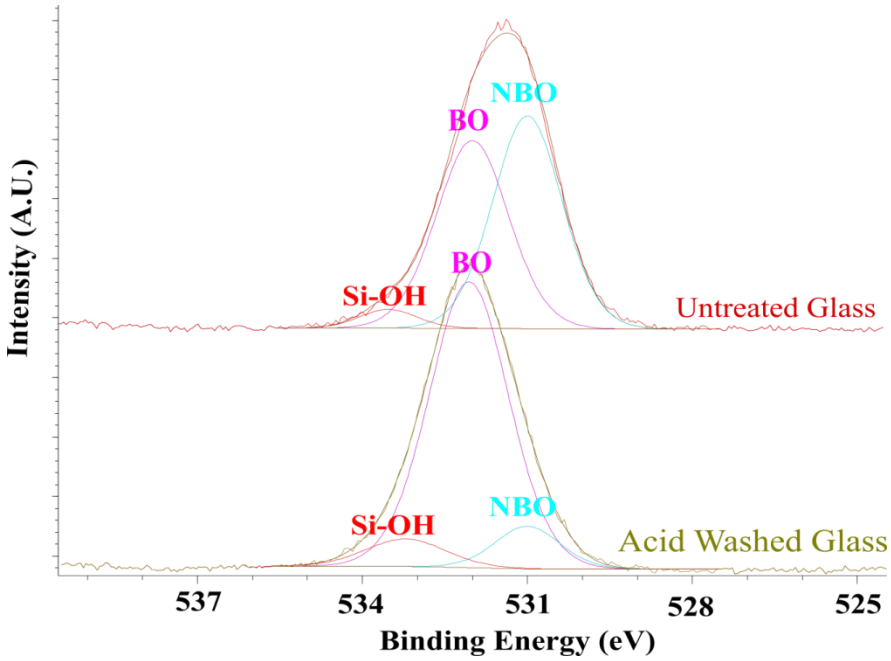

Figure 5.3.2 High resolution O_{1s} spectra for untreated and acid washed glass.

Deconvolution of the O_{1s} spectra also gives a third component peak (> 533eV) that can be assigned to Si-OH groups [368]. There is a doubling of the content of silanol groups on the acid washed glass surface compared to the untreated sample, which is likely to account for the improved homogeneity of the resultant hydrogel sample.

From Figure 5.3.3 it can be seen that the surface Ga_{2p} signal is 1118.2eV for the untreated glass and 1118.6eV for the acid washed glass. These results are both higher than that of β-Ga_2O_3 (1117.9eV) [369], which contains an equal mixture of tetrahedral and octahedral gallium oxide. The binding energy, however, is lower than that of $Ga(PO)_4$ (1119.3 eV) [370], which has a tetrahedral, charge balanced four coordinate structure. This indicates that the surface composition of the acid washed glass has a greater level of tetrahedral gallium compared to octahedral gallium.

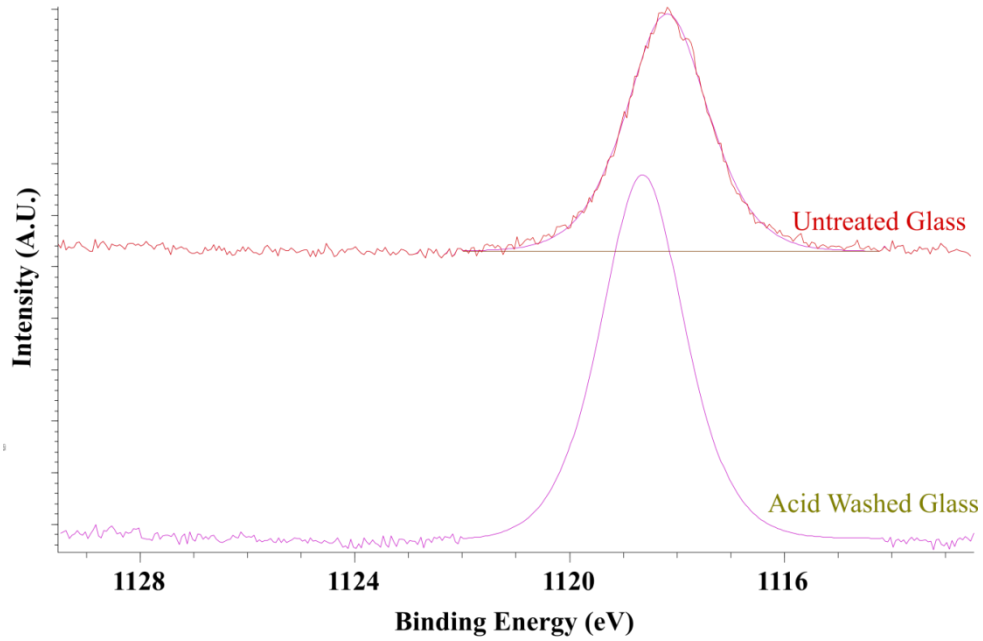

Figure 5.3.3 High resolution $Ga_{2p3/2}$ spectra for untreated and acid washed glass.

From Figure 5.3.4 three peaks can be observed, with the higher binding energy peaks being a result of overlap with the Ga_{3p} binding energies and only the lower Si_{2p} peak (~102eV) being related to the silicate structure. A slight shift in Si_{2p} peak (102.3eV to 102.8eV) is observed with acid washing. The Ga_{2p} is also shifted to higher binding energies with acid washing. The positive shift in binding energy of both $Ga_{2p3/2}$ and Si_{2p} peak can be viewed as reinforcement of the network with more polymerised Si^{4+} and charge balanced Ga^{3+} species.

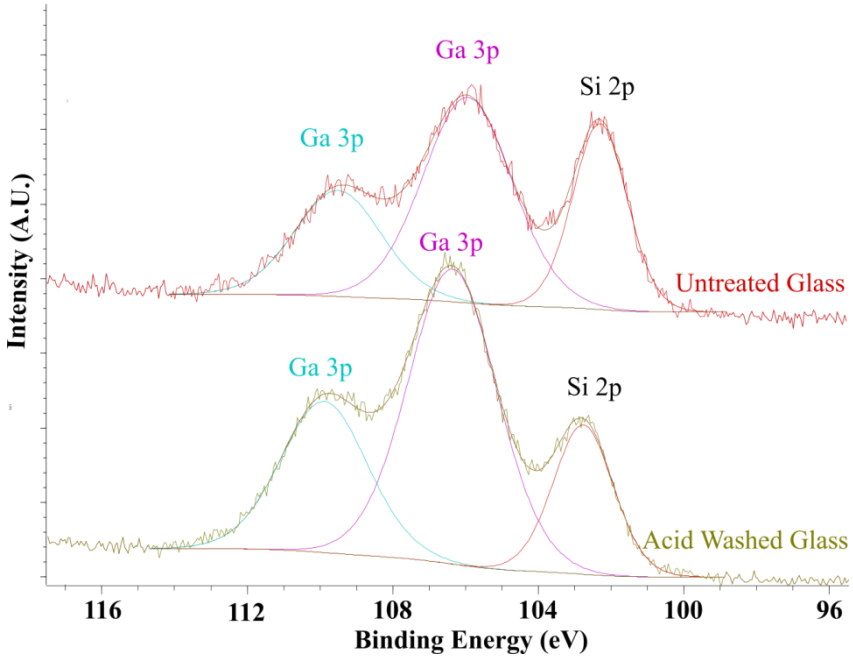

Figure 5.3.4 Si_{2p} X-ray Photoelectron Spectroscopy trace for untreated and acid washed glass

Using Equation 5.3.1 and the method outlined by Sekita et al. we can estimate the percentage of gallium ions tetrahedrally coordinated on the untreated glass surface as 74%, leaving 26%

in an octahedral coordination [371]. These calculations use assumptions that are not valid for the acid washed sample as we are unsure how much gallium remains after acid washing. From the O_{S1} and $Ga_{2p3/2}$ shifts it is likely that an increased number of gallium ions are tetrahedrally coordinated on the surface of the acid washed glass.

Equation 5.3.1 Estimation of the % of tetrahedrally coordinated ions

$$r(O^0) = \frac{n(O^0)}{n(O^0)+n(O^-)} = \frac{4\times n(Si,Ga)-n(O)}{n(O)}$$

Previously it has been seen that in aluminosilicate glasses, chemically similar aluminium ions are observed to convert from tetrahedral to octahedral upon reaching this acid leached silica rich surface layer. As galliumsilicate glasses are similar to aluminosilicate glass, a similar result was expected but it is not seen here. This further adds to the increase in network connectivity of the glass [365] [372].

5.3.5. Fourier Transform Infrared Spectroscopy

ATR-FTIR shows an asymmetric stretching of a Si-O-Si at ~1070cm^{-1} and a hydroxyl peak at 3,500cm^{-1}, which is completely absent in the untreated sample (Figure 5.3.5). This indicates that increased hydroxylation of the surface may have occurred, correlating with the XPS and zeta potential results. This might be expected due to treatment of a silica glass surface with an acidic proton donor.

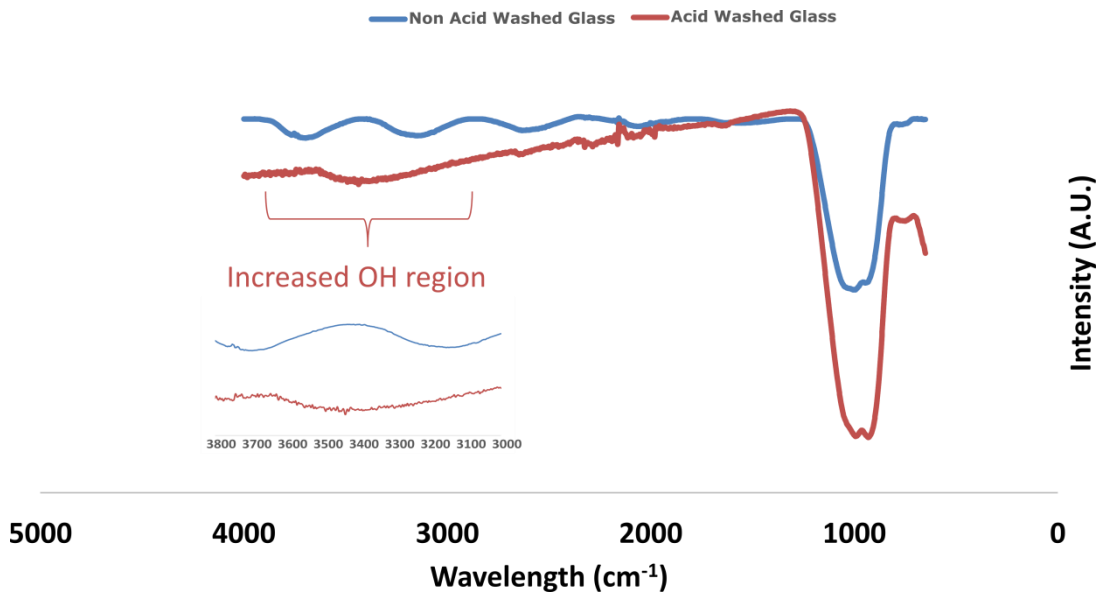

Figure 5.3.5 Attenuated Total Reflectance Fourier Transform Infrared Spectroscopy of acid washed glass particles

5.3.6. Field Emission Scanning Electron Spectroscopy

FE-SEM at 100,000x magnification, shown in Figure 5.3.6, indicates a considerably rougher surface topography for the acid washed glass, compared to the untreated glass surface. This

correlates well with the pore radius found using nitrogen adsorption/desorption results (Table 5.3.1).

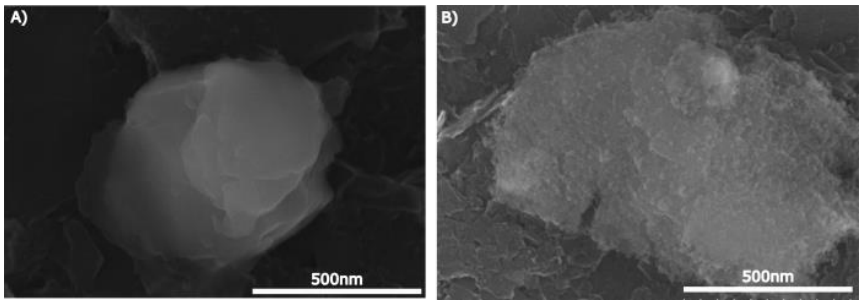

Figure 5.3.6 Field Emission Scanning Electron Microscopy of a) untreated glass and b) acid washed glass at X100k.

5.3.7. Compressive Strength

Figure 5.3.7 and Figure 5.3.8 compares the compressive strength and incremental modulus of the hydrogels produced with untreated and acid washed glass, following storage in DI at 37^0C for 1, 3 & 7 days.

There is a significant difference in strength between hydrogels produced using untreated and acid washed glasses. At day 1 and day 7 the acid washed glass hydrogel is significantly stronger than that of the non-acid washed glass; however the opposite is the case for day 3. It is uncertain what is causing this but it may be the varied kinetics of the release of ions from the glass surface. The acid washed glass has an increased gallium surface content which may account for the improved strength at day 1. At day 3, however, there may be an outflow of the calcium ions from the hydrogel of the acid washed glass. The untreated glass may continue to strengthen due to the higher calcium surface content providing a higher ion concentration and the later release of gallium. At day 7 there is a significant decrease in the hydrogel's strength with the untreated glass. This is likely caused by the glass agglomerations causing areas of varying cross-linking density that reduces the hydrogel's strength, which is commonly observed for inhomogeneous hydrogels. As the cross-linking density increases overtime, the hydrogel will have areas with increasing strength variation. The lower cross-linked areas are likely acting as weak spots in the hydrogel [356] [373]–[376].

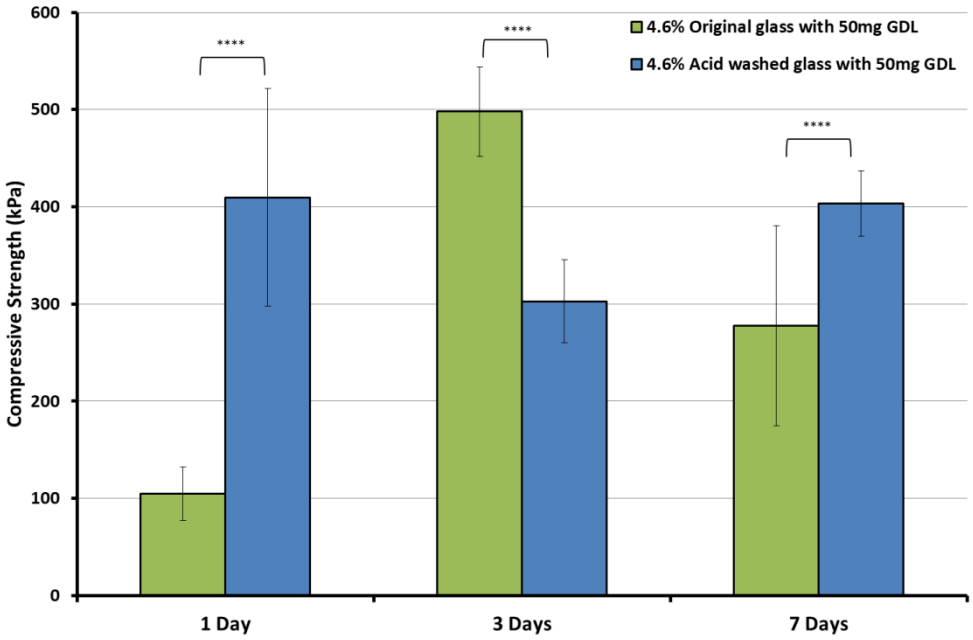

Figure 5.3.7 Compressive stress up to 70% strain of the acid washed and untreated glass following storage at 37^{0}C in DI (n=5)

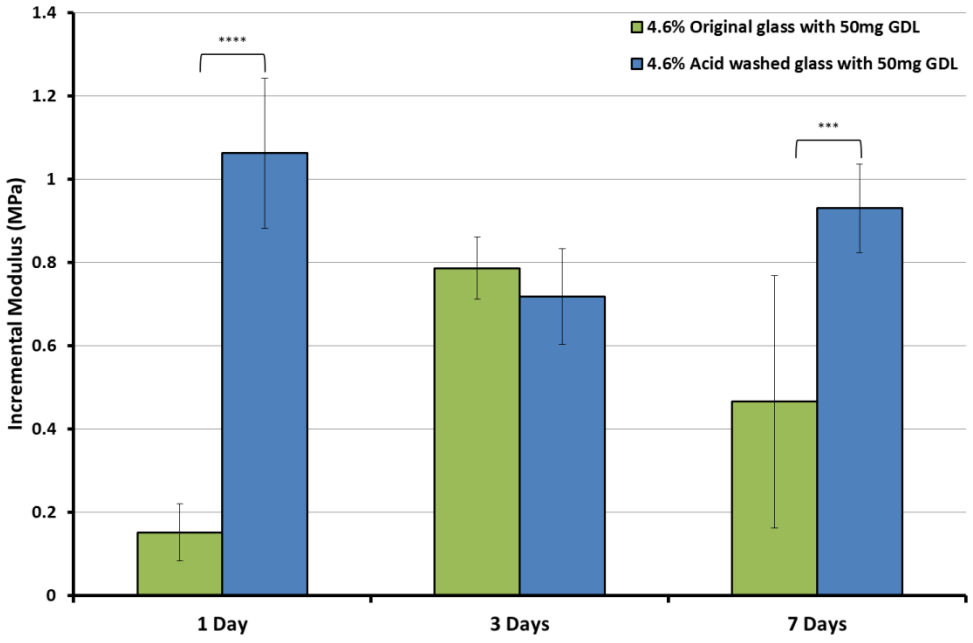

Figure 5.3.8 Incremental modulus (30-50% strain) of the acid washed and untreated glass following storage at 37^{0}C in DI (n=5)

5.3.8. Working and Hardening Time

Figure 5.3.9 and Figure 5.3.10 show that acid washing the glass causes the working and hardening time of the hydrogel to be outside the requirements. To improve this, the hydrogel was examined with increasing glass and GDL contents.

There is no significant change in working time with an increase in glass and 4.15% (w/v) GDL content. As the GDL acidifies the solution to release the ions from the bioactive glass, an increase in GDL is likely needed to maintain the acidic environment with the increasing alkali

ions released at an increased glass content. There is a linear decrease in working time with increasing glass content for both the 6.25% (w/v) (R^2 = 0.97) and 8.3% (w/v) (R^2 = 0.88) GDL content. The working time can be decreased by approximately 10 seconds per 0.045% (w/v) increase in GDL content.

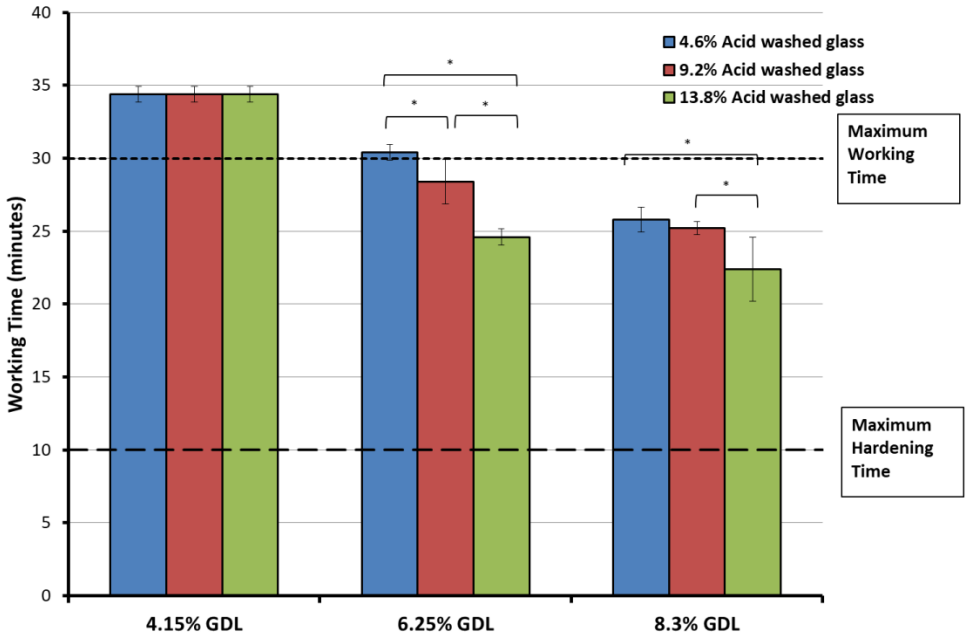

Figure 5.3.9 Acid washed glass working time with varying glass and GDL content (n=5)

Figure 5.3.10 shows the hardening time of the hydrogel with varying glass and GDL content. The hydrogel is within the required hardening time limits at each tested glass content, when the GDL content is 8.3% (w/v). This is not the case for the other GDL contents tested. Although there is a linear decrease in working time with increasing GDL content, this is not observed for the hardening time. At the 4.15% (w/v) GDL content, the 9.2% glass content causes a significant increase in hardening time. There is also a significant increase in hardening time with the 13.8% glass content with 6.25% (w/v) compared to the 4.6 and 9.2% glass content. Yet there is no significant difference compared to the 13.8% glass content with 4.15% (w/v) of GDL. This may be caused by increased glass content releasing an increased alkali ion content. This would increase the pH and slow the release of further ions.

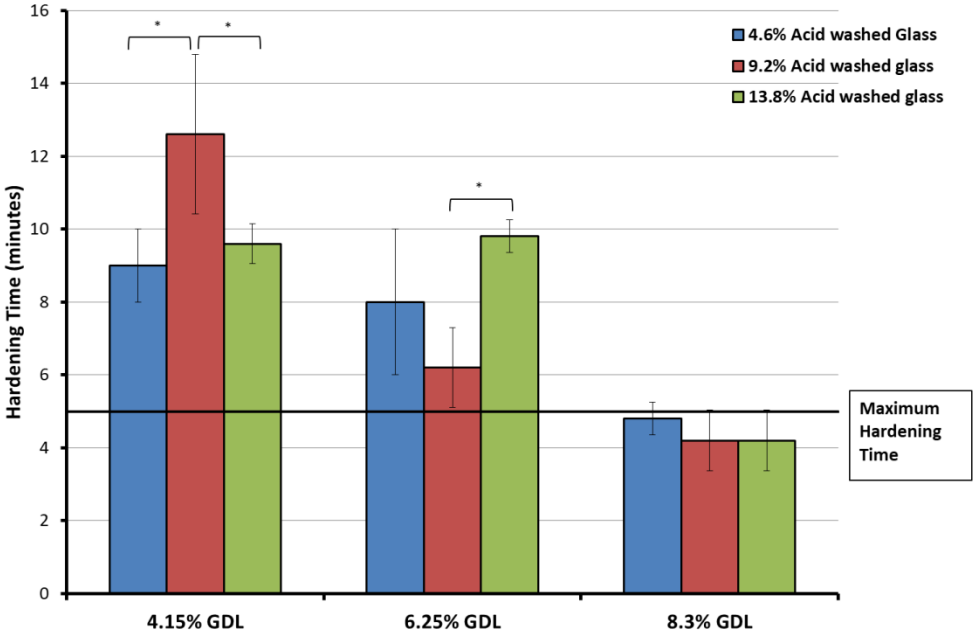

Figure 5.3.10 Acid washed glass hardening time with varying glass and GDL content (n=5)

5.3.9. Compressive Strength

Although the 4.6% and 9.2% glass content were within the working and hardening time limits with 8.3% (w/v) of GDL, increasing the glass content has been shown to increase the strength of the resultant hydrogel (Figure 5.1.10) and will likely increase the radiopacity due to the presence of high density gallium [377]. To examine this further the acid washed glass was increased to the highest content of 13.8%. Figure 5.3.11 and Figure 5.3.12 shows that the increase in the glass and GDL content provides a significant increase in the compressive strength and incremental modulus of the hydrogel.

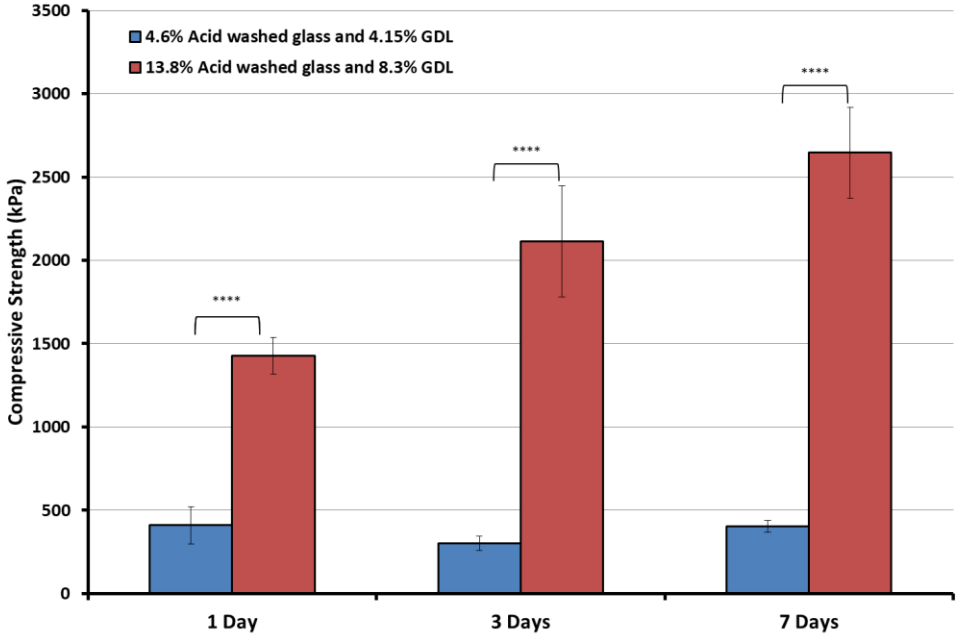

Figure 5.3.11 Compressive stress up to 70% strain of the acid washed glass with varying glass and GDL content following storage at 37^{0}C in DI (n=5)

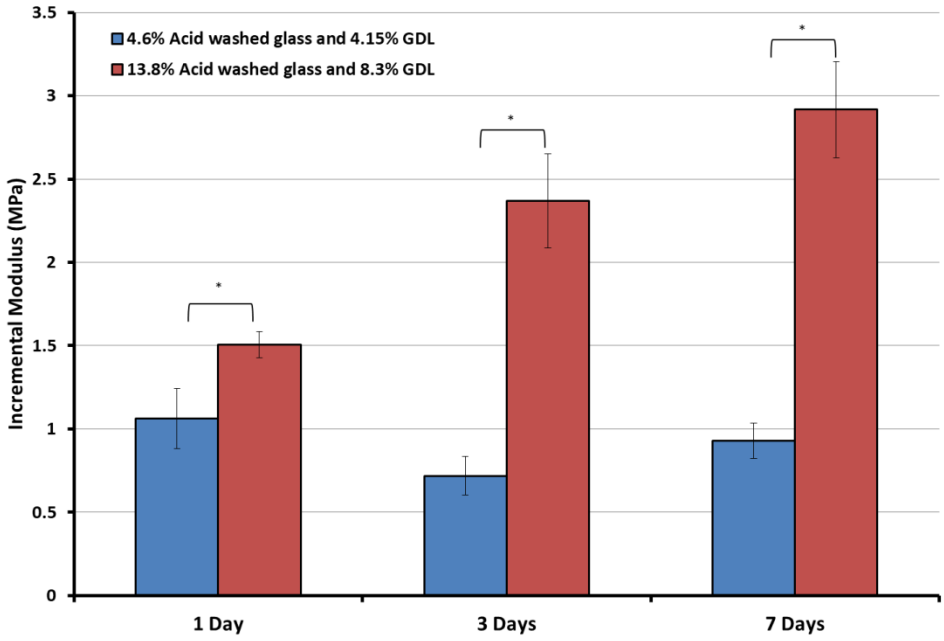

Figure 5.3.12 Incremental modulus (30-50% strain) of the acid washed glass with varying glass and GDL content following storage at 37^{0}C in DI (n=5)

To examine the effects of strength when there is an availability of external cations for ion exchange, as there would be *in vivo*, the samples were compressed following storage in both PBS and SBF at 37^{0}C for 1, 3 and 7 days. Figure 5.3.13 and Figure 5.3.14 shows that the compressive strength and the incremental modulus of the hydrogel decrease significantly in the ionic media compared to DI. Typical stress-strain graphs are shown in Appendix 9.5.2.1 (Figure 9.5.12 - Figure 9.5.15). The strength of the hydrogel continues to increase over time in all media. However, it should be noted that this increase is only significant following

storage in DI. The strength in each storage medium tested exceeds the minimum strength required of the hydrogel.

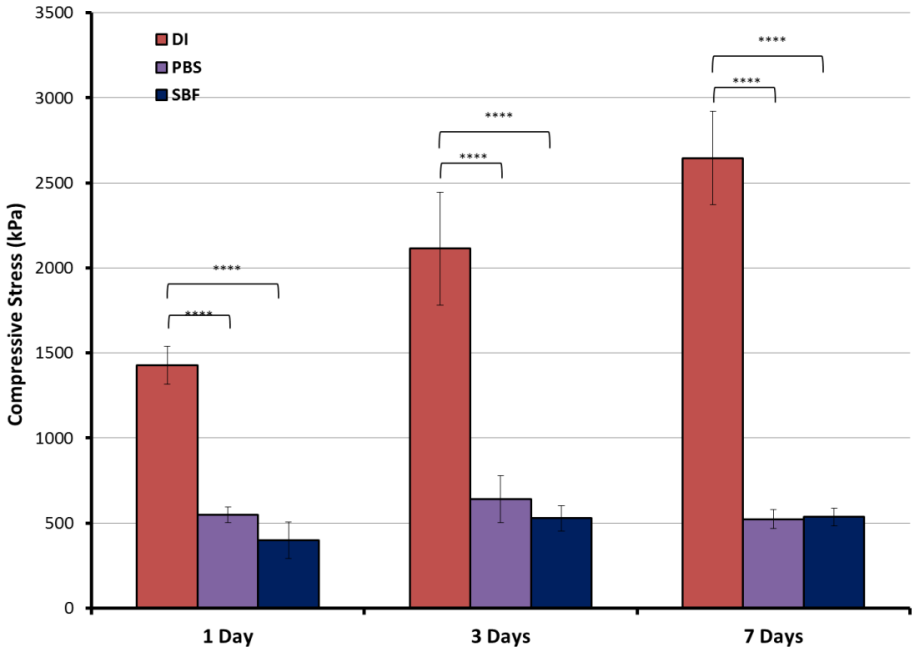

Figure 5.3.13 Compressive stress up to 70% strain of 13.8% acid washed glass with 8.3% (w/v) GDL following storage at 37^{0}C in varying media (n=5)

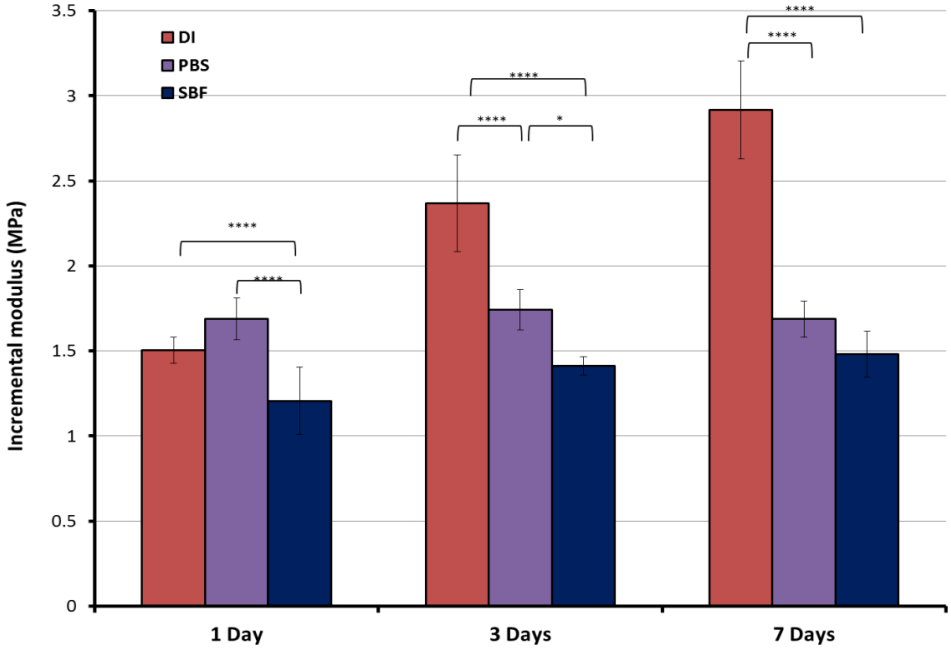

Figure 5.3.14 Incremental modulus (30-50% strain) of 13.8% acid washed glass with 8.3% (w/v) GDL following storage at 37^{0}C in varying media (n=5)

5.3.10. Volume Conservation

There is an expansion of the sample volume when the acid washed glass content is 4.6% with 4.15% (w/v) GDL and a shrinking of the sample with the glass and GDL content is increased, as seen in Figure 5.3.15. This is caused by an increase in cross-linking density.

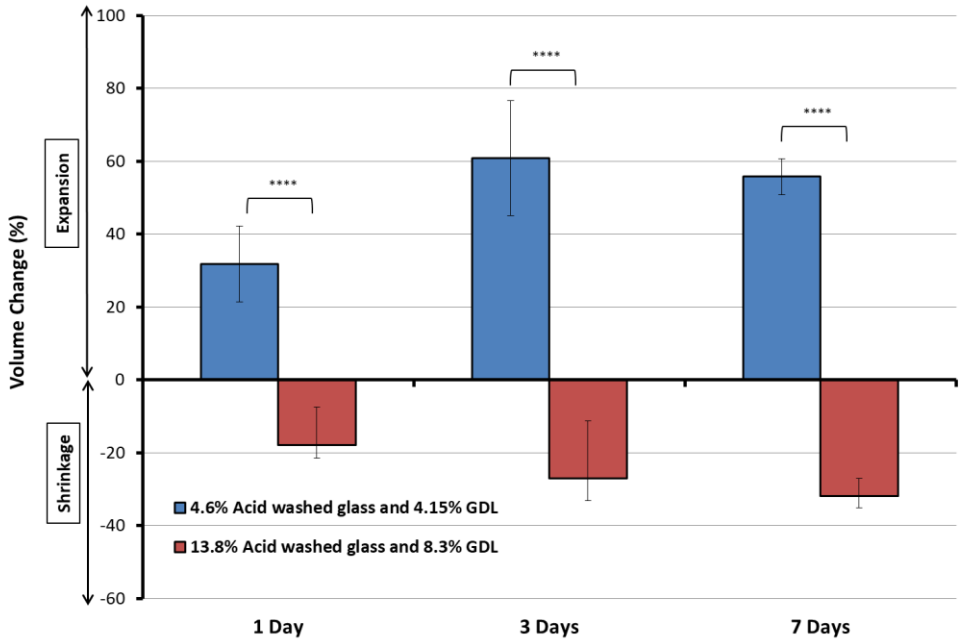

Figure 5.3.15 Acid washed glass with varying glass and GDL content size conservation (n=5)

However, the shrinking of the samples decreases at each time point when the hydrogel is stored in either PBS or SBF, seen in Figure 5.3.16.

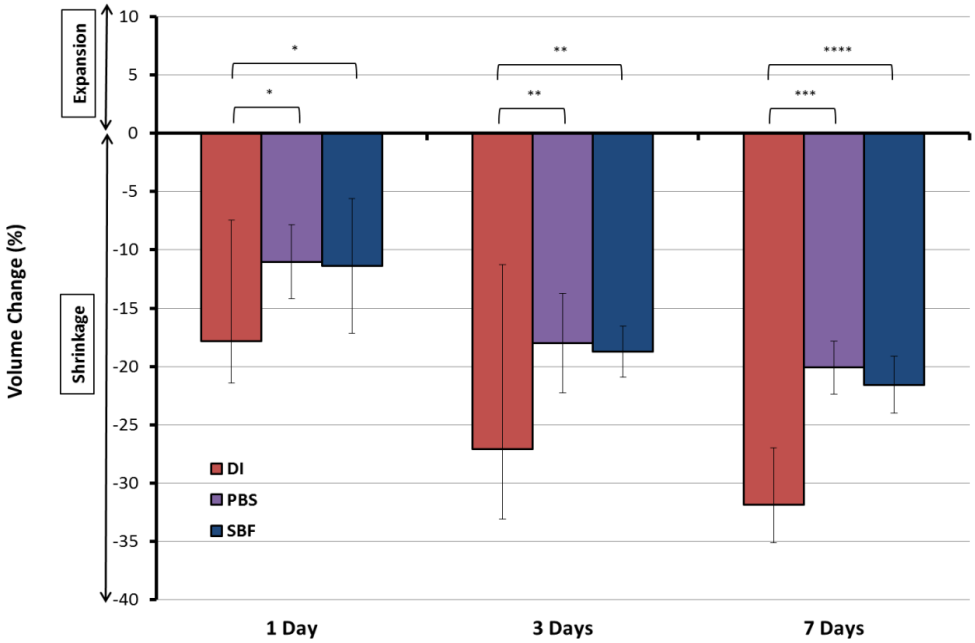

Figure 5.3.16 13.8% acid washed glass with 8.3% (w/v) GDL content size conservation after storage in varying media (n=5)

5.3.11. Homogeneity

Figure 5.3.17 shows the compression testing samples with both untreated and acid washed glass. Visibly, it seems that the acid washed glass produces a more homogenous sample. 3D XMT was carried out to examine the internal structure and agglomeration size.

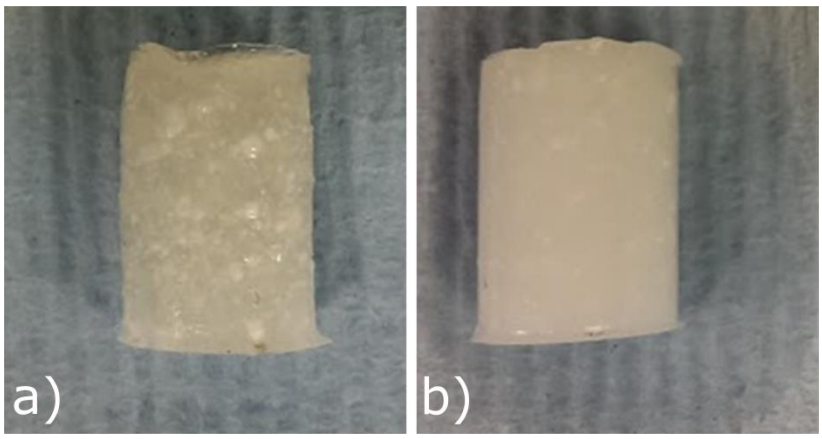

Figure 5.3.17 a) untreated glass compression testing sample and b) acid washed glass compression testing sample

Figure 5.3.18 shows the 3D XMT images of the hydrogel with 4.6% untreated glass with 4.15% (w/v) GDL (a), 4.6% acid washed glass with 4.15% (w/v) GDL (b) and 13.8% acid washed glass with 8.3% (w/v) GDL (c).

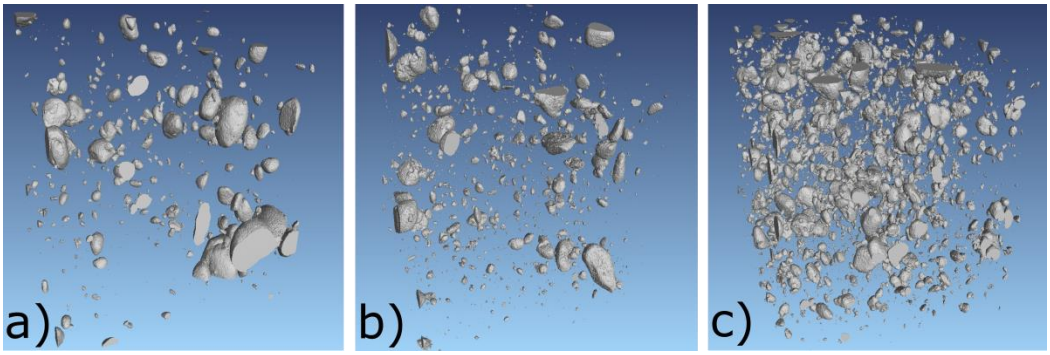

Figure 5.3.18 Sample 3D XMT a) hydrogel with 4.6% untreated glass content and 4.15% (w/v) GDL b) hydrogel with 4.6% acid washed glass content and 4.15% (w/v) GDL c) hydrogel with 13.8% glass content and 8.3% (w/v) GDL

From Table 5.3.4 it can be seen that acid washing the glass greatly reduces the average and maximum particle cluster volume. The untreated glass has larger particle clusters, due to increased agglomeration of the glass particles.

The hydrogel with acid washed glass has an increased number of agglomerates and reduced agglomerate size, resulting in a more homogenous sample compared to the non-acid washed glass sample. This increased homogeneity may contribute to the increased strength observed. A 3-fold increase in the acid washed glass content, from 4.6% to 13.8%, with a 2-fold increase in GDL content, increases the number of agglomerates; however, there is only a 2.2-fold, as opposed to a 3-fold, increase in observable agglomerates in the XMT. This suggests that the increased GDL is breaking down the glass or reducing the size of the agglomerates to <5µm (the minimum size visible using XMT).

The maximum glass agglomerate diameter for the untreated glass (≈1.44mm) is 44% larger than that of the acid washed glass (≈1.0mm). The larger untreated glass agglomerates would

inhibit injection through a 3F catheter (≅1.0mm), therefore, the catheter size would have to be increased to a 4.4F catheter (≅1.47mm) in order to inject without blocking the catheter. This larger catheter size would make navigation through the tortuous cerebral vasculature more difficult.

Table 5.3.4 Sample 3D XMT analysis.

Sample	Particle cluster volume (mm^3)		No. of visible particle clusters	Max particle cluster diameter (mm)
	Average	Max		
4.6% untreated glass (a)	0.0046	0.3654	423	1.4474
4.6% acid washed glass (b)	0.00128	0.1347	1177	0.9621
13.8% acid washed glass (c)	0.00136	0.1931	2628	1.0007

5.3.12. Radiopacity

The radiopacity of the hydrogel was examined in a 5mm wide Eppendorf tube using 2D microtomography. Figure 5.3.19 compares a coil (A), the hydrogel with 4.6% acid washed glass with 4.15% (w/v) GDL (B), the hydrogel with 13.8% acid washed glass with 8.3% (w/v) GDL (C) and a 99% aluminium step wedge with an increasing thickness of 1mm, 2mm and 3mm.

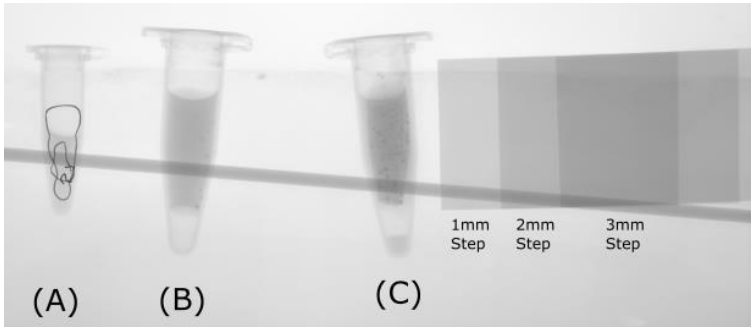

Figure 5.3.19 2D microtomography of a) a coil b) hydrogel with 4.6% glass content and 4.15% (w/v) GDL c) hydrogel with 13.8% glass content and 8.3% (w/v) GDL and a 99% aluminium step wedge

The mean grey scale values were measured using ImageJ (black = 0 and white = 255). It can be seen from the results in Table 5.3.5, that increasing the glass content causes an increase in the radiopacity of the hydrogel. The hydrogel with 13.8% acid washed glass with 8.3% (w/v)GDL has a similar grey scale value to that of the coil and an equal value to 3mm of 99% aluminium.

Table 5.3.5 Mean grey value.

Sample	Mean Greyscale	Greyscale Value	Equivalent aluminium

	Value	range	thickness
Coil (A)	146.7	125 - 199	3.20mm
4.6% acid washed glass (B)	178.4	166 - 188	2.20mm
13.8% acid washed glass (C)	159.2	142 - 190	2.99mm
1mm Step	207.7	204 - 211	1.00mm
2mm Step	183.3	178 - 187	2.00mm
3mm Step	159.9	152 - 165	3.00mm

5.3.13. Discussion

The particle size of the bioactive glass reduced after acid washing. This was supported by the results from nitrogen adsorption/desorption measurements and would indicate that the surface of the glass is eroded, likely caused by the acidic pH.

Pore size results indicate that acid washing increased pore diameter, see Table 5.3.1. The pore size of the acid washed glass samples are approaching mesopore diameter (2-50nm). Mesoporous bioactive glasses are typically produced by a sol-gel method and have surface areas ranging from 200 – 1000 m^2/g. The acid washed glass here has a greatly reduced surface area compared to sol-gel derived bioactive glasses. Although it was not examined here, increasing the acetic acid concentration or acid washing time could potentially increase the porosity of the glass particles. This may improve the use of melt quench glasses, as mesoporous glasses have an improved drug uptake and are being investigated for the delivery of various therapeutics [378].

Zeta potential measurements indicate an increase in hydrophilicity. This increased hydrophilicity of the glass can be attributed to an increase in the protonation of the silanol groups and an increase in Ga^{3+} on the surface of the glass particles which is expected following acid washing [379] [380].

X-ray photoelectron spectroscopy (XPS) indicated a decrease in calcium content and an increase in gallium on the surface of the acid treated glass and an increase in surface connectivity. Glasses which have silanol (Si-OH) groups on their surfaces tend to form hydrogen bonds with water, making them hydrophilic [381]. However, when glasses are fractured or ground their surface may become oxygen deficient due to fracture of Si-O bonds, making hydroxylation more difficult and hence initial hydrophobicity likely. The heat of liquefaction of water, at 44kJ/mol, is a value that has been used in the literature as a measure of the hydrophilicity/hydrophobicity of a surface site. Sites that are stronger that 44kJ/mol are considered hydrophilic, while those weaker than 44kJ/mol are considered hydrophobic [382]. The recondensation of the silicon observed on the surface of the acid washed glass is

likely increasing the number of high energy bonds, such as three coordinated silicon sites (60-200kJ/mol), which have the strongest adsorption, and decrease non-bridging oxygen sites (40-100kJ/mol) and 2 membered ring sites (20-100kJ/mol) [382] [383]. This in turn allows an increased silanol formation on the surface of the glass, resulting in better adsorption and hydrophilicity.

Carbon was observed on the surface of the bioactive glass by XPS. This has been seen previously on the surface of bioactive glasses and was caused by the adsorption of hydrocarbon impurities [384].

As shown in previous studies on aluminosilicate glasses, acid washing reduces the surface calcium concentration [365]. However, previous studies did not show a significant increase in compressive strength due to acid washing [385]. Additionally, previous studies on aluminosilicate glass indicated the increased presence of octahedral modalities on the surface following acid washing, which was not observed in this study with the use of gallium silicate glasses [367].

After 7 days there is a significant increase in strength for the hydrogel containing the acid washed glass. This is likely due to an increase in Ga^{3+} ions on the surface of the acid washed glass compared to the higher Ca^{2+} content on the surface of the untreated glass. Trivalent ions have been shown to produce mechanically stronger hydrogels compared to divalent ions [235] [386] [387] which may contribute to the increased strength observed. The increase in strength may also be caused by an increased homogeneity of the hydrogel, or a combination of both factors.

An increase in network connectivity will reduce the dissolution rate of the glass, which accounts for the increase in working and hardening time of the hydrogel with the acid washed glass. At a glass content of 4.6% and 4.15% (w/v) of GDL both the working time and hardening time of the hydrogel is outside the requirements for its intended application. However, once the glass and GDL content of the hydrogel is increased, the working time and hardening time of the samples decrease. At a glass content of 13.8% with a GDL content of 8.3% (w/v), the hydrogel is within the working and hardening time limits.

Due to increased working and hardening time associated with the acid washing, the glass and GDL content of the hydrogel had to be increased. Increasing the acid washed glass and GDL content further increases the strength of the produced hydrogel. This increase in strength is caused by an increase in availability of cross-linking ions, as shown in Section 5.1. To the best of the author's knowledge, the compressive strength of the hydrogel reported here is stronger than any *in situ* forming ionically cross-linked alginate hydrogels previously reported. *In situ* forming ionically cross-linked alginate hydrogels typically have strengths

ranging from 5 – 800kPa, with strengths varying with alginate type, cross-linker, storage media and time [202] [356] [388] [389]. This high strength is of a great significance, especially when taking into consideration the injectability and the short working and setting time of the hydrogel.

A significant difference is observed in the strength and incremental modulus of the hydrogel when stored in both SBF and PBS compared to DI. This was expected and is due to an ion exchange of the Ca^{2+} with the Na^{+} present in the PBS and SBF [203]. Although there is a significant decrease in strength, the strength of the hydrogel is still above that of the minimum strength required for this application. The incremental modulus of the hydrogel is also increased which will likely cause a reduced transfer of stress to the aneurysm wall.

The sample volume expands in aqueous solutions when the acid washed glass content is 4.6% with 4.15% (w/v), while the 13.8% acid washed glass with 8.3% (w/v) GDL samples shrink (see Figure 5.3.15). This is due to a combination of the increase of available cross-linking ions, as discussed previously, and the presence of trivalent ions. It has been previously observed that divalent ions produce a looser network that encourages swelling compared to trivalent ions [387]. Storage of the sample in SBF or PBS significantly decreases the sample shrinkage due to the exchange of ions causing a reducing of a cross-linking density. However, shrinkage of samples is still larger than would be desired for an aneurysm filler.

3D XMT results show that acid washing the glass produces a more homogenous hydrogel with an increased number of smaller glass agglomerates observed.

2D image by X-ray microtomography shows that increasing the glass content produces a hydrogel sample with a radiopacity equivalent to that of 2.99mm of 99% aluminium when the hydrogel thickness is 5mm. This radiopacity will allow the hydrogel to be easily observed once fully injected. However, the hydrogel's radiopacity may cause issues during the initial stages of injection or if leakage into the parent vasculature occurs when the thickness of the hydrogel is reduced.

It was previously discussed in Section 5.1.8 (page 103) that the untreated glass would inject through a 3F micro-catheter, however, the results shown here would suggest that the untreated glass particles would need the catheter size to be increased to a 4.4F catheter. This may be a result of the agglomerations size being reduced by breaking during injection through the micro-catheter. However, this is not ideal as it likely required an increase in force to inject. Catheters currently used for treating cerebral aneurysms typically have an inner diameter of 0.021" or 0.027". Further optimisation of the hydrogel may be necessary to allow an easy injection of this hydrogel through these reduced catheter dimensions [73].

These results indicate that surface treating the bioactive glass overall improves the hydrogels homogeneity. The increase in hydrophilicity of the surface of the glass reduces the size of the glass agglomerations. The increase in network connectivity and decrease in agglomerations allow for the glass and GDL content to be increased. The increase in these components of the hydrogel, in combination with the improved homogeneity, results in a high strength radiopaque hydrogel that can be formed by *in situ* gelation. Although the combination of bioactive glass and alginate has produced materials with higher strengths, these were scaffolds produced by 3D printing or lyophilisation and would not be suitable for endovascular treatment [248] [390]. The results of sample volume conservation, however, show that increasing glass cause a reduction in sample size. Shrinkage or expansion may cause the hydrogel to migrate or the aneurysm to rupture, respectively and consequently volume conservation of the hydrogel will need to be improved. It can be observed that in Table 5.3.6 that the hydrogel produced using a 13.8% acid washed glass with 8.3% (w/v) of GDL fulfils most of the requirements specified, though material size conservation is less than ideal.

Table 5.3.6 Untreated and acid washed glass design review

Glass and GDL content	Compressive Strength >22kPa?	Is the material size conserved? (<10% expansion with no shrinkage)	Is the hydrogel injectable?	Working Time between 10 and 30 mins?	Hardening Time <5 mins?	Is the material adhesive?	Is the material cytocompatible? (>70% cell viability)	Is the material sterilisable?	Is the material suitably radiopaque?	Is the material haemocompatible?
4.6% untreated glass with 4.15% (w/v) GDL	Yes	No*	Yes	Yes	Yes	TBD	TBD	TBD	No	TBD
4.6% acid washed glass with 4.15% (w/v) GDL	Yes	No	Yes	Yes	Yes	TBD	TBD	TBD	No	TBD
13.8% acid washed glass with 8.3% (w/v) GDL	Yes	No	Yes	Yes	Yes	TBD	TBD	TBD	Yes	TBD

*Will likely expand after storage in SBF as shown with the 4.6% acid washed glass with 4.15% (w/v) GDL (see Figure 5.3.15)

5.4. Effect of the Addition of EDC and NHS

Ideally, the hydrogel should be able to bond to the aneurysm wall to reduce the chance of aneurysm recurrence and the migration of the hydrogel into the parent artery and through the cerebral vasculature [112]. Adhesion of the hydrogel to the aneurysm wall would also reduce WSS within the aneurysm, reducing the risk of rupture. EDC and NHS were added to the hydrogel samples to examine whether the bond strength of the hydrogel could be increased. The alginate concentration, glass content and GDL content have been optimised (see Table 5.3.6, page 135) and are kept constant at 4.5% 700kDa High-M alginate, 13.8% acid washed glass and 8.3% (w/v)of GDL for each sample tested.

5.4.1. Bond Strength

The bond strength of the alginate after 1 hour was examined with an increasing EDC and NHS content shown in Figure 5.4.1. There was a linear increase when the EDC and NHS content was increased from 0% to 0.83% (w/v) (R^2 = 0.997) and linear reduction in bond strength when the EDC and NHS content were increased past 0.83% (w/v) (R^2 = 0.957).

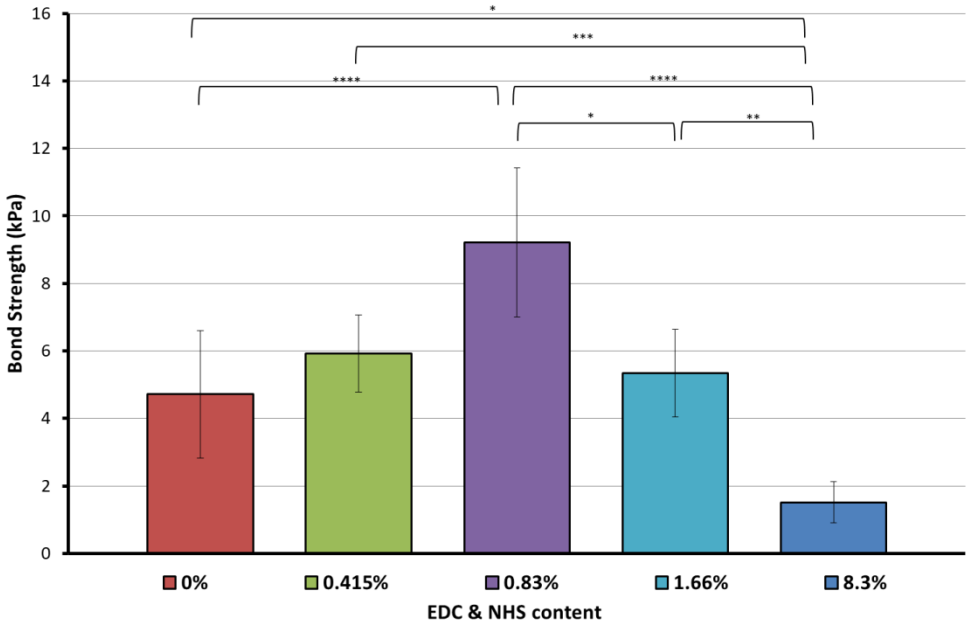

Figure 5.4.1 Bond strength of the hydrogel with varying EDC and NHS content with repeats after 1 hour (n=5)

Following testing of the samples under dry conditions, they were tested after storage in SBF for 1 hour and 1 day. After 1 hour storage in SBF, a significant difference between 0% and 0.83% (w/v) of EDC and NHS is observed. However, after 1 day storage in SBF, it is observed that bond strength increase significantly compared to 1 hour in SBF and a significant difference in bond strength observed with the addition of 0.83% (w/v)of EDC and NHS to the hydrogel, as seen in Figure 5.4.2.

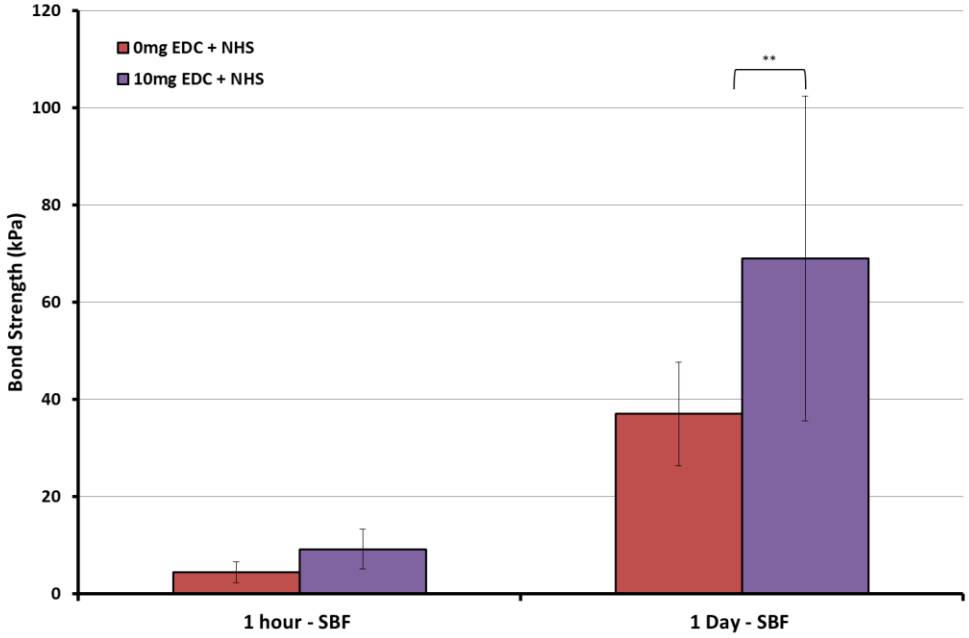

Figure 5.4.2 Bond strength of the hydrogel with 0% and 0.83% (w/v) EDC and NHS following storage in SBF at 37^0C (n=5)

5.4.2. Working and Hardening Time

The working time of the hydrogel significantly increases with the addition of 0.83% (w/v) of EDC and NHS, as seen in Figure 5.4.3, however, the working time is still within the limits for this application.

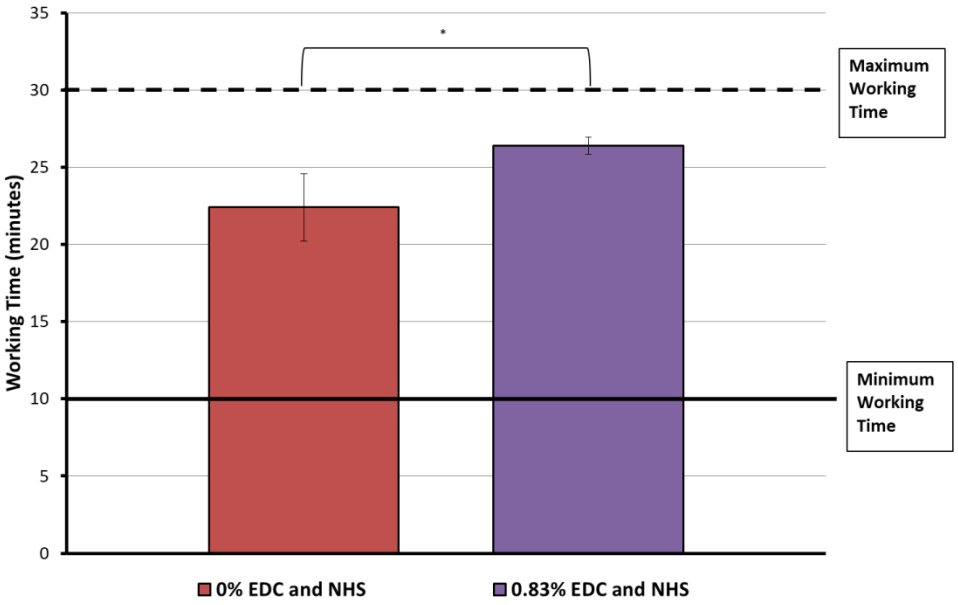

Figure 5.4.3 Working time of the hydrogel with 0% and 0.83% (w/v) EDC and NHS (n=5)

There is no significant change to the hardening time of the hydrogel when EDC and NHS are added, seen in Figure 5.4.4.

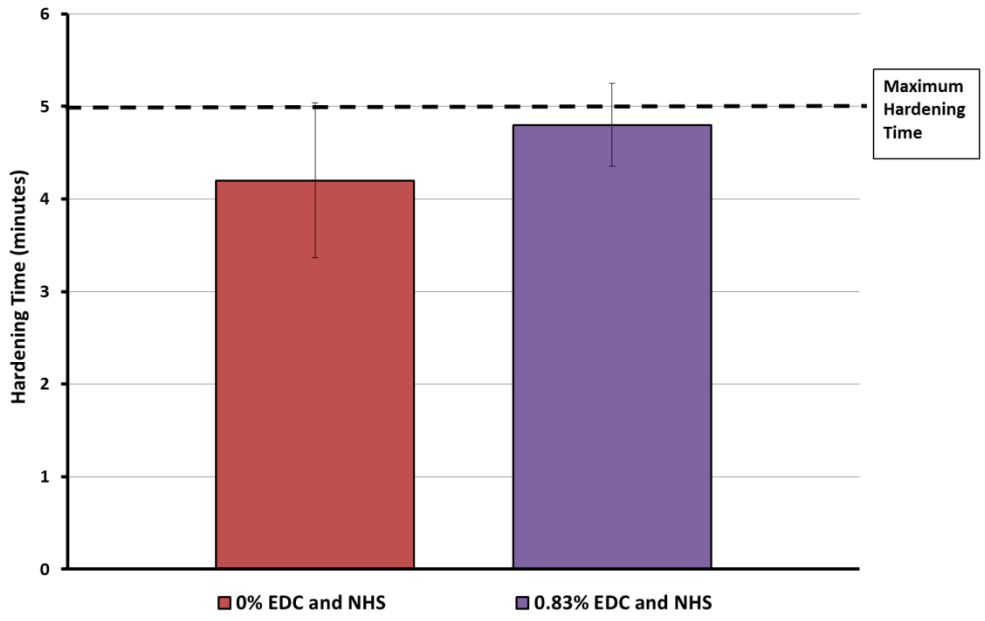

Figure 5.4.4 Hardening time of the hydrogel with 0% and 0.83% (w/v) EDC and NHS (n=5)

5.4.3. Compressive Strength

Figure 5.4.5 and Figure 5.4.6 show that the addition of 0.83% (w/v) of EDC and NHS reduces the compressive strength and incremental modulus of the hydrogel at each time point examined. However, compressive strength still greatly exceeds the minimum strength required for this application.

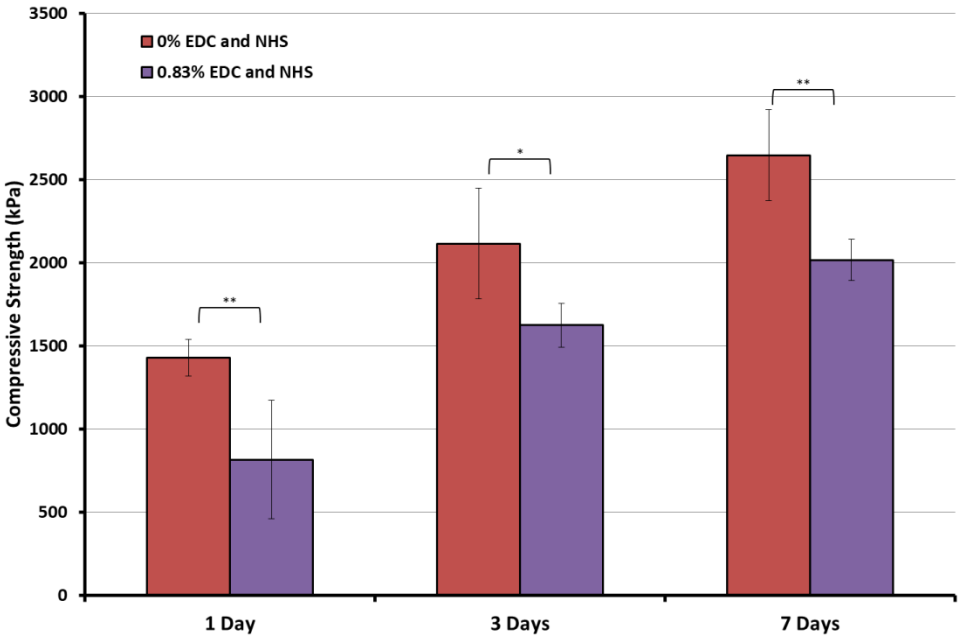

Figure 5.4.5 Compressive stress up to 70% strain of the hydrogel with 0% and 0.83% (w/v) EDC and NHS after storage at 37^0C in DI (n=5)

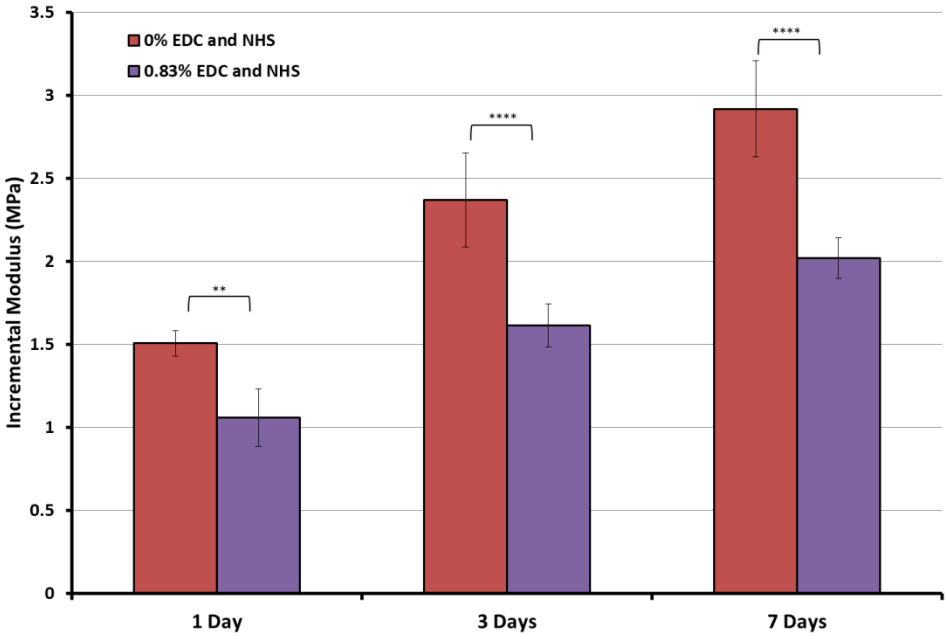

Figure 5.4.6 Incremental modulus (30-50% strain) of the hydrogel with 0% and 0.83% (w/v) EDC and NHS after storage at 37^0C in DI (n=5)

Figure 5.4.7 and Figure 5.4.8 shows the compressive strength and incremental modulus of the hydrogel sample, with 0.83% (w/v) of EDC and NHS, after storage in varying media at 37^0C for 1, 3 and 7 days. Typical stress-strain graphs are shown in Appendix 9.5.2 (Figure 9.5.16 - Figure 9.5.18). From these figures it can be seen that there is a significant difference when the hydrogel is subjected to ion exchange. However, the hydrogel's minimum strength after 7 days exceeds the strength required by the hydrogel for this application. There is a significant increase in the strength over time for the samples stored in DI. However, only a slight and insignificant increase in strength over time is observed for the samples stored in SBF and PBS.

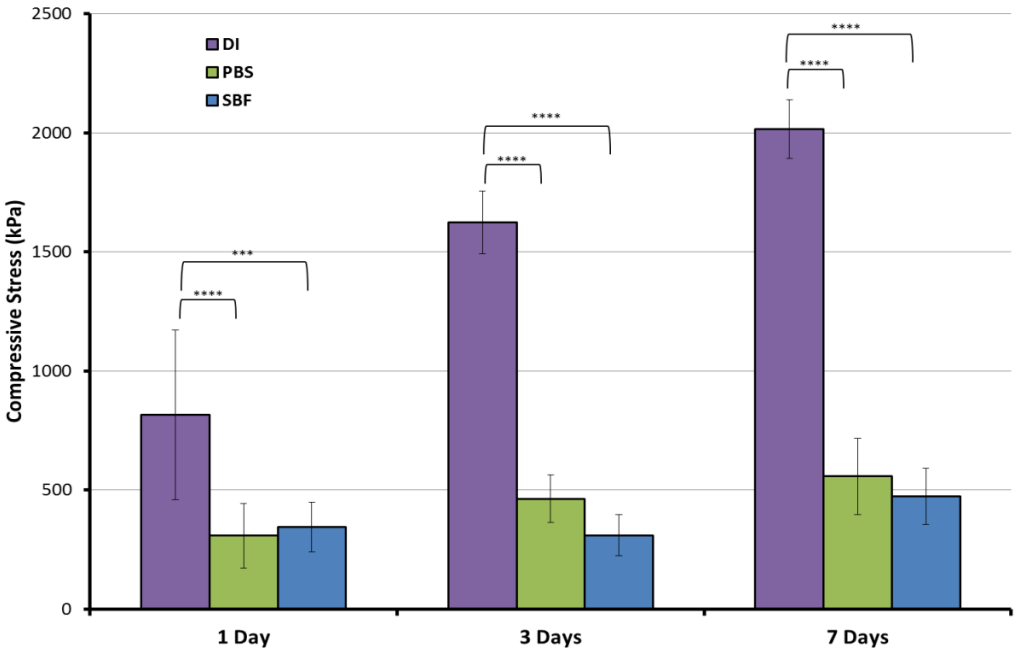

Figure 5.4.7 Compressive stress up to 70% strain of hydrogel with 0.83% (w/v) EDC and NHS after storage at 37^{0}C in varying media (n=5)

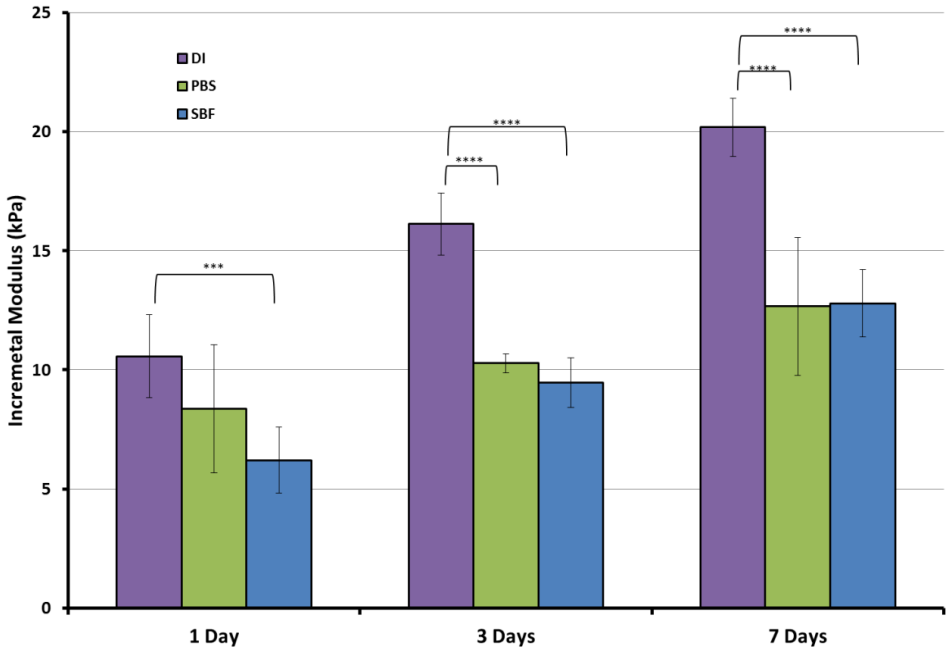

Figure 5.4.8 Incremental modulus (30-50% strain) of the hydrogel with 0.83% (w/v) EDC and NHS after storage at 37^{0}C in varying media (n=5)

The strength of the hydrogel was tested after 30 days storage in both DI and PBS at 37^{0}C. As discussed previous, SBF is not considered stable after 28 days and was therefore not used as a storage medium at 7 days. The strength of the hydrogel continued to increase in both media but was significantly higher for samples stored in DI at each time point examined as shown in Figure 5.4.9.

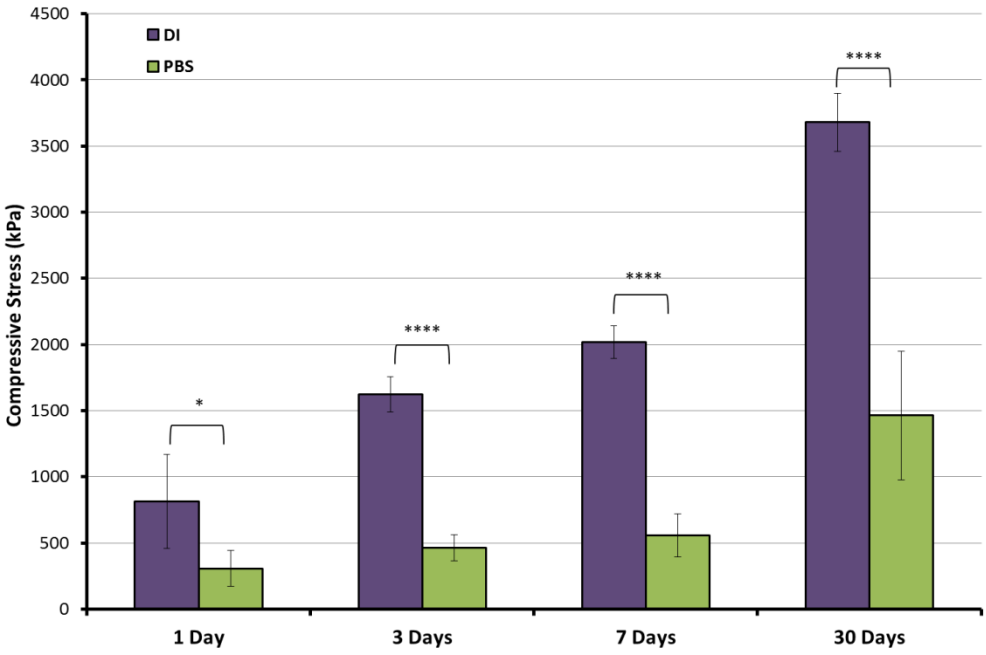

Figure 5.4.9 Compressive stress up to 70% strain of hydrogel with 0.83% (w/v) EDC and NHS after storage at 37^{0}C in varying media (n=5)

5.4.4. Volume Conservation

Figure 5.4.10 shows that there is a continued shrinking of the hydrogels up to 7 days. The samples stored in DI shrink significantly compared to those stored in PBS and SBF. This is likely due to the exchange of calcium ions with sodium present in the ionic solutions. This exchange reduces the hydrogels cross-linking density and causes a decrease in hydrogel shrinkage, as discussed previously.

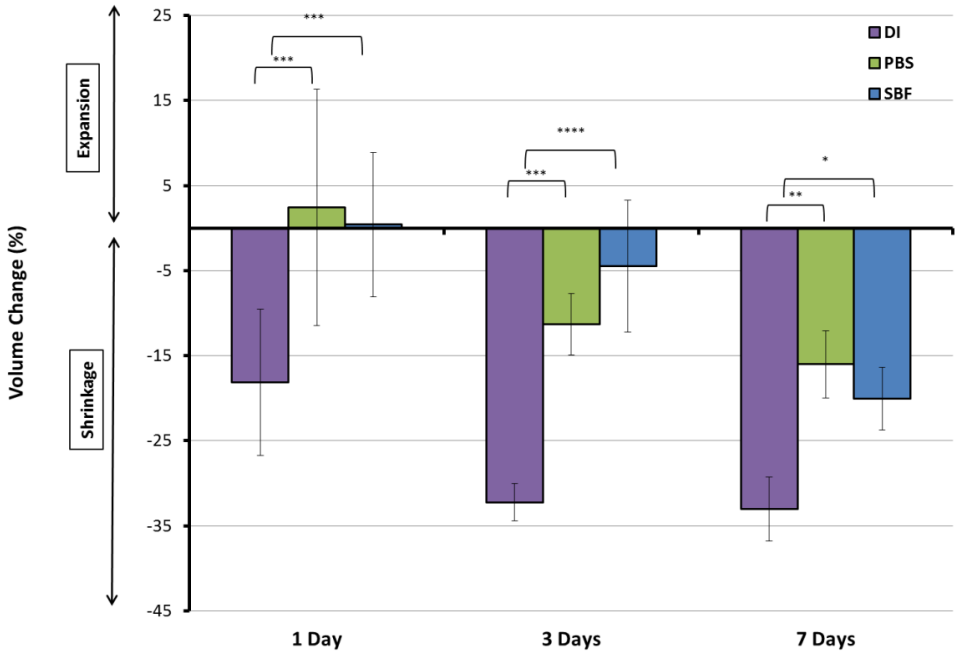

Figure 5.4.10 Volume conservation of the hydrogel with 0.83% (w/v) of EDC and NHS after storage in varying media

However, it can be seen in Figure 5.4.11 that the shrinking of the samples ceases following 7 days, with the volume change between the samples stored for 7 days and 30 days, in both DI and PBS, being insignificant.

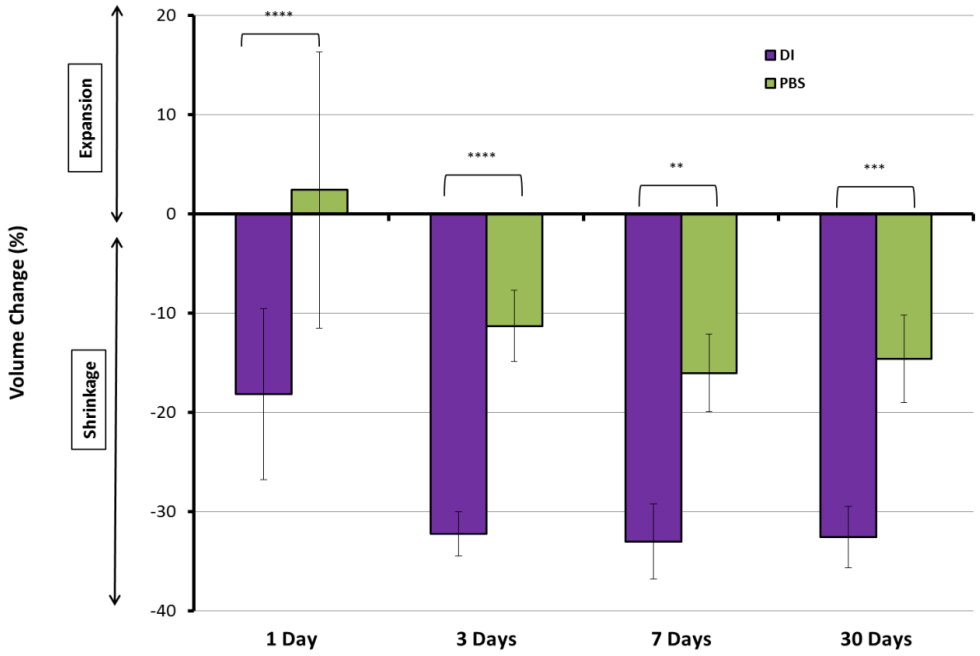

Figure 5.4.11 Volume conservation of the hydrogel with 0.83% (w/v) of EDC and NHS after storage in varying media

5.4.5. Deliverability

The samples tested with the addition of 0.83% (w/v) of EDC and NHS would inject through a 3F micro-catheter into the aneurysm model. Although the hardening time of the hydrogel is close to the time limit, the hydrogel remained in the model once the balloon was deflated, approximately 25 minutes after mixing. The addition of EDC and NHS to the hydrogel did not cause the hydrogel to adhere to the balloon when being injected.

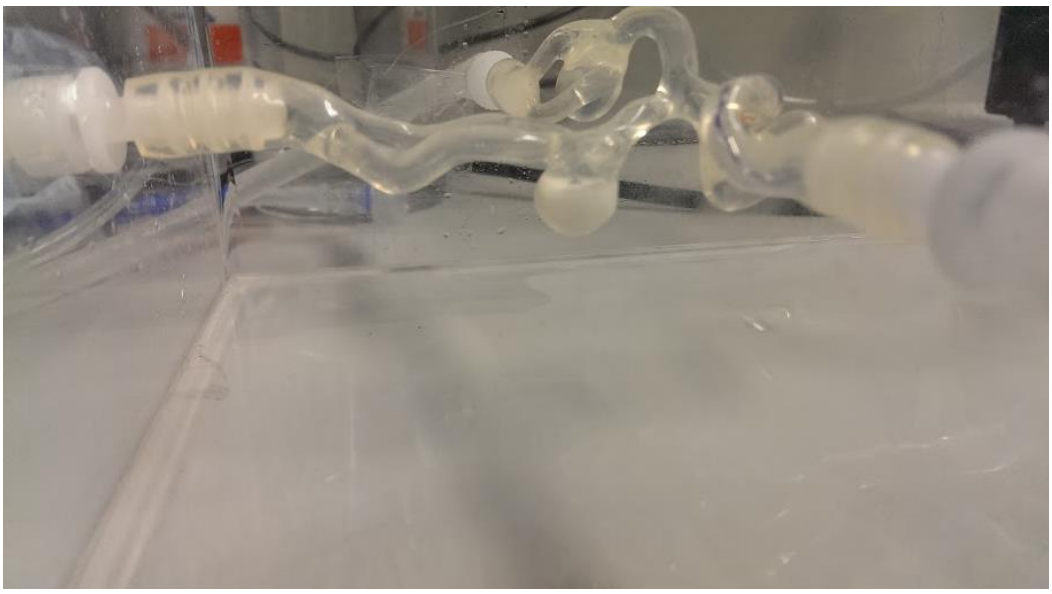

Figure 5.4.12 Hydrogel injected in to the aneurysm model with physiological flow applied

5.4.6. Discussion

EDC and NHS has been used to cross-link alginate with RGD peptides and dopamine to improve cell adhesion [193] [333]. It has also been used to produce cross-linked collagen and collagen-alginate gels [391]–[394]. The results here show that the EDC and NHS amide bond formation can improve the bond strength of an alginate hydrogel to a porcine skin graft without the addition of peptides or polymers. In general, the aneurysm wall mainly consists of the adventitia layer and intima layer with exposed collagen, which will likely allow this cross-linking will occur *in vivo* to the aneurysm wall [20] [33].

Typically, the bond strength of hydrogels increase with an increase in EDC and NHS content [395] [396]. However, in this study we observe a dose dependent increase in bond strength with additions of EDC and NHS up to 0.83% (w/v) and a dose dependent decrease in bond strength with additions exceeding 0.83% (w/v). This may indicate two types of fracture occurring within the hydrogel, causing this dual response. The first type of fracture may be an adhesive failure caused by breaking in the bonds between the porcine skin graft and the hydrogel, which is likely happening for the hydrogel with less than 0.83% (w/v) EDC and NHS content (Figure 9.5.19). The bond strengths of the hydrogels produced here are of similar values to those observed by Cohen *et al* at 0.83% (w/v) of EDC after 1 hour [395].

The second type of fracture may be a cohesive failure caused by reduced strength of the hydrogel with increased EDC and NHS content. In this case, the hydrogel will fracture prior to de-bonding of the hydrogel from the porcine skin graft. The hydrogel's strength can be seen to decrease with the addition of 0.83% (w/v) of EDC and NHS (Figure 5.4.5), which may be decreasing further with increasing EDC and NHS content. The cohesive failure was seen after bond strength testing in Figure 9.5.20.

It can be seen in Figure 5.4.1 and Figure 5.4.2, the hydrogel exhibits a bond strength to the porcine skin graft even without the addition of EDC and NHS (0%). It has been shown that bioactive glass without the addition of an adhesive has the ability to bond with soft and hard tissue [223] [397] [398].

The pH of the solution can also affect the bond strength of the hydrogel, as the EDC and NHS coupling reaction takes place between a pH range of 4.5-7.2 and, therefore, is typically performed in a pH buffer [219]. This suggests why there is a slight increase in the strength of the hydrogel with 0.83% (w/v) of EDC and NHS when it is placed in SBF, as SBF is a 7 pH buffer. The strength continues to increase up to 24 hours which has been likely due to the continued production of amide bonds, which has been previously observed for the coupling of amines and carboxyl group [216].

It has been shown in the literature that the pH of the solutions with varying EDC and NHS contents have a pH of approximately 6 [214] [395]. When the pH of DI was tested with the addition of 8.3% (w/v) GDL, it decreased from 7 to 4. The pH was further decreased with the addition of 0.83% (w/v) of NHS to 3.6, however, when 0.83% (w/v) of EDC was added the pH increased to 5.5. It was also tested with NHS alone, which dropped the pH to 4 and the EDC, again, increased the pH to 6.6. When tested alone the EDC decreased the pH of DI from 7 to 6.8. This suggests that EDC acts as a buffer.

The addition of 0.83% (w/v) of EDC and NHS causes a significant increase in the hydrogel's working time, seen in Figure 5.4.3. This increase may be caused by the increase in pH with the addition of the EDC. This increase in pH would reduce the ability of cross-linking ions to be released from the glass and this decrease in available cross-linking ions would increase the hydrogel working time. Figure 5.4.4 shows no significant difference in the hydrogel's hardening time with an addition of 0.83% (w/v) of EDC and NHS. Overtime, the hydrogel's pH may continue to decrease due to the continued hydrolysis of GDL. Once the buffering capacity of the EDC is exceeded, there is likely an increase the degradation of the glass and the release of cross-linking ions.

Similar to the results shown in Section 5.3.9, a reduced strength is observed when the hydrogel is stored in SBF and PBS (Figure 5.4.7). However, Figure 5.4.9 shows the strength continues to increase over time. This reduction was expected and has been observed elsewhere due to the exchange of Ca^{2+} ions with Na^{2+} ions of the ionic media. Although, unlike in these hydrogels that strength reduces over time due to this continue exchange, the hydrogel here increases due to the continuous ion release from the bioactive glass. It has also been observed that trivalent ions, such as Nd^{3+}, do not exchange with sodium ions present in the media, reducing degradability of alginate hydrogels [203] [387].

Again, the samples shrink over time; however, the shrinkage is decreased when the hydrogel is stored in PBS and SBF due to the reduction in cross-linking density caused by the exchange of calcium ions for sodium. The sample size stays consistent from 7 days up to 30 days. It would be expected there would be a continued shrinkage as the strength increases, due to an increased cross-linking. However, this did not occur and was also observed by Kuo *et al* which indicated an equilibrium with the aqueous environment [209].

The results show that the presence of EDC and NHS can improve the bond strength of the hydrogel to porcine skin graft. This will likely be advantageous *in vivo*. These results indicate that small changes in pH can affect the ion release from bioactive glasses. In this hydrogel, the reduced ion release resulted in a hydrogel with a slower gelation rate and a reduced strength. However, the reduced cross-linking density decreases the sample volume shrinkage which will be required for successfully embolization the aneurysm. Table 5.4.1 shows that the hydrogel with 0.83% (w/v) of EDC and NHS still meets the criteria of an aneurysm treatment but with improved adhesive strength compared to that with 0% EDC and NHS.

Table 5.4.1 0% and 0.83% (w/v) EDC and NHS design review

EDC and NHS content	Compressive Strength >22kPa?	Is the material size conserved? (<10% expansion with no shrinkage)	Is the hydrogel injectable?	Working Time between 10 and 30 mins?	Hardening Time <5 mins?	Is the material adhesive?	Is the material cytocompatible? (>70% cell viability)	Is the material sterilisable?	Is the material suitably radiopaque?	Is the material haemocompatible?
0%	Yes	No	Yes	Yes	Yes	Yes*	TBD	TBD	TBD	TBD
0.83% (w/v)	Yes	No	Yes	Yes	Yes	Yes**	TBD	TBD	TBD	TBD

* has a bond strength of 37kPa and ** has a bond strength of 85kPa after storage for 24 hours in SBF

5.5. *In Vitro* Analysis

Three varying hydrogel formulations have been shown to be potentially useable as an aneurysm embolization treatment (see Table 5.1.2 page 107 and Table 5.4.1 on page 147). Although acid treatment improved the radiopacity and strength of the hydrogel and reduced the number of agglomerations, it had an effect on the surface properties of the glass which may, in turn, affect the ion release rate from and cellular response to the hydrogel. Eluent A and Eluent B will allow for the comparison of the untreated and acid washed glass. Eluent C will contain 0.83% (w/v) of EDC and NHS, which will allow the effects of EDC and NHS to be examined. The hydrogel formulations of which eluents are to be tested are shown in Table 5.5.1. BAECs were dosed for 1 day with 24 hour and 48 hour hydrogel eluent, as discussed in 4.7.

Table 5.5.1 Hydrogel content for cell culture

Eluent	Alginate concentration	Glass type	Glass content	GDL content	EDC and NHS Content
A	4.5% 700kDa alginate	Original, untreated glass	13.8%	8.3% (w/v)	0%
B	4.5% 700kDa alginate	Acid washed glass	13.8%	8.3% (w/v)	0%
C	4.5% 700kDa alginate	Acid washed glass	13.8%	8.3% (w/v)	0.83% (w/v)

5.5.1. Resazurin Blue Assay

Figure 5.5.1 shows, with the 24 hour eluent, a linear decrease (R^2 = 0.97) in cell activity up to 60%, followed by a linear increase in cell activity from 60-100% eluent dose. A significant difference in cell activity is observed for the 48 hour eluent. The cell activity contradicts that of the 24 hour eluent, where the cell activity increases linearly to 230% (R^2 = 0.92) at 60% dose, beyond which a decrease is observed, although not a significant decrease.

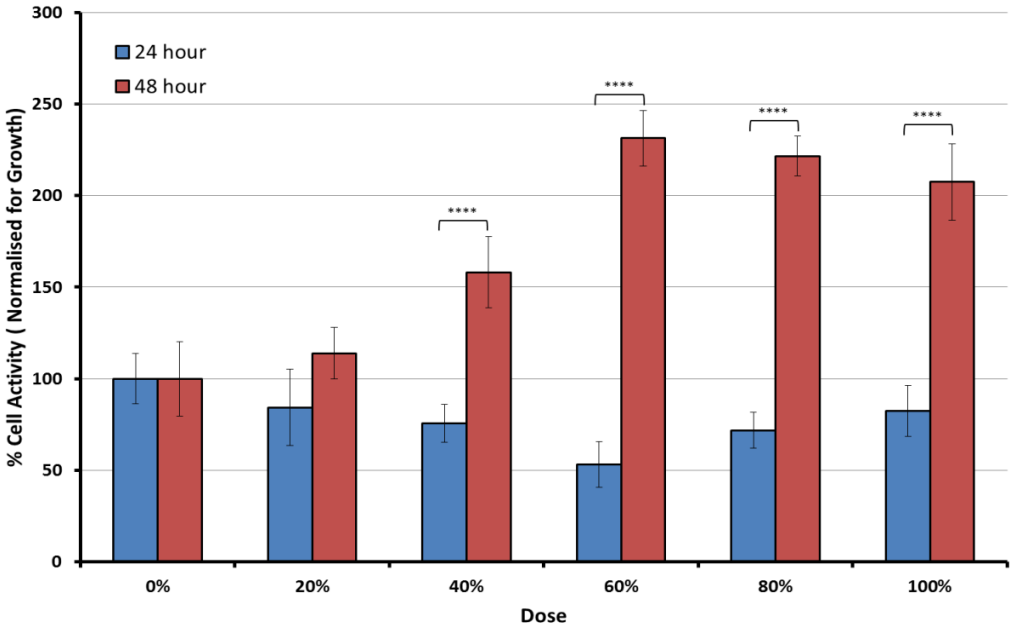

Figure 5.5.1 BAEC cell activity for cells dosed with eluent A at different eluent concentrations (n=3)

Figure 5.5.2 shows Eluent B causes a decrease in cell activity with 20% of the 24 hour eluent. The cell activity increases with increasing dose to 60%, then there is a significant decrease from 60% to 100% eluent dose. The 48 hour eluent shows a significant increase in cell activity for each dose, that increases linearly with increasing dose to a maximum of 332% (R^2 = 0.92).

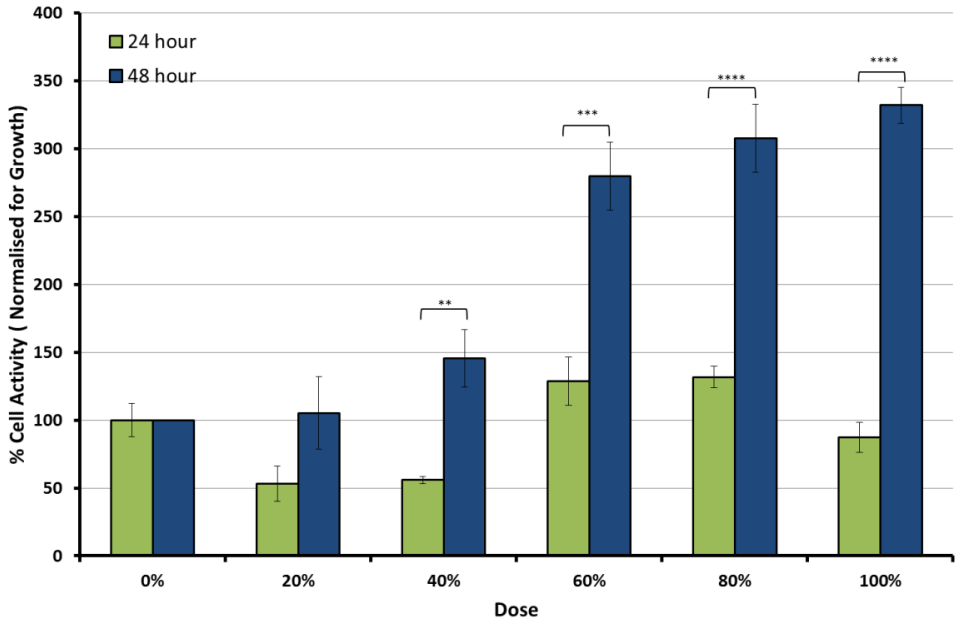

Figure 5.5.2 BAEC cell activity for cells dosed with eluent B at different eluent concentrations (n=3)

There is an initial decrease in the cell activity with a 20% dose of the 24 hour and 48 eluent, however, increasing the dose causes a linear increase of the cell metabolic activity for both

the 24 hour (R^2 = 0.95) and 48 hour (R^2 = 0.97) eluent. There is no significant difference compared to Eluent B when dosed with the 24 hour eluent up to a 80% dose. At a 100% dose Eluent C has an increased metabolic activity. This difference is caused by a decrease in metabolic activity of Eluent B, which may be caused by cell death or the cells reaching confluency. It can be seen in that the addition of 0.83% (w/v) of EDC and NHS (Figure 5.5.3) reduces the cell metabolic activity compared to the cells with 0% (w/v) of EDC and NHS (Figure 5.5.2) at each concentration for the 48 hour eluent. This is increasingly evident with increasing dose, where at 100% there is a decrease from 332% to 257%. This difference in metabolic activity between Eluent B and Eluent C when dosed with the 24 hour and 48 hour eluent may suggest that the EDC has a delayed release from the hydrogel, as EDC can be toxic to cells in high concentrations [214].

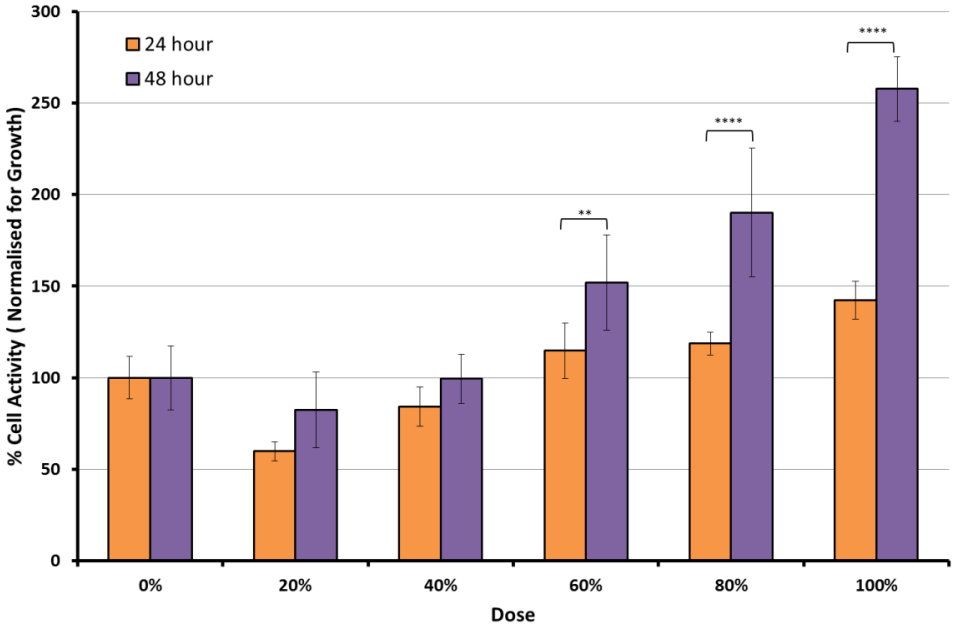

Figure 5.5.3 BAEC cell activity for cells dosed with eluent C at different eluent concentrations (n=3)

5.5.2. Cell Counting

The results of cell counting using DAPI staining follow the same trend as the results of cell metabolic activity for the 24 hour Eluent A, shown in Figure 5.5.1. However, the 48 hour eluent at a 20% and 100% dose causes an increase in metabolic activity but a decrease in cell number is shown. It is unclear what may be causing this discrepancy, though it may be caused by cell death following an increase in metabolic activity due to a lack of nutrients or insufficient dosing time.

Overall, there is a significant decrease in cell number at 20% dose and an increase at a 100% dose (Figure 5.5.4). The cell viability of the cells dosed with 20% of the 24 hour and 48 hour eluent is below the acceptable described in ISO 10993 where 70% cell viability is the limit. It

is unclear which eluent dose will correlate to the effect *in vivo,* yet these results indicate that this hydrogel composition will not be usable for the treatment of cerebral aneurysms.

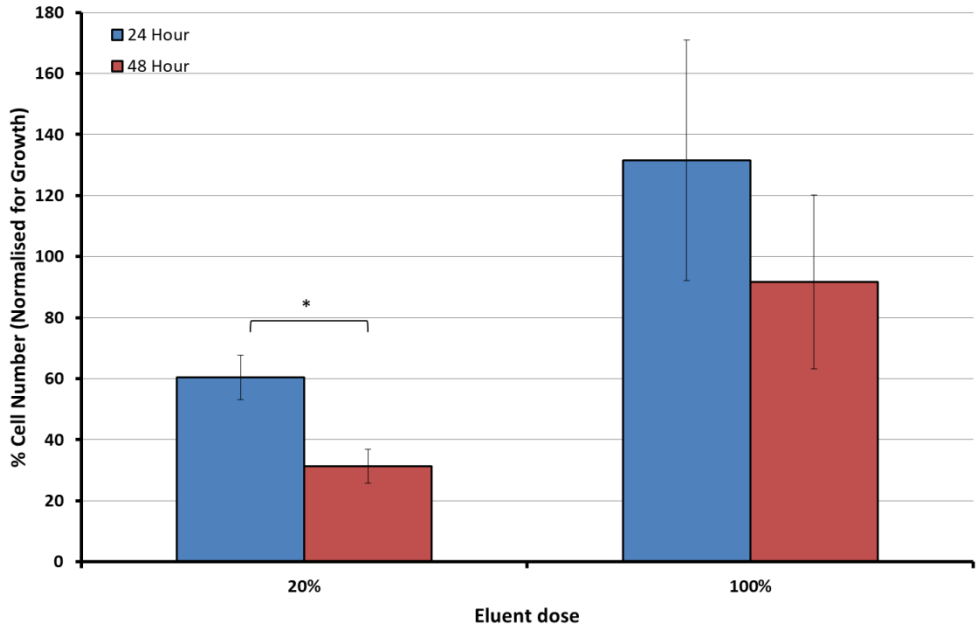

Figure 5.5.4 BAEC cell number change (%) of cells dosed with varying concentrations of eluent A (n=3)

Figure 5.5.5 shows the change in cell numbers for the cells dosed with varying amount of Eluent B. With both the 24 hour and 48 hour eluent, there is an increase in cell numbers with increasing eluent concentration; however, there is no significant difference in cell numbers with 24 hour and 48 hour eluent. Again there is a discrepancy between metabolic activity and cell number, in this circumstance it's a decrease in cell metabolic activity compared to cell number at a 20% and 100% 24 hour eluent dose. There is no increase in cell number at a 20% eluent dose compared to the control, which may indicate the reduction in metabolic activity is caused by the cell undergoing cell cycle arrest to cease apoptosis. At 100% eluent dose, there may be insufficient nutrient in the media to accommodate the increase in cell number. Although there is no significant difference in the 24 hour and 48 hour eluent at a 100% concentration cell number, the 48 hour eluent likely has an increase in glucose released from the hydrogel to support these cells. The cells may also be reaching confluency and undergoing contact inhibition [399] [400].

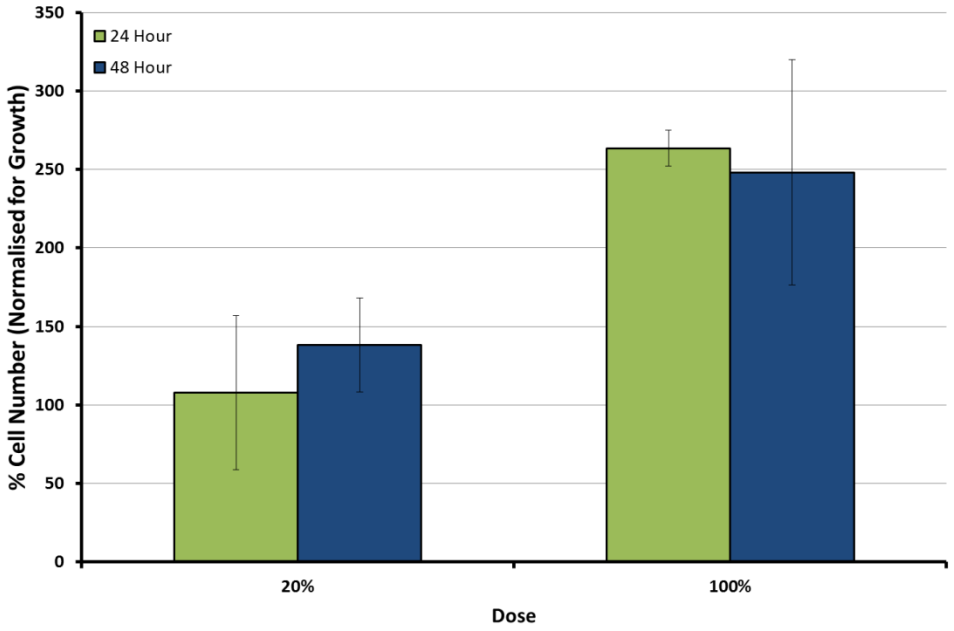

Figure 5.5.5 BAEC cell number change (%) of cells dosed with varying concentrations of eluent B (n=3)

Figure 5.5.6 also shows that although there is initially cell death with the cells dosed with 20% of the 24 hour eluent, however, there is still >70% of cells viable. The cell number then increases with increasing eluent concentration. The 20% 48 hour eluent dose has a decreased metabolic activity compared to that of cell number. This is likely due to the cell cycle arrest again due to a lack of nutrients to accommodate the increase in cell number or insufficient dose time to see significant cell growth, similar to the results of Eluent A and Eluent B.

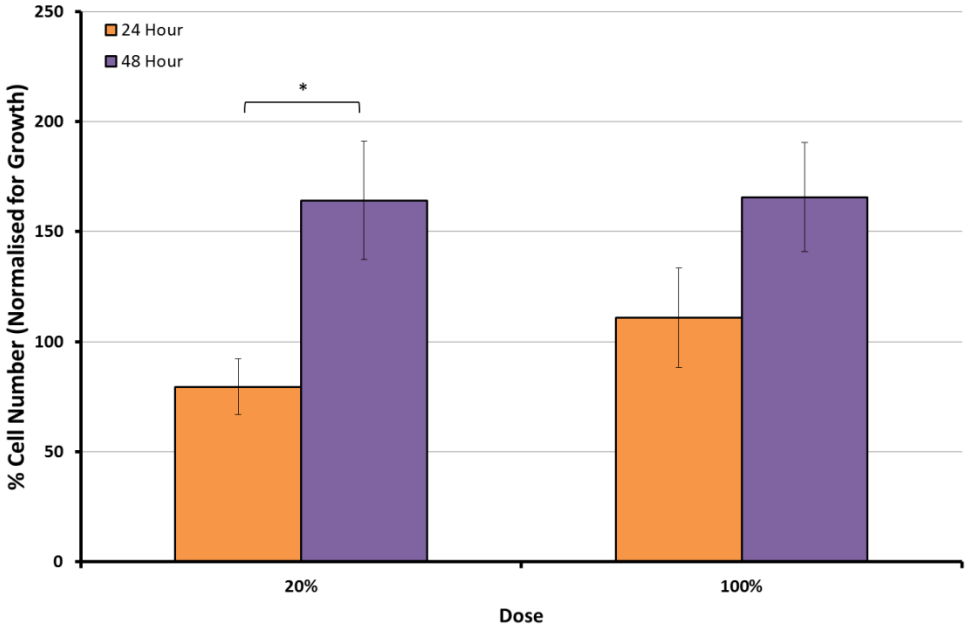

Figure 5.5.6 BAEC cell number change (%) of cells dosed with varying concentrations of eluent C (n=3)

5.5.3. ICP

Figure 5.5.7 shows no significant difference in the ion released from Eluent A after 24 and 48 hours.

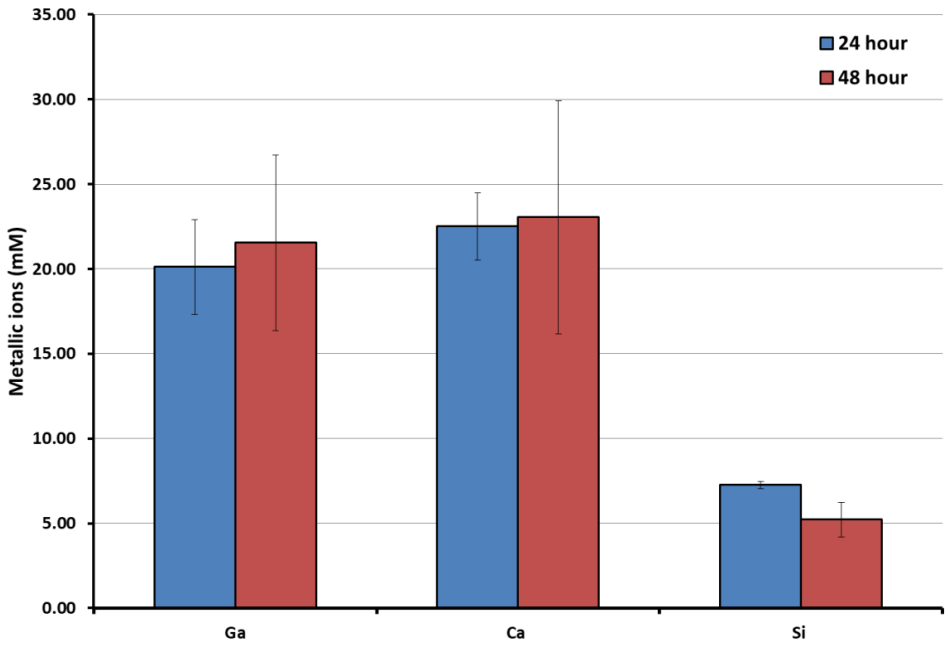

Figure 5.5.7 ICP of eluent A (n=3)

Figure 5.5.8 shows the ICP results of Eluent B shows a significant increase in the release of Ga^{3+} after 48 hours.

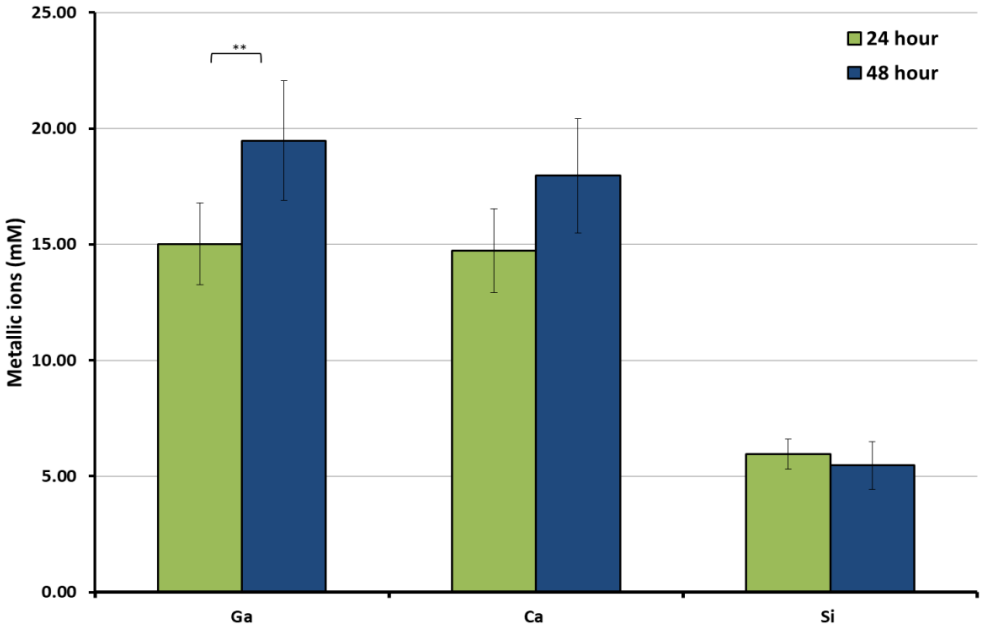

Figure 5.5.8 ICP of eluent B (n=3)

Figure 5.5.9 shows no significant increase in ion release between the 24 hour and 48 hours Eluent C. There is a significant difference in Ga^{3+} content at 48 hours between Eluent B and C

but no difference in the release of Ca^{2+} and Si^{4+}. A significant difference is observed between the release of Ca^{2+} from Eluent A and Eluent C at 48 hours.

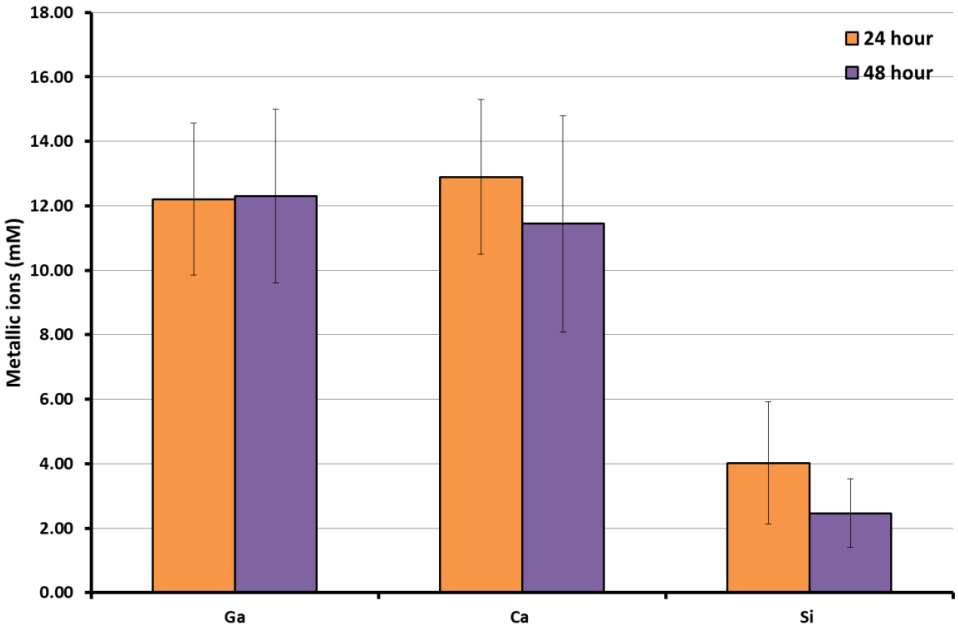

Figure 5.5.9 ICP of eluent C (n=3)

5.5.4. Ion dosing

To examine the effects of the ions released from the hydrogel, BAECs are dosed with gallium, calcium and silica individually at the average content shown by ICP. As the gluconic acid content in the eluent was not determined, the cells were dosed with the GDL content of the hydrogel.

5.5.4.1. Gallium

Figure 5.5.10 shows a significant decrease in cell metabolic activity with cells dosed with varying concentrations of gallium chloride. By at 40% gallium chloride concentration there was a high cytotoxic effect of the gallium chloride on the BAECs.

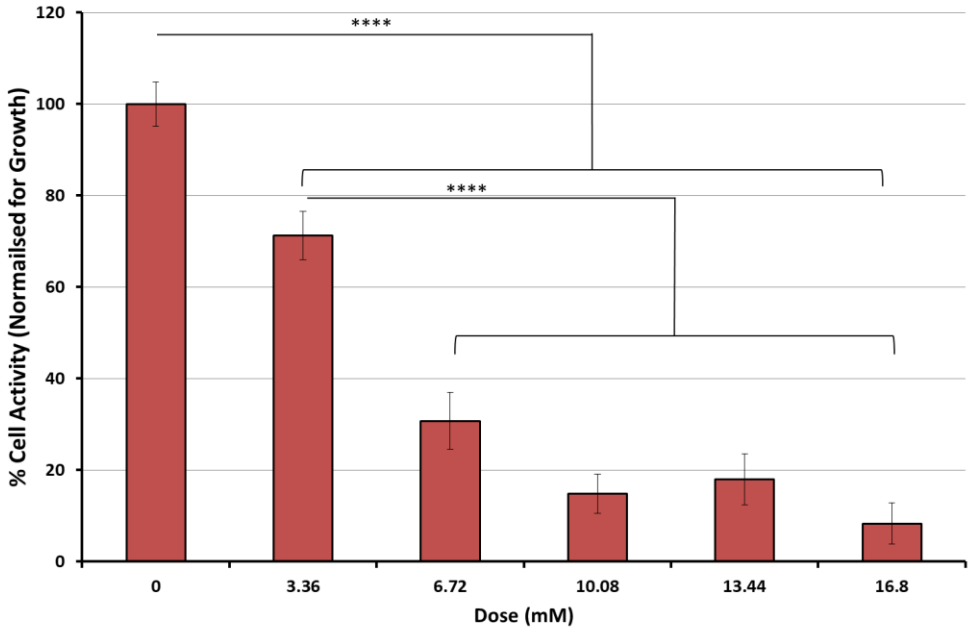

Figure 5.5.10 BAEC cell activity for cells dosed with gallium chloride at different eluent concentrations (n=3)

These cytotoxic effects of gallium chloride was also shown in cell number (see Figure 5.5.11), which correlate with cellular activity data (Figure 5.5.10).

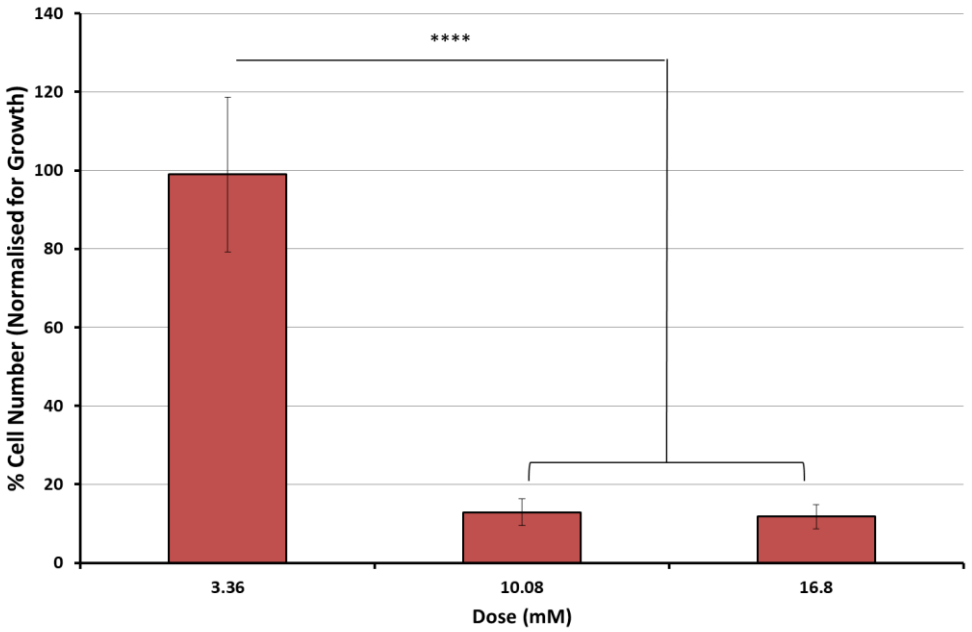

Figure 5.5.11 BAEC cell number change (%) of cells dosed with varying concentrations of gallium chloride (n=3)

Although this does not affect the biocompatibility of the hydrogel, it should be noted that the cellular activity of the BAECs at a 6.72mM concentration is below the ISO 10993 limit of 70% cell activity (see Figure 5.5.10). However, as gallium chloride is extremely acidic, it was

decided to dose the BAEC's with gallium nitrate. This also results in a significant decrease in cell metabolic activity, see Figure 5.5.12.

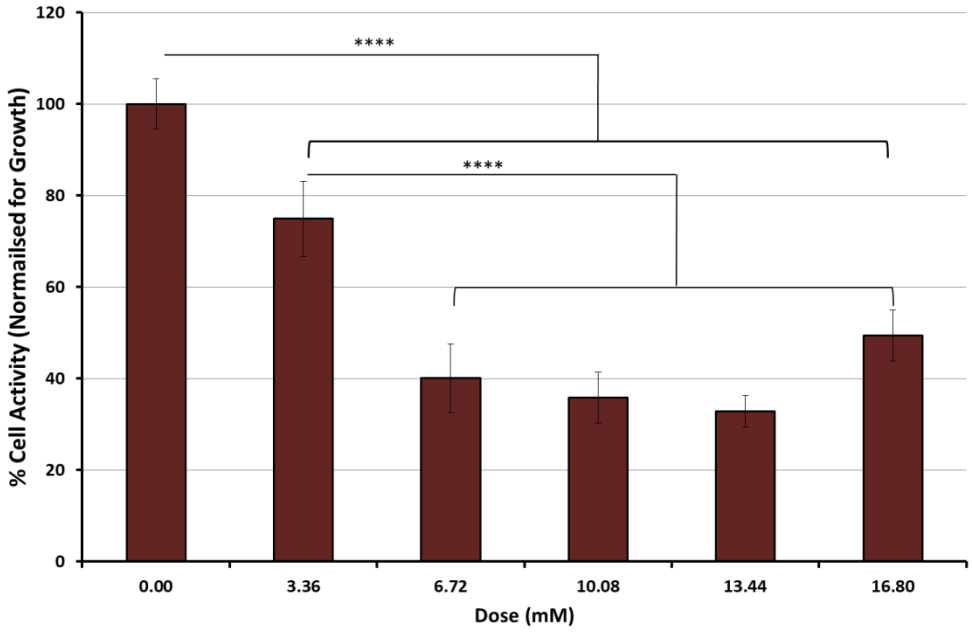

Figure 5.5.12 BAEC cell activity for cells dosed with gallium nitrate at different eluent concentrations (n=3)

Cell number had decreased significantly at each concentration, as shown in Figure 5.5.13. This reduction in cell number at each concentration is significantly reduced compared to the number of cells indicated by the cell activity Figure 5.5.12. Oxidized resazurin blue is converted to a fluorescent pink, which is possibly caused by the metabolisms consumption of oxygen [401]. This increase in metabolic activity is likely caused by the increase in oxygen consumption of the cells due the effects of nitric oxide [402].

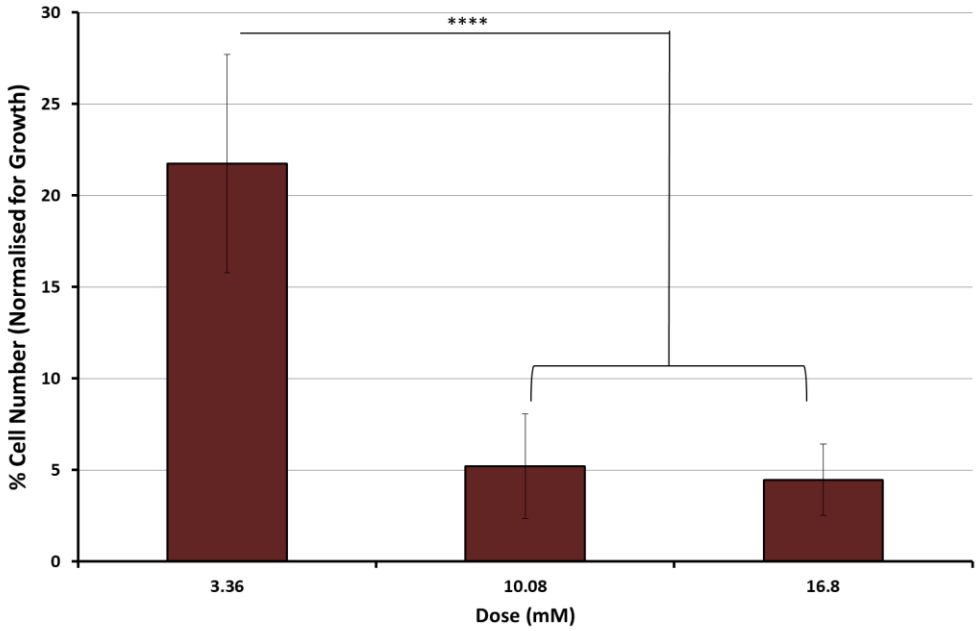

Figure 5.5.13 BAEC cell number change (%) of cells dosed with varying concentrations of gallium nitrate (n=3)

5.5.4.2. Calcium

Figure 5.5.14 shows the metabolic activity of the BAEC's dosed with calcium remained above the 70% limit. However, the metabolic activity decreased slightly with increased calcium concentrations.

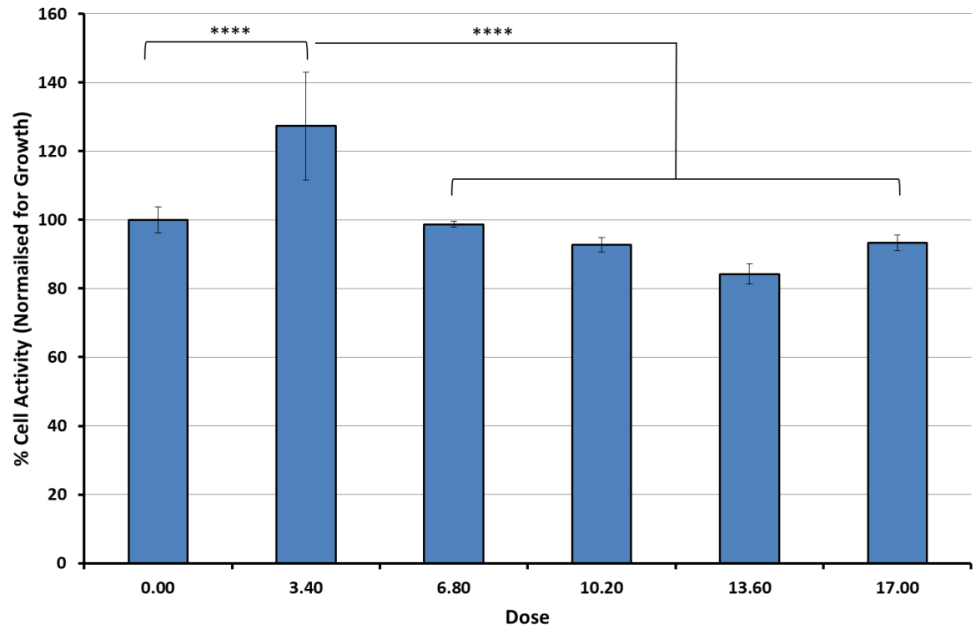

Figure 5.5.14 BAEC cell activity for cells dosed with calcium chloride at different eluent concentrations (n=3)

However, Figure 5.5.15 shows when the cells were dosed with 100% calcium chloride solution, there were significant levels of cell death, of 49% compared to the control.

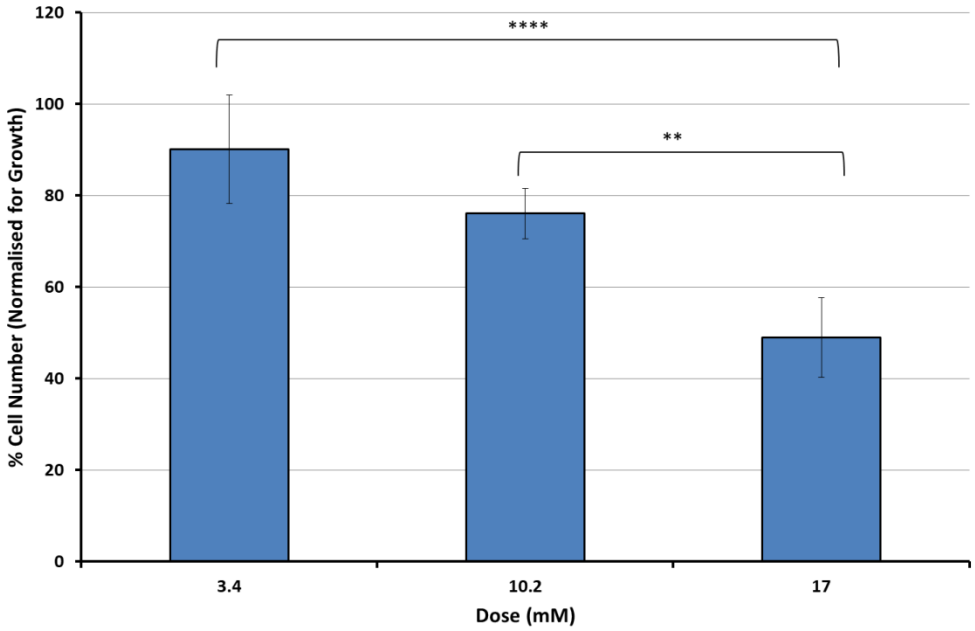

Figure 5.5.15 BAEC cell number change (%) of cells dosed with varying concentrations of calcium chloride (n=3)

5.5.4.3. Silica

Cells dosed with silica showed a significant increase in cell metabolic activity Figure 5.5.16

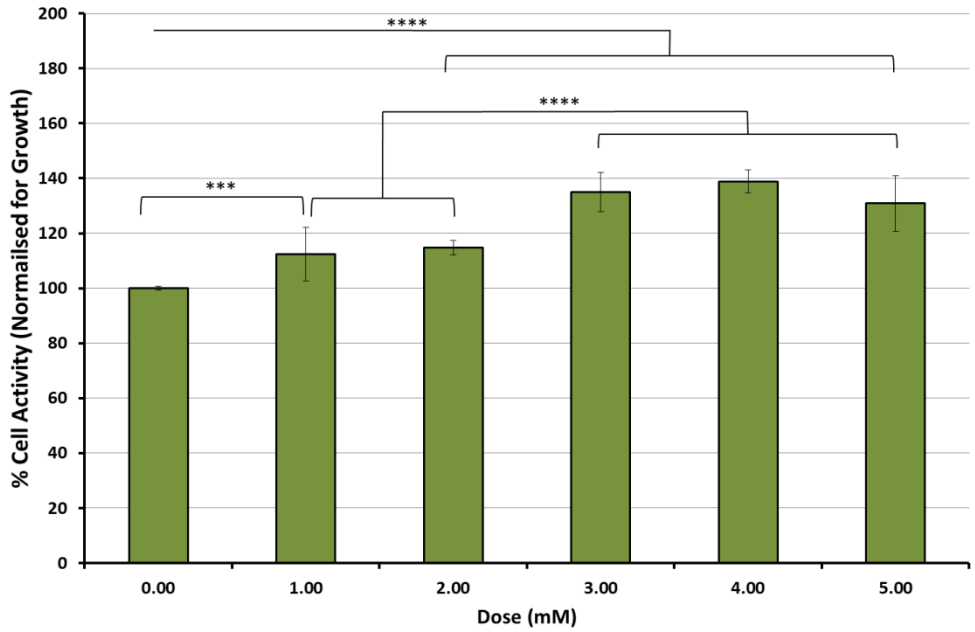

Figure 5.5.16 BAEC cell activity for cells dosed with silicic acid at different eluent concentrations (n=3)

Figure 5.5.17 shows that the increase in metabolic activity is likely caused by an increase in cell number, where the cell number increased 50% compared to that of the control.

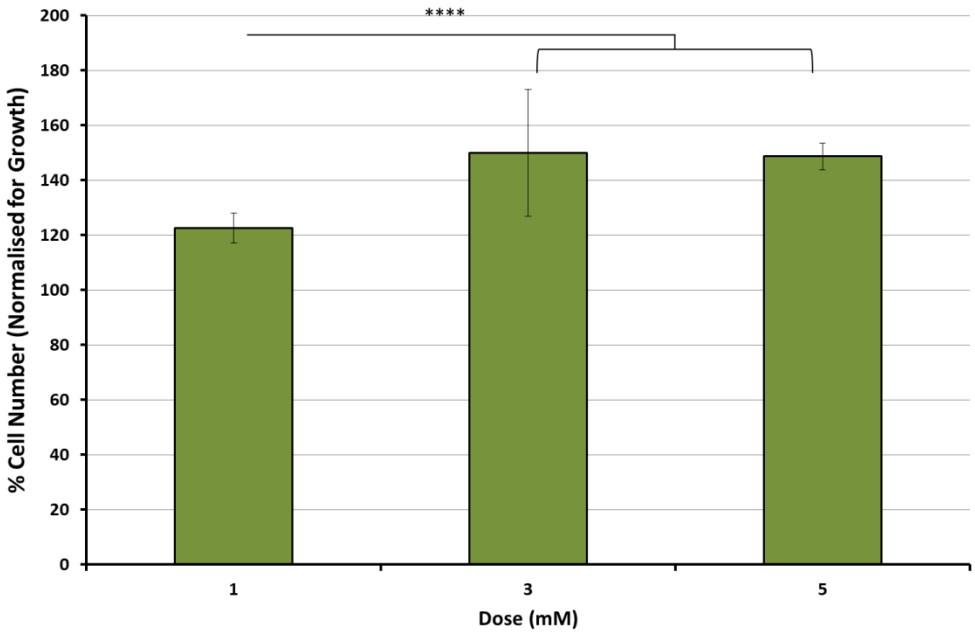

Figure 5.5.17 BAEC cell number change (%) of cells dosed with varying concentrations of silicic acid (n=3)

5.5.4.4. Glucono-Delta-Lactone

There is a significant increase in cells dosed with 20% and 100% GDL. A slight increase was seen in cell activity when dosed with 40%-80% GDL; however, this was not a significant increase (see Figure 5.5.18). This indicates that the increase in cell metabolic activity is not dose dependent for GDL.

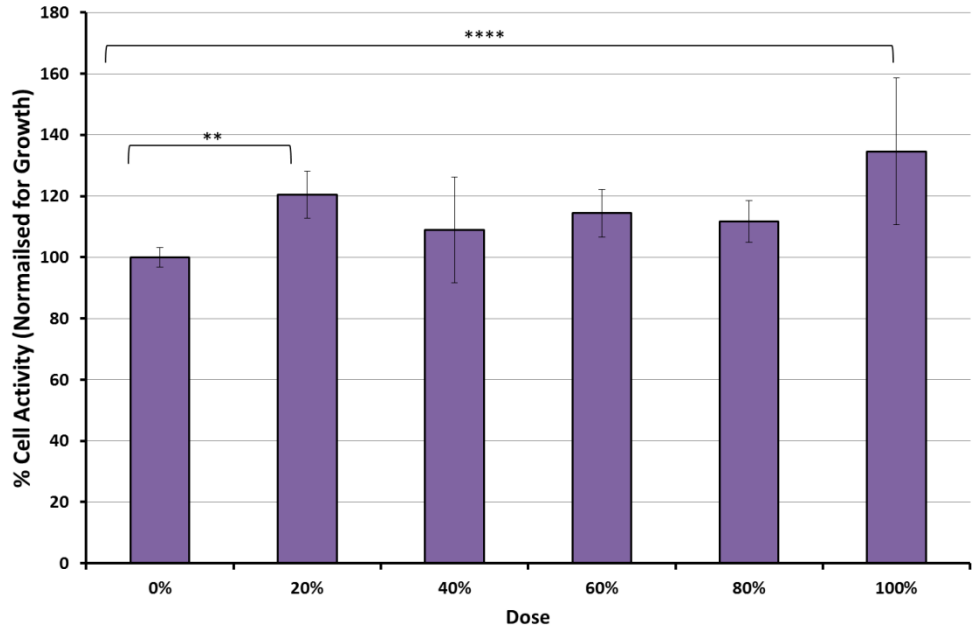

Figure 5.5.18 BAEC cell activity for cells dosed with GDL at different eluent concentrations (n=3)

This plateau was also seen in cell number. Figure 5.5.19 shows that at a 20% concentration there was an increase in cell number that was maintained with increasing GDL concentrations.

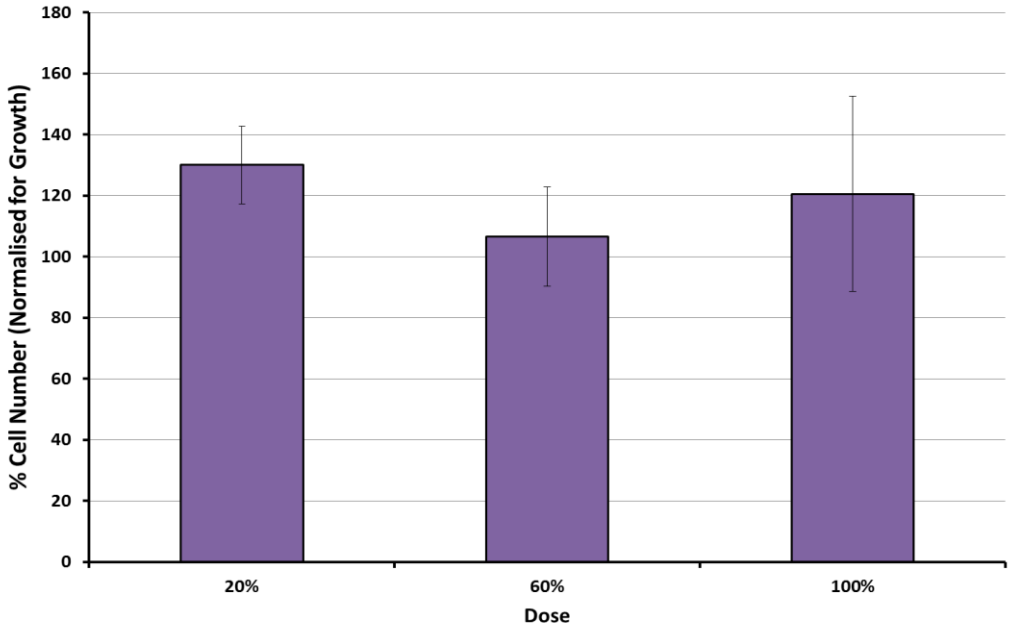

Figure 5.5.19 BAEC cell number change (%) of cells dosed with varying concentrations of GDL (n=3)

5.5.5. Discussion

There was varying results for cell metabolic activity when dosed with each of the 24 hour eluents. There was no significant change in metabolic activity when comparing the 20% and 100% dose of Eluent A and Eluent B (Figure 5.5.1 and Figure 5.5.2), while Eluent C (Figure 5.5.3) causes a dose dependent increase. However, eluent dosing shows a significant increase in metabolic activity when dosed with each 48 hour eluent compared to the 24 hour eluent. Yet, there was no significant increase in the number of cells when comparing 24 and 48 hour eluent at a 100% concentration. This may be caused by resazurin blue typically over estimating the number of cells due to the changes in metabolic activity of cells during their life cycle [300]. The 24 hour dosing time may also not have been sufficient time to see this increase in cell numbers, as doubling time of endothelial cells *in vitro* ranges from 18 - 67 hours [403] [404]. In the presence of growth factors, cells metabolic activity increases to accommodate the energy required for cells to proliferate but the increase in cell number is not seen immediately [399]. Although there is no significant difference in ion content between the 24 hour and 48 hour eluent, there may be an increase in gluconic acid. Gluconic acid can be metabolised as glucose by cells [405]. This increase in glucose may be facilitating the increase in glucose uptake typically caused by growth factor stimuli [399]. If there are insufficient nutrients to accommodate the increase in metabolic activity caused by growth factors, the cells will undergo apoptosis [399]. A lack of glucose or nutrients in the cell culture media may be causing the plateau or reducing the metabolic activity in the 24 hour Eluent A and Eluent B cells (Figure 5.5.1 and Figure 5.5.2). The decrease in cell metabolic activity with the 24 hour eluent compared to the 48 hour eluent may also be caused by the slightly acidic pH of the eluent. The pH of the eluent is lower at 24 hours compared to that of the 48 eluents

due to the neutralising effect of the alkali ions. A decrease in extracellular pH can reduce cell proliferation or result in apoptosis [406] [407].

Although there was no significant change in ion concentrations released from the hydrogel over time, there was a slight increase. This suggests there is a continued release of ions from the glass which is improving the hydrogel's strength over time. Eluent A (untreated glass) has a greater release of Ga^{3+} and Ca^{2+} compared to eluent B (acid washed glass). This decrease in release of ions is likely caused by the increase in network connectivity of the acid washed glass, as discussed in Section 5.3. Eluent C has the lowest release of ions which may be caused by the increase in pH due to the addition of EDC and NHS, as the release of ions from the bioactive glass is reliant on an acidic environment. The ion quantity in the eluent is significantly higher compared to ions typically released from bioactive glasses such as Bioglass 45S5 this is likely caused by alginates ion exchange with sodium in ionic media [408]. The typical calcium content found in blood serum is 2.45mM and the synovial fluid surround the human knee joint has a calcium content of a minimum 4mM [409] [410]. The calcium content of the eluent both greatly exceeds these values.

There is a general trend observed of a dose dependent increase in both cell metabolic activity and cell number at each eluent examined. The increase in cell metabolic activity with increasing eluent concentration suggests there are growth stimulation factors being caused by the ions released from the hydrogel. To examine this dose dependent increase further, BAEC were dosed with GDL and gallium, calcium and silica ions individually at the average concentration each was released from the hydrogel.

Gallium was shown to cause cell death, evident in both cell metabolic activity (Figure 5.5.10 and Figure 5.5.12) and cell number (Figure 5.5.11 and Figure 5.5.13). It has been previously shown that gallium has caused a decrease in cell numbers with increasing gallium content [411]–[413]. These cytotoxic effects may be caused by gallium's interference with cells mitochondria and iron uptake. Apoptosis of cells stored in gallium nitrate for 24 hours has been shown, with effects on the mitochondria evident at 2 hours. However, the cause of changes is cells mitochondria in the presence of gallium is still unknown [414].

Transferrin is a protein that transports iron. Typically, the iron content is approximately 3.3µg/ml, with only one third of available iron binding sites occupied by iron (Fe^{3+}). Fe^{3+} ions are extremely similar to Ga^{3+} ions and for this reason can bind to transferrin when gradually exposed to blood [338]. Cellular activity reduces Fe^{3+} to Fe^{2+}, however, gallium does not exist in a valence state of 2+ and therefore cannot partake in the oxidoreductase reduction [415]. Due to this, gallium can be cytotoxic to iron dependent cells. This provides gallium with

antitumor properties as it causes iron deprivation in malignant cells, which have a high iron requirement [414].

Although there is a significant decrease in cell number and metabolic activity *in vitro,* the effects in *vivo* may not be as damaging. This is due to gallium binding to the larger quantities of transferrin found in blood and a larger supply of iron. Only one third of transferrin has iron bound to it, providing unoccupied binding sites for gallium without decreasing iron content of serum. Gallium can precipitate to become gallate in whole blood and can be excreted by the body [338]. Studies have shown that gallium injected both intravenously and subcutaneously results in an increase in blood clearance and urinary excretion of gallium ions but did not have toxic effects [338]. A solution of 25mg/ml of gallium nitrate has also been approved by the FDA for the treatment of hypercalcemia, which greatly exceeds the amounts released by the hydrogel here [414]. Gallium may reduce inflammation *in vivo*, which was not examined here. This is due to gallium's anti-inflammatory and immunosuppressive activity [338] [416]. Also, the pH of the media when dosing the cells with gallium had to remain slightly acidic, as gallium can precipitate at a neutral pH, as discussed in Materials and Methods 4.8.3. As discussed previously, an acidic extracellular pH results in cell apoptosis.

There was an increase in cell death when dosed with gallium nitrate compared to gallium chloride. This may be due to the increased nitric oxide levels as excessive amounts of nitric oxide can induce apoptosis of endothelial cells by oxidative degradation [417] [418].

There was a significant increase in both cell metabolic activity (Figure 5.5.16) and cell number (Figure 5.5.17) when dosed with up to 3mM silica content. Following this there was a plateau. Calcium shows a significant decrease in cell number (Figure 5.5.15) with only 49% of cell viable after dosing with 17mM of calcium. Extensive research using Bioglass® and other calcium silicate based cements show that these glasses increase the expression of vascular endothelial growth factor (VEGF) and basic fibroblast growth factor (bFGF). This resulted in proliferation of endothelial cells and tubule formation, indicating angiogenesis [131] [183] [241] [408] [419] [420]. It was determined that the increase in cell proliferation was likely caused by the silica ions present, as there was a minimal increase in calcium ions found in the eluent [131] [183] [241]. Intracellular and extracellular calcium content is vital for cell survival and proliferation but the levels of calcium found in the eluent likely exceed the amounts required [421]. There is a 17mM release of calcium ions from the hydrogel. While calcium alginate hydrogels have shown similar or increased release of calcium, these high levels may induce hypercalcemia, as hypercalcemia is classed as a 0.25mmol/l increase in calcium ions of blood [422]–[425]. However, there is no significant difference in the number of ions released from the hydrogel at 24 and 48 hours for each eluent which may suggest that any hypercalcemia will only be temporary.

Figure 5.5.18 and Figure 5.5.19 show a slight increase and a plateau in the metabolic activity of the cells and the cell number when dosed with increasing amounts of GDL. The GDL hydrolysis likely results in an increase in glucose, which has been shown to cause cell proliferation [426], however, without an increase in cell growth factors there may not be a requirement for the increase in glucose by the cells.

Individual ion dosing did not see cell numbers increase as high as eluent dosing. This may be caused by several interactions between the ions and glucose released by the hydrogel. These possible synergistic effects were not examined. When examining the ions individually, there was no increase in the gluconic acid content with increasing ion content. This may have reduced cell proliferation due to a lack of glucose which supports the energy requirements of the proliferating cells. Finally, changes in pH were not taken into consideration, which may have a significant moderating effect on increased cellular activity. The 24 hour eluent had a decreased pH compared to the 48 hour eluent which can result in variations to that which would be experienced *in vivo*.

There are limitations to the cytotoxicity testing carried out here. The cells tested here are bovine aortic endothelial cells rather than human cerebrovascular cells, which is the cell line that the hydrogel would come in contact with *in vivo*. Also, the eluent dose that will exist under *in vivo* conditions is unknown. The testing carried out here is static (unlike *in vivo*) and the media was not changed over the 24 hour period. *In vivo* there will be a continued supply of blood significantly diluting the eluent concentration and reducing the possible damage caused by a reduction in pH. The hydrogel, at the neck of the aneurysm, will be exposed to blood flow which will likely decrease the eluent ion concentration and pH compared to the hydrogel in contact with the fundus of the aneurysm.

Overall, these results indicate that acid washing the glass particles causes a positive response in terms of the proliferation of BAEC, compared to the non-treated glass. This is likely caused by the increase in network connectivity of the glass. Typically, bioactive glasses are designed to have a lower network connectivity to allow for the dissolution of the glass and to promote hydroxyapatite formation. In the hydrogel here, an increased network connectivity reduced the release of gallium and calcium ions (Figure 5.5.7 and Figure 5.5.8). The results of individual ion dosing have shown that both calcium and gallium cause cell apoptosis in a dose dependent manner. There was no significant change in the release of silica from the hydrogel, which has been shown to likely be a cause of the overall cell proliferation (Figure 5.5.17) of Eluent A, Eluent B and Eluent C. Figure 5.5.19 indicates that GDL is likely supporting the energy requirements of the proliferating cells. Figure 5.5.9 shows that Eluent C has a reduced release of gallium, calcium and silica ions from the hydrogel. Although the reduction release of gallium and calcium is reducing cell apoptosis, there is a reduced amount of the cell

proliferation silica. EDC and NHS were also added in the hydrogel formula for Eluent C, which may have a cytotoxicity response such as those exhibited in mice [213]. This combination is likely resulting in the decrease in cell proliferation of cells dosed with Eluent C. These results indicate that the ions released and the rate at which these ions are released from the hydrogel can have an effect of cell growth.

Increases in both endothelial and smooth muscle cells will likely have a positive effect on the procedural outcome with this aneurysm filler, by encouraging cell growth across the neck of the aneurysm. Encouraging cell growth across the neck of the aneurysm will completely occlude the aneurysm from the parent artery and reduce the chance of aneurysm rupture. Apoptosis of smooth muscle cells and endothelial cells is exhibited during the formation of aneurysms; therefore it is likely that the proliferation of these cells will strengthen the aneurysm fundus. Strengthening of the aneurysm dome will reduce aneurysm growth and rupture if aneurysm recurrence occurs due to the compaction of the hydrogel or recanalization [34] [427]–[429].

The cells dosed with Eluent A, at lower concentrations, cause an unacceptable level of cell death and therefore would not be an acceptable treatment for cerebral aneurysms. There was no significant difference in the cells dosed with Eluent B and C; however, in both cases there was increased cell proliferation at higher eluent concentrations. Endothelial cell proliferation is preferable as proliferation at the neck of the aneurysm greatly reduces the chances of recurrence in coiled aneurysm, as the aneurysm is separated from the parent artery [75] [430] [431]. However, excess endothelial cell proliferation within the aneurysm body may cause recanalization of the aneurysm. Endothelial cell proliferation, particularly at the wall of the aneurysm, may cause the aneurysm to recur. The hydrogel composition used for eluent C is therefore the optimum concentration for this application as it causes cell proliferation, which may induce endothelialisation of the neck of the aneurysm, while adhering to the aneurysm wall to reduce the chances of recurrence associated with recanalization of the aneurysm [432]–[435]. Appendix 9.5.3 shows bovine aortic smooth muscle cells (BASMCs) dosed with Eluent C. The results show that this hydrogel is also non-cytotoxic to BASMCs.

Table 5.5.2 Design review table with in vitro analysis results

Sample	Compressive Strength >22kPa?	Is the material size conserved? (<10% expansion with no shrinkage)	Is the hydrogel injectable?	Working Time between 10 and 30 mins?	Hardening Time <5 mins?	Is the material adhesive?	Is the material cytocompatible? (>70% cell viability)	Is the material sterilisable?	Is the material suitably radiopaque?	Is the material haemocompatible?
Eluent A	Yes	No	Yes	Yes	Yes	Not examined	No	TBD	TBD	TBD
Eluent B	Yes	No	Yes	Yes	Yes	Yes*	Yes	TBD	TBD	TBD
Eluent C	Yes	No	Yes	Yes	Yes	Yes**	Yes	TBD	TBD	TBD

* has a bond strength of 37kPa and ** has a bond strength of 85kPa after storage for 24 hours in SBF

5.6. Optimising Sterilisation Techniques

As discussed previously in Section 2.4.5 (page 29), there are many options for material terminal sterilisation. However, not all materials can undergo each sterilisation due to the effects on the material properties. Ethylene oxide and other chemical sterilisation techniques should not be used for neurovascular devices unless residue levels are examined after sterilisation due to their neurotoxicity and possible carcinogenic properties [436].

Several sterilisation techniques have been outlined in the literature for sterilising alginate such as dry heat, autoclaving, gamma irradiating, filtering and UV sterilisation. Sterilisation by filtration causes minimal damage to the alginate but is time consuming and difficult to achieve consistent batches when packaged dry [156]. UV sterilisation has been shown to not produce consistent reduction in endotoxin levels [436]. Dry heat requires exposure to higher temperatures for a prolonged period of time compared to autoclaving and, as a result, causes increased polymer degradation [437] [438]. Section 5.2 has shown that gamma irradiation significantly decreases the molecular weight of the alginate. Gamma irradiating the alginate on dry ice does reduce the irradiation induced damage but still significantly reduced the hydrogel strength [439]. As a result, it was decided to autoclave the dry alginate powder. Autoclaving may not be ideal for steam penetration but it will likely reduce the damage of the alginate due to the reduced temperature of the autoclave compared to dry heat sterilisation [440].

The powder components of the hydrogel (*i.e.* glass, GDL, EDC and NHS) must also be terminally sterilised. Glass can be sterilised by dry heat sterilisation due to its high Tg but GDL, EDC and NHS have melting points of 153^0C, 115^0C and 95^0C, respectively. For effective dry heat sterilisation the material should be heated to 170^0C for 1 hour or 160^0C for 2 hours and 121^0C for 15 minutes for steam sterilisation. These temperatures are above the melting point of these materials and therefore neither technique can be used for sterilisation [441]. Due to these restrictions, it was decided to gamma irradiate the powder samples on dry ice in order to minimise damage, which has been shown to reduce damage to samples during irradiation [166].

5.6.1. Alginate Sterilisation

Although the specific endotoxin level is not stated, raw alginate typically has a high endotoxin level. It has been shown that the purification technique used to produce the 700kDa alginate (Technique 2) does significantly reduce the endotoxin levels but likely not enough to achieve the levels required by the FDA for neurovascular devices [346]. Therefore, the alginate will likely need an increased amount of terminal sterilisation to reduce endotoxin levels, which will cause an increased reduction in the molecular weight of the alginate.

To reduce the initial endotoxin levels present in the alginate and to provide a material suitable for preclinical testing, an ultrapure alginate was purchased from FMC biopolymer. The alginate is a medium viscosity with high M-block content of 55%, a molecular weight of 254kDa and a known endotoxin level of 26EU/g. A 4.5% alginate concentration would give an endotoxin level of 1.17 EU/ml. This alginate will be referred to as MVM.

Analysis from this point forward will continue with the hydrogel composition of 4.5% alginate, 13.8% glass, 8.3% (w/v) of GDL and 0.83% (w/v) EDC and NHS, unless otherwise stated. Although Table 5.5.2 shows the hydrogel with both 0% (w/v) and 0.83% (w/v)of EDC and NHS having potential use as an aneurysm treatment, the addition of 0.83% (w/v) of EDC and NHS improved the adhesive strength and reduced cell proliferation which may reduce recanalization.

5.6.1.1. Compressive Strength

Figure 5.6.1 shows there is a significant difference between the compressive strength of the 700kDa alginate and the MVM at day 1, due to the increased G-block content. However, with further cross-linking of the hydrogel over time, the hydrogels have compressive strengths that are not significantly different. The strength of both hydrogels significantly increases from 1 to 7 days.

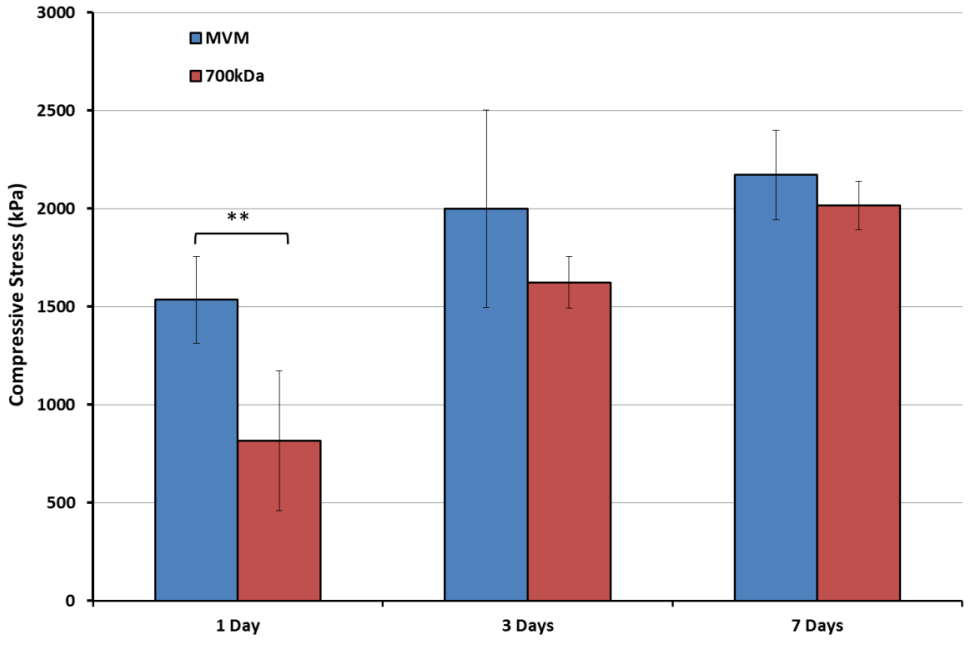

Figure 5.6.1 Compressive stress up to 70% strain of the 700kDa alginate and the ultrapure medium viscosity (MVM) alginate after storage at 37^0C in DI (n=5)

There is a significant difference in the incremental modulus of the hydrogel at each time point (Figure 5.6.2), where the MVM is significantly stiffer than the 700kDa alginate. This was expected due to the increased content of stiff G-blocks [442]. The increased stiffness caused

by the increased G-block may cause the material to undergo brittle failure. However, it may also provide a hydrogel with an increased strength after sterilisation.

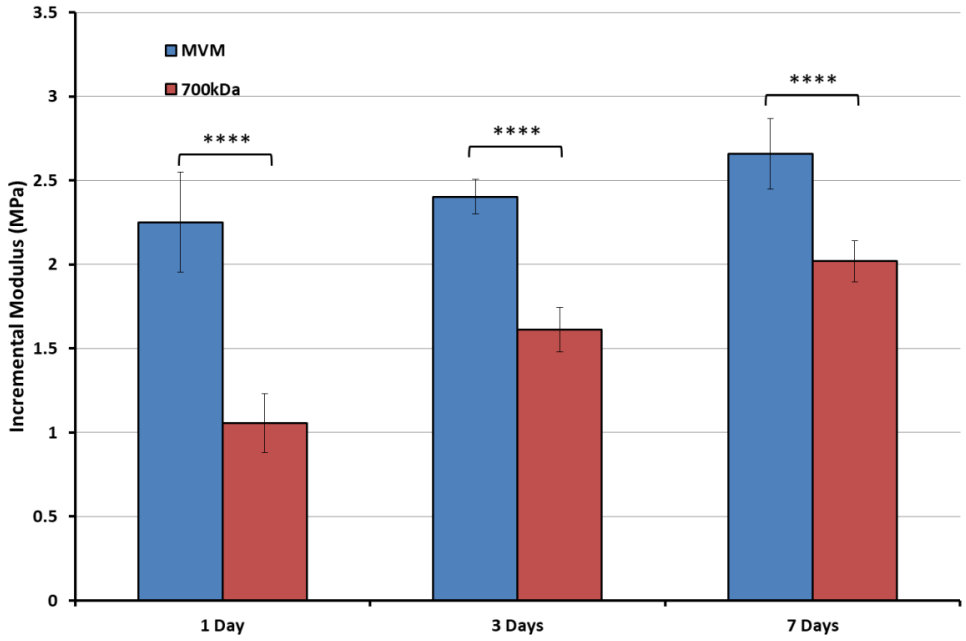

Figure 5.6.2 Incremental modulus (30-50% strain) of the 700kDa alginate and the ultrapure medium viscosity (MVM) alginate following storage at 37^0C in DI (n=5)

BAEC's were also dosed with the eluent of the hydrogel using the MVM alginate and showed no cytotoxic effects (Appendix 9.5.4.2). These results indicate the MVM alginate is a suitable alternative as a replacement for the 700kDa alginate.

As the MVM alginate still had an endotoxin level greater than the acceptable amount and as medical devices must be terminal sterilised after packaging, the alginate was autoclaved. Autoclaving causes a 3-log reduction in endotoxin levels with would give the alginate a final endotoxin content of 0.00117 EU/ml at a 4.5% concentration, which is below the maximum endotoxin level of 0.06EU/ml specified by the FDA [443].

Figure 5.6.3 and Figure 5.6.4 shows that the compressive strength and incremental modulus of the hydrogel decreased when the alginate was autoclaved. This was due to chain scissions reducing the molecular weight of the alginate (see Section 5.6.4.1). It has been previously shown that increasing the alginate concentration can increase the hydrogel's strength if there is a sufficient glass and GDL content (see Figure 5.1.10). As there is a high glass and GDL content it was decided to examine the effects of an increased alginate concentration. Increasing the alginate concentration of the hydrogel to 6.75% increased the strength but a further increase to a 9% alginate concentration reduced the strength. This is likely caused by an inhomogeneous gel being produced due to a lack of cross-linking ions, as was previously observed in Section 5.2. Inhomogeneity may also be the cause of the increase in standard deviation observed.

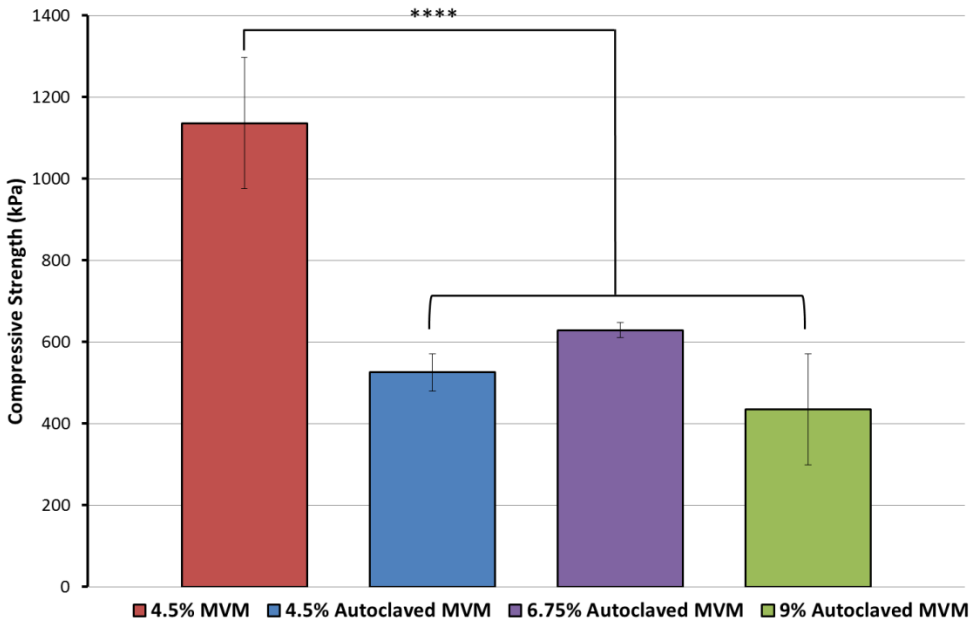

Figure 5.6.3 Compressive strength up to 70% strain of the alginate before and after autoclaving at varying concentrations following storage for 1 day in DI at 37^0C (n=5)

There is no significant decrease it the incremental modulus of the 4.5% alginate after autoclaving (Figure 5.6.4). Similar results have been observed in high G-block alginates, as the stiffness is usually a results of the length of the G-block [192]. Increasing the alginate content up to 6.75% causes an increase in the incremental modulus, likely due to an increased cross-linking density. The compressive strength decreases at 9% alginate concentration which indicates a lack of available cross-linking ions.

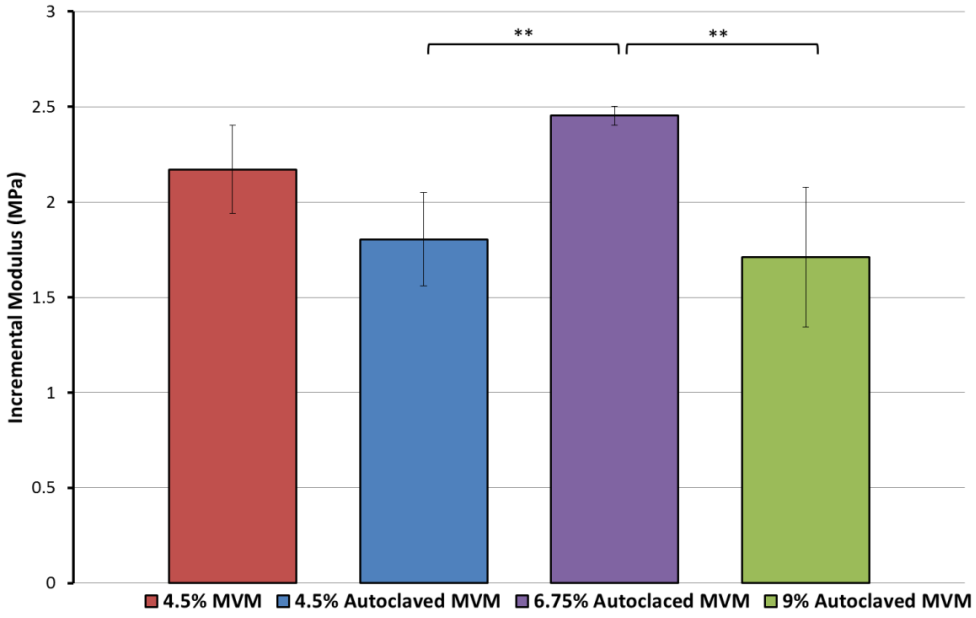

Figure 5.6.4 Incremental modulus (30-50% strain) of the alginate before and after autoclaving at varying concentrations following storage for 1 day in DI at 37^0C (n=5)

There is a significant change in the volume conservation of the hydrogel. The 6.75% alginate concentration has the lowest and most suitable volume change of the hydrogels tested. The expansion of the 9% alginate concentration further indicates that there is a lack of the ions available for cross-linking.

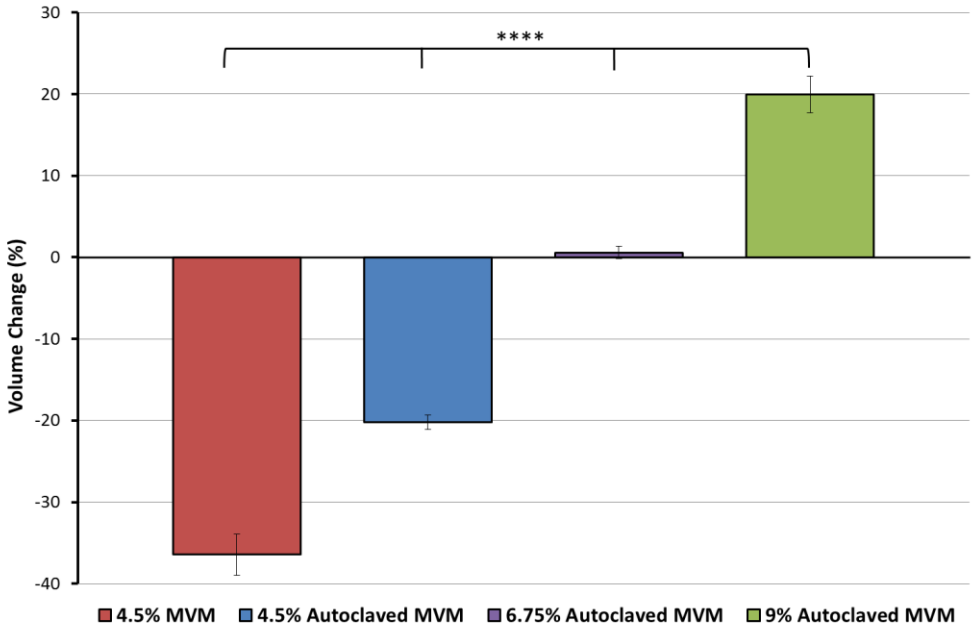

Figure 5.6.5 Alginate size conservation after 1 day following storage for 1 day in DI at 37^0C (n=5)

5.6.1.2. Injectability

To examine the injectability of the hydrogel, it was injected through a 150mm 2F microcatheter, 5, 15 and 20 minutes from the start of mixing. Figure 5.6.6 shows the force required to inject the hydrogel after 5 and 15 minutes. Results from 20 minutes were omitted as the hydrogel at a 6.75% alginate concentration would not inject through a microcatheter. As the hydrogel was not set within 20 minutes it will likely leak into the surrounding vasculature once the balloon is deflated, if the hydrogel was injected at 15 minutes. Due to this, the hydrogel alginate concentration will need to be reduced to cause a reduction in viscosity and allow injection up to the end of working time.

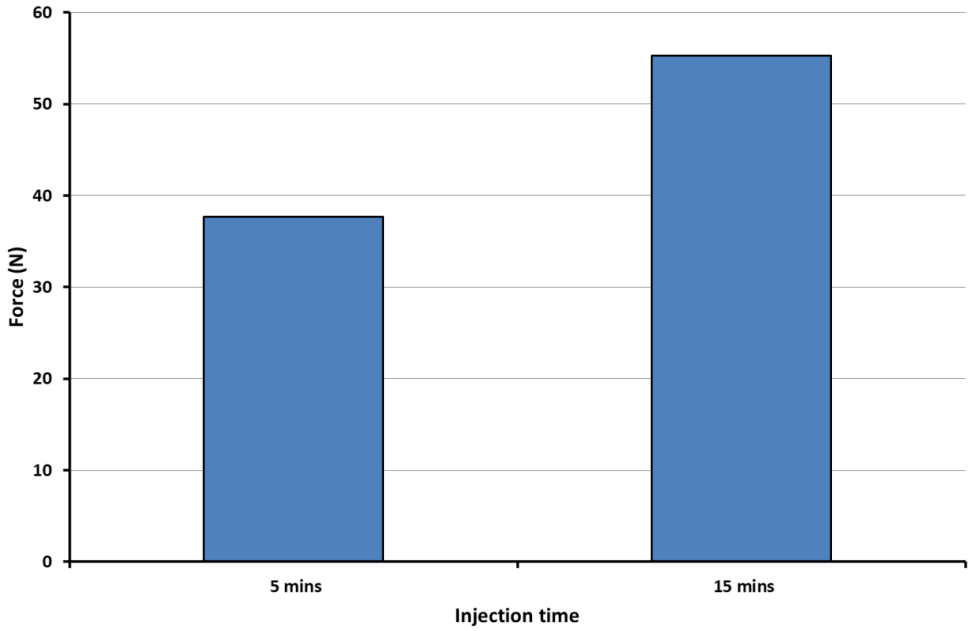

Figure 5.6.6 Force required to inject 6.75% autoclaved MVM hydrogel through a microcatheter 5 and 15 minutes after mixing

The 4.5% autoclaved MVM alginate would inject through the microcatheter but, as shown in Figure 5.6.5, the samples volume decreased significantly after 1 day. This suggests that the cross-linking density was above the required amount. To reduce the cross-linking density the 4.5% autoclaved MVM alginate was tested with a 9.2% glass content and 6.25% (w/v) of GDL. These samples maintained their size after 1 day and had strength exceeding 22kPa so it was decided to continue testing with this hydrogel formulation. Figure 5.6.7 shows that the force required to inject the hydrogel was greatly reduced.

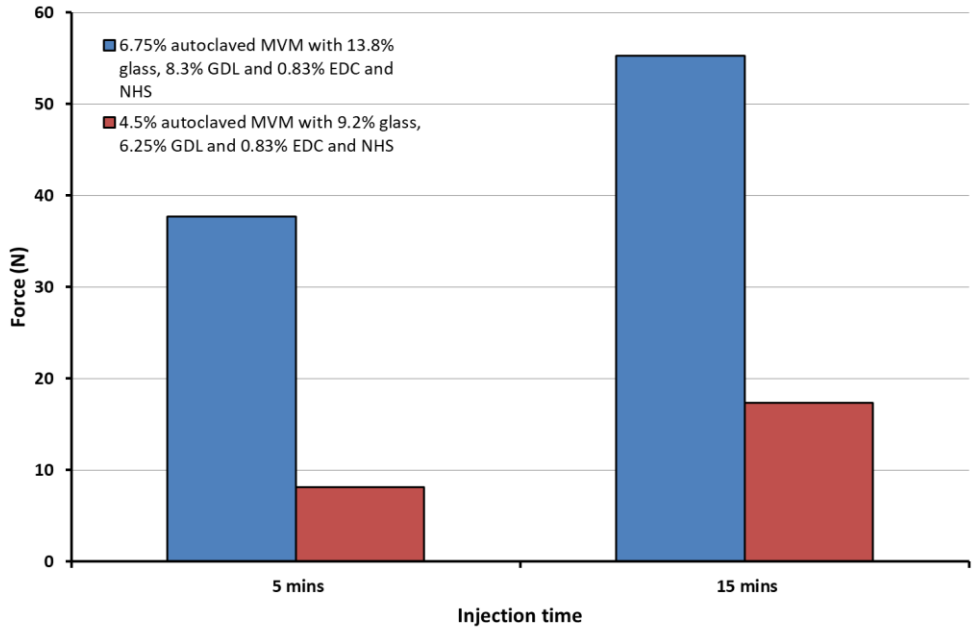

Figure 5.6.7 Force required to inject the hydrogel at various compositions through a microcatheter 5 and 15 minutes after mixing

5.6.2. Powder Components Sterilisation

The powder components of the hydrogel (glass, EDL, EDC and NHS) were gamma irradiated on dry ice. The minimum and maximum gamma irradiated doses were 18.8kGy and 20.5kGy, respectively.

5.6.2.1. Compressive Strength

The results in Figure 5.6.8 show the effects low temperature gamma irradiation of the powder components has on the compressive strength of the hydrogel. It can be seen that gamma irradiation has no effect on the compressive strength of the hydrogel.

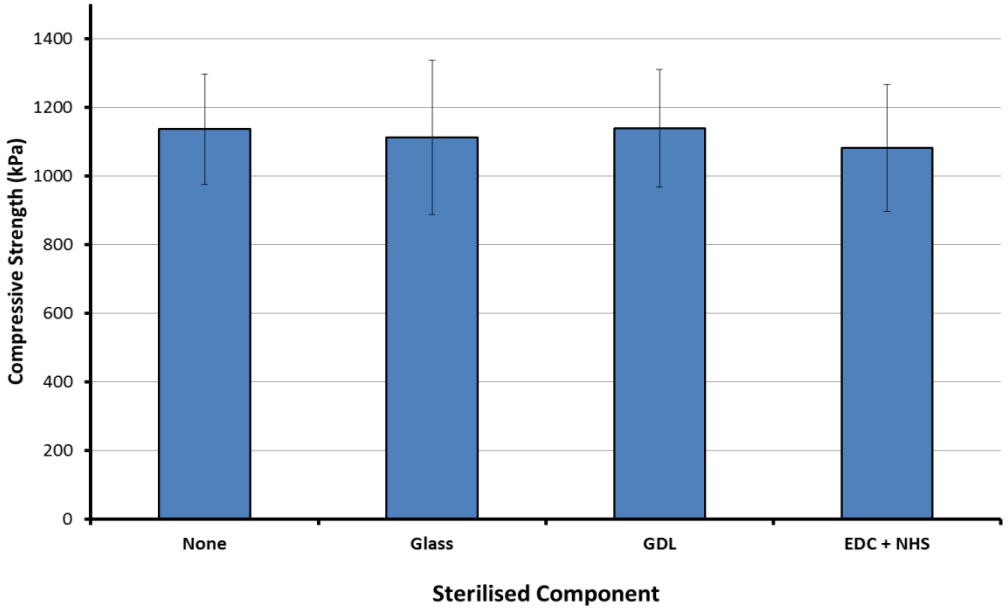

Figure 5.6.8 Compressive strength up to 70% strain of the hydrogel with individual components sterilised using low temperature gamma irradiation following storage for 1 day in SBF at 37^0C (n=5)

5.6.3. All Components Sterilised

5.6.3.1. Compressive Strength

Due to the low volume change and ease of injectability of the hydrogel it was decided to continue testing the hydrogel with a 4.5% alginate concentration of the autoclaved MVM alginate with 9.2% glass and 6.25% (w/v) of GDL. Figure 5.6.9 and Figure 5.6.10 show that the compressive strength and the incremental modulus of the hydrogel increase over time when all the components are sterilised. Figure 9.5.27 shows typical stress-strain graphs. The strength is significantly decreased from that of the non-sterilised 700kDa and MVM alginate (Figure 5.6.1 and Figure 5.6.2), though the change in storage media is likely contributing to these results. However, the hydrogel still greatly exceeds the 22kPa required and increases over time.

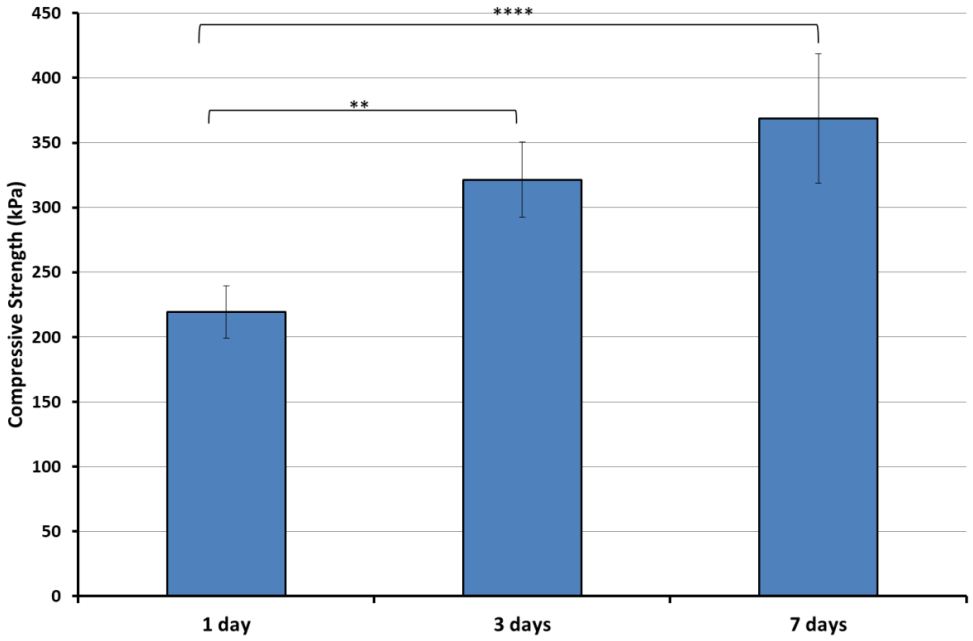

Figure 5.6.9 Compressive strength up to 70% strain of the sterilised hydrogel with 4.5% alginate following storage in SBF at 37^0C (n=5)

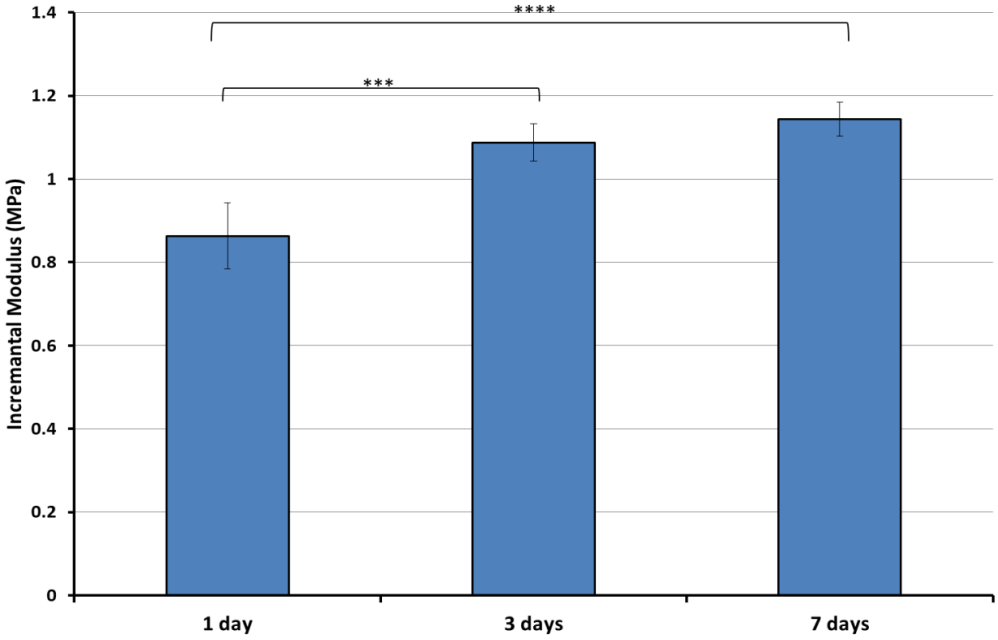

Figure 5.6.10 Incremental modulus (30-50% strain) of the sterilised hydrogel with 4.5% alginate following storage in SBF at 37^0C (n=5)

5.6.3.2. Sample Size Conservation

Typically, as the strengths of the hydrogel increases there is a decrease in sample volume expansion. Figure 5.6.11 shows that these samples slightly increase in volume after storage in SBF. However, there is not significant increase over time.

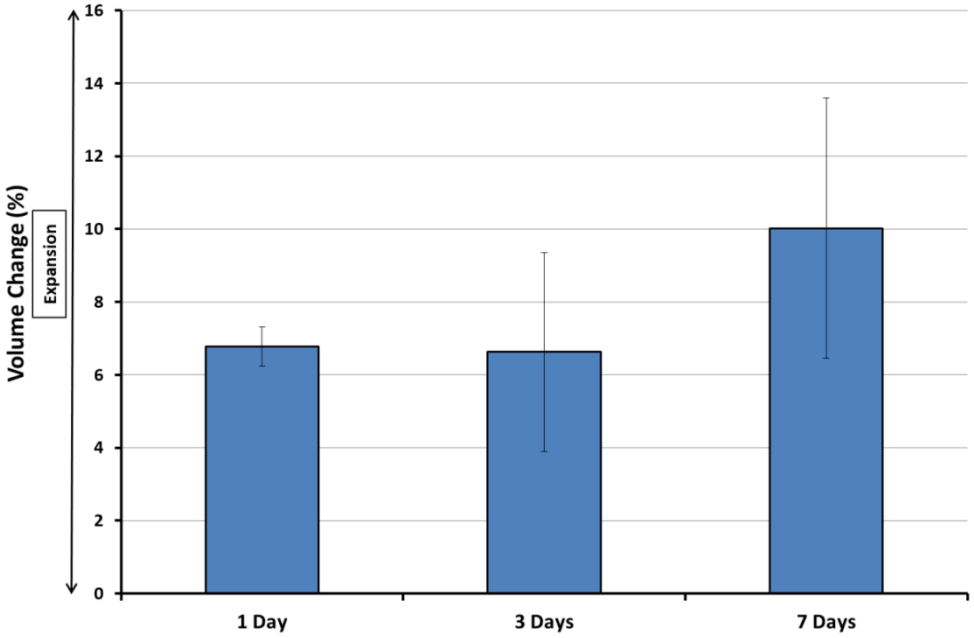

Figure 5.6.11 Sterilised hydrogel with 4.5% alginate size conservation (n=5)

5.6.3.3. Tensile Strength

The tensile strength is significantly reduced by autoclaving the alginate, however, the strength continues to increase over time. As the strength of the hydrogel increases, the strain at which the hydrogels fail increases, indicating the hydrogels are become more ductile over time. The 4.5% MVM alginate fails at a strain of 29.45±7.8 % at day 1 and 43.6±5.2 % at day 7. The 4.5% autoclaved MVM alginate hydrogels are stiffer, failing before 20% strain for each sample tested.

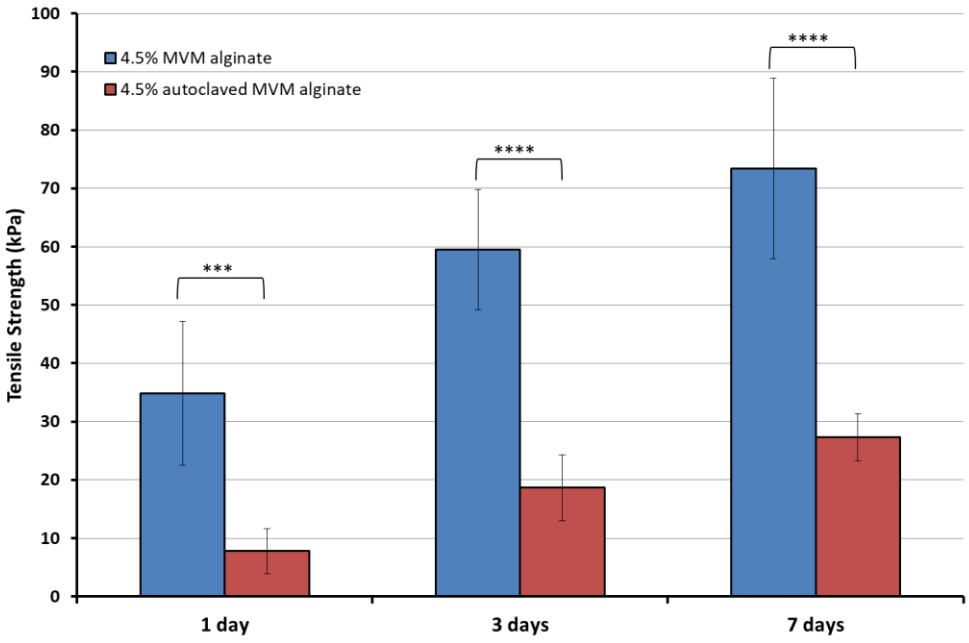

Figure 5.6.12 Ultimate tensile strength of the non-sterilised and sterilised hydrogel with 4.5% alginate following storage in SBF at 37^{0}C (n=5)

5.6.3.4. Bond Strength

Sterilising the hydrogel components has no significant effect on providing a high bond strength, as shown in Figure 5.6.13. Unlike the non-sterilised hydrogel, the sterilised hydrogel failed cohesively rather than adhesively. This is likely due to the reduced strength observed (Figure 5.6.12).

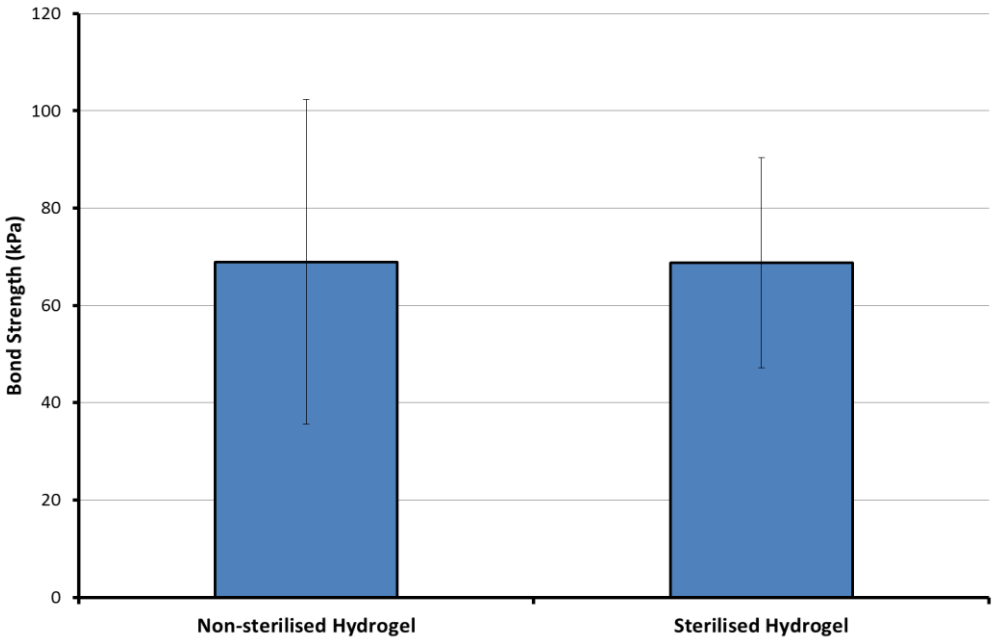

Figure 5.6.13 Bond strength of the hydrogel before and after sterilisation following storage for 1 day in SBF at 37^0C (n=5)

5.6.3.5. Working and Hardening Time

Figure 5.6.14 shows that only sterilising the EDC and NHS powder component has an effect on the hydrogel's working time. The gamma irradiation is likely not reducing the network connectivity of the bioactive glass or increasing the rate of hydrolysis of the GDL, as both of these would result in a quicker release of cross-linking ions and a likely reduction in working time. EDC and NHS have been previously shown to increase the working time of the hydrogel (Figure 5.4.3). These results suggest that the gamma irradiation causes an increase in the buffering effect of the EDC, resulting in an increased pH.

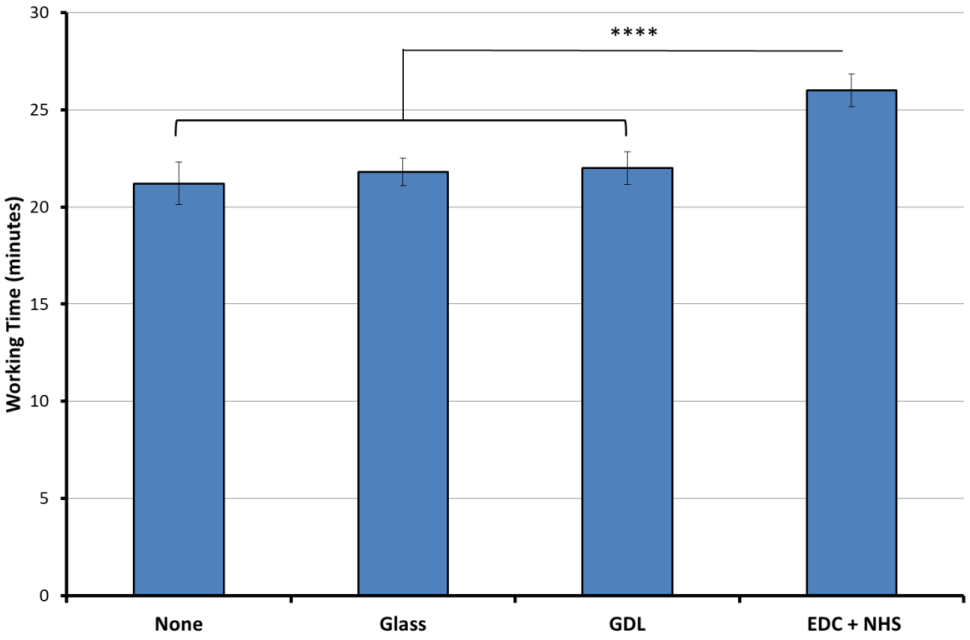

Figure 5.6.14 Working time of hydrogel with individual components sterilised using low temperature gamma irradiation (n=5)

Figure 5.6.15 shows no significant change in hardening time when each of the powder components were sterilised. Although sterilising the EDC and NHS causes an increase in working time, it is not evident in the hardening time. This may due to the continued decrease in pH with the hydrolysis of GDL allowing the glass to release sufficient ions to cross-link the hydrogel, similar to the results shown previously for EDC and NHS hardening time in Figure 5.4.4.

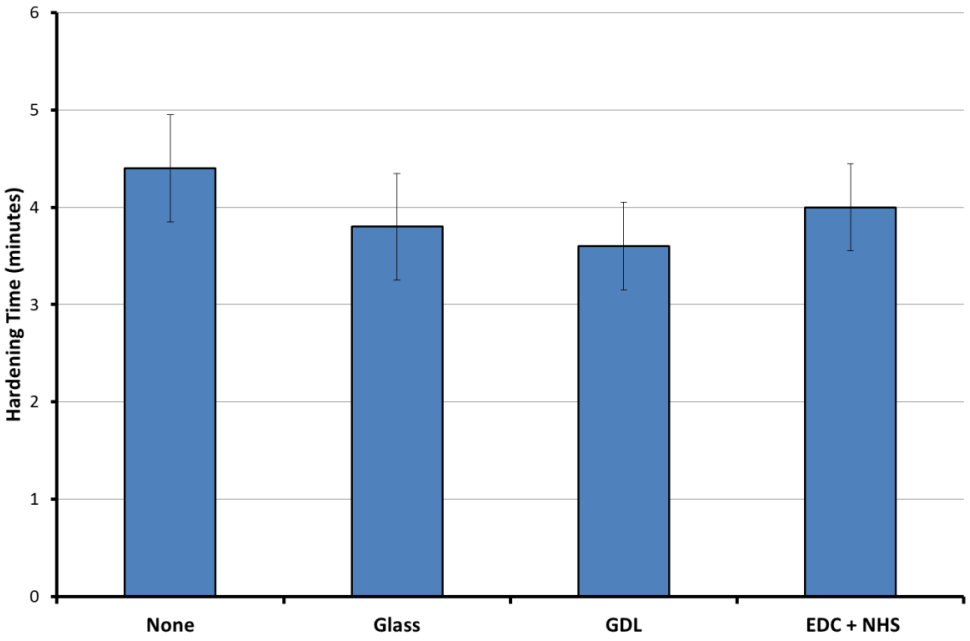

Figure 5.6.15 Hardening time of hydrogel with individual components sterilised using low temperature gamma irradiation (n=5)

The MVM alginate has a significant reduced working time compared to the 700kDa alginate. The working time results presented here support the hypothesis in Section 5.1, that the chemical composition has an increased effect on the working time compared to the molecular weight. Sterilising the hydrogel components increases the working time. This is likely due to the increase caused by the sterilised EDC and NHS (as seen in Figure 5.6.14) and a decrease in molecular weight but it is still within the time limits.

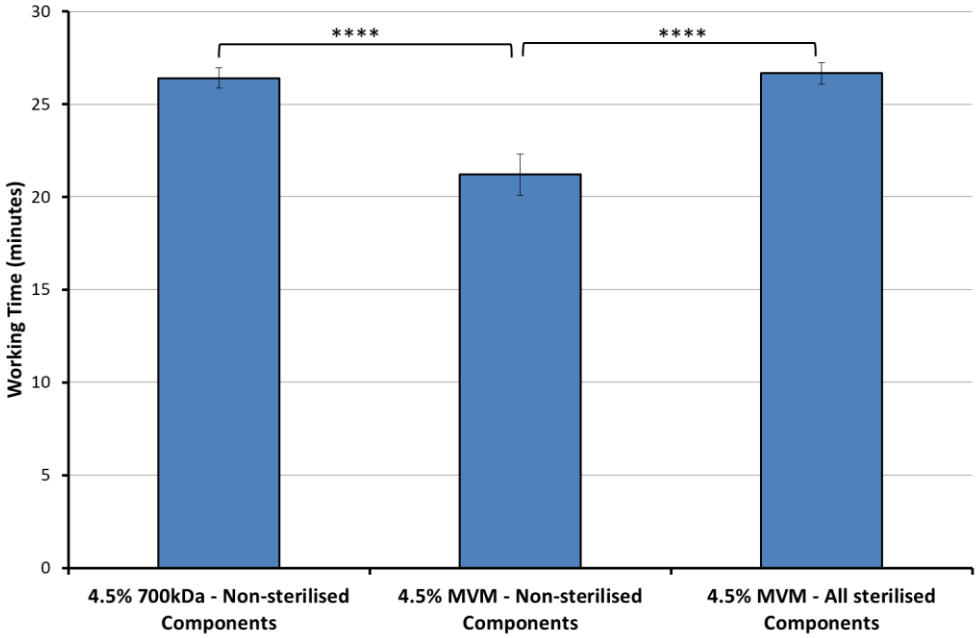

Figure 5.6.16 Hydrogels working time (n=5)

The MVM alginate has the quickest hardening time, likely due to the increases in G-block content of the alginate (see Figure 5.6.17). There was no significant difference in the hydrogel hardening time when comparing the 4.5% MVM alginate with the 4.5% autoclaved alginate. This is likely due to the chemical composition of the alginate remaining the same after sterilisation.

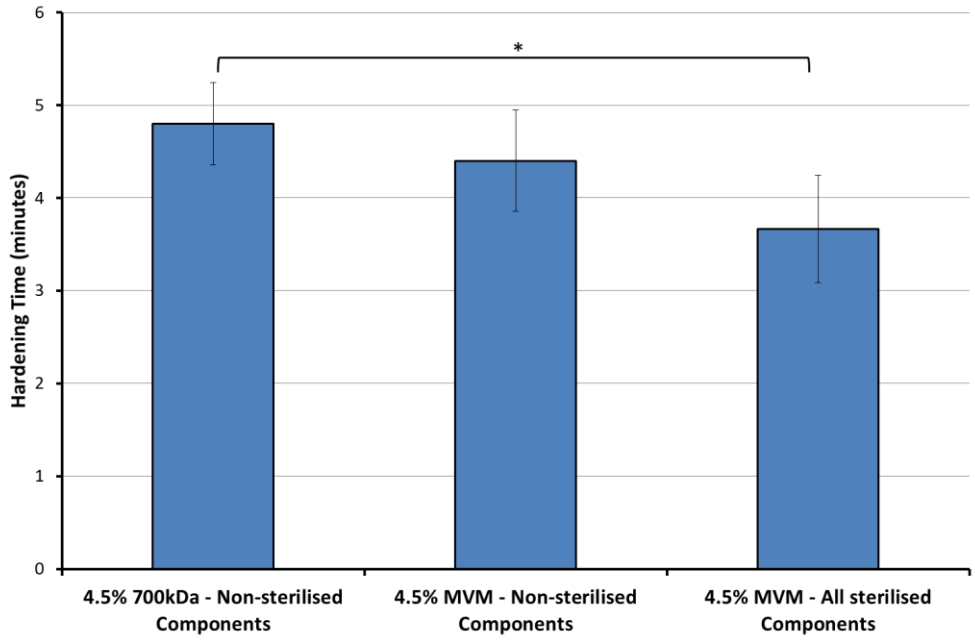

Figure 5.6.17 Hydrogels hardening time (n=5)

5.6.4. Chemical and structural analysis

5.6.4.1. Gel Permeation Chromatography

GPC showed that autoclaving the alginate causes a reduction in the molecular weight of the alginate from 254kDa to 200kDa. This gives a number of 0.27 breaks per molecule.

5.6.4.2. Differential Thermal Analysis

Although not significant, there is a slight decrease in the glass transition temperature of the glass after sterilisation, as shown in Figure 5.6.18.

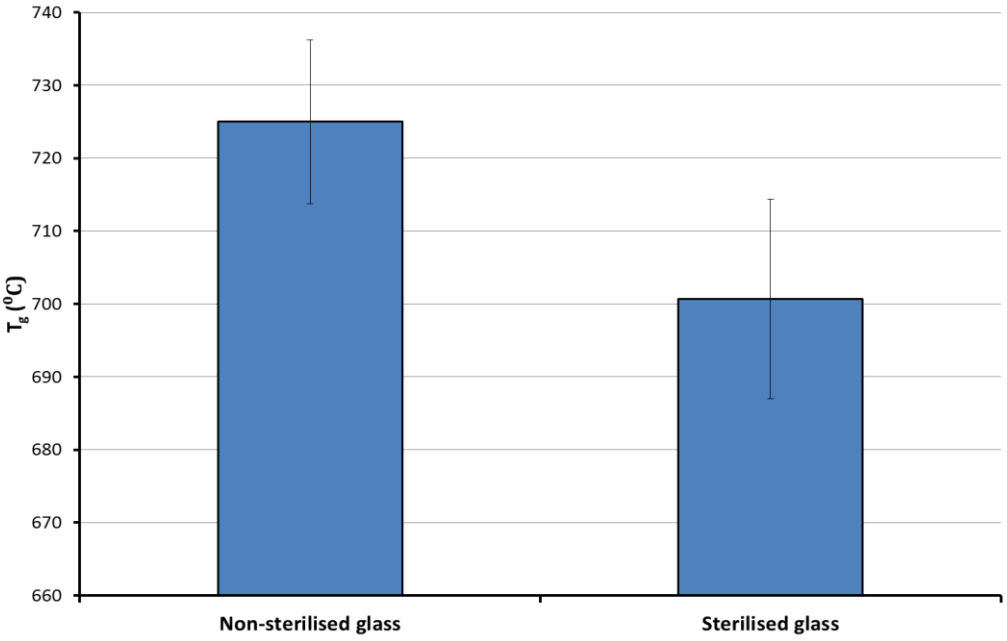

Figure 5.6.18 Glass transition temperature of glass

5.6.5. Discussion

A low endotoxin level is required for a material to be used in neurovascular devices. Ultrapure alginates, such as those available from FMC biopolymer, provide a low endotoxin level at a high molecular weight. The lower endotoxin level of the MVM alginate will reduce the levels of terminal sterilisation required to bring the alginate within the 0.06EU/ml limit specified by the FDA. The results of the 700kDa and MVM alginate hydrogels further support the hypothesis that a low G-block alginates strength can be compensated for with a higher molecular weight alginate, as discussed in Section 5.1.

As expected, autoclaving alginate causes a significant decrease in the molecular weight and strength of the produced hydrogel. However, the effect is less damaging to the alginate compared to gamma irradiation, which has been shown here and reported elsewhere [357] [437] [443]–[445]. The strength can be increased with an increased alginate concentration (Figure 9.5.28) but it remains significantly reduced compared to non-sterilised alginate.

However, this increase in concentration causes an increase in viscosity and results in a hydrogel that cannot be safely injected into the cerebral vasculature. Although there was a reduction in molecular weight compared to the 700kDa alginate, the 6.75% autoclaved MVM alginate supplied had a higher G-block content and an increased concentration. Both these properties can result in an increased viscosity, which increases the force required to inject the hydrogel. Appendix 9.5.4.4 shows that the 6.75% MVM alginate with all sterilised components produces a high strength hydrogel that may be appropriate for embolization through larger microcatheters.

To improve the injectability of the hydrogel, the alginate concentration was decreased to 4.5%. The cross-linking density of the hydrogel increased with a decrease in alginate concentration, indicated by the sample volume change. This increased cross-linking density will likely have a high strength, though a high strength is redundant if the hydrogel cannot remain within the aneurysm due to shrinkage. To improve the hydrogels volume conservation, by reducing the cross-linking density, the glass and GDL content of the hydrogel were reduced.

Reducing the hydrogel's alginate concentration to 4.5% autoclaved alginate with 9.2% glass, 6.25% (w/v) of GDL and 0.83% (w/v) of EDC and NHS decreases the force required to inject the hydrogel. A material that does not require a high pressure to inject is needed as it reduces the chance of migration of the catheter, the catheter rupturing and unexpected embolization [7]. This force of approximately 19N (1080kPa), 15 minutes after mixing, is lower than other injectable shear-thinning biomaterials designed for endovascular embolization [109] [112].

However, it likely requires a higher force to inject compared to contrast agents or Onyx® due to the significant differences in viscosity.

Figure 5.6.9 shows that the hydrogel with the reduced alginate concentration, glass content and GDL content does have a significantly reduced compressive strength (compared to the sterilised hydrogel in Appendix 9.5.4.4). Despite these decreases, the hydrogel still has a sufficiently high strength. Figure 5.6.11 shows that this reduction in cross-linking density improves the size volume conservation of the hydrogel. However, the results to date have shown that as the hydrogel's strength increases, the sample volume reduces. The opposite is occurring here, with the sample insignificantly expanding from day 1 to day 7. This may suggest a reduced rate of cross-linking over time with the hydrogel, which is supported by the insignificant increase in strength of the hydrogel from day 3 to day 7 (Figure 5.6.9). It is unclear what is causing this reduction in cross-linking of this hydrogel with time.

Compression testing, working time and hardening time testing of the hydrogels show that gamma irradiation of the powder components on dry ice does not significantly affect the hydrogel. Although there is a significant increase in the working time of the hydrogel with gamma irradiated EDC, the hydrogel is still within the working time limits. This increase in working time may be caused by the improved dissolution of EDC causing a decrease in pH. This improved dissolution may be caused by a partial degradation of EDC. The hydrogel with 4.5% MVM alginate has tensile strength that exceeds those of typical alginate hydrogels [127]. However, this strength is greatly decreased when the components of the hydrogel are sterilised. Overall, there is a continued increase in strength over time due to a continued release of cross-linking ions.

The tensile strength of Onyx has been shown to range from 3.5kPa to 40kPa [446]. The hydrogel produced here after sterilisation has a tensile strength 7.7kPa to 27.3kPa. The tensile strength of the hydrogel will likely suffice as in vivo the hydrogel will likely not be subjected to high tensile forces, as the two main hemodynamic forces acting on the hydrogel will be compressive stress and shear stress caused by blood flow [447].

There was no significant change in the bond strength of the hydrogel after gamma irradiation (Figure 5.6.13). This was not expected due to the reduced compressive and tensile strength but may be due to the reduced viscosity allowing the hydrogel to fill irregularities on the skin surface, as observed by Foox *et al* [217].

Overall, there is a significant decrease in the strength of the material after sterilisation due to the reduced molecular weight of the hydrogel. However, this reduction in strength is compensated for by an improved sample volume conservation. Overall, the results show an improved hydrogel usability, as the strength still greatly exceeds the minimum strength

required. The working and hardening time are still within the set limits and the hydrogel strengths are, at a minimum, maintained over time. This meets the design review criteria (Table 5.6.1).

Table 5.6.1 Design review table with the hydrogel sterilised

Hydrogel	Compressive Strength >22kPa?	Is the material size conserved? (<10% expansion with no shrinkage)	Is the hydrogel injectable?	Working Time between 10 and 30 mins?	Hardening Time <5 mins?	Is the material adhesive?	Is the material cytocompatible? (>70% cell viability)	Is the material sterilisable?	Is the material suitably radiopaque?	Is the material haemocompatible?
4.5% 700kDa alginate with non-sterilized powders	Yes	No	Yes	Yes	Yes	Yes	Yes	TBD	TBD	TBD
4.5% MVM alginate with all sterilized powders	Yes	Yes	Yes	Yes	Yes	Yes	Yes	Yes	TBD	TBD

5.7. Calcification Results

Calcification of the hydrogel when placed in simulated body fluid will be examined with the optimised sterile hydrogel, shown in Table 5.6.1 (page 183). The composition is 4.5% autoclaved MVM alginate with low temperature gamma irradiated glass at 9.2% concentration, 6.25% (w/v) GDL and 0.83% (w/v)EDC and NHS. Calcification is usually determined by XRD, FTIR or SEM [448]. As standard SEM microscopy cannot be carried out on water swollen hydrogels, it was decided to examine the calcification of the hydrogel by FTIR, XRD and von Kossa staining [449].

A hydrogel that does not result in calcification is not a design requirement set out in Section 2.4; however, calcification of soft tissue can occur in the presence of bioactive glasses. This calcification of the tissue can result in a prolonged inflammatory response and negative soft tissue remodelling. The transfer of nutrients and waste can also be hindered by an apatite layer. Due to these factors, it would be an advantage in the treatment of soft tissue defects if this material remained amorphous [450]–[452].

5.7.1. Attenuated Total Reflectance-Fourier Transform Infrared Spectroscopy

Figure 5.7.1 shows the FTIR peaks of glass particles after storage in DI and SBF. There are no additional peaks located from 890 – 1300cm^{-1} between the glass stored in DI and SBF. These peaks indicate the network connectivity of the glass, with the network connectivity increasing with increasing peak wavelength. As the bioactive glass has a network connectivity of 3, it is assumed the peak at 930cm^{-1} is associated to this [366] [453]–[457].

Peaks at approximately 550cm^{-1} typically indicate the presence of a P-O bending vibration. However, these are usually dual peaks and indicate a crystalline apatite layer. As there is only a signal broad peak, the strong sharp peak at 550cm^{-1} is assigned to the Si-O-Si bending or rocking [453] [458]. The peak at 930cm^{-1} also decreases after storage in SBF, typically this increases with the formation of hydroxyapatite due to the increase presence of phosphate [459].

Small peaks are observed in the SBF samples that are not present in the glass stored in DI. The peaks at 1550cm^{-1} and 1640cm^{-1} on the glass after storage in SBF are likely caused by C-O asymmetric stretching due to the carbonation of the calcium present in glass [456]. Peaks present at 3000cm^{-1} and 3200cm^{-1} are likely water vibrations, which may suggest the glass particles were not dried for a sufficient amount of time after storage or is water bound to the surface [460] [461].

A comparison of a typical FTIR of hydroxyapatite (Figure 9.5.30) compared to the bioactive glass stored in SBF (Figure 5.7.1) would indicate that there is not calcification of the hydrogel.

Hydroxyapatite typically has a number of phosphate bands seen between 500cm^{-1} and 1110cm^{-1}, which are not observed in the FTIR of the bioactive glass. A broad peak at approximately 3500cm^{-1} would indicate the presence of an O-H group, as this is not seen in the samples stored in SBF, it would indicated that there is not carbonated hydroxyl apatite layer [456].

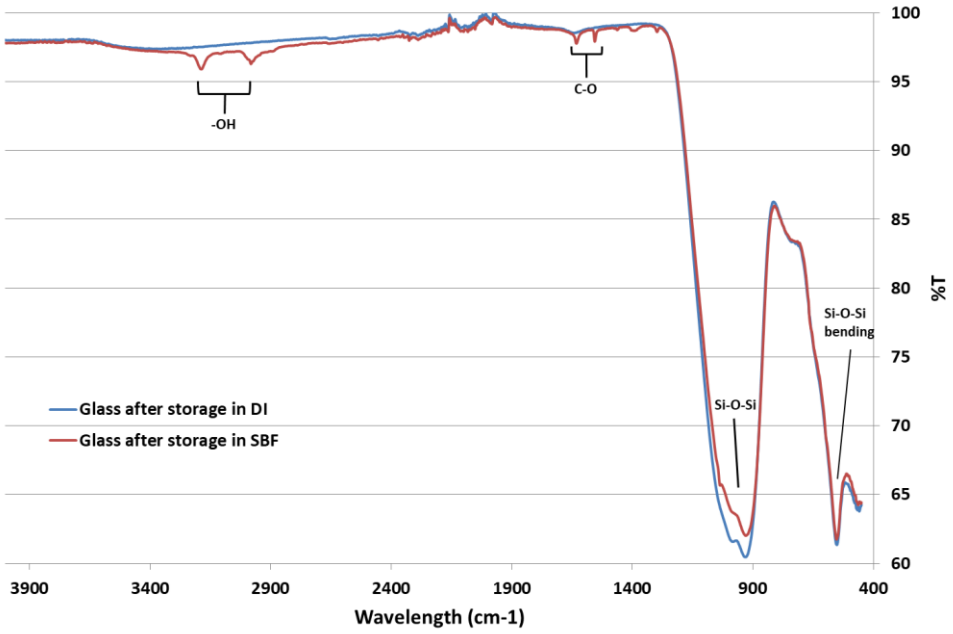

Figure 5.7.1 FTIR of glass after storage in DI (black line) and SBF (blue line) for 7 days

Figure 5.7.2 shows FTIR of raw alginate and the alginate – bioactive glass hydrogel after storage in SBF for 7 days. FTIR shows a strong broad peak at 3242cm^{-1}, which relates to the alginates hydroxyl O-H bonds stretching, which is expected between 3000 and 3600cm^{-1}. Strong peaks at approximately 1594cm^{-1} which corresponds with the asymmetrical stretching of carboxylic groups. Medium sharp peaks at 1408cm^{-1} correspond with symmetrical stretching of carboxyl groups. Strong sharp peaks at 1027cm^{-1} show C-O-C stretching [462]–[466]. Peaks at 1000-1300cm^{-1} can indicate the presence of guluronic and mannuronic acid in the alginate [247].

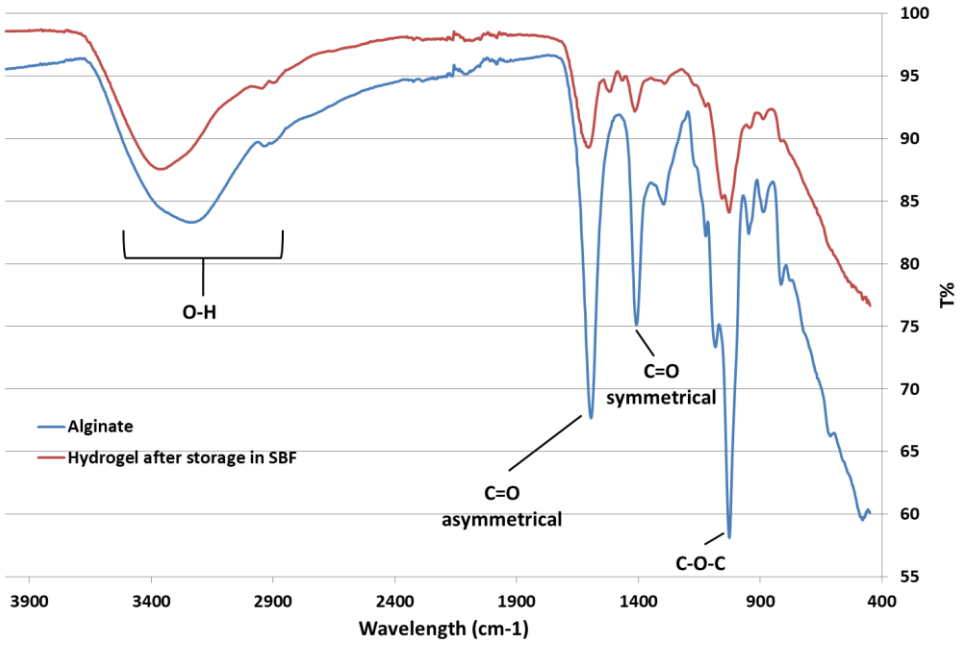

Figure 5.7.2 Raw alginate and alginate – bioactive glass hydrogel after storage in SBF FTIR

Figure 5.7.2 shows there is a reduction in the alginate peaks of the hydrogel after being stored in SBF and lyophilized. However, there is no significant change in peak location. Hydroxyapatite shows strong peaks at 1400-1550cm^{-1} (carbonate) which is observed in the hydrogel following storage in SBF but this may also be attributed to the cross-linking of the alginates carboxyl groups. However phosphate peaks 900-1200cm^{-1} and 450-500cm^{-1} are not seen, indicating no calcification of the hydrogel occurs [235] [452] [467] [468].

5.7.2. X-Ray Diffraction

Figure 5.7.3 shows the glass has a broad amorphous peak after storage in both DI and SBF for 7 days. The sample stored in SBF has two sharp peaks at 22^0 and 41^0. These peaks could indicate the presence of hydroxyapatite. However, the peaks are not broad such as those observed in hydroxyapatite XRD spectra and the broad 100% peak of apatite at approximately 32^0 is not present. This may indicate crystalline structures forming but may be remnants of SBF on the bioactive glass sample after drying [469]–[472].

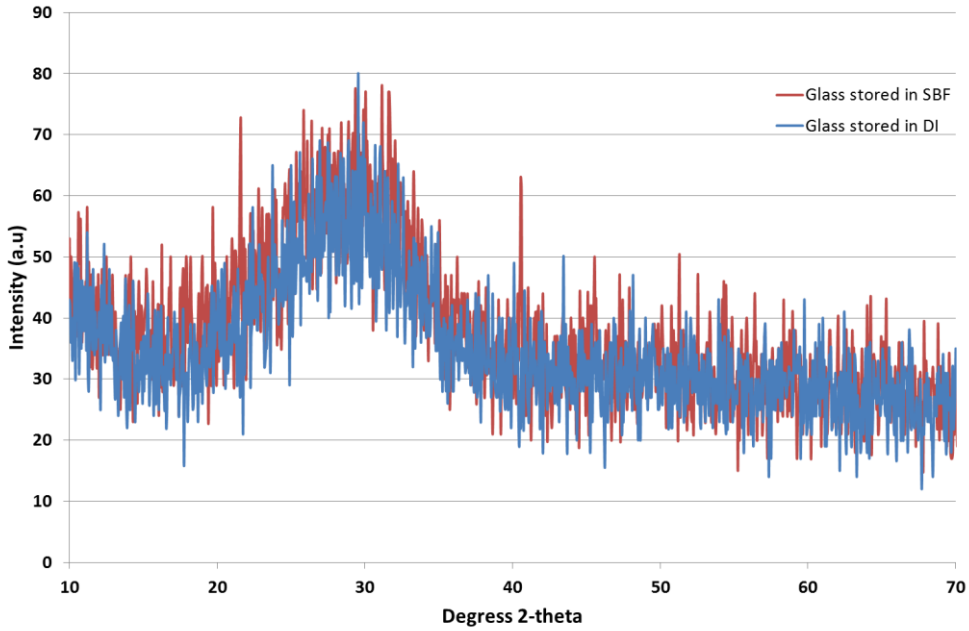

Figure 5.7.3 XRD of glass after storage in DI and SBF

Figure 5.7.4 shows that the bioactive glass – alginate hydrogel remains amorphous after storage in SBF. The hydroxyapatite – alginate sample, as expected, shows crystalline peaks that are associated with hydroxyapatite [473].

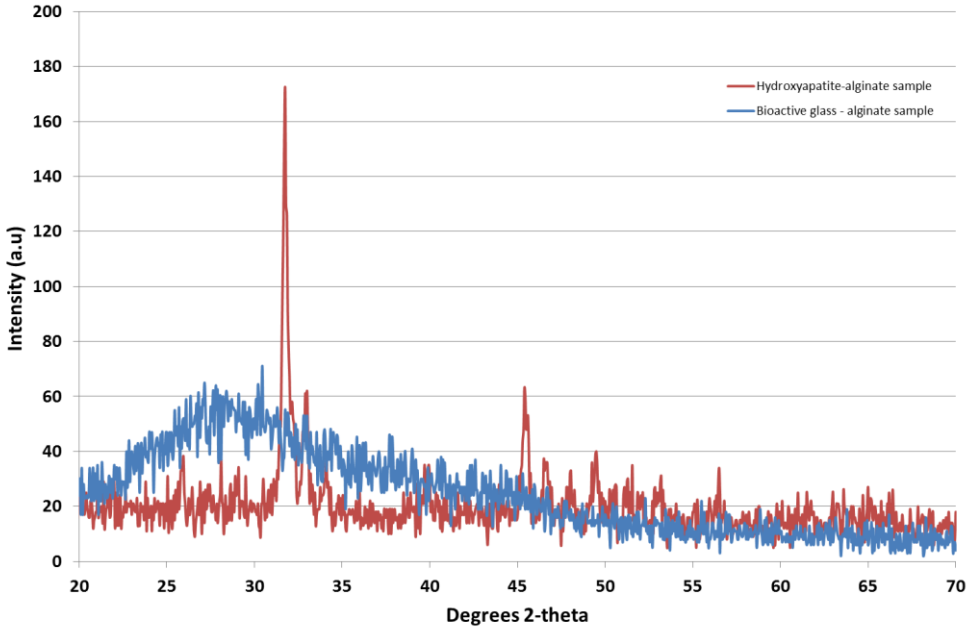

Figure 5.7.4 XRD of hydrogels after storage in SBF for 7 days

5.7.3. Von Kossa Staining

Von Kossa stain reacts with phosphate and can be used to determine calcification [448]. Calcification can be seen a dark brown or black areas caused a reaction between the silver nitrate and phosphate under UV light [474]. Figure 5.7.5 shows the bioactive glass – alginate

hydrogel stains negatively using the Von Kossa stain, suggesting there is no phosphate present on the surface of the hydrogel.

Figure 5.7.5 Bioactive glass - Alginate hydrogel after Von Kossa staining

As expected, the hydroxyapatite - alginate hydrogel shows a strong presence of phosphate on the surface of hydrogel after soaking in SBF, as the Von Kossa stain remains after washing, as seen in Figure 5.7.6 [475].

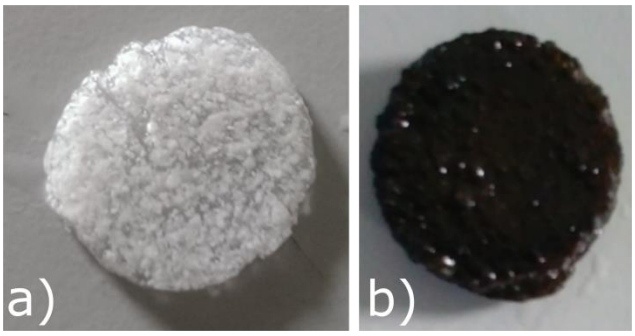

Figure 5.7.6 Hydroxyapatite - Alginate hydrogel before (a) and after (b) Von Kossa staining

5.7.4. Discussion

Typically, glasses and hydrogels, after storage in SBF, have strong splitting peaks between 450cm^{-1} and 600cm^{-1} which relate to a P-O bending vibration. Hydroxyapatite also typically has a broad hydroxyl peak and carbonate peaks, which together is an indication of a crystalline apatite layer [453] [476] [477]. FTIR results show that neither the bioactive glass nor the hydrogel have the typical characteristics of hydroxyapatite after storage in SBF.

There is a clear presence of a dark brown – black stain present on the hydroxyapatite-alginate hydrogel. This is caused by a reaction between the silver nitrate and phosphate in the presence of UV light. In contrast to this, the bioactive glass-alginate hydrogel has no macroscopic dark brown – black spots on the surface. This would indicate that there is no calcium phosphate layer on the surface of the hydrogel.

Although SEM can produce more reliable results when examining the formation of calcification, these hydrogel samples cannot be observed by the technique. The results from

FTIR, XRD and von Kossa staining indicate that calcification of these hydrogels is unlikely to occur.

Bioactive glasses are commonly used for repair of bone defects due to ability to form an apatite layer. Apatite of bioactive glass is initiated by the exchange of cations in the glass with hydrogen in body fluid. Silica dissolves from the glass network resulting in –Si-OH bonds. These –Si-OH bonds repolymerise to form a silica-rich layer. Calcium and phosphate ions move from inside the glass particles and form a calcium phosphate layer on the silica-rich layer. This precipitation is due to the incorporation of hydroxide and carbonate [259].

Apatite formation can depend on the NC of the glass, with the likelihood of apatite formation reducing with increasing NC. It is suggested that glasses with a network connectivity above 2.4 will not form an apatite layer, unless the glass contains a high silica content or the presence of a fluoride. This is due to the rate and amount of ions released will affect the formation of an apatite layer [224] [366] [457] [478] [479]. To achieve this high network connectivity of this bioactive glass, the calcium content of the bioactive glass is used to charge balance the gallium present. This would imply that a certain amount of calcium has remained in the glass. The reduction of apatite formation with the addition of gallium to a bioactive glass has been observed previously [480][481]. Calcium is also required to ionically cross-link the alginate. As apatite formation depends on the amount and release rate of calcium, among other ions, it is clear that the required rate has not been met by this hydrogel.

Although the production of an apatite layer is crucial for the binding of bioactive glasses to bone, it is suggested that binding of soft tissue is influenced by the both an apatite layer and ions released from the glasses interfering with cellular behaviour [238]. Results from Section 5.4 have shown that the hydrogel produced here has the ability to bind with soft tissue and this bond strength can be increased by the presence of EDC and NHS. Although the bond strength may be reduced compared to a hydrogel that forms an apatite layer, the reduced chance of inflammation is of a greater advantage.

Table 5.7.1 Design review table

Hydrogel	Compressive Strength >22kPa?	Is the material size conserved? (<10% expansion with no shrinkage)	Is the hydrogel injectable?	Working Time between 10 and 30 mins?	Hardening Time <5 mins?	Is the material adhesive?	Is the material cytocompatible? (>70% cell viability)	Is the material sterilisable?	Is the material suitably radiopaque?	Is the material haemocompatible?
4.5% MVM alginate with sterilized powders	Yes	Yes	Yes	Yes	Yes	Yes	Yes	Yes	TBD	TBD

5.8. Direct Contact Analysis

As the hydrogel is sterile, direct contact testing can be examined without the risk of contamination. The hydrogel may directly contact endothelial cells in three different ways; directly contacting endothelial cells lining the aneurysm dome, migration of cell from the parent artery wall or blood based progenitor cells attaching to the surface of the hydrogel.

The hydrogel composition examined in this section is a 4.5% autoclaved MVM alginate with low temperature gamma irradiated glass at 9.2% concentration, 6.25% (w/v) GDL and 0.83% (w/v) EDC and NHS. The composition was optimised in Section 5.6

5.8.1. Direct Contact of Hydrogel with Endothelial Cells on a Coverslip

To examine if cells lining the aneurysm dome will survive in direct contact with the hydrogel and to determine if cells will migrate from the parent artery, endothelial cells were seeded onto a slide and the slide was placed on the hydrogel (described in detail in Section 4.10.1).

The surface properties and stiffness of the hydrogel is likely quite different from that of the surface of the well plate. As the material properties and stiffness of the surface that cells are seeded on can greatly affect cell attachment and proliferation, no control was used. Although these results are not comparable to typical *in vitro* cell growth, the results indicate if direct contact of the hydrogel to the cells will result in a cytotoxic effect.

Figure 5.8.1 shows that the number of cells on the slide increased significantly from 1 to 7 days. These results suggest the hydrogel is not causing a significant cytotoxic effect, similar to the results of the cells when dosed with the hydrogel eluent (Section 5.5).

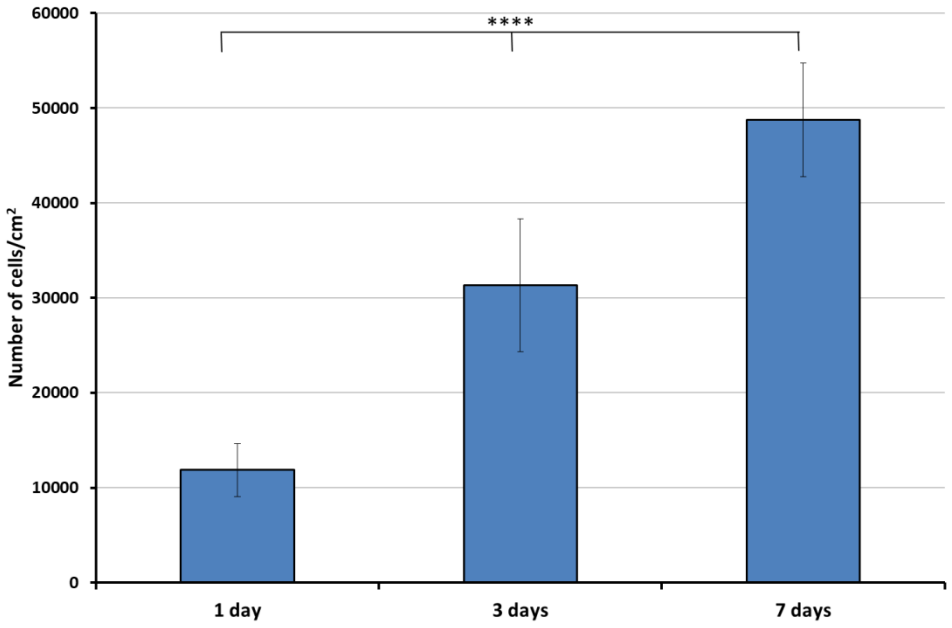

Figure 5.8.1 Number of cells per cm² on the slide in contact with the hydrogel (n=3)

At day 1, 3 and 7, no cells were seen on the hydrogel adjacent to the slide, suggesting that cells would not migrate from the slide to the hydrogel (see Figure 5.8.2). However, at day 3 and day 7, cells were seen in patches across the hydrogel, as shown in Figure 5.8.3. This suggests that the cells are possibly migrating and adhering in patches on the surface of the hydrogel.

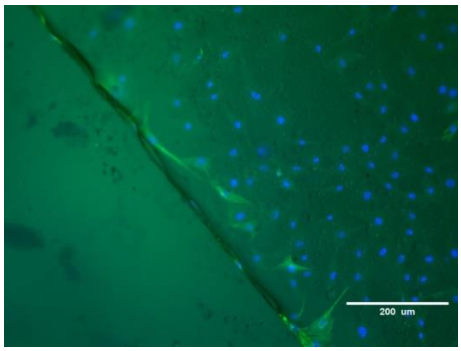

Figure 5.8.2 Cells on the slide in contact with the hydrogel 7 days after seeding

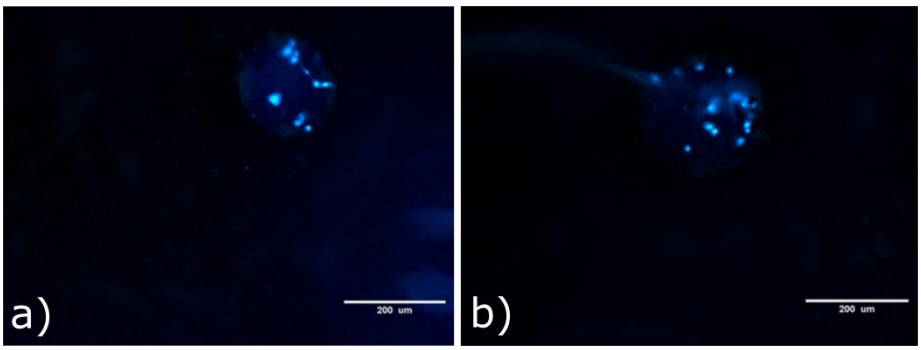

Figure 5.8.3 Cells on the hydrogel after a) 3 days and b) 7 days

5.8.2. Cells Seeded Directly onto the Hydrogel

Again, no control was used to compare the growth or attachment of the cells. However, the number of seeded cells is approximately 9000/cm^2 and these results can be used to quantify the number of cells that adhere.

Approximately 22% of the cells seeded directly onto the hydrogel adhered to the surface of the hydrogel. These results indicate that initial cell attachment to the surface of the hydrogel is poor. Figure 5.8.4 shows that the number of cells adhered to the surface of the hydrogel significant increases over time.

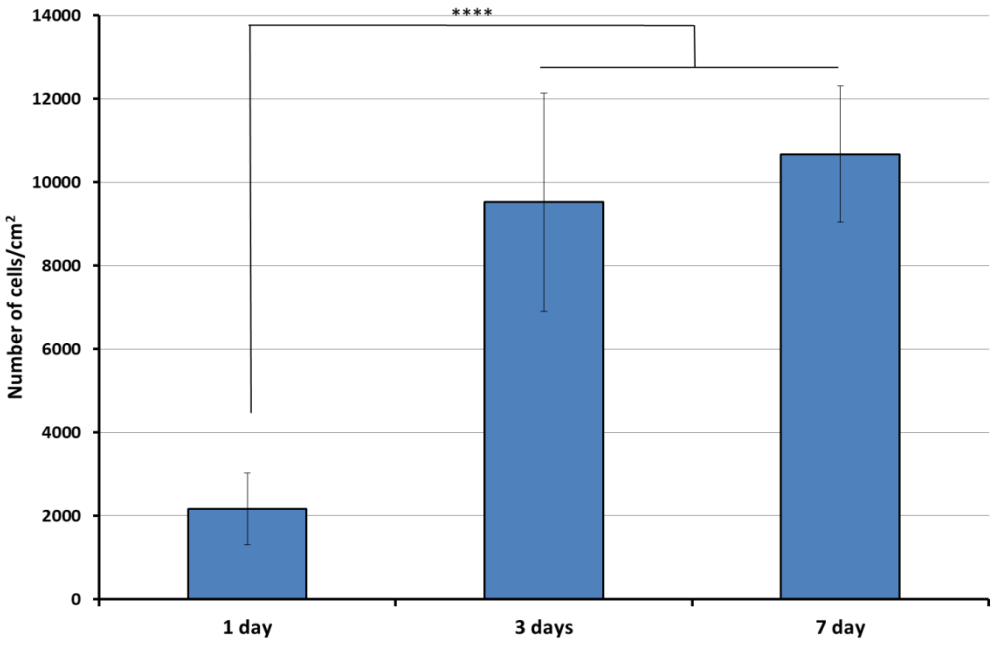

Figure 5.8.4 Number of cells per cm² on the hydrogel (n=3)

5.8.3. Discussion

The hydrogel does not significantly induce apoptosis in cells seeded on a slide and placed in contact with the hydrogel. In fact, the cells are shown to proliferate. These results correlate with the results of eluent dosing (Section 5.5), where cells are likely proliferating due to the ions and gluconic acid released from the hydrogel. The hydrogel's surfaces are typically highly porous, with pore sizes ranging from 5-200nm. These pores allow the nutrients from the media and waste to diffuse through the hydrogel which facilitates cell growth [181]. Surfaces with carboxyl groups, when seeded with cells, have also been shown to result in increased cell proliferation and hydroxyl groups have been shown to provide an increase in oxygen, vital for cell growth [482].

Cells were not seen to spread from the glass coverslip to the hydrogel at day 1, yet at day 3 and day 7 cells were seen in clusters across the hydrogel (Figure 5.8.3). Similar cell agglomerations have been seen previously on other hydrogels and it has been suggested that the cells were weakly attached to the hydrogel but due to strong cell-cell interactions there is a clustering of cells [483]. The cells here appear to be attached to the surface of a particle approximately 200µm in diameter. Particles of this size were seen in acellular hydrogels; see Figure 9.5.31, which are likely agglomerations of the bioactive glass. This may indicate that the cells are migrating from the coverslip to the bioactive glass and adhering. This migration may be caused by the mechano-chemical sensing of the cells [7]. The presence of the glass may also be encouraging cell attachment as bioactive glass and its ions, such as calcium and silica, have also been shown to increase soft tissue bonding and cell attachment [244] [484]–

[486]. Negative zeta potential has also been shown to increase cell attachment, likely due to an increase in surface hydrophobicity [225][379].

Despite a limited number of cells migrating from the surface of the glass slide to the hydrogel, Figure 5.8.4 shows that cells can adhere to the surface of this alginate hydrogel. This variation in results may be caused by the cells preferencing the stiffness of the glass coverslip compared to the lower stiffness hydrogel. However, when the cells are directly seeded on the hydrogel they adhere. Cells typically do not adhere to alginate hydrogels as they are unable to interact due to a lack of receptors that recognise alginate. Alginate's hydrophilic nature furthermore does not allow serum protein adsorption that would promote cell attachment [181] [487] [488]. This improved cell attachment may be caused by the improved strength of this hydrogel compared to typical alginate hydrogels. The presences of ions, such as silica, that improve cell attachment are likely present throughout the hydrogel and may be another explanation for the cell attachment. *In vivo*, a reduced pH can increase the adhesive abilities of endothelial cells. The slightly decreased pH of the media caused by the hydrogel may be contributing to adhesive strength of the endothelial cells here [489].

The number of cells on the surface of the hydrogel increases over time. This may be caused by the continued release of ions and gluconic acid from the hydrogel promoting cell proliferation. This may also be caused by the strength of the hydrogel increasing over time as endothelial cells have been shown to proliferate on stiffer substrates [120] [123] [124]. As the hydrogel strengthens, the cells are likely forming stronger attachments by focal adhesions to the surface of the hydrogel and spreading. At day 1, when focal adhesions are weak, the cells may be washed from the surface of the hydrogel during the fixation and staining process. As the cell adhesion to the surface of the hydrogel strengthens over time, the cells are likely to withstand this process and remain attached to the surface of the hydrogel. This may also explain why cells were seen in agglomerations on the hydrogel when the cells were seeded on a coverslip. This may result in a variance of the number of cells seen attached *in vivo*, due to the presence of a shear stress with constant blood flow. The results here indicate that despite the typical inert properties of alginate hydrogels, the presence of bioactive glass can result in the attachment of cells to the surface of an alginate hydrogel. These improved cell attachment properties may result in the attachment and proliferation of endothelial and smooth muscle cells *in vivo*. This attachment and proliferation will likely reduce the risk of aneurysm rupture post treatment, as endothelialisation or neointima formation across the neck of the aneurysm will result in a complete occlusion.

5.9. Radiopacity

As discussed, the hydrogel needs to be sufficiently radiopaque in order to effectively deliver the hydrogel into the aneurysm endovascularly. Section 5.3 has shown an improved radiopacity due to the increased glass content; however, the glass content has since been reduced during sterilisation (Section 5.6). The hydrogel's radiopacity can be increased by the addition of contrast agents (as discussed in Section 2.4.6) or inclusion of radiopaque ions into the glass phase of the hydrogel, such as tantalum and barium. Tantalum powder is added to Onyx® at a 30% w/v concentration and to N-butyl cyanoacrylates at varying concentrations depending on the desired radiopacity [105] [174]. Tantalum improves the radiopacity but is not ideal as it can stain the skin and produce artefacts at high concentrations under fluoroscopy imaging [174]. In an attempt to overcome this, calcium oxide was partially replaced with tantalum oxide in the bioactive glass formulation. The resultant glass significantly reduced the strength and increased the working and hardening times of the resultant hydrogel (results are shown in Appendix 9.5.8). Due to these negative results, it was decided to examine the effects that tantalum powder had on the hydrogel.

The hydrogel composition tested will be 4.5% autoclaved MVM alginate with low temperature gamma irradiated glass at 9.2% concentration, 6.25% (w/v) GDL, 0.83% (w/v) EDC and NHS and tantalum powder (0%, 20%, 30%, 40%).

5.9.1. Radiopacity

To increase the radiopacity of the hydrogel, tantalum powder was added to the hydrogel at three concentrations; 20%, 30% and 40% (w/v). The radiopacity of the hydrogel was tested at 4 hydrogel thicknesses, as shown in Figure 5.9.1.

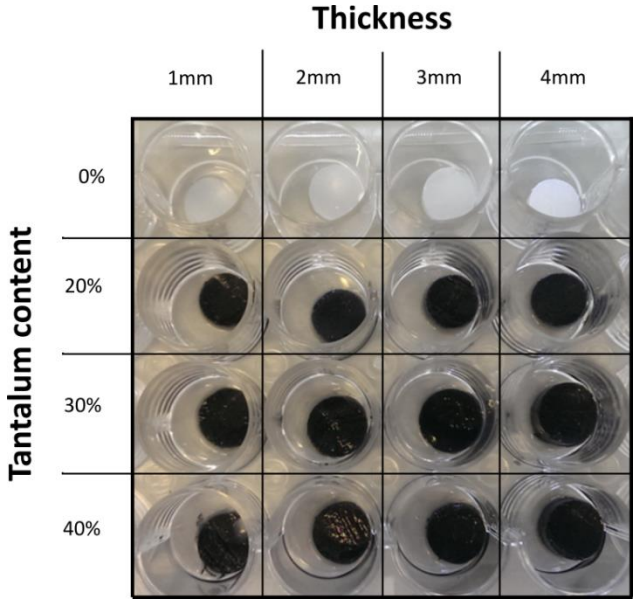

Figure 5.9.1 Hydrogel radiopacity samples

Fluoroscopy images (Figure 5.9.2) of the hydrogel under a full radiosurgery test phantom skull show that hydrogel with 0% tantalum is indecipherable. Increasing the tantalum content and thickness of the hydrogel samples improves the radiopacity.

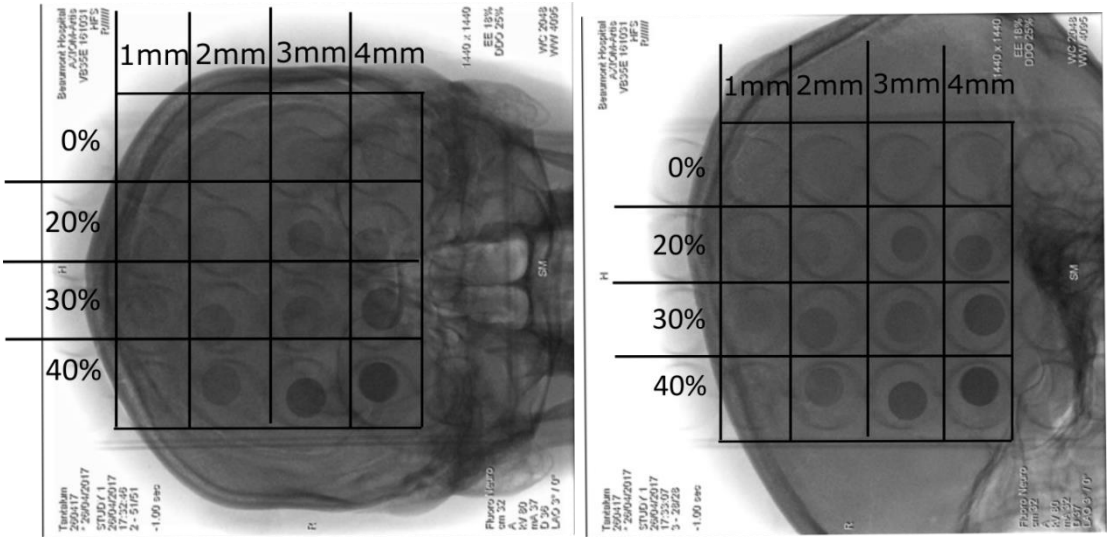

Figure 5.9.2 Fluoroscopy images hydrogel samples of various tantalum content and thickness under a skull model from a) front view and b) side view

The hydrogel with 40% tantalum was injected, under fluoroscopy, through a 150mm long 2.1F microcatheter into an aneurysm model with an iodine filled balloon inflated across the neck. Figure 5.9.3 shows the aneurysm before injection, while the hydrogel was being injected and once the aneurysm was filled. The hydrogel was clearly detectable during injection and visibility improved as the aneurysm continued to fill. Although not as radiopaque as other embolization liquids such as Trufill or Onyx®, the radiopacity was acceptable according to neuroradiologist, Dr. Alan O'Hare (Beaumont Hospital).

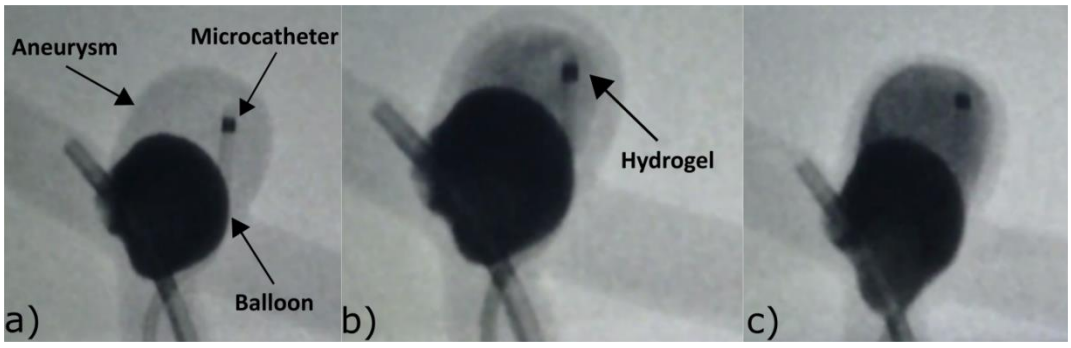

Figure 5.9.3 Fluoroscopy images of the hydrogel with 40% tantalum a) before, b) during and c) after injection into an aneurysm model. A balloon inflated with iodine contrast is placed at the neck of the aneurysm.

5.9.2. Compressive Strength

The addition of tantalum to the hydrogel significantly reduces the strength and incremental modulus of the hydrogel, as shown in Figure 5.9.4 and Figure 5.9.5. Although there is a significant reduction in strength, the hydrogel still greatly exceeds the strengths required to

withstand hypertensive blood pressure. The hydrogel, with the addition of 40% tantalum, also continues to increase in strength over time.

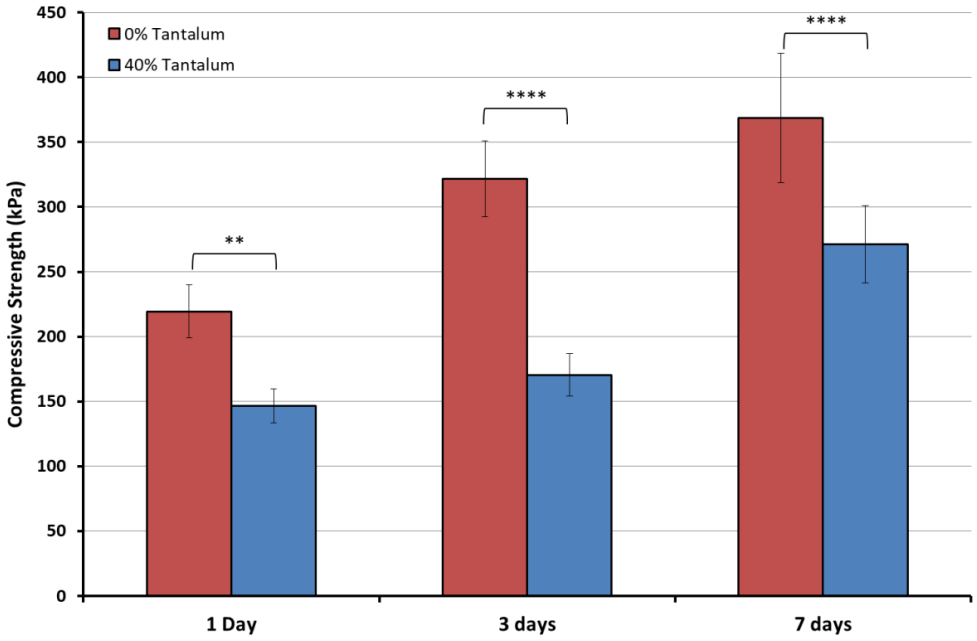

Figure 5.9.4 Compressive strength up to 70% strain of the hydrogel with 0% and 40% (w/v) tantalum following storage for 1, 3 and 7 days at 37^{0}C in SBF (n=5)

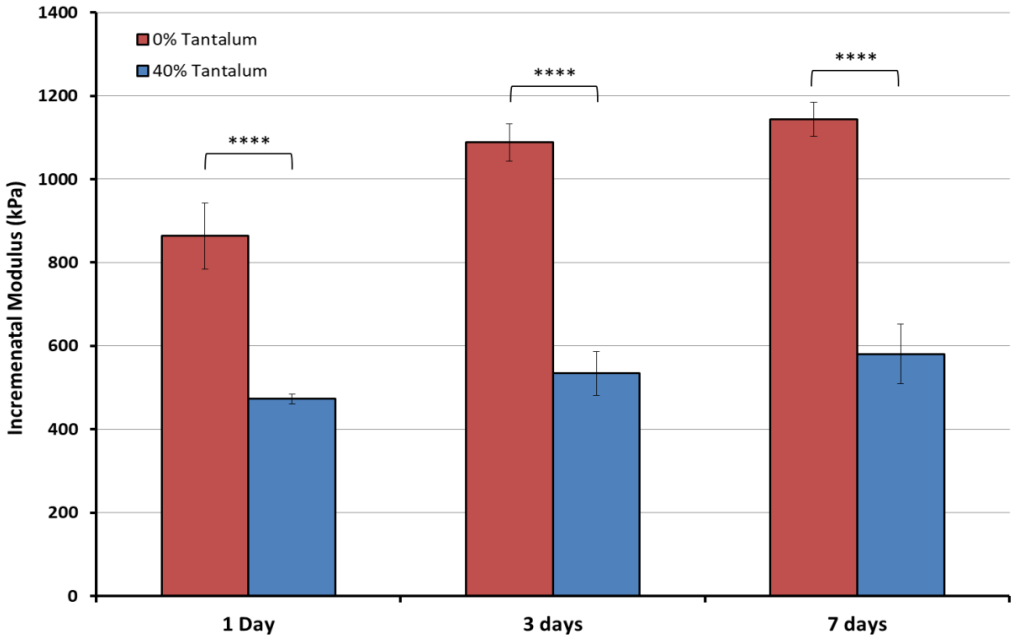

Figure 5.9.5 Incremental Modulus (30-40% strain) of the hydrogel with 0% and 40% (w/v) tantalum following storage for 1, 3 and 7 days at 37^{0}C in SBF (n=5)

5.9.3. Sample Size Conservation

Figure 5.9.6 shows that there is no significant difference between hydrogels with 0% and 40% tantalum content at day 1 or day 3. At day 7, the hydrogel with the addition of 40% tantalum is significantly decreased in volume compared to the hydrogel with 0% tantalum.

The 40% tantalum samples at day 1 are at the maximum acceptable expansion (10%) though by day 1 the expansion is sufficiently reduced.

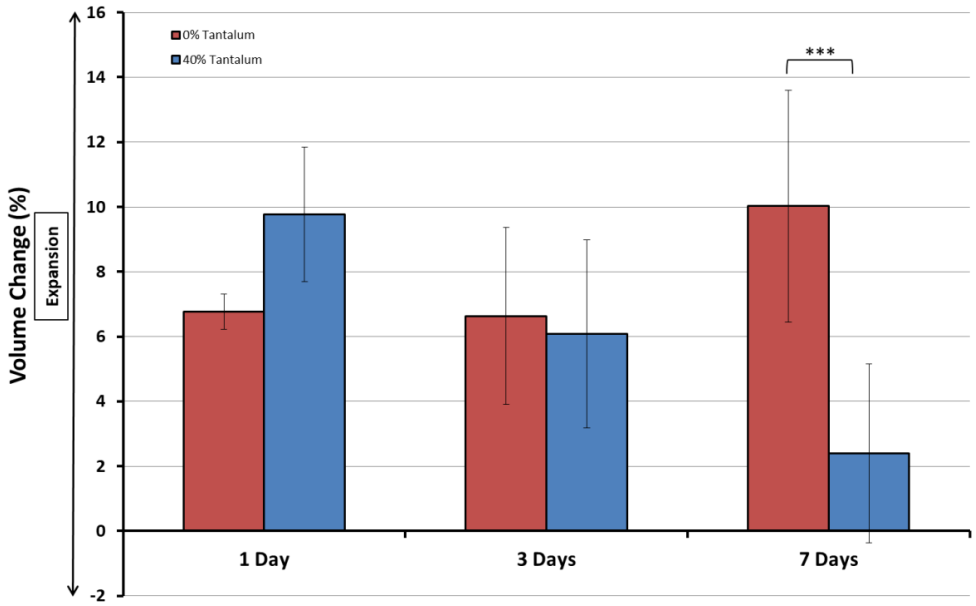

Figure 5.9.6 Hydrogel with 0% and 40% tantalum size conservation after storage for 1, 3 and 7 days at 37^0C in SBF (n=5)

5.9.4. Working and Hardening Time

The addition of tantalum to the hydrogel had no significant effect on the hydrogel's working or hardening time, as shown in Figure 5.9.7.

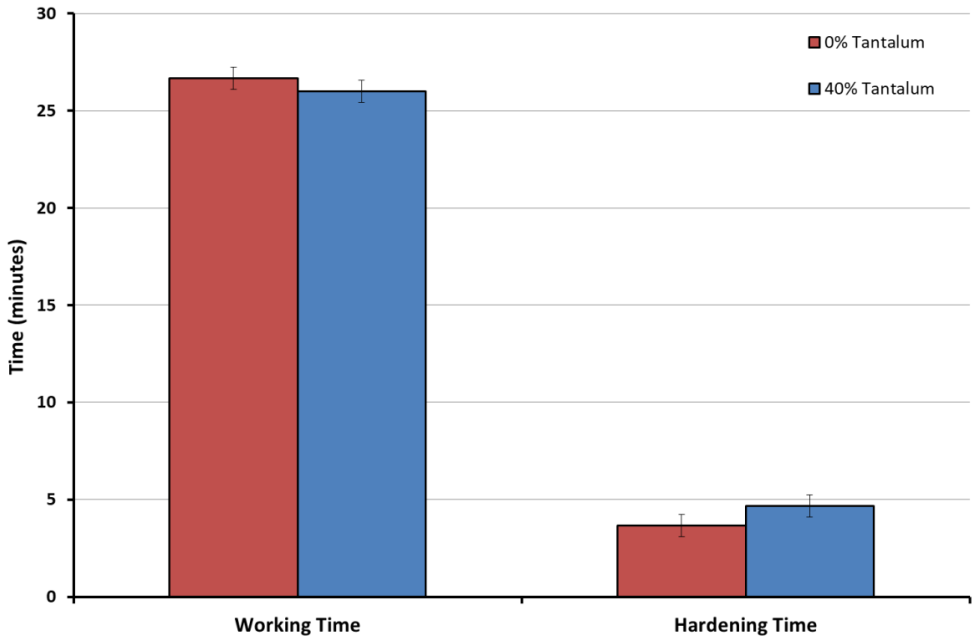

Figure 5.9.7 Working and hardening time with 0% and 40% (w/v) tantalum content (n=5)

5.9.5. Discussion

As expected, increasing the content of tantalum powder in the hydrogel increased its radiopacity. Contrast agents can be added to the hydrogel to further improve the radiopacity, though they will likely increase the viscosity of the hydrogel and increase the force required to inject the hydrogel into the aneurysm.

Although the hydrogel has an increased tantalum powder content compared to Onyx®, the hydrogel does not appear to be as radiopaque (Figure 9.5.32). This may be caused by the variations in tantalum powder. The tantalum powder used for the hydrogel has a particle size of approximately 44µm. Onyx® uses a micronized tantalum powder with a maximum particle size of 22µm but with 68% of the powder having a particle size <5.5µm [105]. This reduced particle size may allow for an increased quantity of tantalum and a more homogenous distribution of the tantalum powder through the Onyx® solution.

The addition of the metallic tantalum particles are likely inducing weak spots in the hydrogel, which may account for this reduction in strength, see Figure 5.9.4. However, the hydrogel's strength exceeds the minimum requirement of 22kPa and continues to increase in strength over time. [19].

The anomaly that occurs with the size conservation in the 0% tantalum does not occur with the 40% tantalum content hydrogel, as the volume reduces overtime with increasing cross-linking density. The sample volume by day 7 is a 2% expansion, if maintained over time, as is shown to do after 7 days in Figure 5.4.11, will reduce possible pressure on the aneurysm wall while providing a high aneurysm dome fill.

For the hydrogel with the addition of 40% tantalum; working and hardening times are within the hydrogel's design limits. Although there was a significant decrease in strength of the hydrogel, the radiopacity of the hydrogel was greatly improved by the addition of 40% tantalum. Table 5.9.1 shows that the hydrogel has met the requirements set out for the optimum hydrogel for the treatment of cerebral aneurysms.

Table 5.9.1 Design review table

Hydrogel	Compressive Strength >22kPa?	Is the material size conserved? (<10% expansion with no shrinkage)	Is the hydrogel injectable?	Working Time between 10 and 30 mins?	Hardening Time <5 mins?	Is the material adhesive?	Is the material cytocompatible? (>70% cell viability)	Is the material sterilisable?	Is the material suitably radiopaque?	Is the material haemocompatible?
0% tantalum	Yes	Yes	Yes	Yes	Yes	Yes	Yes	Yes	No	TBD
40% tantalum	Yes	Yes	Yes	Yes	Yes	Yes	Yes	Yes	Yes	TBD

5.10. Platelet Adhesion

Platelets adhering to the surface of a biomaterial in the cerebral vasculature is typically unwanted as it can result in ischemia. To examine if platelets adhere and become activated, whole human blood was placed on the hydrogel.

Platelet adhesion can be hindered due to sodium citrate in blood collection tubes or induced by vigorous pipetting during experiments. To ensure the experimental set up does not affect platelet adhesion and activation, a positive and negative control is used. A 6 well plate is used as a positive control and a coverslip coated with a siliconizing agent is used as a negative control. The positive, negative and hydrogel samples were stored for 1 hour at 37^0C with 1.5ml of whole human blood.

Dynamic testing provides results more applicable to *in vivo*, as blood flow can affect the adhesion of platelets as blood flow rate and shear rate and stress can influence platelet adhesion. However, experimental set up can be difficult as various tubing materials and roughness can induce platelet adhesion [18] [312] [318]. For this reason static testing was carried out in this study to examine platelet adhesion to the hydrogel, although acknowledged that the results may differ from those obtained *in vivo*.

5.10.1. Positive Control

Figure 5.10.1 shows platelets attached in both their non-activated (red arrows) and activated state (white arrows). The majority of platelets adhering to the surface of the well plate are in their activated state, which can be differentiated from the non-activated platelets by their larger diameter (>3μm). Shape is another indication of platelet activation as the cells lose their spherical shape and the filaments and α-granules move to the platelets periphery. It can be seen in the activated platelets that the fluorescence intensity is increased at the periphery of the platelets.

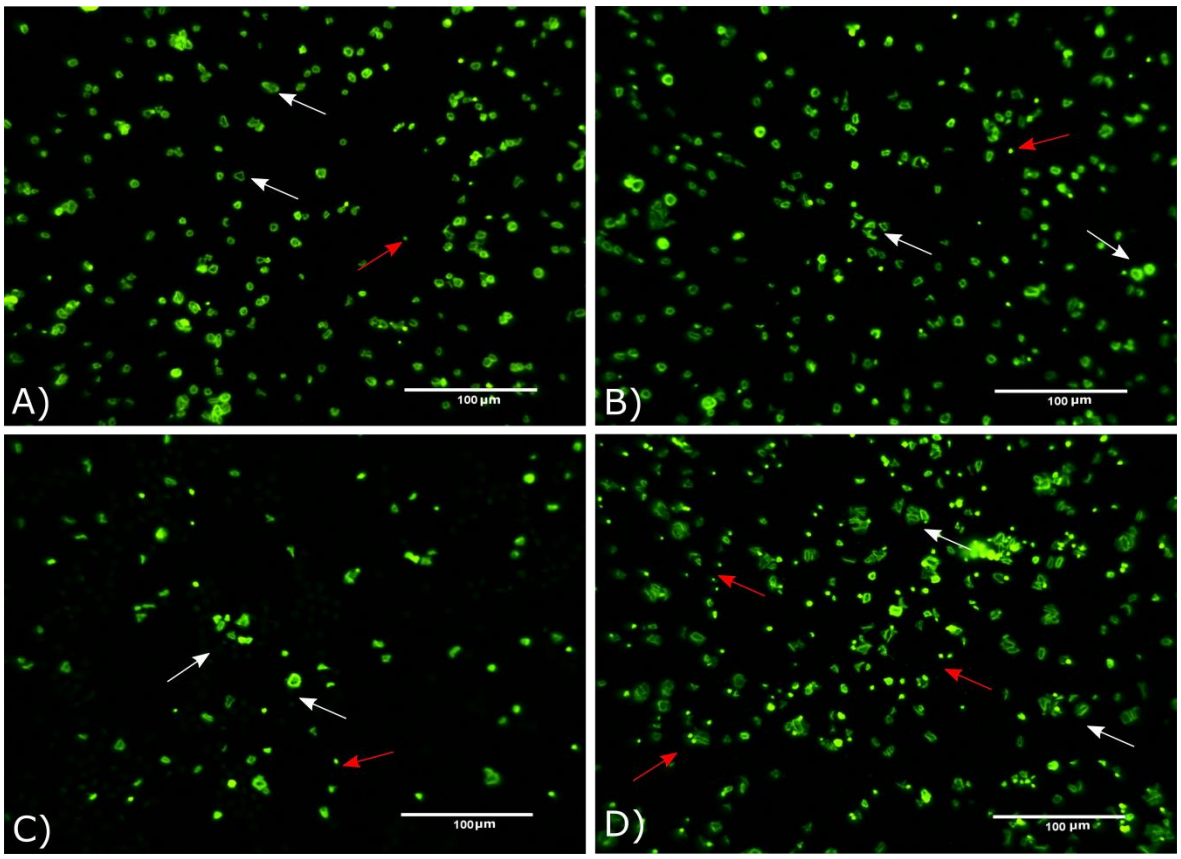

Figure 5.10.1 Platelet attachment to the surface of the positive control (➞ indicates non-activated platelets, ⇨ indicates activated platelets)

5.10.2. Negative Control

A significant reduction in adhered platelets can be seen in the negative control. Of the platelets that did adhere, the majority remained in their non-activated state (Figure 5.10.2C and Figure 5.10.2D). Some of the adhered platelets have a diameter >3µm, which suggest they could have become activated during pipetting.

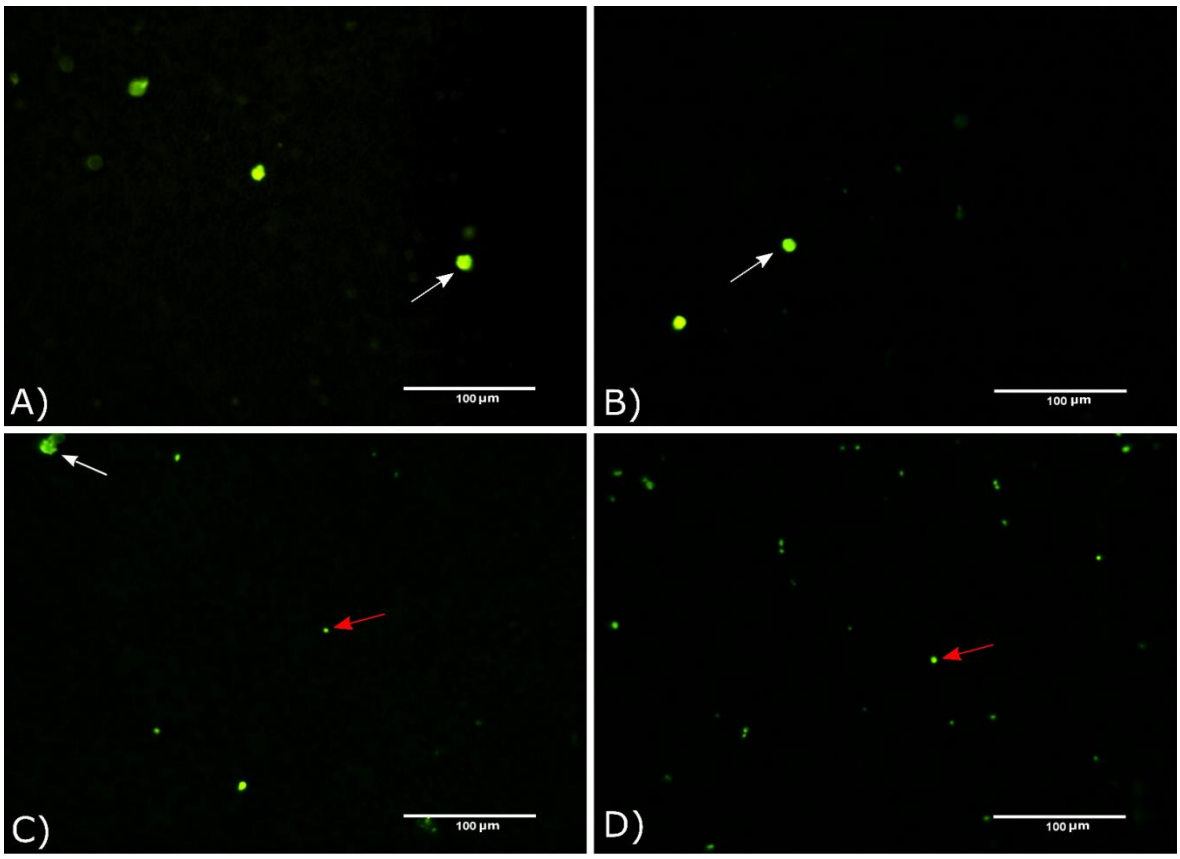

Figure 5.10.2 Platelet attachment to the surface of the negative control (➞ indicates non-activated platelets, ⇨ indicates activated platelets)

5.10.3. Hydrogel Sample

Imaging platelet adhesion and activation on the hydrogel was difficult due to the hydrogel adsorbing the blood and the fluorescent stains. Blood adsorption caused difficulties in focusing the microscope, as platelets in the foreground and background of the image appeared as large circular shape. This makes it difficult to differentiate from activated platelets, as shown in Figure 5.10.3A. The hydrogel adsorbing the stains caused a large background intensity to be present in the images, which again is difficult to differentiate from the platelets with a lower fluorescence intensity.

Even so, it can be seen in Figure 5.10.3A-D that the majority of distinguishable platelets are a small (<3µm) circular shape, indicating the majority are non-activated platelets. The significant number of non-activated platelets adhering to a surface is unusual but is likely caused by the platelets present in the blood adsorbed by the hydrogel and not by the platelets adhering to the hydrogel.

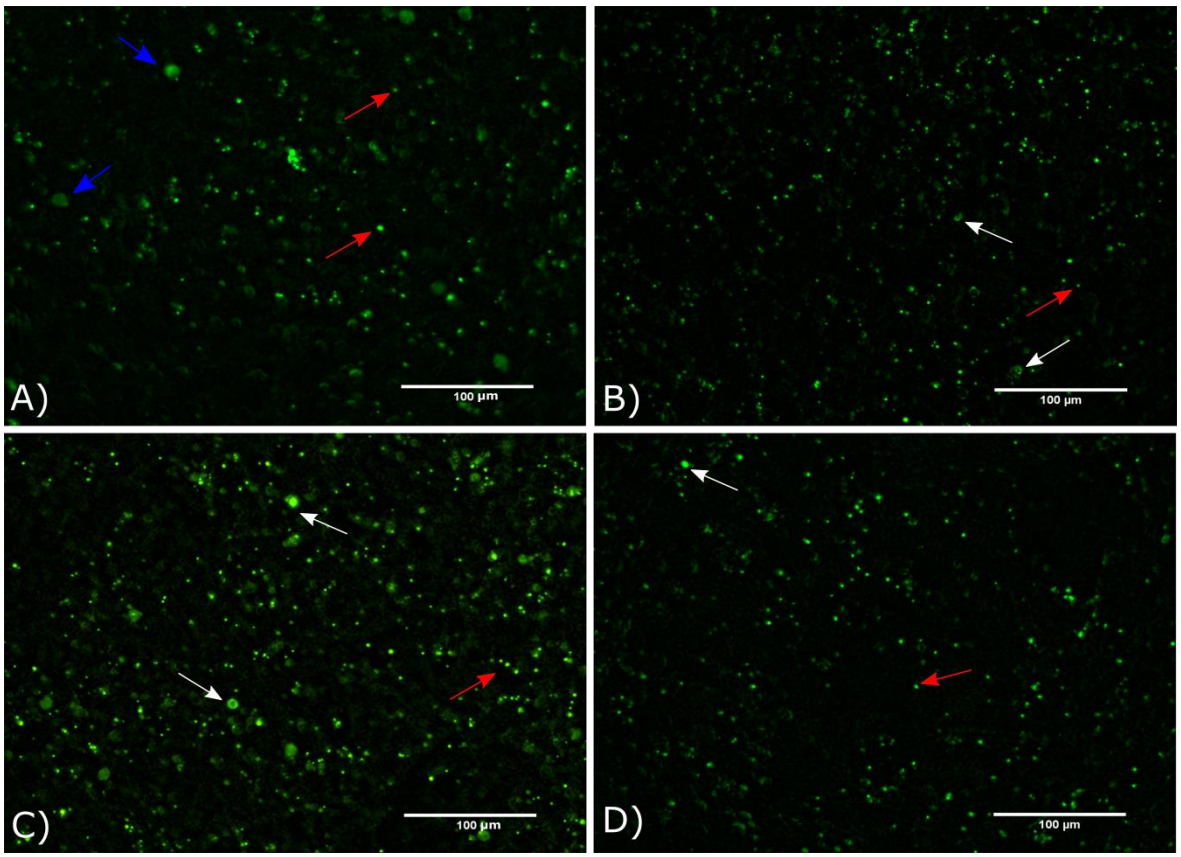

Figure 5.10.3 Platelet attachment to the surface of the hydrogel (➞ indicates non-activated platelets, ⇨ indicates activated platelets, ➟ indicates unfocused platelet)

5.10.4. Discussion

Materials in contact with whole blood may trigger reactions such as inflammation or platelet adhesion [482]. Platelet adhesion and activation is typically a quick response, occurring within 3-5 minutes on the surface of platinum coils and a shear thinning biomaterial designed for aneurysm occlusion [112].

Alginate does not typically adsorb proteins that encourage platelet adhesion, such as fibrinogen as it can't be adsorbed by carboxyl groups due to their negative charge and interactions with water [482]. Although the addition of calcium to the alginate to produce a hydrogel can encourage platelet adhesion, which is evident from its use as a wound dressing [490] [491]. In addition to calcium, the hydrogel discussed here also contains silica and gallium ions, both of which have also been shown to encourage platelet adhesion and activation. Results have shown the silica containing bone substitute material had an increased number of platelets adhering and activating [318] [492]. However, thrombus formation for gallium was dose dependent and decreased at 0.2ppm [380]. Despite the hydrogel containing these ions, platelet adhesion and activation appeared to be reduced compared to that of the control. These variations may be caused by the bioactive glass having a hydrophobic surface, which can reduce platelet attachment [310] [380]. Although the

calcium, gallium and silica content of the hydrogel is unknown, the calcium content of wound dressing hydrogel is known to be approximately 100mg/l [493].

The GDL and EDC components of the hydrogel will likely have an effect on platelet adhesion to the hydrogel. The GDL component of the hydrogel has been used to reduce coagulation [494]. EDC and NHS has also been shown to have a dose dependent effect on platelet attachment, with concentrations about 10% decreasing platelet attachment [495].

The apparent reduced amount of platelet adhesion is highly advantageous for the use of a material intended for vascular applications. As the hydrogel does not rely on thrombus formation to provide a complete occlusion, platelet adhesion is not required. Platelet adhesion and activation would likely have a negative effect, with a clot forming at the neck of the aneurysm. A thrombus in this location may result in irreversible ischemia. Although low, the risk of procedural clot formation still remains since thromboembolic events can occur from blood stagnation due to the presence of the catheter and balloon [306] [496]. Table 5.10.1 indicates that the hydrogel fulfil the requirements of a cerebral aneurysm treatment.

Table 5.10.1 Design review table

Hydrogel	Compressive Strength >22kPa?	Is the material size conserved? (<10% expansion with no shrinkage)	Is the hydrogel injectable?	Working Time between 10 and 30 mins?	Hardening Time <5 mins?	Is the material adhesive?	Is the material cytocompatible? (>70% cell viability)	Is the material sterilisable?	Is the material suitably radiopaque ?	Is the material haemocompatible?
4.5% MVM alginate with sterilised powders	Yes	Yes	Yes	Yes	Yes	Yes	Yes	Yes	Yes	Yes

5.11. *In vivo* Analysis

To examine the injectability *in vivo* and the biological response to the hydrogel, eight rabbits were embolized with either the hydrogel or by coiling. Aneurysms were created either 66 or 90 days prior to treatment, as discussed in more detail in Section 4.13.3 (page 89). The hydrogel was injected into the vessel through a microcatheter with a balloon inflated during treatment, unless otherwise stated. Due to limited success in delivering the hydrogel into the aneurysm it was decided to place the hydrogel in renal arteries to assess if the material had any toxic effects. The treatment each rabbit underwent and location is shown in Table 5.11.1. After fully unsuccessful treatment the animals were euthanized immediately. Rabbits which were treated successfully were euthanized after 28 days and histology was carried out of the treated area.

Table 5.11.1 Embolization treatment tested for each rabbit

Rabbit	Treatment	Hydrogel used (Section)	Area treated
1	Hydrogel	6.75% autoclaved MVM alginate, 13.8% glass, 100mg GDL and 0.83% (w/v) EDC/NHS (9.5.4.4)	Aneurysm
2	Hydrogel	6.75% autoclaved MVM alginate, 13.8% glass, 100mg GDL and 0.83% (w/v) EDC/NHS (9.5.4.4)	Aneurysm
3	Hydrogel	4.5% autoclaved MVM alginate, 9.2% glass, 6.25% (w/v) GDL, 0.83% (w/v) EDC/NHS and 40% tantalum(5.9)	Aneurysm
4	Hydrogel	4.5% autoclaved MVM alginate, 9.2% glass, 6.25% (w/v) GDL, 0.83% (w/v) EDC/NHS and 40% tantalum(5.9)	Aneurysm
5	Hydrogel	4.5% autoclaved MVM alginate, 9.2% glass, 6.25% (w/v) GDL, 0.83% (w/v) EDC/NHS and 40% tantalum(5.9)	Aneurysm
6	Hydrogel	4.5% autoclaved MVM alginate, 9.2% glass, 6.25% (w/v) GDL, 0.83% (w/v) EDC/NHS and 40% tantalum(5.9)	Renal Artery
7	Hydrogel	4.5% autoclaved MVM alginate, 9.2% glass, 6.25% (w/v) GDL, 0.83% (w/v) EDC/NHS and 40% tantalum(5.9)	Renal Artery
8	Coil	N/A	Aneurysm and Renal Artery

Overall, of the rabbits that were successfully treated, there was no evidence of significant weight changes in the rabbits. There was also no indication of toxicity post treatment when examining kidney and liver enzymes and haematology. The delivery of the hydrogel and the results obtained from each rabbit are detailed below.

5.11.1. Rabbit 1 – Aneurysm Treated with Hydrogel

The hydrogel was injected 17 minutes after mixing but was not visible by fluoroscopy. It was uncertain if this was caused by poor radiopacity or the material was too viscous to be injected through the microcatheter. To gain a better understanding, a new hydrogel was prepared and the microcatheter was replaced. The hydrogel was injected at the earlier time of 15 minutes after mixing but again was not visible. The balloon and microcatheter were removed and an angiograph was carried out. The angiograph showed that the aneurysm was partially occluded which may have been caused by the hydrogel or thrombus formation due to blood stagnation. The rabbit was sutured and brought to recovery. Later that day the rabbit woke but with cognitive difficulties. This suggests the material had migrated downstream. The animal was euthanized that day and no histology was carried out after this. This suggests that the material was not sufficiently radiopaque to be observed by fluoroscopy.

5.11.2. Rabbit 2 – Aneurysm Treated with Hydrogel

To increase the radiopacity, the water component of the hydrogel was replaced with the contrast agent Omnipaque™. The hydrogel was injected into the aneurysm 14.5 minutes after mixing. Again, the hydrogel was not visible and the animal was euthanized on the table (non-recovery). No histology was carried out on Rabbit 2.

5.11.3. Rabbit 3 – Aneurysm Treated with Hydrogel

To improve the radiopacity and injectability of the hydrogel, the hydrogel was reformulated (discussed in 5.9). To ensure the balloon was successfully occluding the aneurysm, the microcatheter was placed within the aneurysm and a balloon was placed across the neck. The balloon was inflated and contrast agent was injected into the aneurysm dome. No contrast agent was seen to leak from the aneurysm (Figure 5.11.1). The balloon was deflated until required for embolization of the aneurysm.

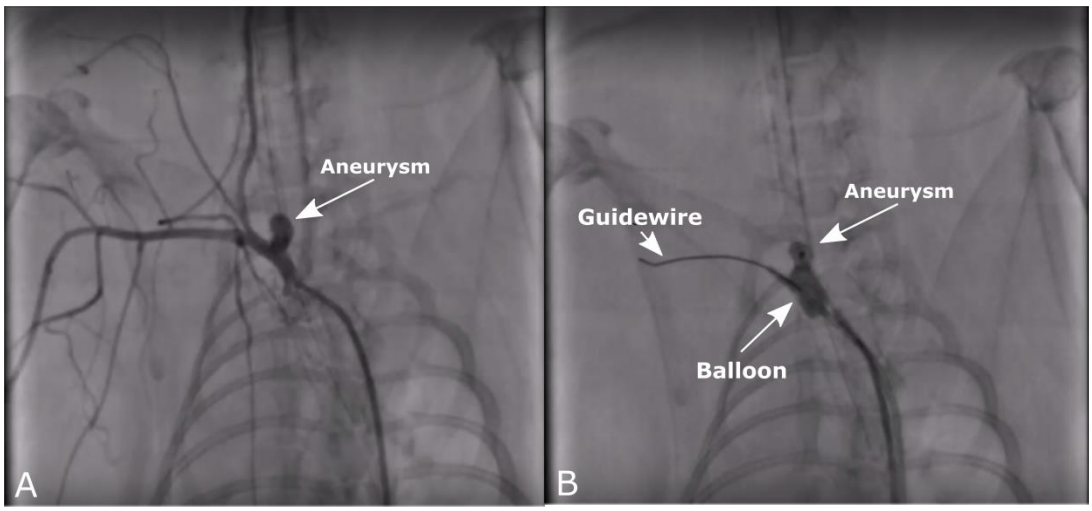

Figure 5.11.1 A) Aneurysm B) Balloon inflated with Omnipaque™ occluding the aneurysm filled with Omnipaque™

The addition of tantalum and the reduced alginate concentration improved visualisation and injectability of the hydrogel (Figure 5.11.2B). However, during injection the material was seen to leak from the proximal side of the balloon and migrate downstream. It was determined that this leaking may be caused by an increase in intrasaccular pressure during injection of the material causing the balloon to deform and the material to migrate (Figure 5.11.2C). The balloon was deflated and no hydrogel was observed within the aneurysm dome (Figure 5.11.2D).

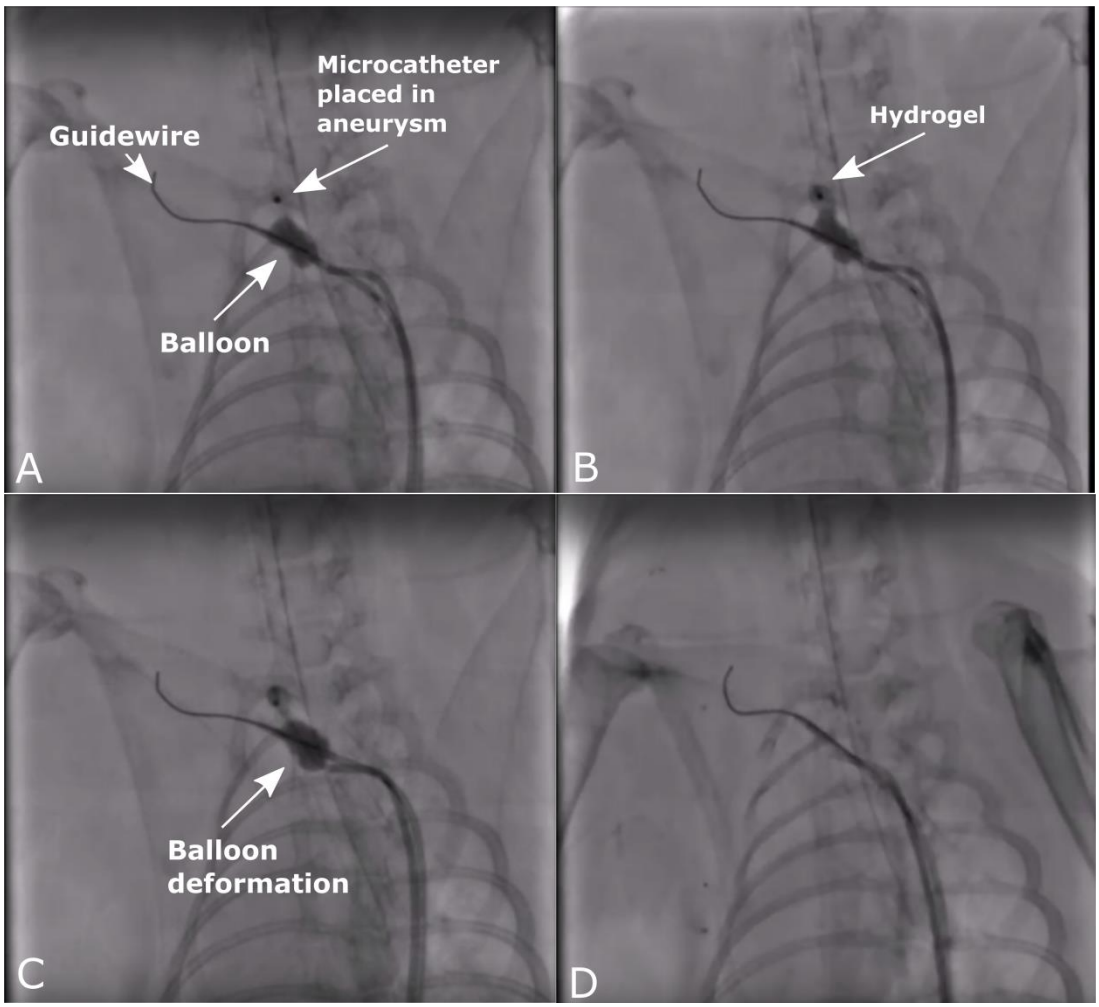

Figure 5.11.2 A) Balloon inflated with Omnipaque™ at the neck of the aneurysm B) Hydrogel being injected through the microcatheter into the aneurysm dome C) Balloon deformation D)No hydrogel observed post treatment

In order to fully utilise this non-recovery animal, the hydrogel was injected again at a later time (23 minutes after mixing began). This later time was used to allow the material to become more viscous, which may reduce the chance of material migration. The aneurysm was completely filled with the hydrogel with no migration during injection observed, as shown in Figure 5.11.3.

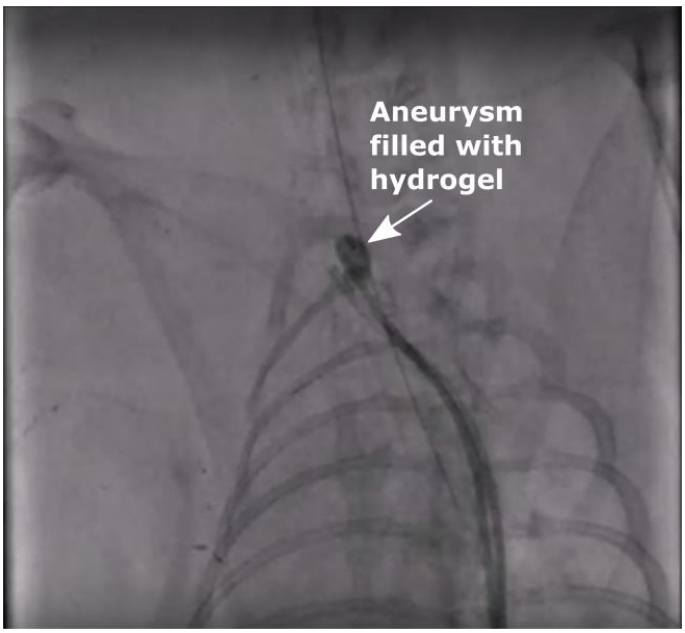

Figure 5.11.3 Hydrogel within the aneurysm dome

The rabbit was euthanized on the table (non-recovery) due to the previous migration of the material. No histology samples were taken for Rabbit 3.

5.11.4. Rabbit 4 – Aneurysm Treated with Hydrogel

In an attempt to reduce intrasaccular pressure, the balloon was placed so that the lumen of the balloon was in the dome of the aneurysm. The purpose of this positioning of the balloon was to allow blood from the aneurysm to travel through the lumen and reduce the pressure within the dome. This method proved successful as the aneurysm dome was filled with the hydrogel without migrating during injection. After 8 minutes the balloon was deflated and the material remained in place. However, the balloon lumen had become trapped in the material and required some force to remove it, see Figure 5.11.4A. During removal of the balloon, some of the hydrogel was removed and migrated, Figure 5.11.4B. It is likely that some material had been forced into the balloon lumen and had become attached to the hydrogel in the aneurysm dome, causing migration during removal.

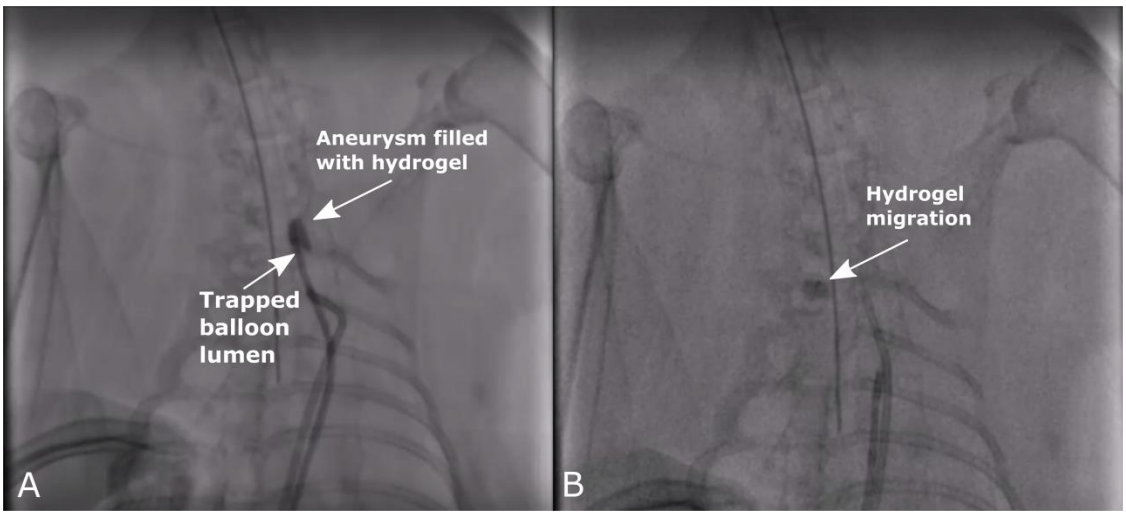

Figure 5.11.4 A) Balloon lumen trapped in aneurysm filled with hydrogel B) Hydrogel migrating downstream

Again, the rabbit was deemed to be non-recovery and was further utilised for acute delivery data. The hydrogel was injected again, in a similar manner to further assess if this method of embolization is more successful. The hydrogel was injected again after 23 minutes but the balloon was deflated earlier, at 5 minutes following inflation. It can be seen in Figure 5.11.5 that the hydrogel remained in place and the balloon was successfully removed. Although the rabbit had to be euthanized, this result showed that the hydrogel can be used to occlude an aneurysm.

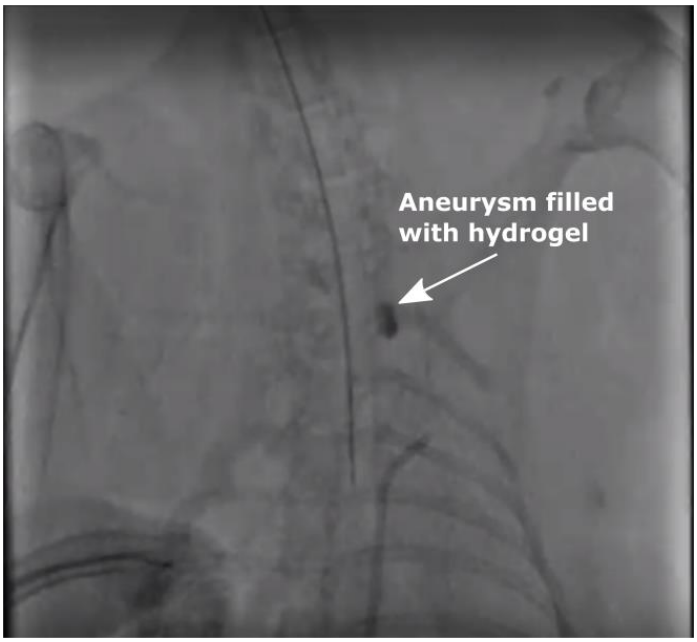

Figure 5.11.5 Aneurysm fully occluded with hydrogel

5.11.5. Rabbit 5 – Aneurysm Treated with Hydrogel

Due to the hydrogel being delivered in Rabbit 4 with the balloon lumen inside the aneurysm, it was decided to attempt this procedure again. Figure 5.11.6 shows that the hydrogel filled the aneurysm without migrating downstream. However, while the balloon was being

removed a small string of the hydrogel was released from the balloon lumen and travelled downstream. The animal was immediately euthanized but histology was carried out.

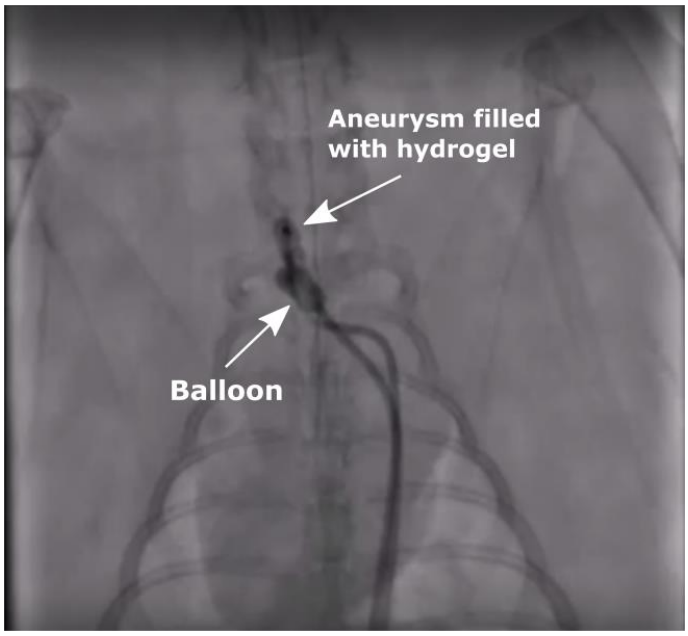

Figure 5.11.6 Hydrogel being injected into the aneurysm

Histology showed a small amount of unorganized fibrin-thrombus at the fundus of the aneurysm dome (Figure 5.11.7). This was likely caused by blood being trapped behind the hydrogel during injection and not caused by blood migrating to behind the hydrogel.

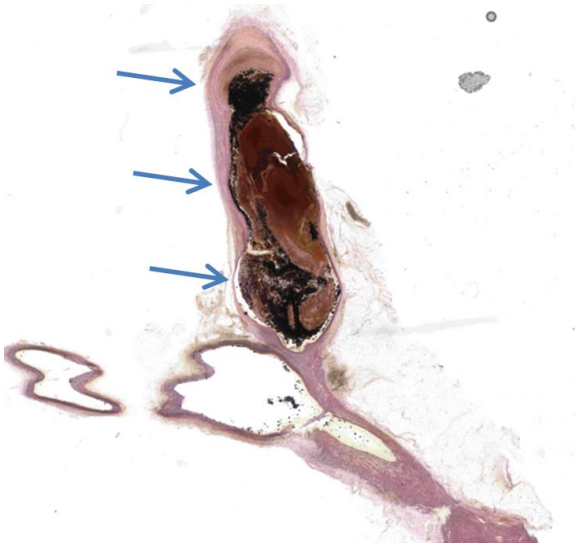

Figure 5.11.7 Histology of the aneurysm treated with the hydrogel

5.11.6. Rabbit 6 – Renal Treated with Hydrogel

Due to limited success with aneurysm embolization it was decided to carry out terminal kidney embolization with the hydrogel on Rabbit 6. The hydrogel was injected 23 minutes after mixing and the balloon was deflated 2 minutes after inflation. The hydrogel remained in place and showed a good occlusion of the vessels with no material migration (Figure 5.11.8).

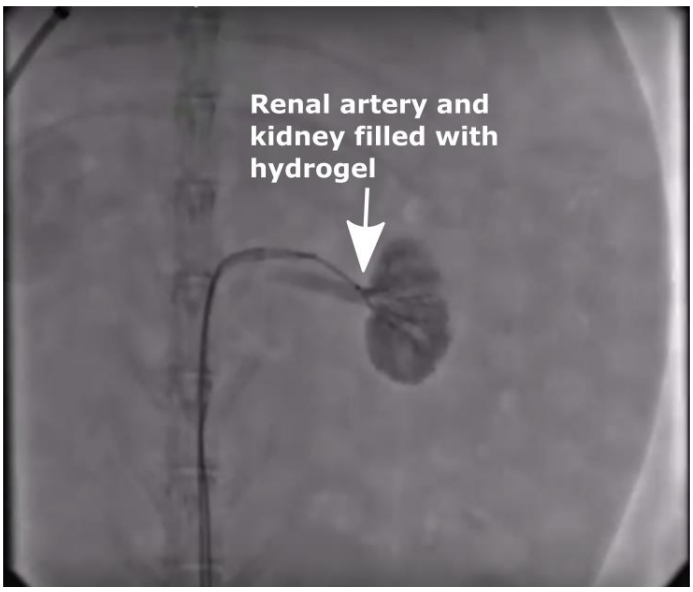

Figure 5.11.8 Kidney and renal artery embolized with hydrogel

The hydrogel remained in the kidney for 30 days without causing a toxic response to the rabbit. At 30 days, the animal was euthanized and the kidney and renal artery were examined. As shown in Figure 5.11.9, the kidney had a length of 31mm and a width of approximately 20mm. The NZW rabbit left kidney typically has a length of 38-40mm and a width of 22-28mm at 8 months [497]. These results show a 25% decrease in the length and a 32.5% reduction in the width of the kidney.

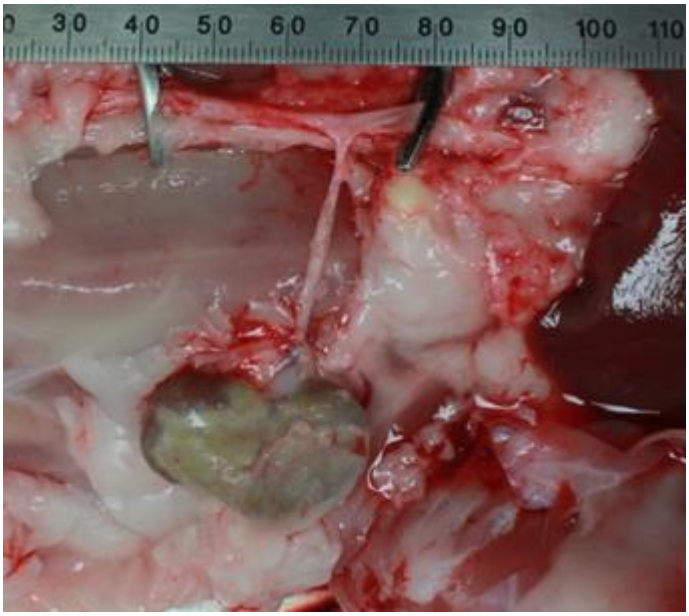

Figure 5.11.9 Macroscopic image of the left kidney treated with the hydrogel

Dissection of the kidney showed that during embolization, the material had filled numerous interlobular, arcuate and intralobular arteries, distal and glomerular afferent arterioles and capillary tufts. This indicates that the material was able to be delivered into small vasculature and remain for a minimum of 30 days. A near-complete occlusion was achieved with

neointima formation evident. Mild recanalization (<20%) was observed in the occluded vessels but there was no evidence of necrosis or inflammation caused by the device.

5.11.7. Rabbit 7 – Renal Artery Treated with Hydrogel

Rabbit 7 had its renal artery embolized with the hydrogel. No balloon was used for embolization of Rabbit 7. Figure 5.11.10A shows the hydrogel is clearly visible during injection. Figure 5.11.10 shows the kidney embolized with the hydrogel.

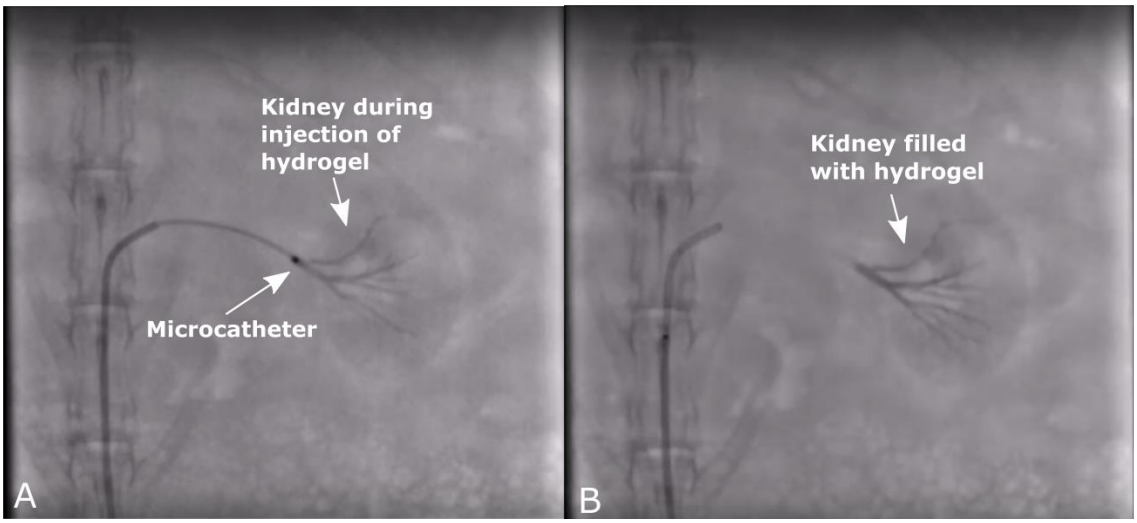

Figure 5.11.10 A) Hydrogel being injected into kidney B) Kidney embolized with hydrogel

30 days after initial treatment, the rabbit was euthanized. Renal artery enlargement (30 x 60mm) was macroscopically observed in Rabbit 7. Embolization of the renal artery with the hydrogel in Rabbit 7 exhibited similar results to Rabbit 6. Though, embolization in rabbit 6 resulted in necrosis of the perirenal adipose tissue, with notable inflammation and fibrosis in that area. This was likely caused by the embolization of the renal artery and not related to the hydrogel.

5.11.8. Rabbit 8 – Renal Artery and Aneurysm Treated with Coil

Rabbit 8 had coils placed in both an aneurysm and the kidneys renal artery. Figure 5.11.11 shows the coils could successfully occlude the aneurysm.

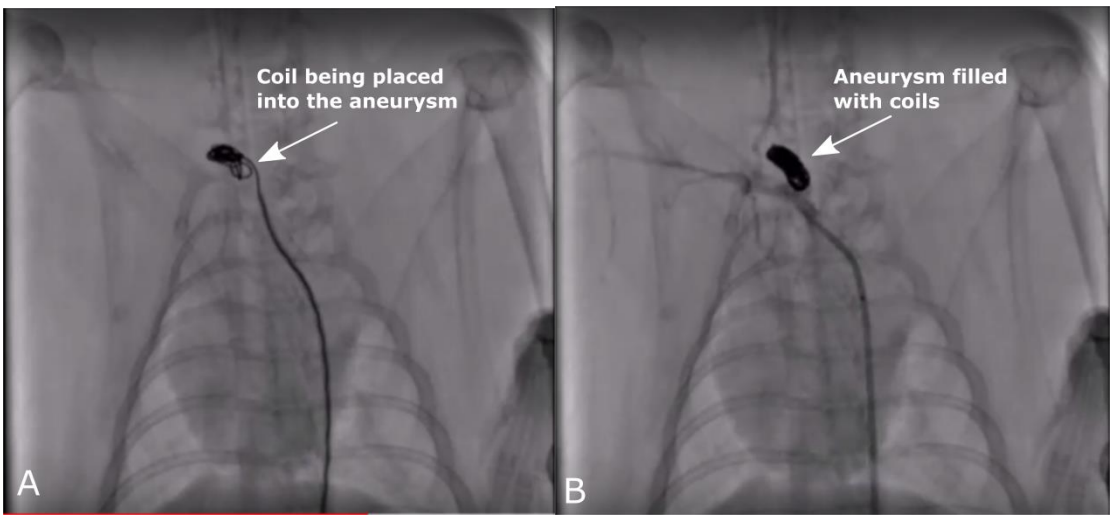

Figure 5.11.11 Aneurysm A) during and B) after coiling

Histology showed that after 30 days, neointimal formation, organizing haemorrhage and non-endothelialized fibrin thrombus in the aneurysm treated with the coils (see Figure 5.11.12). There was no adverse response, such as inflammation or necrosis, observed in the aneurysm. As discussed in Section 2.3.3.1, this is the ideal healing response of a coiled aneurysm.

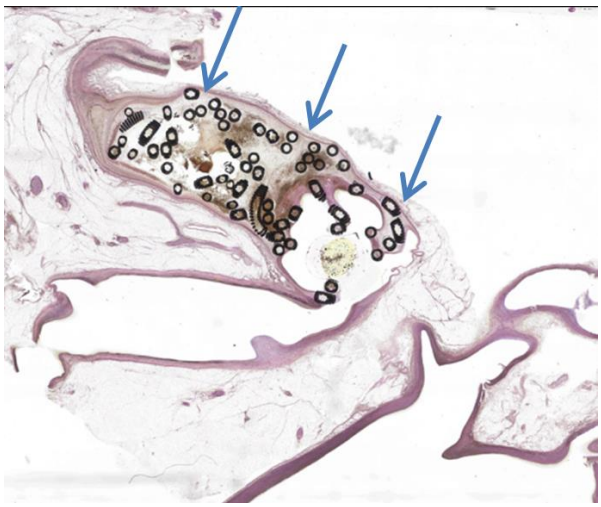

Figure 5.11.12 Histology of coiled aneurysm

To embolize the renal artery of the kidney, coils were placed within the rabbit's renal artery, as shown in Figure 5.11.13.

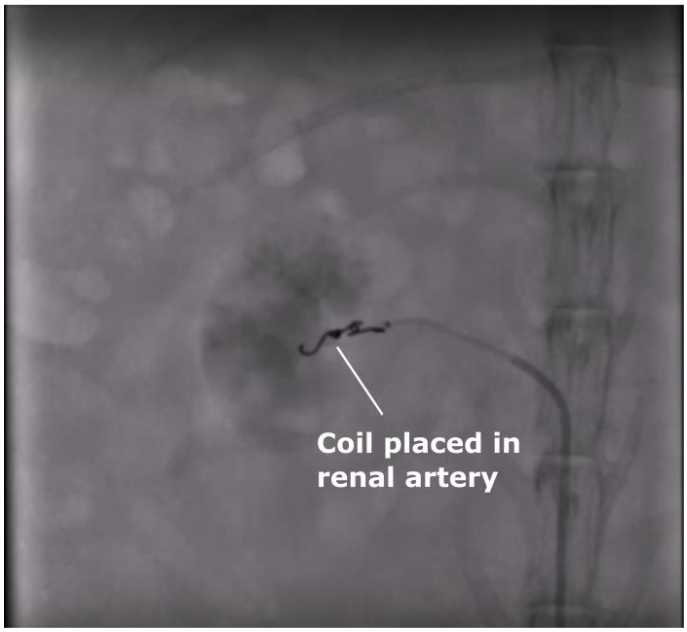

Figure 5.11.13 Coil within renal artery

After 30 days the rabbit was euthanized and dissected. The size of the right kidney is smaller than the left and has a length between 33-37mm and a width of 24-27mm [497]. The kidney treated with the coils had a length of 29mm and a width of approximately 19mm after 30 days, as shown in Figure 5.11.14. This is a 21.5% reduction in the length and 34% reduction in the width of the kidney.

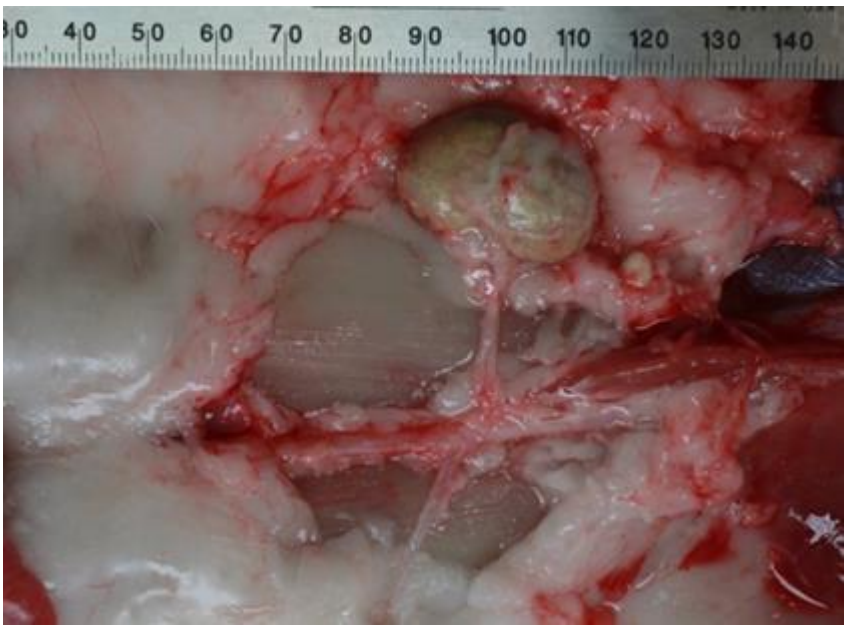

Figure 5.11.14 Macroscopic image of right kidney

Histology samples of the renal artery treated with the coils showed renal cortical necrosis, near-complete occlusion and mature neointima.

5.11.9. Discussion

Initially, the material was too viscous and insufficiently radiopaque. The viscosity was reduced by modifying the hydrogels alginate, glasses and GDL content and the radiopacity was improved by the addition of tantalum. These changes to the hydrogel significantly improved the deliverability and visibility of the hydrogel into the aneurysm. Despite these changes, no surviving rabbit's aneurysm could be embolized with the hydrogel as small amounts of material migrated during injection[5]. The results show that modifications to traditional embolization methods can improve the deliverability of the hydrogel, with the hydrogel successfully occluding the aneurysm in three of the trials.

Migration of liquid embolic material during injection is common, even with the presence of a balloon across the aneurysm neck [119] [498] [499]. This is likely caused by intrasaccular pressure causing the non-compliant balloon to compact, which was observed in Rabbit 3. In this study we have shown that placing the lumen of the balloon into the aneurysm can reduce intrasaccular pressure and improve injectability. Yet, issues can occur if the lumen of the balloon becomes trapped within the set hydrogel. Although not examined, the hydrogel is likely migrating into the balloon lumen during injection. The hydrogel within the balloon lumen and the hydrogel within the aneurysm dome are likely setting together. In this case, the entrapment of the lumen in the hydrogel may be reduced by using a balloon with a reduced lumen inner diameter. This reduced inner diameter will likely allow blood to migrate into the lumen, while the more viscous hydrogel remains in the aneurysm. Other studies have also shown that the injection of embolic materials can be improved by placing a stent across the aneurysm neck during injection [5] [118] [500] [501]

Kidney embolization results indicate that the hydrogel has no toxic response on the host. Although inflammation and tissue necrosis were observed, they were caused by the successful embolization of the arteries and not in response to the hydrogel [502]–[504]

A mild amount of recanalization was observed in the renal artery embolization with the hydrogel. Recanalization is not ideal in aneurysm treatments as it may cause recurrence of the aneurysm. Recanalization is common in aneurysms treated with coils with rates are as high as 25.5% in initially fully occluded coiled aneurysms [434] [505].

Neointima formation was observed in the renal artery embolization with the hydrogel and with the coils. Neointima formation is an advantage in embolization as it will occlude the treated area from the parent artery [172] [506]. Results in aneurysm studies with embolic agents have varying success of neointima formation present 30 days after treatment [118] [500] [507].

5.12. Design of Injection Device

To improve ease of injecting the hydrogel, a syringe must be designed.

The force required to inject a material through a catheter can be calculated using the Hagen-Poiseuille equation

Equation 5.12.1 Hagen-Poiseuielle equation

$$F = \frac{128Q\mu LA}{\pi D^4}$$

Where;
Q = the volumetric flow rate (m^3/s)
μ = the dynamic viscosity of the material (Pa.s)
L = the catheter length (m)
D = the diameter of the needle/catheter (m)
A = the syringe plunger area (m^3) [112] [508].

This equation is useful to predict the force required to inject Newtonian fluids at various viscosities with varying flow rates, syringes and catheters. However, alginate is a Non-Newtonian fluid that undergoes shear thinning and, therefore, it is difficult to predict the changes in force at increasing viscosities and flow rates [197]. However, it is clear from the equation that increasing the flow rate, fluid viscosity, catheter length and syringe size will cause an increase in force required to inject the material. The largest change to the force required will be caused by varying the diameter of the catheter used.

5.12.1. Testing Commercially Available Syringes

Standard push syringes are available in various volumes with the syringe plunger area typically increasing with an increase in syringe volume. Increasing plunger areas result in an increase in force to inject a material. Alternatively, for a larger syringe plunger area, a reduction in the flow rate can allow a material inject through the same catheter at a similar force.

To examine the effect syringe size and flow rate has on the force required to inject the hydrogel, the hydrogel was injected through a 2.4F catheter from a 1ml and 3ml syringe. Figure 5.12.1 shows that the injection force required to inject the hydrogel from a 1ml syringe at 0.5ml/min rate was 60N. The hydrogel could not be injected through the 3ml syringe at 0.5ml/min rate and therefore the flow rate was reduced to 0.1ml/min. The hydrogel could inject at this flow rate with a force of 44N.

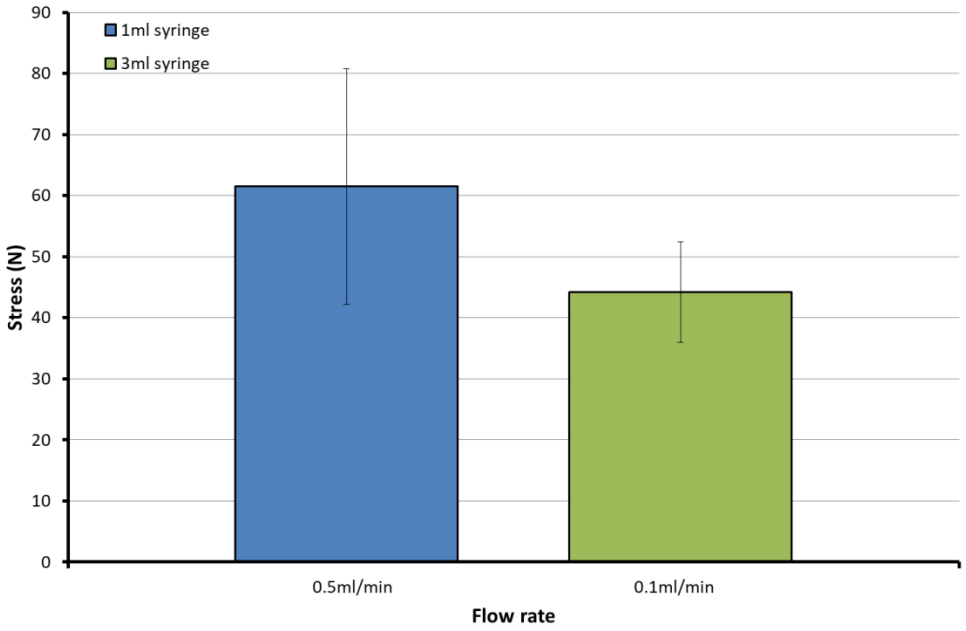

Figure 5.12.1 Injecting 4.5% MVM alginate hydrogel through a 2.4F catheter

5.12.2. Design of Syringe

In order to fill a medium sized aneurysm, approximately 2ml of hydrogel will be required. The results in Figure 5.12.1 show that in order to inject the hydrogel from commercially available syringes, the flow rate must be reduced or a multiple number of 1ml syringes must be used. Due to the hydrogel having a working and setting limit, a reduction in flow rate to reduce the force is not ideal. Use of numerous syringes would not be ideal either, as an air bubble could be introduced into the cerebral vasculature while changing the syringes. Therefore, a syringe was designed to have a 5mm diameter, similar to the 1ml syringe, and a longer length to increase the syringe volume to 2.4ml.

A threaded plunger syringe was designed as this is commonly used in syringes designed to inject high viscosity materials, as the injection force required is reduced compared to a typical push syringe. This design also helps control the injection rate of the material [509]–[512]. This may allow for injection rate to be increases and reduce surgery time. Drawings of the syringe are shown in Appendix 9.5.10.

The results to date have shown the hydrogel mixed to a volume of 1.2ml. However, in order to fill the aneurysm a 2ml hydrogel is required. To examine this, testing was carried out when the hydrogel's components were doubled in weight. The results of scaling up the hydrogel volume indicate that increasing the hydrogel volume has no negative effect on the performance of the hydrogel. The results are shown in Appendix 9.5.10.1.

Chapter 6. Project Discussion

The hydrogel produced here is shown to incorporate a combination of the advantages of *in situ* gelling alginate hydrogels with the advantages of bioactive glasses. *In situ* gelling alginate hydrogels allow the treatment of vascular defects in a minimally invasive manner while providing a high occlusion rate. Alginate hydrogels typically lack sufficient mechanical properties and stability for embolization, however, the incorporation of bioactive glass allows for the slow release of cross-linking ions that result in a high strength homogenous hydrogel that is stable overtime. The incorporation of bioactive glasses can also promote cell growth and adhesion, which is lacking from typical calcium alginate hydrogels.

It can be seen from the results of Section 5.1 and 5.2 that molecular weight, chemical composition and concentration of alginate can significantly affect the compressive strength, viscosity, working time and hardening time of a hydrogel. Typically, alginates with a High-G content will have a higher compressive strength compared to High-M alginates, however, it can be seen in Figure 5.1.8 and Figure 5.1.9 that a high molecular weight can be used to compensate for the lower strength typically observed with a High-M alginate. This difference is likely due to two different cross-linking mechanisms involved. For the High-G, low molecular weight alginate, the cross-linking is likely caused by ionic cross-linking. A considerable portion of the cross-linking of the High-M and high molecular weight alginates is likely caused by the increased chain entanglements.

The results from 5.2 show that gamma irradiation of alginate can significantly decrease the strength and viscosity of the produced hydrogel. The working time and hardening time of the hydrogel is also significantly increased. These effects are caused by the decrease in chain entanglements, resulting from a reduction in molecular weight. This further shows that molecular weight can greatly affect the produced hydrogel when using a High-M content alginate. The results from Section 5.2 show that gamma irradiation of alginate is not a suitable sterilisation technique for the specific intended use of this hydrogel.

Acid washing of the glass phase can affect the surface properties and reduce the agglomeration of glass powders. This results in a hydrogel with a strength higher than that which has been reported in the current literature for *in situ* forming alginate hydrogels. This was likely caused by the increase in trivalent ions on the surface of the glass particles and a better dispersion of glass particles resulting in a more homogenous hydrogel.

The results show that the hydrogel is highly tuneable by varying the alginate type and concentration, glass content and GDL content. The surface properties of the bioactive glass are also a key component in the resulting hydrogel. Although the working time and hardening

time of the hydrogel decreases linearly with the increase in alginate concentration, glass and GDL content, this is not observed for the strength. This is due to longer term interaction such as the cross-linking density of the hydrogel. An increase in alginate concentration will require an increase in glass and GDL to produce a sufficient ion content. Excessive glass content will result in an inhomogeneous hydrogel due to the agglomeration of glass particles. An increase in GDL will decrease the pH further, which may result in significant inflammation and cell apoptosis.

For the hydrogel to have a suitable sample volume conservation and injectability, the strength of the hydrogel has to be reduced. This is due to the strength of the hydrogel increasing with increasing alginate concentration and cross-linking density. Increasing the alginate concentration results in a highly viscous hydrogel that requires an excessive force to inject from a micro-catheter. Increasing the cross-linking density causes water molecules to be removed from the hydrogel due to an increase in elastic forces and results in a loss of volume [209]. The injectability can be improved by reducing the alginate concentration, though the glass and GDL content must be optimised to reduce sample expansion.

EDC and NHS have been used to improve the cell adhesive and bond strength of alginate by cross-linking alginate with peptides or other polymers. Due to the *in situ* gelation of the hydrogel discussed here, the EDC and NHS can provide the formation of an amide bond during gelation to the surface of the aneurysm wall.

The ions released from this hydrogel encourage cell proliferation in a dose-dependent and exposure duration-dependent manner. The results show that the gallium ions released from the glass phase are likely having a cytotoxic effect but this is mediated by cell proliferative ions such as silicon and the gluconic acid released from the hydrogel.

Cells typically do not adhere to the surface of alginate hydrogels. Results here show that the addition of bioactive glass and EDC and NHS to alginate cause the hydrogel to adhere to tissue and encourage cells to attach to the hydrogel surface.

In addition to improving volume conservation and injectability, the strength of the hydrogel will have to be forfeited to improve the bond strength, sterility and radiopacity of the hydrogel. As the hydrogel had an initial high strength, these reductions in strengths still resulted in a hydrogel that greatly exceeds the minimum strength requirement. The resulting hydrogel fulfils each requirement of the “Ideal aneurysm treatment device” described in 2.4 (page 25).

6.1.1. Comparison of the Optimum Composition to Other Aneurysm Treatments

A range of injectable polymer formulations have been developed for soft tissue applications but many contain toxic monomers, activators and free radicals. The gelation rate of the hydrogel described here is slow compared to other alginate hydrogels [201] [357], which allows the hydrogel to be delivered and set, within a clinically applicable time frame.

For an aneurysm filler to be effective it should have sufficient strength in order to behave in a similar manner to native cerebral tissue; diverting flow, withstanding stresses caused by arterial expansion and contraction and haemodynamic forces (static, dynamic and shear). A calcium alginate gel that was designed for embolization was reported to have a compressive strength of 124kPa at 60% strain [109]. Onyx®, a material approved for the treatment of cerebral aneurysms in Europe, has been observed to have a compressive strength of 3MPa after 5 days [130]. However, Onyx® sets rapidly when in contact with blood, which reduces the strength and adhesive properties of the material. The optimised hydrogel in this study exhibits an incremental modulus of up to 472kPa and a compressive strength of 146kPa after storage in SBF for 1 day. Both the incremental modulus and strength increase to 581kPa and 271kPa respectively after 7 days. Although it is not equal in strength to Onyx® or the 1MPa modulus which is likely to reduce WSS (indicated by CFD), it may act to support the existing tissue in its function, without transferring excessive stress to the damaged tissue. This novel material also has a greater mechanical integrity than the currently used coil technology, where coils with clots have a compressive strength of approximately 4.24±1.26kPa.Though these strengths are not optimal, coils continue to function in this mechanical environment [76] [80] [129].

Figure 5.6.12 shows the hydrogel has a significantly reduced tensile strength compared to cerebral vasculature and aneurysms, discussed in Section 2.1.3 and 2.2.3. This strength will have to be improved for the use applications such as the treatment of myocardial infarctions. Though, for the treatment of cerebral aneurysms the strength of the hydrogel will likely suffice.

An advantage of Onyx® as an aneurysm treatment compared to that of coils is that it greatly reduces the vortices, jet flows and WSS stress within the aneurysm without relying on thrombus formation. It is thought that all of these are factors contribute to aneurysm rupture [48]–[50]. It is likely that the produced novel glass-alginate hydrogel will have the same advantages as Onyx® due to the complete embolization of the aneurysm.

Onyx® can cause angiotoxic effects due to the presence of DMSO in the Onyx® solution if not injected at the correct rate. The novel hydrogel discussed here does not require the diffusion of inorganic solvent in order to gel. This hydrogel can also be injected in 5 minutes and does

not require a repeated inflation or deflation of the balloon. This provides a significant advantage of reducing toxicity, surgery time and possible vessel damaged caused by repeated balloon inflation.

The release of multivalent ions from the glass and gluconic acid from the hydrogel has been shown to support cell proliferation. This is ideal for an aneurysm filler as it would encourage endothelialisation of the neck of the aneurysm, causing the aneurysm to fully occlude from the parent artery. This may also improve the strength of the wall of the aneurysm, as aneurysm walls typically have a fragmented endothelial layer. However, an excessive proliferation of endothelial cells may cause recanalization of the aneurysm. While Onyx® and hydrogel coated coils have been shown to cause remodelling at the neck of the aneurysm, endothelialisation is not always observed with bare coils [78] [446]. The literature does not indicate an aneurysm treatment, like the novel hydrogel, that can promote cell proliferation.

Neither Onyx® nor bare coils are adhesive to the aneurysm wall. Here, the addition of 0.83% (w/v) of EDC and NHS increased the adhesion of the hydrogel to a porcine skin graft. This is advantageous as it may reduce the chance of recurrence of the aneurysm and inhibit blood flowing behind the embolic material.

As with Onyx® and other injectable aneurysm treatment materials, the novel hydrogel was seen to migrate from the aneurysm dome during injection [119] [498]. However, the hydrogel was successful delivered into aneurysm non-recovery animals. The hydrogel was injected into the renal artery for kidney embolization and the material was found to successfully embolize the renal artery, with material found in the micro-vasculature. The material was shown to have sufficient mechanical properties to embolize the arteries while supporting neointima formation.

Chapter 7. Conclusion and Future Work

7.1. Conclusions

- Ion releasing bioactive glass can be used to cross-link alginate, resulting in a high strength material. The continued release of ions from glass causes an increase in strength over time. This continued release of ions results in a hydrogel with a compressive strength of 2,645 kPa, higher than any reported for *in situ* gelling alginate hydrogels.

- Alginate concentration, molecular weight and chemical composition affect the sample volume conservation, viscosity, strength, deliverability, working and hardening time of the novel hydrogels such that:
    - The hydrogel working time is predominantly governed by the chemical composition of the alginate.
    - The hydrogel hardening time is predominantly governed by the molecular weight of the alginate.
    - High G-block alginates have a high strength and viscosity, even at a low molecular weight.
    - The strength and viscosity of a high M-block alginate can be compensated for by increasing the alginate's molecular weight.

- The surface properties of glass particles can be modified by acid washing. This has an effect on the particle size, surface topography, pore size, surface ion content and surface network connectivity. These modifications on the surface properties of the glass can reduce glass particle agglomeration due to decreased hydrophobicity. In the case of this hydrogel, modification of the surface ion content resulted in a higher strength hydrogel.

- The inclusion of EDC and NHS in the hydrogel can significantly increase the bond strength of the alginate hydrogel to a porcine skin graft in 1 day without the addition of RGD peptides or collagen.

- The strength of the hydrogel must be sacrificed to improve the injectability and to achieve volume conservation.

- The quantity and release rate of ions from bioactive glass can affect cell viability. In the case of bioactive glasses, the release quantity and rate can be controlled by the

network connectivity of the glass and the glass surface ion content. Gallium and calcium can have cytotoxic effects on endothelial cells but these effects can be mediated by the release of cell proliferative ions such as silica.

- The damaging effect that gamma irradiation has on glass, GDL, EDC and NHS can be reduced if the material is irradiated at low temperatures.

- The addition of glass to an alginate hydrogel can improve the ability of cells to adhere to the surface. This may be caused by the presence of silica ions or a reduction in the hydrophilicity of the alginate due to the hydrophobic glass ions.

- The hydrogel can be effectively used as an embolization treatment and encourage neointima formation without causing any material related inflammation.

7.2. Future Work

- Acid washing the surface of the glass increased the surface area and pore diameter of the glass. Prolonged acid washing times may further increase the pore diameter. This increase may allow the glass particles to be loaded with therapeutic ions, which if incorporated into the hydrogel, could be used for the direct delivery of therapeutics to the required site.

- Production of glass particles by sol-gel will allow for a more controlled particle size. This may further improve the strength of the hydrogel, as these particles are more likely to be evenly distributed throughout the hydrogel.

- The radiopacity of the hydrogel was improved by the addition of tantalum powder; however, it reduced the hydrogel's strength. Other methods may improve the radiopacity without having the same negative effects on strength. These include other forms of tantalum, contrast agents and tantalum containing bioactive glass. The use of a tantalum with a smaller particle size may allow a reduced quantity of tantalum with a better dispersion. No contrast agents were tested to date but have been shown to successfully increase the radiopacity of other polymers. Although tantalum was added to the glass, replacing calcium, it caused negative results likely due to an increased glass network connectivity. Partially replacing gallium or silica in the glass composition may provide a glass with acceptable ion release rates and an increased radiopacity.

- For clinical applications, the hydrogel will have to remain sterile from production to injection. Not alone will sterility need to be maintained in its packaged form, but every effort will need to be made to maintain sterility during mixing. For this, a sterile mixing device will need to be designed.

- Time will likely have a negative effect on the packaged components of the hydrogel, particularly the alginate, which is delicate and liable to degradation. Shelf-life studies should be completed to examine if the properties of the hydrogel, particularly the strength, working time and hardening time, change over a typical product shelf-life.

- The hydrogel's properties can be vastly modified by varying the alginate, glass and GDL content. For this application, increasing these components has a negative effect on the injectability. However, larger catheters may be used in other embolization techniques. These increased catheter sizes will allow for the alginate concentration to

be increased, which will increase the hydrogel's strength particularly if the glass and GDL concentration is also suitably increased. Examining the hydrogel's injectability, strength and setting time at various concentrations should be examined to determine its usability for a range of other applications.

- Polymerase chain reaction of BAECs dosed with the hydrogel's eluent and the individual ions may provide a better insight mechanism by which the eluent encourages cell attachment and proliferation. This will allow tailoring of the hydrogel to improve the biocompatibility of the hydrogel. The ion content and release rate from the hydrogel could be controlled through further surface modification of the bioactive glass or increasing/decreasing the glass and GDL content.

- Incorporating small amounts of thermal responsive cross-linkers into the hydrogel, such as PNIPAAm, may improve its usability for cerebral aneurysm applications by resulting in an initial thermally induced partial gelation/thickening upon delivery, thereby reducing the chance of material migration during delivery.

- *In vitro* or *in vivo* studies with a stent or flow diverter, rather than a compliant balloon, at the neck of the aneurysm may improve the injectability of the material, as it will reduce intrasaccular pressure.

- The design of a partially covered retrievable stent may sufficiently reduce blood flow to allow the material to be injected and set, while reducing intrasaccular pressure and trap any material that migrates.

Chapter 8. Bibliography

[1] J. L. Brisman *et al.*, "Cerebral Aneurysms," *N. Engl. J. Med.*, vol. 355, no. 9, pp. 928–939, Aug. 2006.

[2] E. Crobeddu, G. Lanzino, D. F. Kallmes, and H. J. Cloft, "Review of 2 Decades of Aneurysm-Recurrence Literature, Part 2: Managing Recurrence after Endovascular Coiling," *Am. J. Neuroradiol.*, 2012.

[3] C. R. Brennecka, M. C. Preul, and B. L. Vernon, "In vitro delivery, cytotoxicity, swelling, and degradation behavior of a liquid-to-solid gelling polymer system for cerebral aneurysm embolization," *J. Biomed. Mater. Res. Part B Appl. Biomater.*, vol. 100B, no. 5, pp. 1298–1309, 2012.

[4] F. Zhou *et al.*, "Novel Hydrogel Material as a Potential Embolic Agent in Embolization Treatments," vol. 6, p. 32145, Aug. 2016.

[5] J. N. Rodriguez *et al.*, "Design and biocompatibility of endovascular aneurysm filling devices," *J. Biomed. Mater. Res. A*, vol. 103, no. 4, pp. 1577–1594, Apr. 2015.

[6] L. Lh. Yahia, N. Chirani, L. Gritsch, F. L. Motta, S. Chirani, and S. Fare, "History and Applications of Hydrogels," *J. Biomed. Sci.*, vol. 4, no. 2, pp. 1–23, 2015.

[7] D. Seliktar, "Designing cell-compatible hydrogels for biomedical applications.," *Science*, vol. 336, no. 6085, pp. 1124–1128, 2012.

[8] B. Choi *et al.*, "Introduction to In Situ Forming Hydrogels for Biomedical Applications," in *In-Situ Gelling Polymers: For Biomedical Applications*, X. J. Loh, Ed. Singapore: Springer Singapore, 2015, pp. 5–35.

[9] S. Utech and A. R. Boccaccini, "A review of hydrogel-based composites for biomedical applications: enhancement of hydrogel properties by addition of rigid inorganic fillers," *J. Mater. Sci.*, vol. 51, no. 1, pp. 271–310, 2016.

[10] F. Baino, "How can bioactive glasses be useful in ocular surgery?," *J. Biomed. Mater. Res. Part A*, vol. 103, no. 3, pp. 1259–1275, 2015.

[11] A. R. Boccaccini, M. Erol, W. J. Stark, D. Mohn, Z. Hong, and J. F. Mano, "Polymer/bioactive glass nanocomposites for biomedical applications: A review," *Compos. Sci. Technol.*, vol. 70, no. 13, pp. 1764–1776, Nov. 2010.

[12] V. Miguez-Pacheco, L. L. Hench, and A. R. Boccaccini, "Bioactive glasses beyond bone and teeth: Emerging applications in contact with soft tissues," *Acta Biomater.*, vol. 13, pp. 1–15, Feb. 2015.

[13] A. K. Gaharwar, N. A. Peppas, and A. Khademhosseini, "Nanocomposite hydrogels for biomedical applications.," *Biotechnol. Bioeng.*, vol. 111, no. 3, pp. 441–453, Mar. 2014.

[14] A. R. Boccaccini, J. R. Jones, and Q.-Z. Chen, "Composites Containing Bioactive Glass," in *Bio-Glasses*, John Wiley & Sons, Ltd, 2012, pp. 121–138.

[15] O. Clarkin, "Biomaterial Research Group," 2017. [Online]. Available: www.biomaterials.ie.

[16] Cipolla MJ, "Control of Cerebral Blood Flow," in *The Cerebral Circulation*, San Rafael (CA): Morgan & Claypool Life Sciences, 2009.

[17] T. S. Chang and P. C. Leung, *Principles, Techniques and Applications in Microsurgery*. World Scientific Publishing Company, 1986.

[18] W. Zingg, A. W. Neumann, A. B. Strong, O. S. Hum, and D. R. Absolom, "Effect of surface roughness on platelet adhesion under static and under flow conditions.," *Can. J. Surg.*, vol. 25, no. 1, pp. 16–19, Jan. 1982.

[19] A. P. Ebrahimi, "Mechanical Properties of Normal and Diseased Cerebrovascular System," *J. Vasc. Interv. Neurol.*, vol. 2, no. 2, pp. 155–162, Apr. 2009.

[20] M. J. Thubrikar, *Vascular Mechanics and Pathology*. Springer US, 2007.

[21] J. D. Humphrey and P. B. Canham, "Structure, mechanical properties, and mechanics of intracranial saccular aneurysms," *J. Elast.*, vol. 61, no. 1–3, pp. 49–81, 2000.

[22] K. Ritz, N. P. Denswil, O. C. G. Stam, J. J. van Lieshout, and M. J. A. P. Daemen, "Cause and Mechanisms of Intracranial Atherosclerosis," *Circulation*, vol. 130, no. 16, pp. 1407–1414, Oct. 2014.

[23] E. Bor-Seng-Shu *et al.*, "Cerebral hemodynamics: concepts of clinical importance," *Arq.*

Neuropsiquiatr., vol. 70, pp. 352–356, 2012.
[24] R. Morton and R. G. Ellenbogen, "Chapter 19 - Intracranial Hypertension A2 - Sekhar, Richard G. EllenbogenSaleem I. AbdulraufLaligam N. BT - Principles of Neurological Surgery (Third Edition)," Philadelphia: W.B. Saunders, 2012, pp. 311–323.
[25] P. Vespa, "What is the optimal threshold for cerebral perfusion pressure following traumatic brain injury?," *Neurosurg Focus*, vol. 15, no. 6, p. E4, 2003.
[26] A. Ostadfar, *Biofluid Mechanics: Principles and Applications*. Elsevier Science, 2016.
[27] M. Ibaraki *et al.*, "Cerebral Vascular Mean Transit Time in Healthy Humans: A Comparative Study with PET and Dynamic Susceptibility Contrast-Enhanced MRI," *J. Cereb. Blood Flow Metab.* , vol. 27, no. 2, pp. 404–413, Feb. 2007.
[28] C. M. Houseman, S. A. Belverud, and R. K. Narayan, *Principles of Neurological Surgery*. Elsevier, 2012.
[29] R. F. Santos-Galduróz, O. F. A. Bueno, L. I. Yamaga, F. Armani, and J. C. F. Galduróz, "Influence of blood viscosity to cerebral blood flow in older humans compared to young subjects.," *Clin. Neurophysiol.*, vol. 123, no. 1, pp. 117–20, Jan. 2012.
[30] W. Nichols, M. O'Rourke, and C. Vlachopoulos, *McDonald's Blood Flow in Arteries, Sixth Edition: Theoretical, Experimental and Clinical Principles*. CRC Press, 2011.
[31] C. T. McKee, J. A. Last, P. Russell, and C. J. Murphy, "Indentation Versus Tensile Measurements of Young's Modulus for Soft Biological Tissues," *Tissue Eng. Part B. Rev.*, vol. 17, no. 3, pp. 155–164, Jun. 2011.
[32] K. L. Monson, W. Goldsmith, N. M. Barbaro, and G. T. Manley, "Significance of source and size in the mechanical response of human cerebral blood vessels.," *J. Biomech.*, vol. 38, no. 4, pp. 737–44, Apr. 2005.
[33] J. Frösen *et al.*, "Remodeling of Saccular Cerebral Artery Aneurysm Wall Is Associated With Rupture: Histological Analysis of 24 Unruptured and 42 Ruptured Cases ," *Stroke* , vol. 35, no. 10, pp. 2287–2293, Oct. 2004.
[34] J. Frösen *et al.*, "Saccular intracranial aneurysm: pathology and mechanisms," *Acta Neuropathol.*, vol. 123, no. 6, pp. 773–786, 2012.
[35] C. S. Eddleman, C. C. Getch, B. R. Bendok, and H. H. Batjer, "Chapter 13 - Intracranial Aneurysms A2 - Ellenbogen, Richard G.," in *Principles of Neurological Surgery*, S. I. Abdulrauf and L. N. B. T.-P. of N. S. (Third E. Sekhar, Eds. Philadelphia: W.B. Saunders, 2012, pp. 209–228.
[36] J. G. Isaksen *et al.*, "Determination of wall tension in cerebral artery aneurysms by numerical simulation.," *Stroke.*, vol. 39, no. 12, pp. 3172–3178, Dec. 2008.
[37] J. K. Park, S. H. Kim, B. S. Kim, G. Choi, S. Y. Jeong, and J. C. Choi, "Imaging of intracranial plaques with black-blood double inversion recovery MR imaging and CT.," *J. Neuroimaging*, vol. 21, no. 2, pp. e64-8, Apr. 2011.
[38] A. Selimovic, Y. Ventikos, and P. N. Watton, "Modelling the Evolution of Cerebral Aneurysms: Biomechanics, Mechanobiology and Multiscale Modelling," *Procedia IUTAM*, vol. 10, pp. 396–409, 2014.
[39] G. N. Foutrakis, H. Yonas, and R. J. Sclabassi, "Saccular Aneurysm Formation in Curved and Bifurcating Arteries," *Am. J. Neuroradiol.* , vol. 20, no. 7, pp. 1309–1317, Jul. 1999.
[40] G. A. Holzapfel and R. W. Ogden, *Biomechanics of Soft Tissue in Cardiovascular Systems*. Springer Vienna, 2003.
[41] M. Shojima *et al.*, "Role of the Bloodstream Impacting Force and the Local Pressure Elevation in the Rupture of Cerebral Aneurysms," *Stroke* , vol. 36, no. 9, pp. 1933–1938, Sep. 2005.
[42] Y. Kanematsu *et al.*, "Critical roles of macrophages in the formation of intracranial aneurysm," *Stroke.*, vol. 42, no. 1, pp. 173–178, Jan. 2011.
[43] Y. Nuki *et al.*, "Roles of macrophages in flow-induced outward vascular remodeling.," *J. Cereb. Blood Flow Metab.*, vol. 29, no. 3, pp. 495–503, Mar. 2009.
[44] A. Maradni, A. Khoshnevisan, S. H. Mousavi, S. H. Emamirazavi, and A. Noruzijavidan, "Role of matrix metalloproteinases (MMPs) and MMP inhibitors on intracranial aneurysms: a review article," *Med. J. Islam. Repub. Iran*, vol. 27, no. 4, pp. 249–254, Nov. 2013.
[45] R. Torii, M. Oshima, T. Kobayashi, K. Takagi, and T. E. Tezduyar, "Fluid–structure

interaction modeling of blood flow and cerebral aneurysm: Significance of artery and aneurysm shapes," *Comput. Methods Appl. Mech. Eng.*, vol. 198, no. 45–46, pp. 3613–3621, Sep. 2009.

[46] G. A. Holzapfel and R. W. Ogden, *Mechanics of Biological Tissue*. Springer, 2006.

[47] M. R. Crompton, "Mechanism of Growth and Rupture in Cerebral Berry Aneurysms," *Br. Med. J.*, vol. 1, no. 5496, pp. 1138–1142, May 1966.

[48] S. Dhar *et al.*, "Morphology Parameters for Intracranial Aneurysm Rupture Risk Assessment," *Neurosurgery*, vol. 63, no. 2, pp. 185–197, Aug. 2008.

[49] J. Xiang *et al.*, "Hemodynamic–Morphologic Discriminants for Intracranial Aneurysm Rupture," *Stroke* , vol. 42, no. 1, pp. 144–152, Jan. 2011.

[50] W. Wang, F. Graziano, V. Russo, A. J. Ulm, D. De Kee, and D. B. Khismatullin, "Giant intracranial aneurysm embolization with a yield stress fluid material: insights from CFD analysis.," *Biorheology*, vol. 50, no. 3–4, pp. 99–114, 2013.

[51] L. Boussel *et al.*, "Aneurysm growth occurs at region of low wall shear stress: patient-specific correlation of hemodynamics and growth in a longitudinal study.," *Stroke*, vol. 39, no. 11, pp. 2997–3002, Nov. 2008.

[52] S. Juvela, M. Porras, and K. Poussa, "Natural history of unruptured intracranial aneurysms: probability of and risk factors for aneurysm rupture," *J. Neurosurg.*, vol. 93, no. 3, pp. 379–387, Sep. 2000.

[53] H. J. Steiger, R. Aaslid, S. Keller, and H. J. Reulen, "Strength, elasticity and viscoelastic properties of cerebral aneurysms.," *Heart Vessels*, vol. 5, no. 1, pp. 41–46, 1989.

[54] M. B. Pritz, "Cerebral Aneurysm Classification Based on Angioarchitecture," *J. Stroke Cerebrovasc. Dis.*, vol. 20, no. 2, pp. 162–167, Feb. 2016.

[55] "Cerebral Aneurysms Fact Sheet," *National Institute of Neurological Disorders and Stroke*. [Online]. Available: http://www.ninds.nih.gov/disorders/cerebral_aneurysm/detail_cerebral_aneurysms.htm.

[56] R. A. Hanel and R. F. Spetzler, "Surgical treatment of complex intracranial aneurysms.," *Neurosurgery*, vol. 62, no. 6 Suppl 3, p. 1289, Jun. 2008.

[57] M. Kroon and G. A. Holzapfel, "A model for saccular cerebral aneurysm growth by collagen fibre remodelling.," *J. Theor. Biol.*, vol. 247, no. 4, pp. 775–87, Aug. 2007.

[58] H. Saito, K. Ogasawara, Y. Kubo, N. Tomitsuka, and A. Ogawa, "Treatment of ruptured fusiform aneurysm in the posterior cerebral artery with posterior cerebral artery-superior cerebellar artery anastomosis combined with parent artery occlusion: case report.," *Surg. Neurol.*, vol. 65, no. 6, pp. 621–4, Jun. 2006.

[59] L. W. Wilkins, *Pathophysiology: A 2-in-1 Reference for Nurses*. Lippincott Williams & Wilkins, 2005.

[60] "Brain Aneurysms," *Johns Hopkins Cerebrovascular Center*. [Online]. Available: http://www.hopkinsmedicine.org/neurology_neurosurgery/centers_clinics/cerebrovascular/conditions/aneurysms.html.

[61] J. Sun and H. Tan, "Alginate-based biomaterials for regenerative medicine applications," *Materials (Basel).*, vol. 6, no. 4, pp. 1285–1309, 2013.

[62] C. Vega, J. V Kwoon, and S. D. Lavine, "Intracranial aneurysms: current evidence and clinical practice.," *Am. Fam. Physician*, vol. 66, no. 4, pp. 601–608, Aug. 2002.

[63] D. G. Peters *et al.*, "Molecular anatomy of an intracranial aneurysm: coordinated expression of genes involved in wound healing and tissue remodeling.," *Stroke.*, vol. 32, no. 4, pp. 1036–1042, Apr. 2001.

[64] J. D. Humphrey, *Cardiovascular Solid Mechanics: Cells, Tissues, and Organs*. Springer New York, 2013.

[65] J. B. Bederson *et al.*, "Guidelines for the Management of Aneurysmal Subarachnoid Hemorrhage: A Statement for Healthcare Professionals From a Special Writing Group of the Stroke Council, American Heart Association ," *Stroke* , vol. 40, no. 3, pp. 994–1025, Mar. 2009.

[66] NHS, "Brain aneurysm - Treatment." [Online]. Available: http://www.nhs.uk/Conditions/Aneurysm/Pages/Treatment.aspx.

[67] L. N. Williams and R. D. Brown, "Management of unruptured intracranial aneurysms,"

Neurol. Clin. Pract., vol. 3, no. 2, pp. 99–108, Apr. 2013.

[68] M. Zuccarello and A. Ringer, "Aneurysm Surgery: clipping," 2015. [Online]. Available: https://www.mayfieldclinic.com/PE-Clipping.htm.

[69] K. Tsutsumi, K. Ueki, A. Morita, M. Usui, and T. Kirino, "Risk of aneurysm recurrence in patients with clipped cerebral aneurysms: results of long-term follow-up angiography.," *Stroke.*, vol. 32, no. 5, pp. 1191–1194, May 2001.

[70] S. K. Natarajan, A. H. Siddiqui, L. N. Hopkins, and E. I. Levy, "Chapter 17 – Endovascular Neurosurgery," in *Principles of Neurological Surgery*, 2012, pp. 265–289.

[71] C. Gkogkas, J. Baker, A. M. Norbash, and K. U. Frerichs, "Endovascular Treatment of Intracranial Aneurysms," in *Minimally Invasive Neurosurgery*, Totowa, NJ: Humana Press, 2005, pp. 151–173.

[72] M. R. Harrigan and J. P. Deveikis, "Intracranial Aneurysms and Subarachnoid Haemorrhage," in *Handbook of Cerebrovascular Disease and Neurointerventional Technique*, Totowa, NJ: Humana Press, 2013, pp. 483–569.

[73] H. Henkes and W. Weber, "The Past, Present and Future of Endovascular Aneurysm Treatment.," *Clin. Neuroradiol.*, vol. 25 Suppl 2, pp. 317–324, Oct. 2015.

[74] A. J. Melchiorri, N. Hibino, and J. P. Fisher, "Strategies and techniques to enhance the in situ endothelialization of small-diameter biodegradable polymeric vascular grafts.," *Tissue Eng. Part B. Rev.*, vol. 19, no. 4, pp. 292–307, Aug. 2013.

[75] W. Brinjikji, D. F. Kallmes, and R. Kadirvel, "Mechanisms of Healing in Coiled Intracranial Aneurysms: A Review of the Literature," *AJNR. Am. J. Neuroradiol.*, vol. 36, no. 7, pp. 1216–1222, Jul. 2015.

[76] S. Gallas *et al.*, "Long-term follow-up of 1036 cerebral aneurysms treated by bare coils: a multicentric cohort treated between 1998 and 2003.," *AJNR. Am. J. Neuroradiol.*, vol. 30, no. 10, pp. 1986–1992, Nov. 2009.

[77] J. Y. Chueh *et al.*, "Aneurysm permeability following coil embolization: packing density and coil distribution.," *J. Neurointerv. Surg.*, vol. 7, no. 9, pp. 676–681, Sep. 2015.

[78] M. Reinges *et al.*, "Bare, bio-active and hydrogel-coated coils for endovascular treatment of experimentally induced aneurysms. Long-term histological and scanning electron microscopy results.," *Interv. Neuroradiol.*, vol. 16, no. 2, pp. 139–150, Jun. 2010.

[79] S. Geyik, O. Ertugrul, K. Yavuz, P. Geyik, I. Saatci, and H. S. Cekirge, "Comparison of bioactive coils and bare platinum coils for treatment of intracranial aneurysms: a matched-pair analysis," *J. Neurosurg.*, vol. 112, no. 4, pp. 709–713, Oct. 2009.

[80] M. Sluzewski, W. J. van Rooij, M. J. Slob, J. O. Bescós, C. H. Slump, and D. Wijnalda, "Relation between Aneurysm Volume, Packing, and Compaction in 145 Cerebral Aneurysms Treated with Coils," *Radiology*, vol. 231, no. 3, pp. 653–658, Jun. 2004.

[81] J. B. White, C. G. M. Ken, H. J. Cloft, and D. F. Kallmes, "Coils in a nutshell: a review of coil physical properties.," *AJNR. Am. J. Neuroradiol.*, vol. 29, no. 7, pp. 1242–1246, Aug. 2008.

[82] J. R. Vanzin, D. G. Abud, M. T. S. Rezende, and J. Moret, "Number of coils necessary to treat cerebral aneurysms according to each size group: a study based on a series of 952 embolized aneurysms.," *Arq. Neuropsiquiatr.*, vol. 70, no. 7, pp. 520–523, Jul. 2012.

[83] J. R. Mascitelli *et al.*, "An update to the Raymond-Roy Occlusion Classification of intracranial aneurysms treated with coil embolization," *J. Neurointerv. Surg.*, vol. 7, no. 7, pp. 496–502, 2015.

[84] A. D. Banerjee and H. Guimaraens, Leopoldo Cuellar, *Asymptomatic Delayed Coil Migration from an Intracranial Aneurysm: A Case Report*, vol. 2011. 2011, p. 2.

[85] H. W. Jeong, J. H. Seo, S. T. Kim, C. K. Jung, and S. Suh, "Clinical Practice Guideline for the Management of Intracranial Aneurysms," *Neurointervention*, vol. 9, no. 2, pp. 63–71, Sep. 2014.

[86] T. C. Origitano, "Current options in clipping versus coiling of intracranial aneurysms: to clip, to coil, to wait and watch.," *Neurosurg. Clin. N. Am.*, vol. 19, no. 3, p. 469–76, vi, Jul. 2008.

[87] M. F. K. Suri, M. Z. Memon, and A. I. Qureshi, "Treatment of unruptured intracranial aneurysms using internally expanding coils," *J. Vasc. Interv. Neurol.*, vol. 1, no. 2, pp.

42–45, Apr. 2008.
[88] S. Vaidya, K. R. Tozer, and J. Chen, "An Overview of Embolic Agents," *Semin. Intervent. Radiol.*, vol. 25, no. 3, pp. 204–215, Sep. 2008.
[89] M. Keeley, G. Cruise, M. Constant, S. Warner, and M. Walker, "Embolization device constructed from expansile polymer." Google Patents, 2014.
[90] "Flow Diversion for Aneurysms with Stents," *Johns Hopkins Medicine*. [Online]. Available: http://www.hopkinsmedicine.org/neurology_neurosurgery/centers_clinics/aneurysm/treatment/flow-diversion.html.
[91] H. H. Bearat, M. C. Preul, and B. L. Vernon, "Cytotoxicity, in vitro models and preliminary in vivo study of dual physical and chemical gels for endovascular embolization of cerebral aneurysms.," *J. Biomed. Mater. Res. A*, vol. 101, no. 9, pp. 2515–2525, Sep. 2013.
[92] M. Kojima, K. Irie, T. Fukuda, F. Arai, Y. Hirose, and M. Negoro, "The study of flow diversion effects on aneurysm using multiple enterprise stents and two flow diverters," *Asian J. Neurosurg.*, vol. 7, no. 4, pp. 159–165, 2012.
[93] B. Lubicz *et al.*, "Flow-Diverter Stent for the Endovascular Treatment of Intracranial Aneurysms: A Prospective Study in 29 Patients With 34 Aneurysms ," *Stroke* , vol. 41, no. 10, pp. 2247–2253, Oct. 2010.
[94] L. Pierot, "Flow diverter stents in the treatment of intracranial aneurysms: Where are we?," *J. Neuroradiol.*, vol. 38, no. 1, pp. 40–46, Mar. 2011.
[95] Z. Kulcsár *et al.*, "High-Profile Flow Diverter (Silk) Implantation in the Basilar Artery: Efficacy in the Treatment of Aneurysms and the Role of the Perforators ," *Stroke* , vol. 41, no. 8, pp. 1690–1696, Aug. 2010.
[96] "Pipeline Embolization of Cerebral Aneurysms." [Online]. Available: http://neuroangio.org/neurointerventional-techniques/pipeline-embolization-of-cerebral-aneurysms/.
[97] J. R. Cebral *et al.*, "Aneurysm rupture following treatment with flow-diverting stents: computational hemodynamics analysis of treatment.," *AJNR. Am. J. Neuroradiol.*, vol. 32, no. 1, pp. 27–33, Jan. 2011.
[98] T. Hassan, Y. M. Ahmed, and A. A. Hassan, "The adverse effects of flow-diverter stent-like devices on the flow pattern of saccular intracranial aneurysm models: computational fluid dynamics study," *Acta Neurochir. (Wien).*, vol. 153, no. 8, pp. 1633–1640, 2011.
[99] Y. H. Ding, D. A. Lewis, R. Kadirvel, D. Dai, and D. F. Kallmes, "The Woven EndoBridge: A New Aneurysm Occlusion Device," *Am. J. Neuroradiol.* , vol. 32, no. 3, pp. 607–611, Mar. 2011.
[100] J. Klisch, V. Sychra, C. Strasilla, T. Liebig, and D. Fiorella, "The Woven EndoBridge Cerebral Aneurysm Embolization Device (WEB II): initial clinical experience," *Neuroradiology*, vol. 53, no. 8, pp. 599–607, 2011.
[101] A. K. Wallner, E. Broussalis, T. Hauser, E. Trinka, and M. Killer-Oberpfalzer, "Coiling after Treatment with the Woven EndoBridge Cerebral Aneurysm Embolization Device: A Case Report," *Interv. Neuroradiol.*, vol. 18, no. 2, pp. 208–212, Jun. 2012.
[102] L. Pierot *et al.*, "WEB-DL Endovascular Treatment of Wide-Neck Bifurcation Aneurysms: Long-Term Results in a European Series," *Am. J. Neuroradiol.*, vol. 36, no. 12, p. 2314 LP-2319, Dec. 2015.
[103] B. Jiang, M. Paff, G. P. Colby, A. L. Coon, and L.-M. Lin, "Cerebral aneurysm treatment: modern neurovascular techniques," *Stroke Vasc. Neurol.*, 2016.
[104] L. Pierot *et al.*, "WEB Treatment of Intracranial Aneurysms: Feasibility, Complications, and 1-Month Safety Results with the WEB DL and WEB SL/SLS in the French Observatory.," *AJNR. Am. J. Neuroradiol.*, vol. 36, no. 5, pp. 922–927, May 2015.
[105] Tom Daughters, "PMA 030004 - Onyx® Liquid Embolic System for Treatment of Brain Arteriovenous Malformations," 2003.
[106] C. Pascal and L. Boyer, *Embolization*. Springer London, 2013.
[107] B. H. Lee *et al.*, "In vitro and in vivo demonstration of physically and chemically in situ gelling NIPAAm-based copolymer system.," *J. Biomater. Sci. Polym. Ed.*, vol. 24, no. 13,

pp. 1575–1588, 2013.
[108] C. for D. and R. Health, "Safety Communications - Catheter Entrapment with the ev3 Onyx Liquid Embolic System: FDA Safety Communication," *U.S. Food Drug Adm.*, 2015.
[109] T. A. Becker, D. R. Kipke, and T. Brandon, "Calcium alginate gel: A biocompatible and mechanically stable polymer for endovascular embolization," *J. Biomed. Mater. Res.*, vol. 54, no. 1, pp. 76–86, Jan. 2001.
[110] C. A. Bruno and P. M. Meyers, "Endovascular Management of Arteriovenous Malformations of the Brain," *Interv. Neurol.*, vol. 1, no. 3–4, pp. 109–123, 2013.
[111] "n-Butyl Cyanoacrylate Embolization of Cerebral Arteriovenous Malformations: Results of a Prospective, Randomized, Multi-center Trial," *Am. J. Neuroradiol.*, vol. 23, no. 5, pp. 748–755, 2002.
[112] R. K. Avery *et al.*, "An injectable shear-thinning biomaterial for endovascular embolization," *Sci. Transl. Med.*, vol. 8, no. 365, 2016.
[113] V. Nisha, "Radiopaque Materials from Natural Polymers: Special emphasis on chitosan and natural rubber," Cochin University of Science and Technology, 2006.
[114] B. Richling, "Homologous controlled-viscosity fibrin for endovascular embolization," *Acta Neurochir. (Wien).*, vol. 62, no. 3, pp. 159–170, Sep. 1982.
[115] F. Wang, B. Xu, Z. Sun, C. Wu, and X. Zhang, "Wall shear stress in intracranial aneurysms and adjacent arteries," *Neural Regen. Res.*, vol. 8, no. 11, pp. 1007–1015, 2013.
[116] W. R. Mower, W. J. Quiñones, and S. S. Gambhir, "Effect of intraluminal thrombus on abdominal aortic aneurysm wall stress," *J. Vasc. Surg.*, vol. 26, no. 4, pp. 602–608, 1997.
[117] R. Ramachandran, "A nonlinear stress sensitivity study on role of Coil-thrombus complex in reduction of idealized cerebral aneurysm wall," University of Cincinnati, 2007.
[118] Y. Murayama, F. Viñuela, S. Tateshima, F. Viñuela Jr, and Y. Akiba, "Endovascular Treatment of Experimental Aneurysms by Use of a Combination of Liquid Embolic Agents and Protective Devices," *Am. J. Neuroradiol.*, vol. 21, no. 9, p. 1726 LP-1735, Oct. 2000.
[119] R. T. Dalyai *et al.*, "Redefining Onyx HD 500 in the Flow Diversion Era.," *Int. J. Vasc. Med.*, vol. 2012, p. 435490, 2012.
[120] P. C. Georges and P. A. Janmey, "Cell type-specific response to growth on soft materials.," *J. Appl. Physiol.*, vol. 98, no. 4, pp. 1547–1553, Apr. 2005.
[121] A. J. Engler, L. Richert, J. Y. Wong, C. Picart, and D. E. Discher, "Surface probe measurements of the elasticity of sectioned tissue, thin gels and polyelectrolyte multilayer films: Correlations between substrate stiffness and cell adhesion," *Surf. Sci.*, vol. 570, no. 1–2, pp. 142–154, 2004.
[122] C. M. Lo, H. B. Wang, M. Dembo, and Y. li Wang, "Cell Movement Is Guided by the Rigidity of the Substrate," *Biophys. J.*, vol. 79, no. 1, pp. 144–152, 2000.
[123] D. E. Discher, P. A. Janmey, and Y. L. Wang, "Tissue Cells Feel and Respond to the Stiffness of Their Substrate," *Science (80-.).*, vol. 310, 2005.
[124] W. Guo, M. T. Frey, N. A. Burnham, and Y. Wang, "Substrate rigidity regulates the formation and maintenance of tissues.," *Biophys. J.*, vol. 90, no. 6, pp. 2213–2220, Mar. 2006.
[125] A. Saez, A. Buguin, P. Silberzan, and B. Ladoux, "Is the Mechanical Activity of Epithelial Cells Controlled by Deformations or Forces?," *Biophys. J.*, vol. 89, no. 6, pp. L52–L54, Dec. 2005.
[126] S. Jalali, M. Tafazzoli-Shadpour, N. Haghighipour, R. Omidvar, and F. Safshekan, "Regulation of Endothelial Cell Adherence and Elastic Modulus by Substrate Stiffness.," *Cell Commun. Adhes.*, vol. 22, no. 2–6, pp. 79–89, Apr. 2015.
[127] J. L. Drury, R. G. Dennis, and D. J. Mooney, "The tensile properties of alginate hydrogels," *Biomaterials*, vol. 25, no. 16, pp. 3187–3199, Jul. 2004.
[128] E. Mazza and A. E. Ehret, "Mechanical biocompatibility of highly deformable biomedical materials," *J. Mech. Behav. Biomed. Mater.*, vol. 48, pp. 100–124, 2015.
[129] K. J. Haworth, C. R. Weidner, T. A. Abruzzo, J. T. Shearn, and C. K. Holland, "Mechanical properties and fibrin characteristics of endovascular coil–clot complexes: relevance to

endovascular cerebral aneurysm repair paradigms," *J. Neurointerv. Surg.*, vol. 7, no. 4, pp. 291–296, Apr. 2015.
[130] T. Ohyama, I. K. Ko, A. Miura, H. Iwata, and W. Taki, "ProNectin F-grafted-ethylene vinyl alcohol copolymer (EVAL) as a liquid type material for treating cerebral aneurysm--an in vivo and in vitro study.," *Biomaterials*, vol. 25, no. 17, pp. 3845–52, Aug. 2004.
[131] Y. Han, Q. Zeng, H. Li, and J. Chang, "The calcium silicate/alginate composite: preparation and evaluation of its behavior as bioactive injectable hydrogels.," *Acta Biomater.*, vol. 9, no. 11, pp. 9107–9117, Nov. 2013.
[132] D. A. Stidd, D. K. Lopes, and M. Chen, "Aneurysm Coil Embolization Using a 1.5-Fr Distal Outer Diameter Microcatheter," *Neurointervention*, vol. 9, no. 1, pp. 39–44, Feb. 2014.
[133] P. Kim Nelson and D. I. Levy, "Balloon-assisted Coil Embolization of Wide-necked Aneurysms of the Internal Carotid Artery: Medium-term Angiographic and Clinical Follow-up in 22 Patients," *Am. J. Neuroradiol.* , vol. 22, no. 1, pp. 19–26, Jan. 2001.
[134] J. Curtis and P. Klykken, "A Comparative Assessment of Three Common Catheter Materials," 2008.
[135] B. Y. Seyithanoglu *et al.*, "Compliant vs non-compliant balloons. A prospective randomized study.," *Jpn. Heart J.*, vol. 39, no. 1, pp. 45–54, Jan. 1998.
[136] Creganna, "Technical Capabilities." [Online]. Available: http://www.creganna.com/technologies/medical-balloons/technical-capabilities/.
[137] R. C. Fries, *Handbook of Medical Device Design*. Taylor & Francis, 2000.
[138] D. F. Williams, *The Williams Dictionary of Biomaterials*. Liverpool University Press, 1999.
[139] J. M. Morais, F. Papadimitrakopoulos, and D. J. Burgess, "Biomaterials/tissue interactions: possible solutions to overcome foreign body response.," *AAPS J.*, vol. 12, no. 2, pp. 188–196, Jun. 2010.
[140] K. Vafai, *Porous Media: Applications in Biological Systems and Biotechnology*. CRC Press, 2010.
[141] M. Otto, A. Franzen, T. Hansen, and C. J. Kirkpatrick, "Modification of human platelet adhesion on biomaterial surfaces by protein preadsorption under static and flow conditions.," *J. Mater. Sci. Mater. Med.*, vol. 15, no. 1, pp. 35–42, Jan. 2004.
[142] "ISO 10993 Part 4: Selection of tests for interactions with blood," 2017.
[143] R. F. Wallin and E. F. Arscott, "A practical guide to ISO 10993-5: Cytotoxicity," *Med. Device Diagnostic Ind. Mag.*, pp. 2–4, 1998.
[144] "ISO 10993 Part 5: Tests for in vitro cytotoxicity."
[145] US Food and Drug Administration, "Immunotoxicity Testing Guidance," *Guid. Ind. Fda Rev.*, pp. 1–16, 1999.
[146] J. M. Anderson, "Biological Responses to Materials," *Annu. Rev. Mater. Res.*, vol. 31, no. 1, pp. 81–110, 2001.
[147] J. M. Anderson, A. Rodriguez, and D. T. Chang, "Foreign Body Reaction to Biomaterials," *Semin. Immunol.*, vol. 20, no. 2, pp. 86–100, 2008.
[148] W. Murphy, J. Black, and G. Hastings, *Handbook of Biomaterial Properties*. Springer New York, 2016.
[149] T. B. Wissing, V. Bonito, C. V. C. Bouten, and A. I. P. M. Smits, "Biomaterial-driven in situ cardiovascular tissue engineering—a multi-disciplinary perspective," *npj Regen. Med.*, vol. 2, no. 1, p. 18, 2017.
[150] R. A. Hortensius and B. A. C. Harley, "Naturally derived biomaterials for addressing inflammation in tissue regeneration," *Exp. Biol. Med. (Maywood).*, vol. 241, no. 10, pp. 1015–1024, May 2016.
[151] K. Hosaka and B. L. Hoh, "Inflammation and cerebral aneurysms.," *Transl. Stroke Res.*, vol. 5, no. 2, pp. 190–198, Apr. 2014.
[152] US Food and Drug Administration, "Application of the device good manufacturing practice regulation to the manufacture of sterile devices," *Guid. sterile device*, 1997.
[153] "Medical Device Sterilization." [Online]. Available: http://www.lso-inc.com/sterilization-validation-services/medical-device-sterilization.html.
[154] S. S. Block, *Disinfection, Sterilization, and Preservation*. Lippincott Williams & Wilkins, 2001.

[155] D. Hill, *Design Engineering of Biomaterials for Medical Devices*. Wiley, 1998.
[156] F. Munarin, S. Bozzini, L. Visai, M. C. Tanzi, and P. Petrini, "Sterilization treatments on polysaccharides: Effects and side effects on pectin," *Food Hydrocoll.*, vol. 31, no. 1, pp. 74–84, May 2013.
[157] Priorclave, "Dry Heat Sterilizers vs Steam Autoclaves." [Online]. Available: https://priorclavena.com/steam-autoclave-sterilizers/dry-heat-sterilizers-vs-steam-autoclaves/.
[158] "ISO 17665 Steam Sterilization for Medical Devices." [Online]. Available: http://www.lso-inc.com/sterilization-validation-services/iso17665-steam-sterilization.html.
[159] DuPont, "Sterile Packaging: Start Sterile, Stay Sterile With Tyvek®." [Online]. Available: https://www.google.ie/search?q=dupont&oq=dupont&aqs=chrome..69i57j69i60l4j0.2045j0j7&sourceid=chrome&ie=UTF-8.
[160] "ISO 11135 EtO Sterilization for Medical Devices." [Online]. Available: http://www.lso-inc.com/sterilization-validation-services/iso11135-eto-sterilization.html.
[161] P. L. Hudson, D. Gantt, and J. Brown, "Guidance for Industry and FDA Staff - Class II Special Controls Guidance Document : Vascular and Neurovascular Embolization Devices Class II Special Controls Guidance Document : Vascular," no. 2003, 2004.
[162] "Ethylene Oxide Residual Analysis," *Sanichem*. [Online]. Available: http://www.sanichem.com.my/EtO_residual.html.
[163] A. D. Lucas *et al.*, "Residual ethylene oxide in medical devices and device material.," *J. Biomed. Mater. Res. B. Appl. Biomater.*, vol. 66, no. 2, pp. 548–552, Aug. 2003.
[164] R. Franca *et al.*, "The effect of ethylene oxide sterilization on the surface chemistry and in vitro cytotoxicity of several kinds of chitosan.," *J. Biomed. Mater. Res. B. Appl. Biomater.*, vol. 101, no. 8, pp. 1444–1455, Nov. 2013.
[165] "ISO 11137 Gamma & E-Beam Sterilization for Medical Devices." [Online]. Available: http://www.lso-inc.com/sterilization-validation-services/iso11137-gamma-ebeam-sterilization.html.
[166] M. A. Dobrovolskaia and S. E. McNeil, *Handbook of Immunological Properties of Engineered Nanomaterials*. World Scientific Publishing Company, 2016.
[167] H. Nguyen, D. A. F. Morgan, and M. R. Forwood, "Sterilization of Allograft Bone: is 25 kGy the Gold Standard for Gamma Irradiation?," *Cell Tissue Bank.*, vol. 8, no. 2, p. 81, 2006.
[168] M. W. Jornitz, *Sterile Filtration*. Springer.
[169] M. Hjortso, *Cell Adhesion in Bioprocessing and Biotechnology*. Taylor & Francis, 1994.
[170] T. McGloughlin, *Biomechanics and Mechanobiology of Aneurysms*. Springer Berlin Heidelberg, 2011.
[171] H. Lusic and M. W. Grinstaff, "X-Ray Computed Tomography Contrast Agents," *Chem. Rev.*, vol. 113, no. 3, p. 10.1021/cr200358s, Mar. 2013.
[172] C. R. Brennecka, M. C. Preul, T. A. Becker, and B. L. Vernon, "In vivo embolization of lateral wall aneurysms in canines using the liquid-to-solid gelling PPODA-QT polymer system: 6-month pilot study," *J. Neurosurg.*, vol. 119, no. 1, pp. 228–238, Apr. 2013.
[173] B. H. Lee, C. Leon, R. McLemore, J. V. Macias, and B. L. Vernon, "Synthesis and characterization of thermo-sensitive radio-opaque poly(N-isopropylacrylamide-co-PEG-2-iodobenzoate).," *J. Biomater. Sci. Polym. Ed.*, vol. 22, no. 17, pp. 2357–2367, 2011.
[174] R. J. Rosen and S. Contractor, "The Use of Cyanoacrylate Adhesives in the Management of Congenital Vascular Malformations," *Semin. Intervent. Radiol.*, vol. 21, no. 1, pp. 59–66, Mar. 2004.
[175] G. A. Paleos and D. J. Lloyd, "What are Hydrogels ?," 2012.
[176] S. K. Gulrez, G. O. Phillips, and S. Al-Assaf, *Hydrogels: Methods of Preparation, Characterisation and Applications*. INTECH Open Access Publisher, 2011.
[177] S. J. Buwalda, K. W. M. Boere, P. J. Dijkstra, J. Feijen, T. Vermonden, and W. E. Hennink, "Hydrogels in a historical perspective: From simple networks to smart materials," *J. Control. Release*, vol. 190, pp. 254–273, Sep. 2014.

[178] J. Zhu and R. E. Marchant, "Design properties of hydrogel tissue-engineering scaffolds," *Expert Rev. Med. Devices*, vol. 8, no. 5, pp. 607–626, Sep. 2011.
[179] M. Ebara *et al.*, *Smart biomaterials*, vol. 1992, no. 22. 2014.
[180] N. M. Morteza Bahram and M. Moghtader, "An Introduction to Hydrogels and Some Recent Applications," in *Emerging Concepts in Analysis and Applications of Hydrogels*, D. S. B. Majee, Ed. InTech, 2016.
[181] T. Andersen, P. Auk-Emblem, and M. Dornish, "3D Cell Culture in Alginate Hydrogels," *Microarrays*, vol. 4, no. 2, pp. 133–161, Jun. 2015.
[182] K. Y. Lee and D. J. Mooney, "Hydrogels for Tissue Engineering," *Chem. Rev.*, vol. 101, no. 7, pp. 1869–1880, Jul. 2001.
[183] H. Li and J. Chang, "Stimulation of proangiogenesis by calcium silicate bioactive ceramic," *Acta Biomater.*, vol. 9, no. 2, pp. 5379–5389, Feb. 2013.
[184] R. Jin, B. Lou, and C. Lin, "Tyrosinase-mediated *in situ* forming hydrogels from biodegradable chondroitin sulfate-tyramine conjugates," *Polym. Int.*, vol. 62, no. 3, pp. 353–361, Mar. 2013.
[185] K. Kashima and M. Imai, "Advanced Membrane Material from Marine Biological Polymer and Sensitive Molecular-Size Recognition for Promising Separation Technology," R. Y. B. T.-A. D. Ning, Ed. Rijeka: InTech, 2012.
[186] D. J. McHugh, *Production and utilization of products from commercial seaweeds*, no. nos. 288-289. Food and Agriculture Organization of the United Nations, 1987.
[187] A. N. da Silva and C. H. Garcia-Cruz, "Biopolymers by Azotobacter Vinelandii," in *Biopolymers*, M. Elnashar, Ed. 2010.
[188] T. Andersen, B. L. Strand, K. Formo, E. Alsberg, and B. E. Christensen, "Chapter 9 Alginates as biomaterials in tissue engineering," in *Carbohydrate Chemistry: Volume 37*, vol. 37, The Royal Society of Chemistry, 2012, pp. 227–258.
[189] K. I. Draget, O. Smidsrød, and G. Skjåk-Bræk, "Alginates from Algae," in *Biopolymers Online*, Wiley-VCH Verlag GmbH & Co. KGaA, 2005.
[190] D. S. Morais *et al.*, "Development and characterization of novel alginate-based hydrogels as vehicles for bone substitutes.," *Carbohydr. Polym.*, vol. 95, no. 1, pp. 134–42, Jun. 2013.
[191] K. Y. Lee and D. J. Mooney, "Alginate: properties and biomedical applications," *Prog. Polym. Sci.*, vol. 37, no. 1, pp. 106–126, Jan. 2012.
[192] H. J. Kong, D. Kaigler, K. Kim, and D. J. Mooney, "Controlling rigidity and degradation of alginate hydrogels via molecular weight distribution.," *Biomacromolecules*, vol. 5, no. 5, pp. 1720–1727, 2004.
[193] P. X. Ma and J. Elisseeff, *Scaffolding In Tissue Engineering*. CRC Press, 2005.
[194] M. Fertah, A. Belfkira, E. montassir Dahmane, M. Taourirte, and F. Brouillette, "Extraction and characterization of sodium alginate from Moroccan Laminaria digitata brown seaweed," *Arab. J. Chem.*, May 2014.
[195] R. Popeski-Dimovski, S. Rendevski, and N. Mahmudi, "Change in Gellation Time of Sodium Alginate Biopolymer Hydrogels With Change of Dose of Gamma Irradiation," *Phys. Maced. 61*, pp. 67–72, 2012.
[196] S. Fu *et al.*, "Relevance of Rheological Properties of Sodium Alginate in Solution to Calcium Alginate Gel Properties," *AAPS PharmSciTech*, vol. 12, no. 2, pp. 453–460, Jun. 2011.
[197] T. A. Becker and D. R. Kipke, "Flow properties of liquid calcium alginate polymer injected through medical microcatheters for endovascular embolization," *J. Biomed. Mater. Res.*, vol. 61, no. 4, pp. 533–540, Sep. 2002.
[198] E. Ruvinov and S. Cohen, "Alginate biomaterial for the treatment of myocardial infarction: Progress, translational strategies, and clinical outlook: From ocean algae to patient bedside," *Adv. Drug Deliv. Rev.*, vol. 96, pp. 54–76, 2016.
[199] K. I. Draget, G. Skjåk Bræk, and O. Smidsrød, "Alginic acid gels: the effect of alginate chemical composition and molecular weight," *Carbohydr. Polym.*, vol. 25, no. 1, pp. 31–38, 1994.
[200] Y. A. Morch *et al.*, "Effect of Ca2+, Ba2+, and Sr2+ on Alginate Microbeads," *Biomacromolecules*, vol. 7, no. 5, pp. 1471–1480, May 2006.

[201] B. E. Larsen, J. Bjørnstad, E. O. Pettersen, H. H. Tønnesen, and J. E. Melvik, "Rheological characterization of an injectable alginate gel system," *BMC Biotechnol.*, vol. 15, no. 1, pp. 1–12, 2015.
[202] C. K. Kuo and P. X. Ma, "Ionically crosslinked alginate hydrogels as scaffolds for tissue engineering: Part 1. Structure, gelation rate and mechanical properties," *Biomaterials*, vol. 22, no. 6, pp. 511–521, Mar. 2001.
[203] M. a LeRoux, F. Guilak, and L. a Setton, "Compressive and shear properties of alginate gel: Effects of sodium ions and alginate concentration," *J. Biomed. Mater. Res.*, vol. 47, pp. 46–53, 1999.
[204] H. Liao *et al.*, "Mechanisms of oligoguluronate modulating the calcium-induced gelation of alginate," *Polymer (Guildf).*, vol. 74, pp. 166–175, Sep. 2015.
[205] I. Donati, S. Holtan, Y. A. Mørch, M. Borgogna, M. Dentini, and G. Skjåk-Bræk, "New hypothesis on the role of alternating sequences in calcium-alginate gels," *Biomacromolecules*, vol. 6, 2005.
[206] I. Donati, Y. A. Morch, B. L. Strand, G. Skjak-Braek, and S. Paoletti, "Effect of Elongation of Alternating Sequences on Swelling Behavior and Large Deformation Properties of Natural Alginate Gels," *J Phys Chem B*, vol. 113, 2009.
[207] Y. Fang *et al.*, "Multiple steps and critical behaviors of the binding of calcium to alginate.," *J. Phys. Chem. B*, vol. 111, no. 10, pp. 2456–2462, Mar. 2007.
[208] V. Guarino Tania;Altobelli,Rosaria;Ambrosio,Luigi, "Degradation properties and metabolic activity of alginate and chitosan polyelectrolytes for drug delivery and tissue engineering applications," *AIMS Mater. Sci.*, vol. 2, no. 4, pp. 497–502.
[209] C. K. Kuo and P. X. Ma, "Maintaining dimensions and mechanical properties of ionically crosslinked alginate hydrogel scaffolds in vitro," *J. Biomed. Mater. Res. Part A*, vol. 84A, no. 4, pp. 899–907, 2008.
[210] L. Richert *et al.*, "Improvement of Stability and Cell Adhesion Properties of Polyelectrolyte Multilayer Films by Chemical Cross-Linking," *Biomacromolecules*, vol. 5, no. 2, pp. 284–294, Mar. 2004.
[211] "Chemistry of Crosslinking." [Online]. Available: https://www.thermofisher.com/ie/en/home/life-science/protein-biology/protein-biology-learning-center/protein-biology-resource-library/pierce-protein-methods/chemistry-crosslinking.html.
[212] J. Conde, J. T. Dias, V. Grazú, M. Moros, P. V Baptista, and J. M. de la Fuente, "Revisiting 30 years of biofunctionalization and surface chemistry of inorganic nanoparticles for nanomedicine," *Front. Chem.*, vol. 2, p. 48, Jul. 2014.
[213] Y. Otani, Y. Tabata, and Y. Ikada, "A new biological glue from gelatin and poly (L-glutamic acid)," *J. Biomed. Mater. Res.*, vol. 31, no. 2, pp. 157–166, 1996.
[214] M. Foox, A. Raz-Pasteur, I. Berdicevsky, N. Krivoy, and M. Zilberman, "*In vitro* microbial inhibition, bonding strength, and cellular response to novel gelatin-alginate antibiotic-releasing soft tissue adhesives," *Polym. Adv. Technol.*, vol. 25, no. 5, pp. 516–524, 2014.
[215] B. H. McDonagh, "Optimalised Carbodiimide Chemistry for RGD-coupled Alginate," Norwegian University of Science and Technology, 2012.
[216] D. Sehgal and I. K. Vijay, "A Method for the High Efficiency of Water-Soluble Carbodiimide-Mediated Amidation," *Anal. Biochem.*, vol. 218, no. 1, pp. 87–91, 1994.
[217] M. Foox, M. Ben-Tzur, N. Koifman, and M. Zilberman, "Effect of gamma radiation on novel gelatin alginate–based bioadhesives," *Int. J. Polym. Mater. Polym. Biomater.*, vol. 65, no. 12, pp. 611–618, Aug. 2016.
[218] "Carbodiimide Crosslinker Chemistry." [Online]. Available: https://www.thermofisher.com/ie/en/home/life-science/protein-biology/protein-biology-learning-center/protein-biology-resource-library/pierce-protein-methods/carbodiimide-crosslinker-chemistry.html.
[219] ThermoFisher, "NHS & Sulfo-NHS," pp. 1–4, 2009.
[220] H. Ylänen, *Bioactive Glasses: Materials, Properties and Applications*. Elsevier Science, 2011.
[221] J. E. Shelby, *Introduction to Glass Science and Technology*. The Royal Society of Chemistry, 2005.

[222] X. Zhao, J. M. Courtney, and H. Qian, *Bioactive Materials in Medicine: Design and Applications*. Elsevier Science, 2011.
[223] G. Kaur, G. Pickrell, N. Sriranganathan, V. Kumar, and D. Homa, "Review and the state of the art: Sol–gel and melt quenched bioactive glasses for tissue engineering," *J. Biomed. Mater. Res. Part B Appl. Biomater.*, vol. 4803, pp. 1248–75, 2015.
[224] D. S. Brauer, "Bioactive glasses-structure and properties.," *Angew. Chem. Int. Ed. Engl.*, vol. 54, no. 14, pp. 4160–4181, Mar. 2015.
[225] A. Doostmohammadi, A. Monshi, R. Salehi, M. H. Fathi, Z. Golniya, and A. U. Daniels, "Bioactive glass nanoparticles with negative zeta potential," *Ceram. Int.*, vol. 37, no. 7, pp. 2311–2316, 2011.
[226] M. Santin and G. J. Phillips, *Biomimetic, Bioresponsive, and Bioactive Materials: An Introduction to Integrating Materials with Tissues*. Wiley, 2012.
[227] S. Kohara *et al.*, "Relationship between topological order and glass forming ability in densely packed enstatite and forsterite composition glasses," *Proc. Natl. Acad. Sci.* , vol. 108, no. 36, pp. 14780–14785, Sep. 2011.
[228] A. D. Wilson and J. W. Nicholson, *Acid-Base Cements: Their Biomedical and Industrial Applications*. Cambridge University Press, 2005.
[229] "Volcanic Rocks." [Online]. Available: http://www.alexstrekeisen.it/english/vulc/index.php.
[230] I. Farnan, "Structural chemistry: Oxygen bridges in molten glass," *Nature*, vol. 390, no. 6655, pp. 14–15, Nov. 1997.
[231] P. Hee *et al.*, "Properties and structural investigation of gallophosphate glasses by 71 Ga and 31 P nuclear magnetic resonance and vibrational spectroscopies," *J. Mater. Chem. C*, vol. 2, no. 37, p. 7906, 2014.
[232] M. N. Rahaman *et al.*, "Bioactive glass in tissue engineering," *Acta Biomater.*, vol. 7, no. 6, pp. 2355–2373, Jun. 2011.
[233] V. Krishnan and T. Lakshmi, "Bioglass: A novel biocompatible innovation," *J. Adv. Pharm. Technol. Res.*, vol. 4, no. 2, pp. 78–83, 2013.
[234] P. Ducheyne, K. Healy, D. E. Hutmacher, D. W. Grainger, and C. J. Kirkpatrick, *Comprehensive Biomaterials*. Elsevier Science, 2011.
[235] T. J. Keenan, L. M. Placek, A. Coughlan, G. M. Bowers, M. M. Hall, and A. W. Wren, "Structural characterization and anti-cancerous potential of gallium bioactive glass/hydrogel composites," *Carbohydr. Polym.*, vol. 153, pp. 482–491, 2016.
[236] E. Zeimaran *et al.*, "Antibacterial properties of poly (octanediol citrate)/gallium-containing bioglass composite scaffolds," *J. Mater. Sci. Mater. Med.*, vol. 27, no. 1, pp. 1–11, 2015.
[237] C. Mao, X. Chen, G. Miao, and C. Lin, "Angiogenesis stimulated by novel nanoscale bioactive glasses," *Biomed. Mater.*, vol. 10, no. 2, p. 25005, 2015.
[238] A. R. Boccaccini, D. S. Brauer, and L. Hupa, *Bioactive Glasses: Fundamentals, Technology and Applications*. Royal Society of Chemistry, 2016.
[239] V. Mourino, P. Newby, F. Pishbin, J. P. Cattalini, S. Lucangioli, and A. R. Boccaccini, "Physicochemical, biological and drug-release properties of gallium crosslinked alginate/nanoparticulate bioactive glass composite films," *Soft Matter*, vol. 7, no. 14, pp. 6705–6712, 2011.
[240] V. Mouriño, P. Newby, and A. R. Boccaccini, "Preparation and Characterization of Gallium Releasing 3-D Alginate Coated 45S5 Bioglass® Based Scaffolds for Bone Tissue Engineering," *Adv. Eng. Mater.*, vol. 12, no. 7, pp. B283–B291, 2010.
[241] H. Li and J. Chang, "Bioactive silicate materials stimulate angiogenesis in fibroblast and endothelial cell co-culture system through paracrine effect," *Acta Biomater.*, vol. 9, no. 6, pp. 6981–6991, Jun. 2013.
[242] R. M. Day *et al.*, "Assessment of polyglycolic acid mesh and bioactive glass for soft-tissue engineering scaffolds," *Biomaterials*, vol. 25, no. 27, pp. 5857–5866, Dec. 2004.
[243] J. Wilson, G. H. Pigott, F. J. Schoen, and L. L. Hench, "Toxicology and biocompatibility of bioglasses," *J. Biomed. Mater. Res.*, vol. 15, no. 6, pp. 805–817, 1981.
[244] V. Miguez-pacheco and D. Greenspan, "Bioactive glasses in soft tissue repair," *Am. Ceram. Soc. Bull.*, vol. 94, no. 6, pp. 27–31, 2015.

[245] E. A. Ross, C. D. Batich, W. L. Clapp, J. E. Sallustio, and N. C. Lee, "Tissue adhesion to bioactive glass-coated silicone tubing in a rat model of peritoneal dialysis catheters and catheter tunnels," *Kidney Int.*, vol. 63, no. 2, pp. 702–708, Feb. 2003.
[246] J. A. Killion *et al.*, "Hydrogel/bioactive glass composites for bone regeneration applications: synthesis and characterisation.," *Mater. Sci. Eng. C. Mater. Biol. Appl.*, vol. 33, no. 7, pp. 4203–4212, Oct. 2013.
[247] S. Srinivasan, R. Jayasree, K. P. Chennazhi, S. V. Nair, and R. Jayakumar, "Biocompatible alginate/nano bioactive glass ceramic composite scaffolds for periodontal tissue regeneration," *Carbohydr. Polym.*, vol. 87, no. 1, pp. 274–283, 2012.
[248] F. Zhao, W. Zhang, X. Fu, W. Xie, and X. Chen, "Fabrication and characterization of bioactive glass/alginate composite scaffolds by a self-crosslinking processing for bone regeneration," *RSC Adv.*, vol. 6, no. 94, pp. 91201–91208, 2016.
[249] G. Luo *et al.*, "13-93 bioactive glass/alginate composite scaffolds 3D printed under mild conditions for bone regeneration," *RSC Adv.*, vol. 7, no. 20, pp. 11880–11889, 2017.
[250] T. Lakhanisky, "GLUCONIC ACID AND DERIVATIVES," 2004.
[251] C. Aparicio and M. P. Ginebra, *Biomineralization and Biomaterials: Fundamentals and Applications*. Elsevier Science, 2015.
[252] D. Alves Cardoso, J. J. J. P. van den Beucken, L. L. H. Both, J. Bender, J. A. Jansen, and S. C. G. Leeuwenburgh, "Gelation and biocompatibility of injectable alginate–calcium phosphate gels for bone regeneration," *J. Biomed. Mater. Res. Part A*, vol. 102, no. 3, pp. 808–817, 2014.
[253] O. Clarkin and C. Lally, "A gallium-based glass composition." 2016.
[254] Agilent Technologies, "An Introduction to Gel Permeation Chromatography and Size Exclusion Chromatography," 2014.
[255] "What is NMR?," *The Hebrew University of Jerusalem*. [Online]. Available: http://chem.ch.huji.ac.il/nmr/whatisnmr/whatisnmr.html.
[256] T. James, "Fundamentals of NMR," Department of Pharmaceutical Chemistry, 1998.
[257] A. International, *ASTM Standard Test Method for Determining the Chemical Composition and Sequence in Alginate by Proton Nuclear Magnetic Resonance (1H NMR) Spectroscopy1*. .
[258] M. E. Brown, *Handbook of Thermal Analysis and Calorimetry: Principles and Practice*. Elsevier Science, 1998.
[259] J. Jones and A. Clare, *Bio-Glasses: An Introduction*. Wiley, 2012.
[260] B. Dutrow and C. (Clark, "X-ray Powder Diffraction (XRD)."
[261] S. a Speakman, "Basics of X-Ray Powder Diffraction," in *Basics of X-Ray Powder Diffraction*, 1900, no. 617, pp. 1–97.
[262] S. Johnson, "Advantages & Disadvantages of XRD and XRF," 2017. [Online]. Available: http://sciencing.com/advantages-disadvantages-xrd-xrf-6054766.html.
[263] "Laser Diffraction." [Online]. Available: http://www.malvern.com/en/products/technology/laser-diffraction/.
[264] "Laser Light Scattering Method," 2014. [Online]. Available: https://technologypharmaceutical.wordpress.com/2014/12/10/laser-light-scattering-method/.
[265] J. M. Walls and R. Smith, *Surface Science Techniques*. Elsevier Science, 2013.
[266] J. M. Hollander and W. L. Jolly, "X-ray photoelectron spectroscopy," *Acc. Chem. Res.*, vol. 3, no. 6, pp. 193–200, Jun. 1970.
[267] I. M. Watt, *The Principles and Practice of Electron Microscopy*. Cambridge University Press, 1997.
[268] W. Zhou and Z. L. Wang, *Scanning Microscopy for Nanotechnology: Techniques and Applications*. Springer New York, 2007.
[269] M. A. Ganzoury, N. K. Allam, T. Nicolet, and C. All, "Introduction to Fourier Transform Infrared Spectrometry," *Renew. Sustain. Energy Rev.*, vol. 50, pp. 1–8, 2015.
[270] Malvern, "Zetasizer Nano Z." [Online]. Available: http://www.malvern.com/en/products/product-range/zetasizer-range/zetasizer-nano-range/zetasizer-nano-z/.
[271] K. Sing, "The use of nitrogen adsorption for the characterisation of porous materials,"

Colloids Surfaces A Physicochem. Eng. Asp., vol. 187, pp. 3–9, 2001.
[272] ISO [International Organization for Standardization], "Determination of the specific surface area of solids by gas adsorption - BET method (ISO 9277:2010(E))," vol. 2010, p. 30 pp., 2010.
[273] Micromeritics Instrument Corporation, "Gas Adsorption Theory." [Online]. Available: http://www.micromeritics.com/Repository/Files/Gas_Adsorption_Theory_poster.pdf.
[274] S. Brunauer, P. H. Emmett, and E. Teller, "Adsorption of Gases in Multimolecular Layers," *J. Am. Chem. Soc.*, vol. 60, no. 2, pp. 309–319, Feb. 1938.
[275] W. Pabst and E. Gregorova, "Characterization of particles and particle systems," *ICT Prague*, pp. 1–122, 2007.
[276] E. P. Barrett, L. G. Joyner, and P. P. Halenda, "The Determination of Pore Volume and Area Distributions in Porous Substances. I. Computations from Nitrogen Isotherms," *J. Am. Chem. Soc.*, vol. 73, no. 1, pp. 373–380, Jan. 1951.
[277] "What is Deionized Water?" [Online]. Available: http://puretecwater.com/what-is-deionized-water.html.
[278] A. Oyane, H.-M. Kim, T. Furuya, T. Kokubo, T. Miyazaki, and T. Nakamura, "Preparation and assessment of revised simulated body fluids," *J. Biomed. Mater. Res. Part A*, vol. 65A, no. 2, pp. 188–195, 2003.
[279] Y. Luo, A. Lode, F. Sonntag, B. Nies, and M. Gelinsky, "Well-ordered biphasic calcium phosphate-alginate scaffolds fabricated by multi-channel 3D plotting under mild conditions," *J. Mater. Chem. B*, vol. 1, no. 33, pp. 4088–4098, 2013.
[280] Q. A. Acton, *Advances in Bioartificial Materials and Tissue Engineering Research and Application: 2011 Edition*. ScholarlyEditions, 2012.
[281] T. Kokubo and H. Takadama, "How useful is SBF in predicting in vivo bone bioactivity?," *Biomaterials*, vol. 27, no. 15, pp. 2907–15, May 2006.
[282] M. Vallet-Regi and D. Arcos, *Biomimetic Nanoceramics in Clinical Use: From Materials to Applications*. Royal Society of Chemistry, 2008.
[283] S. Aldrich, "Phosphate buffered saline." [Online]. Available: http://www.sigmaaldrich.com/catalog/product/sigma/p4417?lang=en&region=IE.
[284] G. Perfetti, E. Van De Casteele, B. Rieger, W. J. Wildeboer, and G. M. H. Meesters, "X-ray micro tomography and image analysis as complementary methods for morphological characterization and coating thickness measurement of coated particles," *Adv. Powder Technol.*, vol. 21, no. 6, pp. 663–675, 2010.
[285] B. Dupen, *Applied Strength of Materials for Engineering Technology*. Purdue University, 2012.
[286] I. Roorkee, "Lecture 11 Mechanical Properties." [Online]. Available: http://nptel.ac.in/courses/112107146/11.
[287] L. A. Pruitt and A. M. Chakravartula, *Mechanics of Biomaterials: Fundamental Principles for Implant Design*. Cambridge University Press, 2011.
[288] J. Vincent, *Structural Biomaterials: Third Edition*. Princeton University Press, 2012.
[289] S. Saha, *Biomedical Engineering: I Recent Developments: Proceedings of the First Southern Biomedical Engineering Conference*. Elsevier Science, 2013.
[290] H. H. Winter, "Can the gel point of a cross-linking polymer be detected by the G′ – G″ crossover?," *Polym. Eng. Sci.*, vol. 27, no. 22, pp. 1698–1702, Dec. 1987.
[291] "ISO 9917-1:2007(en) Dentistry — Water-based cements — Part 1: Powder/liquid acid-base cements."
[292] D. R. Heldman, D. B. Lund, and C. Sabliov, *Handbook of Food Engineering, Second Edition*. CRC Press, 2006.
[293] J. Goodwin, R. W. Hughes, and R. S. of Chemistry (Great Britain), *Rheology for Chemists: An Introduction*. Royal Society of Chemistry, 2000.
[294] A. B. Rodd, J. Cooper-White, D. E. Dunstan, and D. V Boger, "Gel point studies for chemically modified biopolymer networks using small amplitude oscillatory rheometry," *Polymer (Guildf).*, vol. 42, no. 1, pp. 185–198, Jan. 2001.
[295] C. A. Bonino, J. E. Samorezov, O. Jeon, E. Alsberg, and S. A. Khan, "Real-time in siturheology of alginate hydrogel photocrosslinking," *Soft Matter*, vol. 7, no. 24, pp. 11510–11517, 2011.

[296] S. Liu, W. L. Chan, and L. Li, "Rheological Properties and Scaling Laws of κ-Carrageenan in Aqueous Solution," *Macromolecules*, vol. 48, no. 20, pp. 7649–7657, Oct. 2015.
[297] ASTM, "ASTM F2255-03 - Standard Test Method for Strength Properties of Tissue Adhesives in Lap-Shear by Tension Loading," vol. 5, no. Reapproved, pp. 1–6, 2010.
[298] ASTM, "ASTM F2256 - 03 - Standard Test Method for Strength Properties of Tissue Adhesives in T-Peel by Tension Loading," vol. 5, no. Reapproved, pp. 1–6, 2010.
[299] ASTM, "ASTM F2258-03 - Standard Test Method for Strength Properties of Tissue Adhesives Tension," vol. 5, no. Reapproved, pp. 1–6, 2010.
[300] V. M. C. Quent, D. Loessner, T. Friis, J. C. Reichert, and D. W. Hutmacher, "Discrepancies between metabolic activity and DNA content as tool to assess cell proliferation in cancer research," *J. Cell. Mol. Med.*, vol. 14, no. 4, pp. 1003–1013, Apr. 2010.
[301] S. N. Rampersad, "Multiple applications of alamar blue as an indicator of metabolic function and cellular health in cell viability bioassays," *Sensors (Switzerland)*, vol. 12, no. 9, pp. 12347–12360, 2012.
[302] B. Chazotte, "Labeling nuclear DNA using DAPI.," *Cold Spring Harb. Protoc.*, vol. 2011, no. 1, p. pdb.prot5556, Jan. 2011.
[303] B. Chazotte, "Labeling cytoskeletal F-actin with rhodamine phalloidin or fluorescein phalloidin for imaging.," *Cold Spring Harb. Protoc.*, vol. 2010, no. 5, p. pdb.prot4947, May 2010.
[304] "ISO 10993-4:2017(en) Biological evaluation of medical devices — Part 4: Selection of tests for interactions with blood," 2017.
[305] S. Moradi, N. Hadjesfandiari, S. F. Toosi, J. N. Kizhakkedathu, and S. G. Hatzikiriakos, "Effect of Extreme Wettability on Platelet Adhesion on Metallic Implants: From Superhydrophilicity to Superhydrophobicity," *ACS Appl. Mater. Interfaces*, vol. 8, no. 27, pp. 17631–17641, Jul. 2016.
[306] M. J. Workman *et al.*, "Thrombus Formation at the Neck of Cerebral Aneurysms during Treatment with Guglielmi Detachable Coils," *Am. J. Neuroradiol.*, vol. 23, no. 9, p. 1568 LP-1576, Oct. 2002.
[307] E. Delivopoulos, M. M. Ouberai, P. D. Coffey, M. J. Swann, K. M. Shakesheff, and M. E. Welland, "Serum protein layers on parylene-C and silicon oxide: Effect on cell adhesion," *Colloids Surf. B. Biointerfaces*, vol. 126, pp. 169–177, Feb. 2015.
[308] L. E. Corum and V. Hlady, "Screening platelet-surface interactions using negative surface charge gradients.," *Biomaterials*, vol. 31, no. 12, pp. 3148–3155, Apr. 2010.
[309] A. Morrison, V. S. Hornsey, C. V Prowse, and I. R. MacGregor, "Use of the DiaMed Impact R to test platelet function in stored platelet concentrates," *Vox Sang.*, vol. 93, no. 2, pp. 166–172, 2007.
[310] K. Adamson, E. Spain, U. Prendergast, R. J. Forster, N. Moran, and T. E. Keyes, "Ligand capture and activation of human platelets at monolayer modified gold surfaces," *Biomater. Sci.*, vol. 2, no. 10, pp. 1509–1520, 2014.
[311] R. E. Rumbaut, *Platelet-Vessel Wall Interactions in Hemostasis and Thrombosis*. Biota Publishing, 2010.
[312] Z. M. Ruggeri and G. L. Mendolicchio, "Adhesion Mechanisms in Platelet Function," *Circ. Res.*, vol. 100, no. 12, p. 1673 LP-1685, Jun. 2007.
[313] N. H. Wallén, M. Ladjevardi, J. Albert, and A. Bröijersén, "Influence of Different Anticoagulants on Platelet Aggregation in Whole Blood; A Comparison between Citrate, Low Molecular Mass Heparin and Hirudin," *Thromb. Res.*, vol. 87, no. 1, pp. 151–157, Jul. 1997.
[314] E. I. B. Peerschke, D. D. Castellone, A. K. Stroobants, and J. Francis, "Reference range determination for whole-blood platelet aggregation using the Multiplate analyzer.," *Am. J. Clin. Pathol.*, vol. 142, no. 5, pp. 647–656, Nov. 2014.
[315] N. Savion and D. Varon, "Impact--the cone and plate(let) analyzer: testing platelet function and anti-platelet drug response.," *Pathophysiol. Haemost. Thromb.*, vol. 35, no. 1–2, pp. 83–88, 2006.
[316] Kenet *et al.*, "Cone and platelet analyser (CPA): a new test for the prediction of bleeding among thrombocytopenic patients," *Br. J. Haematol.*, vol. 101, no. 2, pp. 255–259, 1998.

[317] M. V. Soloviev, Y. Okazaki, and H. Harasaki, "Whole Blood Platelet Aggregation in Humans and Animals: A Comparative Study," *J. Surg. Res.*, vol. 82, no. 2, pp. 180–187, Apr. 1999.

[318] M. O. Klein, P. W. Kammerer, T. Scholz, M. Moergel, C. M. Kirchmaier, and B. Al-Nawas, "Modulation of platelet activation and initial cytokine release by alloplastic bone substitute materials," *Clin. Oral Implants Res.*, vol. 21, no. 3, pp. 336–345, Mar. 2010.

[319] K. Adamson, E. Spain, U. Prendergast, N. Moran, R. J. Forster, and T. E. Keyes, "Peptide-Mediated Platelet Capture at Gold Micropore Arrays," *ACS Appl. Mater. Interfaces*, vol. 8, no. 47, pp. 32189–32201, 2016.

[320] I. A. de Oliveira, "Main Models of Experimental Saccular Aneurysm in Animals," Y. B. T.-A. Murai, Ed. Rijeka: InTech, 2012, p. Ch. 03.

[321] I. Q. Grunwald, B. Romeike, R. Eymann, C. Roth, T. Struffert, and W. Reith, "An Experimental Aneurysm Model: a Training Model for Neurointerventionalists," *Interv. Neuroradiol.*, vol. 12, no. 1, pp. 17–24, Mar. 2006.

[322] M. N. Gurcan, L. Boucheron, A. Can, A. Madabhushi, N. Rajpoot, and B. Yener, "Histopathological Image Analysis: A Review," *IEEE Rev. Biomed. Eng.*, vol. 2, pp. 147–171, 2009.

[323] N. Parry, "A Beginner's Guide to Haematoxylin and Eosin Staining," 2015. [Online]. Available: http://bitesizebio.com/13400/a-beginners-guide-to-haematoxylin-and-eosin-staining/.

[324] V. Kazlouskaya, S. Malhotra, J. Lambe, M. H. Idriss, D. Elston, and C. Andres, "The utility of elastic Verhoeff-Van Gieson staining in dermatopathology," *J. Cutan. Pathol.*, vol. 40, no. 2, pp. 211–225, 2013.

[325] D. Kipke, T. Becker, and V. Collins, "Method for forming an endovascular occlusion," 2001.

[326] A. P. Rauter, F. Djedaini-Pilard, S. Jarosz, and J. P. Kamerling, *Carbohydrate Chemistry: Chemical and Biological Approaches*. Royal Society of Chemistry, 2011.

[327] A. Barbetta, E. Barigelli, and M. Dentini, "Porous Alginate Hydrogels: Synthetic Methods for Tailoring the Porous Texture," *Biomacromolecules*, vol. 10, no. 8, pp. 2328–2337, 2009.

[328] W. Ding, J. Zhou, Y. Zeng, Y. Wang, and B. Shi, "Preparation of oxidized sodium alginate with different molecular weights and its application for crosslinking collagen fiber," *Carbohydr. Polym.*, vol. 157, pp. 1650–1656, 2017.

[329] T. M. Aida, T. Yamagata, M. Watanabe, and R. L. Smith, "Depolymerization of sodium alginate under hydrothermal conditions," *Carbohydr. Polym.*, vol. 80, no. 1, pp. 296–302, Mar. 2010.

[330] Sarah Brady, "To Develop a New Method of Determining the Setting Time and Adhesive Properties of a Novel Hydrogel Composition," Dublin City University, 2014.

[331] L. Corrigan, "Evaluation of material characteristics of a potential novel filler for treatment of aortic aneurysms," Dublin City University, 2013.

[332] H. Iwata, S. Matsuda, K. Mitsuhashi, E. Itoh, and Y. Ikada, "A novel surgical glue composed of gelatin and N-hydroxysuccinimide activated poly(L-glutamic acid): Part 1. Synthesis of activated poly(L-glutamic acid) and its gelation with gelatin.," *Biomaterials*, vol. 19, no. 20, pp. 1869–1876, Oct. 1998.

[333] J. Hou, C. Li, Y. Guan, Y. Zhang, and X. X. Zhu, "Enzymatically crosslinked alginate hydrogels with improved adhesion properties," *Polym. Chem.*, vol. 6, no. 12, pp. 2204–2213, 2015.

[334] M. Matsuda, M. Inoue, and T. Taguchi, "Enhanced bonding strength of a novel tissue adhesive consisting of cholesteryl group-modified gelatin and disuccinimidyl tartarate," *J. Bioact. Compat. Polym.* , vol. 27, no. 1, pp. 31–44, Jan. 2012.

[335] M. Y. Yousif, D. W. Holdsworth, and T. L. Poepping, "A blood-mimicking fluid for particle image velocimetry with silicone vascular models," *Exp. Fluids*, vol. 50, no. 3, pp. 769–774, Mar. 2011.

[336] S. Deutsch, J. M. Tarbell, K. B. Manning, G. Rosenberg, and A. A. Fontaine, "Experimental Fluid Mechanics of Pulsatile Artifical Blood Pumps," *Annu. Rev. Fluid Mech.*, vol. 38, no. 1, pp. 65–86, Dec. 2005.

[337] W. L. Lim, Y. T. Chew, T. C. Chew, and H. T. Low, "Particle image velocimetry in the investigation of flow past artificial heart valves," *Ann. Biomed. Eng.*, vol. 22, no. 3, pp. 307–318, May 1994.
[338] L. R. Bernstein, "Mechanisms of Therapeutic Activity for Gallium," *Pharmacol. Rev.*, vol. 50, no. 4, p. 665 LP-682, Dec. 1998.
[339] N. H. Fujiwara and D. F. Kallmes, "Healing Response in Elastase-Induced Rabbit Aneurysms after Embolization with a New Platinum Coil System," *Am. J. Neuroradiol.*, vol. 23, no. 7, pp. 1137–1144, 2002.
[340] T. A. Altes *et al.*, "Creation of Saccular Aneurysms in the Rabbit," *Am. J. Roentgenol.*, vol. 174, no. 2, pp. 349–354, Feb. 2000.
[341] C. Rodríguez-Rivero, L. Hilliou, E. M. Martín del Valle, and M. A. Galán, "Rheological characterization of commercial highly viscous alginate solutions in shear and extensional flows," *Rheol. Acta*, vol. 53, no. 7, pp. 559–570, 2014.
[342] "Alginates/PGA/Functionality and Rheology." [Online]. Available: http://www.fmcbiopolymer.com/Food/Ingredients/AlginatesPGA/FunctionalityandRheology.aspx.
[343] J. O. Hollinger, *An Introduction to Biomaterials*. Taylor & Francis, 2005.
[344] I. Fernández Farrés and I. T. Norton, "Formation kinetics and rheology of alginate fluid gels produced by in-situ calcium release," *Food Hydrocoll.*, vol. 40, pp. 76–84, Oct. 2014.
[345] F. Mancini, L. Montanari, D. Peressini, and P. Fantozzi, "Influence of Alginate Concentration and Molecular Weight on Functional Properties of Mayonnaise," *LWT - Food Sci. Technol.*, vol. 35, no. 6, pp. 517–525, Sep. 2002.
[346] J. Dusseault *et al.*, "Evaluation of alginate purification methods: effect on polyphenol, endotoxin, and protein contamination.," *J. Biomed. Mater. Res. A*, vol. 76, no. 2, pp. 243–251, Feb. 2006.
[347] M. Menard *et al.*, "Role of protein contaminants in the immunogenicity of alginates.," *J. Biomed. Mater. Res. B. Appl. Biomater.*, vol. 93, no. 2, pp. 333–340, May 2010.
[348] P. Berat *et al.*, "Determination of viscosity-average molecular weight of chitosan using intrinsic viscosity measurement," *J. Nucl. Relat. Technol.*, vol. 45, no. 37, 2013.
[349] H. Kakita and H. Kamishima, "Some properties of alginate gels derived from algal sodium alginate," *J. Appl. Phycol.*, vol. 20, no. 5, pp. 543–549, 2008.
[350] I. T. Norton, F. Spyropoulos, and P. Cox, *Practical Food Rheology: An Interpretive Approach*. Wiley, 2010.
[351] D. J. McHugh, "Alginate," in *A guide to the seaweed industry*, Food and Agriculture Organization of the United Nations, 2003, pp. 39–50.
[352] H. Hecht and S. Srebnik, "Structural Characterization of Sodium Alginate and Calcium Alginate," *Biomacromolecules*, vol. 17, no. 6, pp. 2160–67, 2016.
[353] Y. F. Liangbin Li, Rob Vreeker, and Ingrid Appelqvist, and E. Mendes, "Reexamining the Egg-Box Model in Calcium−Alginate Gels with X-ray Diffraction," *Biomacromolecules*, vol. 8, no. 2, pp. 464–468, 2007.
[354] I. Donati *et al.*, "New Hypothesis on the Role of Alternating Sequences in Calcium−Alginate Gels," *Biomacromolecules*, vol. 6, no. 2, pp. 1031–1040, 2005.
[355] K. I. Draget, K. Steinsvag, E. Onsoyen, and O. Smidsrod, "Na- and K-alginate; effect on Ca2+ −gelation," *Carbohydr Polym*, vol. 35, 1998.
[356] E. A. Nunamaker, K. J. Otto, and D. R. Kipke, "Investigation of the material properties of alginate for the development of hydrogel repair of dura mater," *J. Mech. Behav. Biomed. Mater.*, vol. 4, no. 1, pp. 16–33, Jan. 2011.
[357] D. W. Lee, W. S. Choi, M. W. Byun, H. J. Park, Y.-M. Yu, and C. M. Lee, "Effect of gamma-irradiation on degradation of alginate.," *J. Agric. Food Chem.*, vol. 51, no. 16, pp. 4819–4823, Jul. 2003.
[358] H. L. A. El-Mohdy, "Radiation-induced degradation of sodium alginate and its plant growth promotion effect," *Arab. J. Chem.*, vol. 10, pp. S431–S438, Feb. 2017.
[359] T. Huq, A. Khan, D. Dussault, S. Salmieri, R. A. Khan, and M. Lacroix, "Effect of gamma radiation on the physico-chemical properties of alginate-based films and beads," *Radiat. Phys. Chem.*, vol. 81, no. 8, pp. 945–948, Aug. 2012.

[360] C. Ouwerx, N. Velings, M. . Mestdagh, and M. A. . Axelos, "Physico-chemical properties and rheology of alginate gel beads formed with various divalent cations," *Polym. Gels Networks*, vol. 6, no. 5, pp. 393–408, Oct. 1998.
[361] M. M. Caruso *et al.*, "Mechanically-induced chemical changes in polymeric materials.," *Chem. Rev.*, vol. 109, no. 11, pp. 5755–5798, Nov. 2009.
[362] R. P. Wool, J. L. Willett, O. J. McGarel, and B. L. Yuan, "Strength of Polymer Interfaces.," *Am. Chem. Soc. Polym. Prepr. Div. Polym. Chem.*, vol. 28, no. 2, pp. 38–39, 1987.
[363] A. Martinsen, G. Skjåk-Bræk, and O. Smidsrød, "Alginate as immobilization material: I. Correlation between Chemical and Physical Properties of Alginate Gel Beads," *Biotechnol Bioeng*, vol. 33, 1989.
[364] S. Gorodzha *et al.*, "High-resolution synchrotron X-ray analysis of bioglass-enriched hydrogels," *J. Biomed. Mater. Res. Part A*, vol. 104, no. 5, pp. 1194–1201, 2016.
[365] C. M. Crowley, J. Doyle, M. R. Towler, N. Rushe, and S. Hampshire, "Influence of acid washing on the surface morphology of ionomer glasses and handling properties of glass ionomer cements.," *J. Mater. Sci. Mater. Med.*, vol. 18, no. 8, pp. 1497–1506, Aug. 2007.
[366] M. Araújo, M. Miola, G. Baldi, J. Perez, and E. Verné, "Bioactive Glasses with Low Ca/P Ratio and Enhanced Bioactivity," *Materials (Basel).*, vol. 9, no. 4, 2016.
[367] N. Tsomaia, S. L. Brantley, J. P. Hamilton, C. G. Pantano, and K. T. Mueller, "NMR evidence for formation of octahedral and tetrahedral Al and repolymerization of the Si network during dissolution of aluminosilicate glass and crystal," *Am. Mineral.*, vol. 88, no. 1, pp. 54–67, 2003.
[368] M. E. Simonsen, C. Sønderby, Z. Li, and E. G. Søgaard, "XPS and FT-IR investigation of silicate polymers," *J. Mater. Sci.*, vol. 44, no. 8, pp. 2079–2088, 2009.
[369] G. Hollinger, R. Skheyta-Kabbani, and M. Gendry, "Oxides on GaAs and InAs surfaces: An x-ray-photoelectron-spectroscopy study of reference compounds and thin oxide layers," *Phys. Rev. B*, vol. 49, no. 16, pp. 11159–11167, Apr. 1994.
[370] H. He, C.-F. Cheng, S. Seal, T. L. Barr, and J. Klinowski, "Solid-State NMR and ESCA Studies of the Framework Aluminosilicate Analcime and Its Gallosilicate Analog," *J. Phys. Chem.*, vol. 99, no. 10, pp. 3235–3239, Mar. 1995.
[371] M. Sekita, A. Fujimori, A. Makishima, T. Shimohira, and H. Ohashi, "X-ray photoelectron spectroscopy of a cerium-doped lanthanum aluminosilicate glass," *J. Non. Cryst. Solids*, vol. 76, no. 2–3, pp. 399–407, 1985.
[372] G. S. Henderson, G. Calas, and J. F. Stebbins, "The Structure of Silicate Glasses and Melts," *Elements*, vol. 2, no. 5, pp. 269–273, 2006.
[373] O. Okay, "General Properties of Hydrogels BT - Hydrogel Sensors and Actuators: Engineering and Technology," G. Gerlach and K.-F. Arndt, Eds. Berlin, Heidelberg: Springer Berlin Heidelberg, 2010, pp. 1–14.
[374] J.-Y. Sun *et al.*, "Highly stretchable and tough hydrogels," *Nature*, vol. 489, no. 7414, pp. 133–136, Sep. 2012.
[375] D. Zhang, L. Chen, Z. Wang, and T. Wei, *Recent progress on the research of high strength hydrogels*. 2015.
[376] F. Ikkai and M. Shibayama, "Inhomogeneity control in polymer gels," *J. Polym. Sci. Part B Polym. Phys.*, vol. 43, no. 6, pp. 617–628, 2005.
[377] L. Yi and J. Liu, "Liquid metal biomaterials: a newly emerging area to tackle modern biomedical challenges," *Int. Mater. Rev.*, vol. 62, no. 7, pp. 415–440, Oct. 2017.
[378] S. Pourshahrestani, E. Zeimaran, N. A. Kadri, and M. R. Towler, "In vitro evaluation of thrombogenicity effect of gallium-containing mesoporous bioactive glass," *Front. Bioeng. Biotechnol.*, no. 2812.
[379] A. Bismarck, A. R. Boccaccini, E. Egia-Ajuriagojeaskoa, D. Hülsenberg, and T. Leutbecher, "Surface characterization of glass fibers made from silicate waste: Zeta-potential and contact angle measurements," *J. Mater. Sci.*, vol. 39, no. 2, pp. 401–412.
[380] S. Pourshahrestani *et al.*, "Gallium-containing mesoporous bioactive glass with potent hemostatic activity and antibacterial efficacy," *J. Mater. Chem. B*, vol. 4, no. 1, pp. 71–86, 2016.
[381] S. Takeda, K. Yamamoto, Y. Hayasaka, and K. Matsumoto, "Surface OH group governing

wettability of commercial glasses," *J. Non. Cryst. Solids*, vol. 249, no. 1, pp. 41–46, Jul. 1999.
[382] E. A. Leed, J. O. Sofo, and C. G. Pantano, "Electronic structure calculations of physisorption and chemisorption on oxide glass surfaces," *Phys. Rev. B*, vol. 72, no. 15, p. 155427, Oct. 2005.
[383] E. A. Leed and C. G. Pantano, "Computer modeling of water adsorption on silica and silicate glass fracture surfaces," *J. Non. Cryst. Solids*, vol. 325, no. 1, pp. 48–60, 2003.
[384] J. Serra *et al.*, *FTIR and XPS studies of bioactive silica based glasses*, vol. 332. 2003.
[385] L. H. Prentice, M. J. Tyas, and M. F. Burrow, "Ion leaching of a glass-ionomer glass: an empirical model and effects on setting characteristics and strength.," *J. Mater. Sci. Mater. Med.*, vol. 18, no. 1, pp. 127–131, Jan. 2007.
[386] C. H. Yang *et al.*, "Strengthening Alginate/Polyacrylamide Hydrogels Using Various Multivalent Cations," *ACS Appl. Mater. Interfaces*, vol. 5, no. 21, pp. 10418–10422, Nov. 2013.
[387] S. Liu, M. Kang, I. Hussain, K. Li, F. Yao, and G. Fu, "High mechanical strength and stability of alginate hydrogel induced by neodymium ions coordination," *Polym. Degrad. Stab.*, vol. 133, pp. 1–7, Nov. 2016.
[388] J. Jang, Y.-J. Seol, H. J. Kim, J. Kundu, S. W. Kim, and D.-W. Cho, "Effects of alginate hydrogel cross-linking density on mechanical and biological behaviors for tissue engineering," *J. Mech. Behav. Biomed. Mater.*, vol. 37, pp. 69–77, Sep. 2014.
[389] M. Qiu, D. Chen, C. Shen, J. Shen, H. Zhao, and Y. He, "Preparation of in situ forming and injectable alginate/mesoporous Sr-containing calcium silicate composite cement for bone repair," *RSC Adv.*, vol. 7, no. 38, pp. 23671–23679, 2017.
[390] Y. Luo, C. Wu, A. Lode, and M. Gelinsky, "Hierarchical mesoporous bioactive glass/alginate composite scaffolds fabricated by three-dimensional plotting for bone tissue engineering," *Biofabrication*, vol. 5, no. 1, p. 15005, 2013.
[391] F. Everaerts, M. Torrianni, M. Hendriks, and J. Feijen, "Biomechanical properties of carbodiimide crosslinked collagen: Influence of the formation of ester crosslinks," *J. Biomed. Mater. Res. Part A*, vol. 85A, no. 2, pp. 547–555, 2008.
[392] K. Nam, T. Kimura, and A. Kishida, "Controlling Coupling Reaction of EDC and NHS for Preparation of Collagen Gels Using Ethanol/Water Co-Solvents," *Macromol. Biosci.*, vol. 8, no. 1, pp. 32–37, 2008.
[393] D. V Shepherd, J. H. Shepherd, S. Ghose, S. J. Kew, R. E. Cameron, and S. M. Best, "The process of EDC-NHS Cross-linking of reconstituted collagen fibres increases collagen fibrillar order and alignment.," *APL Mater.*, vol. 3, no. 1, Jan. 2015.
[394] L. Fan *et al.*, "Preparation and characterization of sodium alginate modified with collagen peptides.," *Carbohydr. Polym.*, vol. 93, no. 2, pp. 380–385, Apr. 2013.
[395] B. Cohen, O. Pinkas, M. Foox, and M. Zilberman, "Gelatin-alginate novel tissue adhesives and their formulation-strength effects," *Acta Biomater.*, vol. 9, no. 11, pp. 9004–9011, 2013.
[396] B. Cohen, M. Panker, E. Zuckerman, M. Foox, and M. Zilberman, "Effect of calcium phosphate-based fillers on the structure and bonding strength of novel gelatin–alginate bioadhesives," *J. Biomater. Appl.* , vol. 28, no. 9, pp. 1366–1375, May 2014.
[397] L. L. Hench and H. A. Paschall, "Direct chemical bond of bioactive glass-ceramic materials to bone and muscle," *J. Biomed. Mater. Res.*, vol. 7, no. 3, pp. 25–42, 1973.
[398] K. C. Leung, T. W. Chow, C. W. Woo, and R. K. Clark, "Tensile, shear and cleavage bond strengths of alginate adhesive.," *J. Dent.*, vol. 26, no. 7, pp. 617–622, Sep. 1998.
[399] E. F. Mason and J. C. Rathmell, "Cell metabolism: An essential link between cell growth and apoptosis," *Biochim. Biophys. Acta - Mol. Cell Res.*, vol. 1813, no. 4, pp. 645–654, Apr. 2011.
[400] J. Bereiter-Hahn, A. Munnich, and P. Woiteneck, "Dependence of Energy Metabolism on the Density of Cells in Culture," *Cell Struct. Funct.*, vol. 23, no. 2, pp. 85–93, 1998.
[401] J. O'Brien, I. Wilson, T. Orton, and F. Pognan, "Investigation of the Alamar Blue (resazurin) fluorescent dye for the assessment of mammalian cell cytotoxicity," *Eur. J. Biochem.*, vol. 267, no. 17, pp. 5421–5426, 2000.
[402] G. C. Brown, "Regulation of mitochondrial respiration by nitric oxide inhibition of

cytochrome c oxidase," *Biochim. Biophys. Acta - Bioenerg.*, vol. 1504, no. 1, pp. 46–57, 2001.

[403] D. W. 2nd Lincoln, R. G. Whitney, and J. R. Smith, "In vitro proliferation and lifespan of bovine aorta endothelial cells: response to conditioned media.," *J. Cell Sci.*, vol. 56, pp. 281–292, Aug. 1982.

[404] G. S. Duthu and J. R. Smith, "In vitro proliferation and lifespan of bovine aorta endothelial cells: effect of culture conditions and fibroblast growth factor.," *J. Cell. Physiol.*, vol. 103, no. 3, pp. 385–392, Jun. 1980.

[405] C. of the E. Communities, "Reports of the Scientific Committee for Food."

[406] D. D'Arcangelo *et al.*, "Acidosis Inhibits Endothelial Cell Apoptosis and Function and Induces Basic Fibroblast Growth Factor and Vascular Endothelial Growth Factor Expression," *Circ. Res.* , vol. 86, no. 3, pp. 312–318, Feb. 2000.

[407] M. Pirchl, J. Marksteiner, and C. Humpel, "Effects of acidosis on brain capillary endothelial cells and cholinergic neurons: relevance to vascular dementia and Alzheimer's disease.," *Neurol. Res.*, vol. 28, no. 6, pp. 657–664, Sep. 2006.

[408] A. Hoppe, N. S. Güldal, and A. R. Boccaccini, "A review of the biological response to ionic dissolution products from bioactive glasses and glass-ceramics," *Biomaterials*, vol. 32, no. 11, pp. 2757–2774, Apr. 2011.

[409] J. Burgess and E. Raven, "Calcium in biological systems," *Adv. Inorg. Chem.*, vol. 61, pp. 251–366, 2009.

[410] L. Q. Wan, J. Jiang, D. E. Arnold, X. E. Guo, H. H. Lu, and V. C. Mow, "Calcium Concentration Effects on the Mechanical and Biochemical Properties of Chondrocyte-Alginate Constructs," *Cell. Mol. Bioeng.*, vol. 1, no. 1, pp. 93–102, Mar. 2008.

[411] J. Kovar, P. Seligman, and E. W. Gelfand, "Differential growth-inhibitory effects of gallium on B-lymphocyte lines in high versus low iron concentrations.," *Cancer Res.*, vol. 50, no. 18, pp. 5727–5730, Sep. 1990.

[412] K.-L. Chang, W.-T. Liao, C.-L. Yu, C.-C. E. Lan, L. W. Chang, and H.-S. Yu, "Effects of gallium on immune stimulation and apoptosis induction in human peripheral blood mononuclear cells," *Toxicol. Appl. Pharmacol.*, vol. 193, no. 2, pp. 209–217, Dec. 2003.

[413] C. R. Chitambar, D. P. Purpi, J. Woodliff, M. Yang, and J. P. Wereley, "Development of gallium compounds for treatment of lymphoma: gallium maltolate, a novel hydroxypyrone gallium compound, induces apoptosis and circumvents lymphoma cell resistance to gallium nitrate.," *J. Pharmacol. Exp. Ther.*, vol. 322, no. 3, pp. 1228–1236, 2007.

[414] C. R. Chitambar, "Gallium and its competing roles with iron in biological systems," *Biochim. Biophys. Acta - Mol. Cell Res.*, vol. 1863, no. 8, pp. 2044–2053, Aug. 2016.

[415] P. Melnikov, A. Malzac, and M. de B. Coelho, "Gallium and bone pathology," *Acta Ortopédica Bras.*, vol. 16, no. 1, pp. 54–57, 2008.

[416] C. R. Chitambar, "Medical Applications and Toxicities of Gallium Compounds," *Int. J. Environ. Res. Public Health*, vol. 7, no. 5, pp. 2337–2361, May 2010.

[417] K. Takeuchi *et al.*, "Nitric oxide: inhibitory effects on endothelial cell calcium signaling, prostaglandin I2 production and nitric oxide synthase expression," *Cardiovasc. Res.*, vol. 62, no. 1, pp. 194–201, 2004.

[418] D. Tousoulis, A.-M. Kampoli, C. Tentolouris, N. Papageorgiou, and C. Stefanadis, "The role of nitric oxide on endothelial function.," *Curr. Vasc. Pharmacol.*, vol. 10, no. 1, pp. 4–18, Jan. 2012.

[419] R. M. Day, "Bioactive glass stimulates the secretion of angiogenic growth factors and angiogenesis in vitro.," *Tissue Eng.*, vol. 11, no. 5–6, pp. 768–777, 2005.

[420] Q. Zhao, J. Qian, H. Zhou, Y. Yuan, Y. Mao, and C. Liu, "In vitro osteoblast-like and endothelial cells' response to calcium silicate/calcium phosphate cement," *Biomed. Mater.*, vol. 5, no. 3, p. 35004, 2010.

[421] L. Munaron, "Intracellular Calcium, Endothelial Cells and Angiogenesis," *Recent Patents on Anti-Cancer Drug Discovery*, vol. 1, no. 1. pp. 105–119, 2006.

[422] Y. Li, Y. Han, X. Wang, J. Peng, Y. Xu, and J. Chang, "Multifunctional Hydrogels Prepared by Dual Ion Cross-Linking for Chronic Wound Healing.," *ACS Appl. Mater. Interfaces*, vol. 9, no. 19, pp. 16054–16062, May 2017.

[423] Q. Zeng, Y. Han, H. Li, and J. Chang, "Bioglass/alginate composite hydrogel beads as cell carriers for bone regeneration.," *J. Biomed. Mater. Res. B. Appl. Biomater.*, vol. 102, no. 1, pp. 42–51, Jan. 2014.

[424] O. Aarstad, E. B. Heggset, I. S. Pedersen, S. H. Bjørnøy, K. Syverud, and B. L. Strand, "Mechanical Properties of Composite Hydrogels of Alginate and Cellulose Nanofibrils," *Polymers (Basel).*, vol. 9, no. 8, 2017.

[425] F. F. Siyam and D. M. Klachko, "What Is Hypercalcemia? The Importance of Fasting Samples," *Cardiorenal Med.*, vol. 3, no. 4, pp. 232–238, Dec. 2013.

[426] X. Li *et al.*, "High glucose concentration induces endothelial cell proliferation by regulating cyclin-D2-related miR-98," *J. Cell. Mol. Med.*, vol. 20, no. 6, pp. 1159–1169, Jun. 2016.

[427] S. Kondo, N. Hashimoto, H. Kikuchi, F. Hazama, I. Nagata, and H. Kataoka, "Apoptosis of medial smooth muscle cells in the development of saccular cerebral aneurysms in rats.," *Stroke*, vol. 29, no. 1, p. 181–8; discussion 189, Jan. 1998.

[428] T. Hashimoto, H. Meng, and W. L. Young, "Intracranial aneurysms: links among inflammation, hemodynamics and vascular remodeling," *Neurol. Res.*, vol. 28, no. 4, pp. 372–380, Jun. 2006.

[429] J. Raymond, A. C. Desfaits, and D. Roy, "Fibrinogen and vascular smooth muscle cell grafts promote healing of experimental aneurysms treated by embolization.," *Stroke*, vol. 30, no. 8, pp. 1657–1664, Aug. 1999.

[430] J. Raymond, T. Darsaut, I. Salazkin, G. Gevry, and F. Bouzeghrane, "Mechanisms of Occlusion and Recanalization in Canine Carotid Bifurcation Aneurysms Embolized with Platinum Coils: An Alternative Concept," *Am. J. Neuroradiol.* , vol. 29, no. 4, pp. 745–752, Apr. 2008.

[431] Y. Mitome-Mishima *et al.*, "Endothelial Cell Proliferation in Swine Experimental Aneurysm after Coil Embolization," *PLoS One*, vol. 9, no. 2, p. e89047, Feb. 2014.

[432] *Textbook of Pathology*. Jaypee Brothers, Medical Publishers, 2004.

[433] J. Raymond, V. Lebel, C. Ogoudikpe, A. Metcalfe, M. Chagnon, and O. Robledo, "Recanalization of arterial thrombus, and inhibition with beta-radiation in a new murine carotid occlusion model: MRNA expression of angiopoietins, metalloproteinases, and their inhibitors.," *J. Vasc. Surg.*, vol. 40, no. 6, pp. 1190–1198, Dec. 2004.

[434] I. Y. Tan, R. F. Agid, and R. A. Willinsky, "Recanalization Rates after Endovascular Coil Embolization in a Cohort of Matched Ruptured and Unruptured Cerebral Aneurysms," *Interv. Neuroradiol.*, vol. 17, no. 1, pp. 27–35, Mar. 2011.

[435] C. J. Bettinger and M. B. Horowitz, "Coated vaso-occclusive device for treatment of aneurysms," 2014.

[436] W. L. Stoppel, J. C. White, S. D. Horava, A. C. Henry, S. C. Roberts, and S. R. Bhatia, "Terminal sterilization of alginate hydrogels: Efficacy and impact on mechanical properties," *J. Biomed. Mater. Res. Part B Appl. Biomater.*, vol. 102, no. 4, pp. 877–884, May 2014.

[437] W. J. Leo, A. J. McLoughlin, and D. M. Malone, "Effects of sterilization treatments on some properties of alginate solutions and gels," *Biotechnol. Prog.*, vol. 6, no. 1, pp. 51–53, Jan. 1990.

[438] N. C. Whyte, *Alginate degradation in situ accompanying thermal drying of the marine algae Nereocystis luetkeana and Macrocystis integrifolia*. 1976.

[439] J. Cox, "Examination of the Effect of Extreme Cooling on the Terminal Sterilisation of Sensitive Biomedical Hydrogel Components," Dublin City University, 2016.

[440] L. C. Anderson, G. Otto, K. R. Pritchett-Corning, M. T. Whary, and J. G. Fox, *Laboratory Animal Medicine*. Elsevier Science, 2015.

[441] T. Sandle, *Sterility, Sterilisation and Sterility Assurance for Pharmaceuticals: Technology, Validation and Current Regulations*. Elsevier Science, 2013.

[442] O. Aarstad, B. L. Strand, L. M. Klepp-Andersen, and G. Skjak-Braek, "Analysis of G-block distributions and their impact on gel properties of in vitro epimerized mannuronan.," *Biomacromolecules*, vol. 14, no. 10, pp. 3409–3416, Oct. 2013.

[443] L. Li, C. L. Wilbur, and K. L. Mintz, "Kinetics of Hydrothermal Inactivation of Endotoxins

,” *Appl. Environ. Microbiol.*, vol. 77, no. 8, pp. 2640–2647, Apr. 2011.
[444] O. Gautier, “Sterilized, Validated, Documented and Pyrogen Tested Wipers.”
[445] T. Hu, Y. Yang, L. Tan, T. Yin, Y. Wang, and G. Wang, “Effects of gamma irradiation and moist heat for sterilization on sodium alginate.,” *Biomed. Mater. Eng.*, vol. 24, no. 5, pp. 1837–1849, 2014.
[446] “Summary of Safety and Probable Benefit - Onyx® Liquid Embolic System Onyx® HD-500,” 2007.
[447] W. Jeong and K. Rhee, “Hemodynamics of Cerebral Aneurysms: Computational Analyses of Aneurysm Progress and Treatment,” *Comput. Math. Methods Med.*, vol. 2012, p. 782801, Feb. 2012.
[448] L. F. Bonewald *et al.*, “Von Kossa Staining Alone Is Not Sufficient to Confirm that Mineralization In Vitro Represents Bone Formation,” *Calcif. Tissue Int.*, vol. 72, no. 5, pp. 537–547, 2003.
[449] C. Marmorat, A. Arinstein, N. Koifman, Y. Talmon, E. Zussman, and M. Rafailovich, “Cryo-Imaging of Hydrogels Supermolecular Structure,” vol. 6, p. 25495, May 2016.
[450] D. Zhu, N. Mackenzie, C. Farquharson, and V. Macrae, “Mechanisms and Clinical Consequences of Vascular Calcification,” *Front. Endocrinol. (Lausanne).*, vol. 3, p. 95, 2012.
[451] X. H. Wu, X.-Y. Chen, L. J. Wang, and K. S. Wong, “Intracranial Artery Calcification and Its Clinical Significance,” *J. Clin. Neurol.*, vol. 12, no. 3, pp. 253–261, Jul. 2016.
[452] C. S. Lee *et al.*, “Regulating in vivo calcification of alginate microbeads,” *Biomaterials*, vol. 31, no. 18, pp. 4926–4934, Jun. 2010.
[453] R. Veres, D. L. Trandafir, K. Magyari, S. Simon, D. Barbos, and V. Simon, “Gamma irradiation effect on bioactive glasses synthesized with polyethylene-glycol template,” *Ceram. Int.*, vol. 42, no. 1, pp. 1990–1997, 2016.
[454] M. M. Farag, W. M. Abd-Allah, and A. M. Ibrahim, “Effect of gamma irradiation on drug releasing from nano-bioactive glass,” *Drug Deliv. Transl. Res.*, vol. 5, no. 1, pp. 63–73, 2015.
[455] A. G. Kalampounias, “IR and Raman spectroscopic studies of sol–gel derived alkaline-earth silicate glasses,” *Bull. Mater. Sci.*, vol. 34, no. 2, pp. 299–303, 2011.
[456] T. Himanshu and K. B. and S. S. Sampath KA, Himanshu T, “Structural, Magnetic and In Vitro Bioactivity of Co-Cu Ferrite and Bioglass Composite for Hyperthermia in Bone Tissue Engineering,” *Bioceram. Dev. Appl.*, vol. 6, no. 1, pp. 1–7, 2016.
[457] J. Serra *et al.*, “Influence of the non-bridging oxygen groups on the bioactivity of silicate glasses.,” *J. Mater. Sci. Mater. Med.*, vol. 13, no. 12, pp. 1221–1225, Dec. 2002.
[458] D. C. Clupper, J. E. Gough, P. M. Embanga, I. Notingher, L. L. Hench, and M. M. Hall, “Bioactive evaluation of 45S5 bioactive glass fibres and preliminary study of human osteoblast attachment.,” *J. Mater. Sci. Mater. Med.*, vol. 15, no. 7, pp. 803–808, Jul. 2004.
[459] L. Radev, N. Y. Mostafa, I. Michailova, I. M. M. Salvado, and M. H. V. Fernandes, “In Vitro Bioactivity of Collagen/Calcium Phosphate Silicate Composites, Cross-Linked with Chondroitin Sulfate,” *Int. J. Mater. Chem.*, vol. 2, no. 1, pp. 1–9, 2012.
[460] F. Margha and A. Abdelghany, *Bone bonding ability of some borate bio-glasses and their corresponding glass-ceramic derivatives*, vol. 6. 2012.
[461] P. K. Khan *et al.*, “Influence of single and binary doping of strontium and lithium on in vivo biological properties of bioactive glass scaffolds,” vol. 6, p. 32964, Sep. 2016.
[462] M. O. Taha, K. M. Aiedeh, Y. Al-Hiari, and H. Al-Khatib, “Synthesis of zinc-crosslinked thiolated alginic acid beads and their in vitro evaluation as potential enteric delivery system with folic acid as model drug.,” *Pharmazie*, vol. 60, no. 10, pp. 736–742, Oct. 2005.
[463] H. Daemi and M. Barikani, “Synthesis and characterization of calcium alginate nanoparticles, sodium homopolymannuronate salt and its calcium nanoparticles,” *Sci. Iran.*, vol. 19, no. 6, pp. 2023–2028, 2012.
[464] C. Sartori, “The Characterisation of Alginate Systems for Biomedical Applications,” Brunel University, 1997.
[465] R. S. Banegas, C. F. Zornio, A. de M. G. Borges, L. C. Porto, and V. Soldi, “Preparation, characterization and properties of films obtained from cross-linked guar gum,”

Polmeros, vol. 23, pp. 182–188, 2013.

[466] P. Li, Y.-N. Dai, J.-P. Zhang, A.-Q. Wang, and Q. Wei, "Chitosan-Alginate Nanoparticles as a Novel Drug Delivery System for Nifedipine," *Int. J. Biomed. Sci.*, vol. 4, no. 3, pp. 221–228, Sep. 2008.

[467] A. Ślósarczyk, Z. Paszkiewicz, and C. Paluszkiewicz, "FTIR and XRD evaluation of carbonated hydroxyapatite powders synthesized by wet methods," *J. Mol. Struct.*, vol. 744, pp. 657–661, 2005.

[468] Y. Luo, A. Lode, C. Wu, J. Chang, and M. Gelinsky, "Alginate/Nanohydroxyapatite Scaffolds with Designed Core/Shell Structures Fabricated by 3D Plotting and in Situ Mineralization for Bone Tissue Engineering," *ACS Appl. Mater. Interfaces*, vol. 7, no. 12, pp. 6541–6549, Apr. 2015.

[469] R. Narayan, P. Colombo, T. Ohji, and A. Wereszczak, *Advances in Bioceramics and Porous Ceramics*. Wiley, 2009.

[470] A. F. Fraga, E. de A. Filho, E. C. da S. Rigo, and A. O. Boschi, "Synthesis of chitosan/hydroxyapatite membranes coated with hydroxycarbonate apatite for guided tissue regeneration purposes," *Appl. Surf. Sci.*, vol. 257, no. 9, pp. 3888–3892, 2011.

[471] T. J. Ribeiro *et al.*, "Sol-gel as methodology to obtain bioactive materials," *An. Acad. Bras. Cienc.*, vol. 86, pp. 27–36, 2014.

[472] P. P. Lopes *et al.*, "In vitro bioactivity of PMMA-based composite in simulated plasma with albumin," *Mater. (Rio Janeiro)*, vol. 12, pp. 128–133, 2007.

[473] P. Parhi, A. Ramanan, and A. R. Ray, "Preparation and characterization of alginate and hydroxyapatite-based biocomposite," *J. Appl. Polym. Sci.*, vol. 102, no. 6, pp. 5162–5165, 2006.

[474] Y.-H. Wang, Y. Liu, P. Maye, and D. W. Rowe, "Examination of Mineralized Nodule Formation in Living Osteoblastic Cultures Using Fluorescent Dyes," *Biotechnol. Prog.*, vol. 22, no. 6, pp. 1697–1701, 2006.

[475] A. C. Akman, R. Seda Tığlı, M. Gümüşderelioğlu, and R. M. Nohutcu, "Bone Morphogenetic Protein-6-loaded Chitosan Scaffolds Enhance the Osteoblastic Characteristics of MC3T3-E1 Cells," *Artif. Organs*, vol. 34, no. 1, pp. 65–74, 2010.

[476] G. Poologasundarampillai *et al.*, "Cotton-wool-like bioactive glasses for bone regeneration," *Acta Biomater.*, vol. 10, no. 8, pp. 3733–3746, 2014.

[477] D. Sriranganathan, N. Kanwal, K. A. Hing, and R. G. Hill, "Strontium substituted bioactive glasses for tissue engineered scaffolds: the importance of octacalcium phosphate," *J. Mater. Sci. Mater. Med.*, vol. 27, p. 39, Dec. 2016.

[478] M. Mneimne, R. G. Hill, A. J. Bushby, and D. S. Brauer, "High phosphate content significantly increases apatite formation of fluoride-containing bioactive glasses," *Acta Biomater.*, vol. 7, no. 4, pp. 1827–1834, 2011.

[479] F. A. Shah, D. S. Brauer, R. G. Hill, and K. A. Hing, "Apatite formation of bioactive glasses is enhanced by low additions of fluoride but delayed in the presence of serum proteins," *Mater. Lett.*, vol. 153, pp. 143–147, 2015.

[480] G. Kaur, O. P. Pandey, K. Singh, D. Homa, B. Scott, and G. Pickrell, "A review of bioactive glasses: Their structure, properties, fabrication and apatite formation.," *J. Biomed. Mater. Res. A*, vol. 102, no. 1, pp. 254–274, Jan. 2014.

[481] T. J. Keenan, L. M. Placek, T. L. McGinnity, M. R. Towler, M. M. Hall, and A. W. Wren, "Relating ion release and pH to in vitro cell viability for gallium-inclusive bioactive glasses," *J. Mater. Sci.*, vol. 51, no. 2, pp. 1107–1120, Jan. 2016.

[482] P. Thevenot, W. Hu, and L. Tang, "Surface chemistry influences implant biocompatibility.," *Curr. Top. Med. Chem.*, vol. 8, no. 4, pp. 270–280, 2008.

[483] B. Sarker *et al.*, "Evaluation of Fibroblasts Adhesion and Proliferation on Alginate-Gelatin Crosslinked Hydrogel," *PLoS One*, vol. 9, no. 9, pp. 1–12, 2014.

[484] N. Cao, X. Chen, and D. Schreyer, "Influence of Calcium Ions on Cell Survival and Proliferation in the Context of an Alginate Hydrogel," *ISRN Chem. Eng.*, vol. 2012, pp. 242–247, 2012.

[485] V. Torres-Costa *et al.*, "Engineering of silicon surfaces at the micro- and nanoscales for cell adhesion and migration control," *Int. J. Nanomedicine*, vol. 7, pp. 623–630, Feb. 2012.

[486] B. J. Kirby, A. R. Wheeler, R. N. Zare, J. A. Fruetel, and T. J. Shepodd, "Programmable modification of cell adhesion and zeta potential in silica microchips," *Lab Chip*, vol. 3, no. 1, pp. 5–10, 2003.
[487] J. A. Rowley, G. Madlambayan, and D. J. Mooney, "Alginate hydrogels as synthetic extracellular matrix materials," *Biomaterials*, vol. 20, no. 1, pp. 45–53, Jan. 1999.
[488] K. J. Smetana, "Cell biology of hydrogels.," *Biomaterials*, vol. 14, no. 14, pp. 1046–1050, Nov. 1993.
[489] C. V Serrano *et al.*, "pH dependence of neutrophil-endothelial cell adhesion and adhesion molecule expression.," *Am. J. Physiol.*, vol. 271, no. 3 Pt 1, pp. C962–C970, 1996.
[490] J.-D. Rembe *et al.*, "Comparison of hemostatic dressings for superficial wounds using a new spectrophotometric coagulation assay," *J. Transl. Med.*, vol. 13, p. 375, Nov. 2015.
[491] M. Rinaudo, "Biomaterials based on a natural polysaccharide: alginate," *TIP*, vol. 17, no. 1, pp. 92–96, Jun. 2014.
[492] S. Pourshahrestani *et al.*, "Potency and Cytotoxicity of a Novel Gallium-Containing Mesoporous Bioactive Glass/Chitosan Composite Scaffold as Hemostatic Agents," *ACS Appl. Mater. Interfaces*, Aug. 2017.
[493] K. Kawai *et al.*, "Calcium-Based Nanoparticles Accelerate Skin Wound Healing," *PLoS One*, vol. 6, no. 11, p. e27106, Nov. 2011.
[494] C. R. Spillert and D. Persaud, "Hemostatic effects of glucono-delta-lactone." Google Patents, 2013.
[495] N. Davidenko *et al.*, "Control of crosslinking for tailoring collagen-based scaffolds stability and mechanics," *Acta Biomater.*, vol. 25, pp. 131–142, Oct. 2015.
[496] K. F. Layton, H. J. Cloft, L. A. Gray, D. A. Lewis, and D. F. Kallmes, "Balloon-Assisted Coiling of Intracranial Aneurysms: Evaluation of Local Thrombus Formation and Symptomatic Thromboembolic Complications," *Am. J. Neuroradiol.*, vol. 28, no. 6, p. 1172 LP-1175, Jun. 2007.
[497] R. Dimitrov, D. Kostov, K. Stamatova, and V. Yordanova, "Anatomotopographical and Morphological Analysis of Normal Kidneys of Rabbit (Oryctolagus Cuniculus)," vol. 10, no. 2, pp. 79–84, 2012.
[498] J. Ueno and N. Tohma, "Endovascular Treatment of Cerebral Aneurysm with Coils and Onyx: in-vivo experiment," *Interv. Neuroradiol.*, vol. 10, no. Suppl 1, pp. 51–56, Mar. 2004.
[499] H. Takao *et al.*, "Endovascular Treatment of Experimental Aneurysms Using a Combination of Thermoreversible Gelation Polymer and Protection Devices: Feasibility Study," *Neurosurgery*, vol. 65, no. 3, p. 601, 2009.
[500] A. Berenstein, "Treatment of experimental aneurysms with a new liquid embolic agent and a retrievable stent: proof of concept and feasibility study.," *J. Neurointerv. Surg.*, vol. 8, no. 9, pp. 934–939, Sep. 2016.
[501] I. Szikora, L. R. Guterman, S. C. Standard, A. K. Wakhloo, and L. N. Hopkins, "Endovascular treatment of experimental aneurysms with liquid polymers: the protective potential of stents.," *Neurosurgery*, vol. 38, no. 2, pp. 339–347, Feb. 1996.
[502] H. Zielinski, T. Syrylo, and S. Szmigielski, "Renal Artery Embolization in Treatment of Renal Cancer with Emphasis on Response of Immune System," J. B. T.-R. T. Chen, Ed. Rijeka: InTech, 2013, p. Ch. 06.
[503] R. Loffroy *et al.*, "Transcatheter Arterial Embolization in Patients with Kidney Diseases: an Overview of the Technical Aspects and Clinical Indications," *Korean J. Radiol.*, vol. 11, no. 3, pp. 257–268, Apr. 2010.
[504] M. Omodon, G. Ayuba, and I. J. Patel, "Review of renal artery embolization for treatment of renal angiomyolipoma," *Clin. Nephrol. Urol. Sci.*, vol. 3, no. 1, p. 1, Feb. 2016.
[505] I. Q. Grunwald *et al.*, "Recanalization after endovascular treatment of intracerebral aneurysms," *Neuroradiology*, vol. 49, no. 1, pp. 41–47, Jan. 2007.
[506] J. N. Rodriguez *et al.*, "Design and biocompatibility of endovascular aneurysm filling devices.," *J. Biomed. Mater. Res. A*, vol. 103, no. 4, pp. 1577–1594, Apr. 2015.
[507] J. N. Rodriguez *et al.*, "In vivo tissue response following implantation of shape memory

polyurethane foam in a porcine aneurysm model," *J. Biomed. Mater. Res. A*, vol. 102, no. 5, pp. 1231–1242, May 2014.
[508] A. Fry, "Injecting Highly Viscous Drugs," *Pharmaceutical Technology*, 2014. [Online]. Available: http://www.pharmtech.com/injecting-highly-viscous-drugs.
[509] S. H. Kerr and M. T. Fulmer, "Threaded syringe for delivery of a bone substitute material," 2004.
[510] B. Strauss, B. Smith, B. Canfield, A. Conner, D. Hayman, and E. Olsen, "Threaded syringe with quick stop," 2003.
[511] G. Aurin and W. Porter, "Bone cement syringe," 2004.
[512] E. O. Brian M. Strauss, Brock H. Smith, Brian Canfield, Amanda Conner, Douglas R. Hayman, "Threaded syringe with quick stop," US7018365 B2, 2006.
[513] D. Yang and K. S. Jones, "Effect of alginate on innate immune activation of macrophages.," *J. Biomed. Mater. Res. A*, vol. 90, no. 2, pp. 411–418, Aug. 2009.
[514] H. Gheisari, E. Karamian, and M. Abdellahi, *A novel hydroxyapatite –Hardystonite nanocomposite ceramic*, vol. 41. 2015.
[515] A. S. Aronson, N. Jonsson, and P. Alberius, "Tantalum markers in radiography," *Skeletal Radiol.*, vol. 14, no. 3, pp. 207–211, 1985.
[516] D. C. Chan, H. W. Titus, K. H. Chung, H. Dixon, S. T. Wellinghoff, and H. R. Rawls, "Radiopacity of tantalum oxide nanoparticle filled resins.," *Dent. Mater.*, vol. 15, no. 3, pp. 219–222, May 1999.
[517] L. Cordeiro *et al.*, "Thermal and structural properties of tantalum alkali-phosphate glasses," *J. Non. Cryst. Solids*, vol. 402, pp. 44–48, Oct. 2014.
[518] A. M. Alhalawani and M. R. Towler, "A novel tantalum-containing bioglass. Part I. Structure and solubility," *Mater. Sci. Eng. C*, vol. 72, pp. 202–211, Mar. 2017.
[519] W. Kriz and B. Kaissling, "Chapter 20 - Structural Organization of the Mammalian Kidney A2 - Alpern, Robert J.," O. W. Moe and M. B. T.-S. and G. T. K. (Fifth E. Caplan, Eds. Academic Press, 2013, pp. 595–691.
[520] B. M. Koeppen and B. A. Stanton, "2 - Structure and Function of the Kidneys BT - Renal Physiology (Fifth Edition)," Philadelphia: Mosby, 2013, pp. 15–26.
[521] S. Sauk and D. Zuckerman, "Renal Artery Embolization," *Semin. Intervent. Radiol.*, vol. 28, no. 4, pp. 396–406, 2011.
[522] R. W. Schrier, *Schrier's Diseases of the Kidney*. Wolters Kluwer Health, 2012.

Chapter 9. Appendix

9.1. Appendix A

9.1.1. Publications and Presentations

9.1.1.1. Optimisation of a Novel Glass-Alginate Composite for Treatment of Cerebral Aneurysms

Optimisation of a Novel Glass-Alginate Hydrogel for the Treatment of Intracranial Aneurysms

S.A. Brady[a], E.K. Fox[a], C. Lally[b], O.M. Clarkin[a]
[a]School of Mechanical & Manufacturing Engineering, Dublin City University, Dublin 9, Ireland
[b]Mechanical & Manufacturing Engineering, Trinity College Dublin, Dublin 2, Ireland

Abstract

The current gold standard for aneurysm treatment is endovascular coiling. However, recurrence is observed in over 20% of cases. A novel hydrogel has been developed to treat aneurysms. This hydrogel is composed of a polymeric alginate, a novel ion releasing glass and glucono-delta-lactone. This is an internally setting alginate hydrogel, wherein the setting rate can be controlled by both the glass and the alginate chemistry. The aim of this work is to examine the effect of each component of the hydrogel and optimise the composition of the hydrogel, specifically the alginate molecular weight, M/G ratio and concentration. The effects of gamma sterilisation will also be examined. The results show that alginate concentration, chemical composition and molecular weight affect the compressive strength, working time, hardening time and deliverability of the hydrogel. Gamma irradiation of the alginate reduces the molecular weight, which has a negative effect on the usability of this hydrogel.

Keywords

Alginate, molecular weight, chemical composition, concentration, hydrogel, intracranial aneurysm

1. Introduction

An intracranial aneurysm is an irregular out-pouching of a cerebral artery. It is estimated that 1% to 6% of the adult population has an intracranial aneurysm (Brisman et al., 2006). A ruptured aneurysm can lead to stroke, resulting in disability or death. Treatments such as clipping and coiling are currently used to prevent an aneurysm from rupturing; however, there are a number of problems associated with these. Clipping the aneurysm involves a craniotomy and carries the risks of infection and scarring (Brisman et al., 2006). In the United States, the most common treatment method for intracranial aneurysms is coiling. However, recurrence is common, happening in 20.8% of endovascular coiling cases (Crobeddu, Lanzino, Kallmes, & Cloft, 2012), indicating that it is a suboptimal treatment method.

In this study we explore the possibility of delivering a hydrogel which will fill the aneurysm more completely and prevent rupture. This novel hydrogel composite is composed of a polymeric alginate, a novel ion releasing glass and glucono-delta-lactone (GDL).

Ideally, the hydrogel should adhere to the aneurysm wall preventing migration and aneurysm recurrence. Additionally, the hydrogel must be able to withstand a compressive stress of at least 22kPa, which relates to hypertensive blood pressure (Cipolla MJ, 2009). The envisaged hydrogel delivery procedure will involve inflating a compliant balloon adjacent to the aneurysm neck, as with endovascular coiling. The novel hydrogel will then be injected through a micro-catheter into the aneurysm whilst the inflated balloon prevents leakage of the filler into the blood stream (see Figure S 1). To allow for delivery, an optimum working time of between 10 and 30 minutes has been determined by clinical observation (Brady et al. 2017) It has been determined that the novel hydrogel must be set within 5 minutes of injection (based on the maximum inflation time for a balloon in the cerebral vasculature. A balloon inflated for greater than 5 minutes may result in cerebral ischemia (Kim Nelson & Levy, 2001). The alginate sterility must also be considered and this can ordinarily be achieved by moist heat sterilization, gamma-irradiation or ethylene oxide sterilization (Munarin, Bozzini, Visai, Tanzi, & Petrini, 2013).

Alginate is a polysaccharide composed of β-D-mannuronic acid (M) and α-L-guluronic acid (G), giving alginate an M/G block structure. Alginate has the ability to gel when cross-linked with multivalent ions. Alginate is typically described in terms of molecular weight and the M/G ratio. G-rich alginates are stiffer and more brittle than M-rich alginates (Morais et al., 2013).

The role of the glass in this hydrogel is to deliver a steady release of multivalent ions, controlling the rate of gelation and the strength of the hydrogel. The more stable the glass the slower the rate of gelation. A glass that releases a higher quantity of ions will form a stronger hydrogel. Bioactive glasses have also traditionally been used to deliver therapeutic ions, which encourage cell growth and extracellular matrix production. This hydrogel formulation could also, in the future, be used to deliver therapeutic ion doses.

GDL is a lactone that hydrolyses in water to form a gluconic acid, its role in the novel hydrogel is to acidify the solution. This in turn releases multivalent ions, contained in the glass, allowing them to cross-link with the alginate. The gelation rate of the hydrogel can be tightly controlled by both the composition of the glass phase and the ratio of constituent components of the gel. An increased amount of GDL results in increased acidity, causing a more rapid glass ion release and a more rapid gelation.

The aim of this work is to individually vary the concentration of two different alginates, with similar viscosities but differing molecular weights and M/G ratios and to examine the effect on the mechanical properties, sample volume conservation, working time, hardening time and deliverability of a hydrogel. We hypothesise that the strength of the hydrogel will increase with increasing alginate concentration but the sample size will reduce over time due to the increased cross-linking density. Although alginate is a Non-Newtonian liquid that undergoes shear thinning, there will likely be a large increase in viscosity with increasing alginate concentration and this will affect the deliverability of the hydrogel. In addition, the effect of a reduction in molecular weight by sterilisation on the most suitable alginate is subsequently examined. Gamma irradiation is known to

greatly reduce the molecular weight of alginate and will likely cause a significant reduction in the hydrogel's strength. This will also reduce the viscosity which may help with the deliverability of the hydrogel. Gamma irradiation will be chosen as a possible sterilisation technique for future work, provided there is a positive outcome of these results. This optimisation is designed to improve the novel hydrogel's performance for the treatment of cerebral aneurysms.

2. Material and Methods

2.1. Materials

2.1.1. Alginate Purification

All reagents used were purchased from Sigma-Aldrich (Wicklow, Ireland), unless stated otherwise. Two different techniques were used to produce the two different potassium alginates; a medium viscosity High-G content alginate (MVG) and a medium viscosity High-M content alginate (MVM). The hydrogel was purified from a sodium salt and alginate to a potassium alginate to reduce the endotoxin levels found in the supplied alginate (Dusseault et al., 2006). All acid/base solutions were made up in 20 mmol/L of NaCl in deionised water (DI), unless stated otherwise.

MVG was produced by dissolving 8g of a sodium salt from brown algae in 400 mL of DI. The alginate pH was raised to 7.0 by adding a 0.5 M potassium hydroxide (KOH). The alginate was then precipitated by adding 200 mL of methanol per 100 mL of alginate. The alginate was filtered through a 500 µm sieve after 10 minutes. The alginate was then freeze-dried.

MVM was produced by dissolving 9 g of sodium alginate was dissolved in 900 mL of 1 mmol/L sodium EGTA. The solution was then filtered through 11 µm and 2.5 µm filter paper respectively. The alginate was then precipitated on ice by reducing the pH to 1.5 using a 2 M hydrochloric acid (HCl). The alginate was decanted through a 500 µm stainless sieve and stirred 30 minutes in 200 mL of a 0.01 M HCl solution and decanted again. This stirring and decanting was repeated three times. To remove proteins the alginate was stirred for 30 minutes in 100 mL of a 0.01 M HCl solution with 20 mL of chloroform and 5 mL of 1-butanol, and collected in a 500 µm stainless steel sieve. This washing and collecting was repeated three times. 350 mL of DI was added and the pH was raised to 7.0 by adding a 0.5 M KOH. The alginate was stirred in a solution of 20 mL chloroform and 5 mL of 1-butanol per 100 mL of alginate and centrifuged at a rate of 5,000 rpm for 5 minutes. The alginate was then separated using a pipette from the chloroform/1-butanol solution. This washing and centrifuging was repeated once. Finally, the alginate was precipitated by adding 200 mL of ethanol per 100 mL of alginate and filtered after 10 minutes. The alginate was then freeze-dried.

A sample of the porous freeze-dried solid MVM alginate was gamma irradiated at Synergy Healthcare (Westport, Ireland) by exposing the sample to a cobalt 60 source until a final irradiation dose of 25kGy was achieved.

The required amount of freeze-dried alginate, to make the required alginate concentration, was then added to 12 mL of DI.

2.1.2. Glass

The glass had a mole fraction composition of $0.33SiO_2 \bullet 0.18Ga_2O_3 \bullet 0.23CaO \bullet 0.11P_2O_5 \bullet 0.15CaCl_2$. A glass frit of this composition was produced by melting the appropriate raw materials in a platinum 10% rhodium crucible at 1480 °C for 1 hour. The molten mixture was then shock quenched into

water. A glass powder was then produced by grinding 30 g of glass frit using 15 mm diameter zirconia balls in a ball mill (Pulverisette 6 classic Mono planetary ball mill, Fritsch GmbH, Germany) at 500 rpm for 10 minutes. Particles over 500 µm were removed by sieving the glass powder through a 500 µm sieve. 7.5 g of the <500 µm particles were ground in 22.5 mL of DI using 5 mm zirconia balls in a ball mill at 500 rpm for 10 minutes. The glass mixture was dried in the oven at 130 ºC.

2.1.3. Glucono-Delta-Lactone

D-(+)-Gluconic acid δ-lactone was purchased from Sigma Aldrich. The GDL particle size was reduced by grinding 30 g at 500 rpm for 5 minutes using a ball mill. Particle size analysis is shown in Figure S 2.

2.1.4. Hydrogel preparation

The required amount of freeze-dried alginate was dissolved in 1.2 mL of DI. The novel hydrogel was produced by mixing 4.6% of glass powder, 50 mg of GDL with the 1.2 mL of the alginate solution for 1 minute, unless otherwise stated. Design Expert 9 (Stat-Ease, Minneapolis, USA) was used to determine the four alginate concentrations to be tested; 0.5%, 2.5%, 4.5% and 6.0%.

2.2. Methods

2.2.1. Alginate Characterisation

Gel permeation chromatography (GPC) and nuclear magnetic resonance spectroscopy (^{1}H NMR) were carried out as follows in order to characterise the alginates produced.

GPC was carried out using a liquid chromatography system (Agilent 1200, Agilent, USA) equipped with a Suprema Linear GPC column (PSS, Germany). The mobile phase used consisted of 0.1 M disodium hydrogen phosphate containing 0.5 g/L of sodium nitrate buffered to pH 9. All samples were injected at a concentration of 1 mg/mL, at a flow rate of 0.5 mL/min. Pullulan standards were used to construct the calibration curves as alginate standards are not available. This is not an ideal standard as it can overestimate the molecular weight (Andersen, Strand, Formo, Alsberg, & Christensen, 2012). However, they are commonly used in determining molecular weights of alginates with a refractive index detector (Aida, Yamagata, Watanabe, & Smith, 2010; Barbetta, Barigelli, & Dentini, 2009; Ding, Zhou, Zeng, Wang, & Shi, 2017).

^{1}H NMR analysis of the potassium alginate was carried out using a modified version of the standard ASTM F2259–03. The alginate solution was prepared by mixing the alginate to a 0.1% (w/v) in DI. HCl was used to bring the alginate pH to 5.6 and the alginate solution was stored in a water bath at 100 °C for 1 hour. HCl was used to further adjust the pH of the alginate to 3.8. The solution was stored again in a water bath at 100°C for 30 minutes. The pH was then raised to 7 using NaOH and the alginate was freeze dried. The alginate was then dissolved in 5 mL of 99% D_2O and freeze dried overnight. 12 mg of alginate was dissolved in 1 mL of D_2O and placed in a NMR tube. The NMR of the alginate was tested using a Bruker Advance 400 (Bruker, Massachusetts, USA) at 80°C. 64 scans were carried out using a 2s relaxation delay. The M-block, G-block and alternating block sequences content were then calculated as per the equations in ASTM F2259-03 using the produced spectrum.

2.2.2. Viscosity

The viscosity of each alginate at varying concentrations was determined at 24ºC using a SV-10 tuning forks Vibro Viscometer (A&D Company, Japan)

running a sine wave formation at a constant frequency of 30Hz and amplitude of less than 1 mm. The viscometer measures up to 10,000 mPa.s.

2.2.3. Volume Conservation

To examine whether the 1.2 mL hydrogel volume was conserved over time, the samples volumes were measured after storage in 20 mL of DI for 1, 3 and 7 days. The hydrogel was mixed and poured into a cylindrical mould (10 mm diameter and 14 mm height). The hydrogel was left to set for 1 hour and incubated in DI at 37°C for the required amount of time. After the required time the hydrogel was removed from the DI and dimensions were measured using callipers. 'Volume conservation' was calculated by calculating the change in volume compared to the original (pre-incubated) volume.

2.2.4. Compression testing

To examine the mechanical properties of the novel hydrogel, compression testing was carried after storing the novel hydrogel for 7 days in DI. The compression testing samples were made as described above. After the required amount of time the hydrogel sample was compressed using a mechanical testing machine (Z005, Zwick Roell, Germany) equipped with a 5 kN load cell. A 0.005 N pre-load was applied. The samples were compressed up to 70% strain at a crosshead speed of 2 mm/min.

2.2.5. Working and Hardening Time

The working and setting time of each alginate was determined using a modified version of ISO 9917. The setting time was found by mixing the hydrogel and placing a circular indenter (diameter: 6 mm, weight: 20 g) on the sample every 60 seconds. The hydrogel was considered set when it held the indenter without causing an indentation in the hydrogel.

The working time was determined by stirring the hydrogel every 1 minute until the hydrogel would not return to its original shape.

The hardening time is defined as the difference between the setting time and working time of the hydrogel.

2.2.6. Deliverability

The deliverability of each alginate was tested by injecting the hydrogel by hand at the varying alginate concentrations through a 3F micro catheter, using a quick stop syringe.

The optimum hydrogel was then injected through a 2.7F micro-catheter into a silicone side wall aneurysm, (neck size of 2.5 x 6 mm, model H+N-S-A-005, Elastrat, Switzerland). A pulsatile blood pump (1423, Harvard Apparatus, Mass., USA) was used to pump a 36:64 water:glycerol solution through the aneurysm and to provide physiologically correct blood pressure (140/80 mmHg) and flow rates (700 mL l/min). The pressure was measured at the aneurysm inlet and outlet using pressure transducers (DTX Plus Disposable Pressure Transducer, Argon) which was amplified using a bridge analogue input (NI9237, National Instrument) and the pressure was monitored using LabView. A 5 mm diameter balloon (Trek, Abbott) was inflated adjacent to the aneurysm neck, to facilitate placement.

2.2.7. Statistical analysis

Student T-tests ($p<0.05$) and ANOVA with Bonferroni's post hoc test was carried out using IBM SPSS (IBM, Armonk, NY).

3. Results

3.1. Effect of alginate molecular weight and chemical composition

3.1.1. Alginate Characterisation

GPC was carried out to determine the molecular weight (MW) of each alginate and ^{1}H NMR spectra of the alginates were used to determine the guluronic acid (F_G), mannuronic acid (F_M) and alternating block (F_{GM}) fractions, which were calculated as per ASTM F2259 – 03.

Table 1 gives the calculated results of the alginates produced; see Figure S 3 and Figure S 4 for graphs. MVG produced a low molecular weight (60kDa) alginate with a High-G content. MVM produced a high molecular weight (700kDa) alginate with a High-M content.

3.1.2. Volume Conservation

The volume of the samples with a low alginate concentration reduced in size, see Figure 1. A 4.5% alginate concentration approximately maintains its size or slightly expands (<5%) whilst the samples at the 6.0% alginate concentration expanded after 7 days.

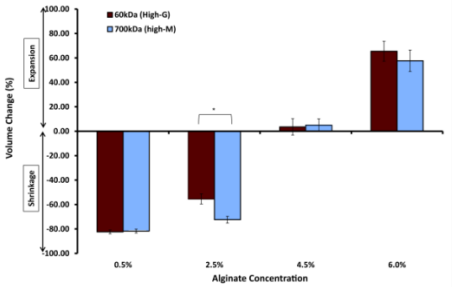

Figure 1 Volume conservation after storage for 7 days in DI at 37°C (n=5)

3.1.3. Viscosity

Both alginates have a similar viscosity at each concentration and the viscosity increases with increasing alginate concentration (Figure S 5). Both the alginates have viscosity greater than 10,000 mPa.s at the 6.0% alginate concentration.

3.1.4. Compression testing

Both hydrogel compositions at each concentration far exceed the minimum compressive strength (22 kPa) required.

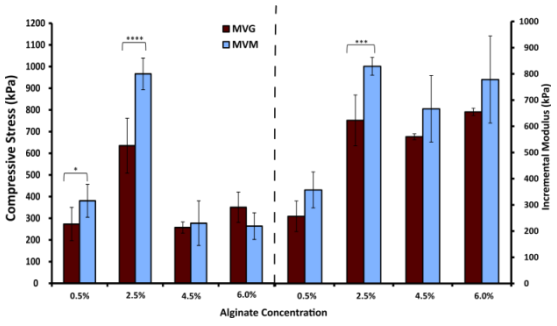

Figure 2 (a) Compressive stress up to 70% strain and (b) Incremental modulus (30 to 50% strain) of the alginates at the 4 concentrations after storage for 7 days in DI at 37°C

The strength of the hydrogel was observed to increase from 0.5% to 2.5% alginate concentration. This was expected to continue with increased alginate concentration, as observed elsewhere (Draget, Skjåk Bræk, & Smidsrød, 1994; C K Kuo & Ma, 2001; Becker, Kipke, & Brandon, 2001), however, this is not observed here. The decreased strength observed at 4.5% and 6.0% may be caused by shortage of cross-linking cations. As there is no increase in GDL or glass content there will be no increase in ion availability to cross-link with increasing number of chains provided by the increased alginate concentration.

Figure 3 shows that increasing the glass content increases the modulus and strength of the hydrogel at a 4.5% alginate concentration. Increasing the glass content from 4.6% to 9.2% more than doubles both the strength and modulus of the

Sample	Molecular weight	F_G	F_M	M/G	F_{GG}	F_{MM}	F_{GM}	$\bar{N}_{G>1}$
MVG	60kDa	0.52	0.48	0.92	0.38	0.33	0.14	7.08
MVM	700kDa	0.37	0.63	1.7	0.18	0.45	0.18	3.59

hydrogel, with no further increase being observed with further glass addition (13.8%). This may be increased further with an increase in GDL content.

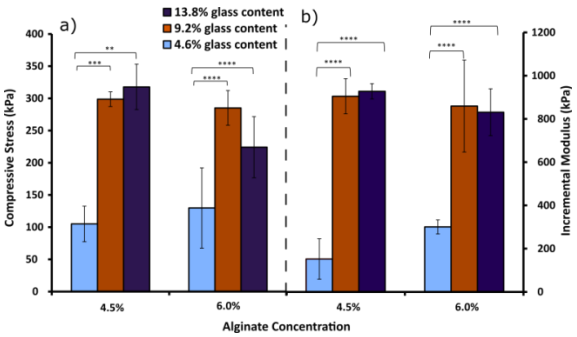

Figure 3 (a)Compressive stress up to 70% strain and (b) Incremental modulus (30 to 50% strain) of 4.5% and 6.0% MVM alginate with 50 mg GDL and an increased glass content after storage for 1 day in DI at 37°C (n=5)

3.1.5. Working Time and Hardening Time

Figure 4 shows the working and hardening time of each composition. For both alginates only the 4.5% and 6.0% alginate concentrations are within the required working and hardening time. There is an approximately linear decrease in working time for the MVG and MVM alginate (R^2 = 0.91 and R^2 = 0.94, respectively) and hardening time for the MVM alginate (R^2 = 0.93) with increasing alginate concentration. As there is no significant difference between the 0.5% and 2.5% hardening time ($p < 0.05$), there is not a linear reduction for the MVG alginate.

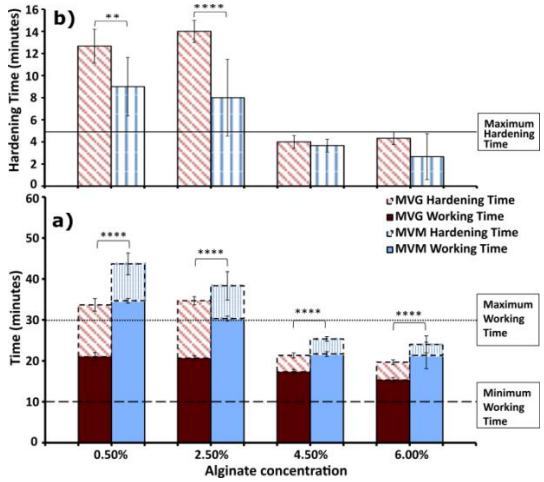

Figure 4 Alginate a) working and b) hardening time (n=5)

3.1.6. Deliverability

The alginate concentration of 0.5% (either MVG or MVM) gave insufficient viscosity (41-44mPas) to remain in the aneurysm when blood flow was applied. The 2.5% and 4.5% alginate concentration of both MVG and MVM alginates (<10,000 mPa.s) would inject through the micro-catheter easily, up to 20 minutes after mixing. The MVG and MVM alginates at 6.0% alginate concentration (>10,000 mPa.s) would not inject through the micro-catheter, blocking it 2 minutes after mixing the hydrogel.

As the 4.5% concentration of the MVM alginate had the correct strength, sufficient volume conservation, and correct working and hardening times it was selected to inject into the aneurysm model. With the balloon inflated and the flow pump on, the hydrogel was injected into the 10 mm aneurysm with a 2.5x2.5 mm neck two minutes before the end of the working time (22 minutes after mixing). The hydrogel was fully injected by the working time and the balloon remained inflated for two minutes. The hydrogel stayed within the aneurysm and remained in the aneurysm with no perceptible erosion once the balloon was deflated for the time tested (30 minutes).

3.2. Effect of Gamma Irradiation

As previously stated, the MVM alginate was the more suitable of the two alginates examined for treatment of cerebral aneurysms and hence was selected for gamma irradiation. A sample of the alginate was gamma irradiated by Synergy Healthcare (Westport, Ireland) at 25kGy to examine the effects of a change in molecular weight alone and for sterilisation purposes.

3.2.1. Alginate Characterisation

GPC and ^{1}H NMR showed that gamma irradiation causes a reduction in alginate

molecular weight to 180kDa without a change to the alginate chemical composition (Table 1).

3.2.2. Volume Conservation

Figure 5 shows that, again, the lower irradiated alginate concentrations shrink in volume whilst the 6.0% alginate concentration increases in volume over 7 days for both alginates. The 4.5% alginate concentration has minimal expansion in volume.

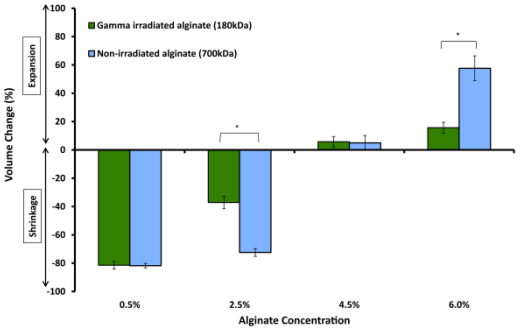

Figure 5 Volume conservation after storage for 7 days in DI at 37°C (n=5)

3.2.3. Viscosity

The results show that gamma irradiation reduces alginate viscosity, with values ranging from 2.83 to 86.43 mPa.s. The viscosity increases by approximately 6.25 mPa.s for each 1% increase in alginate concentration for the gamma irradiated alginate, see Figure S 8.

3.3. Compression testing

Reduction in molecular weight caused by gamma irradiation greatly affects the compressive stress and incremental modulus of the hydrogel compared to the non-irradiated sample ($p > 0.05$). Although the gamma irradiated alginate has a compressive strength that exceeds the limit discussed in the introduction (22 kPa), the incremental modulus of the alginate decreases with increasing alginate concentration and at each concentration has a decreased strength compared to the non-irradiated alginate, see Figure 6.

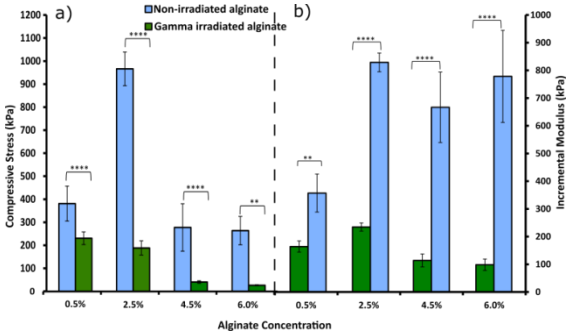

Figure 6 (a) Compressive stress up to 70% strain and (b) Incremental modulus (30 to 50% strain) of irradiated and non-irradiated alginate compositions after storage for 7 days in DI at 37°C

3.3.1. Working Time and Hardening Time

The reduction in molecular weight of the gamma irradiated alginate significantly increases the working and hardening time ($p > 0.05$), see Figure 7. The working and hardening times decrease linearly with increasing alginate concentration for both irradiated and non-irradiated samples, i.e. R^2 = 0.91, 0.91 and R^2 = 0.91, 0.92, respectively. However, at each concentration test, the gamma irradiated alginate is not within the time limits for its intended application.

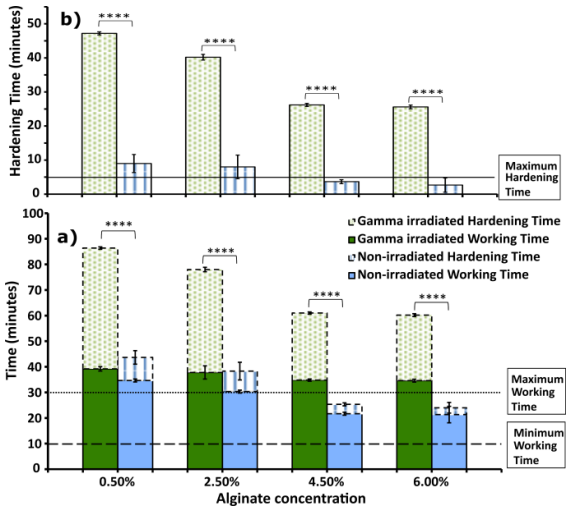

Figure 7 Hydrogel a) working and b) hardening time (n=5)

3.3.2. Deliverability

None of the gamma irradiated alginate concentrations had sufficient viscosity to remain in the aneurysm when blood flow was applied, similar to that of the 0.5%

alginate concentration of the non-irradiated alginate.

4. Discussion

From the GPC and ^{1}H NMR results we can see that two different alginates were produced, a MVM with a high molecular weight and a MVG with a low molecular weight. Though the molecular weight of the MVG alginate is over ten times less than that of the MVM alginate, the viscosities are similar (Figure S 5). This is not typical but may be due to differences in M/G ratios and G-block length, with higher G content and length alginates being typically stiffer and more viscous compared to alginates with a High-M content (Jothisaraswathi & Rengasamy, 2006; Nedovic & Willaert, 2013; Schmid, Fariña, Rehm, & Sieber, 2016; Smith & Miri, 2011). It has been shown that varying the alginate purification method results in alginates with significantly different viscosities. The varying alginates and purification methods used here may have an additional effect on the viscosity of the alginate due variances in residual salts and impurities and the resulting pH of the alginate solution (Dusseault et al., 2006; K. Y. Lee & Mooney, 2012; McHugh, 2003).

It is clear from the results that the cross linking density of the hydrogel is important to control the strength and volume conservation. At the 0.5% alginate concentration there is likely a shortage of alginate chains and an excess of cations. At a 4.5% and 6.0% alginate concentration there is a shortage of cross-linking ions and, as a result, there are alginate chains that are not optimally cross-linked.

The sample volume conservation exhibits results similar to those described by Kuo *et al* (Catherine K Kuo & Ma, 2008). At a 0.5% and 2.5% alginate concentration the samples shrink and the 4.5% and 6.0% alginate concentration samples expand (Figure 1). This may be due to the hydrogel's cross-linking density decreasing with increasing alginate concentration as a result of the glass content, and hence ion content, remaining constant. The lower concentration alginates have an increased cross-linking density. This increased cross-linking increases the elastic forces that can resist the swelling caused by water molecules diffusing into the hydrogel. As the concentration increases the cross-linking density decreases allowing water to diffuse through the hydrogel and swell. Neither significant shrinkage nor expansion is desired, as shrinkage may contribute to aneurysm recurrence and excessive sample expansion may cause aneurysm rupture. Samples produced from 4.5% alginate concentration exhibit minimal swelling, which suggests that this alginate concentration provides a cross-linking density that provides a high strength while conserving sample volume.

For both the MVG and MVM alginate the incremental modulus and compressive strength increase from 0.5% to 2.5% alginate concentration (Figure 2). The incremental modulus and compressive strength then decreases with further increased alginate concentration (≥2.5%). The decrease above 2.5% alginate was unexpected and may be due to a shortage of cross-linking ions. This shortage of ions may reduce the cross-linking density and result in an inhomogeneous hydrogel that is prone to fracture. To explore this further, the glass content was increased. This increased the strength for the 4.5% and 6.0% alginate concentration whereby the increase in cations provided a higher cross-linking density (Figure 3). For each of the concentrations, the MVM alginate had the highest modulus and compressive strength for each alginate concentration.

Typically, the High-G alginate would have the higher strength (Draget et al., 1994); however, the increased molecular weight of the MVM alginate may compensate for the lower G-block content and provides increased entanglements.

Though the MVG alginate has the shortest working time, the MVM alginate has the shortest hardening time at each alginate concentration (Figure 4). This indicates that the working time is governed mostly by the chemical composition of the alginate with a High-G content providing a decreased working time. The hardening time of the alginate is governed mainly by the molecular weight of the alginate with a high molecular weight alginate having decreased hardening time. Increasing the alginate concentration of each alginate provides an increased number of ionic cross-linking locations and increased likelihood of chain entanglements, causing working and hardening time to reduce in each hydrogel.

The deliverability of the hydrogel can be determined from the viscosity, with ungelled alginates up to 9,000 mPa.s being injectable through a micro-catheter. For the intended applications of this hydrogel; the strength, conservation of sample volume, working time and hardening time, along with the deliverability of this hydrogel must be considered. The 4.5% concentration of the MVM alginate met each of the requirements and was tested in an aneurysm model with physiological pressures. This hydrogel remained in the aneurysm without migrating.

Gamma irradiation of the MVM alginate was shown to have no effect on the M/G ratio of the alginate. However, it does cause scissions of the glycosidic bonds, which reduces the molecular weight of the alginate.

As expected, viscosity was seen to decrease with gamma irradiation of the MVM alginate, as expected, due to decreased chain entanglements (Dusseault et al., 2006; C K Kuo & Ma, 2001; Ouwerx, Velings, Mestdagh, & Axelos, 1998; Popeski-Dimovski, Rendevski, & Mahmudi, 2012).

From the alginate working and hardening time data it can be seen that the gamma irradiated alginate has the longest working and hardening time due to the High-M content and low molecular weight having a reduced number of ionic cross-linking locations (Popeski-Dimovski et al., 2012). Although usability of the gamma irradiated alginate may be improved by increasing alginate concentration and optimising the glass and GDL content, an alternative method of sterilization may be more efficient, such as sterilisation by filtration in a sterile manufacturing environment.

A range of injectable polymer formulations have been developed for soft tissue applications but many contain toxic monomers, activators and free radicals. The gelation rate of the hydrogel described here is slow compared to other alginate hydrogels (Larsen, Bjørnstad, Pettersen, Tønnesen, & Melvik, 2015; Lee et al., 2003), which allows the hydrogel to be delivered and set, within a clinically applicable time.

Though GDL can be used with alginate to produce acid gels, this is likely not the case with the current hydrogel due to the high strengths and relatively rapid gelation rates observed. The addition of GDL results in a reduced pH during setting, which may affect the hydrogel's biocompatibility. The pH of the storage medium drops by 0.50 with the 4.5% High-M alginate. However, the presence of alkali ions in the bioactive glass has a neutralizing effect over 24 hours. It should

be noted that this temporary reduction in pH, as occurs with many synthetic biomaterials, may result in an increased inflammatory and fibrotic response *in vivo* (Edgar et al., 2016).

For an aneurysm filler to be effective it should have sufficient strength in order to behave similarly to native cerebral tissue; diverting flow and withstanding haemodynamic stresses caused by arterial expansion and contraction and blood flow forces (static, dynamic and shear). A low elastic modulus is required to insure stress caused by blood flow is not transferred to the damaged tissue, causing aneurysm rupture. A calcium alginate gel that was designed for embolization was reported to have a compressive strength of 124kPa at 60% strain (Becker et al., 2001). Onyx®, is a non-adhesive material approved for the treatment of cerebral aneurysms in Europe, has been observed to have a maximum compressive strength of 3 MPa (Ohyama, Ko, Miura, Iwata, & Taki, 2004). However, Onyx® sets rapidly when in contact with blood, which combined with the slow injection rate, is not ideal for placement.

The optimised hydrogel in this study exhibits a compressive strength of 280 kPa. Although it is not equal in strength to Onyx®, it may act to support the existing tissue in its function, without transferring excessive stress to the damaged tissue. The optimised hydrogel reported herein has higher incremental modulus and compressive strength compared to those of other ionically cross-linked alginate hydrogels described in the literature at similar alginate concentrations and chemical compositions (Becker et al., 2001; C K Kuo & Ma, 2001). This novel material reported herein likely has a greater mechanical integrity than the currently used coil technology that can compact with blood flow, which though not optimal, continues to function in this mechanical environment (Gallas et al., 2009; Sluzewski et al., 2004).

Agglomerates were clearly visible in the hydrogel both during and after setting, which may affect consistency of strength and setting, therefore, future testing will be carried out to minimise these agglomerates. The adhesive nature of the hydrogel will also be examined as this is important to reduce aneurysm recurrence. Further optimisation of the sterilisation techniques for each hydrogel component of the hydrogel will also need prior to commercial application.

5. Conclusion

From the results it can be seen that alginate concentration, molecular weight and chemical composition affect the sample volume conservation, viscosity, strength, deliverability, working and hardening time of the novel hydrogels. An alginate with an increased molecular weight and High-M content provides a hydrogel with an increased working time and decreased hardening time while providing the required strength which is advantageous for a cerebral aneurysm filler. Alginates with a viscosity between 2,000 mPa.s and 9,000 mPa.s can be injected through a micro catheter while providing sufficient viscosity to remain within an aneurysm without migration.

Sterilisation by gamma irradiation causes a reduction of molecular weight which decreases the alginate's viscosity and strength and increases the hydrogel's working and hardening time. This is undesirable for the treatment of cerebral aneurysms. For this application, an alternative, less aggressive method of sterilisation will be required.

Acknowledgements

This work was supported by Enterprise Ireland Commercialization Fund through the grant CF/2013/3364.

References

Aida, T. M., Yamagata, T., Watanabe, M., & Smith, R. L. (2010). Depolymerization of sodium alginate under hydrothermal conditions. Carbohydrate Polymers, 80(1), 296–302. http://doi.org/10.1016/j.carbpol.2009.11.032

Andersen, T., Strand, B. L., Formo, K., Alsberg, E., & Christensen, B. E. (2012). Chapter 9 Alginates as biomaterials in tissue engineering. In Carbohydrate Chemistry: Volume 37 (Vol. 37, pp. 227–258). The Royal Society of Chemistry. http://doi.org/10.1039/9781849732765-00227

Barbetta, A., Barigelli, E., & Dentini, M. (2009). Porous Alginate Hydrogels: Synthetic Methods for Tailoring the Porous Texture. Biomacromolecules, 10(8), 2328–2337. http://doi.org/10.1021/bm900517q

Becker, T. A., Kipke, D. R., & Brandon, T. (2001). Calcium alginate gel: A biocompatible and mechanically stable polymer for endovascular embolization. Journal of Biomedical Materials Research, 54(1), 76–86. http://doi.org/10.1002/1097-4636(200101)54:1<76::AID-JBM9>3.0.CO;2-V

Brady, S. A., Fox, E. K., Lally, C., & Clarkin, O. M. (n.d.). Surface modification of a novel glass to optimise strength and deliverability of an injectable alginate composite. Journal of Materials Science. http://doi.org/https://doi.org/10.1007/s10853-017-1466-y

Brisman, J. L., Song, J. K., & Newell, D. W. (2006). Cerebral Aneurysms. New England Journal of Medicine, 355(9), 928–939. http://doi.org/10.1056/NEJMra052760

Cipolla MJ. (2009). Control of Cerebral Blood Flow. In The Cerebral Circulation. San Rafael (CA): Morgan & Claypool Life Sciences.

Clarkin, O. (2017). Biomaterial Research Group. Retrieved from www.biomaterials.ie

Crobeddu, E., Lanzino, G., Kallmes, D. F., & Cloft, H. J. (2012). Review of 2 Decades of Aneurysm-Recurrence Literature, Part 2: Managing Recurrence after Endovascular Coiling. American Journal of Neuroradiology . http://doi.org/10.3174/ajnr.A2958

Ding, W., Zhou, J., Zeng, Y., Wang, Y., & Shi, B. (2017). Preparation of oxidized sodium alginate with different molecular weights and its application for crosslinking collagen fiber. Carbohydrate Polymers, 157, 1650–1656. http://doi.org/10.1016/j.carbpol.2016.11.045

Draget, K. I., Skjåk Bræk, G., & Smidsrød, O. (1994). Alginic acid gels: the effect of alginate chemical composition and molecular weight. Carbohydrate Polymers, 25(1), 31–38. http://doi.org/10.1016/0144-8617(94)90159-7

Dusseault, J., Tam, S. K., Menard, M., Polizu, S., Jourdan, G., Yahia, L., & Halle, J.-P. (2006). Evaluation of alginate purification methods: effect on polyphenol, endotoxin, and protein contamination. Journal of Biomedical Materials Research. Part A, 76(2), 243–251. http://doi.org/10.1002/jbm.a.30541

Edgar, L., McNamara, K., Wong, T., Tamburrini, R., Katari, R., & Orlando, G. (2016). Heterogeneity of Scaffold Biomaterials in Tissue Engineering. Materials, 9(5).

Gallas, S., Januel, A. C., Pasco, A., Drouineau, J., Gabrillargues, J., Gaston, A., Herbreteau, D. (2009). Long-term follow-up of 1036 cerebral aneurysms treated by bare coils: a multicentric cohort treated between 1998 and 2003. AJNR. American Journal of Neuroradiology, 30(10), 1986–1992. http://doi.org/10.3174/ajnr.A1744

Jothisaraswathi, S., & Rengasamy, B. B. R. (2006). Seasonal studies on alginate and its composition II: Turbinaria conoides (J.Ag.) K¨utz. (Fucales, Phaeophyceae). J Appl Phycol. http://doi.org/DOI 10.1007/s10811-006-9089-8

Kim Nelson, P., & Levy, D. I. (2001). Balloon-assisted Coil Embolization of Wide-necked Aneurysms of the Internal Carotid Artery: Medium-term Angiographic and Clinical Follow-up in 22 Patients. American Journal of Neuroradiology, 22(1), 19–26. Retrieved from http://www.ajnr.org/content/22/1/19.abstract

Kuo, C. K., & Ma, P. X. (2001). Ionically crosslinked alginate hydrogels as scaffolds for tissue engineering: Part 1. Structure, gelation rate and mechanical properties. Biomaterials, 22. http://doi.org/10.1016/S0142-9612(00)00201-5

Kuo, C. K., & Ma, P. X. (2008). Maintaining dimensions and mechanical properties of ionically crosslinked alginate hydrogel scaffolds in vitro. Journal of Biomedical Materials Research Part A, 84A(4), 899–907. http://doi.org/10.1002/jbm.a.31375

Larsen, B. E., Bjørnstad, J., Pettersen, E. O., Tønnesen, H. H., & Melvik, J. E. (2015).

Rheological characterization of an injectable alginate gel system. BMC Biotechnology, 15(1), 1–12. http://doi.org/10.1186/s12896-015-0147-7

Lee, D. W., Choi, W. S., Byun, M. W., Park, H. J., Yu, Y.-M., & Lee, C. M. (2003). Effect of gamma-irradiation on degradation of alginate. Journal of Agricultural and Food Chemistry, 51(16), 4819–4823. http://doi.org/10.1021/jf021053y

Lee, K. Y., & Mooney, D. J. (2012). Alginate: properties and biomedical applications. Progress in Polymer Science, 37(1), 106–126. http://doi.org/10.1016/j.progpolymsci.2011.06.003

McHugh, D. J. (2003). Alginate. In A guide to the seaweed industry (pp. 39–50). Food and Agriculture Organization of the United Nations.

Morais, D. S., Rodrigues, M. A., Silva, T. I., Lopes, M. A., Santos, M., Santos, J. D., & Botelho, C. M. (2013). Development and characterization of novel alginate-based hydrogels as vehicles for bone substitutes. Carbohydrate Polymers, 95(1), 134–42. http://doi.org/10.1016/j.carbpol.2013.02.067

Munarin, F., Bozzini, S., Visai, L., Tanzi, M. C., & Petrini, P. (2013). Sterilization treatments on polysaccharides: Effects and side effects on pectin. Food Hydrocolloids, 31(1), 74–84. http://doi.org/10.1016/j.foodhyd.2012.09.017

Nedovic, V., & Willaert, R. (2013). Alginate as a Carrier for Cell Immobilisation. In Fundamentals of Cell Immobilisation Biotechnology (pp. 33–53). Springer Netherlands. Retrieved from https://books.google.ie/books?id=ts7tCAAAQBAJ

Ohyama, T., Ko, I. K., Miura, A., Iwata, H., & Taki, W. (2004). ProNectin F-grafted-ethylene vinyl alcohol copolymer (EVAL) as a liquid type material for treating cerebral aneurysm--an in vivo and in vitro study. Biomaterials, 25(17), 3845–52. http://doi.org/10.1016/j.biomaterials.2003.10.021

Ouwerx, C., Velings, N., Mestdagh, M. ., & Axelos, M. A. . (1998). Physico-chemical properties and rheology of alginate gel beads formed with various divalent cations. Polymer Gels and Networks, 6(5), 393–408. http://doi.org/10.1016/S0966-7822(98)00035-5

Popeski-Dimovski, R., Rendevski, S., & Mahmudi, N. (2012). Change in Gellation Time of Sodium Alginate Biopolymer Hydrogels with Change of Dose of Gamma Irradiation. Physica Macedonica 61, 67–72.

Schmid, J., Fariña, J., Rehm, B., & Sieber, V. (2016). Alginate-modifying enzymes: biological roles and biotechnological uses. In Microbial Exopolysaccharides: From Genes to Applications: (pp. 70–79). Retrieved from https://books.google.ie/books?id=EJFADgAAQBAJ

Sluzewski, M., van Rooij, W. J., Slob, M. J., Bescós, J. O., Slump, C. H., & Wijnalda, D. (2004). Relation between Aneurysm Volume, Packing, and Compaction in 145 Cerebral Aneurysms Treated with Coils. Radiology, 231(3), 653–658. http://doi.org/10.1148/radiol.2313030460

Smith, A. M., & Miri, T. (2011). Alginates in Foods. In Practical Food Rheology (pp. 113–132). Wiley-Blackwell. http://doi.org/10.1002/9781444391060.ch6

Supplementary Material

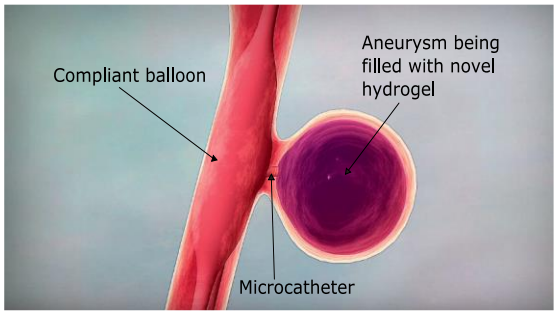

Figure S 1 Schematic of novel hydrogel being injected into a cerebral aneurysm [17]

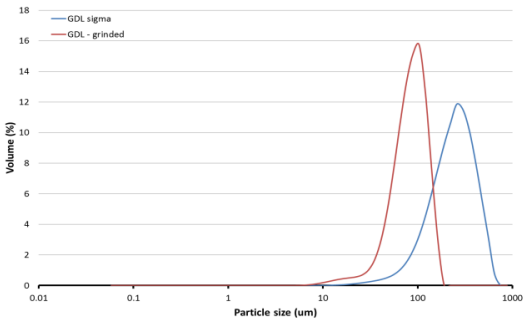

Figure S 2 Particle Size Analysis of GDL purchased from sigma before and after grinding

Effect of alginate molecular weight and chemical composition

Alginate Characterisation

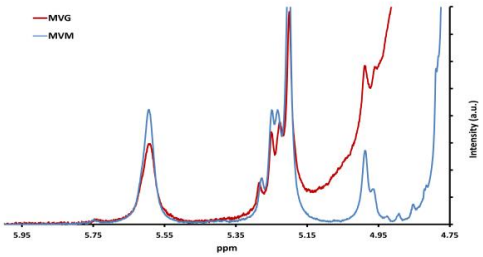

Figure S 3 ^{1}H NMR of MVG and MVM alginate

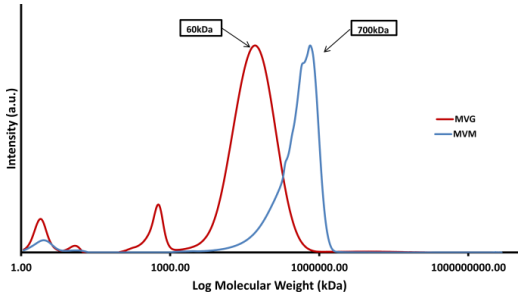

Figure S 4 GPC of MVG and MVM alginate

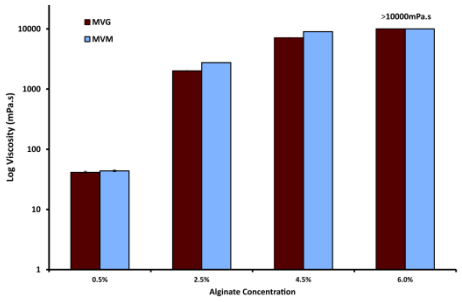

Figure S 5 Viscosity of the alginates at each of the four concentrations (n=5)

Effect of Gamma Irradiation

Alginate Characterisation

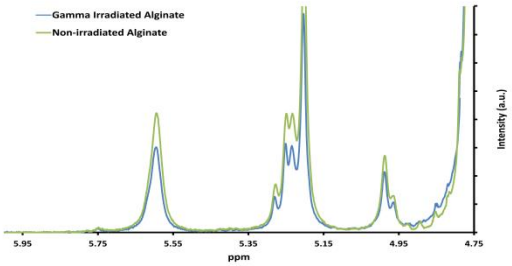

Figure S 6 ^{1}H NMR of gamma irradiated and non-irradiated alginate

The GPC, Figure S 7, shows that gamma irradiation causes scissions of the glycosidic bonds, reducing the molecular weight of the alginate.

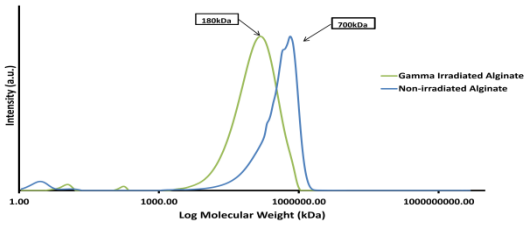

Figure S 7 GPC of gamma irradiated and non-irradiated alginate

Using Equation S1 it was calculated that gamma irradiation causes approximately 3.3 chain breaks per molecule.

$$N = \frac{M_o}{M} - 1$$

Equation S 1 Calculating chain breaks per molecule

Where M_o is the original molecular weight and M is the molecular weight of the alginate following irradiation.

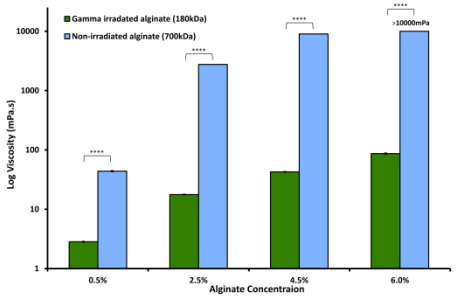

Figure S 8 Viscosity of alginates at each of the four concentrations (n=5)

9.1.1.2. Surface Modification of a Novel Glass for an Optimised Dispersion and Strength of an Injectable Alginate Composite

Surface Modification of a Novel Glass to Optimise Strength and Deliverability of an Injectable Alginate Composite

S.A. Brady[1], E.K. Fox[1], F.R. Laffir[2], B. Phelan[3], A. O'Hare[4], C. Lally[5], O.M. Clarkin[1]
[1]School of Mechanical & Manufacturing Engineering, Dublin City University, Dublin 9, Ireland
[2]Materials and Surface Science Institute, University of Limerick, Limerick, Ireland
[3]South Eastern Applied Materials Research Centre, Waterford Institute of Technology, Waterford, Ireland
[4]Department of Neuroradiology, Beaumont Hospital, Dublin, Ireland
[5]Mechanical & Manufacturing Engineering, Trinity College Dublin, Dublin 2, Ireland

Abstract
It is estimated that 1% to 6% of the adult population have an intracranial aneurysm. Aneurysm coiling is the current preferred treatment method; however, over 20% of coiled aneurysms recur. A novel glass-alginate composite hydrogel has been developed to treat aneurysms, which is designed to completely fill the aneurysm space and prevent aneurysm recurrence. This hydrogel is composed of a polymeric alginate, a novel bioactive glass and glucono-delta-lactone. This novel injectable hydrogel exhibits characteristics suitable for the treatment of cerebral aneurysms. However, poor hydrophilicity of the glass phase results in inhomogeneity and agglomerate formation within the composite, resulting in sub-optimal deliverability and strength. This study examines the effect of surface modification of the glass particles using an acid washing technique, designed to increase glass surface hydrophilicity resulting in a homogeneous sample. This study found that acid washing of the glass not only decreased agglomeration and inhomogeneity but also lengthened working times and increased strength of the resultant hydrogel. This lengthened working time, allowed for an increased glass content and, as a result, further increased compressive strength and radiopacity of the resultant hydrogel. Glass particle size analysis revealed that the relative quantity of fine particles was reduced. Surface analysis of the glass particles revealed an increase in hydrophilic silanol groups and increased surface network connectivity. These factors, combined with a decreased surface calcium and increased surface gallium content are postulated as the likely reasons for the observed increased strength, working time and hardening time.

Keywords: Alginate, bioactive glass, surface modification, silanol, hydrogel, intracranial aneurysm

1. Introduction

1% to 6% of the adult population has an intracranial aneurysm (IA), which is an irregular out-pouching of a cerebral artery. A ruptured aneurysm can lead to stroke, causing disability or death. Current treatments involve clipping or coiling the aneurysm. Clipping the aneurysm involves a craniotomy and carries the risks of infection and scarring [1]. In the United States the most common treatment of IA's is coiling, however, the biggest problem with coiling is aneurysm recurrence, which happens in 20.8% of endovascular coiling cases [2]. We propose the possibility of using a hydrogel which will fill the aneurysm and prevent rupture. To fill the aneurysm with this novel hydrogel, a compliant balloon will be inflated adjacent to the aneurysm, as with endovascular coiling (Figure 1). The novel hydrogel will then be injected through a micro-catheter into the aneurysm whilst the inflated balloon prevents leakage of

the unset filler into the blood stream. To allow for delivery, an optimum working time of between 10 and 30 minutes has been determined for the novel hydrogel, based on discussion with clinical collaborators. In addition, the novel hydrogel must be set within a maximum of 5 minutes following injection, based on the maximum inflation time for a balloon in the cerebral vasculature. A balloon inflated for greater than 5 minutes will result in cerebral ischemia [3].

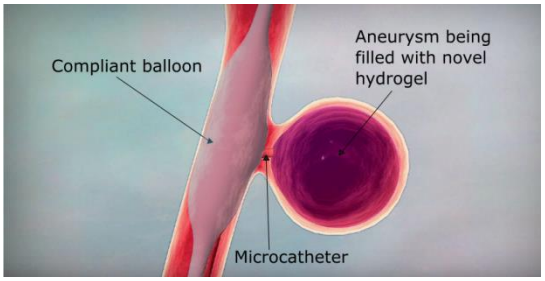

Figure 1 Schematic of novel hydrogel being injected into a cerebral aneurysm [4]

This novel hydrogel composite is composed of a polymeric alginate, a novel bioactive glass and glucono-delta-lactone (GDL).

Alginate is a polysaccharide composed of β-D-mannuronic acid (M) and α-L-guluronic acid (G), giving alginate a M/G block structure. Alginate has the ability to gel when cross-linked with certain multivalent ions. Alginate is typically described in terms of molecular weight and the M/G ratio. G-rich hydrogels are stronger than M-rich hydrogels, but are more brittle [5].

The role of the glass particles is to supply multivalent ions and control the rate of gelation and strength of the hydrogel. A more stable glass will slow the rate of gelation and one that releases more ions into solution will form a more highly cross-linked hydrogel.

GDL is a lactone that hydrolyses in water to form a gluconic acid. Its role in the novel hydrogel is to acidify the solution. This in turn encourages release of multivalent ions from the glass, allowing them to cross-link with the alginate.

Gelation of the hydrogel can be controlled by both the composition of the glass phase and the ratio of constituent components of the hydrogel.

However, it was observed that the novel hydrogel produced had agglomerates caused by the glass clumping together, which is commonly observed [6]. This study examines the effect of acid washing on the structure and composition of the glass sample and the effect that this surface modification has on agglomeration formation, sample homogeneity, compressive strength, working time, hardening time and deliverability of the hydrogel samples. The study uses the modified surface and compositional characteristics to optimise the hydrogel formulation for use in the treatment of cerebral aneurysms.

2. Materials & Methods

2.1. Alginate Production

All reagents used were purchased from Sigma-Aldrich. Alginate was produced and purified by dissolving 9g of sodium alginate in 900ml of 1mmol/l sodium EGTA. The solution was then filtered through 11µm and 2.5µm filter paper respectively. The alginate solution was precipitated on ice by reducing the pH to 1.5 using a 2M hydrochloric acid (HCl), 20mmol/l sodium chloride (NaCl) solution. The alginate was decanted through a 500µm stainless steel sieve and stirred for 30 minutes in 200ml of a 0.01M HCl, 20mmol/l NaCl solution and decanted again. This stirring and decanting was repeated three times. To remove proteins the alginate was stirred for 30 minutes in 100ml of a 0.01M HCl, 20mmol/l NaCl solution with 20ml of chloroform and 5ml

of buthanol, and collected in a 500µm stainless sieve. This washing and collecting was repeated three times. 350ml of deionised water (DI) was added and the pH was raised to 7.0 by adding a 0.5M potassium hydroxide (KOH), 20mmol NaCl solution. The alginate was stirred in a solution of 20ml chloroform and 5ml of buthanol per 100ml of alginate for 30 minutes and centrifuged at a rate of 5000rpm for 5 minutes. The alginate was then separated using a pipette from the chloroform/buthanol solution. This washing and centrifuging was repeated once. Finally, the alginate was precipitated by adding 200ml of ethanol per 100ml of alginate and filtered after 10 minutes. The alginate was then freeze-dried. 0.54g of the freeze dried alginate was added to 12ml of DI to produce a 4.5% alginate solution.

2.2. Glass

The bioactive glass had a composition of $0.33SiO_2 \bullet 0.18Ga_2O_3 \bullet 0.23CaO \bullet 0.11P_2O_5 \bullet 0.15CaCl_2$. The glass frit was produced by melting the raw materials in a platinum 10% rhodium crucible at 1480°C for 1 hour. The molten mixture was then shock quenched into water. A glass powder was then produced by grinding 30g of glass frit using 15mm zirconia balls in a planetary ball mill (Pulverisette 6 classic Mono, Fritsch GmbH, Germany) at 500rpm for 10 minutes. Particles over 500µm were removed by sieving the glass powder through a 500µm sieve. 7.5g of the <500µm particles were mixed with 22.5ml of DI and milled using 5mm zirconia balls in a ball mill at 500rpm for 10 minutes. The glass mixture was dried in the oven at 180ºC.

2.3. Acid Washing Treatment of Glass

7g of glass was stirred in 280ml of 2 vol.% acetic acid for 1 hour. Glass was then centrifuged at 5,000 RPM for 5 minutes and the supernatant was removed. The glass was then stirred in 560ml of DI for 1 hour and then centrifuged at 5,000 RPM for 5 minutes. Glass was then separated and dried in a convection oven at 160˚C for 1.5 hours.

2.4. Glucono-Delta-Lactone

D-(+)-Gluconic acid δ-lactone was purchased from Sigma Aldrich. The GDL was reduced by grinding 30g at 500rpm for 5 minutes using a ball mill and 15mm zirconia balls (Pulverisette 6 classic Mono planetary ball mill, Fritsch GmbH, Germany).

2.5. Hydrogel preparation

The novel hydrogel was produced by mixing 4.6% of glass powder, 50mg of GDL with 1.2ml of alginate for 1 minute, unless otherwise stated. Potassium alginate solutions were made up in bulk prior to mixing.

2.6. Alginate Classification

Gel permeation chromatography (GPC) and proton nuclear magnetic resonance spectroscopy (^{1}H-NMR) was carried out to determine the molecular weight and chemical composition of the alginate respectively.

GPC was carried out on the alginate using a liquid chromatography system (Agilent 1200, Agilent, USA) equipped with a Suprema Linear GPC column (PSS, Germany). The mobile phase used consisted of 0.1M disodium hydrogen phosphate containing 0.5g/l of sodium nitrate buffered to pH 9. All samples were injected at a concentration of 1mg/ml and at a flow rate of 0.5ml/min. Pullulan standards were injected to construct a calibration curve.

^{1}H-NMR of the potassium alginate was tested using a modified version of the standard ASTM F2259–03. The alginate

solution was prepared by mixing the alginate to a 0.1% (w/v) in DI. HCI was used to bring the alginate pH to 5.6 and the alginate solution was stored in a water bath at 100°C for 1 hour. HCl was used to further adjust the pH of the alginate to 3.8. The solution was stored again in a water bath at 100°C for 30 minutes. The pH was then raised to 7 using NaOH and the alginate was freeze dried. The alginate was then dissolved in 5ml of 99% D_2O and freeze dried overnight. 12mg of alginate was dissolved in 1 ml of D_2O and placed in a NMR tube.

The NMR of the alginate was tested using a Bruker Advance 400 (Bruker, Massachusetts, USA) at 80°C. 64 scans were carried out using a 2s relaxation delay. The M/G ratios were then calculated as outlined in ASTM F2259–03.

2.7. Particle Size Analysis

Particle size analysis was carried out using a 632.8nm He-Ne laser Malvern Mastersizer S (Malvern Instruments, Malvern, UK). Particles were pre-sonicated for 15 seconds and analysed in a DI dispersion medium. Laser obscuration was in the range 10-15% and particles were analysed in the range 0.05 μm to 900.00μm.

2.8. Working and Hardening Time

The working time (WT) and setting time (ST) of each alginate was determined using a modified version of ISO 9917. The setting time was found by mixing the hydrogel and placing a circular indenter (diameter: 6mm, weight: 20g) on the sample every 1 minute. The hydrogel was considered set when the hydrogel held the indenter without causing a permanent indentation. The WT was determined by stirring the hydrogel every 1 minute until the hydrogel would not return to its original shape. The hardening time (HT) is defined as the difference between ST and WT of the hydrogel.

2.9. Compression Testing

To examine the mechanical properties of the novel hydrogel, compression testing was carried after storing the novel hydrogel for 1, 3 and 7 days in DI. The novel hydrogel was mixed and poured into a cylindrical mould (10mm diameter and 14mm height). The hydrogel was left to set for 1 hour and stored in DI at 37°C for the required amount of time. After the required amount of time the hydrogel sample was compressed using a mechanical testing machine (Z005, Zwick/Roell, Germany) equipped with a 5kN load cell. A 0.005N pre-load was applied. The samples were compressed up to 70% strain at a crosshead speed of 2mm/min.

2.10. Nitrogen Adsorption/Desorption Measurements

Accelerated surface area and porosimetry measurements were carried out by nitrogen gas adsorption in a Micromeritics Gemini V gas adsorption analyser (Micromeritics, Ottawa, Canada). The surface area was then calculated using Brunauer, Emmett and Teller (BET) and pore size distribution and pore volume were estimated using the Barrett-Joyner-Halenda (BJH) scheme [7].

2.11. Zeta Potential Measurements

Zeta potential measurements were performed at 25°C in DI using a Zetasizer NanoZS (Malvern Instruments, Malvern, UK). The values reported are averages of three measurements, each measurement consisting of an average of >30, 10 second runs.

2.12. X-Ray Photoelectron Spectroscopy

X-Ray Photoelectron Spectroscopy (XPS) was carried out on glass powders in a Kratos Axis 165 Spectrometer (Kratos Analytical, Manchester, UK) using monochromatic Al Kα radiation of energy 1486.6eV. Surface charge was efficiently neutralised by flooding the sample surface with low energy electrons. C 1s peak at 284.8eV was used as the charge reference in determining the binding energies. Elemental analyses were obtained from a survey spectrum scanning the entire binding energy and then high resolution spectra were taken at a number photoelectron transitions, including O_{1s}, Ga_{2p} and Si_{2p}, with a 20eV pass energy. The Ga_{2p} region was chosen instead of the more commonly used Ga_{3d} region to avoid interference of the Ga_{3d} peaks with the O_{2s} peak. Photoelectrons were collected at a normal take off angle relative to the sample surface. Construction and peak fitting in the narrow range spectra used a Shirley type background and the synthetic peaks were of a mixed Gaussian-Lorenzian type.

2.13. Attenuated Total Reflectance-Fourier Transform Infrared Spectroscopy (ATR-FTIR)

Glass samples were analysed using a Spectrum 100 ATR-FTIR (Perkin Elmer, Waltham, USA) equipped with Grams Analyst data analyser. All spectra were obtained between 600 and 4000cm^{-1} at 4cm^{-1} resolution after averaging four scans.

2.14. Field emission scanning electron spectroscopy (FE-SEM)

Glass samples were embedded in graphene resin, attached to sample stubs and analysed using a Hitachi S5500 (Hitachi, Tokyo). Images were captured at 100,000X magnification. An accelerating voltage of 25kV and a current of 4300nA were applied.

2.15. X-ray Microtomography

X-ray Microtomography (XMT) was carried out using a Phoenix Nanotom S (GE Measurement & Control Solutions, Billerica, USA) in order to determine the homogeneity and radiopacity of the glass particles in the hydrogel. A voltage of 80kV and a current of 220μA were maintained to achieve a voxel size of 4.30μm. A 4.725mm^3 image was taken for 3D XMT.

To determine the radiopacity of the samples, ImageJ (National Institutes of Health, MD) was used to find the mean greyscale value of the 2D XMT samples. Note: 255=White and 0=Black.

2.16. Deliverability

The optimised hydrogel composition was injected through a 3F micro-catheter into a silicone side wall aneurysm (neck size of 2.5 x 2.5mm, model H+N-S-A-005, Elastrat, Switzerland)(Figure S1). A pulsatile blood pump (1423, Harvard Apparatus, Holliston, USA) was used to pump a 36:64 water:glycerol solution through the aneurysm and to provide physiologically correct blood pressure (120/80mmHg) and flow rates (700ml/min). The pressure was measured at the aneurysm model inlet and outlet using pressure transducers (DTX Plus Disposable Pressure Transducer, Argon, Plano, USA) which were amplified using a bridge analogue input (NI9237, National Instrument, Austin, USA) and the pressure was monitored using LabView (National Instruments). A 5mm diameter balloon (Trek, Abbott) was inflated adjacent to the aneurysm neck, to facilitate placement.

2.17. Statistical analysis

Student T-test ($p<0.05$) and ANOVA with Bonferroni's post hoc test was carried out using IBM SPSS (IBM, Armonk, NY).

3. Results

3.1. Alginate Classification

Table 1 shows the molecular weight and chemical composition of the alginate determined by the GPC and ^{1}H-NMR. From the results we can see that the sample is a high-M content high molecular weight alginate.

Table 1 Molecular weight and chemical composition of the potassium alginate

Molecular weight	F_G	F_M	M/G	F_{GG}	F_{MM}	F_{GM}
700kDa	0.37	0.63	1.7	0.18	0.45	0.18

3.2. Particle Size Analysis

The particle size of the acid washed glass indicates a bimodal particle distribution, with acid washing decreasing the relative quantity of fine particles and decreasing the size of larger particles (Figure S2).

3.3. Working and Hardening Time

Acid washing the glass resulted in a 63% increase in WT and a 42% increase in HT, see Figure 2. This increased WT and HT brings the hydrogel outside the clinically relevant time limits, discussed previously.

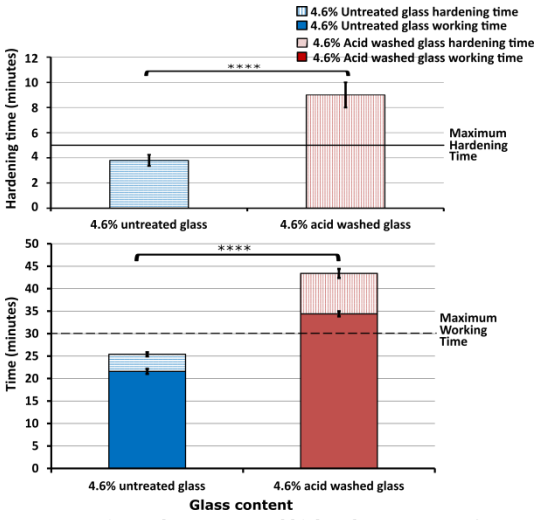

Figure 2 a) Working time and b) hardening time of 4.6% untreated and acid washed glass (n=5)

However, WT and HT can be reduced by increasing the glass and GDL content, as displayed in Figure 3. Increasing the glass and GDL content to 13.8% and 100mg, respectively, brings the acid washed glass hydrogel within the WT and HT limits for this application. This reduction in WT and HT is attributed to the increase of available cross-linking ions, associated with the increased glass and GDL content.

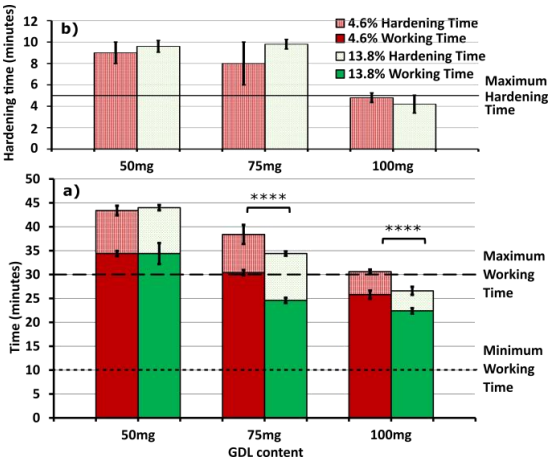

Figure 3 a) Working time and b) hardening time for increasing acid washed glass and GDL content (n=5)

3.4. Compression testing

Acid washing of glass particles significantly increases the compressive strength of the resultant hydrogel after 7 day of incubation, see Figure 4.

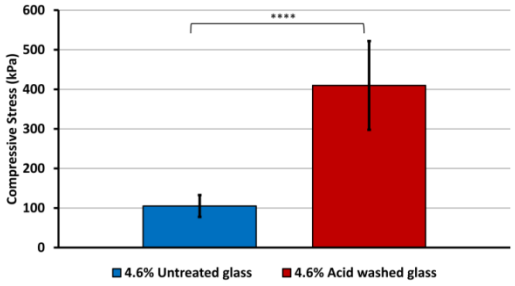

Figure 4 Compressive strength of untreated and acid washed glass following storage for 7 days in DI at 37ºC (n=5)

Further increase of the glass and GDL content increases the strength of the resultant hydrogel over 6.5 times, as seen in Figure 5. The increase in strength is likely caused by the increased cross-link density of the hydrogel due to an increased ion concentration, as with the hydrogel WT and HT.

Table 2 Brunauer Emmett Teller (BET)[1] adsorption and Barrett-Joyner-Halenda (BJH)[2] desorption pore volume analysis.

Sample:	Surface Area[1] (m^2/g):	Pore Volume[2] (cc/g):	Pore Radius[2] (nm):
Untreated Glass	2.375	0.009	1.5466
Acid washed Glass	2.552	0.007	1.9399

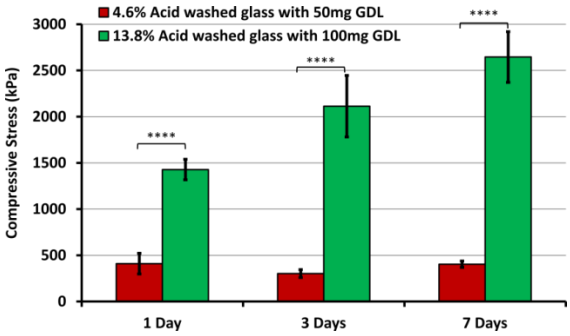

Figure 5 Compressive strength of varying acid washed glass contents following storage for 1, 3 and 7 days in DI at 37ºC (n=5)

3.5. Nitrogen Adsorption/Desorption Measurements

The nitrogen adsorption/desorption results (Table 2) indicates an increased surface area of the acid washed glass particles compared to that on the untreated glass. Nitrogen adsorption results, calculated by BJH, indicate an increased pore diameter and decreased pore volume, which would indicate a widening of the pores and a decrease in depth, most likely indicating some surface erosion.

3.6. Zeta Potential Measurements

Results from the zeta potential measurements are outlined in Table 3. Results indicate a decrease in the negative zeta potential of the acid washed glass, which is indicative of increased hydrophilicity. This increased hydrophilicity can be attributed to an increase in the protonation of the silicate groups on the surface of the glass particles following acid washing [8].

Table 3 Zeta potential measurements of untreated and acid washed glass.

Sample:	Zeta (mV):	Zeta Stdev:
Untreated Glass	-18.8	0.603
Acid Washed Glass	-9.31	0.276

3.7. X-Ray Photoelectron Spectroscopy

Quantitative XPS was carried out on untreated and acid washed glass. Table 4 indicates the elemental composition with some carbon and nitrogen contamination, most likely from the atmosphere. The surface Ca/Ga ratio decreases from 1.5 in the untreated glass to 0.3 in the acid washed glass, indicating that calcium is being preferentially leached from the surface of the glass particles. This may also indicate migration of Ga^{3+} from the internal structure to the surface of the glass, as the Ga/Si ratio is also observed to increase from 0.9 to 1.5 with acid washing.

Figure 6 depicts high resolution O 1s XPS spectra for the untreated and acid washed glasses, indicating a peak at 531.4eV for the untreated sample and 532.0eV for the acid washed sample. This shift in O_{1S} to a higher binding energy with acid washing indicates a higher glass network connectivity (NC) of the acid washed glass surface. Deconvolution of these peaks into their bridging oxygen (BO, 532.0eV) and non-bridging oxygen (NBO, 531.0eV) components indicates considerably lower non-bridging oxygen content on the surface of the acid washed sample. The

Table 4 Composition (atomic %) from XPS of untreated and acid washed glass

Sample:	O	Ga	Ca	Si	P	C
Untreated Glass	55.4	5.7	8.7	6.0	3.9	20.4
Acid Washed Glass	58.6	9.0	2.9	5.8	5.9	17.7

ratio of non-bridging oxygens to bridging oxygens on the surface of the untreated glass is calculated as 1.1, indicating a Q_2 type surface structure, however, after acid treatment this decreases to 0.1, indicating a shift to a higher network connectivity type surface structure (Q_3/Q_4). This higher network connectivity may be the result of silica condensation or repolymerisation in the surface layer following removal of divalent calcium ions, which usually act in a network modifying role. Similar results were observed by Tsomaia *et al.* in aluminosilicate glasses [9].

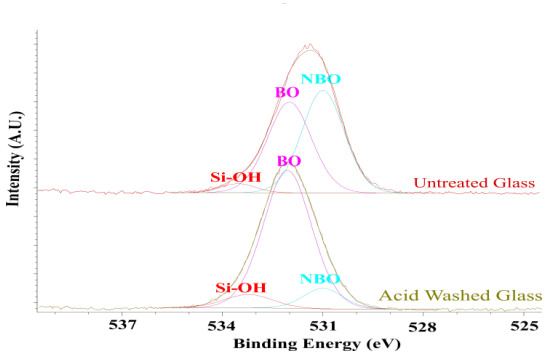

Figure 9.1.1 High resolution O 1s spectra for untreated and acid washed glass

Further deconvolution of the O 1s spectra gives a third component peak (> 533eV) that can be assigned to Si-OH groups [10]. There is doubling of the content of silanol groups on the acid washed glass surface compared to the untreated sample and likely to account for the improved homogeneity of the resultant hydrogel sample.

From Figure 7 it can be seen that the surface Ga_{2p} signal is 1118.2eV (untreated) and 1118.6eV (acid washed), which are both higher than the reported values of β-Ga_2O_3 (1117.9eV) [11], which contains an equal mixture of tetrahedral and octahedral gallium oxide. The binding energy, however, is lower than that of the reported values of $Ga(PO)_4$ (1119.3eV) [12], which has a tetrahedral, charge balanced four coordinate structure. This indicates a surface composition with a greater level of tetrahedral gallium compared to octahedral gallium.

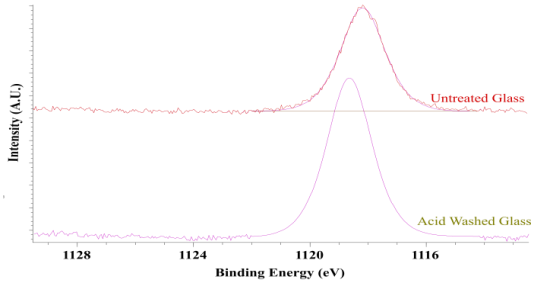

Figure 7 High resolution Ga $2p_{3/2}$ spectra for untreated and acid washed glass

From Figure 8 we can see the surface Si_{2p} signal , in which three peaks can be observed, with the higher binding energy peaks being a result of overlap with the Ga_{3p} binding energies and only the lower Si_{2p} peak (~102eV) being related to the silicate structure. A slight shift in Si_{2p} peak (102.3eV to 102.8eV) is observed with acid washing. The Ga_{2p} is also shifted to higher binding energies with acid washing. The positive shift in binding energy of both Ga $2p_{3/2}$ and Si 2p peak can be viewed as reinforcement of the network with more polymerised Si and Ga species.

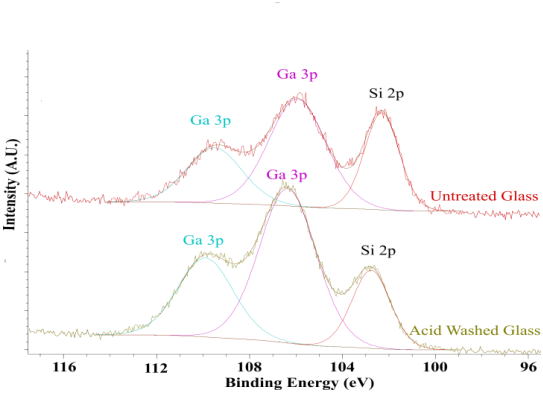

Figure 8 Si_{2p} X-ray Photoelectron Spectroscopy trace for untreated and acid washed glass

Using Equation 1 and the method outlined by Sekita *et al*. we can estimate the percentage of gallium ions tetrahedrally coordinated on the untreated glass surface as 74%, leaving 26% in an octahedral coordination [13]. These calculations use assumptions that are not valid for the acid washed sample as we cannot be certain the quantity of gallium remaining in the surface of the glass after acid washing. From the O1s and $Ga2p_{3/2}$ shifts it is likely that an increased number of gallium ions are tetrahedrally coordinated on the surface of the acid washed glass.

$$r(O^0) = \frac{n(O^0)}{n(O^0)+n(O^-)} = \frac{4\times n(Si,Ga)-n(O)}{n(O)} \quad (1)$$

Contrary to this observation, previously it has been seen that in aluminosilicate glasses, chemically similar aluminium ions are observed to convert from tetrahedral to octahedral upon reaching this acid leached silica rich surface layer [14].

3.8. Fourier transform infrared spectroscopy (FTIR)

ATR-FTIR showed an asymmetric stretching of a Si-O-Si at ~1070 cm^{-1} and a hydroxyl peak at 3,500 cm^{-1}, which is completely absent in the untreated sample (Figure S4). This indicates that increased hydroxylation of the surface may have occurred, correlating with the XPS results. This might be expected due to treatment of a silica glass surface with an acidic proton donor.

FE-SEM at 100,000x magnification indicates a considerably rougher surface topography for the acid washed glass, compared to the untreated glass surface (Figure S5). This correlates well with the pore radius found using nitrogen adsorption results (Table 2).

3.9. Radiopacity

Figure 9 shows a 2D image of a platinum aneurysm coil (A), the hydrogel 4.6% acid washed glass with 50mg GDL (B), the hydrogel with 13.8% glass with 100mg GDL (C) and 1-3mm 99% aluminium step wedge.

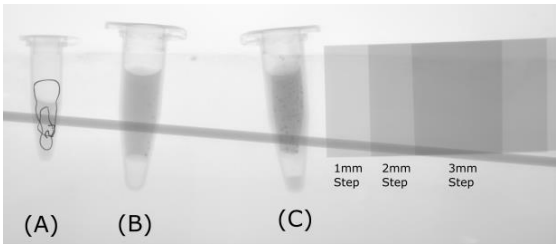

Figure 9 2D X-ray Microtomography of hydrogel samples

Table 5 shows the mean grey values (MGV) calculated using ImageJ. It can be seen that the radiopacity of the hydrogel increases with increasing glass content. This increase in glass content to 13.8% produces a hydrogel with a radiopacity equivalent to 2.99mm of 99% aluminium.

Table 5 ImageJ calculated mean grey values

Sample	MGV	Gray Value range	Equivalent aluminium thickness
Coil (A)	146.7	125 - 199	3.20mm
4.6% acid washed glass (B)	178.4	166 - 188	2.20mm
13.8% acid washed glass (C)	159.2	142 - 190	2.99mm
1mm Step	207.7	204 - 211	1.00mm
2mm Step	183.3	178 - 187	2.00mm
3mm Step	159.9	152 - 165	3.00mm

3.10. Homogeneity

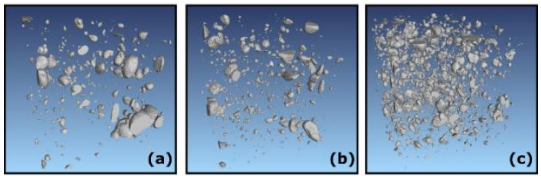

Figure 10 Sample 3D X-ray Microtomography of (a) 4.6% untreated glass with 50mg GDL(b) 4.6% acid washed glass with 50mg GDL(c) 13.8% acid washed glass with 100mg

It can be seen in the 3D XMT images (Figure 10) that both the untreated glass (Figure 10a) and acid washed glass (Figure 10b and 10c) samples contain agglomerates. From the agglomerate size results (Table S1) both the maximum and average particle for the 4.6% untreated glass with 50mg GDL (a) is larger than that of both 4.6% acid washed glass with 50mg GDL (b) and 13.8% acid washed glass with 100mg GDL (c). This suggests the untreated glass is agglomerating more compared to that of the acid washed glass.

The hydrogel with acid washed glass has an increased number of agglomerates and reduced agglomerate size, resulting in a more homogenous sample. This increased homogeneity may contribute to the increased strength observed. A 3-fold increase in the acid washed glass content, from 4.6% to 13.8%, with concomitant increase in GDL content, increases the number of agglomerates; however, there is only a 2.2-fold, as opposed to a 3-fold, increase in observable agglomerates in the XMT. This suggests that the increased GDL is breaking down the glass or reducing the size of the agglomerates to below the detectable size (<5μm). The maximum glass agglomerate diameter for the untreated glass (≃1.44mm) is 44% larger than that of the acid washed glass (≃1.0mm). The larger untreated glass agglomerates would inhibit injection through a 3F catheter (≃1.0mm), therefore, the catheter size would have to be increased to a 4.4F catheter (≃1.47mm) in order to inject without blocking the catheter. This larger catheter size would make navigation through the tortuous cerebral vasculature more difficult.

3.11. Deliverability

With the balloon inflated and the solution flowing at physiological pressure and flow rate, the hydrogel was injected into the ∅10mm (2.5x2.5mm neck) aneurysm of the silicone model two minutes before the end of the hydrogel WT (22 minutes after mixing). The hydrogel was fully injected by the WT and the balloon remained inflated for two minutes. The hydrogel stayed within the aneurysm for the 30 minutes tested once the balloon was deflated.

4. Discussion

Acid washing of the glass particles results in a prolonged WT and HT. The prolonged WT and HT are likely due to the decreased surface calcium content and increased

surface network connectivity. This increased WT and HT is outside the clinically applicable time limits for this specific application. However, due to an increased hydrophilicity and particle dispersion caused by acid washing, the glass content of the hydrogel can be increased. This resulting increase in available ions reduces the WT and HT, which can be further reduced with an increase in GDL content, bringing the composite within the required WT and HT requirements.

Increased strength observed in the set hydrogel composites are likely due to the increased quantity of trivalent gallium ions on the surface of the glass and the reduced calcium content. This increase may also be caused by the increased homogeneity of the hydrogel. The strength can be further increased by increasing the glass and GDL content of the hydrogel. This increased strength is caused by the increase of available ions for an improved cross-linking density. The strength of this produced hydrogel is similar to that of a current embolization treatment, Onyx®, which has a compressive strength of 3MPa [15].

Pore size of acid washed glass samples are approaching mesopore diameter (2-50nm), indicating that further acid treatment may tailor the pore size for the purpose of delivery of various therapeutics. From particle and surface analysis techniques it seems that this increased hydrophilicity is mainly caused by the increased surface concentration of silanol groups.

As shown in previous studies on aluminosilicate glasses, acid washing reduces the surface calcium concentration [14]. However, previous studies did not show a significant increase in compressive strength due to acid washing [16]. Additionally, previous studies on aluminosilicate glass indicated the increased presence of octahedral modalities on the surface following acid washing, which was not observed in this study with the use of gallium silicate glasses [9].

Glasses which have silanol (Si-OH) groups on their surfaces tend to form hydrogen bonding with water, making them hydrophilic [17]. However, when glasses are fractured or ground their surface may become oxygen deficient due to fracture of Si-O bonds, making hydroxylation more difficult and hence initial hydrophobicity likely. The heat of liquefaction of water, at 44kJ/mol, is a value that has been used in the literature as a measure of the hydrophilicity/hydrophobicity of a surface site. Sites that are stronger that 44kJ/mol are considered hydrophilic, while those weaker than 44kJ/mol are considered hydrophobic. The recondensation of the silicon observed on the surface of the acid washed glass is likely increasing the number of high energy bonds, such as three coordinated silicon sites (60-200kJ/mol), which have the strongest adsorption, and decrease non-bridging oxygen sites (40-100kJ/mol) and 2 membered ring sites (20-100kJ/mol) [18][19]. This in turn allows an increased silanol formation on the surface of the glass, resulting in better adsorption and hydrophilicity.

2D XMT showed that increasing the glass content produces a hydrogel sample with a radiopacity equivalent to that of 2.99mm of 99% aluminium. 3D XMT results show that acid washing the glass produces a more homogenous hydrogel with smaller agglomerates of glass.

This reduced agglomerate size allows the hydrogel to be injected into the aneurysm through a 3F catheter. Catheters currently

used for treating cerebral aneurysms typically have an inner diameter of 0.021" or 0.027". Further optimisation of the hydrogel may be necessary to allow an easy injection of this hydrogel through these reduce catheter dimensions [20].

5. Conclusion

Acid washing of the gallium silicate glass increases wettability and allows better mixing with an alginate solution. The resultant hydrogel has a prolonged working and hardening time and forms a hydrogel with a higher compressive strength. The longer working and hardening time may be reduced by increasing glass and GDL content to reduce them to within the clinically applicable limits. This in turn increases the hydrogel's compressive strength and radiopacity. Acid washing of the glass has an effect on the particle size, surface topography, pore size, surface ion content and surface network connectivity, all of which likely have an effect on the working and hardening time of the resultant hydrogel. The increased compressive strength observed is likely an effect of the reduced divalent ion content of the surface and increased trivalent ion content, resulting in more complete and homogenous cross-linking of the alginate hydrogel.

Acknowledgements

This work was supported by Enterprise Ireland Commercialization Fund through the grant CF/2013/3364.

Conflict of interest statement

There are no conflicts of interest for any authors.

References

1. Brisman JL, Song JK, Newell DW (2006) Cerebral Aneurysms. N Engl J Med 355:928–939. doi: 10.1056/NEJMra052760
2. Crobeddu E, Lanzino G, Kallmes DF, Cloft HJ (2012) Review of 2 Decades of Aneurysm-Recurrence Literature, Part 2: Managing Recurrence after Endovascular Coiling. Am J Neuroradiol . doi: 10.3174/ajnr.A2958
3. Kim Nelson P, Levy DI (2001) Balloon-assisted Coil Embolization of Wide-necked Aneurysms of the Internal Carotid Artery: Medium-term Angiographic and Clinical Follow-up in 22 Patients. Am J Neuroradiol 22:19–26.
4. Biomaterial Research Group. www.biomaterials.ie.
5. Morais DS, Rodrigues MA, Silva TI, et al (2013) Development and characterization of novel alginate-based hydrogels as vehicles for bone substitutes. Carbohydr Polym 95:134–42. doi: 10.1016/j.carbpol.2013.02.067
6. Gorodzha S, Douglas TEL, Samal SK, et al (2016) High-resolution synchrotron X-ray analysis of bioglass-enriched hydrogels. J Biomed Mater Res Part A 104:1194–1201. doi: 10.1002/jbm.a.35642
7. Barrett EP, Joyner LG, Halenda PP (1951) The Determination of Pore Volume and Area Distributions in Porous Substances. I. Computations from Nitrogen Isotherms. J Am Chem Soc 73:373–380. doi: 10.1021/ja01145a126
8. Bismarck A, Boccaccini AR, Egia-Ajuriagojeaskoa E, et al Surface characterization of glass fibers made from silicate waste: Zeta-potential and contact angle measurements. J Mater Sci 39:401–412. doi: 10.1023/B:JMSC.0000011493.26161.a6
9. Tsomaia N, Brantley SL, Hamilton JP, et al (2003) NMR evidence for formation of octahedral and tetrahedral Al and repolymerization of the Si network during dissolution of aluminosilicate glass and crystal. Am Mineral 88:54–67.
10. Simonsen ME, Sønderby C, Li Z, Søgaard EG (2009) XPS and FT-IR investigation of silicate polymers. J Mater Sci 44:2079–2088. doi: 10.1007/s10853-009-3270-9
11. Hollinger G, Skheyta-Kabbani R, Gendry M (1994) Oxides on GaAs and InAs surfaces: An x-ray-photoelectron-spectroscopy study of reference compounds and thin oxide layers. Phys Rev B 49:11159–11167. doi:

10.1103/PhysRevB.49.11159
12. He H, Cheng C-F, Seal S, et al (1995) Solid-State NMR and ESCA Studies of the Framework Aluminosilicate Analcime and Its Gallosilicate Analog. J Phys Chem 99:3235–3239. doi: 10.1021/j100010a039
13. Sekita M, Fujimori A, Makishima A, et al (1985) X-ray photoelectron spectroscopy of a cerium-doped lanthanum aluminosilicate glass. J Non Cryst Solids 76:399–407. doi: 10.1016/0022-3093(85)90014-6
14. Crowley CM, Doyle J, Towler MR, et al (2007) Influence of acid washing on the surface morphology of ionomer glasses and handling properties of glass ionomer cements. J Mater Sci Mater Med 18:1497–1506. doi: 10.1007/s10856-007-0128-z
15. Ohyama T, Ko IK, Miura A, et al (2004) ProNectin F-grafted-ethylene vinyl alcohol copolymer (EVAL) as a liquid type material for treating cerebral aneurysm--an in vivo and in vitro study. Biomaterials 25:3845–52. doi: 10.1016/j.biomaterials.2003.10.021
16. Prentice LH, Tyas MJ, Burrow MF (2007) Ion leaching of a glass-ionomer glass: an empirical model and effects on setting characteristics and strength. J Mater Sci Mater Med 18:127–131. doi: 10.1007/s10856-006-0670-0
17. Takeda S, Yamamoto K, Hayasaka Y, Matsumoto K (1999) Surface OH group governing wettability of commercial glasses. J Non Cryst Solids 249:41–46. doi: 10.1016/S0022-3093(99)00297-5
18. Leed EA, Sofo JO, Pantano CG (2005) Electronic structure calculations of physisorption and chemisorption on oxide glass surfaces. Phys Rev B 72:155427. doi: 10.1103/PhysRevB.72.155427
19. Leed EA, Pantano CG (2003) Computer modeling of water adsorption on silica and silicate glass fracture surfaces. J Non Cryst Solids 325:48–60. doi: 10.1016/S0022-3093(03)00361-2
20. Henkes H, Weber W (2015) The Past, Present and Future of Endovascular Aneurysm Treatment. Clin Neuroradiol 25 Suppl 2:317–324. doi: 10.1007/s00062-015-0403-1

9.1.1.3. Bioengineering in Ireland Conference 2015.

Development of a novel hydrogel filler to treat cerebral aneurysms; Determination of the influence of molecular weight and alginate concentration

Sarah Brady[1], Caitríona Lally[1], Eoin K. Fox[1] and Owen M. Clarkin[1]
[1]School of Mechanical and Manufacturing Engineering, Dublin City University, Dublin 9.

It is estimated that 1-6% of the adult population have a cerebral aneurysm (1). Aneurysm treatments include clipping and coiling, however, recurrence occurs in 20.8% of endovascular coiling cases (2). A novel hydrogel, called EnduraGel, has recently been developed at DCU to treat aneurysms and prevent rupture. This hydrogel is composed of a polymeric alginate, a novel bioactive glass and glucono-delta-lactone. The role of the bioactive glass is to control the working and setting time as well as to encourage bioactivity of the gel.

The aim of this work is to optimise the composition of the hydrogel, specifically the alginate molecular weight (MW) and concentration, to achieve the most suitable mechanical properties, and injectability.

Two MW alginates, denoted low molecular weight (LMW) and high molecular weight (HMW), have been tested at three different concentrations. Design Expert was used to determine the best concentrations to be tested. The mechanical properties of the alginate were found by compression testing of cylindrical samples (height 14mm and diameter 10mm). Injectability was determined by injecting the hydrogel through a microcatheter into an aneurysm flow model.

After 7 days the LMW alginate had compressive strengths of 273 kPa, 634 kPa and 257 kPa for the three increasing concentrations whilst the HMW alginate had compressive strengths of 380 kPa, 966 kPa and 277 kPa. The reduced compressive strengths at higher alginate concentrations are unexpected and may result from a shortage of available crosslinking cations. An increase in the glass and/or GDL content for these increased alginate content gels may counteract this issue.

Work to-date indicates that both concentration and MW have an effect on the performance of the hydrogel with concentration having the greatest influence. Although the two lowest alginate concentrations have greater compressive strengths for both MWs, they do not inject as well as the higher concentration and generally flow out of the aneurysm. It can be seen from the compression, that the HMW gives improved performance.

Future work will include testing the setting and working times of the hydrogel and further examining why the HMW alginates have lower compressive strengths. Working times will be

determined using a MFR 2100 Micro Fourier Rheometer (GBC Scientific, Victoria). Setting times will be determined by indention in increments of 1 minute (modification of ISO9917). FTIR will be carried out on the high concentration alginate to determine the number of free carboxylic groups present compared to the number of bound carboxylic groups.

References

1. Cerebral Aneurysms. Jonathon L.Brisman, et al. 9, s.l. : New England Journal of Medicine 2006, 2006, Vol. 355.

2. Review of 2 Decades of Aneurysm-Recurrence Literature, Part 2: Managing Recurrence after Endovascular Coiling. al, E. Crobeddu et. 3, s.l. : AJNR, Vol. 34.

9.1.1.4. UK Society for Biomaterials Conference 2015.

DETERMINATION OF THE INFLUENCE OF GAMMA IRRADAITION, MOLECULAR WEIGHT AND ALGINATE CONCENTRATION ON THE PROPERTIES OF A NOVEL HYDROGEL FOR VASCULAR APPLICATIONS

Sarah Brady, Caitríona Lally, Eoin K. Fox and Owen M. Clarkin
School of Mechanical & Manufacturing Engineering, Dublin City University, Glasnevin, Dublin 9, Ireland
Corresponding author: sarah.brady33@mail.dcu.ie – 1st year Research Masters Student

Introduction

A novel injectable hydrogel, called EnduraGel™, has been developed to prevent cerebral aneurysm rupture. The hydrogel will be injected through a microcatheter into the aneurysm. To allow for delivery of the gel, an optimum working time has been identified of between 10 and 30 minutes. The hydrogel must be set within 5 minutes of injection to prevent cerebral ischemia. In addition the gel must be capable of withstanding hypertensive blood pressure levels (22kPa, 180 mm Hg), to be a suitable filler for cerebral aneurysms.

The aim of this work is to optimise the gel composition, specifically the alginate molecular weight (MW) and concentration, to achieve the most suitable mechanical properties, injectability, working and hardening time.

Materials and Methods

This hydrogel is composed of alginate, bioactive glass and glucono-delta-lactone. Three MW alginates, denoted low molecular weight (LMW), mid-molecular weight (MMW) and high molecular weight (HMW), have been tested at four increasing alginate concentrations; A, B, C and D. The LMW alginate is a G-rich alginate (FG= 0.52) and the HMW alginate is an M-rich alginate (FG= 0.37). The MMW was achieved by gamma irradiating solid HMW alginate at 25kGy.

The MW of each alginate was determined by GPC. The working and setting time were established using a modified version of ISO9917. The hardening time is defined as the time difference between the working and setting time. Mechanical properties were found by compression testing cylindrical samples (ø-10mm, h-14mm) to failure. The injectability was tested by injecting the gel through a 2F microcatheter.

Results and Discussion

Figure 1(a) shows that each of the hydrogels exceeds the minimum compressive strength required. As per reptation theory, it was expected that the strength increase would continue for Concentration C and D, however this was not the case. This decrease in strength may be due to an increased alginate concentration with no increase in the GDL or glass content, causing a shortage of crosslinking cations. The strength may be increased by increasing the glass content. Although the gamma irradiated alginate has a mid-molecular weight, its compressive strength is greatly reduced compared to the LMW and HMW alginate. The

lowered strength compared to the HMW alginate may be a result of scissions of the glycosidic bonds during gamma irradiation (1). The lower strength compared to the LMW alginate may be caused by the lower G-Block ratio.

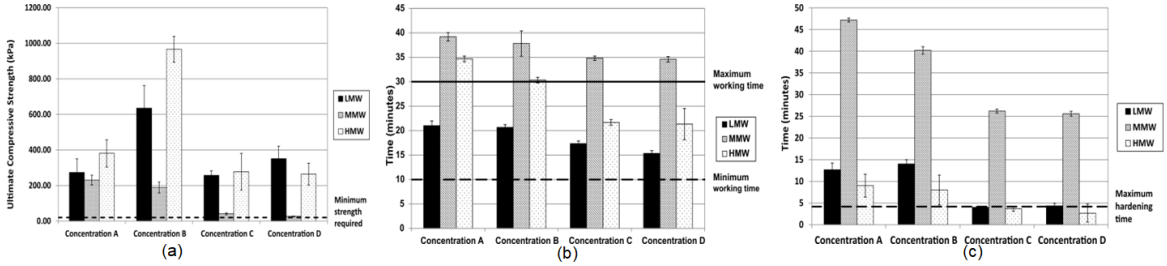

Figure 1: (a) *Ultimate Compressive Strength*, (b) *Working Time*, (c) *Hardening Time*

For the LMW and HMW alginate, Concentration C and D are within the working and hardening time limits, shown in Fig 1 (b) and (c). Each concentration of the MMW alginate is outside the working and hardening time limits. Anecdotally, the MMW alginate clearly has a lower viscosity compared to that of both the HMW and LMW alginate. This reduction in viscosity may cause the increase in working and hardening time.

During injection testing it was found that Concentration D would not inject through the microcatheter as it was too viscous. Concentration A was not viscous enough and would most likely not remain in the aneurysm when blood flow is applied. Both Concentrations B and C could be injected through the microcatheter.

Conclusions

Each of the alginate concentrations have compressive strengths above the minimum required strength. Concentrations C and D of both the LMW and HMW alginates have working time and hardening times within the required limits, however, Concentration D does not inject through the microcatheter. Therefore of the gels studied Concentration C of the HMW is the optimum alginate for this application.

References

1. Lee D.W et al. Agric. Food Chem. 4819−4823, 2003.

9.1.1.5. UK Society for Biomaterials Conference 2016.

OPTIMISED DISPERSION AND STRENGTH OF AN INJECTABLE GLASS-ALGINATE COMPOSITE

Sarah A. Brady[1], Fathima R. Laffir[2], Brendan Phelan[3], Caitríona Lally[4], Owen M. Clarkin[1]
[1]School of Mechanical & Manufacturing Engineering, Dublin City University, Dublin 9, Ireland
[2]Materials and Surface Science Institute, University of Limerick, Limerick, Ireland
[3]South Eastern Applied Materials Research Centre, Waterford Institute of Technology, Waterford, Ireland
[4] Mechanical & Manufacturing Engineering, Trinity College Dublin, Dublin 2, Ireland
Corresponding author: sarah.brady33@mail.dcu.ie – 2nd year Research Masters Student

Introduction

A novel injectable hydrogel has been developed to fill cerebral aneurysms and prevent rupture. The hydrogel will be injected through a microcatheter into the aneurysm. To allow for delivery of the hydrogel, an optimal working time has been identified of between 10 and 30 minutes. The hydrogel must be set within 5 minutes to prevent cerebral ischemia. In addition, the gel must be capable of withstanding hypertensive blood pressure (22 kPa, 160 mm Hg). This hydrogel is composed of alginate, bioactive glass and glucono-delta-lactone (GDL).

We have previously identified the optimum hydrogel composition with the required working and hardening time and compressive strength. However, this hydrogel had agglomerates caused by the glass clumping together. This study examines the effect acid washing has on the structure and composition of the glass and the influence such surface modification has on homogeneity, working time, hardening time and compressive strength with a view to further optimising the hydrogel formulation for use in cerebral aneurysm treatment.

Materials and Methods

The alginate used is a High-M (Fm = 0.63) 700 kDa potassium alginate. The glass has a composition of 0.33SiO2•0.18Ga2O3•0.23CaO•0.11P2O5•0.15CaCl2 and is acid washed by stirring 7 g of glass in 280 ml of 2 vol.% acetic acid for 1 hour. This is then centrifuged at 5,000 RPM for 5 minutes and the supernatant is removed. The glass is then stirred in 560 ml of DI for 1 hour and centrifuged again. The glass is separated and dried at 160 ˚C for 1.5 hours. The novel hydrogel is produced by mixing the glass powder and GDL with 1.2 ml of 4.5 % alginate for 1 minute. Potassium alginate solutions were made up in bulk prior to mixing.

Surface modification of the glass was determined using X-Ray Photoelectron Spectroscopy (XPS) and 3D X-ray Microtomography (XMT). The working and setting time were established using a modified version of ISO9917. The hardening time is defined as the time difference between the working and setting time. Mechanical properties were found by compression testing cylindrical samples (ø-10 mm, h-14 mm) to failure.

Results and Discussion

The surface Ca/Ga ratio decreases from 1.53 in the untreated glass to 0.32 in the acid washed glass, indicating that calcium is being preferentially leached from the surface of the glass particles. This may also indicate migration of the Ga3+ from the internal structure to the surface, as the Ga/Si ratio increases from 0.94 to 1.5 with acid washing. The XPS spectra produces a peak at 531.3 eV for the untreated sample and 531.8 eV for the acid washed sample. This shift in O1S to a lower binding energy with acid washing indicates a higher glass network connectivity (NC) on the acid washed glass surface. This higher network connectivity may be the result of silica condensation or repolymerisation in the surface layer following removal of divalent calcium ions. Further deconvolution of the Si-OH groups (533 eV) indicates a doubling of the content of silanol groups on the acid washed glass surface compared to the untreated glass

XMT results show that both the untreated and acid washed glass particles clump, however, the untreated glass produces larger agglomerates compared to that of the acid washed glass. The acid washed glass hydrogel has an increased number of particle clusters which causes a more homogenous hydrogel with an even distribution of glass particles.

Acid washing the glass resulted in an increase in working time from 22 to 34 minutes and an increase in hardening time from 4 to 9 minutes. Increased working and hardening times are likely due to decreased surface calcium content and increased surface NC. The increased homogeneity and reduced agglomerates allows the glass content of the hydrogel to be increased which can reduce the working and hardening time.

Acid washing of the glass particles significantly increases the compressive strength of the resultant hydrogel. Increased strength of the hydrogel is likely due to the increased quantity of trivalent gallium ions on the surface of the glass and the reduced calcium content, though improved particle bonding and dispersion cannot be ruled out as a contributory factor in increasing strength. The strength of the hydrogel can be further increased with an increase in glass and GDL content.

Conclusions

Acid washing of the glass increases wettability and allows better mixing with an alginate solution. Acid washing also has an effect on the surface ion content and surface network connectivity, all of which have an effect on the working and hardening time of the resultant hydrogel. The resultant gel has a longer working and hardening time and forms a gel with a higher compressive strength. The longer working and hardening time allowed for an increased glass content, which in turn increased the hydrogel's compressive strength.

9.1.1.6. RSC Biomaterials Special Interest Group Annual Meeting 2017

IMPROVED ADHESIVE STRENGTH OF A NOVEL ANEURYSM FILLER

Sarah A. Brady[1], Caitríona Lally[2], Owen M. Clarkin[1]
[1] School of Mechanical & Manufacturing Engineering, Dublin City University, Dublin 9, Ireland
[2] Mechanical & Manufacturing Engineering, Trinity College Dublin, Dublin 2, Ireland
email: sarah.brady33@mail.dcu.ie

INTRODUCTION

The current gold standard for treating cerebral aneurysms is endovascular coiling; however, over 20% of these treated aneurysms recur. Coiled aneurysms recur due to poor packing density and the inability of coils to adhere to the aneurysm wall.

A novel hydrogel with mechanical properties capable of withstanding arterial blood pressure has been developed to fill and occlude the aneurysm. This hydrogel is composed of a polymeric alginate, a novel bioactive glass (Ga2O3-CaO-SiO2-P2O5-CaCl2) and glucono-delta-lactone. The aim of this work is to improve the hydrogel's adhesive strength to natural tissue by the addition of N-(3-Dimethylaminopropyl)-N′-ethylcarbodiimide hydrochloride (EDC) and N-Hydroxysuccinimide (NHS). Once an optimum EDC/NHS content was found, the cytotoxic effect of the hydrogel on bovine aortic endothelial cells (BAEC) was assessed.

MATERIALS AND METHODS

The adhesive strength to a skin xenograft was tested in accordance with ATSM F2255-03. EDC and NHS were added to the hydrogel in 1:1 (w/w) ratio and tested at five increasing contents; 0mg, 5mg, 10mg, 20mg and 100mg.

Resazurin blue elution assays were performed to examine the cells metabolic activity with the optimum EDC and NHS content. DAPI staining was used to examine the cells viability.

RESULTS

The adhesive strength of the hydrogel increased from 0mg to 10mg EDC/NHS. However, there was a decrease in adhesive strength for EDC/NHS contents above 10mg. Mechanical testing showed the addition of EDC/NHS caused a reduction in strength. These results combined may indicate two types of fracture occurring; adhesive failure occurring for the hydrogel with <10mg EDC/NHS content and a cohesive failure caused by reduced strength of the hydrogel with increased EDC/NHS content. As the 10mg EDC and NHS content was optimum, further adhesive strength testing after 1 day of storage was carried out. This showed a continued increase in adhesive strength with time.

BAEC metabolic activity increases with increasing concentrations of eluent. However, addition of 10mg of EDC/NHS reduced BAEC proliferation. DAPI staining showed that the change in cell metabolic activity is caused by a change in the number of viable cells.

9.2. Appendix B

Table 9.2.1 Hydrogel formulae for corresponding sections

Section	Alginate concentration (w/v (mg/1.2ml))	Glass content (w/v (mg/1.2ml))	GDL content (w/v (mg/1.2ml))	EDC and NHS content (w/v (mg/1.2ml))	Tantalum (w/v (mg/1.2ml))
5.1	0.5% (6mg) 60kDa alginate	4.6% (55mg) Original, untreated glass	4.15% (50mg)	0% (0mg)	0% (0mg)
5.1	2.5% (30mg) 60kDa alginate	4.6% (55mg) Original, untreated glass	4.15% (50mg)	0% (0mg)	0% (0mg)
5.1	4.5% (54mg) 60kDa alginate	4.6% (55mg) Original, untreated glass	4.15% (50mg)	0% (0mg)	0% (0mg)
5.1	6% (72mg) 60kDa alginate	4.6% (55mg) Original, untreated glass	4.15% (50mg)	0% (0mg)	0% (0mg)
5.1	0.5% (6mg) 700kDa alginate	4.6% (55mg) Original, untreated glass	4.15% (50mg)	0% (0mg)	0% (0mg)
5.1	2.5% (30mg) 700kDa alginate	4.6% (55mg) Original, untreated glass	4.15% (50mg)	0% (0mg)	0% (0mg)
5.1	4.5% (54mg) 700kDa alginate	4.6% (55mg) Original, untreated glass	4.15% (50mg)	0% (0mg)	0% (0mg)
5.1	6% (72mg) 700kDa alginate	4.6% (55mg) Original, untreated glass	4.15% (50mg)	0% (0mg)	0% (0mg)
5.2	0.5% (6mg)180kDa alginate	4.6% (55mg) Original, untreated glass	4.15% (50mg)	0% (0mg)	0% (0mg)
5.2	2.5% (30mg) 180kDa alginate	4.6% (55mg) Original, untreated glass	4.15% (50mg)	0% (0mg)	0% (0mg)
5.2	4.5% (54mg) 180kDa alginate	4.6% (55mg) Original, untreated glass	4.15% (50mg)	0% (0mg)	0% (0mg)
5.2	6% (72mg)	4.6% (55mg)	4.15% (50mg)	0% (0mg)	0% (0mg)

	180kDa alginate	Original, untreated glass			
5.3	4.5% (54mg) 700kDa alginate	4.6% (55mg) Acid washed glass	4.15% (50mg)	0% (0mg)	0% (0mg)
5.3	4.5% (54mg) 700kDa alginate	13.8% (166mg) Acid washed glass	8.3% (100mg)	0% (0mg)	0% (0mg)
5.4	4.5% (54mg) 700kDa alginate	13.8% (166mg) Acid washed glass	8.3% (100mg)	0% (10mg)	0% (0mg)
5.5	4.5% (54mg) 700kDa alginate	13.8% (166mg) Original, untreated glass	8.3% (100mg)	0% (0mg)	0% (0mg)
5.5	4.5% (54mg) 700kDa alginate	13.8% (166mg) Acid washed glass	8.3% (100mg)	0% (0mg)	0% (0mg)
5.5	4.5% (54mg) 700kDa alginate	13.8% (166mg) Acid washed glass	8.3% (100mg)	0.83% (10mg)	0% (0mg)
5.6	4.5% (54mg) MVM alginate	13.8% (166mg) Acid washed glass	8.3% (100mg)	0.83% (10mg)	0% (0mg)
5.6	4.5% (54mg) Autoclaved MVM alginate	13.8% (166mg) Acid washed glass	8.3% (100mg)	0.83% (10mg)	0% (0mg)
5.6	4.5% (54mg) Autoclaved MVM alginate	9.2% (110mg) gamma irradiated acid washed glass	6.25% (75mg) gamma irradiated	0.83% (10mg) gamma irradiated	0% (0mg)
5.7	4.5% (54mg) Autoclaved MVM alginate	9.2% (110mg) gamma irradiated acid washed glass	6.25% (75mg) gamma irradiated	0.83% (10mg) gamma irradiated	0% (0mg)
5.8	4.5% (54mg) Autoclaved MVM alginate	9.2% (110mg) gamma irradiated acid washed glass	6.25% (75mg) gamma irradiated	0.83% (10mg) gamma irradiated	0% (0mg)
5.9	4.5% (54mg) Autoclaved MVM	9.2% (110mg) gamma	6.25% (75mg) gamma	0.83% (10mg)	40% (480mg)

	alginate	irradiated acid washed glass	irradiated	gamma irradiated	
5.10	4.5% (54mg) Autoclaved MVM alginate	9.2% (110mg) gamma irradiated acid washed glass	6.25% (75mg) gamma irradiated	0.83% (10mg) gamma irradiated	0% (0mg)
5.11	6.75% (81mg) Autoclaved MVM alginate	13.8% (166mg) gamma irradiated acid washed glass	8.3% (100mg) gamma irradiated	0.83% (10mg) gamma irradiated	0% (0mg)
5.11	4.5% (54mg) Autoclaved MVM alginate	9.2% (110mg) gamma irradiated acid washed glass	6.25% (75mg) gamma irradiated	0.83% (10mg) gamma irradiated	40% (480mg)

9.3. Appendix C

Gallium is a semi-metallic ion that is trivalent in aqueous solutions. This ion has been used in a wide variety of treatments such as bone resorption, cancer and autoimmune diseases. Gallium has also been incorporated in materials due to its antibacterial and anti-tumour effects [338].

Gallium has been shown to cross-link alginate, as shown in Figure 9.3.1. The strength of gallium-alginate hydrogels can be improved by the addition of bioactive glass and vice versa [239] [240].

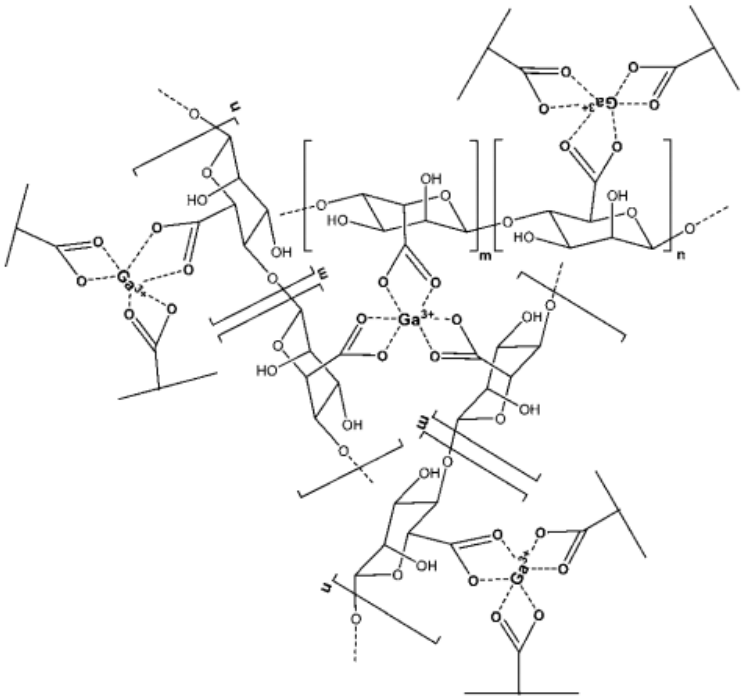

Figure 9.3.1 Predicted mechanism of gallium ions cross-linking alginate [239]

9.4. Appendix D

9.4.1. Rheology

9.4.1.1. Materials and Methods

Rheology of the hydrogel was carried out from the time of mixing, at room temperature, on a Micro Fourier Rheometer (MRF 2100, GBC Scientific Equipment, Victoria, Australia) at a frequency range of 0.5Hz – 200Hz and an amplitude of 0.4mm. The time was measured from the start of mixing using a stopwatch.

9.4.1.2. Storage and Loss Cross Point

There were several issues with the results when determining the gel point using the storage and loss method. The gel point should be relatively similarly when tested at different frequencies; however, this was not the case.

Figure 9.4.1shows the gel point determined at a frequency of 40Hz, which gives one crossing point at 7 minutes.

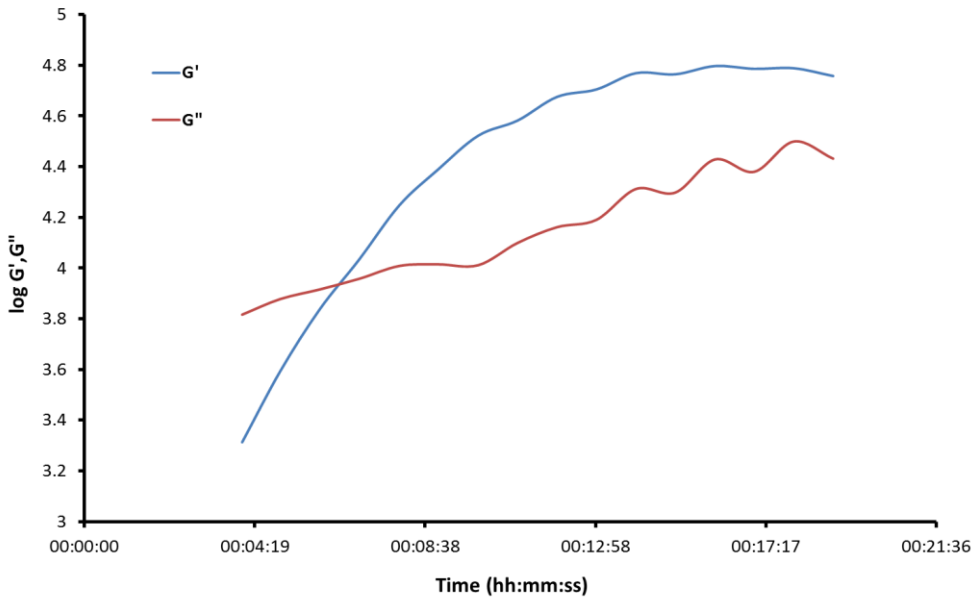

Figure 9.4.1 Gel point of the 0.5% 700kDa alginate at a frequency of 40Hz

However, when the frequency is reduced to 5Hz the graph produced has several crossing points (Figure 9.4.2). Although there is a crossing point at approximately 6 minutes, this time is likely too short to be the gelling point of a low viscosity material such as the 0.5% 700kDa alginate. This problem was evident in all materials tested.

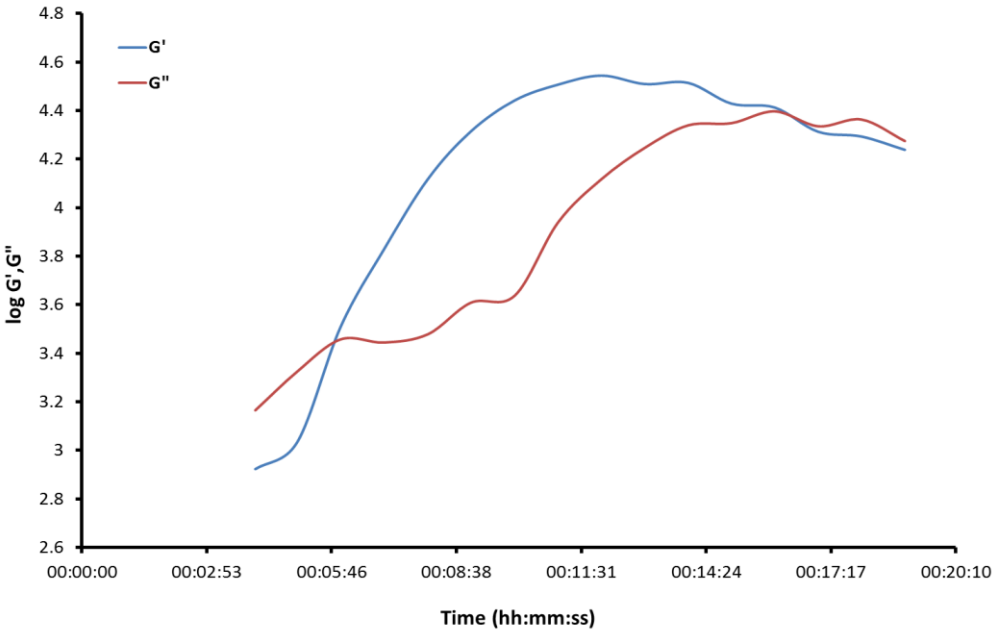

Figure 9.4.2 Gel point of the 0.5% 700kDa alginate at a frequency of 5Hz

At higher concentrations of alginate there was no cross over point at any frequency. As the G" is below the G' it suggests that the gel point was reached before the sample was tested (Figure 9.4.3 and Figure 9.4.4). These results do not correlate with what was physically observed or the results obtained using methods outlined in ISO 9917. It is also evident in each graph that either the G' or the G" line produced is a wave when the line should be straight.

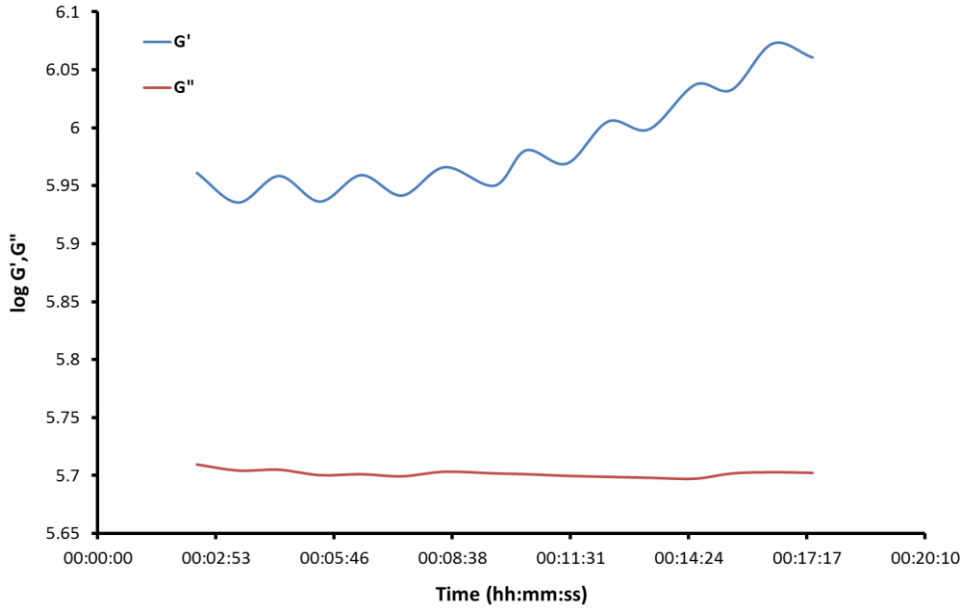

Figure 9.4.3 Gel point of the 4.5% 700kDa alginate at a frequency of 40Hz

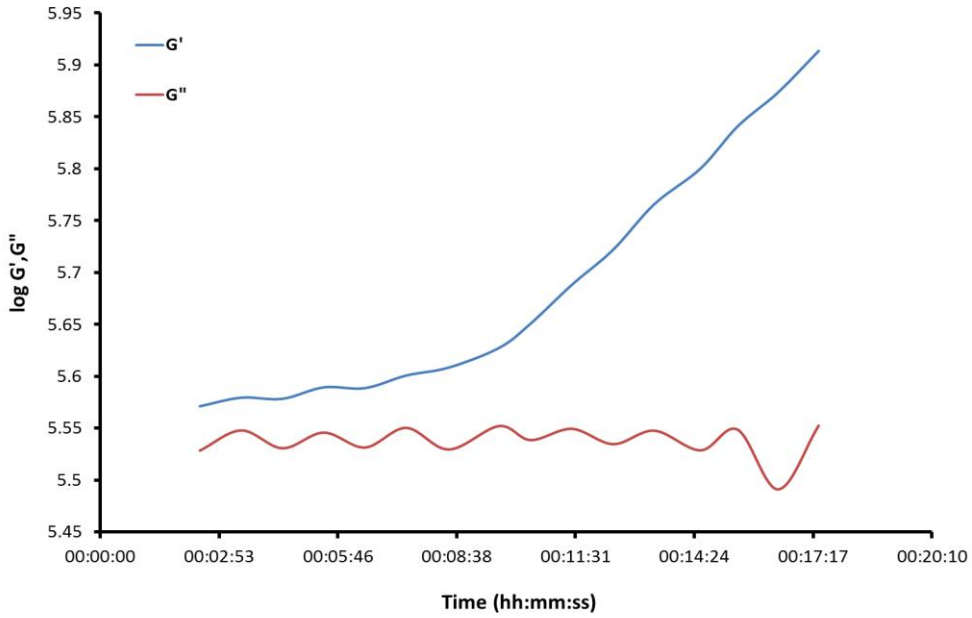

Figure 9.4.4 Gel point of the 4.5% 700kDa alginate at a frequency of 5Hz

9.4.1.3. Winter-Chambon Criterion

Issues are also present when testing the gel point using the Winter-Chambon method. The Winter-Chambon method should indicate the gel point of a material by the crossing point of linear viscoelastic curves (see Figure 3.3.2).

Figure 9.4.5 shows that, again, there are waves produced by the graph rather than lines. This causes the results to show several gel points.

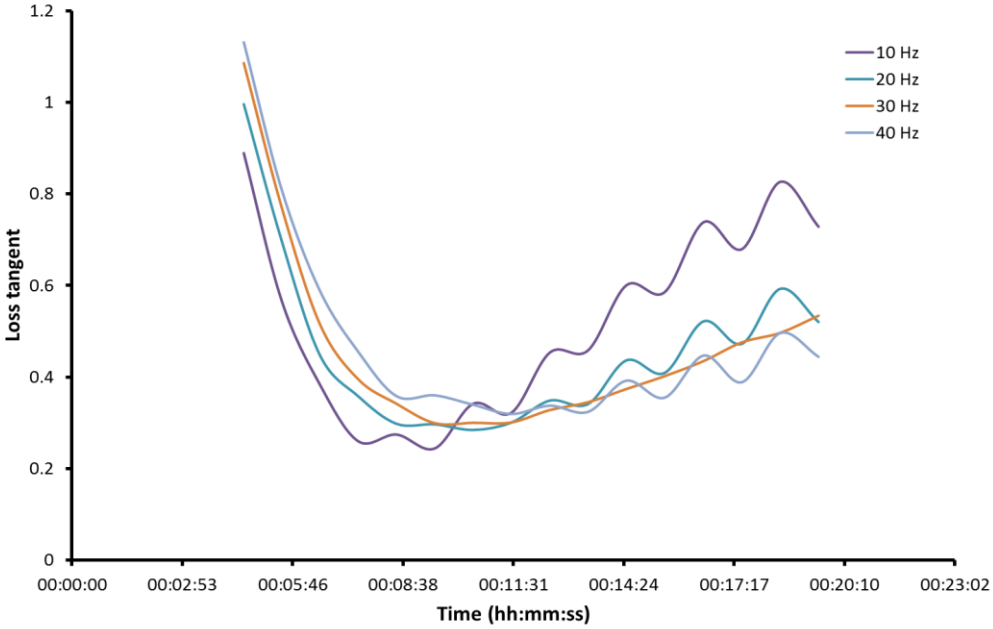

Figure 9.4.5 Gel point of the 0.5% 700kDa using the Winter-Chambon Criterion

Figure 9.4.6 shows that the hydrogel with a 4.5% alginate concentration has not reached its gel point by the end of the test. This result does not correlate with Figure 9.4.3 and Figure 9.4.4 that suggests the gel point has already passed.

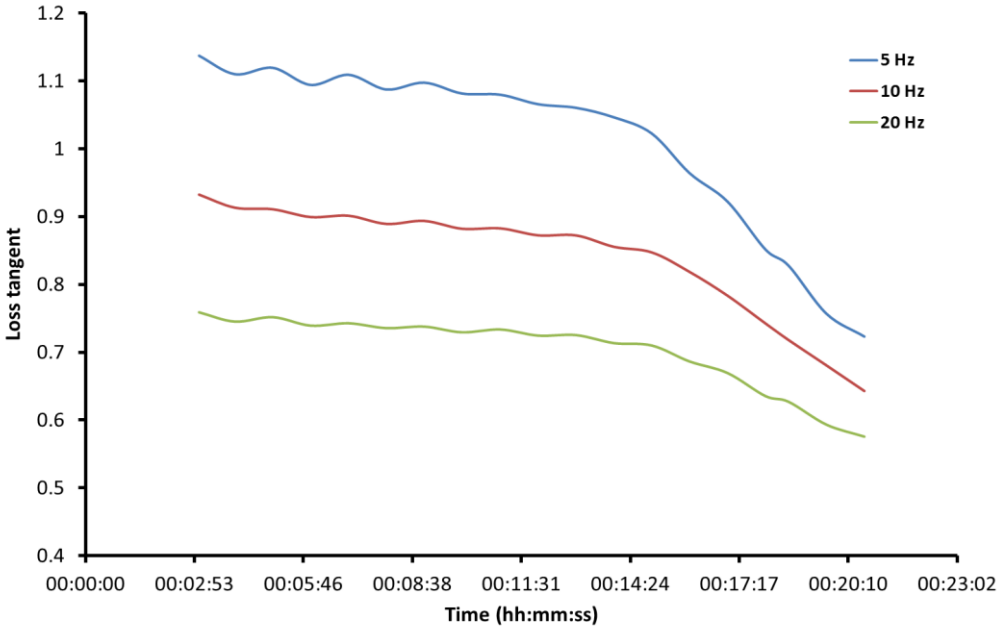

Figure 9.4.6 Gel point of the 4.5% 700kDa using the Winter-Chambon Criterion

9.4.1.4. Discussion

The results from the storage and loss cross point method may suggest the hydrogel is setting in two parts. The original cross point may show when the hydrogel is homogenous. After this there is a continued cross-linking of the hydrogel; however, this is not a homogenous cross-linking and the more viscous material of the hydrogel is being pushed towards the rheometer plates, which caused a 'slipping'. This 'slipping' is only seen in the lower frequencies as the plates of the rheometer moves at a higher amplitude, which allows the more viscous material to move outwards.

Due to the wave results for each sample, the Winter-Chambon criterion could not be used to calculate the gel point of the hydrogel. The relaxation exponent of the hydrogel could not be calculated as there was no clear gel point determined.

These results suggest that neither the storage and loss cross point nor the Winter-Chambon criterion can be used to determine the gel point of this hydrogel.

9.4.2. Flow Model

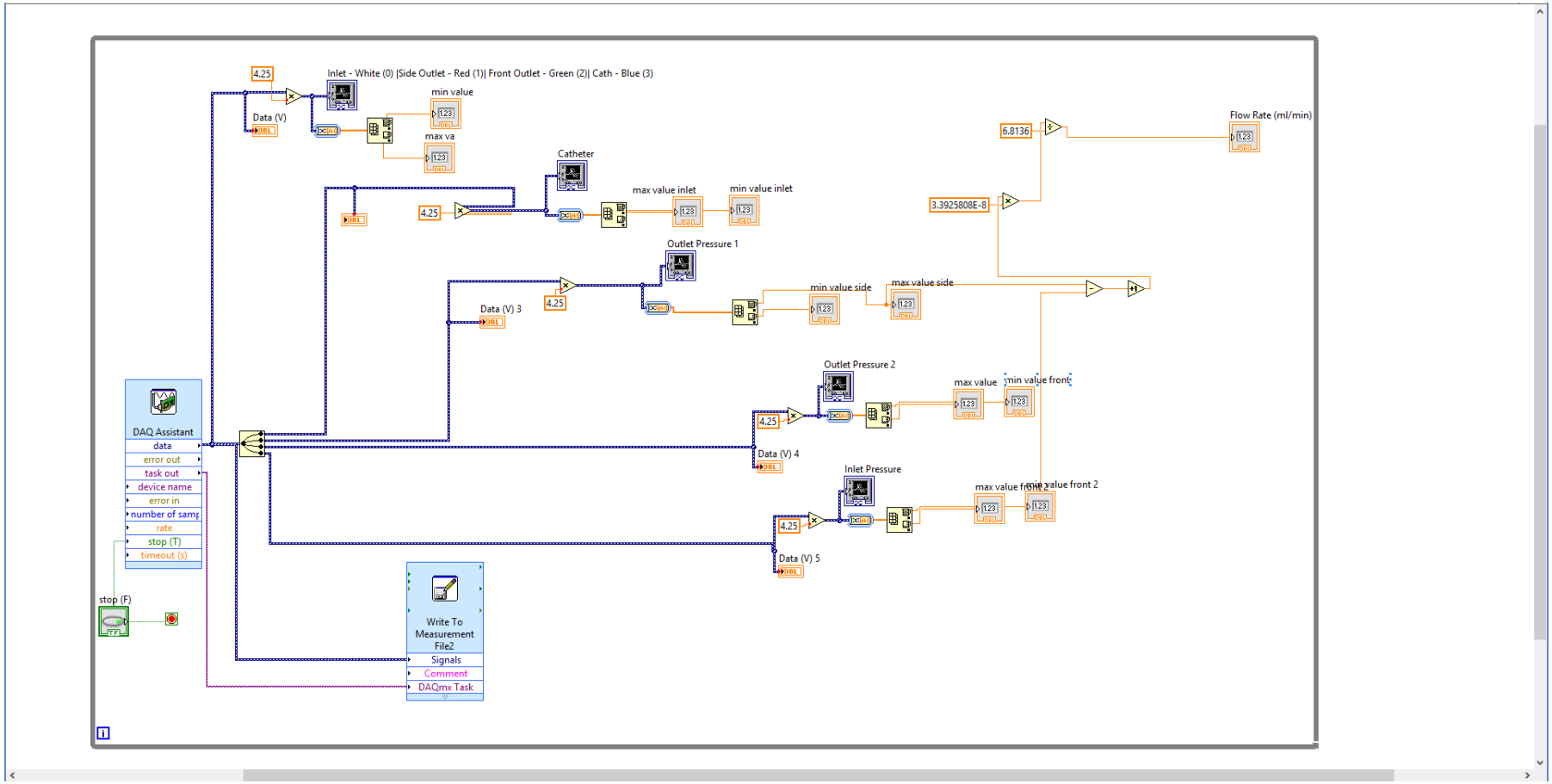

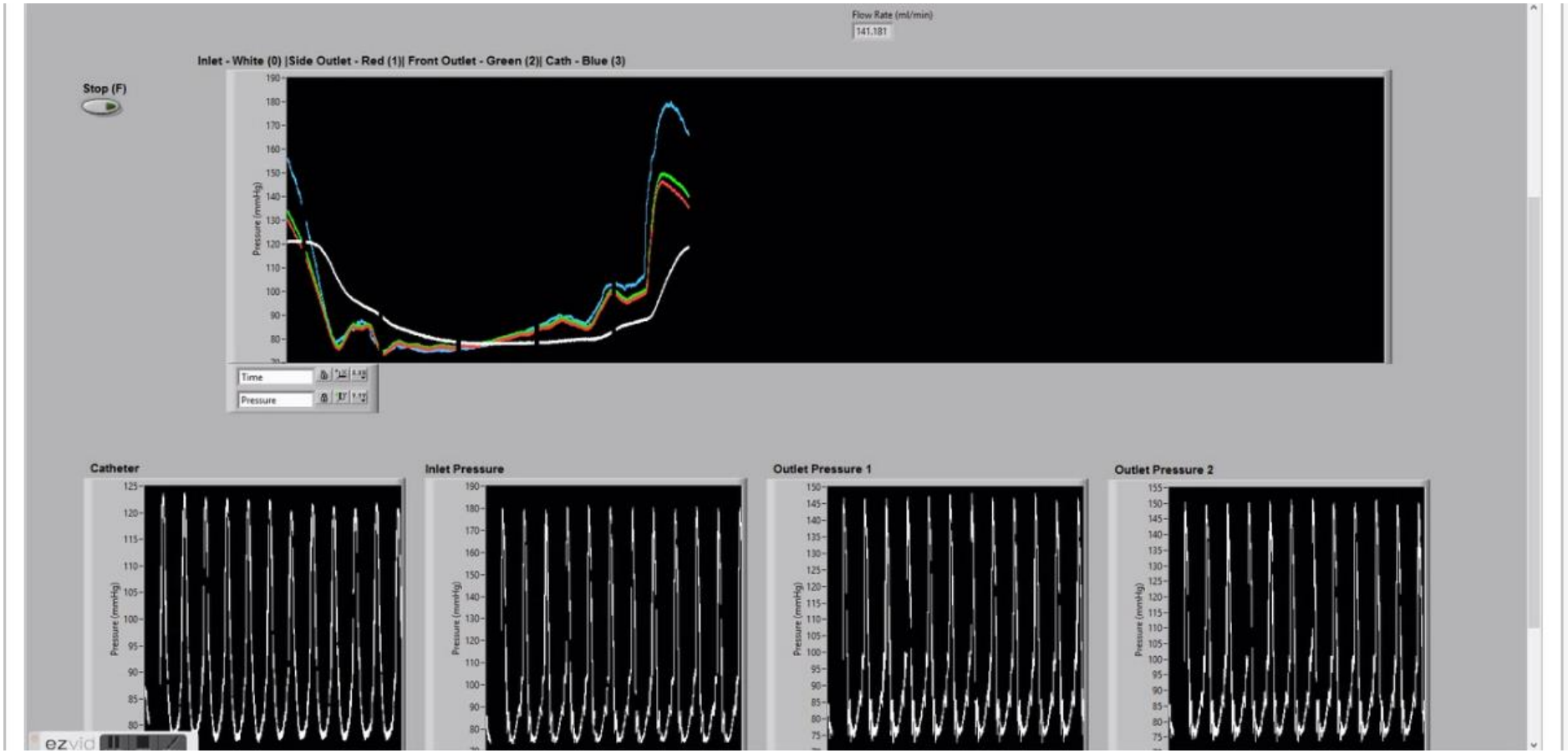
Flow Rate (ml/min)
141.181
Inlet - White (0) |Side Outlet - Red (1)| Front Outlet - Green (2)| Cath - Blue (3)
Stop (F)
Pressure (mmHg)
Time
Pressure
Catheter
Inlet Pressure
Outlet Pressure 1
Outlet Pressure 2
ezvid

9.4.3. Bond Strength

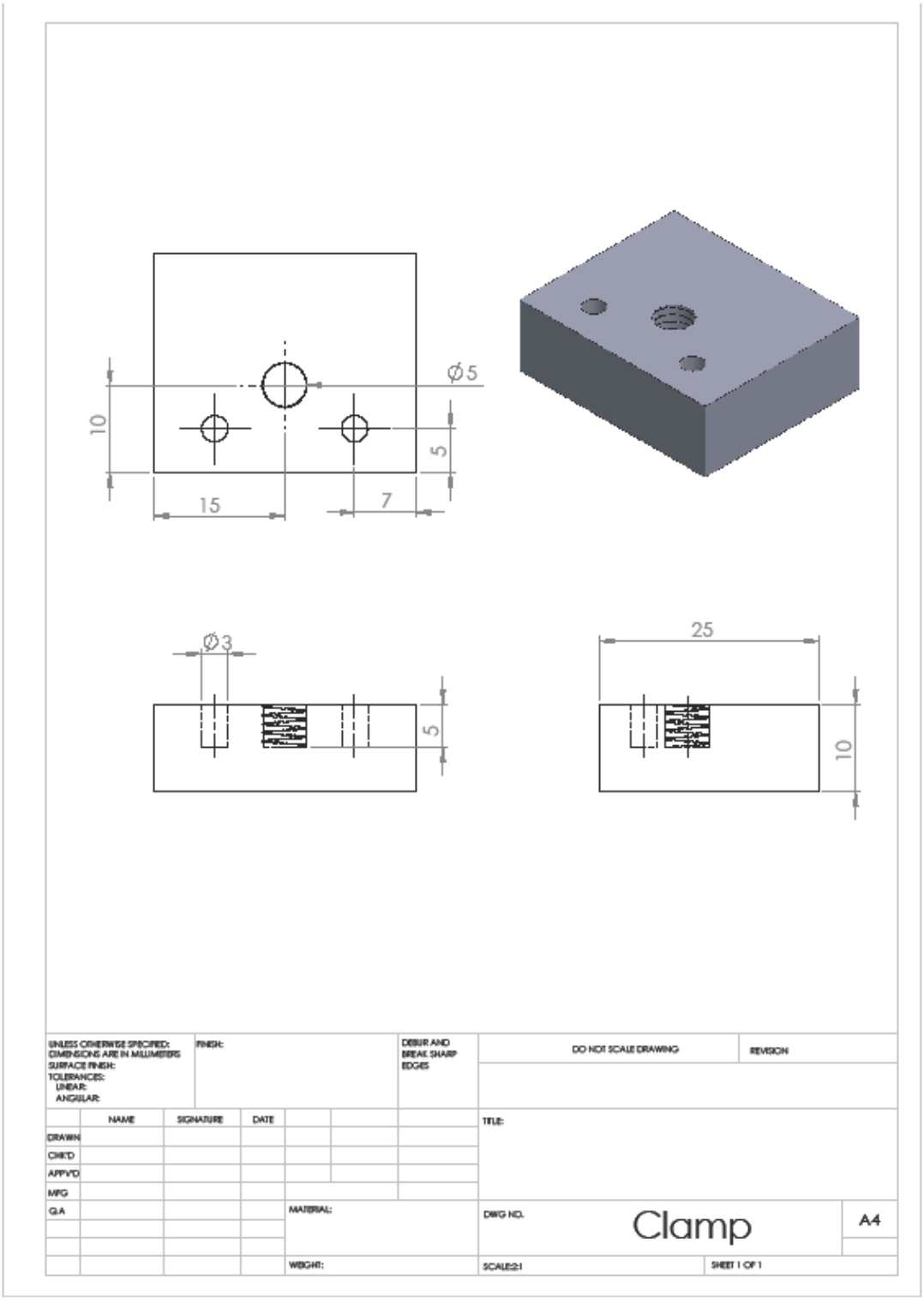

Figure 9.4.7 Drawing of clamp used to keep the plate parallel

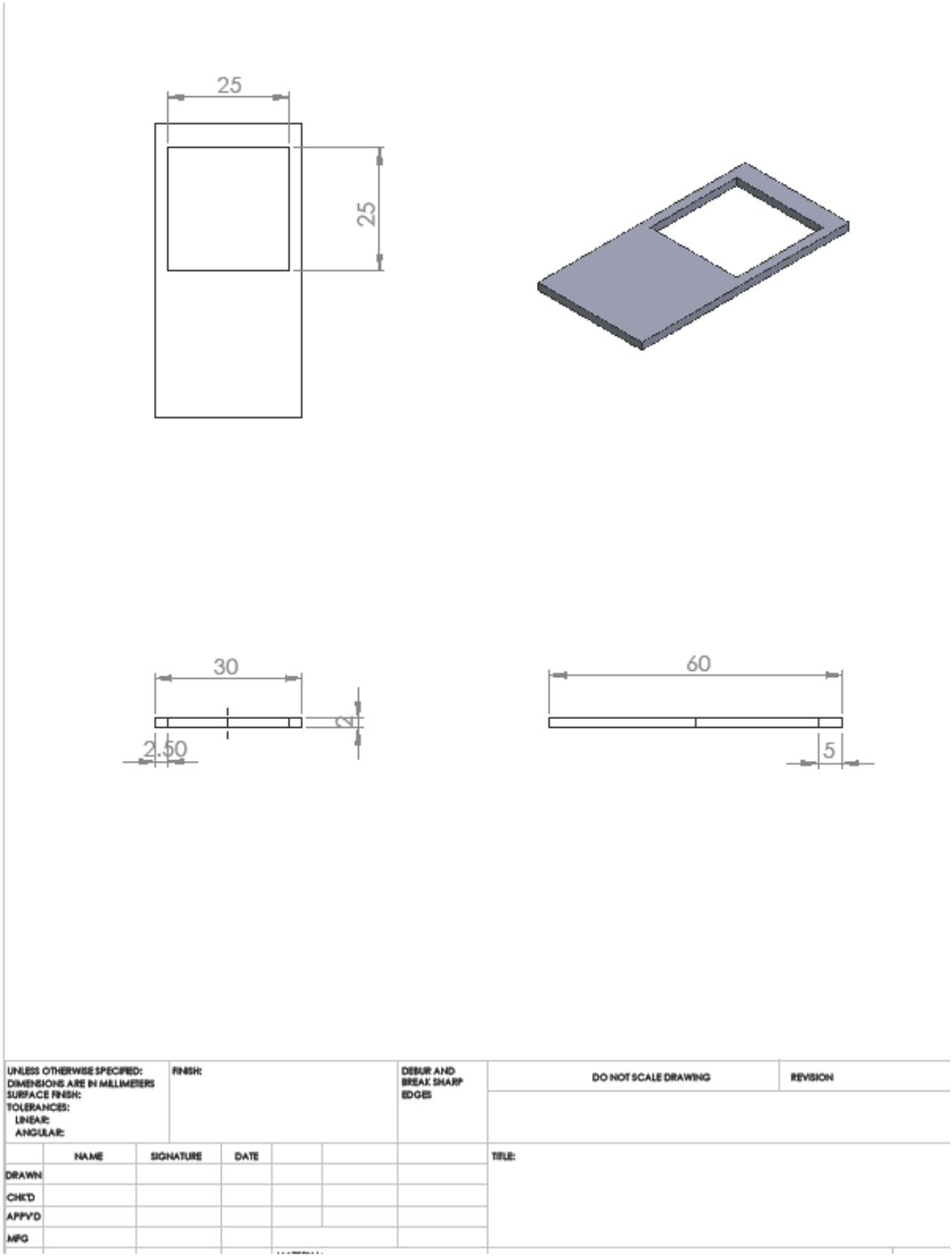

Figure 9.4.8 Drawing of the plate with template for placing hydrogel

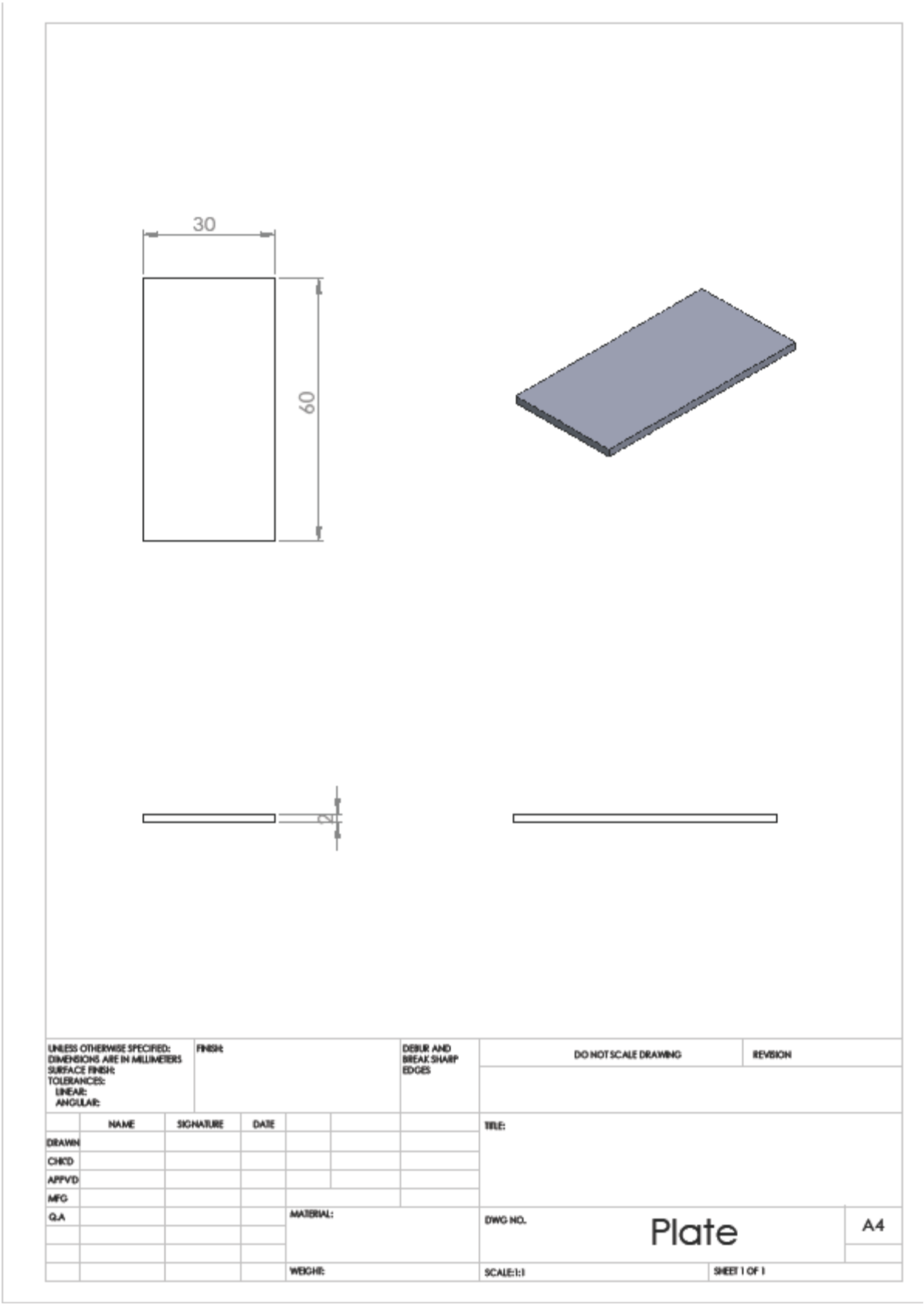

Figure 9.4.9 Drawing of the plates used for bond strength testing

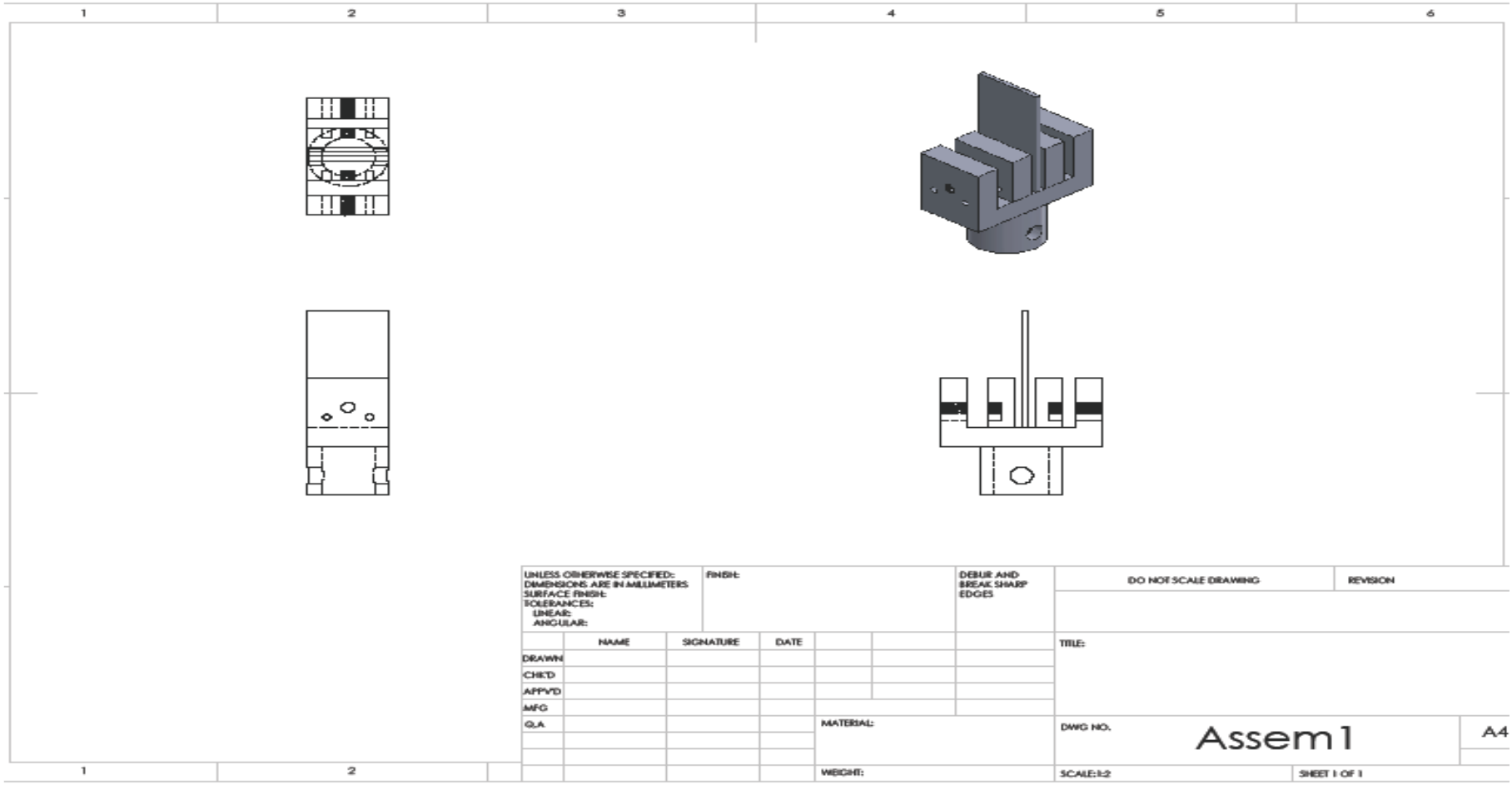

Figure 9.4.10 Assembly drawing of the bond strength testing clamp with plate

9.4.4. Ion Dosing Calculations

9.4.4.1. Calcium

The average calcium content of the hydrogels eluent is 17mM or 0.68mg/mL.

$$\frac{Calcium\ chloride\ molecular\ weight}{Calcium\ molecular\ weight} = \frac{\frac{110.98g}{mol}}{\frac{40.078g}{mol}} = 2.77$$

$$2.77 \times \frac{0.68mg}{ml} = 1.88mg/mL$$

9.4.4.2. Gallium

The average gallium content of the hydrogels eluent is 16.8mM or 1.17mg/mL.

$$\frac{Gallium\ nitrate\ molecular\ weight}{Gallium\ molecular\ weight} = \frac{\frac{255.74g}{mol}}{\frac{69.723g}{mol}} = 3.67$$

$$3.67 \times \frac{1.17mg}{ml} = 4.3mg/mL$$

9.4.4.3. Silicon

The average silicon content of the hydrogels eluent is 5mM or 0.14mg/mL.

$$\frac{Silicic\ acid\ molecular\ weight}{Silicon\ molecular\ weight} = \frac{\frac{96.113g}{mol}}{\frac{28.0855g}{mol}} = 3.422$$

$$3.422 \times \frac{0.14mg}{ml} = 0.5mg/mL$$

9.5. Appendix D

9.5.1. Effect of Molecular Weight and Chemical Composition

9.5.1.1. ^{1}H-NMR

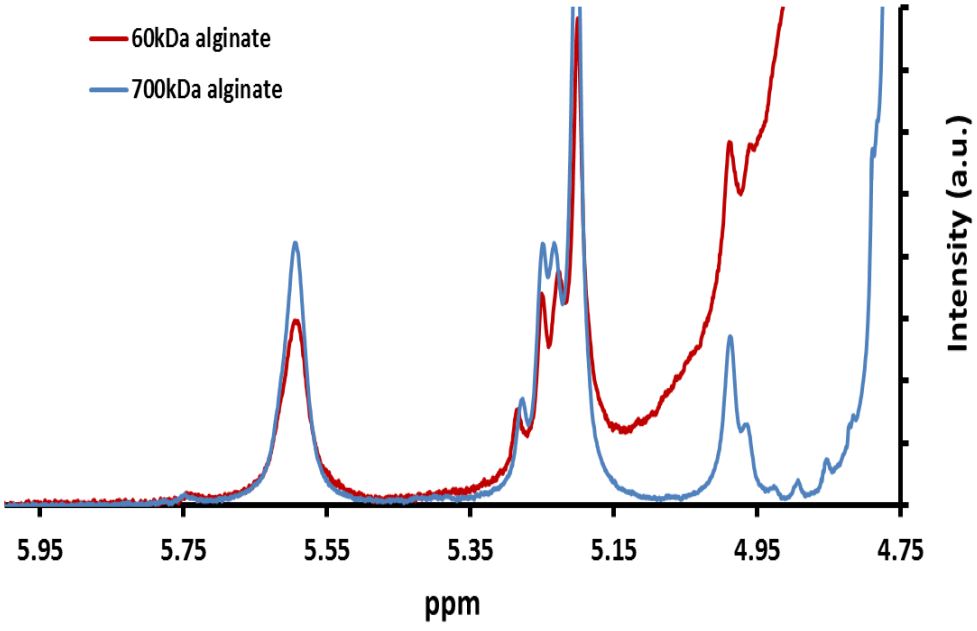

Figure 9.5.1 ^{1}H-NMR spectra of the 60kDa and 700kDa alginate

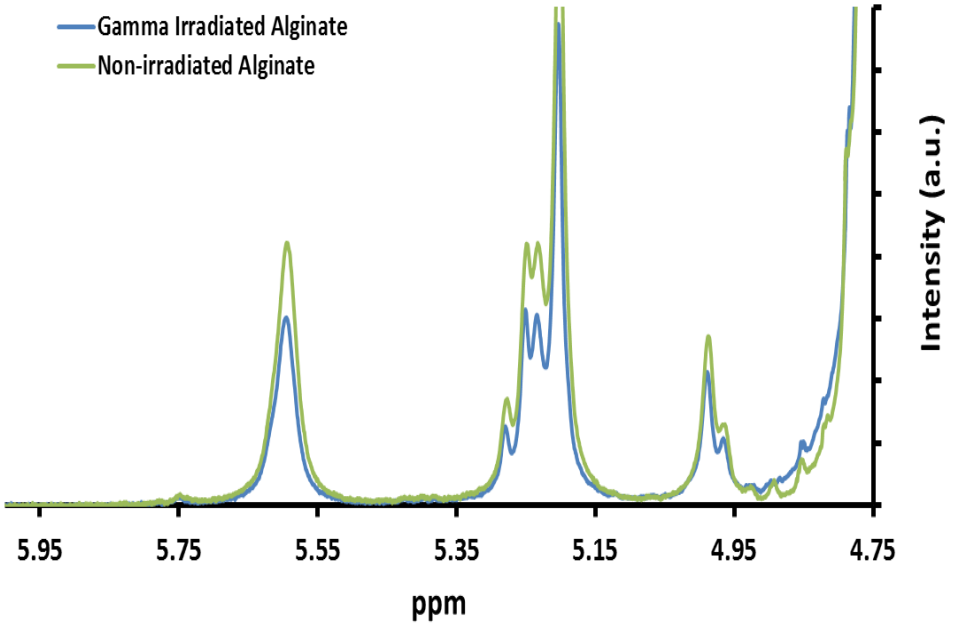

Figure 9.5.2 ^{1}H-NMR spectra of the non-irradiated (700kDa) and gamma irradiated (180kDa) alginate

9.5.1.2. Typical Stress-Strain graphs

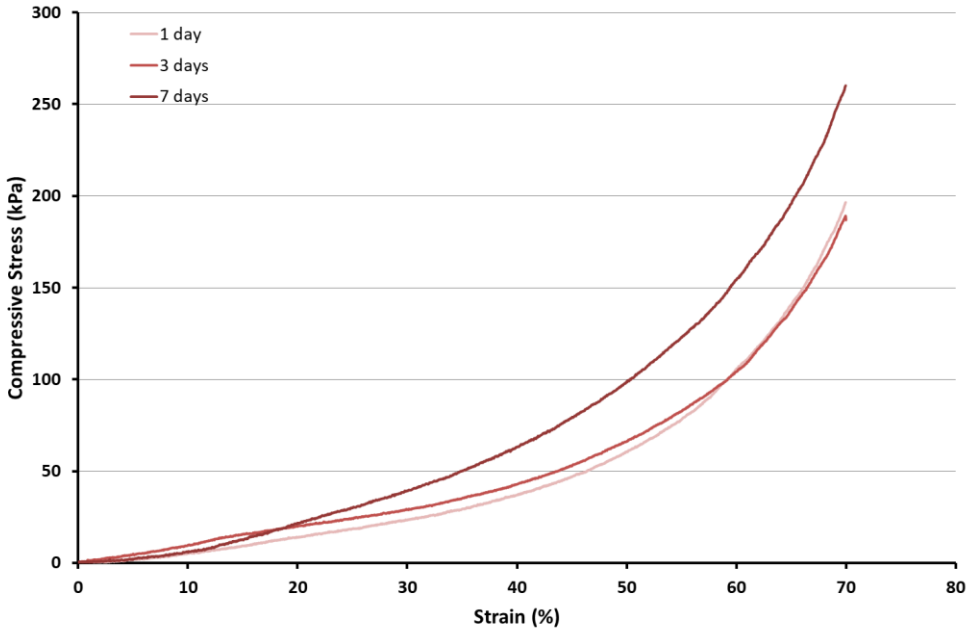

Figure 9.5.3 Typical stress-strain graph of a 0.5% concentration of the 60kDa (High-G) alginate following storage for 1, 3 and 7 at 37^{0}C in DI

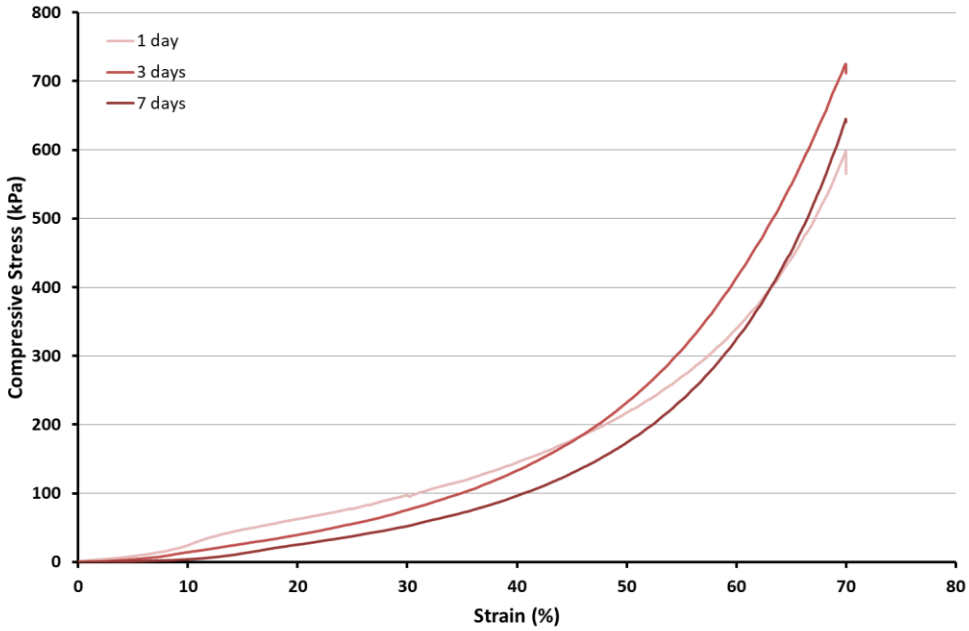

Figure 9.5.4 Typical stress-strain graph of a 2.5% concentration of the 60kDa (High-G) alginate following storage for 1, 3 and 7 at 37^{0}C in DI

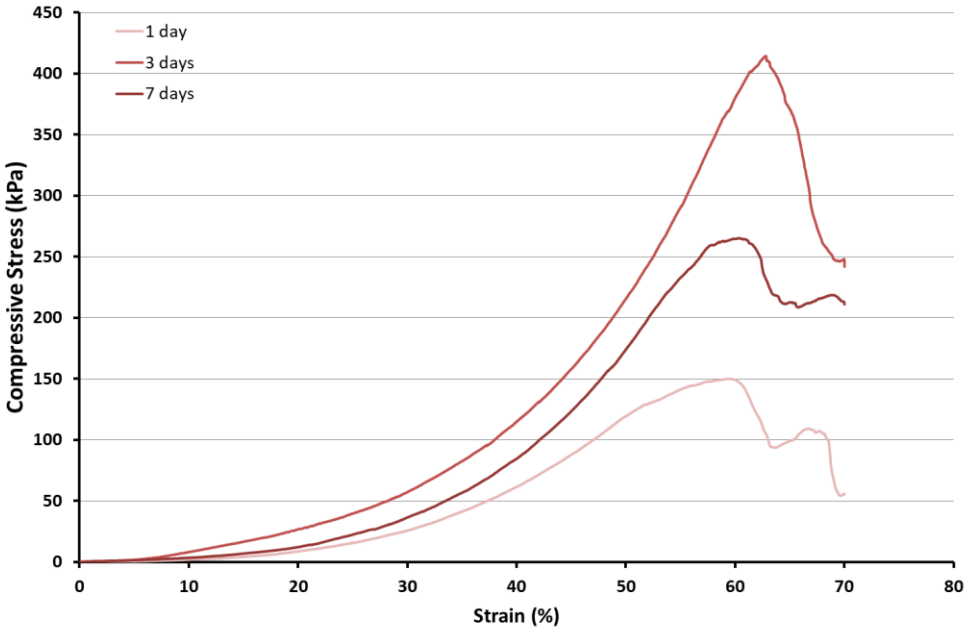

Figure 9.5.5 Typical stress-strain graph of the 4.5% concentration of the 60kDa (High-G) alginate following storage for 1, 3 and 7 at 37^0C in DI

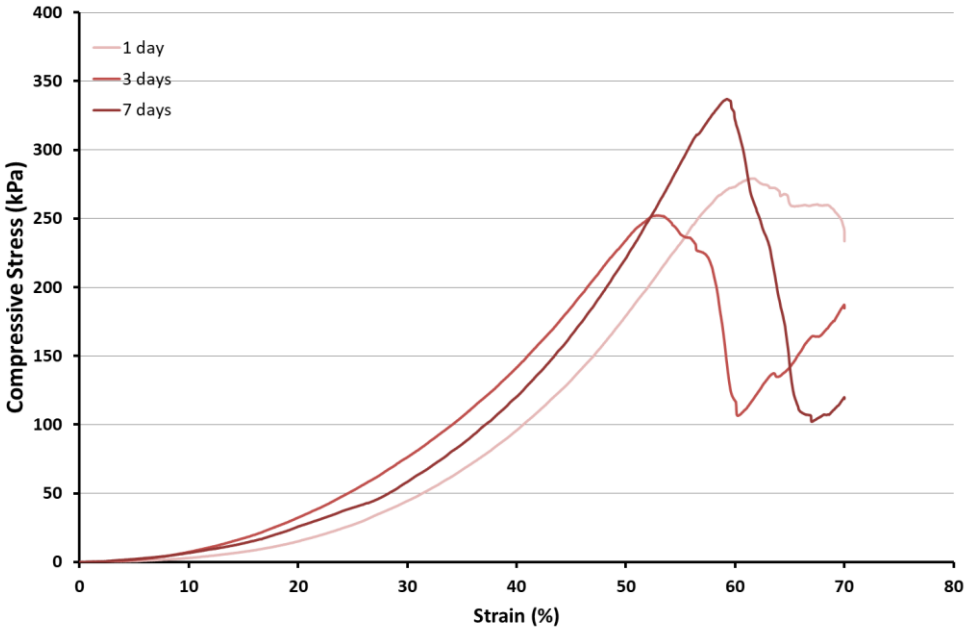

Figure 9.5.6 Typical stress-strain graph of the 6.0% concentration of the 60kDa (High-G) alginate following storage for 1, 3 and 7 at 37^0C in DI

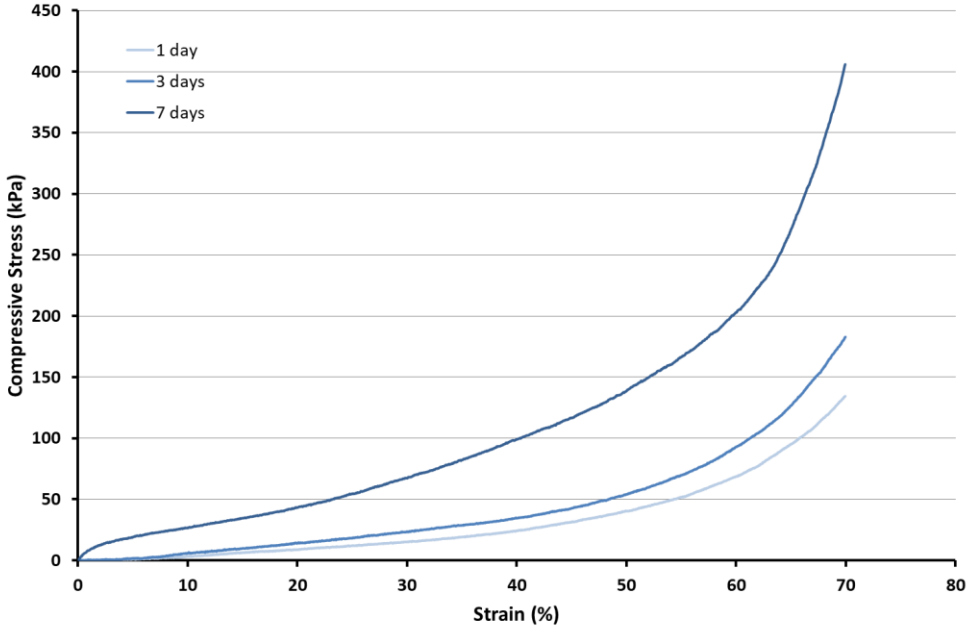

Figure 9.5.7 Typical stress-strain graph of a 0.5% concentration of the 700kDa (High-M) alginate following storage for 1, 3 and 7 at 37^0C in DI

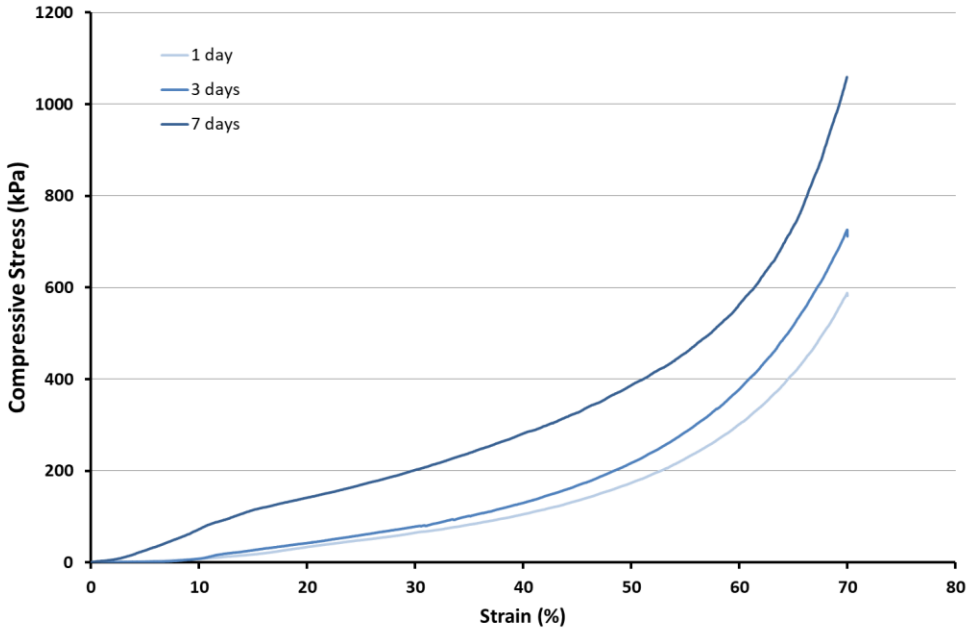

Figure 9.5.8 Typical stress-strain graph of the 700kDa (High-M) alginate following storage for 1, 3 and 7 at 37^0C in DI

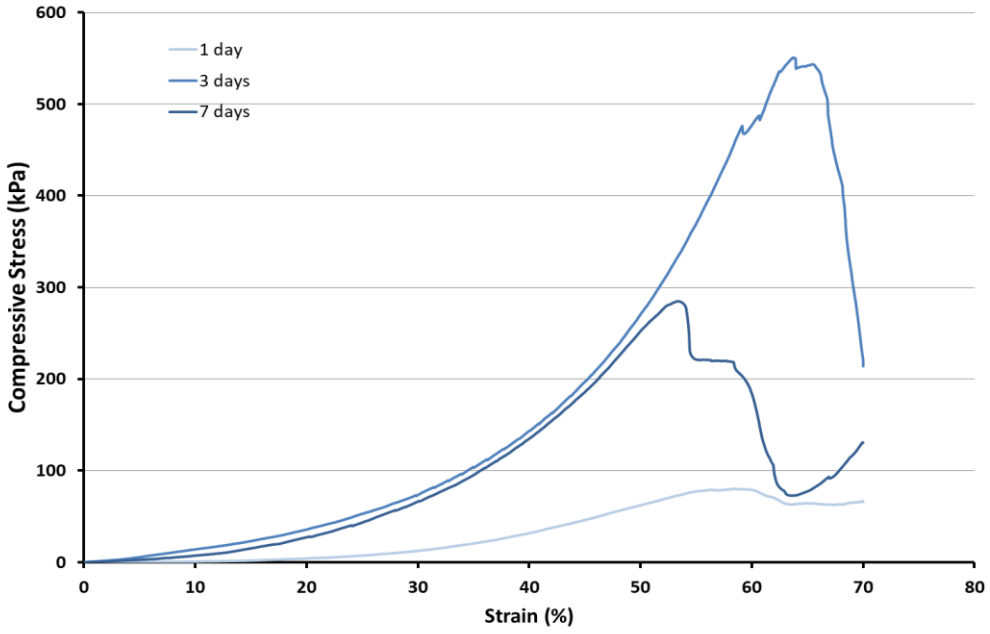

Figure 9.5.9 Typical stress-strain graph of a 4.5% concentration of the 700kDa (High-M) alginate following storage for 1, 3 and 7 at 37^0C in DI

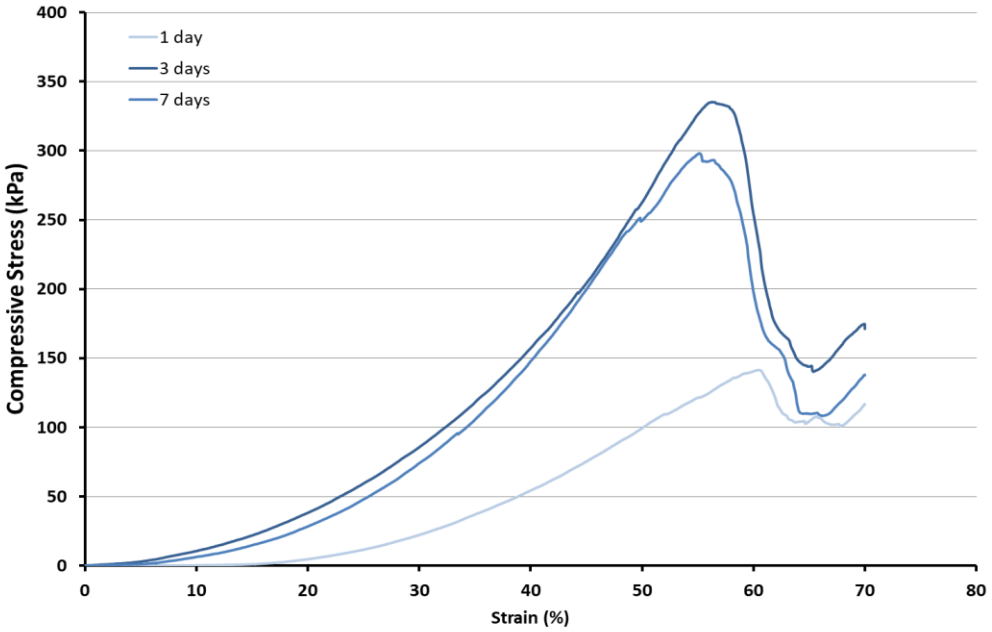

Figure 9.5.10 Typical stress-strain graph of a 6.0% concentration of the 700kDa (High-M) alginate following storage for 1, 3 and 7 at 37^0C in DI

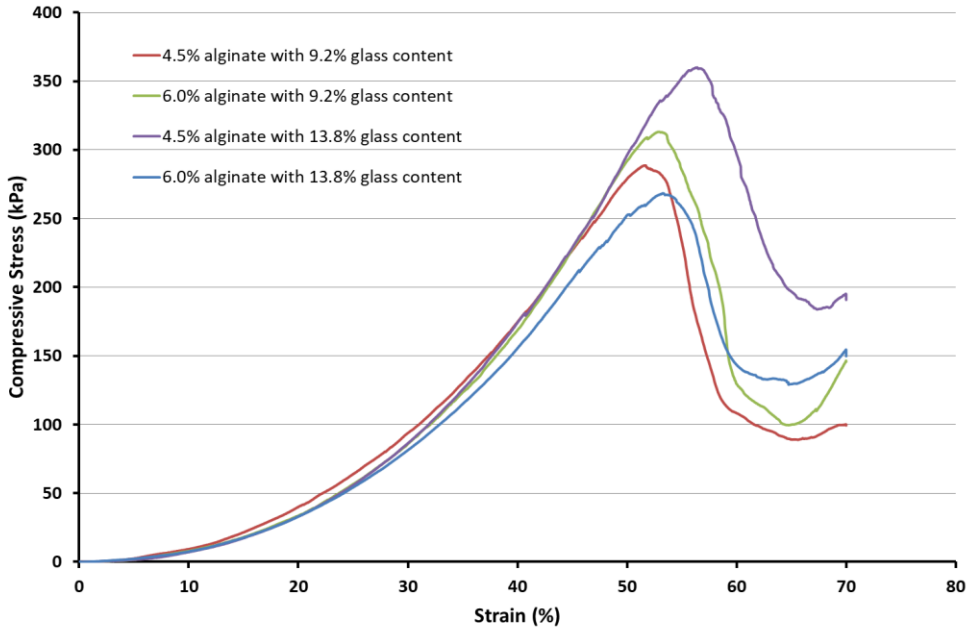

Figure 9.5.11 Typical stress-strain graph of the 700kDa (High-M) alginate with varying glass content following storage for 1 at 37^{0}C in DI

9.5.2. Effect of Acid Washing Glass and Increasing Glass Content

9.5.2.1. Typical Stress-Strain graphs

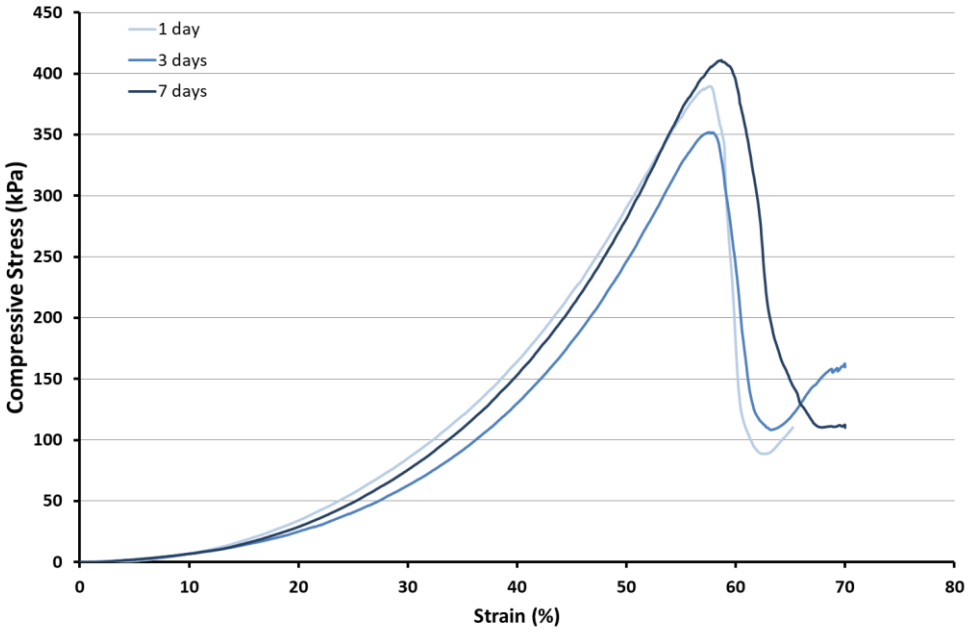

Figure 9.5.12 Typical stress-strain graph of the acid washed glass (4.6% content) following storage for 1, 3 and 7 days at 37^0C in DI

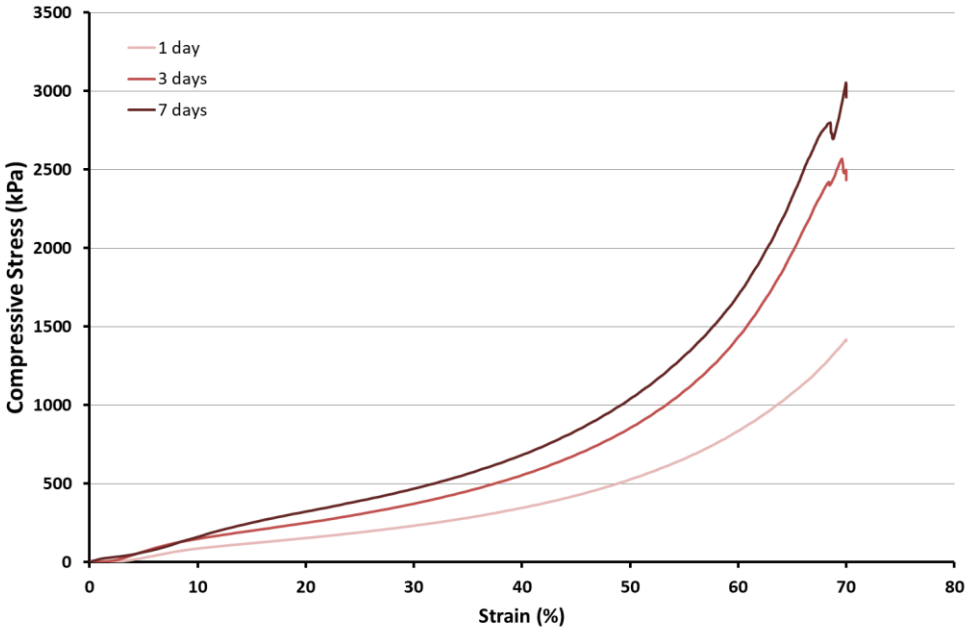

Figure 9.5.13 Typical stress-strain graph of the acid washed glass (13.8% content) following storage for 1, 3 and 7 days at 37^0C in DI

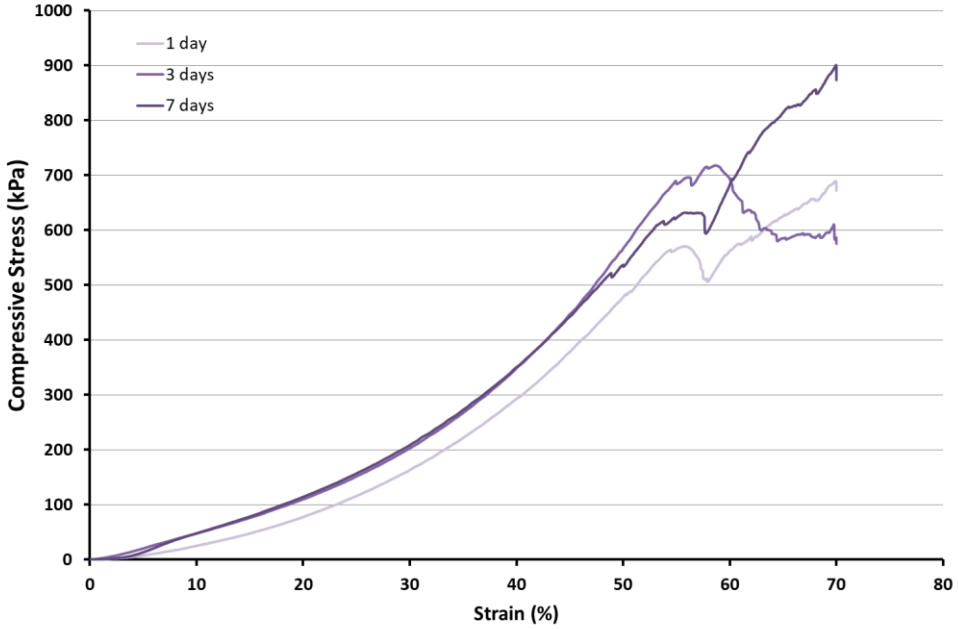

Figure 9.5.14 Typical stress-strain graph of the acid washed glass (13.8% content) following storage for 1, 3 and 7 days at 37^{0}C in PBS

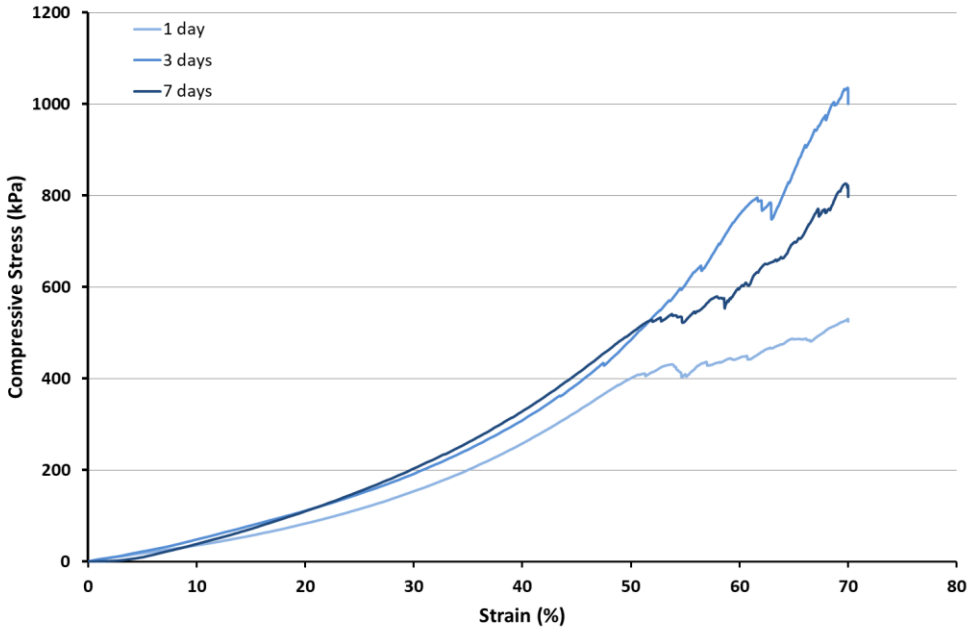

Figure 9.5.15 Typical stress-strain graph of the acid washed glass (13.8% content) following storage for 1, 3 and 7 days at 37^{0}C in SBF

9.5.2.2. *Effect of the Addition of EDC and NHS*

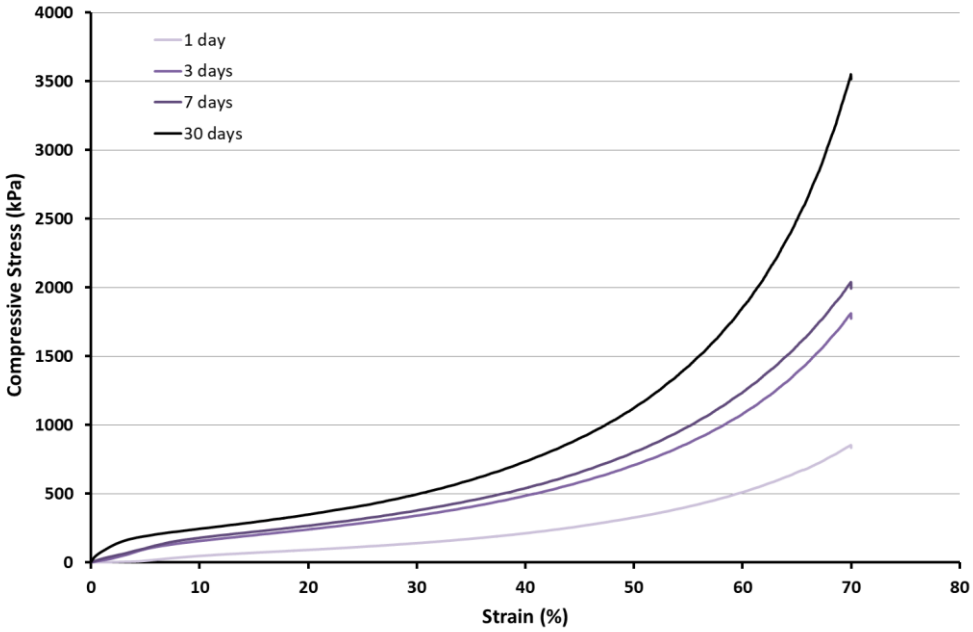

Figure 9.5.16 Typical stress-strain graph of the hydrogel with 0.83% (w/v) of EDC and NHS following storage for 1, 3, 7 and 30 days at 37^0C in DI

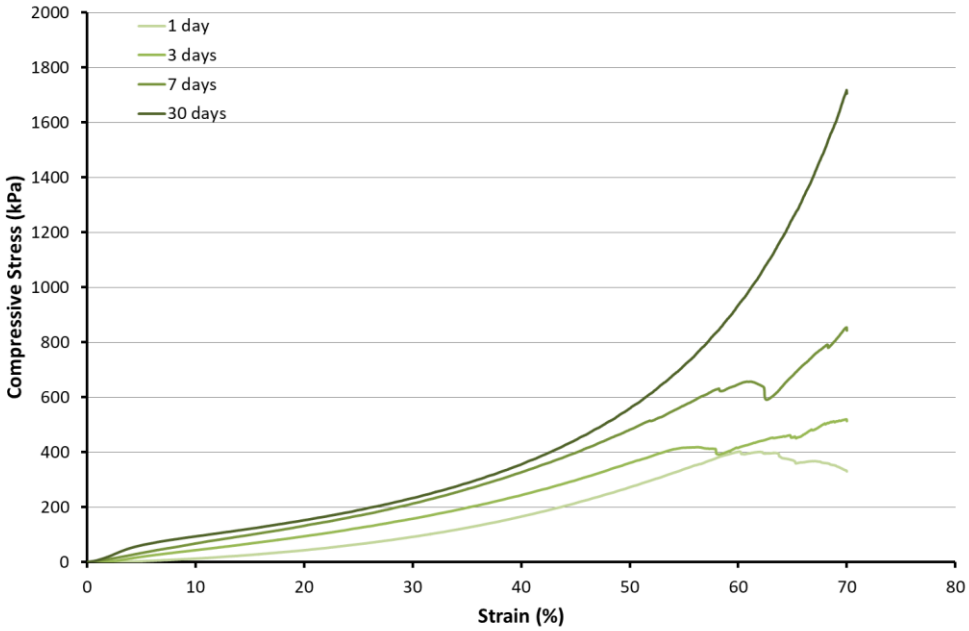

Figure 9.5.17 Typical stress-strain graph of the hydrogel with 0.83% (w/v) of EDC and NHS following storage for 1, 3, 7 and 30 days at 37^0C in PBS

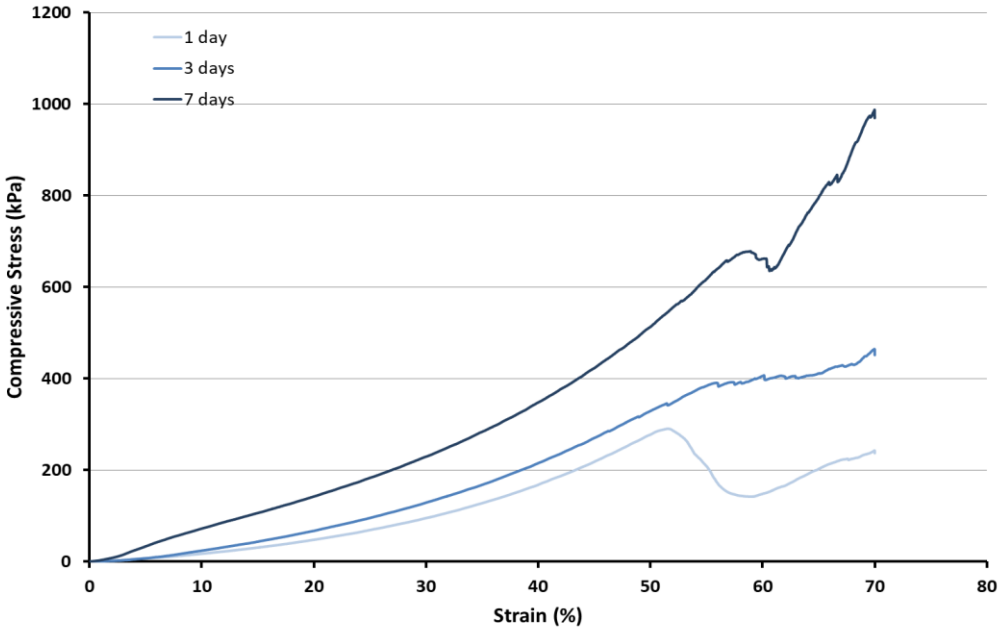

Figure 9.5.18 Typical stress-strain graph of the hydrogel with 0.83% (w/v) of EDC and NHS following storage for 1, 3, 7 and 30 days at 37^0C in SBF

9.5.2.3. Bond Strength Testing

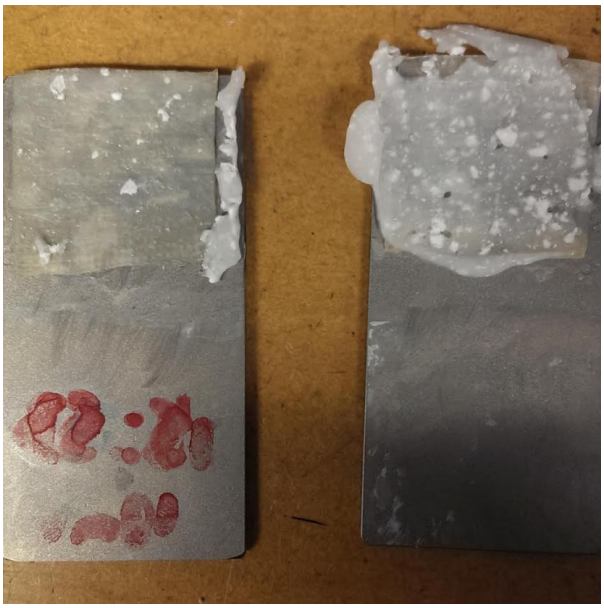

Figure 9.5.19 Adhesive failure of hydrogel with 0.83% (w/v) of EDC and NHS

Figure 9.5.20 Cohesive failure of hydrogel with 0% (w/v) of EDC and NHS

9.5.3. *In Vitro* Analysis

Figure 9.5.21 shows that BASMCs dosed with Eluent C. There was no significant difference between the cells dosed with 24 hour eluent or 48 hour eluent. There was a significant increase in cell metabolic activity when dosed with 60% of the 24 hour and 48 hour eluent. Compared to the BAECs, there is an increase in 24 hour eluent up to 60% and a decrease in 48 hour eluent at 80% and 100%.

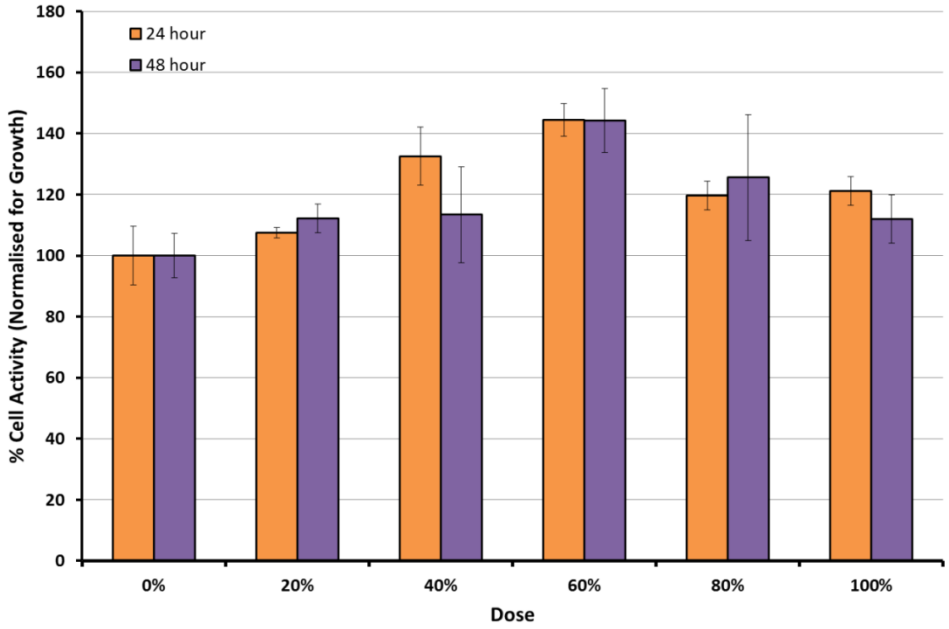

Figure 9.5.21 BASMC cell activity for cells dosed with Eluent C at different eluent concentrations (n=3)

There is a slight decrease in cell number with cells dosed with 20% 24 hour eluent, as shown in Figure 9.5.22. There was a significant increase in cell number of cells dosed with 48 hour eluent. Overall, increasing the eluent concentration caused cell proliferation. There is no significant difference in cell number of BASMCs dosed with 24 hour eluent compared to BAECs. But there was a slight decrease in cell number compared to BAECs dosed with 48 hour at 20%.

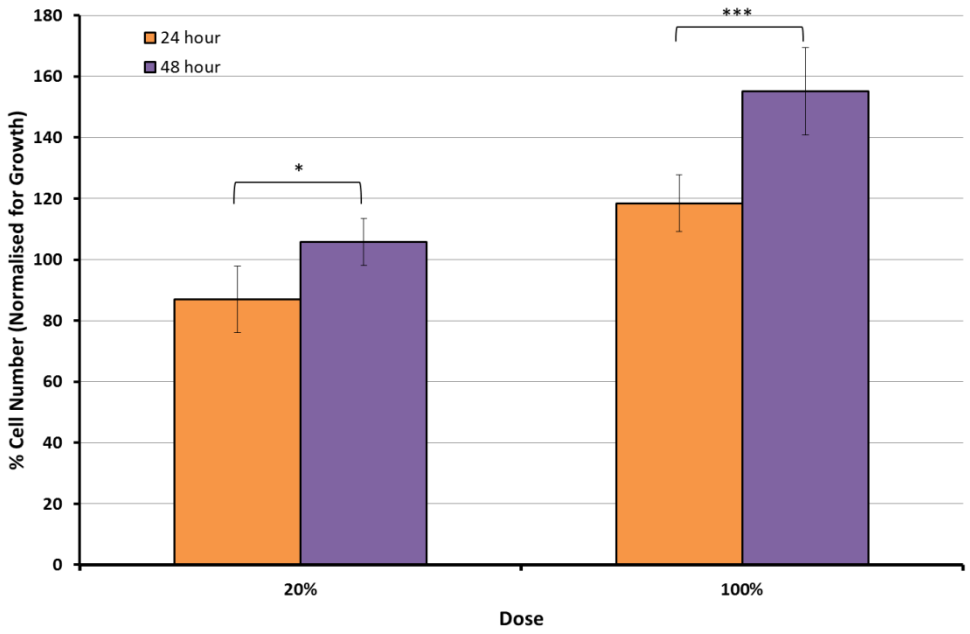

Figure 9.5.22 BASMC cell number change (%) of cells dosed with varying concentrations of Eluent C (n=3)

9.5.4. Optimising Sterilisation Techniques

9.5.4.1. Alginate Sterilisation

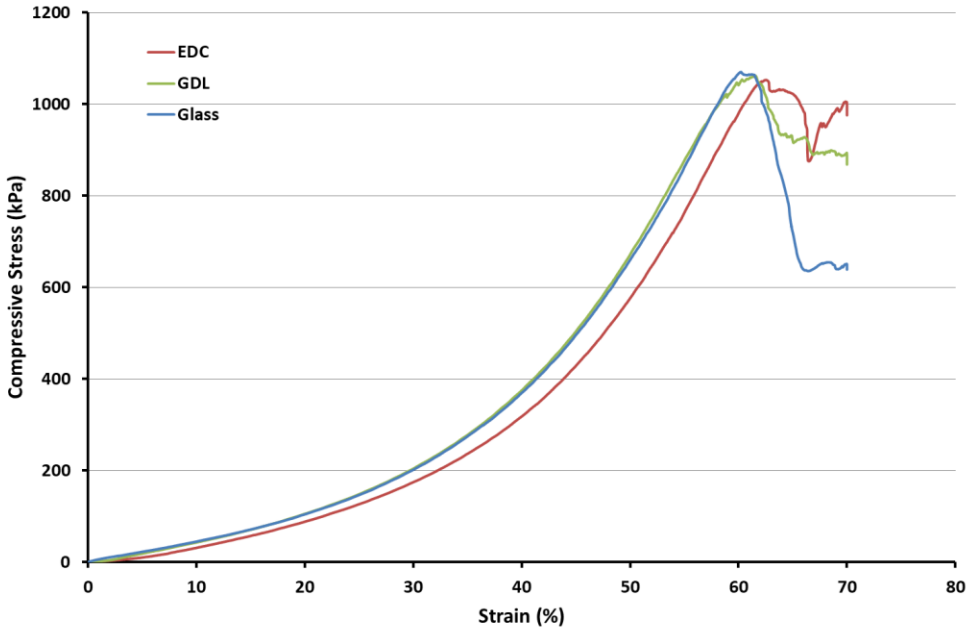

Figure 9.5.23 Typical stress-strain graph of the hydrogel with various components sterilised following storage for 1, 3 and 7 days at 37^0C in DI

9.5.4.2. BAEC's Dosed with MVM Alginate Hydrogel

There was a significant increase in cells dosed with 48 hour eluent compared to the 24 hour eluent between 40% and 100%. Overall, the cell activity increased with increasing eluent concentration (see Figure 9.5.24). Similar increases in metabolic activity were observed for BAECs dosed with the 700kDa alginate hydrogel (Figure 5.5.3).

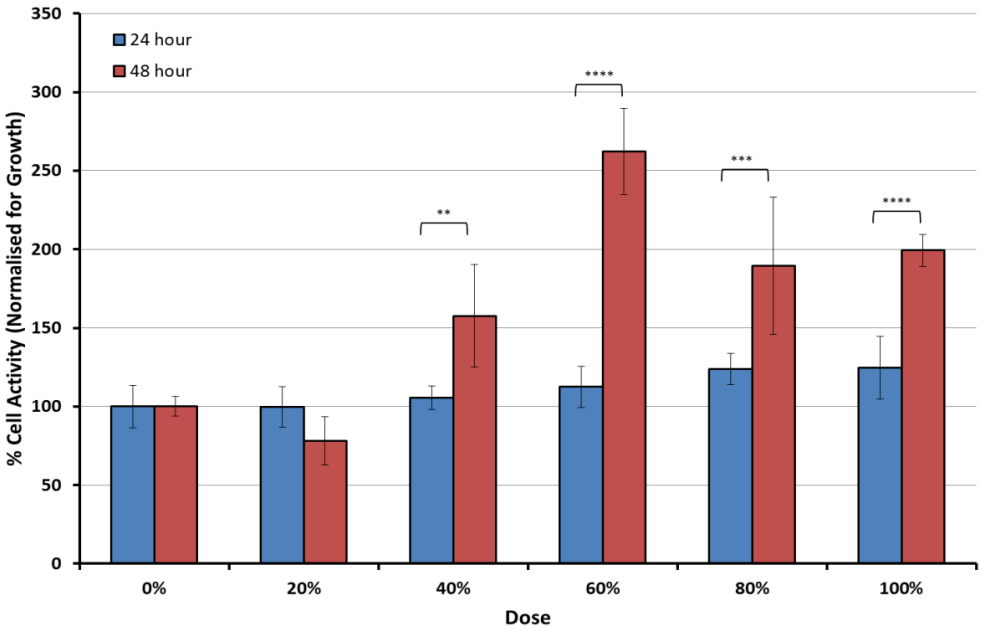

Figure 9.5.24 BAEC cell activity for cells dosed with the hydrogel with MVM alginate at different eluent concentrations (n=3)

There was no significant difference between the cells dosed with 24 hour and 48 hour eluent, as shown in Figure 9.5.25. There was a significant decrease ($p < 0.05$) in the BAECs cell activity with the MVM alginate when compared to the 700kDa alginate; however, there were no cytotoxic effects on the BAECs. There is a significant difference between metabolic activities observed when the cells are dosed with the eluent compared to cell number. Similar results were seen previously (Section) and is likely due to there being insufficient time for considerable cell growth between the cells being dosed and counted.

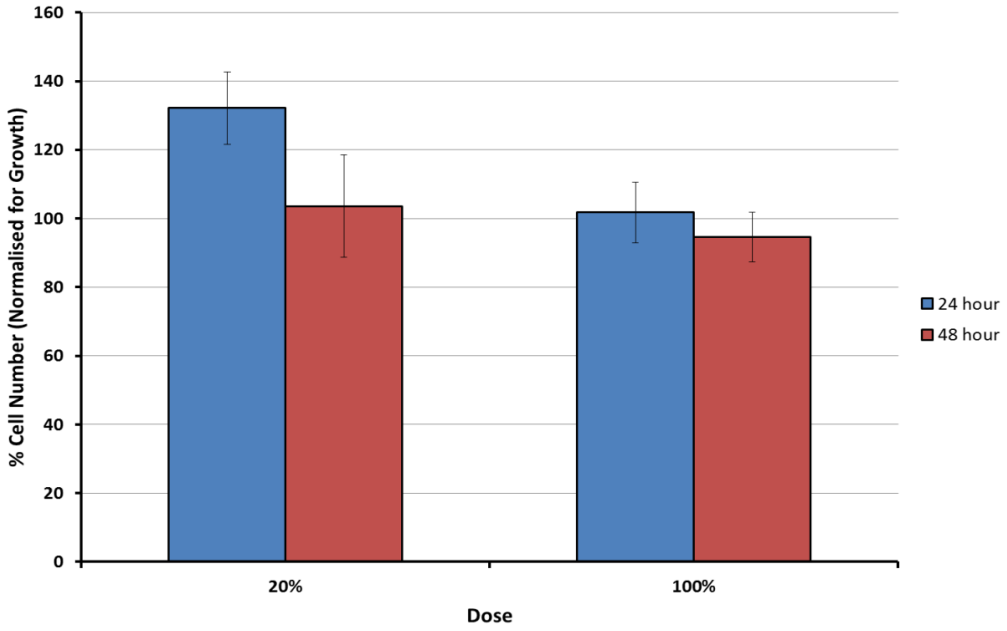

Figure 9.5.25 BAEC cell number change (%) of cells dosed with varying concentrations of the hydrogel with MVM alginate (n=3)

This reduction in cell number may be caused by a change in ions released from the hydrogel. The compressive strength results indicate a high cross-linking density, which may reduce the quantity of ions release from the hydrogel. Although there is a reduction in cell proliferation of the BAEC, the reduced endotoxin levels and M-block content will likely reduce the chances of chronic inflammation or infection *in vivo* [513].

9.5.4.3. *Typical Stress-Strain Graphs*

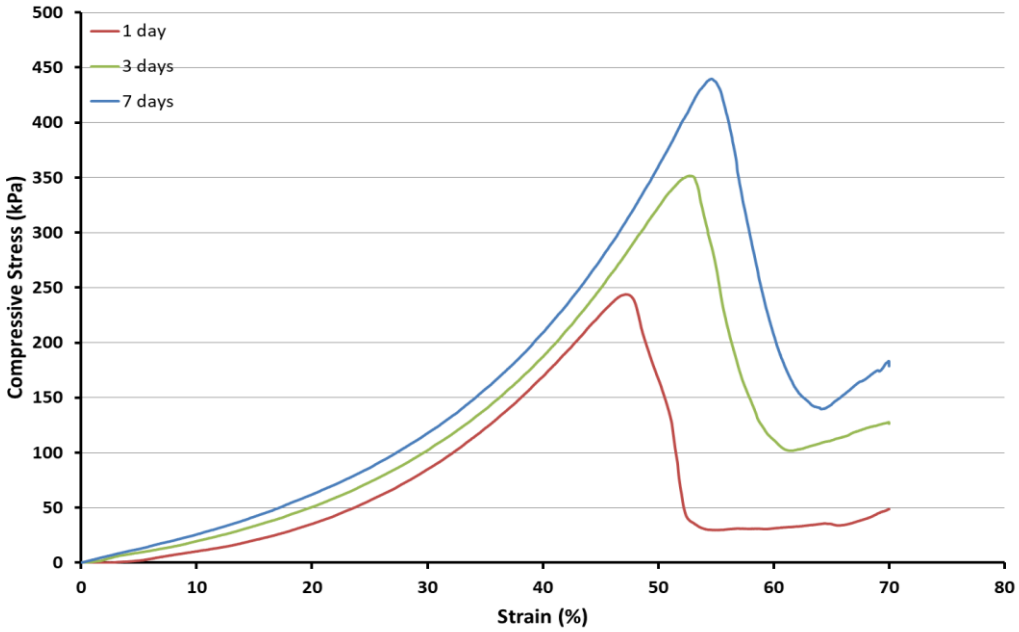

Figure 9.5.26 Typical stress-strain graph of the hydrogel with all components sterilised with 4.5% alginate following storage for 1, 3 and 7 days at 37^0C in SBF

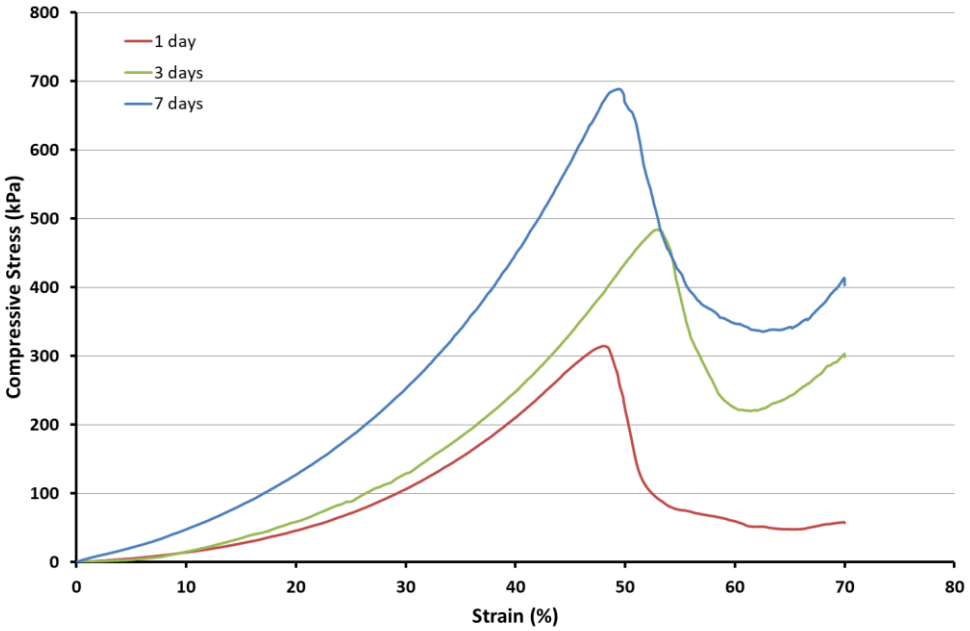

Figure 9.5.27 Typical stress-strain graph of the hydrogel with all components sterilised with 6.75% alginate following storage for 1, 3 and 7 days at 37^0C in SBF

9.5.4.4. 6.75% Autoclaved MVM alginate

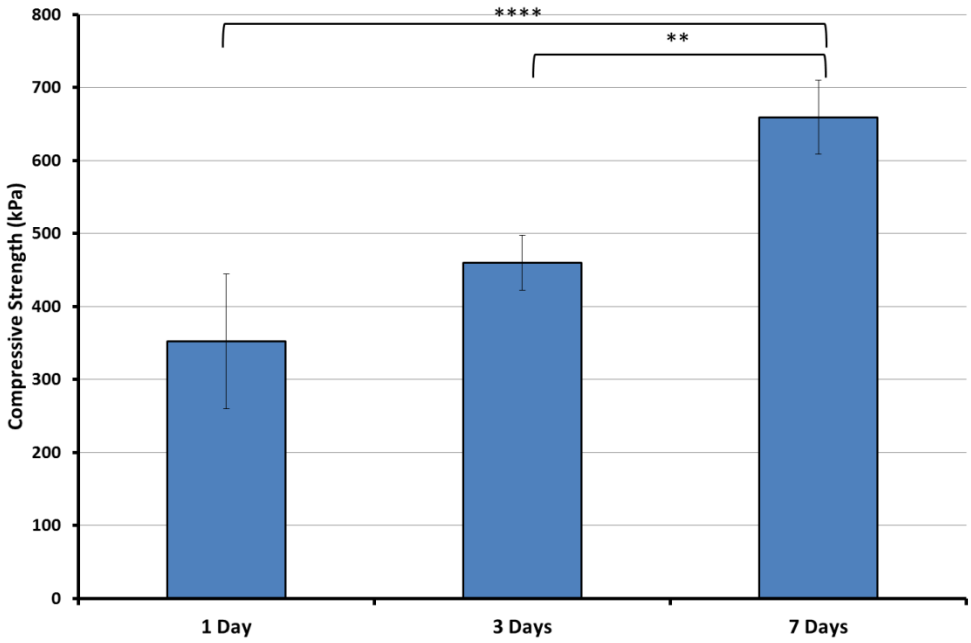

Figure 9.5.28 Compressive strength up to 70% strain of the sterilised hydrogel with 6.75% alginate following storage in SBF at 37^0C (n=5)

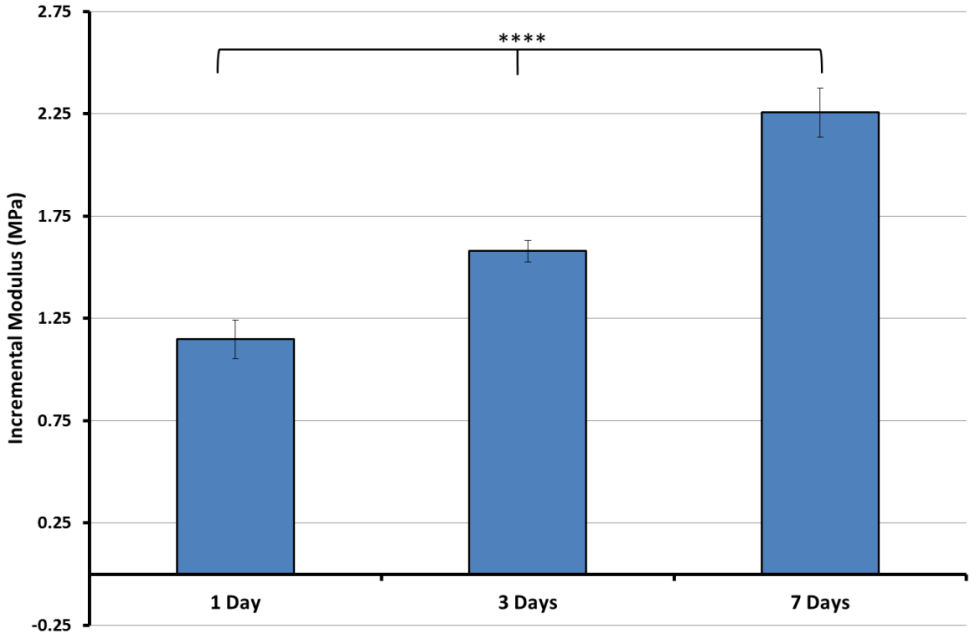

Figure 9.5.29 Incremental modulus (30-50% strain) of the sterilised hydrogel with 6.75% alginate following storage in SBF at 37^0C (n=5)

9.5.5. Direct Contact Testing

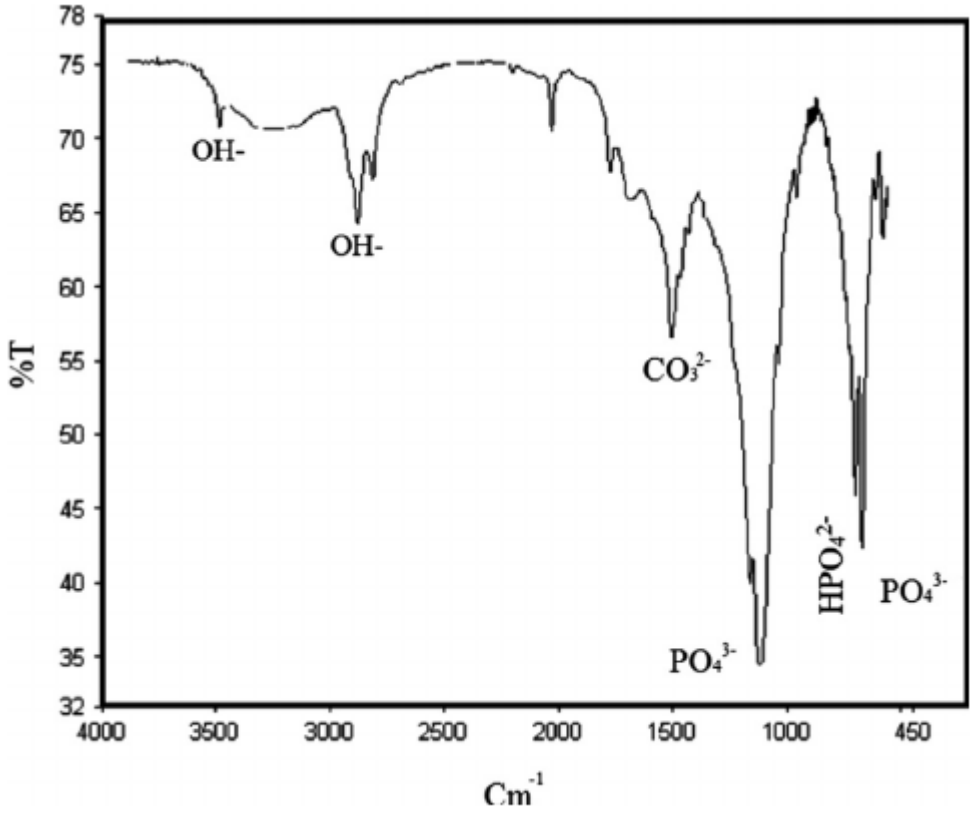

Figure 9.5.30 FTIR of hydroxyapatite powder [514]

9.5.6. Direct Contact Testing

Figure 9.5.31 shows an acellular hydrogel stained with DAPI. Dark spots are seen throughout the hydrogel with a diameter of approximately 200µm. These are likely agglomerations of bioactive glass in the hydrogel. As these agglomerations appear as dark spots, the surface of the glass is likely not adsorbing the stain and interfering with the number of cells observed. The hydrogel itself is seen to adsorb the stain and have a low fluorescence intensity.

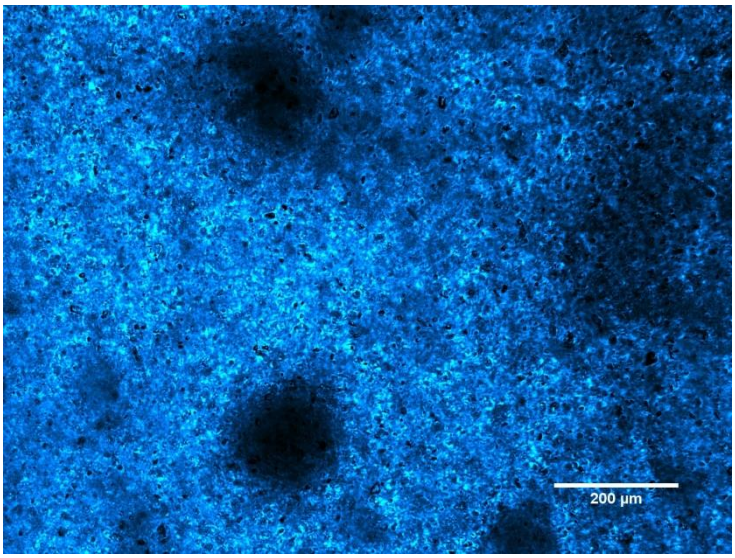

Figure 9.5.31 Acellular DAPI stained hydrogel

9.5.7. Radiopacity

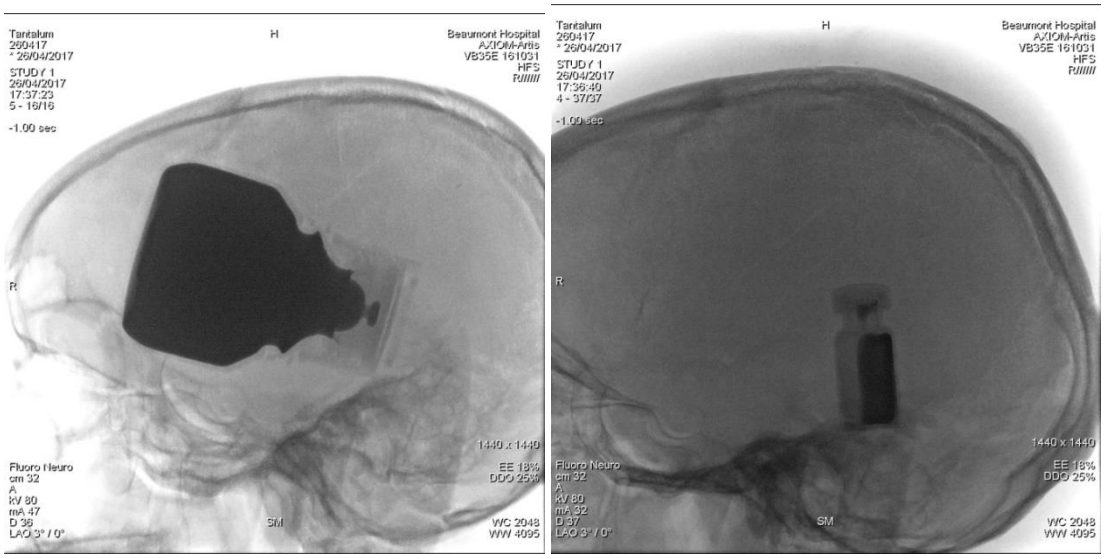

Figure 9.5.32 Fluoroscopy images of an Iodine contrast agent and Onyx® under a skull model

9.5.8. Effect of the Addition of Tantalum

To increase the radiopacity of the hydrogel, the calcium oxide content of the glass was partially replaced with tantalum oxide, see Section 4.3.2 for composition. Tantalum was selected as it is biocompatible and radiopaque [515] [516]. From the results of Section 5.1 and 5.2 it was decided to test the effect of tantalum glass on the hydrogel with the 700kDa High-M alginate at a 4.5% alginate concentration. We have shown that increasing the glass content can increase the hydrogels strength and so the tantalum glass content was varied to further examine the effects increased glass has on the hydrogel strength and the radiopacity of the hydrogel. The GDL content of the hydrogel remained at 4.15% (w/v) for each sample.

9.5.8.1. X-ray Diffraction

Figure 9.5.33 shows that addition of tantalum to the glass does not cause crystallisation of the glass.

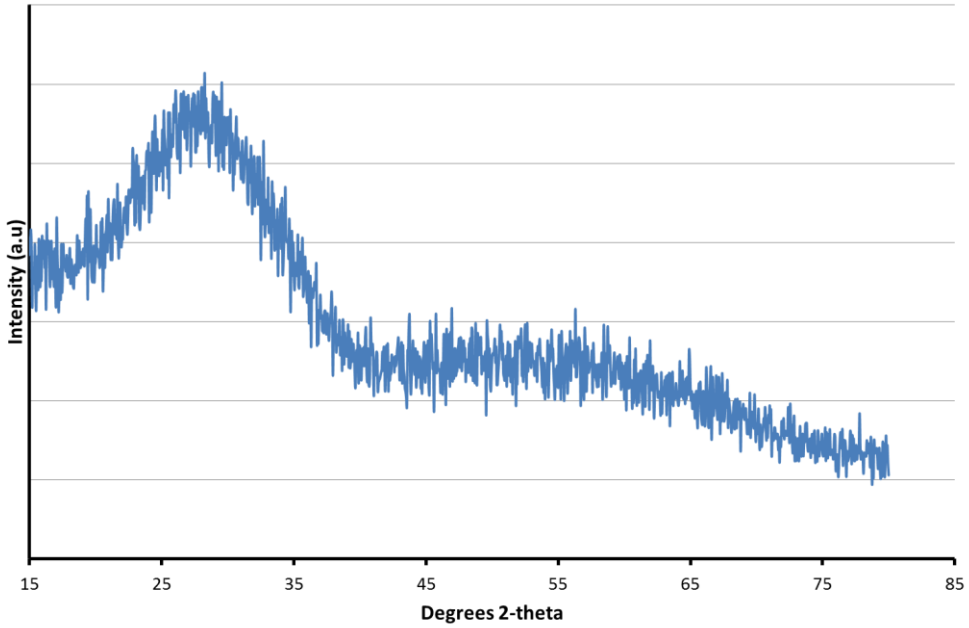

Figure 9.5.33 X-ray diffraction of tantalum glass

9.5.8.2. Compressive Strength

Figure 9.5.34 shows the hydrogel's compressive strength following storage in DI at 37^0C after 1, 3 and 7 days. Increasing the glass content of the hydrogel significantly increases the compressive strength of the hydrogel. However, after 7 days, the hydrogel does not have the minimum strength required (22kPa) at each glass content tested.

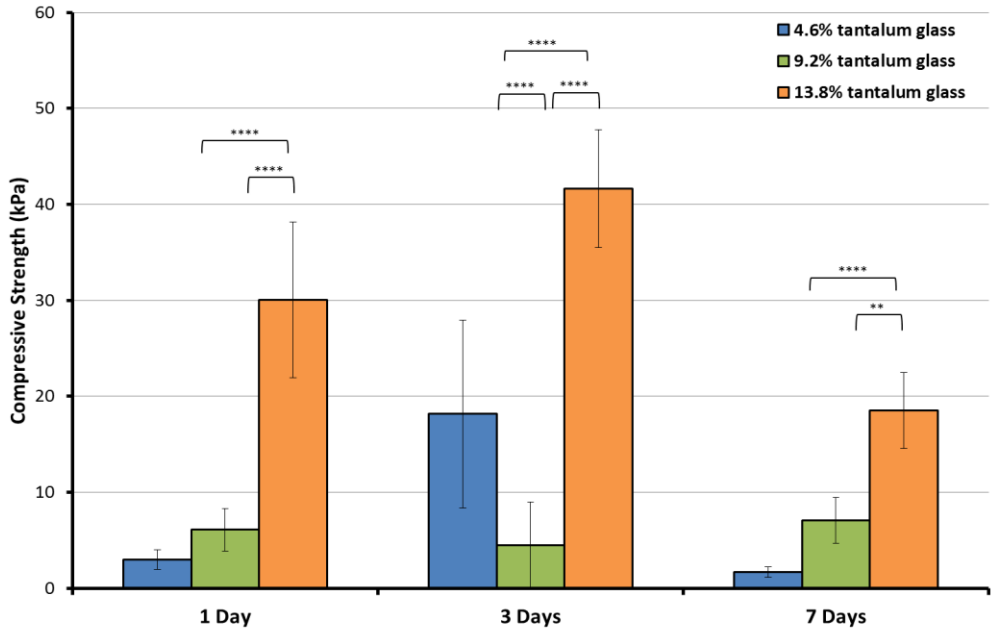

Figure 9.5.34 Compressive strength of 700kDa alginate with varying glass content following storage in DI at 37^0C (n=5)

Figure 9.5.35 compares the tantalum glass to the original glass used in Section 5.1 using a 4.5% alginate concentration, 4.6% glass content with 4.15% (w/v) of GDL. There is a significant decrease in compressive strength at each time point.

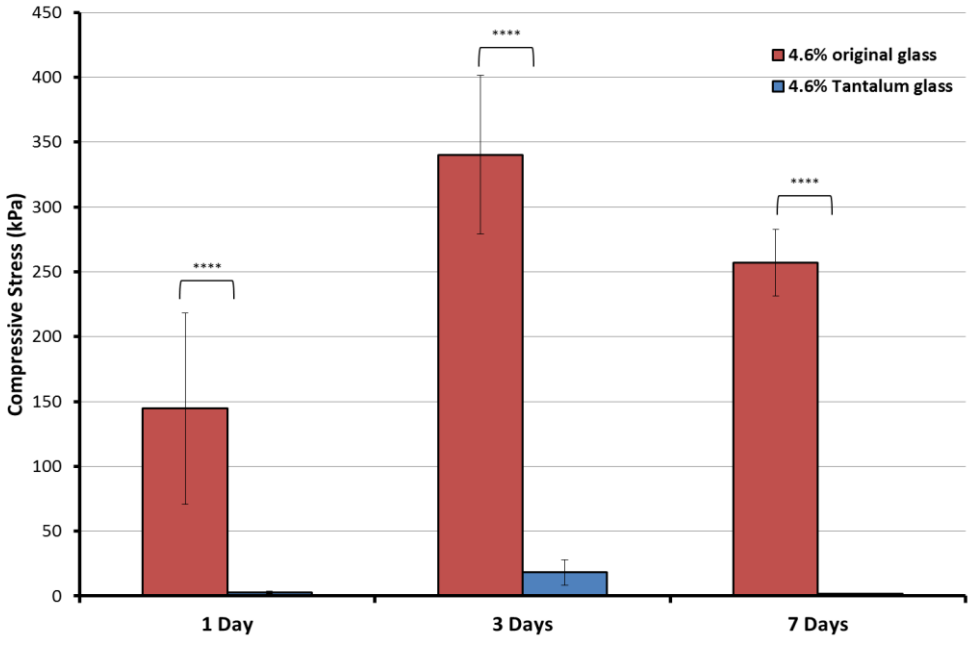

Figure 9.5.35 Compressive stress up to 70% strain of tantalum glass and original glass following storage in DI at 37^0C for 7 days (n=5)

9.5.8.3. Volume Conservation

Figure 9.5.36 shows there is a large increase in sample volume following storage in DI at 37^0C for 7 days. The samples stored for 7 days showed the smallest increase in size, showing that

cross-linking is continuing over time. The mean sample volume does decrease with increasing glass content but not significantly. The minimum expansion of the hydrogel is 85%.

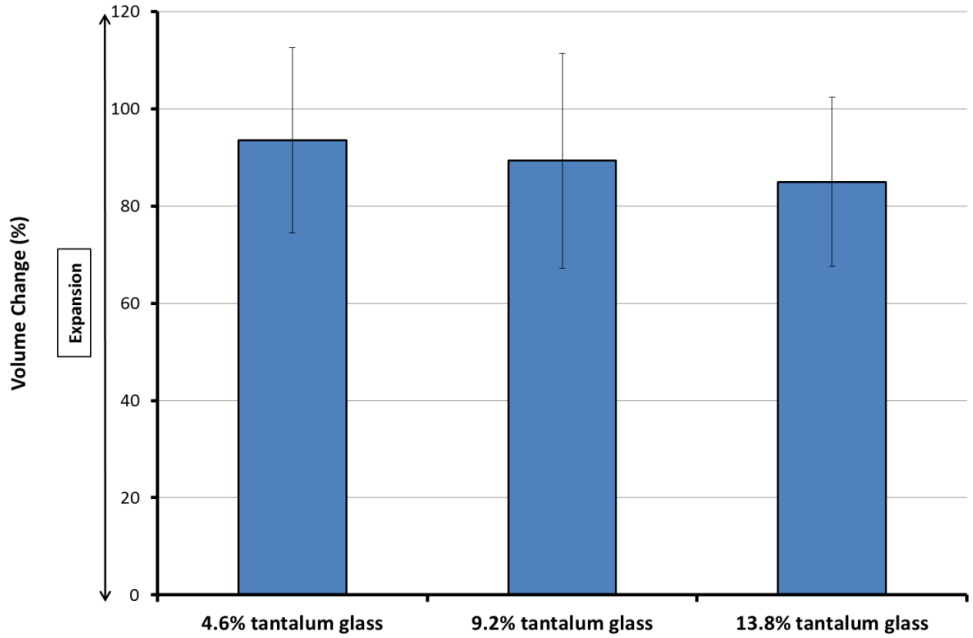

Figure 9.5.36 Tantalum glass with 4.5% alginate size conservation following storage in DI at 37^0C for 7 days (n=5)

9.5.8.4. Discussion

The significantly reduced strength of hydrogel with the tantalum glass, compared to the original glass, may be caused by a reduction in cross-linking density of the alginate. The addition of tantalum to glass has also previously been shown to increase the network connectivity of the glass [517] [518]. Therefore, the reduced strength may be a caused by the reduced release of cross-linking ions from the bioactive glass caused by an increase in the glasses network connectivity.

Further evidence of the weak cross-linking of the alginate is shown in the volume conservation results (Figure 9.5.36). As discussed in Section 5.1.9, alginate hydrogels swell when there is a weak cross-linking of the hydrogel.

Due to the significant decreased strength of the hydrogel, with the strength not reaching the minimum strength required after 7 days, and the significant increase in sample volume it was decided to not complete any further testing with this glass and return to testing with the original glass.

9.5.9. Kidney Embolization

The kidney is an organ which maintains the volume and composition of the body's fluids. The blood supply to the kidneys is through the renal artery. The renal artery divides into the interlobar arteries. As the interlobar arteries enter the renal tissue, the shape of the arteries becomes arc-like; these arteries are the arcuate arteries. The microvasculature of the kidneys is composed of afferent arterioles that divide into cortical radial arteries which supply blood to the glomerular tufts. Efferent arterioles are present to drain the glomeruli [519] [520].

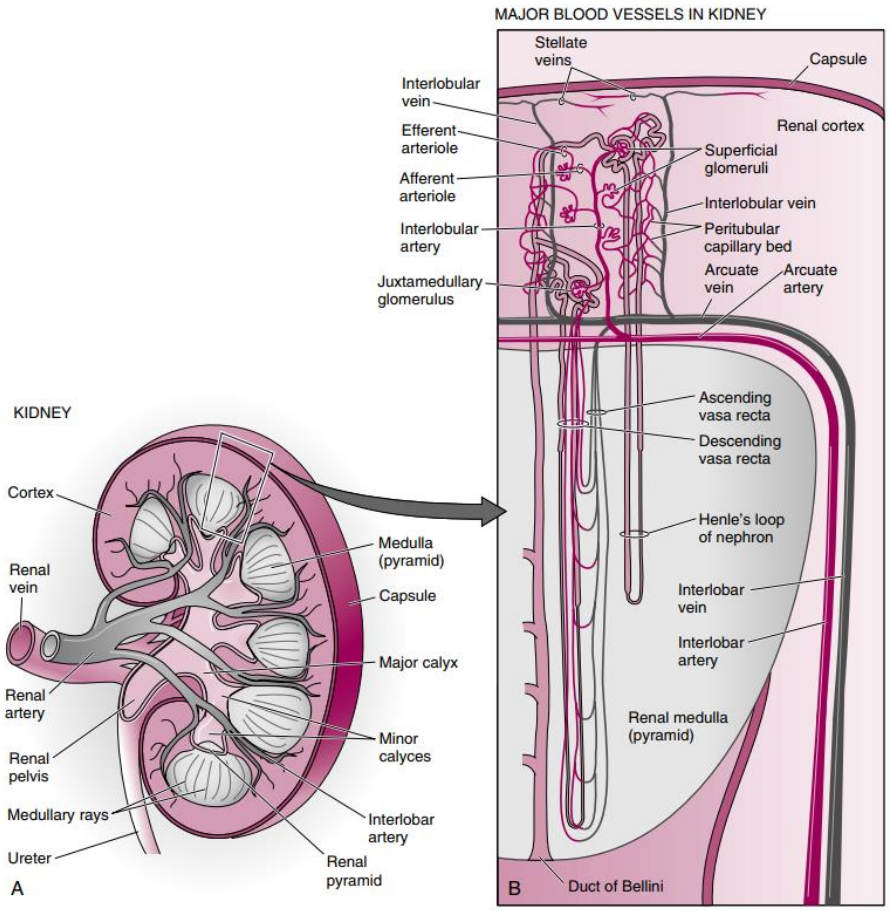

Figure 9.5.37 A) Structure of the kidney and B) the major blood vessels of the kidney [520]

Renal artery embolization is carried out as a treatment for numerous problems such as renal cancer, vascular malformations or to medicate complications from a renal transplant. Renal artery embolization typically involves embolizing the vessels of the kidney. This is carried out by using an embolic agent and in some cases the addition of a coil in the main renal artery. Several embolic agents are used for the embolization of renal arteries. Examples of these are ethanol, PVA particles, microspheres and Gelfoam [521] [522].

9.5.10. Design of injection device

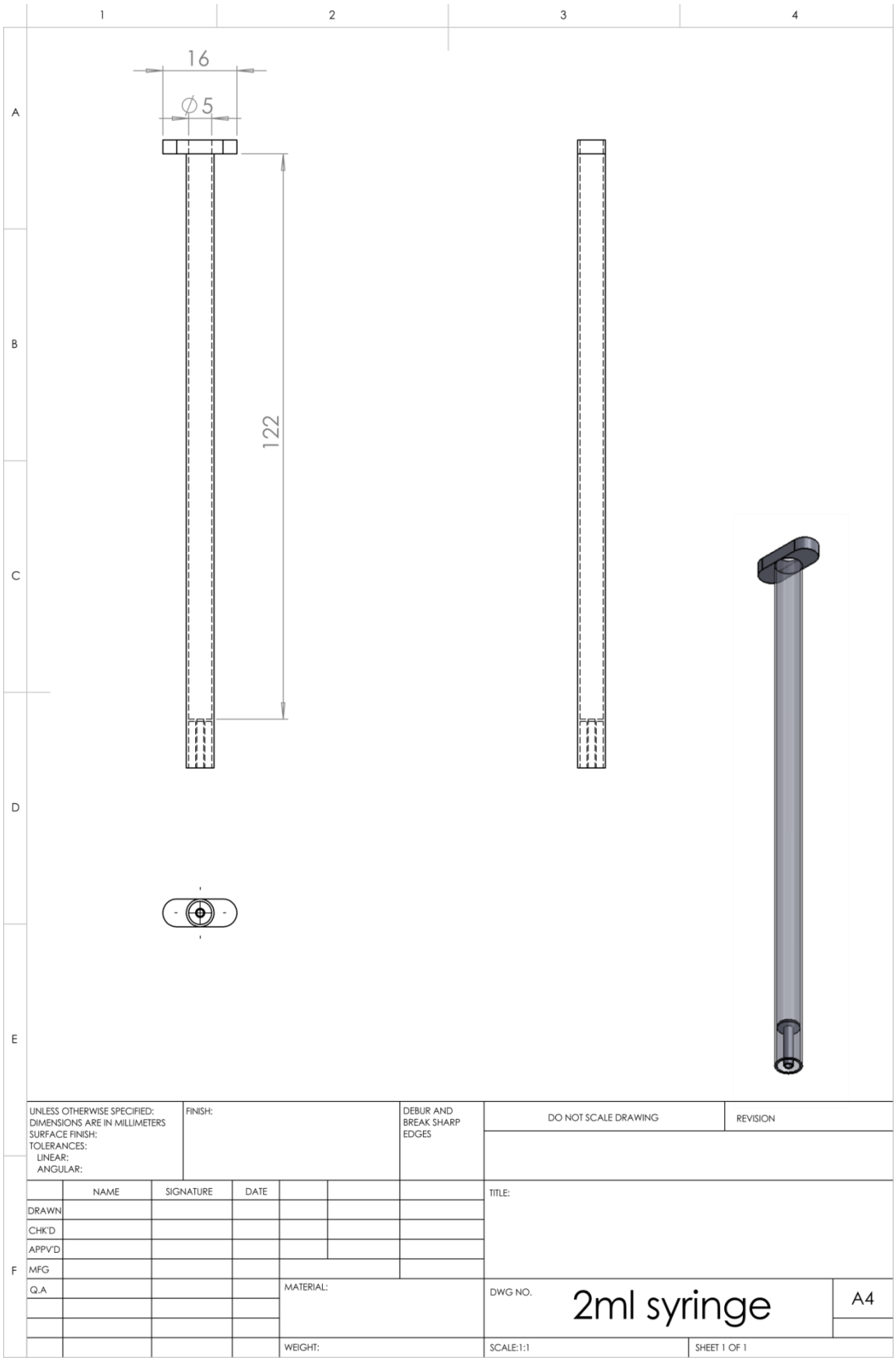

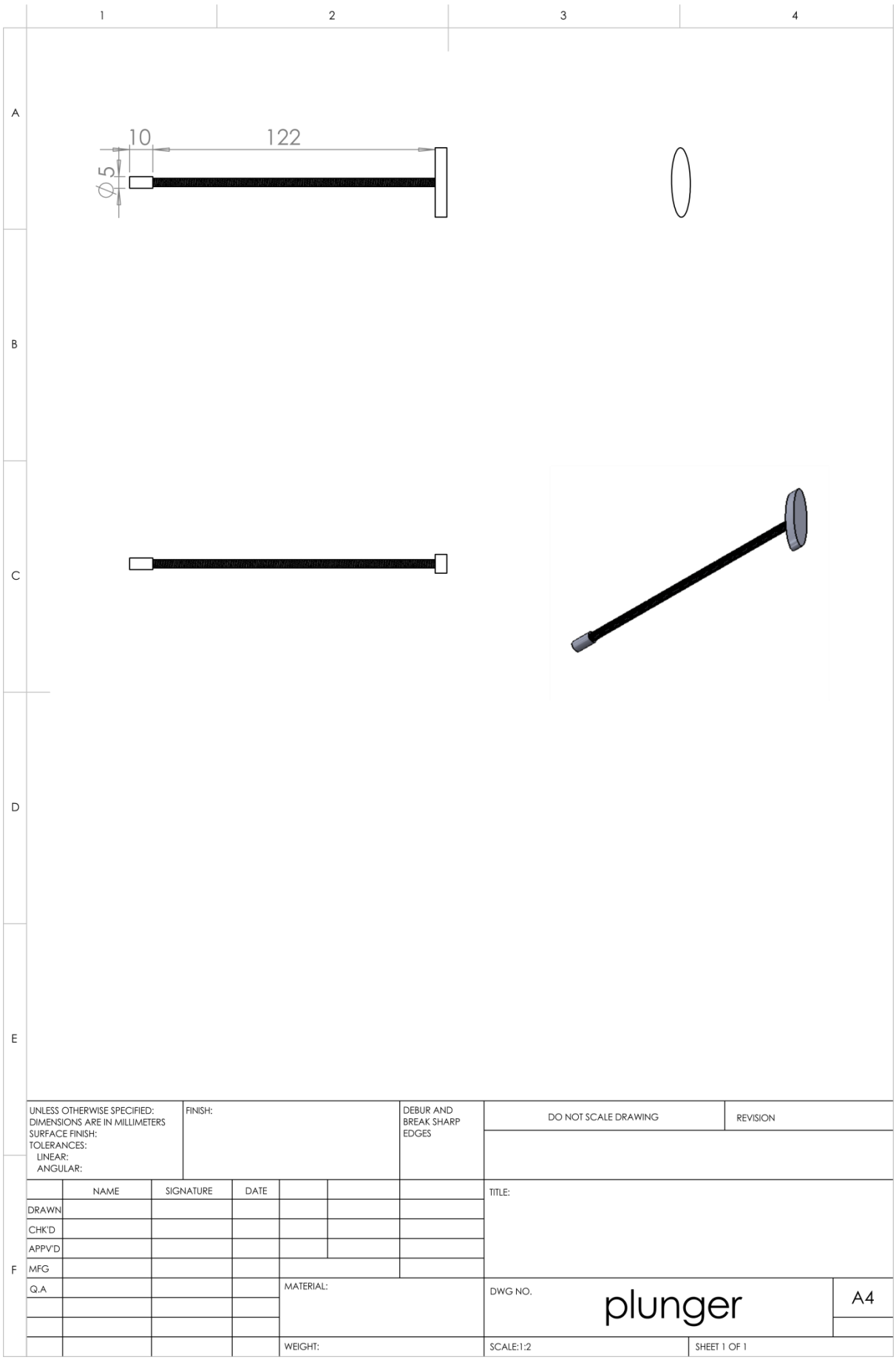

UNLESS OTHERWISE SPECIFIED: DIMENSIONS ARE IN MILLIMETERS SURFACE FINISH: TOLERANCES: LINEAR: ANGULAR:	FINISH:			DEBUR AND BREAK SHARP EDGES	DO NOT SCALE DRAWING	REVISION
	NAME	SIGNATURE	DATE			TITLE:
DRAWN						
CHK'D						
APPV'D						
MFG						
Q.A				MATERIAL:	DWG NO. plunger	A4
				WEIGHT:	SCALE:1:2	SHEET 1 OF 1

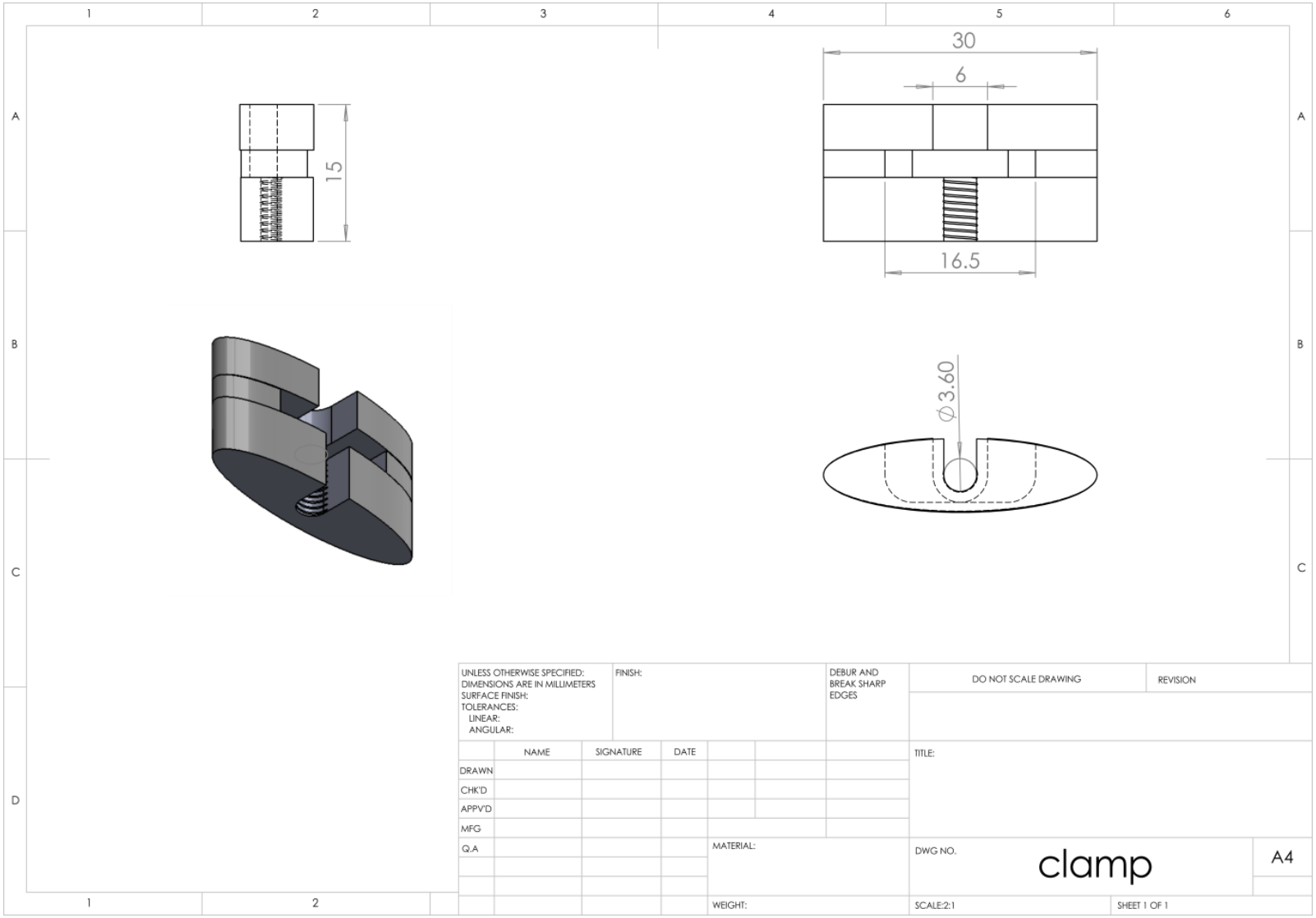
30
6
15
16.5
⌀3.60
UNLESS OTHERWISE SPECIFIED:
DIMENSIONS ARE IN MILLIMETERS
SURFACE FINISH:
TOLERANCES:
LINEAR:
ANGULAR:
FINISH:
DEBUR AND BREAK SHARP EDGES
DO NOT SCALE DRAWING
REVISION
NAME
SIGNATURE
DATE
DRAWN
CHK'D
APPV'D
MFG
Q.A
MATERIAL:
WEIGHT:
TITLE:
DWG NO.
clamp
A4
SCALE:2:1
SHEET 1 OF 1


1
2
3
4
A
B
C
D
E
F
142.50
UNLESS OTHERWISE SPECIFIED:
DIMENSIONS ARE IN MILLIMETERS
SURFACE FINISH:
TOLERANCES:
LINEAR:
ANGULAR:
FINISH:
DEBUR AND BREAK SHARP EDGES
DO NOT SCALE DRAWING
REVISION
NAME
SIGNATURE
DATE
DRAWN
CHK'D
APPV'D
MFG
Q.A
TITLE:
MATERIAL:
DWG NO.
syringe plunger and clamp
A4
WEIGHT:
SCALE:1:2
SHEET 1 OF 1

9.5.10.1. Hydrogel Scale-up

In order to have a sufficient amount of material to fill the microcatheter dead space and the aneurysm, the hydrogel volume will need to be approximately 2ml. The work to date has been completed using 1.2ml of the hydrogel.

To insure there is no change to the hydrogel when scaled up (increased volume), the compressive strength and hydrogel's working and hardening times were examined when the hydrogel's alginate, glass, GDL, EDC and NHS contents were doubled (by weight). There was no change to the alginate concentration.

A reduced strength due to an inhomogeneous gel was expected due to the larger volume to mix, however, Figure 9.5.38 shows that there was no significant change in strength at 1 and 3 days. A significant increase in strength was seen at day 7. The cause of this increase in strength is unknown. It was not expected that the cross-linking density would be affected by the scaling up process.

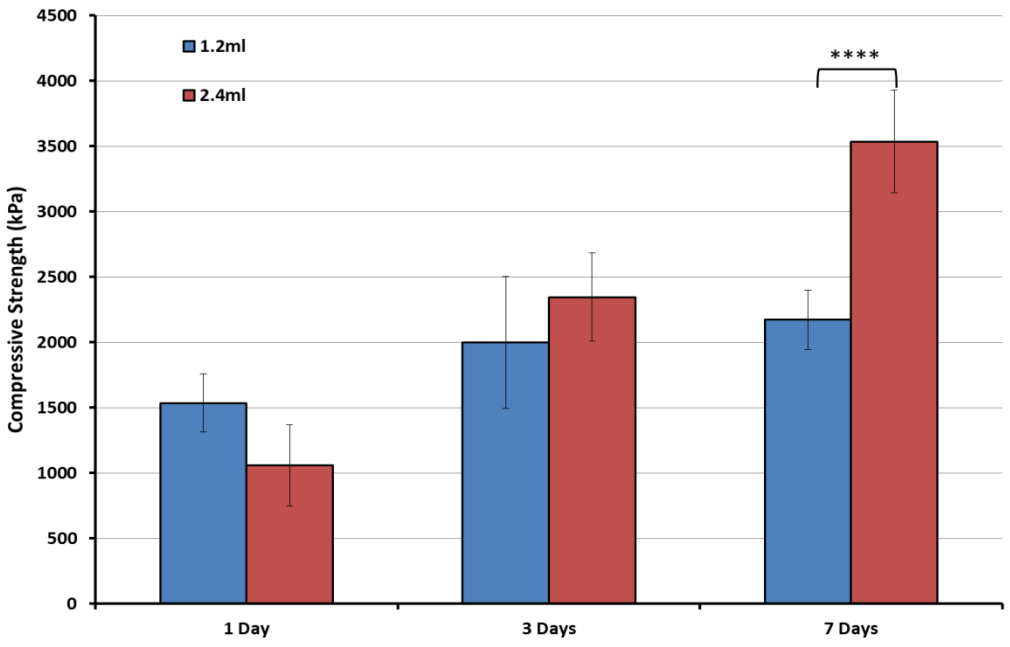

Figure 9.5.38 Compressive stress up to 70% strain of the hydrogel mixed at a 1.2ml and 2.4ml volume following storage at 37^{0}C in DI (n=5)

Figure 9.5.39 shows the increased volume had no significant effect on the hydrogels working or hardening time.

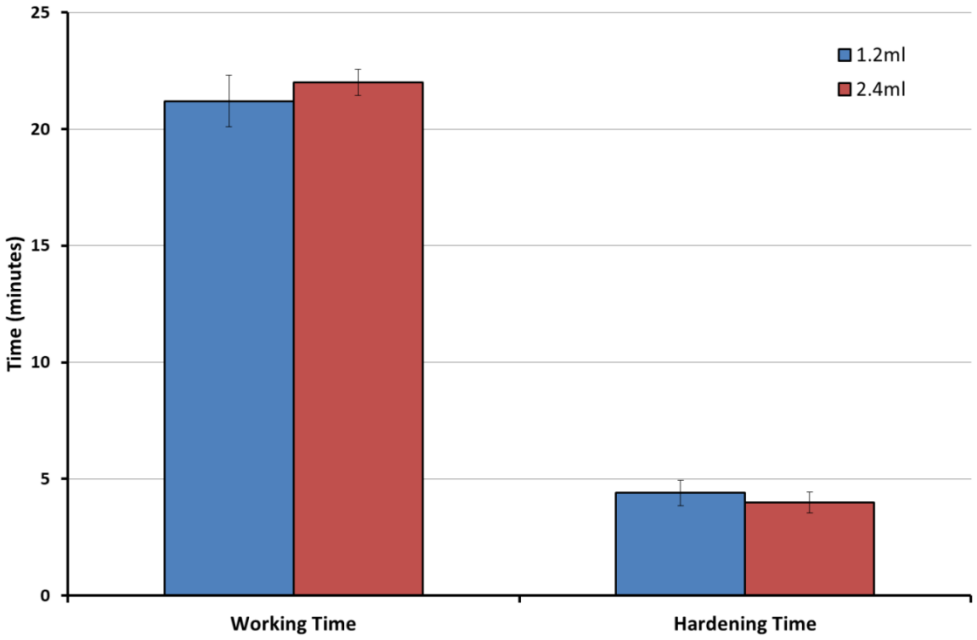

Figure 9.5.39 Hydrogels working and hardening time mixed at a 1.2ml and 2.4ml volume (n=5)